Oligonucleotide Conjugates in DNA Nanotechnology: Applications in Drug Delivery and Gene Silencing

by
Alexander Lee Prinzen

A thesis submitted to McGill University in partial fulfillment of the requirements of the degree of

Doctor of Philosophy

Department of Chemistry
McGill University
Montreal, Quebec, Canada

To my wife Laura Lotfi,

and my family Kimberly Prinzen, William Prinzen,

Kaulin Prinzen and Aleida Prinzen

For your unwavering love and support

Abstract

Oligonucleotides, in the form of DNA and RNA are primarily known as the information and messenger molecules of the cell. Roles beyond this informational molecule have seen oligonucleotides used as structural materials, therapeutics, and molecular recognition components. Combining many of these different roles, the field of DNA nanotechnology has emerged, to generate an unprecedented number of different devices, for applications in sensing, diagnostics, gene silencing and drug delivery. Especially in the case of gene silencing and drug delivery, the biocompatibility, and recognition abilities of DNA place these nanostructures as advantageous carriers for the transport and selective release of these agents. However, by its nature, DNA is chemically inert and to gain more function, chemical modifications are generally needed. This thesis presents new oligonucleotide conjugates used in combination with DNA nanotechnology for the selective delivery/release of both small molecule drugs and antisense oligonucleotides. At first, the evolution of a DNA device that was engineered to selectively amplify the release of small molecule therapeutics, in response to a molecular recognition event is described. A detailed investigation into the design, conjugation chemistry, and kinetics of release are presented. Furthermore, integrating structural DNA nanotechnology and the drug release platform together allows for the generation of well-defined nanostructures which can act as standalone devices without multiple components. Secondly, a new antisense oligonucleotide conjugated with hydrophobic disulfide modifications is generated for their ability to self-assemble into spherical nucleic acids and produce stimuli responsive gene silencing under reducing conditions. The stability of these structures in cellular media and uptake into cells of these structures is thoroughly investigated. Finally, different strategies to improve the drug release device from Chapter 2 for transitioning it into real biological drug delivery applications is developed. Factors such as off-target degradation/activation, delivery to the site of action, rate of metabolism and overall drug specificity are addressed.

Résumé

Les oligonucléotides, sous forme d'ADN et d'ARN, sont principalement connus comme les molécules messagères d'information de la cellule. Au-delà de leur rôle dans la transmission de l'information les oligonucléotides sont utilisés comme matériaux structurels, thérapeutiques et composants de reconnaissance moléculaire. Caractérisés pas ces différents rôles, la nanotechnologie de l'ADN a émergé, pour produire un nombre inédit de dispositifs variés, pour des applications dans les domaines de détection, du diagnostic, l'inactivation génique ou répression génique et l'administration de médicaments. La biocompatibilité et les capacités de reconnaissance de l'ADN placent ces nanostructures comme supports avantageux pour le transport et la libération sélective de ces agents, surtout au niveau du répression génique et du traitement thérapeutique. Etant donné sa nature, l'ADN est chimiquement inerte, cependant pour s'activer, des modifications chimiques sont généralement nécessaires. Cette thèse présente de nouveaux conjugués d'oligonucléotides utilisés en combinaison avec la nanotechnologie de l'ADN pour l'administration/libération ciblée de médicaments à petites molécules et des oligonucléotides anti-sens. En premier lieu, on décrit l'évolution d'un dispositif à ADN qui a été conçu pour amplifier la libération sélective de petites molécules thérapeutiques, en réponse d'un événement de reconnaissance moléculaire. Une étude détaillée de la conception, de la chimie de conjugaison et de la cinétique de libération est présentée. En plus, l'intégration de la nanotechnologie structurelle de l'ADN et de la plate-forme de libération de médicaments permet la génération de nanostructures bien définies qui peuvent agir comme des dispositifs autonomes sans composants multiples. En second lieu, un nouvel oligonucléotide anti-sens conjugué à des modifications disulfure hydrophobes est généré due à leur capacité de s'auto-assembler en acides nucléiques sphériques et à produire une répression génique sensible aux stimuli dans des conditions réductrices. La stabilité de ces structures dans les milieux cellulaires et leurs absorptions dans les cellules sont minutieusement étudiées. Enfin, différentes stratégies sont développées pour améliorer le dispositif de libération de médicament du chapitre 2, dans le but de les transformés en applications concrètes dans le domaine libération de médicament

biologique. Des facteurs tels que la dégradation/l'activation hors cible, l'administration au site d'action, le taux de métabolisme et la spécificité globale du médicament sont abordés.

-Translated by Laura Lotfi-

Acknowledgments

Six years has passed so quickly. Thank you to all the people who have made these last six years unforgettable. First and foremost, I would like to thank my beautiful wife Laura Lotfi for all her love and support during my degree and especially during the writing process. We did it and I love you Habibi! Secondly, I would like to thank my supervisor Dr. Hanadi Sleiman for all her guidance and support throughout my research. I always look forward to our meetings to discuss new ideas and directions for the research. Her hard work, dedication, and motivation inspire me.

I would like to thank Dr Karine Auclair and Dr Paul Wiseman for actively being great committee members over the last six years. As well as Dr Anthony Mittermeir for all his guidance and invaluable insight into modelling kinetic processes.

I am grateful to each person that I have had the privilege of working with. I would like to thank Daniel Saliba for all his hard work and dedication in collaborating on the nanostructures for small molecule release. As well as Christopher Hennecker for hybridization kinetics and Dr Tuan Trinh for all the AFM images and motivational speeches. I would like to also thank Jathavan Asohan for all his valuable insight into *in vitro* gene silencing and collaborating on the disulfide spherical nucleic acid project. Violeta Toader for the innumerable times she has synthesized various phosphoramidites. Alexander Wahba for running all the oligonucleotide m/s and all insights in m/s analysis. Tyler Brown for all his work on the antibody oligonucleotide conjugates.

I am grateful to all Sleiman lab members who I have had the privilege of getting to know these past six years as both friends and colleagues. Alexander Rousina-Webb, Amani Hariri, Amine Garci, Aurélie Lacroix, Casey Platnich, Christophe Lachance-Brais, Danny Bousmail, Daniel Krauss, Daniel Saliba, Donatien de Rochambeau, Empar Vengut Climent, Fangzhou Zhao, Felix Rizzuto, Ghufran Rafique, Hammond Sun, Hassan Fakih, Janane Rahbani, Jathavan Asohan Johans Fakhoury, John Hsu, Justin Conway, Kai Lin Lau, Kamila Mustafina, Katherine Bujold, Maciej Barlog, Michael Dore, Mohammad Askari, Nicole Avakyan, Paty Islas Garcia, Shayne Gracious, Shaun Anderson, Sean Laxton, Sepideh Kaviani, Son Bui, Tuan Trinh, Tyler Brown, Violeta Toader and Xin Luo. Good Luck everyone!

Thank you to all the faculty and staff in the department as well for all your friendships and company. I would also like to thank Chantal Marotte keeping me up to date on deadlines. I would like to thank the department of Chemistry, McGill University, and NSERC for all the financial support over this time. Thank you to the many people outside of research, especially my friends from Western University for all their support as well.

Finally, I would like to thank my entire family for their love and support during my PhD journey. A special thank you to Dr. Henry Stronks for his words of encouragement during my degree and reminding me that it is all worth it. Thank you to my parents Will and Kim as well as my brother Kaulin, sister in-law Tana, sister Aleida and her boyfriend Tom for their support and love, and my extended family who are always there, especially my Opa, Oma and Grandma. To my family in Lebanon as well Hamo (Mamito), Tony (Papito), Bedouin, Bernedette and Sayed, I am looking forward to all seeing you soon. Once again, I would like to thank my wife Laura Lotfi, because I cannot thank her enough for her patience, love, kindness and being my other half. Love you always.

Table of Contents

Table of Figures

List of Tables

List of Abbreviations

1D One dimensional
2D Two dimensional
3D Three dimensional
A Adenine
AGE Agarose gel electrophoresis
AFM Atomic force microscopy
AuNP Gold nanoparticle
bp Base pair
C Cytosine
CLL Chronic lymphocytic leukemia
CLSM Confocal laser scanning microscopy
CMC Critical micelle concentration
CPG Controlled pore glass
Cy3 Cyanine 3
Cy5 Cyanine 5
Cy5.5 Cyanine 5.5
D-DNA Dendritic DNA amphiphile
DLS Dynamic light scattering
DMEM Dulbecco's modified eagle's medium
DMT Dimethoxytrityl
DNA Deoxyribonucleic acid
Ds Double-stranded
DS Disulfide
DTT Dithiothreitol
EDTA Ethylenediaminetetraacetic acid
ESI Electrospray ionization
FACS Fluorescence-activated cell sorting
FBS Fetal bovine serum
FRET Förster resonance energy transfer
G Guanine
HEG Hexaethylene glycol
HE12 Dodecane
HPLC High performance liquid chromatography
HSA Human serum albumin
L_n Number-average contour length
L_w Weight-average contour length
LC-MS Liquid chromatography-mass spectrometry
LNA Locked nucleic acid
miRNA Micro RNA
MW Molecular weight
OD Optical density xxii

PAGE Polyacrylamide gel electrophoresis
PBS Phosphate-buffered saline
PPO Polypropylene oxide
PCR Polymerase chain reaction
PEG Polyethylene glycol
RH Hydrodynamic radius
ROMP Ring opening metathesis polymerization
RNA Ribonucleic acid
RT Room temperature
SDS Sodium dodecyl sulfate
siRNA Small interfering RNA
ss Single-stranded
T Thymine
TAMg Tris-acetate-magnesium buffer
TBE Tris-boric acid-EDTA buffer
TEM Transmission electron microscopy
TEMED Tetramethylethylenediamine
Tris Tris(hydroxymethyl)aminomethane
UV-Vis Ultraviolet-visible

|1|

Introduction

1.1. Preface

Oligonucleotides in the form of DNA and RNA are primarily known in biology as information and messenger molecules. Over the last thirty years of research, oligonucleotides have found functions beyond information, storage and processing and have been used as structural materials, therapeutics, and recognition components. This progression into these other areas has been primarily due to the physical and chemical properties of oligonucleotides such as: biocompatibility, predictable and programmable molecular recognition, and water solubility. While remarkable achievements have been made using unmodified oligonucleotides, the continued advancement of these functions has been, and will be, greatly facilitated through chemical modification. This chapter gives an overview of how the physical and chemical properties of oligonucleotides have allowed for them to be taken out of their biological role and used as a structural material. Current methods for synthesizing and chemically modifying oligonucleotides are then discussed. Finally, a discussion on how chemical modifications are facilitating greater applications for oligonucleotides as structural materials, therapeutics, and recognition components, will be the focus.

1.2. DNA as the Information Molecule and Structural Features

Heredity, or the transfer of information from parents to offspring had entered debates among scientists in the early 1800's. Through his now famous pea experiments, patterns of inheritance were established by Gregor Mendel in the 1860's, however they were largely ignored.[1] Charles Darwin formulated his theory of evolution based on natural selection and heredity as its mechanisms in 1859.[2] Although both Darwin and Mendel had different takes on how heredity worked, they both imagined that there must be a particle of heredity; Darwin called this particle "gemmules" and Mendel "factors". Only a few years later after Darwin had formed his theory of natural selection, DNA was first isolated by the Swiss chemist Friedrich Miescher.[3] Interestingly, after its discovery, Miescher did not expect it to be the molecule of heredity, as in his opinion it lacked the variability needed to generate the diversity among organisms. Like most chemists of

the day, he thought heredity was passed through proteins which were known to exist in a wide variety of forms.

DNA was first identified as the information molecule through the experiments of Avery, Macleod and McCarty in 1944 which demonstrated that DNA (not protein) could transform the properties of cells.[4] Not even a decade later in 1953, Watson, Crick and Franklin determined the structure of DNA as being the double helix structure we know today.[5-6]

Chemically, DNA is a biopolymer made up of four nucleoside monomers (Figure 1.1). Each monomer consists of a nucleobase, connected to a five-membered deoxyribose sugar, which are then connected through, phosphodiester bonds to form the polymer. Nucleobases can be split between the purines (adenine (A) and guanine (G)) and the pyrimidines (thymine (T) and cytosine

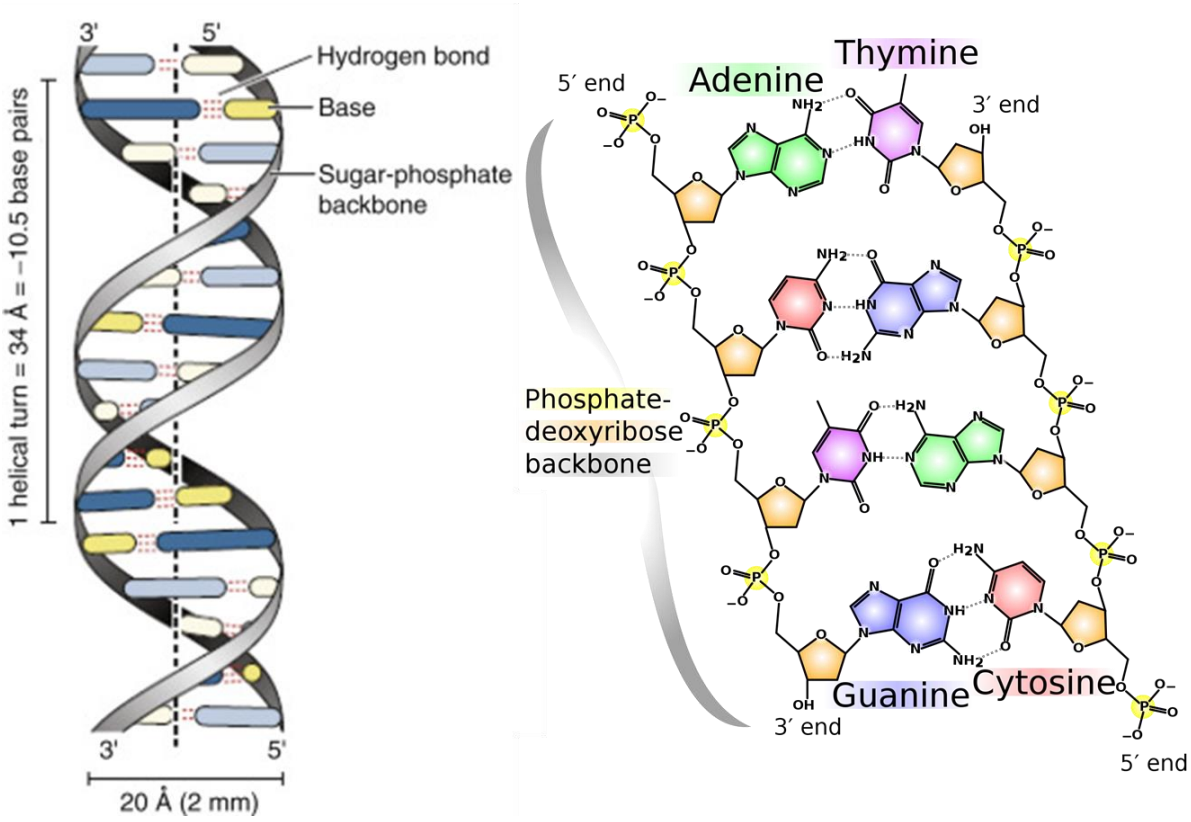

Figure 1. 1 Structural Features of DNA. (Wikipedia)

(C)). The 5’ and 3’ ends of DNA are sugar designations and point to whether the terminal OH is on the 5’ or 3’ carbon. Hydrogen bonding occurs between A:T and G:C forming an antiparallel (3’ of one strand is on the same side as the 5’ end of the other) double helix of two strands of DNA, this bonding is otherwise known as Watson-Crick base pairing.

Binding of DNA is highly co-operative and is assisted by other interactions such as base stacking (π-π interactions), hydrophobic effects and van der Waals forces.[7] Additionally, cations are needed to balance electrostatic repulsion between charged phosphates. The exact order or “sequence” that these monomers are connected is the code that determines how proteins are ultimately made. The double helix itself appears as a rigid molecule over 10nm, with a persistence length of 50nm.[8] Though many different forms of DNA exist, the most common form of DNA found in nature is call B-form, which has well defined size parameters such as; 3.4nm per turn of the helix made of approx. 10.5 bases and a diameter of 2.0nm.[9] Thermodynamically, the relative stability of double stranded DNA can be roughly estimated by the percentage of G:C base pairing in the strand, as there are more hydrogen bonds between these bases and, the order of hydrogen bond donors and acceptors provides attractive secondary interactions.[10] Overall, it is these structural features, and programmability of DNA that have allowed for DNA to be taken out of its biological context and used as an assembly material for various nanostructures.

1.3. Structural DNA Nanotechnology

During a biological process called genetic recombination, two double-stranded DNA molecules become separated into four strands to exchange segments of genetic information. These separated single strands, result in base pairing that leads to a four-stranded DNA structure. The “Holliday junction” (named after the British geneticist Robin Holliday) travels along the DNA duplex by “unzipping” one strand and reforming the hydrogen bonds on the second strand.[11] Inspired by the Holiday junction, in 1982 Nadrian Seeman established the field of DNA nanotechnology by making 3- and 4- way junctions that were able to self-assemble further into networks with repeating patterns.[12-14](Figure 1.2A) As this junction was based on genetic recombination, the sequences used in the initial report were self-complementary, which allowed

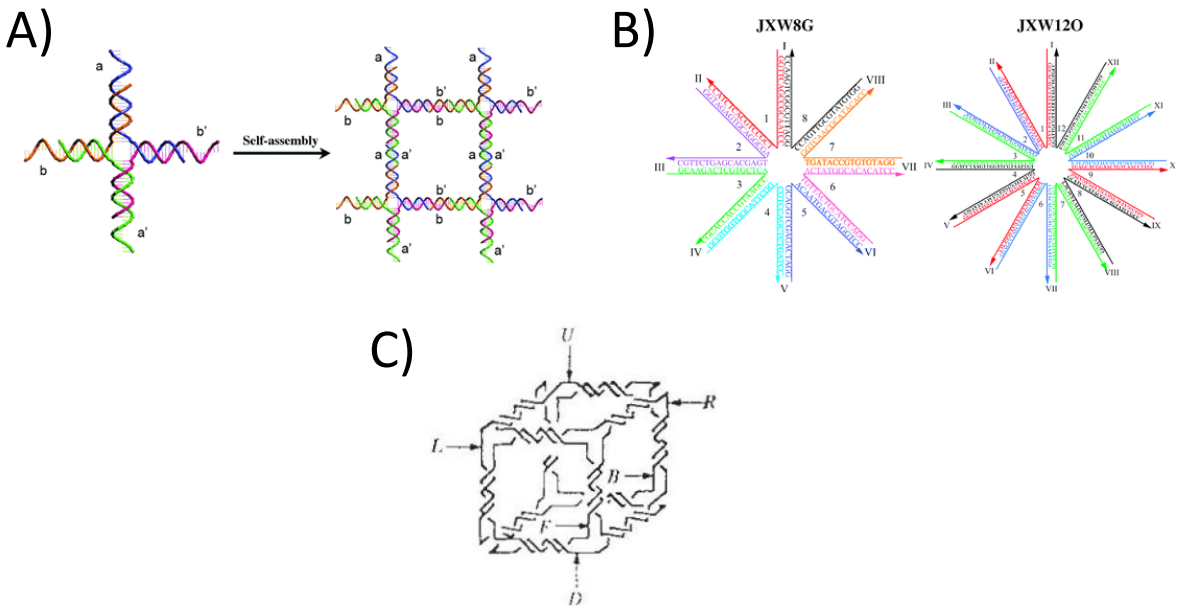

Figure 1. 2 Early DNA structures made in DNA Nanotechnology.

A) Holliday Junction for generating 2D networks. Reproduced with permission ref [25] (John Wiley and Sons 2006) B) Multiarm DNA junctions design. Reproduced with permission ref [18] (American Chemical Society (ACS) 2007) C) Design of first discrete 3D DNA cube. Reproduced with permission ref [19] (Nature Publishing Group (NPG) 1991)

the branching point to migrate, destroying the junction. To make static junctions, Seeman introduced sequence asymmetry, by generating junctions with all unique sequences which could not migrate, and with this was able to further make 5-, 6-, 8- and 12- way junctions.[15-18](Figure 1.2B) The use of multiway junctions would then go on to further generate the first discrete 3D DNA cube in 1991.[19](Figure 1.2C) Extending from Seeman's original work three different areas in structural DNA nanotechnology have been established over time.

1.3.1. Tile Arrays

As the first type of DNA nanostructure, the use of tile arrays in the literature has been extensively explored. To address the flexibility issues that the original junctions had, additional crossover motifs were proposed, in which strands within duplex DNA "crossover" to another strand and these became known as double crossover (DX) junctions.[20] (Figure1.3A) The motif consists of two double helical domains as well as two crossover points, and these new tiles showed a much

greater stiffness than their linear counterparts.[21-22] This extra stiffness allowed for these DX tiles to be assembled into 2D lattices through the use of "sticky ends" and formed the foundation for further types of tiles, including the even more rigid triple crossover (TX) junction.[23-26](Figure 1.3B) Other types of tiles that came out of this work include 3-[27-28] (Figure 1.3C) and 6-helix bundles[29], tensegrity triangles[30], cross-shaped tiles[31] and three-point stars[32].(Figure 1.3D)

To create higher complexity and addressability of these tile based assemblies, while limiting the number of strands, sequences which can be reused, better known as "sequence symmetry" was introduced by Mao et al.[33] Sequence symmetry avoids the challenge of needing perfect stoichiometry of the DNA strands for self-assembly, leading to less defects. The Mao group was

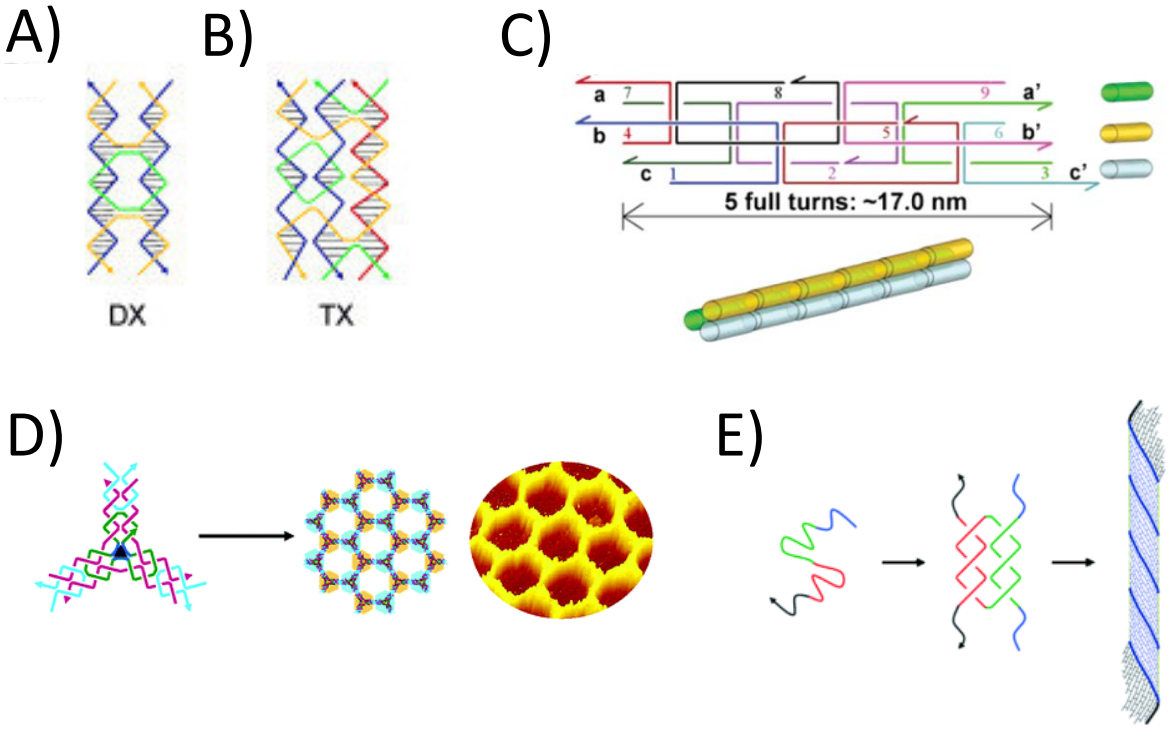

Figure 1. 3 Producing of more complex DNA structures using DNA tile assemblies.

A) and B) Double and Triple crossover tiles. Reproduced with permission ref [25] (John Wiley and Sons 2006) **C)** Assembly of 3-Helix bundles. Reproduced with permission ref [27] (ACS 2005) **D)** Assembly of three-point star. Adapted with permission from ref [32] (ACS 2005) **E)** Assembly of nanotubes from minimal number of DNA strands. Reproduced with permission ref [34] (John Wiley and Sons 2006)

able to generate tile arrays only using one or two strands, generating assemblies on the millimeter scale.[34-35](Figure 1.3E)

Other methods to increase complexity of tile arrays include hierarchical assembly[36-38], algorithmic[39-42] and nucleated self-assembly[43-44]. While over time the complexity of tile arrays has improved, the main constraint of these structures is that they are limited to being periodic in nature. Additionally, as these structures are typically formed through step-growth polymerization processes, there is poor control over their final size. While progress has been made to overcome these issues[44-46], another form of structural DNA nanotechnology has emerged, deemed DNA origami, allowing for completely addressable assemblies.

1.3.2. DNA Origami

Paper origami is thought to have been invented by the Japanese about 1000 years ago, it is the process of folding paper into decorative shapes and figures. While origami, when first invented, was for decorative purposes, today the overarching principle of folding has found applications ranging from robotics[47] to retinal implants[48]. Paul Rothemund was the first person to bring the origami concept into the world of DNA nanotechnology.[49] In 2006, Rothemund used an isolated long genomic single stranded DNA from a bacteriophage and, akin to paper origami, folded this long strand into a pre-determined shape. He was able to fold the genomic DNA using hundreds of short oligonucleotide strands deemed “staple strands”, which (advantageously), did not need to be added with precise stoichiometry or even with high purity.[49-50](Figure 1.4A) With the assistance of computational modelling[51-53], the use of this origami method has allowed for the assembly of any 2D shape imaginable, including; happy smiles, stars and rectangles.[49, 54](Figure 1.4B)

To bring origami into the 3rd dimension, two different methods were proposed in 2009, by William Shih and Ned Seeman’s student, Hao Yan. In the method developed with Shih, DNA-dense nanostructures were assembled through the formation of multi-layered origami by packing the DNA-helices in 3 dimensions.[55-56](Figure 1.4C) Using this approach, many origami shapes could be made that were curved, by selectively deleting base pairs.[57-58] Hao Yan’s

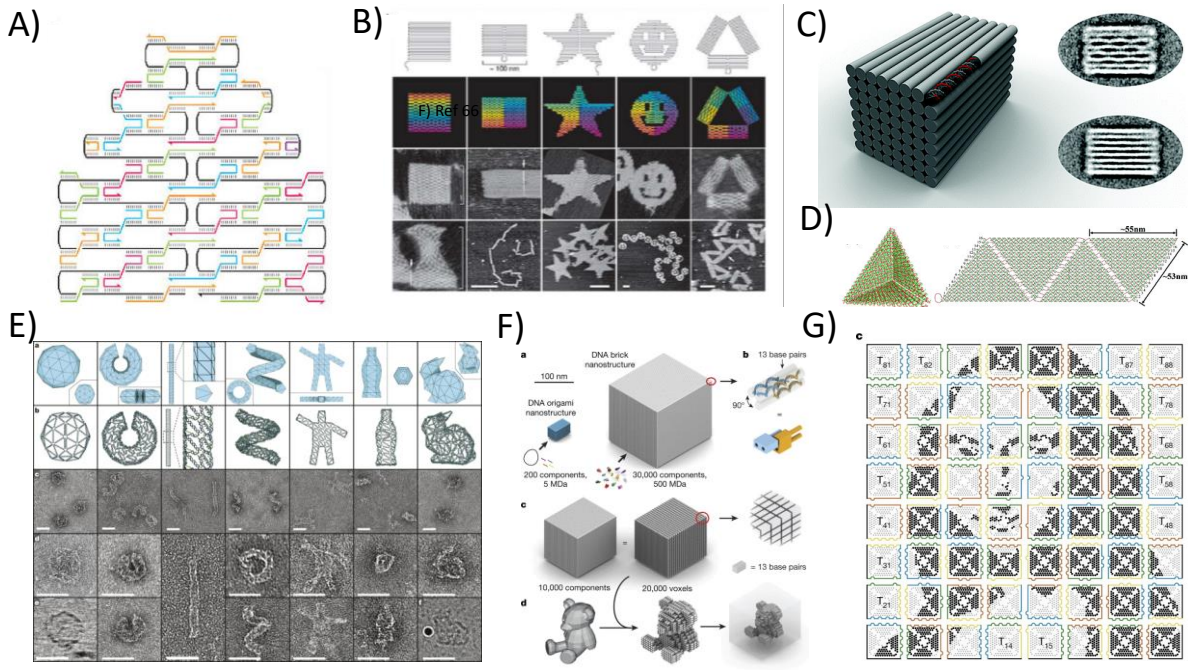

Figure 1. 4 DNA nanostructures from DNA origami.

A) and B) Outline and initial structures made using the DNA origami approach. Reproduced with permission ref [49] (NPG 2006) **C)** 3D DNA origami made using multiple layers. Reproduced with permission ref [55] (ACS 2009) **D)** 3D DNA origami made by stitching origamis together. Reproduced with permission ref [62] (ACS 2009) **E)** 3D origami made using a wireframe approach. Reproduced with permission ref [53] (NPG 2015) **F)** DNA brick assembly Reproduced with permission ref [66] (NPG 2017) **G)** Fractal assembly of DNA origami. Reproduced with permission ref [67] (NPG 2017)

approach was to create hollow topologies by stitching separate pre-assembled origamis together with linking strands, forming well defined boxes. [59-62] (Figure 1.4D) This strategy was also used by Gothelf and Kjems, to make DNA boxes with controllable lids.[63] In 2015, wireframe origami was proposed by Zhang *et. al.* as an alternative method to generate 3D structures, where a 3D object is converted into a minimal, mesh, scaffold and each edge is a DNA duplex.[61] By using the scaffold strand once along each edge, more complex structures are able to be formed including a DNA bunny and waving person.[53](Figure 1.4E)

Still, while a vast number of structures can be formed using these methods, limitations to origami remain. One of the most obvious limitations is that the structures formed are confined to the length of the genomic DNA scaffold. To address this, Yin *et al.* developed “DNA bricks” which use

single-stranded tiles with four binding sites, to be assembled as pixels that, when combined together make the desired shape.[64] This approach has also been expanded to rival the complexity of 3D origami to make various shapes including a DNA brick teddy bear.[65-66](Figure 1.5F) Moreover, the scaffold strand itself may not have the most optimal sequences for efficient folding. Qian and coworkers address this by generating multiple DNA origami arrays, linking them together in a multistage assembly process called "fractal assembly".[67] Using this method, they were able to make many images including the Mona Lisa.(Figure 1.5G)

Another limitation to origami is the number of strands used for assembly. Considering that the cost of DNA has been drastically reduced over time, this may not seem like that much of a drawback. However, as the sequence pool of strands increases, there is a marked decrease in the uniqueness of these strands. This reduced uniqueness can result is malformed structures and reduced yields. A few groups have tried to address this limitation by introducing design principles that promote well-folded origami as opposed to misfolded structures[68] and minimize sequence space with reusable sequences[69]. The bio-production of DNA origami has also been achieved by the Dietz group, using bacteriophages and built-in DNAzyme "scissors", allowing them to generate 163mg of an origami nanorod.[70] Additionally, Yin et al. have described single stranded origami, which they were able to replicate in vitro, and assemble into complex structures.[71] Overall, DNA origami is a powerful method in DNA nanotechnology to generate a plethora of structures. While the complexity of origami has increased over time, still the large number of strands and waste may hinder its applicability in many instances. Therefore, it may be beneficial to generate simpler structures that are more well defined.

1.3.3. DNA Minimal Assemblies

The philosophy of minimalism has gained popularity today, and is about living with less, to make room for more important things in life. Like this lifestyle philosophy, DNA minimal structures are assembled using the least number of strands possible. DNA minimal structures can keep their function while reducing design complexity, which could aid their transition into clinical applications, as current FDA regulations require safety profiles for individual components. In

some of Seeman's original work a DNA cube was made only using 10 DNA strands.[19] Since then other DNA minimal structures have been developed such as Turberfield's tetrahedron[72] (Figure 1.5A)(made of 4 strands), as well as DNA minimal cages with various geometries[73] (Figure 1.5B) and nanotubes[74] with controlled lengths[75] developed in the Sleiman group(Figure 1.5C&D).

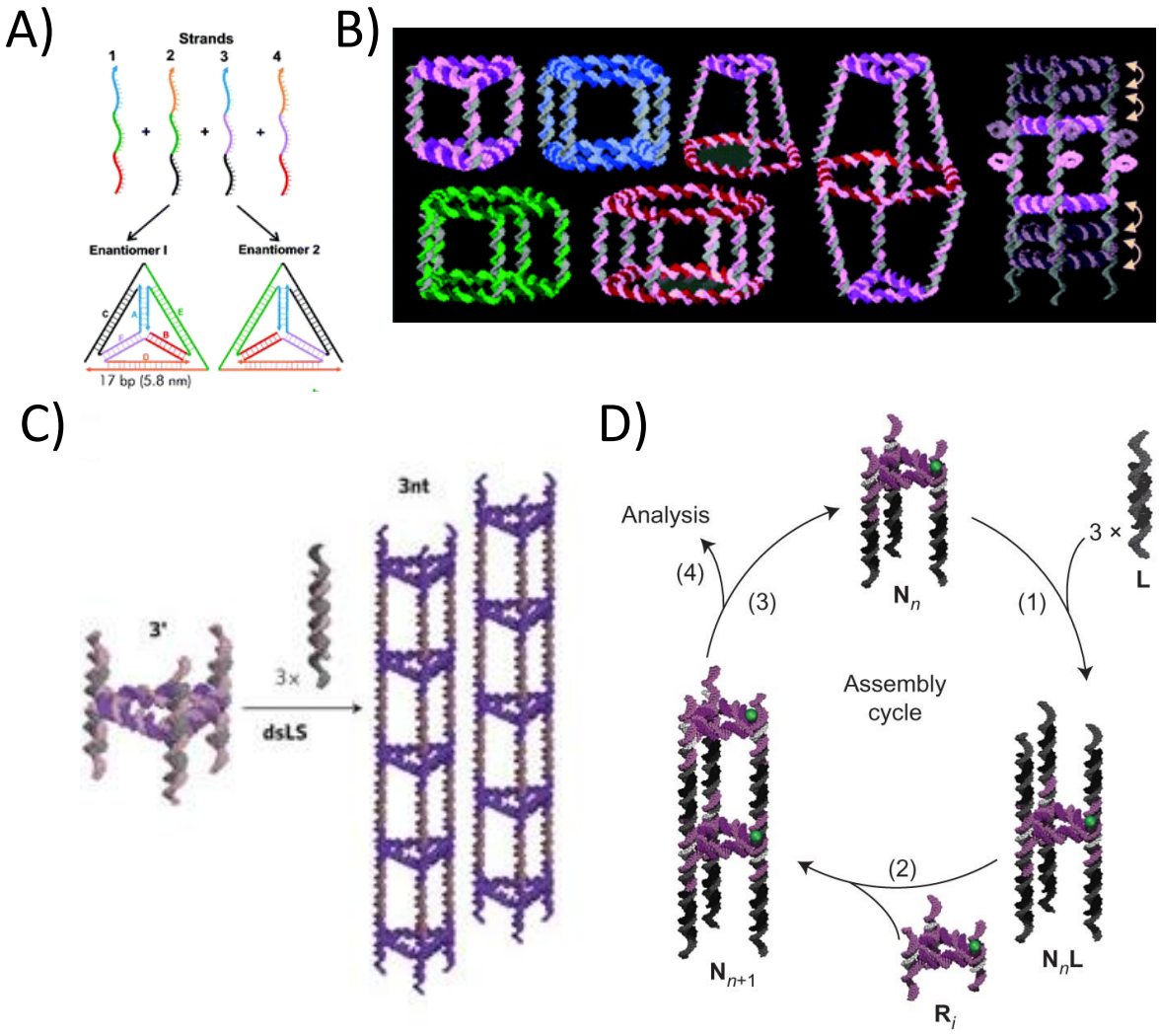

Figure 1. 5 DNA Minimal Assemblies.

A) DNA tetrahedron produced by 4 strands. Reproduced with permission ref [72] (Royal Society of Chemistry (RSC) 2004) **B)** DNA minimal cages. Reproduced with permission ref [73] (ACS 2007) **C)** DNA minimal nanotubes. Reproduced with permission ref [74] (NPG 2009) **D) DNA** minimal nanotubes with controlled lengths. Reproduced with permission ref [75] (NPG 2015)

1.3.4. DNA Nanotechnology Perspective

Overall, by its nature, unmodified DNA is chemically inert, and as such, applications of unmodified DNA nanostructures have been limited. To increase the functionality of DNA, chemical modifications can be made which can be used to improve stability, add targeting ability, improve binding, and organize more functional materials. While many of these modifications can be made directly to the DNA structure itself, a large subset of the modifications includes conjugating DNA with molecules with varied molecular weights. These oligonucleotide conjugates have formed the basis for many of the applications observed by oligonucleotides and DNA nanotechnology and allowed for their use outside of purely as information and structure-based materials. Seeman himself saw the potential for these structures from the very beginning when he proposed to use his structures to help with protein crystallization. Here, we will initially go through some of the DNA conjugation strategies, followed by how these conjugates are enabling DNA to be used further outside of its traditional biological context, often in combination with DNA nanotechnology.

1.4. Conjugation to Oligonucleotides

Almost as early as DNA was identified as the genetic material by Avery *et. al.* it was noticed that there were chemical variations in nucleosides of the same type. In 1948, Rollin Hotchkiss, using paper chromatography, discovered methylated cytosine.[76] Many researchers thought these biological DNA modifications were to regulate gene expression, with confirmation of this coming through a series of experiments in the 1980's by Holliday and Compere, forming the chemical basis for epigenetics.[77-78] The importance of DNA modification in biology cannot be understated as nature processes mRNA post-synthesis as well, leading to a greater number of functions a single mRNA transcript can have. As chemists, we can modify DNA outside of biological systems through chemical reactions. Bio-conjugation in general is the process of conjugating two molecules together, at least one being a biomolecule, such as a protein, carbohydrate, or nucleic acid. Chemists through years of development are now able to generate and modify DNA in unparalleled ways, the origins of which begin with DNA synthesis.

1.4.1. DNA Synthesis

Biologically, DNA synthesis occurs during cell replication and RNA synthesis during transcription. Synthesis is achieved used triphosphate nucleotides and DNA/RNA polymerases which synthesize the oligonucleotides in the 5' to 3' direction. Chemically, the first dinucleotide synthesis was carried out by Michelson and Todd in 1955 with the preparation of a dithymidinyl nucleotide.[79](Figure 1.6A) To generate the phosphate link between two thymidine nucleosides, a 5' benzyl protected thymidine was activated on the 3' end with phenylphosphoryl dichloride and reacted with the 5' hydroxyl of a 3' protected thymidine. While the reaction gave a reasonable yield it did take some time to react. As well, the stability of the phosphoryl chloride intermediate was an issue, as it was sensitive to hydrolysis. In terms of synthesizing *oligo*nucleotides, the challenge was being able to achieve high sequence fidelity i.e. control over the exact sequence. Due to this, traditional polymerization techniques could not be used as they do not provide enough control over monomer addition and length.

Two important concepts were introduced by Khorana in the 1950's, that helped to address this issue and made possible the synthesis of oligonucleotides more than just a few monomers long. The first concept was the "on-off" protection scheme, where monomers are added sequentially one after the other, by selectively deprotecting the 5' end of the growing oligonucleotide.[80-81] Remarkably, the mild acid sensitive dimethoxytrityl (DMT) protecting group Khorana used in his synthesis is still in use today. The other concept was to use a stable 3' phosphorylated nucleosides to condense with the 5' hydroxyl of another 3' protected nucleoside using condensation reagents such as dicyclohexyl carbodiimide (DCC).[82](Figure 1.6B) These two concepts together allowed for the synthesis of a 72mer t-RNA, and this "on-off" cycle remains virtually the same today, except for the addition of an oxidation step.[83] In additon, the nucleosidyl exocyclic amine protecting groups Khorana used are still the same today.

Three major improvements to Khorana's synthesis were made by Letsinger and Kelvin Ogilvie in the 1960's and 70's; solid-phase synthesis[84], the phosphotriester approach[85] and the introduction of the phosphite-triester method[86]. Solid phase synthesis allowed for the high throughput of

reagents and swift purification. Introduction of a β-cyanoethyl protecting group to the

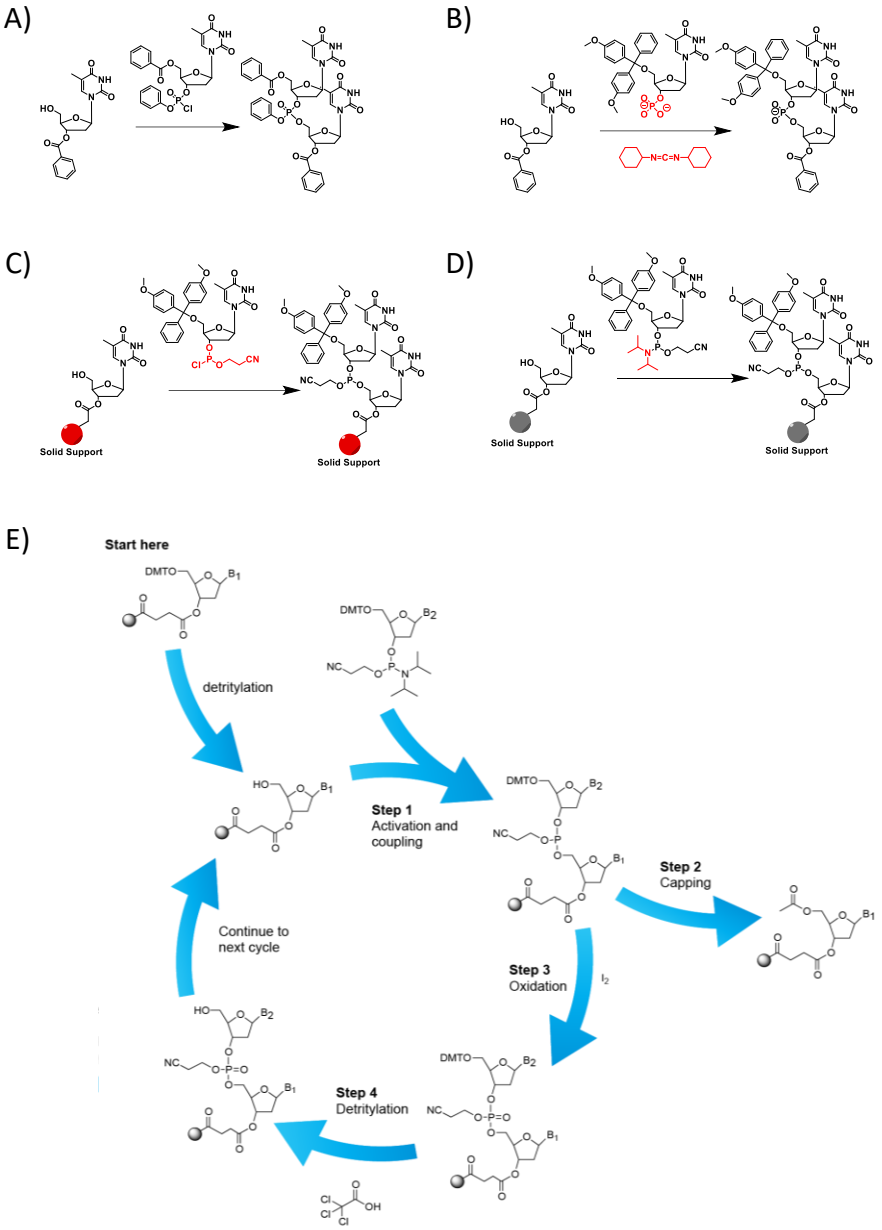

Figure 1. 6 Evolution of DNA Synthesis.

A) First dinucleotide synthesized by Michelson and Todd ref [79] **B)** Scheme for Khorana's dinucleotide synthesis using DCC. ref [82] **C)** Improvements made by Letsinger to DNA synthesis; solid phase synthesis, phosphotriester and phosphite-triester. ref [84], [85], and [86] **D)** Caruthers improvement of replacing chloride with amino leaving group ref [87] **E)** The automated solid phase synthesis of DNA; Begins with the detritylation of the 5' hydroxyl, 1) Activation and coupling 2) Capping failed sequences, 3) Oxidation of the P(III) to P(V), and 4) the cycle repeats by detritylation of the next base.

phosphate in the phosphodiester approach avoided unwanted branching. Finally, using reactive phosphorus in the P(III) state, and adding an oxidation step to the cycle, greatly enhanced the coupling yields between nucleosides.(Figure 1.6C) The currently used phosphoramidite approach by Caruthers provided a seemingly small improvement to the phosphite-triester method, by replacing the chloride leaving group in the phosphite-triester with an amino leaving group.[87] (Figure 1.6D) This simple leaving group replacement was significant because now the nucleoside 3'-phosphoramidites were stable enough to be made in advance and existed as solids allowing for their long term storage. These two properties made automated oligonucleotide synthesis ultimately viable and the mass production of oligonucleotides.[88]

The current, standard automated phosphoramidite method has 4 main steps, 1) Deblocking or Detritylation (removal of the trityl protecting group) 2) Coupling, 3) Capping and 4) Oxidation (Figure 1.6E). In the first step, mild acidic conditions are used to remove the 5'-dimethoxytrityl group (DMT). Following this, the coupling step where two nucleosides are joined together through the incoming 3'phosphoramidite and the 5' primary hydroxyl terminus of the previously deprotected base. Interestingly, this coupling reaction uses an acidic activator and the selection of this activator was crucial, not have to high a pKa to prematurely deprotect the incoming base. Tetrazole's are used for this, where the donation of the proton forms a stable anionic aromatic ring, and the pKa is appropriate to activate without deprotecting the DMT group. Capping is done next, to terminate any growing oligonucleotide that did not react in the coupling step, limiting side products. The oxidation step converts the P(III) phosphorus to P(V), to make it more stable for repeated cycling of these steps. Once the oligonucleotide is complete, it is cleaved from the solid support using ammonium hydroxide, which also removes the nucleosidyl exocyclic amine and β-cyanoethyl protecting groups. For RNA synthesis the cycle is the same, except there is an added step after ammonium hydroxide deprotection to remove the 2'OH silyl protecting group, using fluoride ions.

Having a reliable chemical method for the generation of oligonucleotides was revolutionary. Using the same type of chemistry for introducing building blocks other than the 4 nucleosides is now one of the primary ways that oligonucleotide conjugates are made.

1.4.2. In-Synthesis Modification of DNA

The phosphoramidite approach to oligonucleotide synthesis has now gone well beyond the basic oligonucleotide building blocks. Virtually any molecule can be incorporated into the oligonucleotide as long as it is compatible with the synthesis cycle, final deprotection steps, and has a phosphoramidite group.[89-90] (Figure 1.7. i.) The ease at which chemical moieties can be

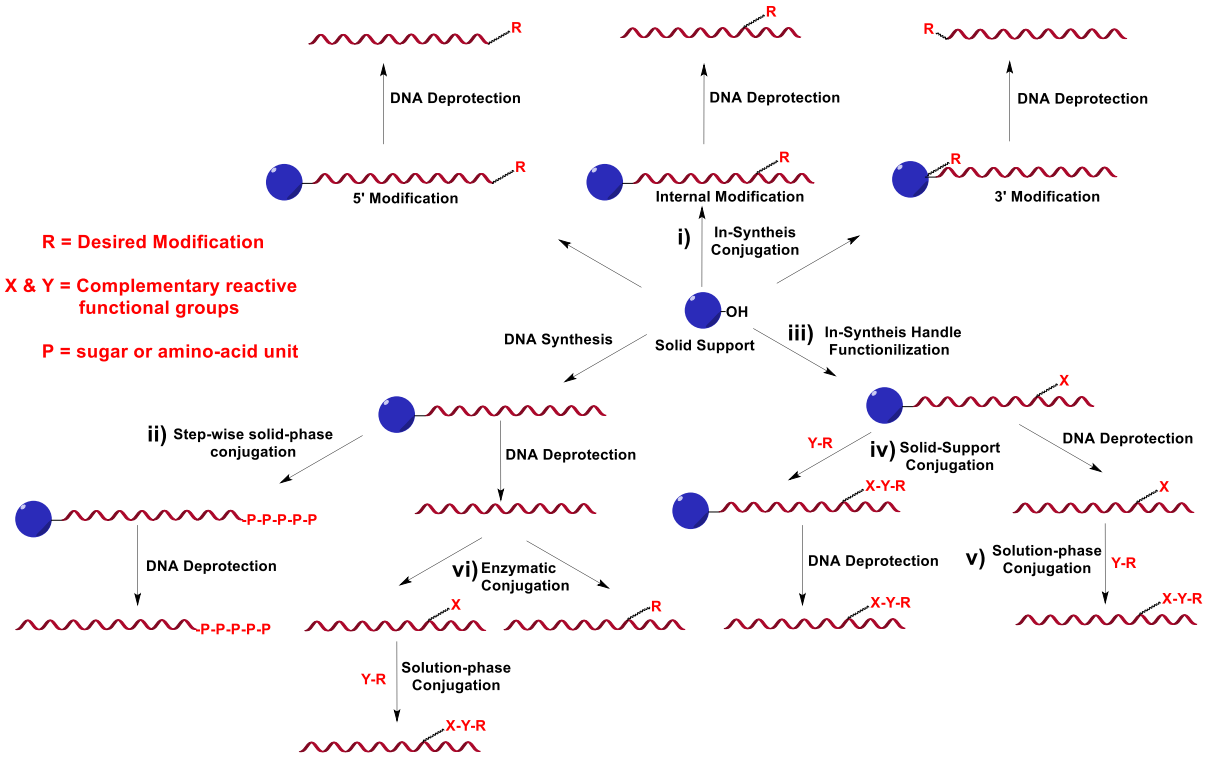

Figure 1. 7 Synthetic routes to functionalizing and conjugating oligonucleotides starting from the solid support.

i) in-synthesis conjugation; modifications are introduced during the oligonucleotide synthesis cycle at either internally or at the 3' and 5' ends, **ii)** Stepwise solid-phase conjugation; a secondary polymer is grown from the oligonucleotide using solid phase methodologies **iii)** in-synthesis handle functionalization; a reactive handle is introduced into the oligonucleotide sequence for later conjugation **iv)** Solid-support conjugation; conjugation to the functional handle is done while the oligonucleotide is still connected to the solid support **v)** Solution-phase conjugation; conjugation to the functional handle is done after the oligonucleotide has been cleaved from the solid support. **vi)** Enzymatic conjugation; either a functional handle or desired modification can be introduced enzymatically on unmodified oligonucleotides. Partially adapted with permission ref [111] (RSC 2010)

introduced to oligonucleotides using solid phase synthesis, has had a direct effect on the applications for DNA and DNA nanotechnology. In synthesis modifications can be introduced at any point in the oligonucleotide synthesis but are generally defined as 5' and 3' (terminus) modifications or internal modifications. Making a modification at the 5' is very attractive as they this occurs at the end of the synthesis cycle, and as such only full-length products should have the modification, which can somewhat help with purification by RP-HPLC.

3' modifications also work well, however care must be taken in the final deprotection depending on what the modification is, as solid support linkers are optimized to cleave best with the 3' hydroxyl group of nucleosides and may require longer times to fully deprotect. To introduce internal modifications, while maintaining base pairing can be done with modified bases such as C8-modified dA and C5-modified dU/dT, as well as dG and dC, but these are less common.

1.4.2.1. Ultra-Mild Bases

Some modifications to oligonucleotides may be able to be conjugated using in-synthesis methods and are stable to the activation, oxidation, capping and deprotecting steps of the DNA synthesis cycle, but not to the final harsh alkali deprotecting step.[91] Additionally, this step in the DNA synthesis procedure, is often the longest step compared to the cycle itself, taking upwards of 17hr at 60°C to fully deprotect. To address this issue, Schulhof *et al.* introduced more labile phenoxyacetyl (pac) protecting groups for adenine and guanine and acetyl for cytosine.[92] Although, the PAC-dG monomer is quite insoluble and is commercially available with the iPr-Pac

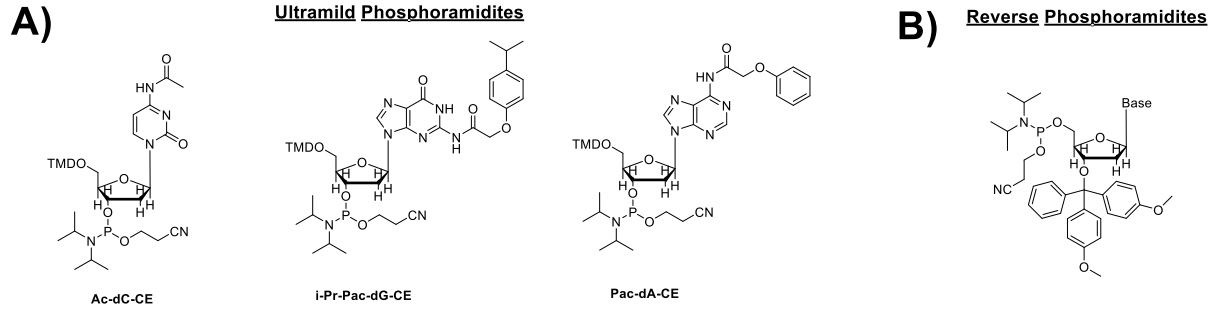

Figure 1. 8 Structure of synthetically relevant phosphoramidites

A) Ultra-mild Phosphoramidites B) Reverse Phosphoramidites

protecting group for this reason[93] (Figure 1.8A). The use of ultra-mild bases has allowed for the better introduction of some dye modifications, which are known to have high instability.[94] Additionally, the introduction of alkene modifications into oligonucleotide strands was achieved by Boles et al. who developed the commercially available Acrydite™ 5' modification for integration DNA into hydrogels.[95] Recently, Allabush et al. were able to make internal alkene modifications and polymerize the oligonucleotide conjugates in polyacrylamide gels.[96] It is recommended when using these types of bases to use phenoxyacetic anhydride, as the capping reagent instead of acetic anhydride to avoid exchange of the Pac protecting group on guanine with acetate.[97]

1.4.2.2. Reverse Phosphoramidites

For many structural nanotechnology applications oligonucleotide directionalities are very important. Typical solid support DNA synthesis occurs from 3' to 5' and introducing 3' modifications can be done simply by adding it as the first modification. However, many modifications are fragile to repeated synthesis cycling, and purification of 3' modified strands can be difficult, as all truncated sequences retain the initial modification.[98] Reverse phosphoramidites address this by having the 3' OH protected with a DMT, while having the 5' OH as the phosphoramidite, and have become a facile method for synthesizing 3'modified DNA oligonucleotides.[99](Figure 1.8B) With Reverse phosphoramidites as well, creating 3'-3' or 5'-5' conjugated oligonucleotides is relatively straightforward[100], and has found a few applications in antisense oligonucleotide therapeutics[100-103] (due to its stability to 3' exonucleases), studies on hairpin loops[104-105], as well as DNA microarray synthesis.[106-107]

1.4.2.3. Stepwise solid-phase conjugation

Stepwise solid-phase conjugation involves synthesizing the complete oligonucleotide, followed by the solid phase synthesis of another biopolymer, or *vice versa*.(Figure 1.7 ii.) This type of conjugation is primarily used to generate oligonucleotide-peptide and oligonucleotide-sugar conjugates.[108-110] Purification using this method is the primary advantage, as all reagents can be separated from the solid support. However, when combining these solid support chemistries,

protecting group compatibility, and stability under deprotection conditions must be strictly adhered to.[111]

In the case of peptide-oligonucleotide conjugates, the linkage between the solid support and the conjugate is usually base labile and the synthesis starts with the peptide. Most peptide linkers are acid-labile and thus incompatible with standard oligonucleotide synthesis.[112] Linkers with ester functionalities have been introduced to circumvent this and peptide synthesis is done using either tert-butyloxycarbonyl (Boc-) or fluorenylmethoxycarbonyl (Fmoc-) protected amino acids.[113-116] In these cases, peptide side chain protection chemistries must be carefully considered, to not cleave under both the peptide synthesis and oligonucleotide synthesis conditions or interfere with other protecting groups present on the oligonucleotide once removed. Alternatively, oligonucleotide synthesis can be done first, however this limits peptide synthesis to the Fmoc- strategy to not cause depurination of the oligonucleotide, and non-standard peptide side chain protecting chemistries must be used.[117-120] Efforts are continuing in this area, however, a vigorous solid phase procedure has yet to be developed.

Further in-synthesis modifications will be discussed later that address the stability requirements for oligonucleotide therapeutics (Section 1.4). However, even with this ease of integration, many functional materials are not compatible with the synthesis cycle and alkali deprotection steps and must be introduced post-synthesis.

1.4.3. Post-synthesis Modification

Post-synthesis modification can be introduced either chemically or enzymatically. For the most part, the post-synthesis modification of oligonucleotides is done after the oligonucleotide has been synthesized and often requires the in-synthesis or enzymatic addition of functional handles to do the conjugation. Many of these handles have found their way into the mainstream and are readily available for purchase. Most handles can be introduced at both the 3’ or 5’ terminal positions or internally. (Figure 1.7 iii.)

1.4.3.1. Handles for Post-synthesis Modification

1.4.3.1.1. Amino Handles

One of the most common handles for post-synthesis modification is the amino handle, which reacts with activated carboxylates to form stable amide bonds (Figure 1.9A). Activated carboxylates in the form of N-hydroxysuccinimide (NHS) esters of many different functionalities are widely commercially available, giving amino conjugation high utility. As the amino group is nucleophilic, it must be protected during DNA synthesis, using groups such as monomethoxytrityl (MMT), trifluoroacetyl (TFA) and Fmoc- groups. Care must be taken when deprotecting amino handles, as the β-cyanoethyl protecting group can add to the amino handle during deprotection. Therefore, pre-deprotecting the β-cyanoethyl groups of amino modified strands with 10% diethylamine in acetonitrile is often useful. For solution phase conjugation, when coupling NHS esters, proper buffers must be used which are basic enough to make sure that the amine is not protonated, but not too basic to hydrolyze the NHS ester. Additionally, purification of amine modified strands before conjugation, is incompatible with polyacrylamide gel electrophoresis (PAGE), as unpolymerized acrylamide reacts preferentially with the amine modification. Using 5' hydrophobic amines can assist in their purification by reverse phase HPLC (RP-HPLC), before conjugation. Amino handles can also be used for the conjugation of isothiocyanates and aldehydes to the oligonucleotide.[121]

1.4.3.1.2. Alkyne Handles

Alkyne handles are another useful handle that can be incorporated into an oligonucleotide at any position, to react with azides in copper(I)-catalyzed alkyne-azide cycloaddition (CuAAC) or "click" reactions.[122-126](Figure 1.9B) Although no protecting groups are required for the alkyne during oligonucleotide synthesis, an interesting report by Gramlich *et al.* introduced orthogonal alkyne protecting groups for the multiple functionalization of DNA using three different alkynes.[127] Copper can be quite toxic for biological applications and due to this requirement for CuAAC, the synthesis of copper-free strain-promoted alkyne-azide cycloaddition (SPAAC) phosphoramidites was done.[128] In particular, the dibenzocyclooctyne group (DBCO), is used most commonly and is commercially available.[129-130] While DBCO modifications exist for functionalization at any position

as well, it should be noted that the use of a DBCO modification at the 3' end, or internally requires the use of non-aqueous oxidizing agent, commonly (1S)-(+)-(10-Camphorsulfonyl)-oxaziridine (CSO).[131] DBCO handles are used for their simple reaction conditions, however, some care should be taken if purifying them pre-reaction using RP-HPLC conditions, as they may be susceptible to dimerization.[132]

1.4.3.1.3. Thiol Handles

Thiol handles are in general quite useful for their reactivity with maleimides, α-halocarbonyls, vinylsulfones and disulfides.[133-136](Figure 1.9C) Of these reacting partners, maleimides are the most popular, as coupling can be done in the presence of reactive primary amines, has a fast reaction rate and uses neutral pH conditions. However, the reaction is reversible when other thiols are present in a more complex mixture, but the products can be stabilized by hydrolytic ring-opening.[137] Primarily, thiol handles are introduced as disulfides, though there are some instances where benzoyl and MTT groups are used. Some caution must be used when introducing the thiol handles, as spontaneous dimerization between oligonucleotide strands can occur during base deprotection, and reduction with dithiothreitol (DTT) or tris(2-carboxyethyl) phosphine (TCEP) may be necessary before further conjugation. To avoid dimerization with disulfide protected thiols, it is recommended that the strand be deprotected using room temperature ammonium hydroxide over a longer period of time. Unprotected thiol handles are unable to be purified by gel electrophoresis, as non-polymerized acrylamide can be readily reacted with the handle. Keeping a disulfide protected thiol is beneficial as the strand can be purified readily, by either RP-HPLC or gel electrophoresis, without unintentional thiol dimerization. However, current commercially available disulfide modifications are only available for the 3' and 5' terminus and not internally. Lipoic acid-based cyclic disulfides, and Dithiol phosphoramidite (Dtpa) are another popular source of thiol handles and are generally used for enhanced gold surface binding.[138-139]

1.4.3.1.4. Azide Handles

To react oligonucleotides with alkynes in CuAAC or SPAAC, azide functionalization of oligonucleotides must be done (Figure 1.9D). Introduction of azide handles into an oligonucleotide sequence can be quite difficult, the phosphite P(III) reagents that are used to make phosphoramidites are able to react with azides in a Staudinger reduction to the corresponding amine.[140] However, an important result by the Lonnberg group that showed a Staudinger reaction did not disturb the azide group in a support-bound growing nucleotide, and allowed for the production of 3'-azide-modified oligonucleotides.[141] Additionally, the Micura

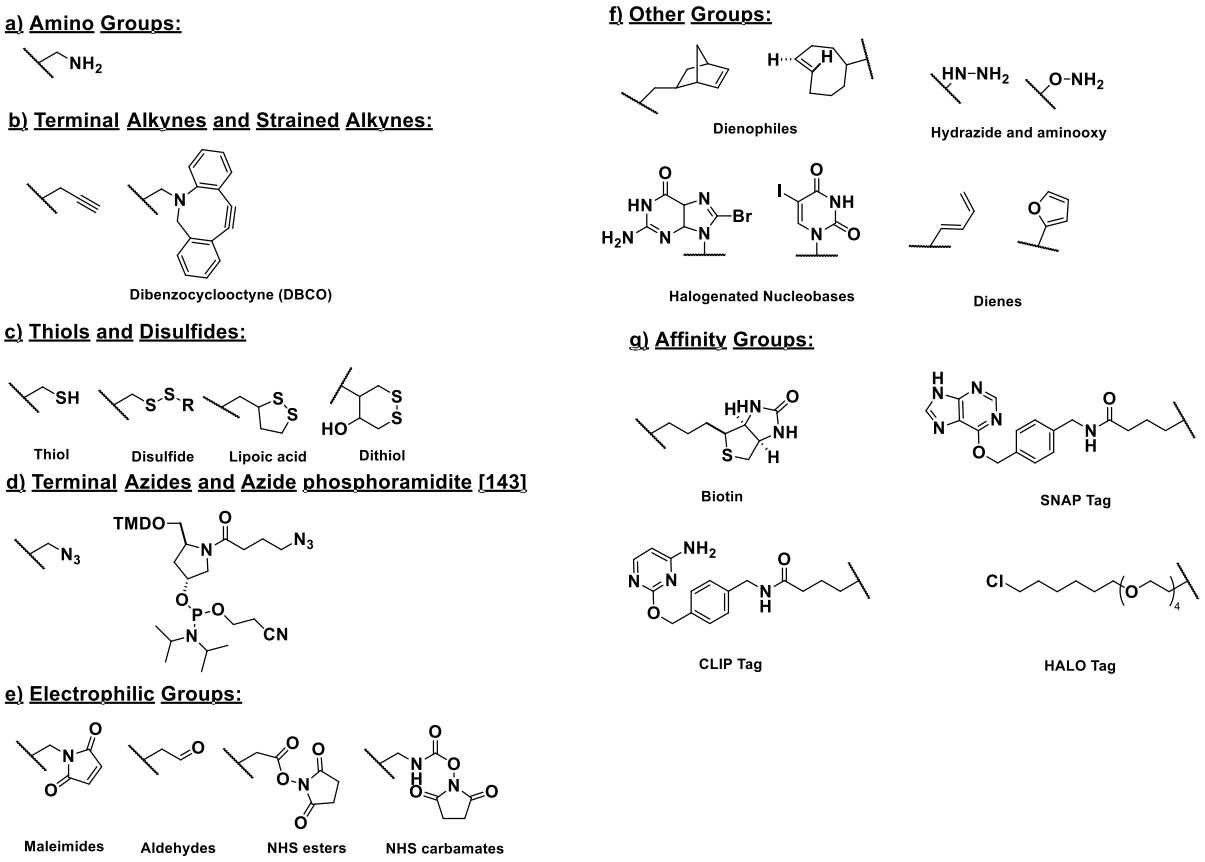

Figure 1. 9 Structure of functional handles which can be incorporated into oligonucleotides on the oligonucleotide synthesizer.

a) Amino groups, b) Terminal alkynes and strained alkynes, c) Thiols and disulfide, d) Terminal azides and azide phosphoramidite, e) Electrophilic groups, f) Other groups, g) Affinity groups. Partially adapted with permission ref [90] (ACS 2019)

group used 2'-O-(2-azidoethyl) modified oligoribonucleotide in the solid-phase synthesis of cyanine labelled siRNA.[142] Following these reports, Maksim et al. were able to make an azide phosphoramidite, of which they could insert multiple copies, without loss of function.[143](Figure 1.9D) Lingala et al. expanded on this and were able to find optimal conditions to make azide functionalized phosphoramidite nucleosides.[144] Other than making azido phosphoramidites, many times azide functionality is introduced into an oligonucleotide through the use of bi-functional linkers.[145] Additionally, conversion of the 5' hydroxyl to an iodo- functional group[146] followed by treatment with sodium azide[147] can be done, or diazo transfer to an amine modification[148].

1.4.3.1.5. Electrophilic Handles

Many conjugating species have nucleophilic functional groups already built into their structure, as such, having oligonucleotides modified with electrophilic handles would be useful for conjugation in such cases (Figure 1.9E). Maleimides are attractive handles to be integrated into oligonucleotide sequences to react with thiols, however, are not compatible with final ammonium hydroxide deprotection conditions. To overcome this, Grandas *et. al.* used maleimide-dimethyl furan Diels-Alder exo adduct phosphoramidites to protect the maleimide during the final deprotection.[149] This was followed by a retro-Diels-Alder reaction to reveal the maleimide, reactivity of the oligonucleotides was assessed by reacting with different thiols. Another electrophilic handle that can be readily incorporated into oligonucleotides are aldehyde functionalities. Using 3-formylindole nucleosides, aldehyde function can be introduced internally or terminally, and allows for reductive amination reactions with amines as well as conjugation to various other functional groups.[150] Carboxylate functional groups have also been used as electrophilic handles for the conjugation of amines to oligonucleotides. NHS-ester phosphoramidites are available for the "on support" (section 1.3.3.2) conjugation of amines to oligonucleotides. Multiple internal labelling can be achieved when using the correct oxidizing conditions.[151] Additionally, activation of amines with N,N-disuccinimdyl carbonate (DSC) has been used for the formation of a urea in a similar manner. This method was especially useful for the conjugation of oligonucleotide-peptide conjugates.[152]

1.4.3.1.6. Other Covalent Coupling Handles

Some other less common, covalent coupling handles have also been introduced to oligonucleotides (Figure 1.9F). Diels-Alder reactions have been used by conjugating a diene[153-154] or trans-cyclooctene[155] to oligonucleotides and reacting with molecules functionalized with maleimide or 1,2,4,5-tetrazine moieties. Hydrazide and aminooxy handles, as well as handles for palladium-catalyzed coupling have also been used in select circumstances. Hydrazides and aminooxy functional groups can be incorporated using phosphoramidite chemistry and offer a nice alternative to amines, as they have lower pKa's for coupling reactions.[156-157] Aminooxy functional groups also offer a more stable linkage than imines when reacting with aldehydes.[158-159] 8-bromoguanine or 5-iodouracil constitute the starting materials for many nucleoside modified phosphoramidites, but can be used themselves for palladium-catalyzed cross-coupling reactions, on or off the solid support.[160-163] Recently as well, Wang et al. introduced another post-synthetic method of conjugation using the oxidative amination of 4-thio-2'deoxyuridine at internal oligonucleotide positions.[164]

1.4.3.1.7. Affinity Handles

Affinity handles can be used to conjugate different species together as well (Figure 1.9G). The most common affinity handle introduction is by far the biotinylation of oligonucleotides. Biotin is a small molecule, which can be easily incorporated into oligonucleotides at any position using phosphoramidite chemistry.[165-166] Biotin- avidin and streptavidin interactions are well established and have been used for conjugating oligonucleotides to quantum dots[167], proteins[168], and carbon nanotubes[169]. Streptavidin is most commonly used for bridging between two biotinylated species, as it one of the strongest non-covalent interactions known (kd $\approx 10^{-14}$mol/L) ; however, some attention should be paid to the binding valency of streptavidin. Streptavidin naturally has 4 binding pockets, which could give mixtures of conjugated products, therefore modified streptavidin with 2 or 3 binding pockets may be necessary.[170]

Affinity handles can also take the form of enzymatic substrates in ligation reactions or tags which are recognized by specific protein domains to create covalent conjugates. Many small molecule

tags have also been conjugated to oligonucleotides such as the; HaloTag[171], SNAP-tag[172] and CLIP-tag[173], for the labelling of modified proteins.[174] Recently, a small tripeptide affinity handle was introduced, for the post-enzymatic modification of oligonucleotides to make protein- & peptide-oligonucleotide conjugates. Using a peptide ligase, Tan *et al.* conjugated cyan fluorescent protein and other small peptides to oligonucleotides synthesized with two tripeptide handles at internal and terminal positions.[175]

1.4.3.2. On support Conjugation

Conjugation to the oligonucleotide can sometimes be done by reacting the functional handle while it is still connected to the solid support.[109, 124, 176-177] (Figure 1.7 iv.) The main requirement for this type of conjugation is that the molecular label is compatible with the final basic deprotection step. While on support, organic solvent conditions can be continued to be used, which is advantageous if the conjugates are highly insoluble in aqueous conditions. Additionally, since the oligonucleotide is still connected to the solid support, purification is relatively straightforward, and can be accomplished by simple filtration and washing.

1.4.3.3. Solution Phase Conjugation

Oligonucleotide conjugation in solution typically requires that the species being conjugated are water soluble. However, if the species being conjugated is not affected by the presence of organic solvents (i.e. folded proteins) using miscible organic solvents (DMSO, DMF, THF, methanol, ethanol) allows for some flexibility for this requirement. Indeed, there are even cases where conjugates have been made using full organic solvent conditions.[178] Alternatively, work in the Sleiman lab has demonstrated the use of hydrophobic micellar cores for the conjugation of highly hydrophobic groups to oligonucleotides using amine and DBCO handles in aqueous conditions.[179-180] (Figure 1.7 v.)

1.4.3.4. Enzymatic Conjugation

Chemical conjugation methods are somewhat limited as high amounts of reagents are generally needed, which can still lead to relatively lower yields. Additionally, even though DNA synthesis is

very robust there is still a limit to the length at which oligonucleotides can be grown by solid support, and modifications at the end of a long synthesis may not be in very high yield. Enzymatic conjugation addresses some of these limitations, by working at low concentrations with high efficiency.[181-182] (Figure 1.7 vi.) To use enzymatic conjugation methods however, phosphorylation of oligonucleotides at either the 3' or 5' ends may be required for the enzymes to work. Phosphorylation reagents and enzymatic phosphorylation kits are readily available for these purposes.

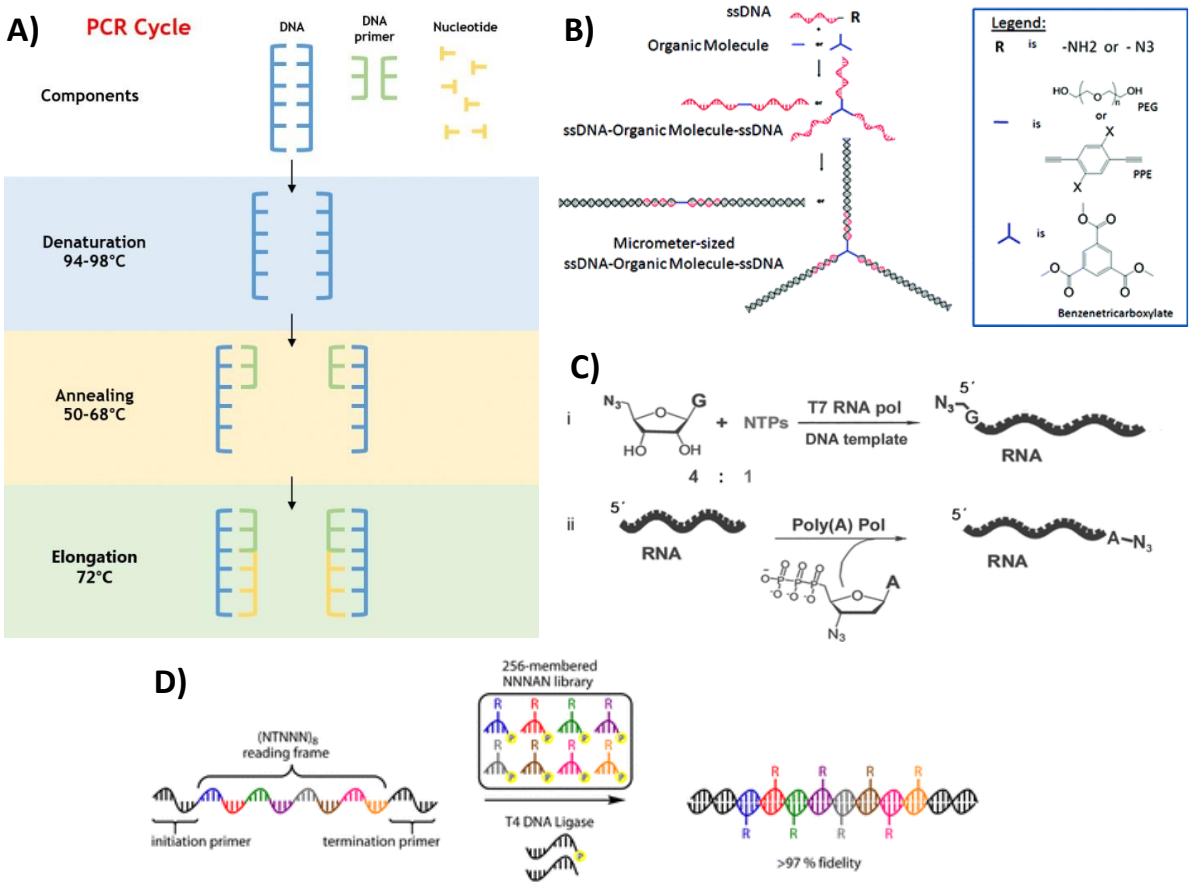

Figure 1. 10 Conjugation of DNA using polymerases and ligases.

A) PCR Cycle consisting of 3 steps; 1) denaturation, 2) annealing and 3) elongation. Ref [183] **B)** Integration of synthetic vertices using modified PCR primers to generate large DNA structures. Reproduced with permission ref [185] (ACS 2011) **C)** addition of an azide handle to the 5' or 3' end of RNA using a T7 RNA polymerase. Reproduced with permission ref [189] (John Wiley and Sons 2011) **D)** Generation of a molecular library using modified oligonucleotide and T4 DNA ligase. Reproduced with permission ref [193] (ACS 2015)

1.4.3.4.1. DNA Polymerase

DNA polymerase is well known as the enzyme of replication in biology. The method of polymerase chain reaction (PCR) has revolutionized biology, and used to make multiple copies of a segment of DNA.[183] (Figure 1.10A) Briefly, there are three steps to PCR; 1) denaturing, 2) annealing and 3) extension. In the denaturing step, double stranded DNA is heated to split apart the duplex into its single stranded form. During the annealing step, short primer sequences are used to hybridize to the end of the sequence of interest to act as starting points for the DNA polymerase. Finally, in the extension step a DNA polymerase (often from a thermophile bacteria) is used to polymerize the DNA between the primer sequences, and the process repeats, exponentially amplifying the DNA segment. Currently, two methods exist for introduction of oligonucleotide modifications using PCR: a) introducing modifications to the primers of PCR and b) using modified nucleotides during the polymerization process.

a) Primer Based Functional Group Introduction

Using pre-modified primers in PCR has been shown to be an efficient method for the introduction of different functionalities to oligonucleotides. Generally, small primer sequences can be made by solid-phase synthesis, introducing functional handles, which are then used in PCR. Handle conjugation can be performed pre- or post- PCR. Using this method, the Herrmann group used PCR primers modified with hydrophobic units to generate DNA multiblock co-polymers.[184] Lee and coworkers, were able to extend DNA arms from small molecule cores by PCR[185] (Figure 1.10B) and Trinh *et. al.* used a synthetic, asymmetric DNA trimer for the simultaneous PCR amplification of 3 different oligonucleotides.[186] The most prominent limitation of this method is that modifications can only be made at terminal positions, limiting the scope of modifications that can be made.

b) Unnatural Nucleotides

The use of unnatural nucleotides for the introduction of modifications to oligonucleotides is relatively straightforward and can be done by simply adding the modified triphosphate during the PCR process. The most important disadvantage of this method is that it is not site-specific,

resulting in partial or complete labeling of the oligonucleotide at a specific nucleotide type. Recently however, some groups have started to use unnatural base pairs (UBP) to overcome this limitation by first synthesizing DNA with UBPs by solid support and then amplifying by PCR with the UBP complementary nucleotide added.[187]

Modifications of unnatural bases are typically done on the nucleosidyl base to remain compatible with the DNA polymerase.[188] This in itself is another limitation, as it limits the scope of modifications that can be made using this method. In an interesting case, an azido handle can be introduced selectively at the 5' or 3' end of an oligonucleotide. Paredes et al. used a modified uracil nucleotide with an azide in place of the 5' or 3' hydroxyl.[189](Figure 1.10C) Using RNA polymerase, if this modified base gets introduced anywhere other than the terminal position, polymerization is terminated. Therefore, full length product will only have one azido handle. Dore *et. al.* used this method of azide functionalization to generate RNA conjugates that were amphiphilic and assembled into spheres.[180]

1.4.3.4.2. DNA Ligase

The Hili group has actively pursued the use of DNA ligases for the introduction of chemical modifications to DNA.[190] Similar to the primer based method, smaller sections of modified oligonucleotides can be synthesized using standard solid phase synthesis, but then are stitched together using a DNA template and DNA ligase. Using their "LOOPER" (Ligase-catalyzed oligonucleotide polymerizations) method the Hili group has been able to generate large chemical libraries of modified oligonucleotides with diverse functional groups.[191-193](Figure 1.10D) Careful consideration had to be made as to which ligase to use when ligating shorter or longer lengths of oligonucleotides, and it was discovered that the T3 DNA ligase could not accommodate certain base modifications of adenosine.[194]

1.4.3.4.3. Oligonucleotide Modifying Enzymes

Other enzymatic approaches have been developed which use enzymes to recognize specific sequences on oligonucleotide strands to directly incorporate modifications at desired sites. For example, the Weinhold group developed a DNA functionalization strategy, through engineering a modified cofactor for M.Taq1 (a DNA methyl transferase enzyme from *Thermus aquaticus)*.[195] (Figure 1.11A) Under normal conditions the methyl group from the cofactor S-adenosyl-L-methionine (AdoMet) is transferred by M.Taq1 to the exocyclic amine of adenosine, only at double stranded positions with the sequence 5'-TCGA-3'. However, the modified cofactor contained an aziridinyl residue, and as such, the entire nucleoside was transferred onto the exocyclic amine. Another strategy to transfer only functional groups and not the entire cofactor was later developed by the same group using cofactor analogues which carry a sulfonium-bound extended side chain with a terminal functional group.[196] Other enzymes are also able to site selectively transfer functional groups to oligonucleotides such as; Beta-glucosyltransferase[197], tRNA-agmatine synthetase[198] and tRNA guanine transglycosylase[199]. These enzymes, along with their cofactors, and functional groups that can be introduced can be found in Figure 1.11B.

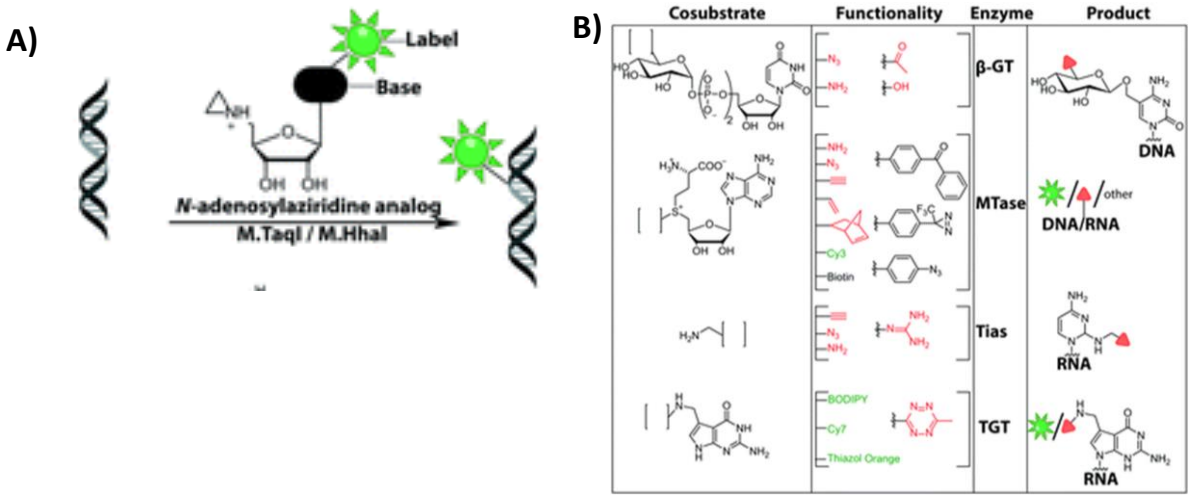

Figure 1. 11 Methods for functionalizing DNA with oligonucleotide modifying enzymes.

A) Labelling of an oligonucleotide using a modified cofactor for M.Taq1. Reproduced with permission ref [182] (RSC 2020) **B)** Co-substrates, functional groups and enzymes able to enzymatically modify oligonucleotides. Reproduced with permission ref [182] (RSC 2020)

From these handles and methods, conjugation of various small molecules, bio-macromolecules, polymers, and particles to oligonucleotides has led to an endless number of different DNA nanostructures/devices. Out of all the DNA nanodevices developed, three functions of oligonucleotides beyond its use as the information molecule have been identified, all which use modified or conjugated DNA to enhance or generate new functions; 1) Structural, 2) Therapeutic and 3) Recognition. Combinations of these different functions are what allow for the construction of many different devices for therapeutic, diagnostic and nanomaterial applications.

1.5. Modifications for Structure

While using strictly unmodified DNA has given rise to a large variety of different structures with precisely defined geometries, varying in shape and size, using oligonucleotide conjugates has expanded this library of structures even further. In DNA nanotechnology DNA primarily generates its structures through Watson-Crick base pairing, limiting the scope of assembly. Conjugating DNA with other functionalities to access structures without using Watson-Crick base pairing, using both other supramolecular interactions and synthetic structural insertions, has generated a plethora of structures for various applications. Additionally, the ability to have complete control of the positioning of other materials other than DNA, has given more applications to the structural use of pure DNA constructs.

1.5.1. Material Positioning

The ability to use DNA conjugated with other organic or inorganic materials and place them in a precisely defined manner on DNA scaffolds has expanded the utility of structural DNA nanotechnology. For example, DNA conjugated to gold nanoparticles have found utility in developing hotspots[200-201] or well-defined nanoelectronic devices[202-203].(Figure 1.12A) In a somewhat reverse manner, instead of positioning already functionalized gold particles on origami scaffolds, the Sleiman group was able to “print” lipoic acid modified DNA onto gold in a spatially defined manner.[204](Figure 1.12.B) Building on this, Luo et al. encapsulated gold nanoparticles and positioned them on DNA origami in 3D spatial arrangements.[205] (Figure 1.12.C) Fu *et al*. were able to study the enzyme cascades of glucose oxidease(GOx)/horseradish

peroxidase (HRP) by linking these enzymes to oligonucleotides and positioning them on DNA

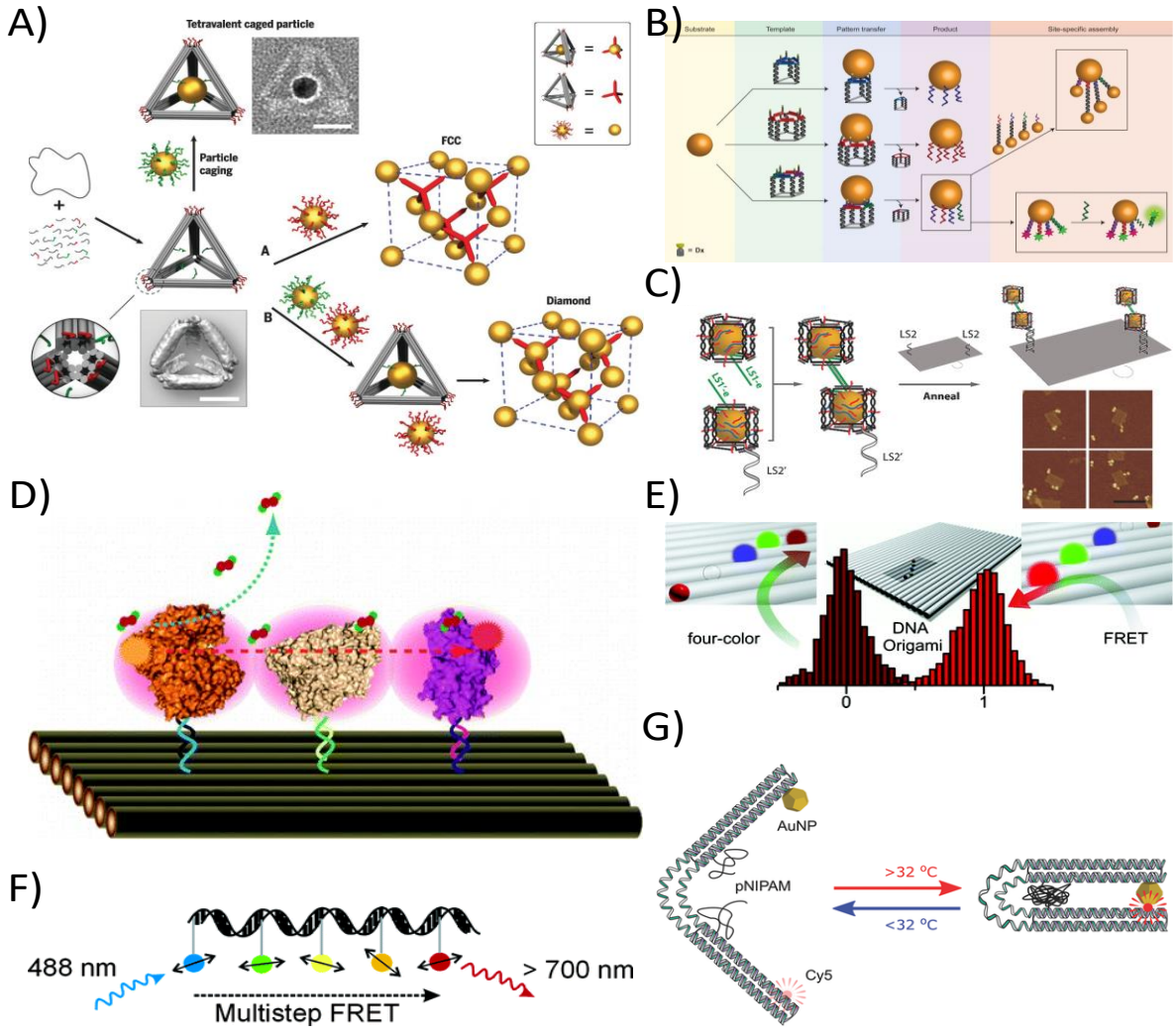

Figure 1. 12 Applications of DNA Nanostructures for precise positioning other materials.

A) DNA origami used to generate diamond superlattices of gold nanoparticles. Reproduced with permission ref [200] (Association for the Advancement of Science (AAAS) 2016) **B)** Printing of DNA onto a GNP from DNA cages. Reproduced with permission ref [204] (NPG 2016) **C)** Organization of GNP's in 3D on DNA origami. Reproduced with permission ref [205] (John Wiley and Sons 2018) **D)** GOx and horseradish peroxidase tethered to DNA origami. Reproduced with permission ref [206] (ACS 2012) **E)** FRET cascade on DNA origami. Reproduced with permission ref [207] (ACS 2011) **F)** DNA photonic wires Reproduced with permission ref [208] (ACS 2004) **G)** DNA tweezers actuated by temperature dependent PNIPAM polymer. Reproduced with permission ref [209] (John Wiley and Sons 2018)

origami scaffolds.[206] (Figure 1.12.D) They were able to systematically vary the distance between enzymes, which revealed distance-dependent kinetic processes.

Cascades of fluorescent energy transfer (FRET) on DNA origami were performed by the Tinnefeld group, by carefully positioning the dyes 9nm apart to minimize direct FRET, but to allow for successive FRET.[207](Figure 1.12.E) Additionally, DNA photonic wires were made with quantum dots by Heilemann et al. using DNA scaffolds.[208](Figure 1.12.F) Another interesting application was done by the Baumberg group, where by positioning two poly(N-isopropylacrylaamide) (PNIPAM) DNA conjugates on each arm of DNA origami tweezers, the activity of the tweezers could be modulated by changes in temperature.[209] (Figure 1.12.G) Overall, conjugation of oligonucleotides with other materials and situating them in spatially defined ways, is a valuable tool that is gained from the combination of these conjugates and structural DNA nanotechnology.

1.5.2. Supramolecular DNA Assemblies

Supramolecular chemistry, broadly defined, is the chemistry beyond the covalent bond. It includes interactions such as hydrogen bonding (H-bonding), electrostatic, hydrophobic, π-π stacking, metal coordination and Van der Waals interactions. Since oligonucleotides already use well defined H-bonding interactions for hybridization, the most common ways that other supramolecular interactions are introduced to DNA is through the hydrophobic interactions, π-π interactions and metal co-ordination.

1.5.2.1. Hydrophobically Modified DNA

Amphiphiles are probably best known in the field of block co-polymer self-assembly. These polymers contain both hydrophilic and hydrophobic groups and have been extensively studied for their potential in applications such as drug delivery vehicles, imaging agents and nanoreactors.[210] Introduction of hydrophobic moieties to DNA to make DNA amphiphiles can be done either in-synthesis[211-212] or post-synthesis[213], on solid support or in solution[214]. However, a big challenge with generating DNA amphiphiles for self-assembly is the conjugation of the hydrophobic and hydrophilic blocks, as these large blocks, have incompatible solubility's and

need high yielding chemistries to conjugate. While some groups have tried to overcome this using surfactants[214], the Sleiman group in particular has addressed this limitation by introducing smaller hydrophobic units sequentially in-synthesis.[215](Figure 1.13.A) These "sequence defined"

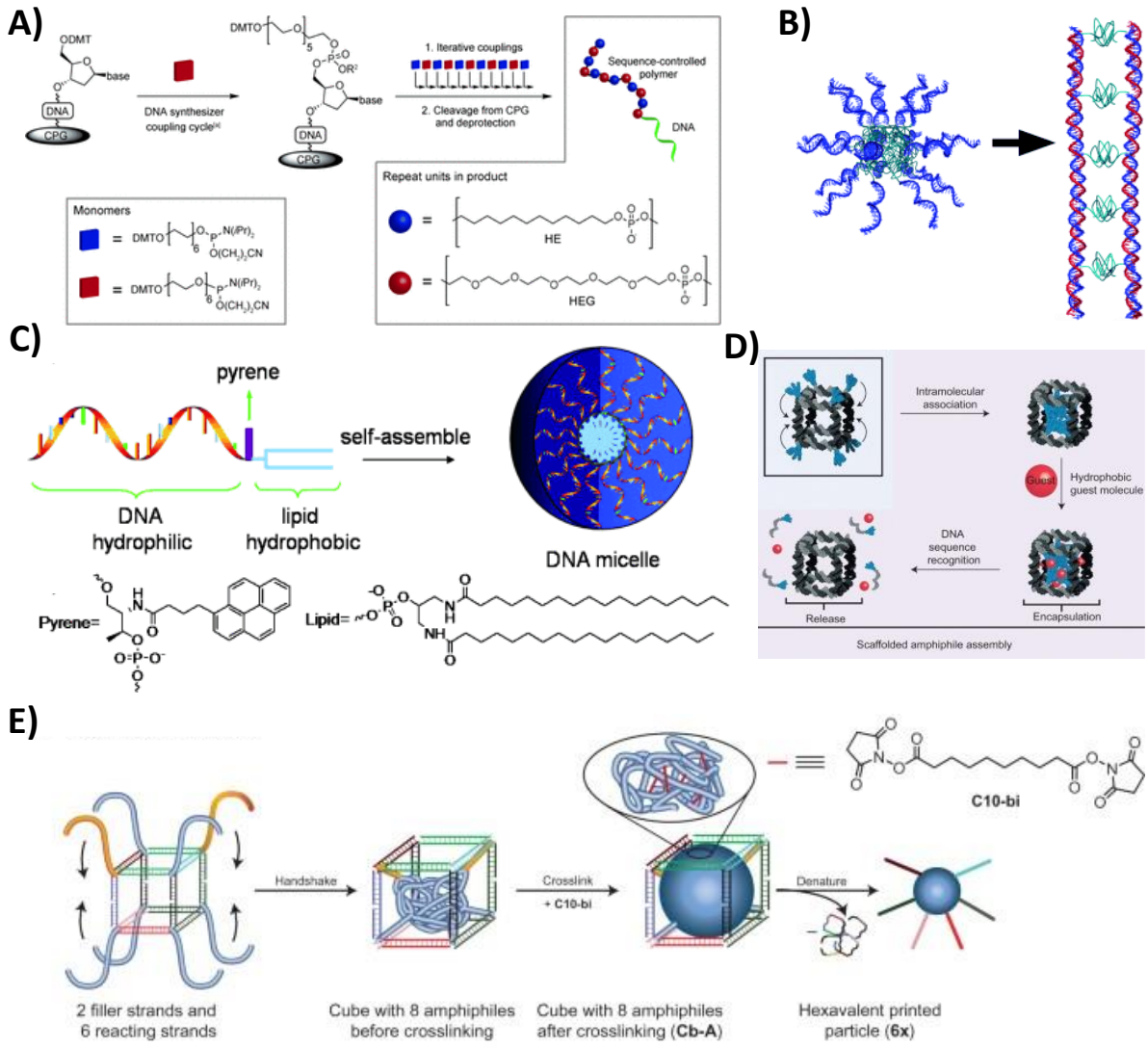

Figure 1. 13 Hydrophobically modified oligonucleotides for generating new structures.

A) Synthesis of sequence-defined DNA-polymers. Reproduced with permission ref [215] (John Wiley and Sons 2014) **B)** Structure switching of SNA's to rods. Reproduced with permission ref [221] (John Wiley and Sons 2007) **C)** DNA-pyrene-lipid amphiphile. Reproduced with permission ref [220] (John Wiley and Sons 2010) **D)** Hydrophobic core inside a DNA cube for drug encapsulation. Reproduced with permission ref [222] (NPG 2013) **E)** Printing on DNA-hydrophobes. Reproduced with permission ref [223] (NPG 2018)

DNA amphiphiles, have been used for applications in drug delivery[216] and the study of different assembly modes[217-218].

DNA integrated with hydrophobic building blocks have been used to generate many structures, which can be modulated by varying the ratio between hydrophilic and hydrophobic blocks. Out of all the different morphologies these amphiphiles can generate, spherical shapes are the most common geometry and are otherwise known as spherical nucleic acids (SNA's).[211, 215, 219-220] In an interesting study by the Tan group it was shown that the size of SNA's could be modulated by changing the length if the DNA block.[220](Figure 1.13.C) Additionally, the Hermann group demonstrated that structure switching can occur, by adding a long DNA strand, complementary to the SNA corona, to make rod-like aggregates.[221](Figure 1.13.B) Using hydrophobic interactions, Edwardson et. al. was able to synthesize dendritic DNA which when hybridized to a DNA cube scaffold, generated a hydrophobic core, which was able to encapsulate small molecule cargo.[222](Figure 1.13.D) With the same template Trinh et al. was able to make "printed" SNA's with defined 3D geometries that were only able to be hybridized back to the template in the correct orientation.[223](Figure 1.13.E)

π-π interactions have also been used in conjunction with DNA have been taken advantage of by different groups. Haner et al., through the use of DNA-oligo pyrene conjugates were able to generate DNA-grafted supramolecular polymers.[224](Figure 1.14.A) Moreover, DNA conjugated with poly[3-(2,5,8,11-tetraoxatridecanyl)thiophene] (PTTOT) assembled into vesicles in aqueous solutions, retaining their optoelectronic properties.[225](Figure 1.14.B) The Sleiman group was even able to generate sheets, nanofibers, and DNA "hockey sticks" using the π-π interaction between DNA conjugated to cyanine 3 dyes.[226](Figure 1.14.C)

Cholesterol, is a common hydrophobic modification used to enhance silencing of antisense oligonucleotides but is also interesting in its use as a DNA amphiphile.[227] Using cholesterol conjugated DNA, the immobilization of vesicles on membranes was achieved by Hook et al.[228] Furthermore, Li, Fan and coworkers used surface anchored DNA nanostructures to study substrate-enhanced diffusion of enzymes.[229] Cholesterol conjugation has also led to the formation of artificial membrane channels by Langecker et al.[230] and Chidchob et al.[231] which were able to translocate DNA molecules and fluorescent dyes across membranes

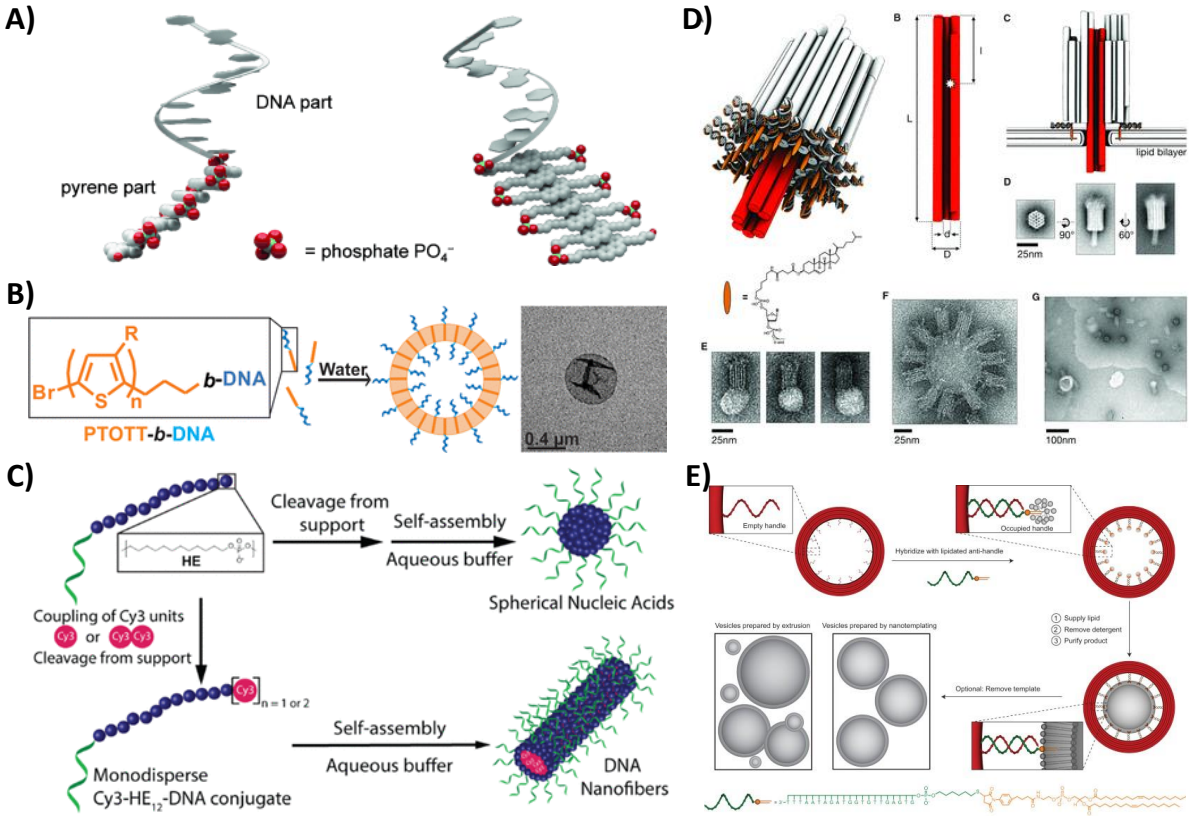

Figure 1. 14 DNA nanostructures accessed by π-π and membrane interactions.

A) DNA-pyrene conjugates. Reproduced with permission ref [224] (John Wiley and Sons 2015) **B)** DNA-PTTOT conjugates assemble into vesicles. Reproduced with permission ref [225] (ACS 2014) **C)** Cyanine 3-DNA conjugates for nanofiber formation. Reproduced with permission ref [226] (ACS 2014) **D)** Artificial membrane channel made of DNA-cholesterol conjugates. Reproduced with permission ref [230] (AAAS 2012) **E)** Formation of defined liposomes using lipid conjugated-DNA origami. Reproduced with permission ref [232] (ACS 2014)

respectively.(Figure 1.14.D) Outside the use of cholesterol-membrane insertions, the groups of Shih and Lin, were able shape liposomes using DNA templates conjugated with lipid moieties.[232-233](Figure 1.14.E)

1.5.2.2. Synthetic Vertices & DNA Metal Co-ordination

In addition to using other types of interactions to generate structures, the introduction of covalently linked synthetic vertices, opened more structural space for DNA nanostructures. Often these synthetic vertices are inert and used purely for structural purposes. As in the cases of

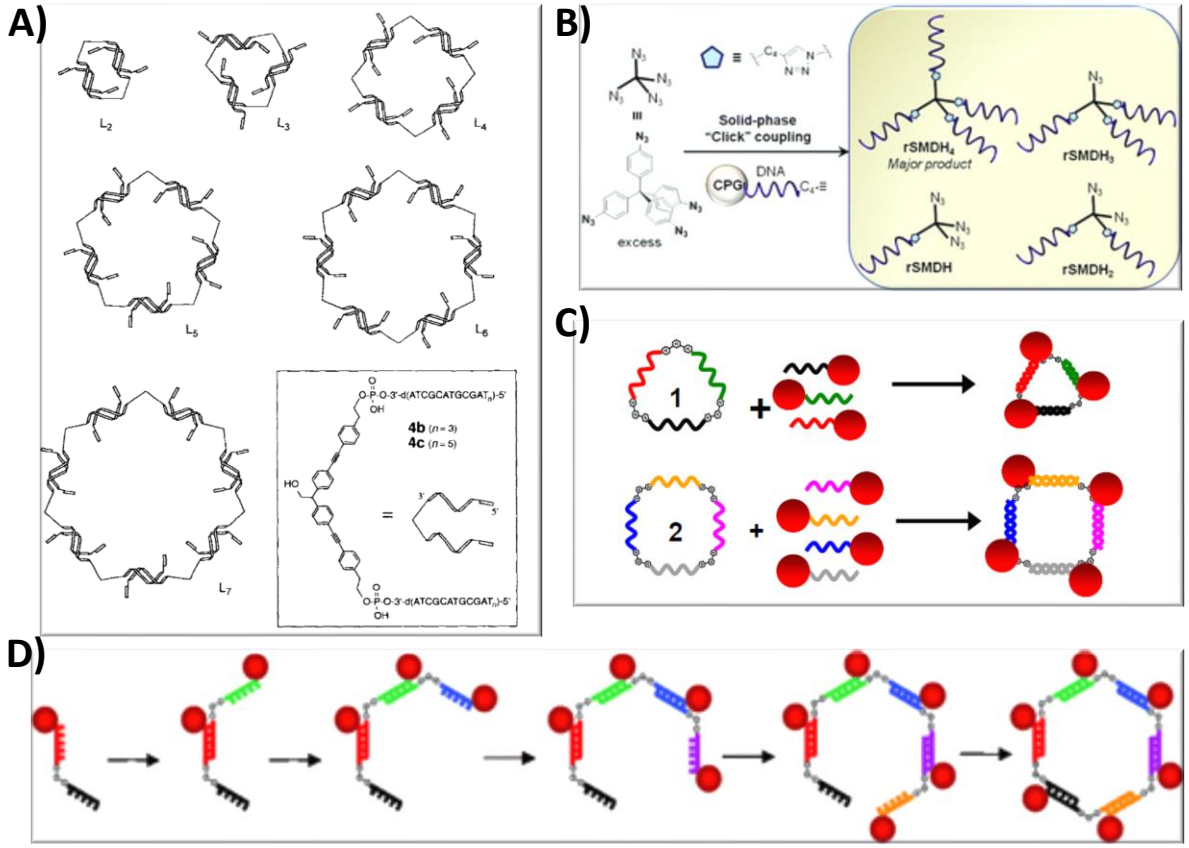

Figure 1. 15 DNA nanostructures with synthetic vertices.

A) Assembly of complementary DNA with synthetic vertices to generate macrocycles. Reproduced with permission ref [234] (John Wiley and Sons 1997) **B)** Synthesis of branched DNA with a synthetic vertex on solid support. Reproduced with permission ref [236] (RSC 2014) **C)** Asymmetric DNA macrocycles for gold nanoparticle templation Reproduced with permission ref [237] (John Wiley and Sons 2006) **D)** Synthesis of a structure switching DNA hexagon with synthetic vertices. Reproduced with permission ref [238] (ACS 2007).

Bergstrom and von Kiedrowski, where the introduction of synthetic vertices was able to break the linearity of DNA.[234-235](Figure 1.15.A) Their synthetic vertices could direct angles, and ultimately resulted in the generation of 2D DNA nanostructures. Tetravalent molecule-DNA conjugation was achieved by Thaner et al. whereby using CuAAC chemistry on solid support between a tetra azide molecule and alkyne functionalized DNA, improved yields of the tetra DNA significantly.[236](Figure 1.15.B) In these two examples however, the vertices where made as 5' modifications using a synthetic vertex, with either di-phosphoramidite or tetra azido functionality, thereby connecting identical sequences together. It was Sleiman et al. who first demonstrated the in-synthesis modification of DNA with an internal synthetic vertex modification, a terphenyl diol phosphoramidite, protected with an MMT group.[237](Figure 1.15.C) The use of this modification allowed for the group to generate dynamic scaffolds for gold nanoparticle templation[238](Figure 1.15.D), as well as DNA minimal cages, with well-defined DNA polygonal faces[73] and DNA nanotubes, for the encapsulation of gold nanoparticles.[239-240]

To potentially add more function to synthetic vertices, metal co-ordination has been extensively investigated as another supramolecular interaction being integrated into DNA nanostructures. In general, to co-ordinate metals with DNA, the in-synthesis modification of DNA with metal coordinating ligands is performed. Co-ordination of transition metals to ligand-functionalized DNA/DNA nanostructures has seen applications in photosynthesis, sensing, catalysis and nanoelectronics.[241-242] From a purely structural point of view, the incorporation metals into DNA nanostructures has produced many new assembly modes, including; cyclic structures using co-ordination with ruthenium[243], DNA triangles[244], 3D metal –nucleic acid cages[245](Figure 1.16.A) and chiral metal-DNA junctions[246](Figure 1.16.B) using the co-ordination of Cu(I) to each corner and at the center of the junction. Interestingly the Sleiman group has also reported the incorporation of metals into DX-tiles, which enhanced their stability and assembled into fiber-like structures.[247] Sleiman had previously found that the incorporation of metal ions into duplex DNA, exhibited a higher Tm than normal DNA duplex's as well.[248](Figure 1.16.C) Moreover, through the site selective incorporation of metal-ligand complexes along a DNA duplex's, charge transport could be modulated.[249-250]

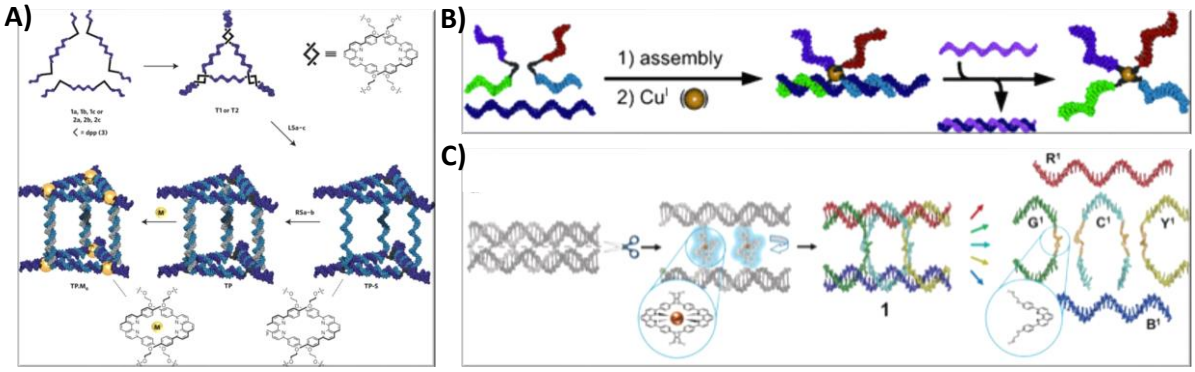

Figure 1. 16 DNA Metal Vertices.

A) 3D metal-nucleic acid cages using Cu(I) corners. Reproduced with permission ref [245] (NPG 2009) **B)** Synthesis of a DNA junction using Cu(I) Reproduced with permission ref [246] (John Wiley and Sons 2011) **C)** DX-tile incorporating Cu(I) centers. Reproduced with permission ref [248] (John Wiley and Sons 2020)

In summary, the modification and conjugation of oligonucleotides to other materials in combination with structural DNA nanotechnology, and the use of other supramolecular interactions with DNA has opened a large variety of new structures, and applications for DNA nanotechnology.

1.6. Modifications for Therapeutics

From the proposal of the central dogma of biology in 1958 by Watson, the potential for oligonucleotides to be used as therapeutic targets had been recognized. Using unmodified DNA, however poses many challenges to the overall success of these therapeutics and as such therapeutic oligonucleotide have been modified extensively with nucleic acid analogues and as conjugates to improve their efficacy.[251] Combining the fields of DNA nanotechnology and oligonucleotide therapeutics has shown even greater potential for better therapeutic outcomes. To get a better understanding of the importance of these modifications, we will first go through how the most relevant oligonucleotide therapeutics work and what some of the challenges are for their success. Following this will be a description of some of the most important modifications and conjugates that have helped to overcome these challenges. As well, how in combination with DNA nanotechnology are helping to improve their effects further.[252-255]

1.6.1. Gene Silencing

While there are many different types of oligonucleotide therapeutics, with different modes of action, this thesis will focus on one type in particular; gene silencing. Gene silencing is perhaps the most common method for oligonucleotide therapeutics and dates back to the first report of antisense oligonucleotides (ASO's) to inhibit viral replication by Zamecnik et al. in 1978.[256-257] Many targets on the post-translational level are undruggable, often because they do not have active sites for small molecules to bind and generate an effect.[258-259] Oligonucleotide therapeutics on the other hand, make many of these targets druggable as they act on the post-transcriptional level. Even among this one type of oligonucleotide therapeutic, various sub-types exist and are categorized by their mode of action, including; ASO's[260], siRNA[261-262], DNA/RNAzymes[263-264], and others[265]. ASO's and siRNA are particularly attractive, as they are simple short oligonucleotides and their mechanisms of action are well understood.

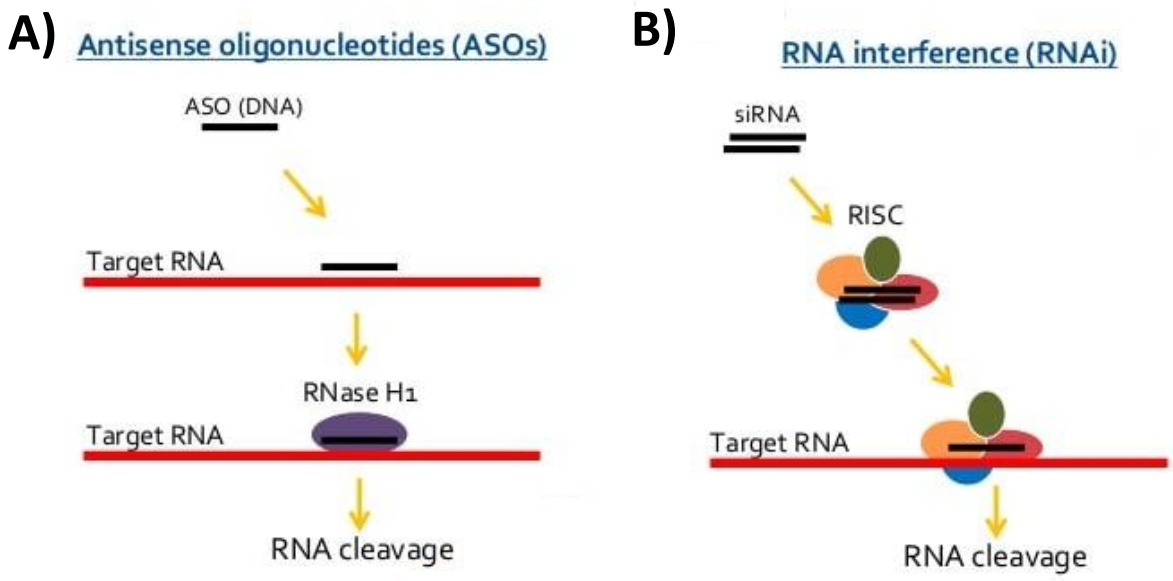

Figure 1. 17 Mechanisms of gene silencing

by: A) Antisense oligonucleotides (ASO)**, B)** silencing RNA (siRNA) Adapted with permission from (Lennox KA, Behlke MA. J Rare Dis Res Treat. (2016) 1(3): 66-70). (BioMed Central 2016).

In general, these therapeutic oligonucleotides work by base-pairing to a specific mRNA target. More specifically, ASO's modulate gene expression when hybridized, by two mechanisms; 1) sterically blocking a target mRNA from being read by a ribosome, disrupting translation, and 2) an RNase H-dependent approach, where once hybridized to the target mRNA the RNase H enzyme is recruited and cleaves the mRNA.[266](Figure 1.17.A) siRNA takes advantage of the RNA interference pathway which is natively used by endogenous miRNA for gene regulation. siRNA is introduced exogenously and mimics miRNA; siRNA are double stranded RNA duplexes, with one strand being deemed the guide or antisense strand and the other the passenger or sense strand. The antisense strand is what hybridizes to the mRNA target and is loaded into the RNA-induced silencing complex (RISC). This complex is then able to dictate gene silencing by either translational arrest or mRNA cleavage.[267](Figure 1.17.B) A relevant advantage of ASO's over siRNA is that since the siRNA mechanism integrates the antisense strand into the RISC complex, the number of modifications that can be tolerated in siRNA is reduced, as the enzyme must be able to recognize the siRNA. However, siRNA results in higher turnovers than ASO's, meaning less need to be delivered to generate similar effects. Overall, these two types of oligonucleotide therapeutics are the most widely used strategies for gene silencing. However, while remarkable, their progress into the clinic has been slow; it and took the first ASO drug (Vitravene) until 1998 to reach the market[268], and challenges remain for their overall success.

1.6.2. Challenges in Oligonucleotide Therapeutics

Due to oligonucleotide's high specificity, easy synthesis and biocompatible properties, the promise for oligonucleotide therapeutics is obvious. Not as obvious however are some of the properties that make it difficult for oligonucleotide therapeutics to be translated into clinical success. The major challenges to using oligonucleotides as therapeutics include; poor biostability, cellular uptake, and *in vivo* distribution.

Poor biostability comes from the ready exposure to nucleases present in serum and in vivo, which can degrade the oligonucleotides. Nucleases are a class of enzyme that degrade DNA/RNA either at the 5' or 3' end of the sequence (exonucleases) or internally (endonucleases). Extracellularly,

3’-exonucleases are responsible for most degradation, while inside cells, both 5’ and 3’ exonucleases, as well as endonucleases are present.[269] Additionally, oligonucleotides are sensitive to both acidic and basic environments, which can be found in different locations throughout an organism. Under acidic conditions, depurination of oligonucleotides can occur and in the case of RNA, the 2’-OH can hydrolytically cleave the strand quite readily under basic conditions.[270]

Cellular uptake is another challenge for oligonucleotide therapeutics, because unlike small molecules (which can diffuse through membranes), oligonucleotides are large negatively charged species, which are repelled by the negatively charged cell membrane.[271] Due to this, oligonucleotides are uptaken in active processes, called endocytosis. There are several

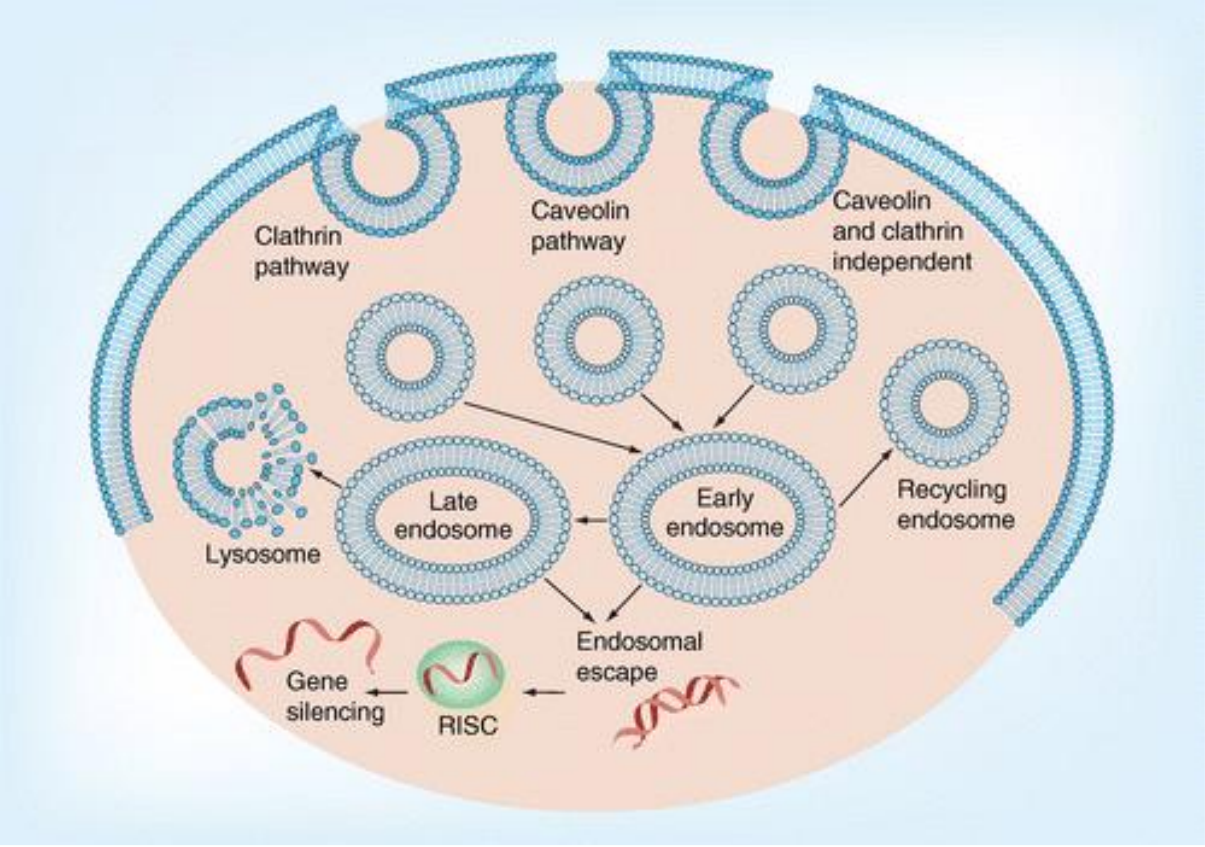

Figure 1. 18 Cellular internalization pathways of oligonucleotide therapeutics.

Adapted with permission from ref [307] (Future Science 2013).

mechanisms of receptor-mediated endocytosis, distinguished by the proteins used in the uptake process. In the main pathway, polymerization of a clathrin protein coat, facilitates changes in the curvature of a membrane, forming a vesicle for oligonucleotide internalization. This vesicle (otherwise known as the endosome) becomes acidic (pH 5-6) and is either directed towards the lysosome for recycling (degradation), or back to the outside of the cell via exocytosis.(Figure 1.18) Since nucleic acid therapeutics act in the cytosol, one of the most paramount challenges is releasing them from this compartment, so that they can generate their effect.[272]

Most of the oligonucleotide therapeutic, when injected finds its way to the liver, kidneys or it is taken up by macrophages.[273-274] Overall the biodistribution of the oligonucleotide therapeutic will determine its efficacy. Targeting oligonucleotide therapeutics to specific tissues, and especially the brain is an ongoing challenge. Accumulating the therapeutic to the brain would be very beneficial for the treatment of many neurological diseases, yet the blood brain barrier presents a giant obstacle that is difficult to overcome.[275] Many oligonucleotide therapeutics are directed towards the treatment of cancer.[276-277] This is because tumors possess leaky vasculature and endothelium, allowing for the accumulation of therapeutics, known as the enhanced permeability and retention (EPR) effect.[278] The EPR effect is an explanation for the observed phenomenon that molecules of certain sizes accumulate in tumor tissues, however, the extent to which this effect works outside mice models is being debated.[279] Off-target effects are another challenge for oligonucleotide therapeutics and must be considered. Geary *et al.* found that many oligonucleotides do have systemic distribution profiles, and silencing could be observed in many tissues, highlighting the need to mitigate off-target effects.[274] Sometimes the challenge of distribution can be overcome through using localized injections like intrathecal, and intra-articular administration, which was the case for the antisense therapeutic Milasen.[280]

It should be noted that in many cases, to overcome these barriers, transfection agents, viruses and other carriers, especially in the form of lipid nanoparticles are showing great promise to deliver oligonucleotide therapeutics. In a select example, ASO's encapsulated in glucose-coated nanoparticles were shown to cross the blood-brain barrier.[281] However, a detailed description of

these carriers is outside the scope of this thesis, and the reader is referred to the relevant reviews.[265, 282-283]

1.6.2.1. Nucleic Acid Analogues

To overcome some of the challenges associated with oligonucleotide therapeutic delivery, many nucleic acid analogues have been developed. In general, most modifications aim to increase stability of the oligonucleotide therapeutic and reduce immune responses, either through base, sugar, or backbone modifications. Probably one of the most common modifications has been the introduction of phosphorothioated (PS) oligonucleotides.[284] Using Beaucage's reagent during the oxidation step of the synthesis cycle introduces a sulfur atom in place of an oxygen to the phosphorus backbone, making it chiral.[285](Figure 1.19.A) The exchange of this atom makes oligonucleotides much more resistant to nuclease degradation, as the enzymes can no longer recognize the PS backbone.[286]

Switching between sulfurization and oxidation is a common practice for generating oligonucleotide therapeutics. This is often done to mitigate properties of PS DNA such as; lower DNA binding affinity, increased hydrophobicity, and higher toxicity than PO DNA.[284] Many efforts have been made to control the stereochemistry of PS DNA, and only within the past two years have scalable methods for the synthesis of stereochemically pure PS DNA been found. A method by Iwamoto *et. al.* uses a chiral phosphoramidite for the synthesis of stereochemically pure phosphorothioate DNA.[287](Figure 1.19.B) In another study by the Baran group a P(V) reagent was used to generate chiral phosphorothioates in DNA.[288] (Figure 1.19.C) The use of stereochemically enriched ASO's have reported higher nuclease resistance for S isomers, and better incorporation into RNase H for the R isomers.[289-291]

Modifying the sugar or nucleobases of DNA is another resource to improve their therapeutic properties. Unlike the PS modification many of these modifications can increase double helix stability and have higher affinity for their targets. This increased stability, may also be useful for applications outside of strictly therapeutics, and may have some value in structural DNA nanotechnology.[90] In addition to better stability and higher affinity, these modifications can also

be used to increase cellular uptake and have better integration into enzymatic machinery. There are many different sugar modifications for these purposes and many are commercially available.[251, 292-293] For example, locked nucleic acid (LNA), first reported in 1997-1998 by both the Imanishi[294] and Wengel[295] groups, is a bicyclic sugar modification, where the 2' hydroxyl and 4' carbon are linked through a methylene bridge.(Figure 1.19.D) This methylene essentially "locks" the RNA and pre-organizes it for hybridization. The addition of a single LNA base modification can increase the Tm of a DNA duplex by 5-10°C, and without the 2' hydroxyl group, stabilizes the strand to hydrolytic cleavage.[296]

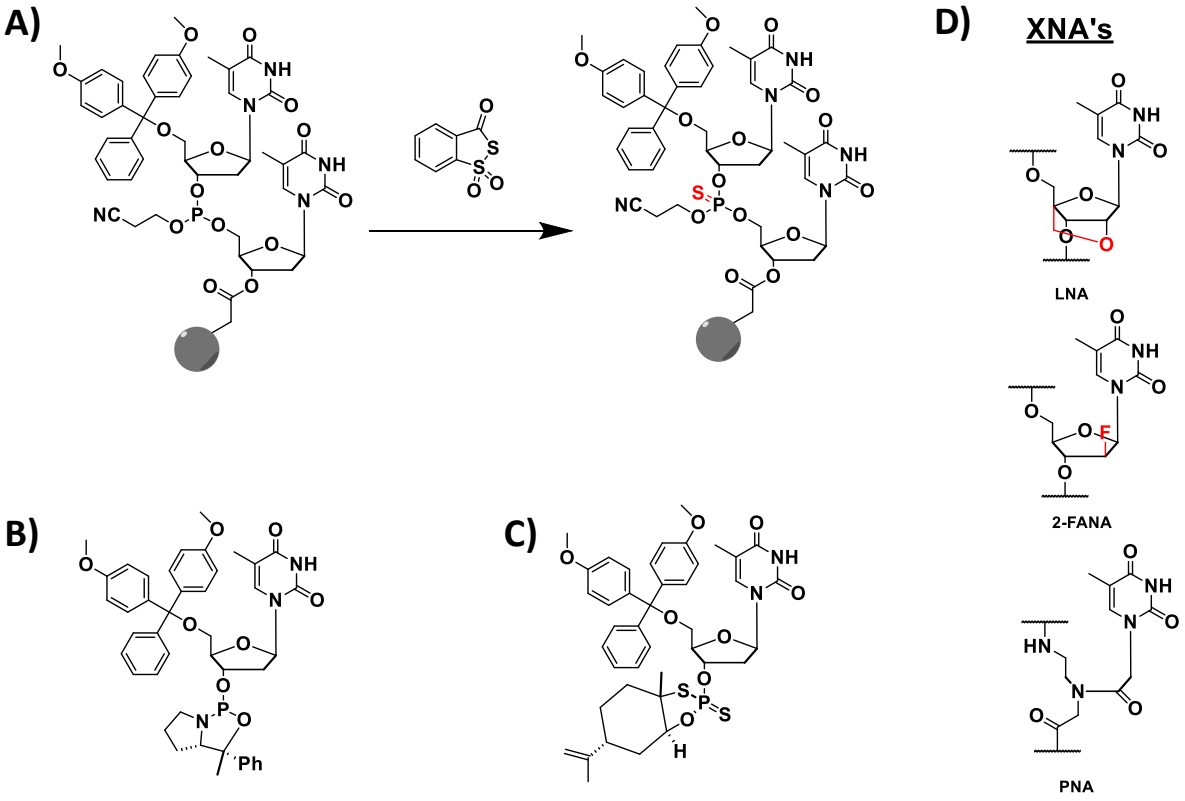

Figure 1. 19 Nucleic acid analogues.

A) Phosphorothioate formation using Beaucage's reagent **B)** Phosphoramidite for chiral Phosphorothioate formation by Iwamoto *et al*. ref [287] **C)** Reagent for chiral Phosphorothioate formation from the Baran group ref [288] **D)** Select XNA nucleic acid modifications (LNA, 2-FANA and PNA).

2’-deoxy-2’-fluoroarabino (2’F-ANA) is another modification used which enhances oligonucleotides stability towards nucleases and improves silencing (Figure 1.19.D). 2’F-ANA is the 2’epimer of 2’F-RNA, but as the fluorine is in the arabino configuration, it adopts a South (C2’-endo) pucker conformation, mimicking the structure of DNA.[297] Interestingly, due to being a mimic of DNA, 2’F-ANA modified oligonucleotides are known to also work through the RNase H-mediated cleavage mechanism.[298] 2’F-ANA modified strands have been shown to silence through gymnosis i.e. without transfection agents.[299] Additionally, siRNA with combinations of 2’F-ANA and LNA, were shown to be more potent and have reduced immunostimulation profiles.[300]

Peptide nucleic acid (PNA), is an analogue of DNA, which does not use phosphate linkages, and is instead made through peptide synthesis protocols (Figure 1.19.D). It is worth mentioning in this section, because as it lacks phosphates, the potential for it to cross cellular membranes is greatly enhanced. First described by Nielsen *et al.,* PNA has a very strong binding affinity to DNA and RNA, and does not require cations to stabilize the duplex.[301-302] Another advantage of PNA is, since PNA is made using solid-phase peptide synthesis, the integration of peptides is relatively straightforward and does not require changes to reaction chemistries.[303-304] PNA-peptide conjugates made in this way, have allowed for the selective transport of antisense therapeutics into tumors.[305] While the advantages of PNA are clear, as longer PNA strands are made, solubility becomes the limiting factor of this analogue. More conjugates will be discussed in the next section 1.5.2.2.

Many other modifications exist beyond what has been presented here, and for a more complete review on the subject the reader is referred to the relevant material.[292-293] While these modifications have been found to improve the half-life of oligonucleotides, DNA binding and cellular uptake, there is still much room for improvement. The use of conjugated small molecules and macromolecules to oligonucleotides can help to further enhance the function of oligonucleotide therapeutics.

1.6.2.2. Conjugates

To further overcome the challenges associated with oligonucleotide therapeutics, many conjugates have been developed, and can be broadly categorized as either uptake-enhancing, or targeting conjugates.[306-307] Additionally, conjugating to the terminal positions of oligonucleotides has, in general, been shown to increase biostability, by virtue of blocking the termini from being recognized by exonuclease's.

1.6.2.2.1. Uptake-enhancing conjugates

Hydrophobic modifications are by far the most common uptake-enhancing ligands for oligonucleotide conjugates and can be readily conjugated to oligonucleotides by solid-phase means.(Figure 1.20.A) Cholesterol, in particular has found widespread use throughout the literature.[306] It was shown to help in silencing of an endogenous apoB gene *in vivo* when appended to an siRNA.[308] When introduced into the siRNA the conjugate resulted in 50% reduction of the apoB target, and siRNA without cholesterol showed no effect. Other conjugates with stearoyl ligands and the lipid docasanyl showed similar effects.[309] α-tocopherol is another hydrophobic modification that has been shown to enhance gene silencing in the liver. Nishina *et al.* demonstrated that a lower concentration of α-tocopherol conjugated siRNA was needed than cholesterol-siRNA, and serum was necessary for *in vitro* uptake.[310] This suggests that the interaction with tocopherol binding proteins plays an important role.

Tissue distribution profiles can also be altered through the conjugation of hydrophobic units to oligonucleotides, by differential binding to serum proteins, such as high-density and low-density lipoproteins (HDL & LDL) as well as albumin.[311] In the Sleiman lab dendritic DNA (D-DNA) ASO's, were made through the in-synthesis addition of branching units and hydrophobic building blocks.[312] These ASO's were shown to bind to albumin with a Kd of approx. 50nM, and helped protect the ASO from nuclease degradation when bound to albumin.[313](Figure 1.20.B)

Cell penetrating peptides (CPP), are another uptake-enhancing conjugate, currently being explored.[314-315] These are peptides with usually high amounts of cationic amino acids, with the ability to cross cellular membranes. The mechanism of uptake is still not well understood, but it is established that CPPs associate with anionic cell-surface molecules and are subsequently internalized into the endosome.[316] Some previous solid phase methods of conjugation peptides were previously mentioned in section 1.3.2.3. and 1.5.2.1, however, CPP's can also be conjugated to oligonucleotides though solution-phase means.[112] Using oligonucleotide-CPP conjugates can be somewhat challenging because the high amount of cationic charge from the CPP, tends to lead to the formation of large aggregates between the oligonucleotide and the CPP. Due to this, the best results of CPP's have been when used in conjunction with uncharged oligonucleotide

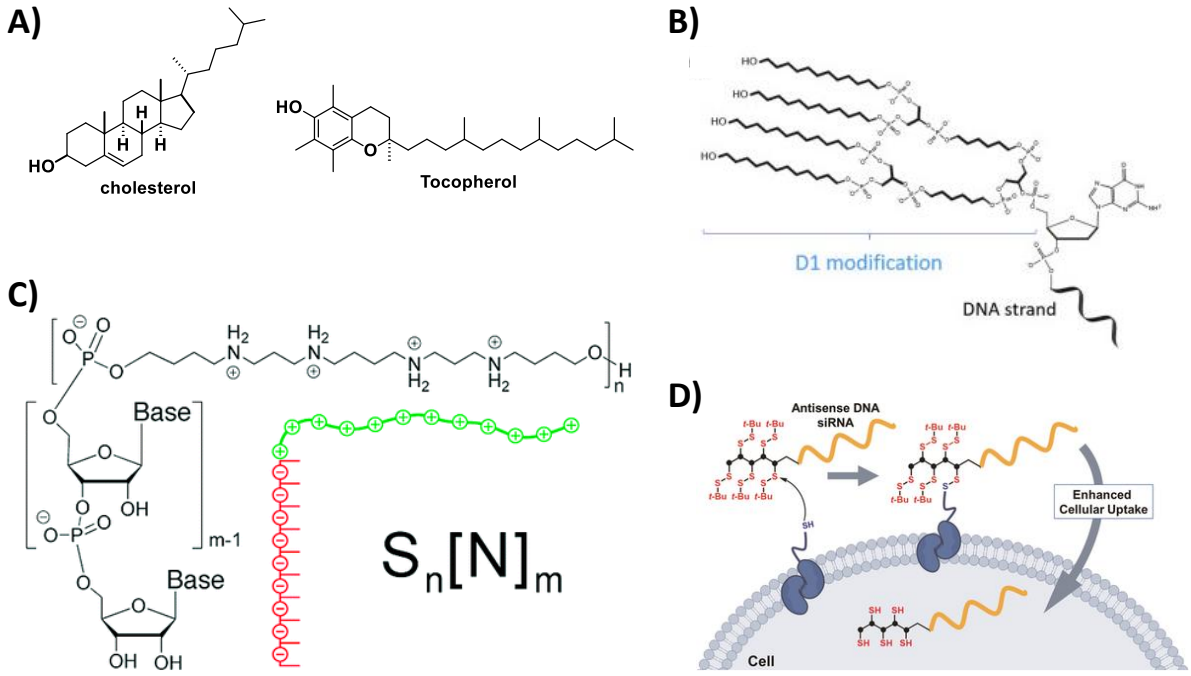

Figure 1. 20 Ligands for enhanced uptake of oligonucleotide therapeutics.

A) Structure of hydrophobic ligands for enhanced uptake; cholesterol and tocopherol. **B)** Structure of Dendritic modified DNA (D-DNA) Reproduced with permission ref [313] (Elsevier 2020). **C)** DNA-Spermine conjugate for endosomal escape. Reproduced with permission ref [319] (ACS 2009) **D)** Enhanced uptake of DNA-disulfide conjugates. Reproduced with permission ref [323] (John Wiley and Sons 2019)

analogues. Morpholino oligonucleotides (PMO) are such oligonucleotide analogues, and when conjugated to CPP's were found to have higher uptake than the non-conjugated counterparts.

Polyamines such as spermine, are like CPP's in that they use large amounts of positive charge to alleviate the consequences of having many anionic charges. Conjugation of many spermine molecules to an oligonucleotide can increase its affinity for its target, acting as "Zip DNA". A spermine phosphoramidite was produced by the Kotera group in 2007, and when conjugated with siRNA, was shown to induce luciferase gene silencing.[317] Importantly, for efficient silencing the N:P (nitrogen : phosphate) ratio of the spermine-siRNA conjugate had to be > 1.5 in order for the conjugate to be released from the endosome.[317-319](Figure 1..20.C) The same group used was able to successfully deliver splice switching oligonucleotides conjugated with oligospermine into monolayer cells and spheroids.[320] This phosphoramidite is now commercially available, which will help facilitate its use further.

The protein coronae of a therapeutic is the shell of proteins that adhere to the therapeutic once injected into the blood stream and heavily influences the therapeutics biodistribution. PEGylation is a strategy commonly used in the formulation of nanoparticles to prevent protein coronae from forming. Hexathylene glycol (HEG), and triethylene glycol (TEG) phosphoramidites are readily available for use and PEG conjugation protocols to oligonucleotides have been well established. PEGylation has been shown to increase half-life but not to assist with cellular uptake. Pegaptinib is a PEGylated oligonucleotide therapeutic currently approved by the FDA.[321] It is an aptamer which is conjugated to a branched 40kDa PEG chain at the 5' end for the treatment of age-dependent macular degeneration. Administration is done directly in the eye, and PEGylation helps in retention of the therapeutic to that location.[322]

Recently, disulfide modified oligonucleotides have been shown to have increased uptake and silencing properties.[323-324](Figure 1.20.D) The proposed mechanism for this is through disulfide mediated uptake, which provides direct cytosolic internalization. This is hugely beneficial and helps to overcome one of the biggest barriers in oligonucleotide therapeutics, endosomal release. Although, the studies used in vitro conditions which were free of serum proteins which may influence overall applicability but nonetheless should be studied further.

1.6.2.2.2. Targeting Conjugates

In contrast to uptake-enhancing conjugates, conjugating targeting ligands to oligonucleotide therapeutics to improve tissue targeting is current under investigation. Of the targeting ligands under investigation, small molecule targeting ligands offer relatively easy conjugation chemistry to oligonucleotides and have been used to improve therapeutic efficacy. The folate receptor protein on the surface of cells has a high affinity to folic acid (vitamin B9), and once bound, triggers endosomal cellular uptake.[325] Oligonucleotide-folic acid conjugates have been generated to target this receptor, which is overexpressed in many cancer cell types.(Figure 1.21.A) The Wagner group found receptor-specific gene silencing could be achieved with their conjugates, as no silencing was observed without the folate ligand, however still needed a polycationic transfection agent for effective endosomal escape.[326] In 2017 Orellana et al. found that carrier-free silencing could be achieved over 72hr in mouse models using folate conjugates.[327] Interestingly, in this study they found that detachment of the folate ligand after internalization was not necessary to achieve silencing.

N-acetyl galactosamine (GalNac) ligands have also been used to improve tissue targeting towards hepatocytes through binding the asialoglycoproetin receptor. Due to multivalent effects, conjugating three GalNac ligands to an siRNA using a trebler-branching unit, has been shown to improve silencing over the single monosaccharide ligand.[328] (Figure 1.21.B) These ligands are relatively straightforward to conjugate to oligonucleotides via solid phase methods. For conjugation of the triantennary GalNac cluster, a few different strategies have been pursued; direct conjugation of the cluster, coupling of a trebler phosphoramidite, followed by a

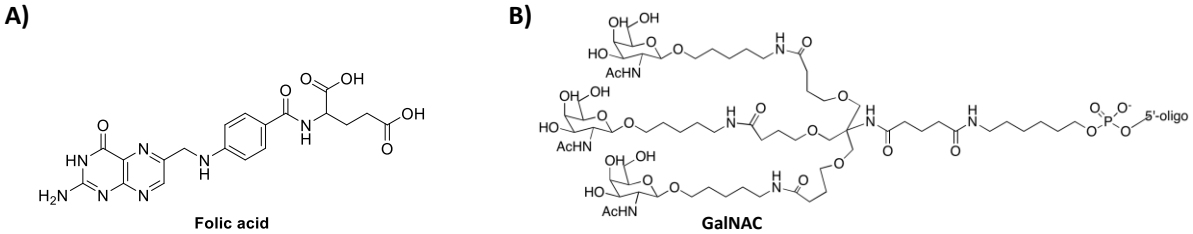

Figure 1. 21 Targeting ligands for oligonucleotide therapeutics.

A) Structure of Folic Acid **B)** Structure of GalNac ligand used by Alnylam inc. ref [328]

monosaccharide GalNac phosphoramidite[329], and coupling 3 successive nucleotidic monomers of GalNAc.[330] In all cases, gene silencing was enhanced in the hepatocytes of in vivo mouse models.

Conjugation with proteins and antibodies (Ab) is very attractive, as it holds the promise of antigen-dependent and cell-type specific targeting of oligonucleotides. siRNAs were conjugated with different Abs by the Siebel group and were shown target specific antigens, but endosomal escape remained a barrier in the study.[331]

While these conjugates are showing great potential, conjugation chemistries to Abs can be quite challenging.[332] Antibody-oligonucleotide conjugates (AOC's) can be made in a multitude of different ways i.e. through electrostatic interactions, biotin-avidin interactions, hybridization or direct conjugation.[333] (Figure 1.22.A) However, these methods all still require the direct chemical conjugation of linker molecule to the antibody, for subsequent oligonucleotide conjugation. Characteristics of AOC's such as the degree of conjugation (DoC) and the linkage site, influence the conjugates overall properties, such as; solubility, toxicity and affinity, but can be hard to control. Introduction of the linker, on the Ab is a great challenge in developing well defined AOC's.

Both in vitro and chemical methods exist for functionalizing Abs, each with their advantages and disadvantages. In general, in vitro techniques use gene editing and natural/unnatural amino acids or peptide tags to introduce unique or site-specific functional handles. For example, Thiomab technology uses the genetic incorporation of additional cysteine residues into monoclonal antibodies to generate site-specific thiol handles for conjugation.[331, 334] While gene editing techniques can generate well defined antibodies for conjugation, the method is not very accessible to non-experts and is quite costly.

Chemical conjugation methods, on the other hand are much more accessible and many bi-functional linkers exist for the conjugation of various species to Ab's at lysine, or cysteine residues. Unfortunately, these methods suffer from the opposite problem, and conjugation is not well controlled, thereby generating conjugates with large DoC's in often ill-defined locations.[335] DoC in chemical conjugation can be somewhat controlled at the expense of overall yield, by

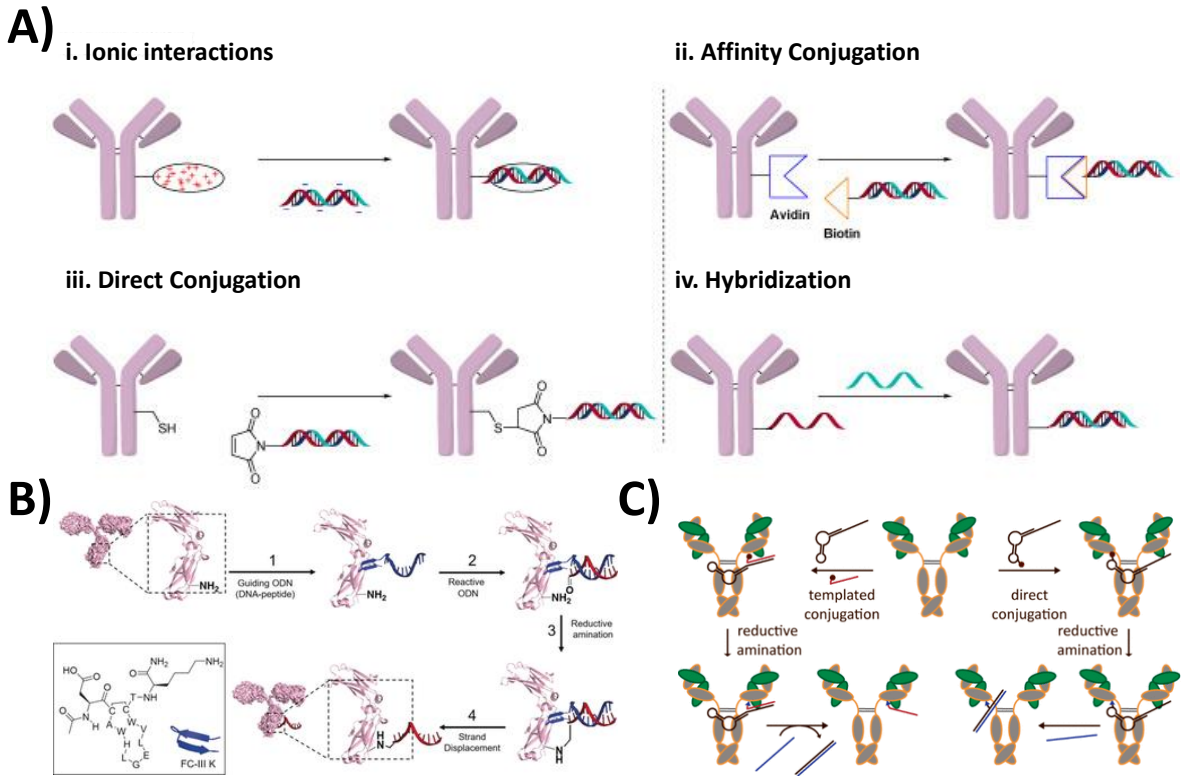

Figure 1. 22 Methods for oligonucleotide conjugation to antibodies

A) Standard antibody-oligonucleotide conjugations; ionic, affinity, direct and hybridization. Adapted with permission ref [333] (Multidisciplinary Digital Publishing Institute (MDPI) 2021) **B)** DNA-Ab conjugation guided by an FC region binding peptide. Adapted with permission ref [337] (John Wiley and Sons 2019) **C)** DNA-Ab conjugation guided by an FC region binding aptamer. Adapted with permission ref [338] (ACS 2019)

selecting a ratio between reacting species that centers the Poisson distribution of products around the desired DoC.[336] Although, high concentrations of antibody are generally needed to generate AOC's in reasonable yields. The Gothelf group has made great progress towards the site-specific chemical conjugation of antibodies with oligonucleotides at low concentrations. Using peptide[337] or aptamer[338] guided reactive oligonucleotides, the group was able to bind to the constant region of a diverse set of Abs and make AOC's in a high conversion yield (60-90%). (Figure 1.22.B&C)

The use of aptamers as targeting ligands are another avenue that has been well developed and will be discussed in Section 1.6.1.

1.6.2.2.3. Conjugate Linkers

The linker chemistry between the oligonucleotide and the conjugating species, is an important aspect that must also be considered. Generally, linker chemistries can be classified as degradable, or non-degradable. Degradable linkers can be further broken down as either being traceless or not. Non-degradable linkages form a covalent bond between the oligonucleotide and the conjugating species which cannot be cleaved. This can be advantageous, as un-intended degradation before reaching the desired target can be mitigated. However, by not cleaving, the conjugate could interfere with its ability to silence. For example, Ye *et al.* demonstrated that conjugating siRNA to CPPs using PEG spacers, cleavable disulfides and non-cleavable thiolmaleimide chemistry, influenced their overall knockdown and efficacy, with the disulfide generating the most potent effects.[339] (Figure 1.23.A) Stimuli responsive linkers, which can be cleaved through exogenous stimuli have also gained a lot of attention recently, as they can be tailored to cleave with spatio-temporal control. A photoresponsive 5'-cholesterol linked siRNA conjugate was produced by Yang et al. which targeted *firefly luciferase, gfp* and *Eg5* genes.[340]

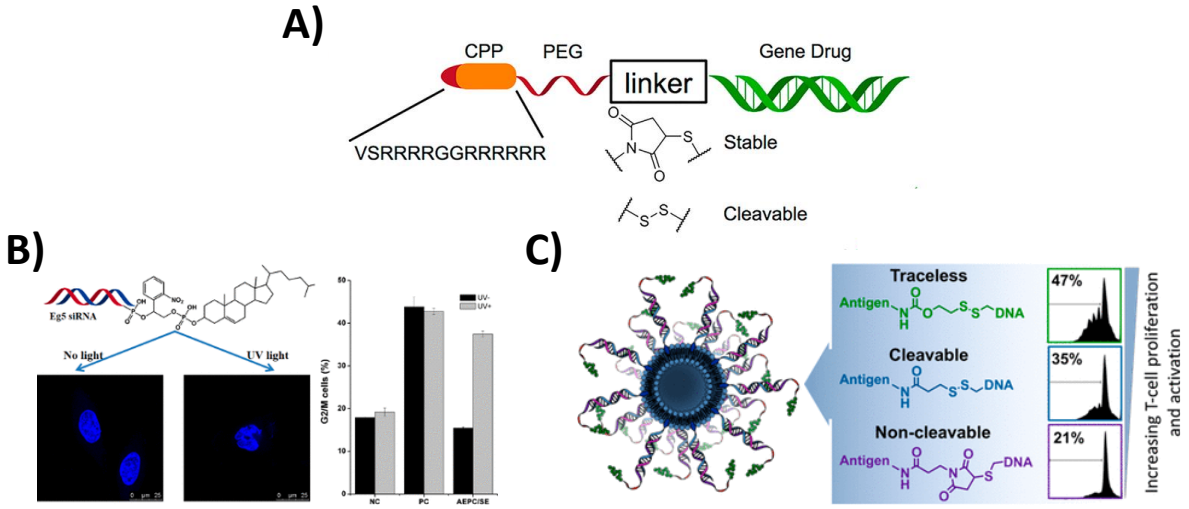

Figure 1. 23 Oligonucleotide conjugate linkers.

A) Stable and cleavable linkers in a CPP-oligonucleotide conjugate. Adapted with permission ref [339] (Ivyspring International Publisher 2017) **B)** siRNA conjugated to cholesterol through a UV-labile linker. Adapted with permission ref [340] (ACS 2018) **C)** Effect of; traceless, cleavable and non-cleavable linkers in oligonucleotide therapeutic effect. Adapted with permission ref [341] (ACS 2018)

They found that the gene silencing of their conjugates was temporarily masked when the conjugate was made on the antisense strand of the siRNA, until light activated. (Figure 1.23.B)

Moreover, many linkers when they are cleaved, leave a piece of the linker still connected to the active compound, which can still influence the efficacy of the therapeutic to a degree. Therefore, traceless linkers have been introduced, which, when cleaved, only result in the active oligonucleotide therapeutic. Mirkin *et al*. exemplified this concept by comparing three different linker chemistries of antigens coupled to a TLR9 agonist oligonucleotide adjuvant.[341] (Figure 1.23.C) They used traceless, cleavable and non-cleavable linkers connecting the antigen and found that the choice of linker significantly affected the immunostimulatory effects of these conjugates. These findings highlight the critical role that the linker chemistry plays in the overall efficacy of the oligonucleotide therapeutic.

1.6.2.3. Merging with DNA Nanotechnology

The marriage of DNA nanotechnology with therapeutic oligonucleotides is just beginning. Having complete control over the structure of DNA nanomaterials and addressing them with oligonucleotide therapeutics for delivery is a promising area. Mirkin *et al.* were the first to introduce the idea of spherical nucleic acids (SNA's), which use the shape of a gold nanoparticle conjugated with ASO's for enhanced uptake and increased nuclease resistance.[342](Figure 1.24.A)) SNA's have been expanded with the use of targeting ligands such as antibodies[343] and using other materials for the core of the SNA's[216, 342]. Fakhoury *et al*. found that SNA's assembled by a hydrophobic core needed less transfection agent to achieve the same level of silencing than unmodified ASO's.[344] (Figure 1.24.B) Additionally, Fakih *et. al.* demonstrated that 2'-FANA modified SNA's with hydrophobic cores could silence better than the unsubstituted FANA strands without the use of transfection agents.[216, 345](Figure 1.24.C) The Sleiman group also demonstrated using DNA prisms with 6 ASOs, which due to the additional stability of the bound antisense strands, silenced better than unbound controls.[346] siRNA conjugated to nanotubes were used by Ju *et al.* in combination with double aptamer "smart key", which required the recognition of two cell surface markers. [347](Figure 1.24.D) The first aptamer activated the

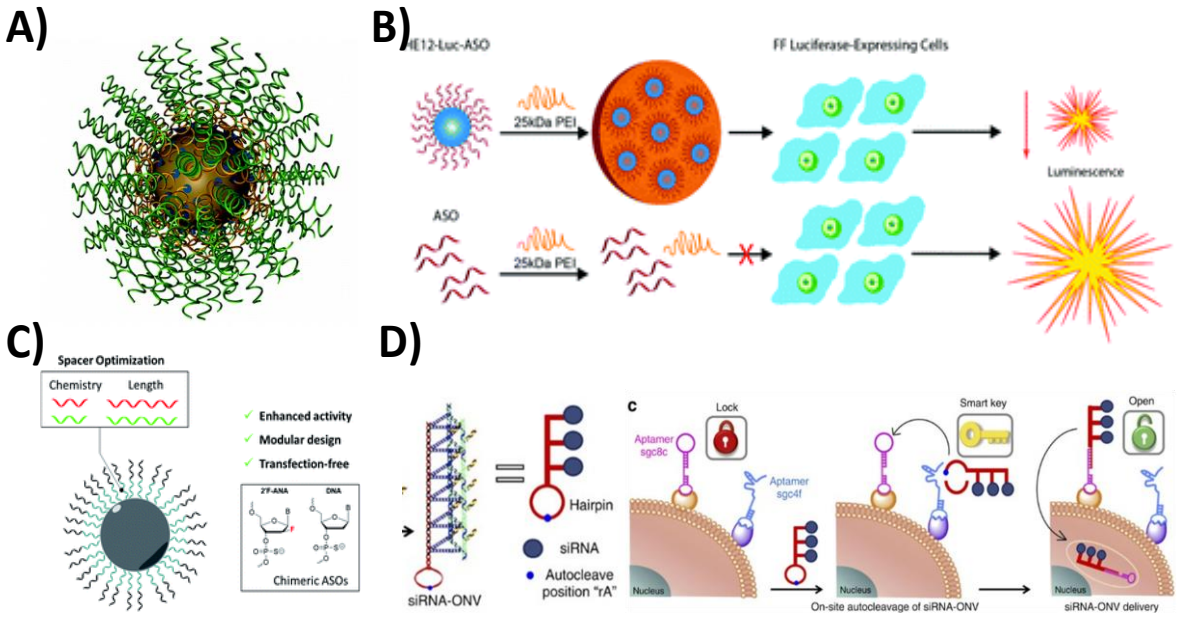

Figure 1. 24 Therapeutic DNA nanotechnology.

A) Structure of an SNA with a gold nanoparticle core. Adapted with permission ref [342] (ACS 2012) **B)** SNA's with a hydrophobic core silence better than unmodified DNA. Adapted with permission ref [344] (RSC 2015) **C)** Structure of 2' F-ANA SNA's Adapted with permission ref [345] (RSC 2021) **D)** DNA nanotube functionalized with siRNA. Adapted with permission ref [347] (NPG 2016)

nanotube using a DNAzyme to cleave a hairpin integrated within the nanotube, and once cleaved the second aptamer could recognize the nanotube to internalize the structure, selectively delivering the therapeutic. Furthermore, conjugation of folate to a DNA tetrahedron hybridized with siRNA, resulted in reduced gene expression in mouse tumor models.[348-349] Even DNA origami was used for the delivery of siRNAs against the Bc12 protein, which shrank tumors in xenograft mouse models.[350]

Presently, many of the modifications made for oligonucleotide therapeutics are finding their way into the DNA nanotechnology for applications other than therapeutics, where stability and targeting are important. In a recent study, the Mirkin group used LNA modified oligonucleotides to generate superlattices of nanoparticles of various shapes.[351] The use of LNA modifications increased the melting temperature only in the sticky end regions of their constructs. William Shih's group have also used DNA nanostructures conjugated with oligolysine and found that the oligolysine protected the structures themselves from denaturation and nuclease degradation.[352]

Moreover, PNA modifications have also been used to increase hybridization stability[353], as well as allowed for easy integration of peptides into DNA nanostructures[354].

1.7. Modifications for Molecular Recognition

1.7.1. Aptamers Modifications

Probably one of the most interesting functions that DNA can have is its ability to not only recognize complementary strands, but other small molecules and proteins as well. Aptamers are single-stranded DNA or RNA which can fold into a 3D structure for recognition, and have been used as both targeting moieties, and therapeutics. Aptamers are made in a process called SELEX (systematic evolution of ligands by exponential enrichment) where through a series of incubation, separation and amplification cycles, high affinity aptamers can be evolved.[355-356](Figure 1.25.A) SELEX has increased in efficiency over time and has been expanded to include cell-SELEX[357], cell-internalization SELEX[358] and in-vivo SELEX[359]. Unfortunately, the molecular recognition properties of oligonucleotides when compared to antibodies have not been able to achieve the same level of binding efficiency, mostly due to the limited chemical interactions that DNA can make. To address this and increase chemical diversity, modified oligonucleotides have been used in the form of SOMAmer (Slow Off-rate Modified Aptamers) technology, where dU residues are variably modified in the 5-position.[360-361] However, modifications made to the oligonucleotides this way are still limited as they need to be compatible with the DNA

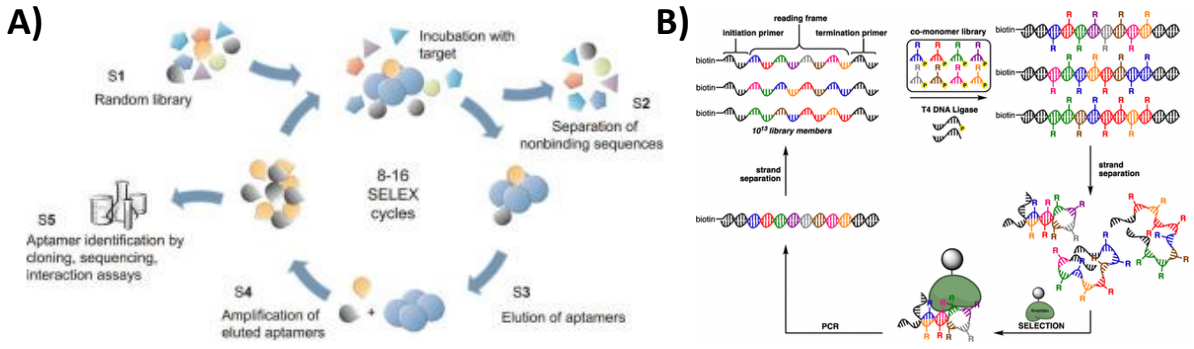

Figure 1. 25 Evolution of oligonucleotides for recognition.

A) Process of SELEX with incubation, separation and amplification steps. Adapted with permission ref [355] (NPG 2014) **B)** Molecular evolution LOOPER. Adapted with permission ref [362] (ACS 2017).

polymerase. Additionally, the number of unique modifications that can be introduced is limited to the number of nucleobases used in the genetic code. The Hili group has worked towards addressing this second problem through their LOOPER technology, using a DNA scaffold to template short, modified oligonucleotides with diverse functionality in multiple positions and then ligating these fragments together.[362] A selection step followed by PCR amplification allows for the evolution of the library. (Figure 1.25.B) Initial research efforts are being made to use completely synthetic oligomers for binding, in combination with DNA barcoding.[363]Binding synthetic oligomers to a target followed by amplification, and sequencing of an appended barcode, aptamers would no longer have a limited chemical operational space.

1.7.2. DNA Templated Organic Synthesis

The recognition of t-RNA building blocks to the ribosome/mRNA complex during the process of translation is what allows them to produce of all the proteins in nature. Nature can achieve this production at very low monomer concentrations uM or nM, due to the high degree of affinity and specificity between reacting components, resulting in increased effective concentrations. Typically, in organic synthesis high amounts of reagents are used at M and mM concentrations to achieve chemical transformations. Inspired by how nature performs chemical transformations, Liu *et al.* pioneered the use of reactive DNA conjugates in combination with recognition to DNA templates, to perform chemical reactions. This process called "DNA Templated Synthesis" (DTS) has found uses in many fields such as polymer formation, diagnostics, drug and reaction discovery.[364](Figure 1.26.A)

In their original proof of principle study in 2001, Liu et al. investigated reactions between DNA conjugates with appended nucleophiles (amines and thiols), and DNA conjugated with electrophiles (iodoacetimides, bromoacetimides, vinylsulfones and maleimides).[365] Product formation was only observed when the DNA was complementary to each other, and when the sequences were mismatched no reaction took place. The addition of spacers between reacting groups, did not show decreases in reactivity, and therefore it was concluded that local concentration is what facilitated reactions, rather than better alignment of reagents. Due to the

remarkable DNA recognition ability multiple incompatible reactions were able to be achieved in tandem.[366] From the original study a vast number of other chemical reactions have been facilitated by DTS such as; Wittig olefination, Heck coupling, reductive amination and Huisgen cycloadditions.[367](Figure 1.26.B)

With this large toolbox of reactions, multistep syntheses were able to be achieved, as well as the production of large macrocycles. Sixty-five[368] and 256,000[369]-membered libraries of macrocycles were produced using DTS, to screen for lead compounds of pharmacological relevance. Different template architectures have also been explored, being particularly useful for distance-dependent reactions.[370] Placing building blocks in the middle of 3- and 4-way junctions, the Gothelf group also generated a "Yoctoreactor" platform for the generation of high throughput small molecule drug libraries.[371] (Figure 1.26.C.)

To mimic the complex synthesis found in nature, efforts have been made to use DTS for sequence-controlled synthesis. In some of the first work towards this, the Liu group performed an ordered multistep synthesis of a triolefin and tripeptide by using a DNA template that could change its secondary structure, through changes in temperature.[372](Figure 1.26.D) Changing between temperatures, exposed different hybridization sites to modulate the order of DTS. Other sequence-controlled synthesis methodologies have been investigated by the Turberfield, and O'Reilly laboratories, using series of Wittig reactions leading to the generation of sequenced-controlled oligomers up to 10 building blocks long.[373] In 2010, autonomous DTS was achieved using a DNA walker that was able to do sequential amine acylation reactions as it moved along a DNA track.[374] (Figure 1.26.E)

Apart from using DTS for the synthesis of complex small molecules, Czlapinski and Sheppard formed metal-salen bridges[375], which inspired the Gothelf group in their synthesis of linear and branched nanowires.[376] Using elongated linear building blocks and cleavable linkers, nanowires and DNA could be separated from each other, expanding the utility of the approach further.[377-378](Figure 1.26. F) Furthermore, Lo *et al*. was able to template the formation of nanowires through the use of a template formed in a ring opening polymerization (ROMP), which could hydrogen bond with the corresponding nanowire monomers, and be subsequently

polymerized.[379] . Ligation reactions are another interesting avenue heavily pursued by DTS for stabilization of DNA nanostructures. Various forms of photocrosslinking have been used to ligate DNA strands together[380-381], and very recently, this method was used to stabilize whole origami

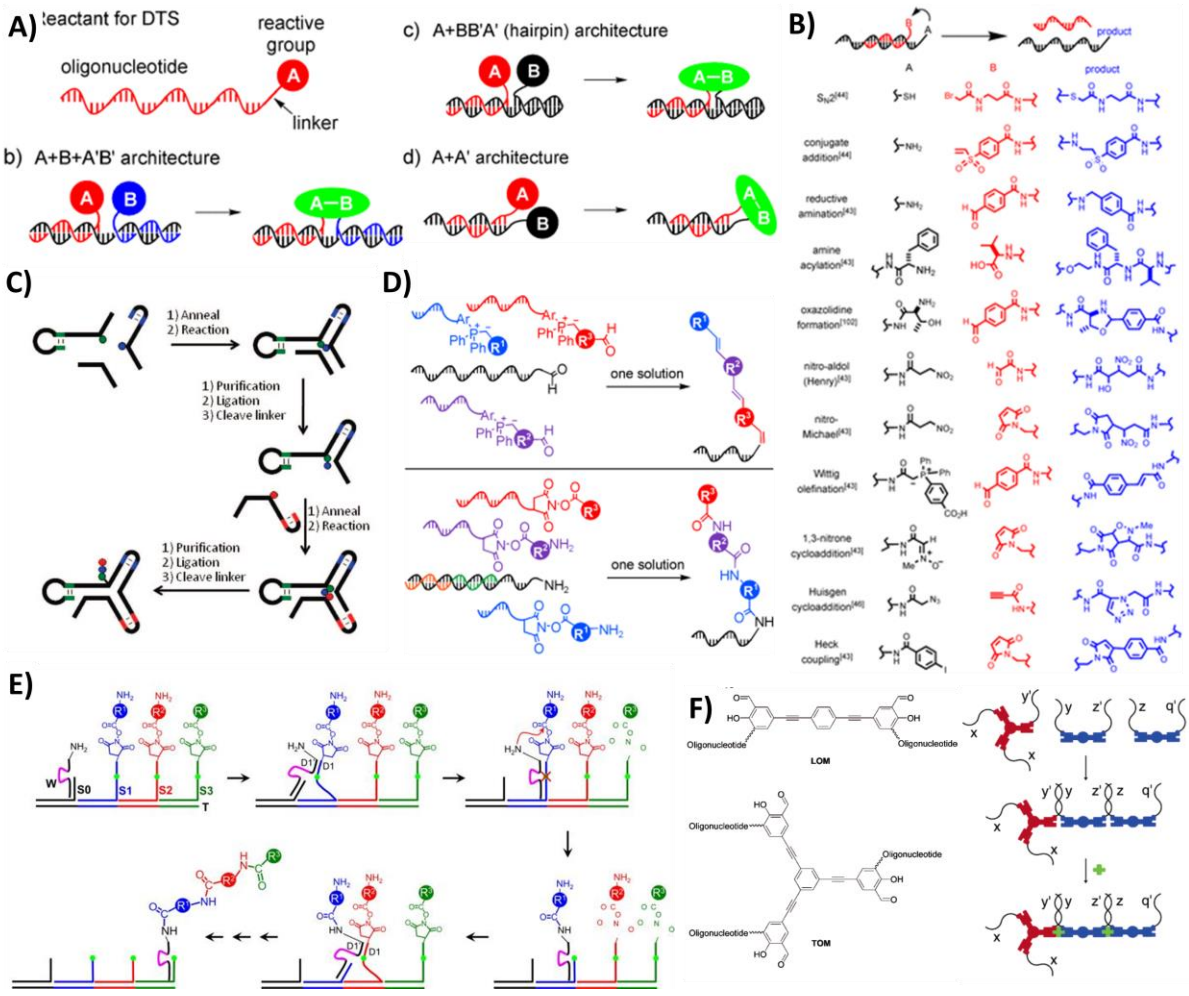

Figure 1. 26 DNA templated reactions.

A) Types of DNA templated reactions. Adapted with permission ref [364] (John Wiley and Sons 2004) **B)** Chemistry of different DNA templated reactions. Adapted with permission ref [367] (John Wiley and Sons 2002) **C)** Yoctoreactor platform for generating high throughput drug libraries. Adapted with permission ref [371] (ACS 2009) **D)** Generation of triolefin and tripeptides using a DNA template. Adapted with permission ref [372] (John Wiley and Sons 2005) **E)** Automated DNA templated synthesis using a DNA walker. Adapted with permission ref [374] (NPG 2010) **F)** Branched and linear DNA nanowires using metal-salen bridges. Adapted with permission ref [377] (ACS 2004)

structures[382]. Gothelf *et. al.* have also shown the crosslinking of DNA DX-tiles using a disulfide crosslinking approach.[383]

Overall, DTS clearly demonstrates how the recognition properties of DNA can be taken advantage of in conjunction with chemical modifications, to build new materials and generate new functions.

1.7.3. Strand Displacement & Aptamer Switches

In the previous two examples of using the molecular recognition properties of DNA, recognition for the most part remained static and unchanging. Using DNA to generate dynamic motion has been an area of incredible interest to produce many molecular probes and diagnostics. Toehold mediated strand displacement is the primary mechanism by which dynamic function can be achieved with DNA. The idea of strand displacement was originally inspired by the unzipping of the Holliday junction found in replication.[384-385] While there are a few different types of strand displacement the most common is toehold-mediated strand displacement (illustrated in Figure

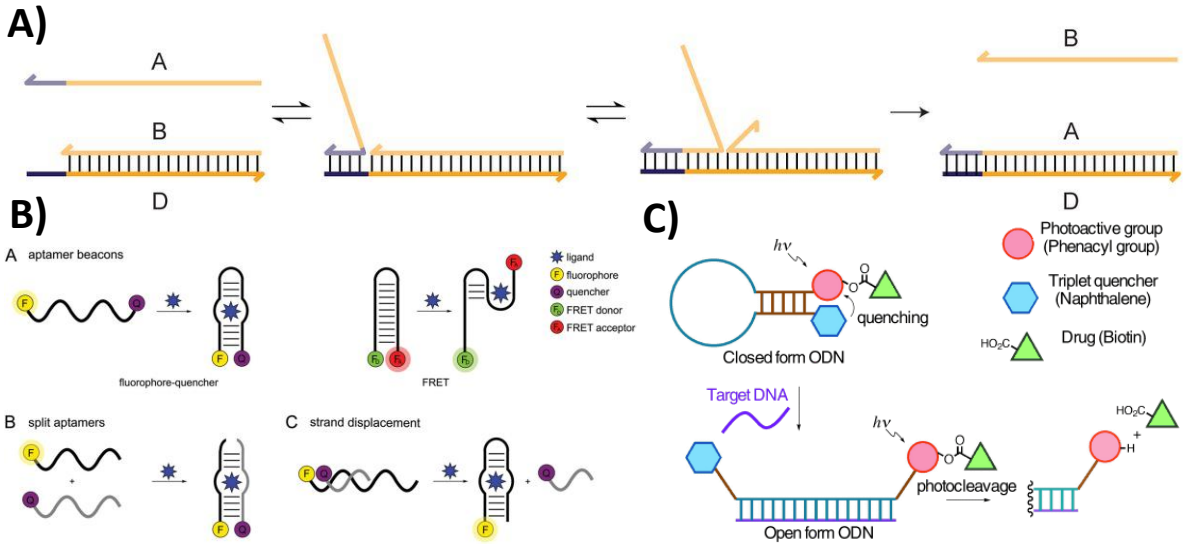

Figure 1. 27 Strand Displacement mechanism and applications.

A) Mechanism of Strand displacement**.** Adapted with permission ref [384] (ACS 2019) **B)** Methods of aptamer switching beacons Adapted with permission ref [388] (John Wiley and Sons 2020) **C)** Molecular beacon for the release of small molecule payloads. Adapted with permission ref [390] (John Wiley and Sons 2003)

1.27.A). In toehold mediated strand displacement, an “invader” strand (A) binds to the toehold overhang of a target duplex (B:D) and replaces the “incumbent” strand (B) to generate a new (A:D) duplex single stranded (B). This process is ultimately driven by the greater thermodynamic stability of (A:D) duplex opposed to the (B:D) duplex. Measuring the dynamic motion using a spectroscopic output is probably the biggest contribution oligonucleotide conjugation has given to study this dynamic process, through the conjugation of various dye molecules to DNA FRET or quenching pairs. However, some groups have started to move towards using other DNA modifications. For example, Olson *et al*. have demonstrated that the integration of LNA

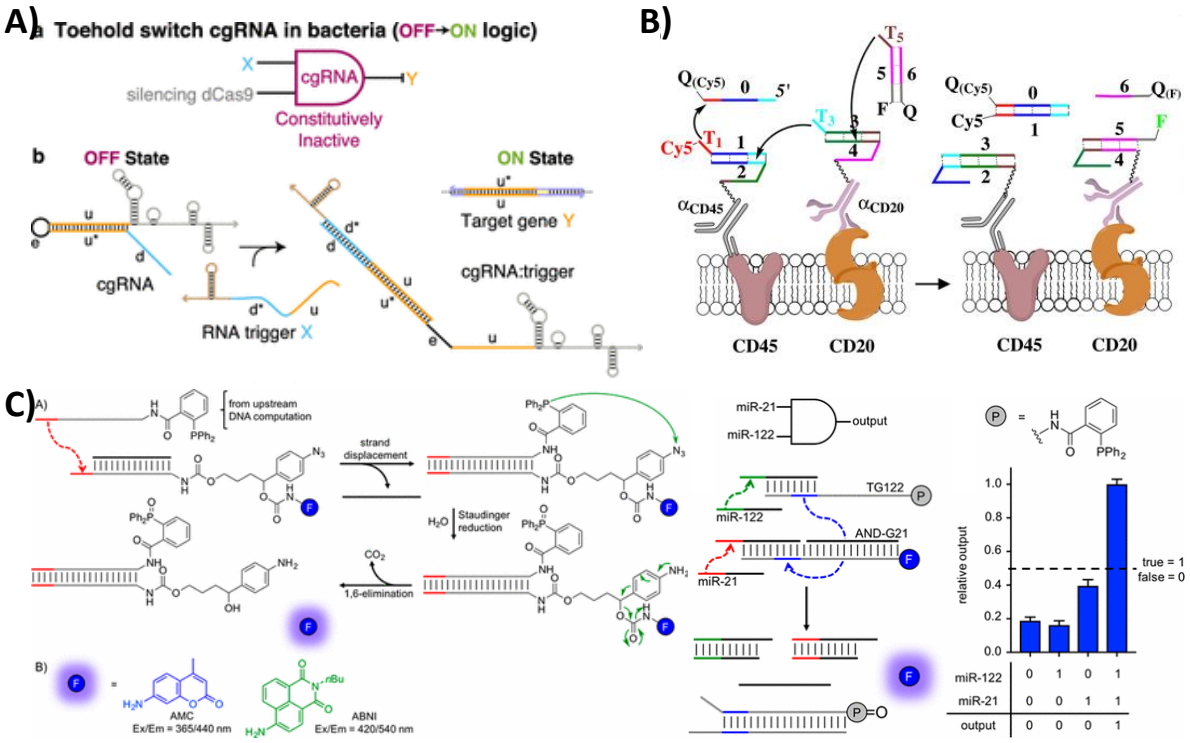

Figure 1. 28 Applications of strand displacement in DNA computation.

A) DNA logic gate for CRISPR activation. Both dCas9 and RNA trigger strand X are necessary to turn “on” the conditional guide RNA (cgRNA) for integration into CRISPR. RNA trigger X displaces a portion of the cgRNA revealing the gRNA sequence for CRISPR activation. Adapted with permission ref [393] (ACS 2019) **B)** DNA computation on cell membrane biomarkers. AOC’s are used to bind CD45 and CD20 biomarkers and an oligonucleotide strand displacement cascade reveals whether these markers are present on the cell, by giving a spectroscopic output if the cascade is successful. Adapted with permission ref [395] (NPG 2013) **C)** Release of small molecules from a DNA AND gate. Adapted with permission ref [396] (ACS 2017)

modifications into strand displacement can have profound effects on the selectivity and rate of the mechanism.[386]

One of the simplest devices to use a strand displacement mechanism, are molecular beacons, which are hairpin shaped DNA with large loops and short stems and have conjugated fluorescent and quencher dyes at the 5' and 3' ends.[387] When an input target strand is introduced to a molecular beacon it hybridizes to the loop portion of the hairpin, and displaces the stem, separating the dye pair and providing a measurable output signal. MB can be made that recognize other inputs as well in the form of aptamer beacons or split aptamers[388], where the aptamer complex is more thermodynamically stable than the original duplex or single strand.(Figure 1.27.B)

There are a wide range of molecular beacons that have been developed to respond to a vast array of input sequences, with many different conjugation chemistries to enhance their function.[389] An interesting application of molecular beacons from a drug delivery and conjugation point of view was the development of a molecular beacon by Okamoto *et al*., where they were able to trigger the release of small molecules in response to a target sequence and light.[390](Figure 1.27.C) In their molecular beacon, a photoactive probe and quencher were tethered to either end of the molecular beacon, and only when the target sequence was present, did the molecular beacon open up and the photoactive probe triggered by light.

Another direct application of strand displacement has been the development DNA computation circuits. Instead of using directly 1 input with 1 output, using series of strand displacement networks cascades in tandem, allows for complex calculations to be made with DNA.[391] Like an electronic computer these systems use series of strand displacement logic gates to perform their calculations. The use of DNA logic gates has allowed for the generation of DNA computers which can calculate square roots[392], produce CRISPR inputs[393-394], and perform cell surface biomarker analysis[395].(Figure 1.28.A & B) Again, this field has been greatly facilitated by the conjugation of organic dyes to oligonucleotides, to give measurable outputs. However, efforts have been recently made to generate more functional outputs with the help of conjugated oligonucleotides.

A great example of this was by Morihiro *et al.* who generated a DNA AND gate and used a DNA templated Wittig reaction to release small molecules.[396](Figure 1.28.C)

1.7.4. Dynamic DNA Nanotechnology

The combination of structural DNA and dynamic recognition by stimuli responsive oligonucleotides, has given more function to the simple DNA structures previously explored in this chapter.[397] In addition to the use of DNA as the input stimulus, other stimuli can also be used to generate dynamic functions with DNA. While there are many examples in the field of dynamic DNA nanotechnology which use pure DNA, these are primarily for producing dynamic containers[63], tweezers[398], and walkers[399], with limited applications.[400] Increased function has been gained with DNA conjugates.[401]

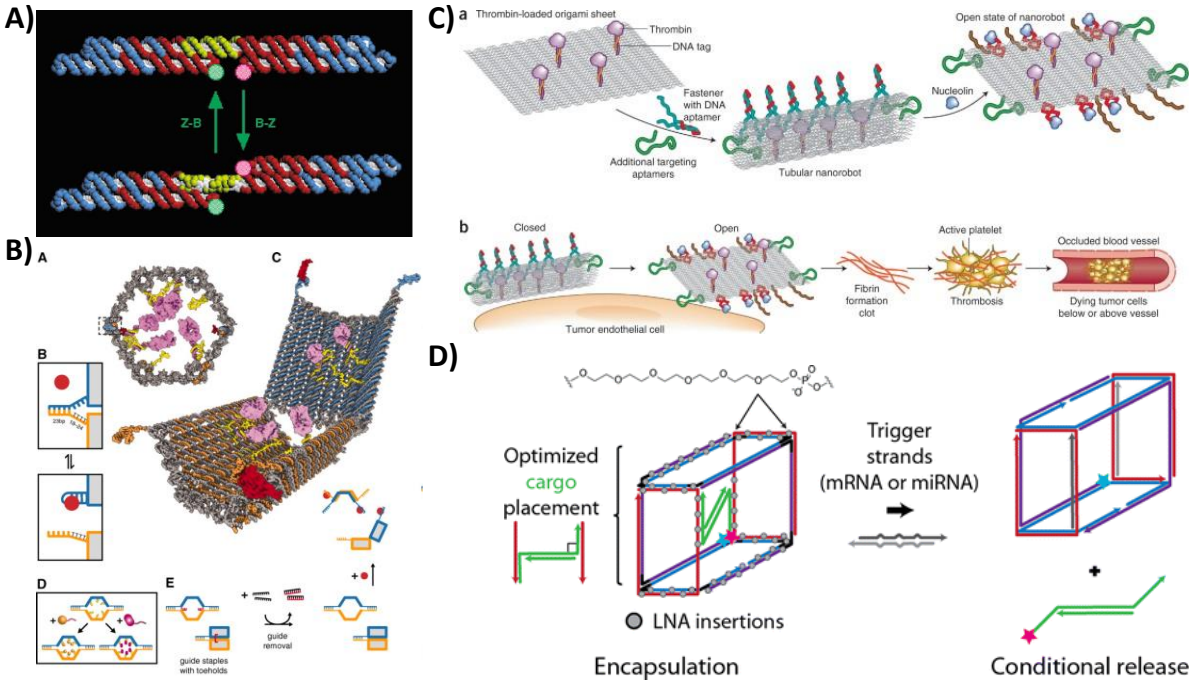

Figure 1. 29 Dynamic DNA nanostructures.

A) B to Z transition monitored with conjugated dyes. Adapted with permission ref [402] (NPG 1999) **B)** DNA logic gated nanorobot for the delivery of molecular payloads. Adapted with permission ref [403] (AAAS 2012) **C)** DNA nanorobot responsive to nucleolin, reveals a thrombin payload, causing clotting in cancer tissue. Adapted with permission ref [404] (NPG 2018) **D)** Triggered release of an siRNA from a DNA nanosuitcase. Adapted with permission ref [407] (ACS 2016)

In one of the first applications of dynamic DNA nanotechnology, reported by Seeman *et al.*, two double-crossover tiles were actuated by small molecules to switch between B- and Z-form DNA.[402] (Figure 1.29.A) A pair of conjugated FRET dyes was used to monitor this conformational change. In 2012 a seminal publication by Church et al demonstrated the construction of a logic gated "nanorobot", which was able to encapsulate and selectively deliver molecular payloads.[403](Figure 1.29.B) Later, Li et al. were inspired by this, and designed a "nanorobot" as a cancer therapeutic.[404](Figure 1.29.C) The nanorobot, was made to be responsive to nucleolin inputs, which are present in high concentration in cancerous tissue. Through the encapsulation of a thrombin-DNA conjugate, the nanorobot remained inactive until opened by the binding of nucleolin to an integrated aptamer switch. This revealed the thrombin enzyme, which resulted in selective blood clotting only at the tumor site. More recently, DNA origami containers that are responsive to pH have been developed by the Linko group, which opened to expose both gold nanoparticles and HRP enzymes.[405]

In the Sleiman group the hydrophobic core of a DNA cube was made to be disrupted in response to biological markers, paving the way for selective drug release applications.[406] Bujold et al. then used a logic gated "DNA nanosuitcase" that through strand displacement using two biomarkers, ejected a modified siRNA strand for selective gene silencing.[407](Figure 1.29.D) This device was later followed up with a simpler version based on SNA's, which ejected the effector strand in a similar manner.[408] These two devices exemplify all three functions DNA can have outside of purely information; structural, therapeutic and recognition.

DNA microspheres were developed by the Willner group which were able to encapsulate cargo and be selectively released in response to ATP using multiple layered aptamer switches.[409] DNA walkers, that were modified with reactive handles were also able to use DNA templated reactions to generate sequence defined small molecule outputs. Urban et al. demonstrated using DNA conjugated gold nanocrystals, they could create dynamic motion and "slide" DNA origami filaments. Moreover, through coupling an enzyme to the end of molecular tweezers, the group of Hao Yan was able to actuate the activity of an enzyme/cofactor pair, using strand displacement.[410]

1.7.5. Catalytic DNA Recognition

While the molecular recognition applications within DNA nanotechnology are incredible, for biological applications such as imaging, bio-detection and therapeutic delivery, the lack of amplification mechanisms can hinder the overall applicability of such systems, as biomarkers are generally present at low concentrations. To improve the sensitivity of these devices, catalytic DNA recognition mechanisms have been developed, and many of these mechanisms are also enhanced through the introduction of DNA modifications and conjugates.[411]

1.7.5.1. Catalytic Strand Displacement

1.7.5.1.1. Hybridization chain Reaction

The hybridization chain reaction (HCR) developed by Dirks and Pierce is perhaps the most well-known catalytic strand displacement mechanism and has seen a huge number of applications ranging from diagnostics to drug delivery.[412-413](Figure 1.30.A) In HCR, potential energy is stored using two metastable hairpins, each DNA hairpin has a partial overhang, that is complementary to the loop on the next hairpin. When an initiator strand is introduced, toehold mediated strand displacement occurs on one of the hairpins, which reveals the loop sequence. The loop sequence is then able to hybridize to the toehold of the second hairpin and vice-versa. The process continually repeats generating a new long double stranded oligonucleotide.[414]

Besides oligonucleotides, through the use of aptamers and other strategies HCR can be made responsive to a multitude of different stimuli including small molecules[415-416], proteins[417-418], and even whole cells[419]. Branched HCR has been introduced to generate exponential amplification from binding the initiator sequence.[420-421] Improvements to HCR have been able to multiplex multiple HCR's simultaneously, giving it better signal gain with less noise[422-423], and design parameters for the hairpins have been investigated.[424] Diffusion of the HCR hairpins to the growing double stranded polymer limits the rate at which HCR can occur. To address this, various groups have templated HCR using DNA origami, and DNA minimal nanostructures, localizing the hairpins and increasing the rate of polymerization. Very recently, an investigation into replacing

the HCR components with PNA was done and shown to be suitable in the detection of a cancer biomarker.[425]

Most applications of HCR have been for improved detection applications, and this is achieved through the conjugation of the HCR hairpins with various dyes[426], enzymes[427], and metals[428-429] to give, fluorescent[430-431], chemiluminescent[432-433], colorimetric[428], or electrochemical[434] outputs.

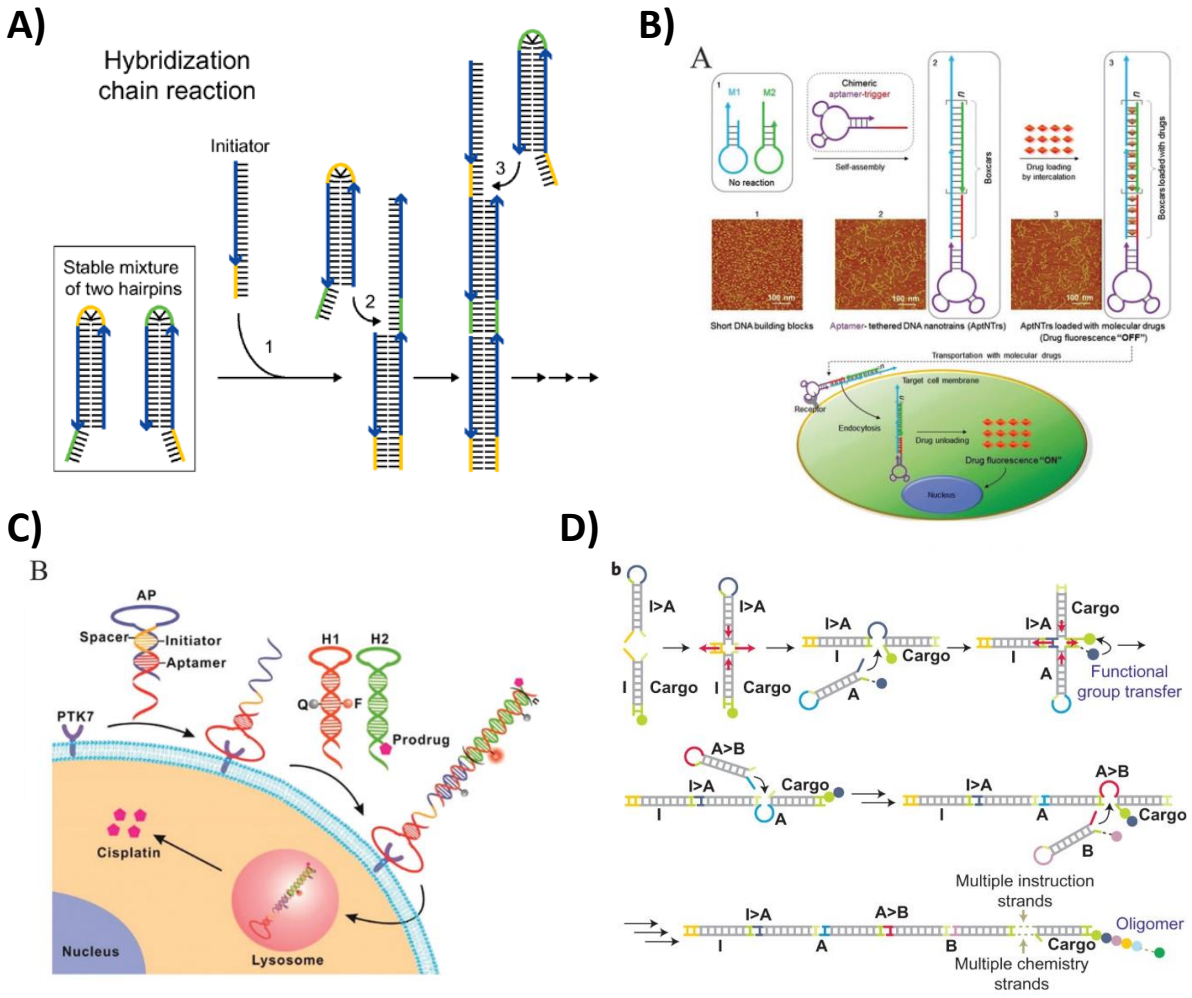

Figure 1. 30 Hybridization Chain Reaction (HCR)

A) Mechanism of HCR. Adapted with permission ref [414] (NPG 2004) **B)** DNA nanotrains for the delivery of doxorubicin (Dox) Adapted with permission ref [436] (United States National Academy of Sciences (USNAS) 2013) **C)** Theragnostic device for delivery of cisplatin with HCR. Adapted with permission ref [438] (ACS 2015) **D)** Automated DNA templated synthesis of oligomers using HCR. Adapted with permission ref [440] (NPG 2016)

In vitro delivery of HCR hairpins into living cells has also been achieved for the detection of mRNA through FRET pairs and electrostatic conjugation to gold nanoparticles.[435]

There are a few drug delivery applications of HCR; DNA "nanotrains" were produced to respond to specific cell surface receptors, and through the intercalation of doxorubicin, demonstrated potent antitumor effects in xenograft mouse models.[436-437](Figure 1.30.B) In another example, a theranostic approach was taken by Wang et al. by conjugating a fluorescent dye and quencher to one of the HCR hairpins, as well as conjugating cisplatin post synthesis.[438](Figure 1.30.C) Upon recognition of the PTK7 receptor, the HCR system polymerized separating the dye pair, giving a fluorescent readout and internalizing the drug. More recently Tan et al. conjugated chlorin e6 to the HCR hairpins, which acts as a photosensitizer, to provide photodynamic therapy, when internalized by HeLa cells.[439] In a combination between DNA templated synthesis and HCR, Meng and co-workers were able to generate an HCR amplification circuit, in which multiple reactions could be done sequentially with only a small amount of input.[440](Figure 1.30.D)

1.7.5.1.2. Catalytic Hairpin & Entropy-Driven Catalytic Assembly

Similar to HCR, Catalytic hairpin assembly (CHA), developed by Turberfield *et al*., uses two metastable hairpins, an initiator strand, as well as an output duplex.[441](Figure 1.31.A) Instead of irreversibly consuming the initiator strand CHA catalytically turns over the initiator strand, to produce amplification. This amplification process has been used primarily for the development of bio-detection devices. Li *et al.* used CHA for the detection of microRNAs in live cancer cells.[442](Figure 1.31.B) They conjugated the hairpins of CHA to a gold nanoparticle using a reduction sensitive bio-degradable linker to deliver the components. Once internalized the hairpin fuel was cleaved from the particle and the initiation of the CHA cycle was induced by a miRNA trigger, eventually resulting in a FRET output. Other nanocarrier platforms have also been used to for miRNA detection using CHA hairpins conjugated on MoS_2 nanosheets[443], graphite[444] and lanthanide-doped upconversion nanoparticles[445].

Finally, Entropy-Driven Catalytic Assembly (EDC) is another amplification circuit which recycles the initiator strand but uses simple duplex DNA as opposed to metastable hairpins[446] (Figure

1.31.C). Like CHA, this amplification mechanism has been primarily used for detection purposes. In a relevant example, He *et. al*. used EDC in combination with DNA nanotechnology to enhance the uptake of the EDC components into living cells for the detection of mRNA[447].(Figure 1.31.D) Overall, the fuel requirement, as well as the low operation speed of these catalytic strand displacement circuits may be the greatest barriers for their use in more applications.

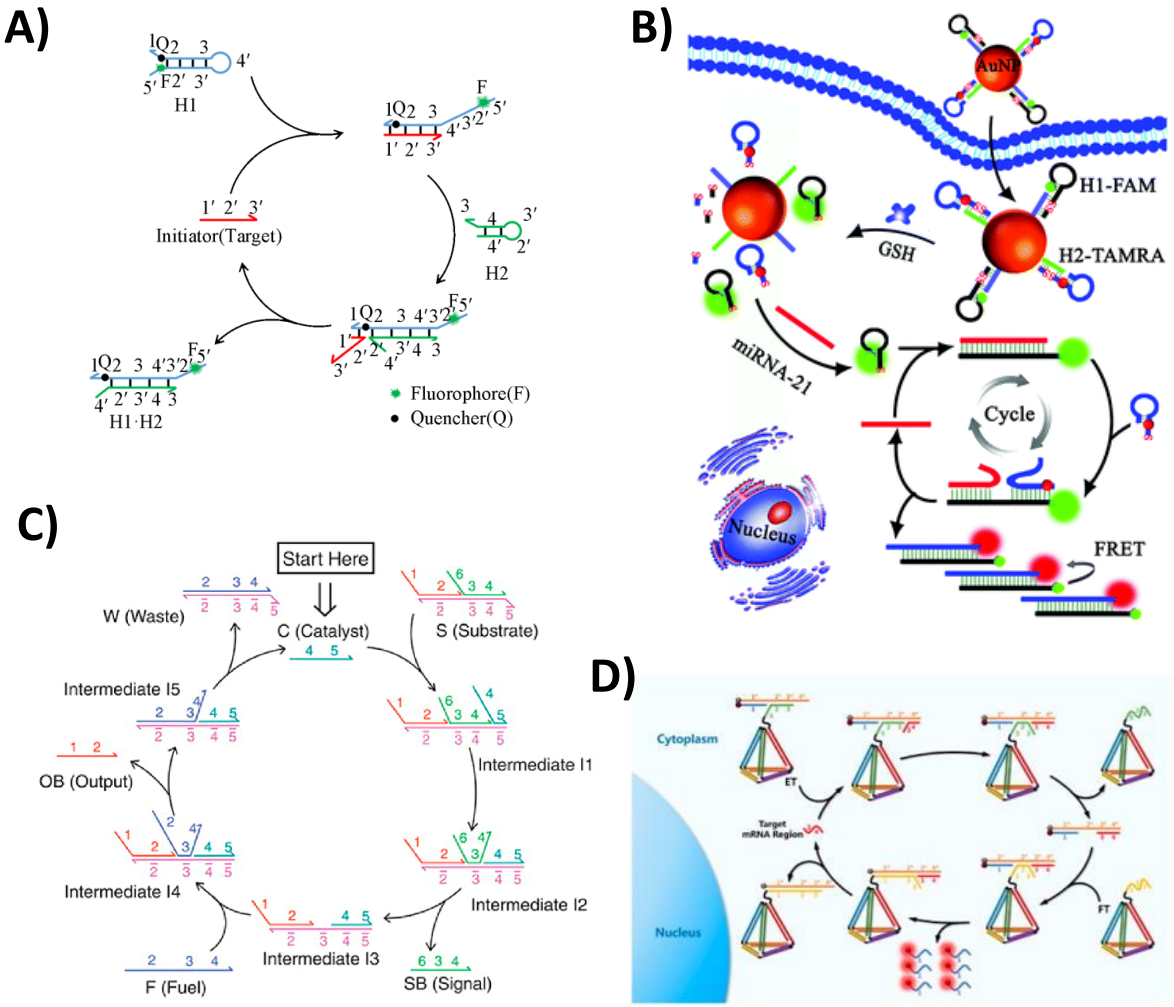

Figure 1. 31 DNA recycling catalytic mechanisms.

A) Catalytic hairpin assembly (CHA) mechanism. Adapted with permission ref [441] (Cell Press 2006) **B)** Delivery of CHA components conjugated to a gold nanoparticle for the detection of mRNA. Adapted with permission ref [442] (RSC 2018) **C)** Entropy Driven Catalytic assembly mechanism. Adapted with permission ref [446] (AAAS 2007) **D)** Enhanced delivery of EDC components using a DNA tetrahedron nanostructure for the detection of mRNA. Adapted with permission ref [447] (ACS 2018)

1.7.5.2. Dynamic Strand Exchange

1.7.5.2.1. DNA/RNAzymes

Instead of using fuel to drive catalytic activity, dynamic strand exchange uses the reversible association of short oligonucleotide strands with low melting temperatures to temporarily hybridize with a given DNA/RNA template. Catalysis using DNA/RNAzymes may be one of the best examples of a dynamic strand exchange process.[448-449](Figure 1.32.A) These catalytically active oligonucleotides hybridize to a strand target and induce cleavage of the strand at a particular site. This now cleaved strand, has a much lower melting temperature than the non-cleaved strand and dissociates from the DNA/RNAzyme, allowing the DNA/RNAzyme to find another full-length product, generating catalytic turnover. DNA/RNAzymes have been made which are only active in the presence of metals, or ions. Additionally, modifications to DNA/RNAzymes have been pursued to improve or generate new, catalytic ability.[450]

Since their discovery many efforts have been made to use them as therapeutic oligonucleotides, and, unique devices based on this turnover have also been developed.[451-452] For example, DNAzymes that are only active at low pH have been used to selectively degrade Dox loaded SNA's for drug delivery.[453](Figure 1.32.B) In another example, fluorophores were encapsulated in SiO_2 mesoporous nanoparticles, capped with DNAzymes, which only released the cargo when the DNAzymes were activated by metals.[454](Figure 1.32.C) Overall, integrating DNAzymes into DNA nanostructures were also shown to improve their gene silencing abilities.[455](Figure 1.32.D)

An interesting design which combined HCR and DNAzymes, improved enzyme-free signal amplification of a DNA sequence.[456] In this design, each of the HCR hairpins contained half the DNAzyme and upon polymerization, the two halves came together to form the complete DNAzyme. The now complete DNAzyme was then able to catalytically metabolize an oligonucleotide containing a fluorophore-quencher pair to generate a spectroscopic output. While many devices have been produced using DNA/RNAzymes, a limitation is that they remain mainly strand cleavage devices and require narrow conditions to operate. To expand this type of turnover further, addressing short oligonucleotides/ oligonucleotide analogues with chemical

modifications has been useful in generating multiple diagnostic probes, imaging devices and drug delivery systems.

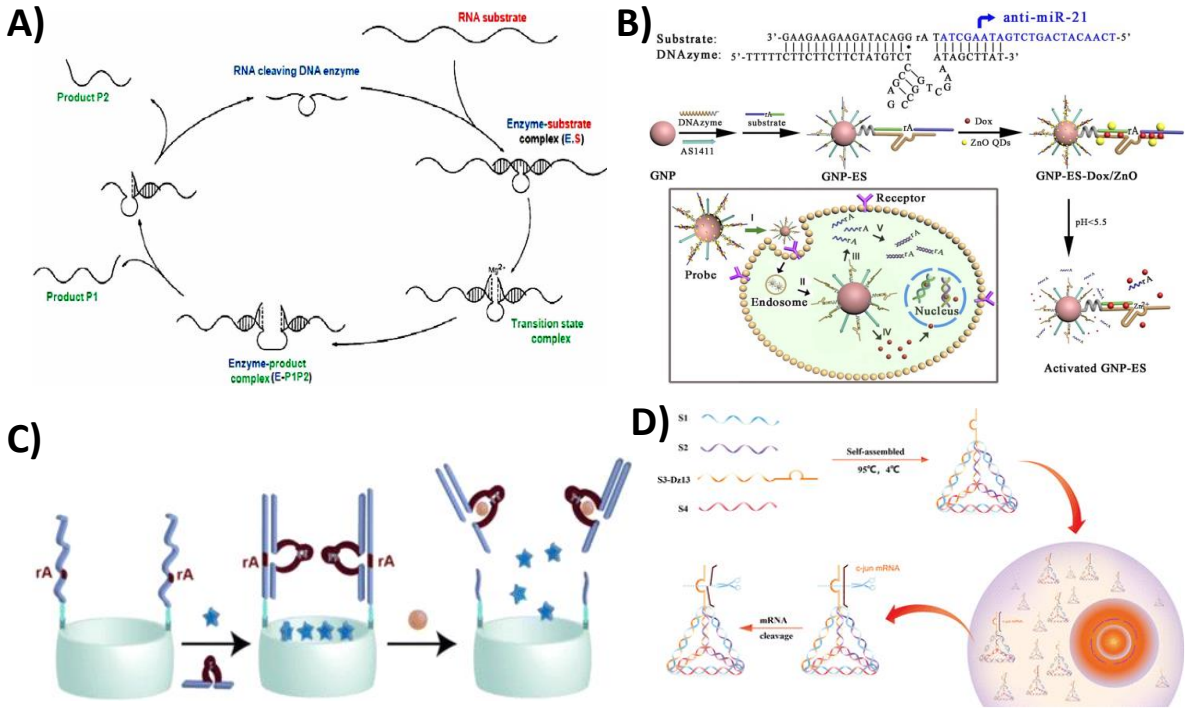

Figure 1. 32 DNA Nanostructures using DNAzymes.

A) DNAzyme mechanism; bind, cleave, dissociate. Adapted with permission ref [448] (Elsevier 2006) **B)** DNAzyme conjugated to a GNP or the selective release of Dox. Adapted with permission ref [453] (AAAS 2016) **C)** Opening of a SiO_2 mesoporous nanoparticle with DNAzymes. Adapted with permission ref [454] (ASC 2013) **D)** Enhanced uptake of a DNAzyme coupled to a DNA tetrahedron nanostructure. Adapted with permission ref [455] (ACS 2019)

1.7.5.2.2. Nucleic Acid-Triggered Catalytic Drug Release

In a similar way that DNA/Ribozymes can generate turnover, Taylor *et. al.* was the first to combine DNA templated reactions with a catalytic turnover mechanism. Named nucleic acid-triggered catalytic drug release, two reactive strands (trigger and substrate) are brought into close proximity with each other on a DNA template, allowed to react and result in the release of a cytotoxic drug.[457-459](Figure 1.33.A) Interestingly, they showed that their catalytic DNA followed Michaelis-Menten kinetics, and was susceptible to added inhibitors. Though, it was originally envisioned for drug release, this work has sparked the development of many bioimaging and

detection probes, as well as prodrugs.[460-461] To reduce the number of components, a follow up study was performed, where the template and catalytic trigger components were merged into one hairpin structure.[462] Non-specific hydrolysis in the original system, could lead to poor performance of the device, therefore other bio-orthogonal chemistries were explored to mitigate this.

The Winssinger group replaced the chemistry with a bio-orthogonal Staudinger reduction, using PNA functionalized with P(III) and self-immolative azide linkers.[463](Figure 1.33.B) Franzini and Kool also used a templated Staudinger reduction with turnover to make what they called Q-STAR probes (quenched-Staudinger trigger α-azidoether release) for the detection of specific RNA targets.[464] Templated tetrazine cycloadditions have also been used by the Devaraj research group in live cells to detect specific oligonucleotide sequences and more recently unmask the fluorescence of near-IR emitting fluorophore caged with vinyl ethers.[465-466] In these reactions however, both substrate and trigger are consumed, meaning that both trigger and substrate components needed to dissociate to generate turnover, as opposed to just the substrate component in the original system.

Winssinger *et al.* addressed this by replacing their P(III) trigger strand with a strand modified with $[Ru(bpy)_3]^{2+}$, which, when photoexcited catalyzed the photoreduction of an azide to aniline, leading to self-immolative degradation and substrate release.[467] 4000 turnovers where able to be achieved, and enabled them to use their system in vitro and in vivo for selective imaging of miR-21 and miR-31 in cancer cells and for the detection of specific mRNA in wild-type zebrafish.[468-469] This group was also able to improve their system further by replacing the azide moiety with a pyridinium-based immolative linker. With this change, the photocatlytic reaction had remarkable turnover ($10\ h^{-1}$) and enzyme-like efficiencies ($10^{-5}\ \underline{M}^{-1}\ s^{-1}$).[470] Coupling of this release method with an HCR circuit was able to achieve even higher levels of amplification.[471] More recently, a notable improvement to their release system has seen the introduction of bioluminescence, to replace the device dependence on external light sources.[472](Figure 1.33.C)

Furthermore, the group of Oliver Seitz, instead of releasing active compounds in bond breaking reactions have used dynamic exchange to catalytically produce compounds from non-toxic or

non-emissive starting materials in bond forming reactions.[473-474] For example, they were able to use acyl transfer reactions of amino acids to short peptides on a DNA template to generate active peptides, which disrupted protein-protein interactions.[475-476](Figure 1.33.D) This represents an improved approach to using native mRNA as the template for these reactions as side degradation reactions can break bonds and result in the non-specific release of active compounds, in the bond breaking approach.

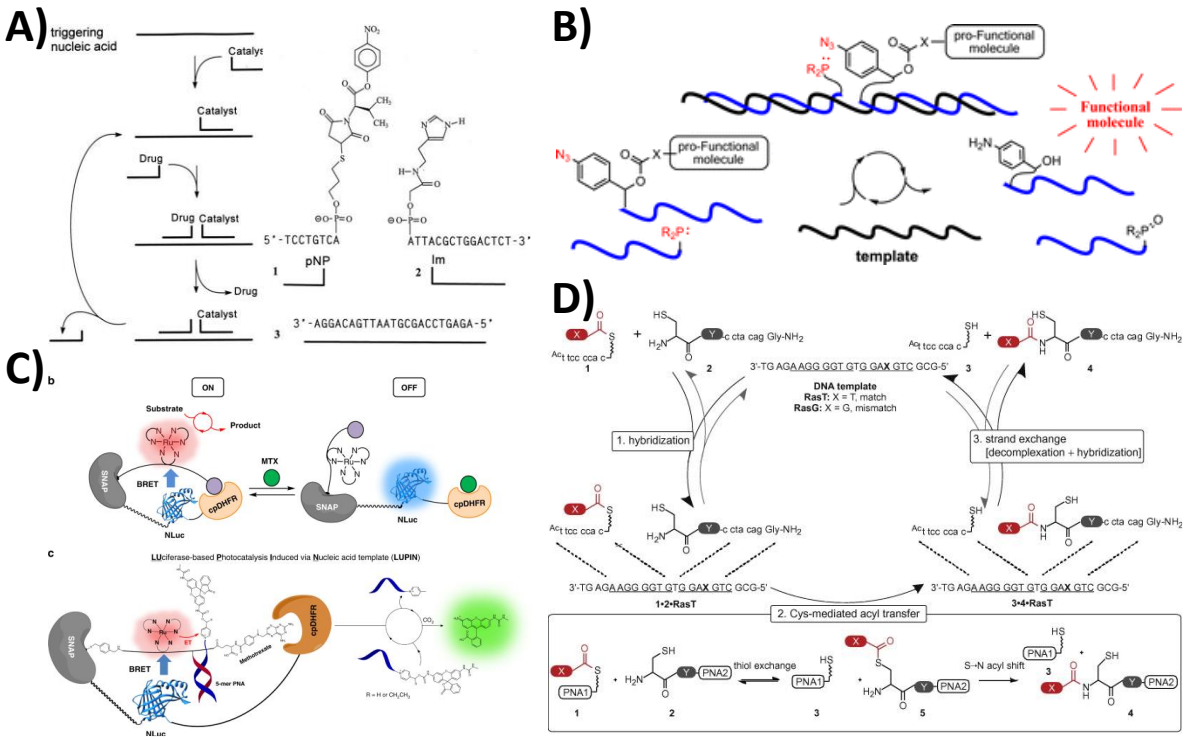

Figure 1. 33 Nucleic acid-triggered catalytic drug release.

A) First report of nucleic acid-triggered catalytic drug release by Taylor *et al*. Adapted with permission ref [457] (USNAS 2013) **B)** Release of functional molecules with turnover using a DNA templated Staudinger reduction. Adapted with permission ref [463] (RSC 2011) **C)** Catalytic release of functional molecules using a $[Ru(bpy)_3]^{2+}$, light catalyst, activated by Bioluminescence Resonance Energy Transfer (BRET). Adapted with permission ref [472] (NPG 2018) **D)** Catalytic production of therapeutic peptides by a DNA templated acyl transfer reaction. Adapted with permission ref [475] (Elsevier 2011)

1.8. Scope of Thesis

Oligonucleotides have gone well beyond their role as the information carrier of the cell and are able to be used as therapeutics, structural building blocks, and recognition components. Though in many cases significant applications can be achieved using strictly unmodified DNA, the use of modified and/or conjugated DNA is at the center of expanding this utility, to generate therapeutics, diagnostic, imaging, and drug delivery devices. In general, this thesis uses oligonucleotide conjugates, to generate new DNA nanodevices for both small molecule and oligonucleotide therapeutic delivery in conditional, stimuli-responsive ways.

Chapter 2 utilizes oligonucleotide-small molecule conjugates, for the development of a DNA nanodevice designed for conditional, amplified release of the small molecule from the conjugate, in response to a biological trigger. The evolution of the design for this device will be described, ultimately leading to the use of nucleic acid templated disulfide exchange for release and the hybridization chain reaction (HCR) for amplification. Further integration of the multiple components of HCR into a DNA nanostructure, localizes both trigger and substrate together, which remain unreacted until the proper biomarker is introduced.

While Chapters 2 was focused on the selective release of small molecules from conjugates and DNA Nanostructures, using biological markers, Chapter 3 focuses on the delivery of antisense-oligonucleotide conjugates for gene silencing. Disulfide modifications are added to an ASO in a sequence defined manner to make reduction sensitive SNA's, for stimuli responsive gene silencing and the mechanism of uptake and action are investigated.

Moreover, building from the findings in chapter 2, Chapter 4 looks at improving and developing ways to bring the drug delivery device into a more biologically relevant setting, by changing the chemistry of release to be more bio-orthogonal and to be responsive to extracellular signals through the development of DNA-Antibody conjugates. Methods to improve the signal gain from the original system are also explored. Additionally, amplification can often be compensated for by increased selectivity. Therefore, new templates for selective release of small molecules are investigated in the form of fully templated amplifiers and logic gates. Similar strand displacement

amplification technology is also applied for the release of antisense oligonucleotides in an amplified manner from SNA's.

Finally, appendices i-viii present some preliminary experiments, small molecule synthesis protocols and collaborations for work beyond what is presented in the body of this thesis.

Overall, this thesis takes DNA out of its biological context and with the help of chemical modification enhances its structural, therapeutic and recognition properties for applications in targeted and conditional small molecule drug and gene therapy.

1.9. References

1. Mendel, G., Experiments in plant hybridization. Read at the February 8th, and March 8th, 1865, meetings of the Brünn Natural History Society. Abhand-lungen: 1866.
2. Darwin, C., *On the origin of species by means of natural selection, or preservation of favoured races in the struggle for life*. London : John Murray, 1859: 1859.
3. Miescher-Rüsch, F., Ueber die chemische Zusammensetzung der Eiterzellen. . **1871**.
4. Avery, O. T.; Macleod, C. M.; McCarty, M., STUDIES ON THE CHEMICAL NATURE OF THE SUBSTANCE INDUCING TRANSFORMATION OF PNEUMOCOCCAL TYPES : INDUCTION OF TRANSFORMATION BY A DESOXYRIBONUCLEIC ACID FRACTION ISOLATED FROM PNEUMOCOCCUS TYPE III. *J. Exp. Med.* **1944,** *79* (2), 137-58.
5. Watson, J. D.; Crick, F. H. C., Molecular Structure of Nucleic Acids: A Structure for Deoxyribose Nucleic Acid. *Nature* **1953,** *171* (4356), 737-738.
6. Franklin, R. E.; Gosling, R. G., Evidence for 2-chain helix in crystalline structure of sodium deoxyribonucleate. *Nature* **1953,** *172* (4369), 156-7.
7. Yakovchuk, P.; Protozanova, E.; Frank-Kamenetskii, M. D., Base-stacking and base-pairing contributions into thermal stability of the DNA double helix. *Nucleic Acids Res.* **2006,** *34* (2), 564-74.
8. Bustamante, C.; Bryant, Z.; Smith, S. B., Ten years of tension: single-molecule DNA mechanics. *Nature* **2003,** *421* (6921), 423-427.
9. Ussery, D. W., DNA Structure: A-, B- and Z-DNA Helix Families. In *eLS*.
10. Stofer, E.; Chipot, C.; Lavery, R., Free Energy Calculations of Watson−Crick Base Pairing in Aqueous Solution. *J. Am. Chem. Soc.* **1999,** *121* (41), 9503-9508.
11. Holliday, R., A mechanism for gene conversion in fungi. *Genetical Research* **1964,** *5* (2), 282-304.
12. Seeman, N. C., Structural DNA nanotechnology: an overview. *Methods Mol Biol* **2005,** *303*, 143-166.
13. Seeman, N. C., Another Important 60th Anniversary. In *Hierarchical Macromolecular Structures: 60 Years after the Staudinger Nobel Prize I*, Percec, V., Ed. Springer International Publishing: Cham, 2013; pp 217-228.
14. Seeman, N. C., Nucleic acid junctions and lattices. *J. Theor. Biol.* **1982,** *99* (2), 237-247.

15. Seeman, N. C.; Kallenbach, N. R., Design of immobile nucleic acid junctions. *Biophys. J.* **1983,** *44* (2), 201-209.
16. Ma, R. I.; Kallenbach, N. R.; Sheardy, R. D.; Petrillo, M. L.; Seeman, N. C., Three-arm nucleic acid junctions are flexible. *Nucleic Acids Res.* **1986,** *14* (24), 9745-9753.
17. Wang, Y. L.; Mueller, J. E.; Kemper, B.; Seeman, N. C., Assembly and characterization of five-arm and six-arm DNA branched junctions. *Biochemistry* **1991,** *30* (23), 5667-74.
18. Wang, X.; Seeman, N. C., Assembly and characterization of 8-arm and 12-arm DNA branched junctions. *J. Am. Chem. Soc.* **2007,** *129* (26), 8169-8176.
19. Chen, J. H.; Seeman, N. C., Synthesis from DNA of a molecule with the connectivity of a cube. *Nature* **1991,** *350* (6319), 631-3.
20. Li, X.; Yang, X.; Qi, J.; Seeman, N. C., Antiparallel DNA Double Crossover Molecules As Components for Nanoconstruction. *J. Am. Chem. Soc.* **1996,** *118* (26), 6131-6140.
21. Fu, T. J.; Seeman, N. C., DNA double-crossover molecules. *Biochemistry* **1993,** *32* (13), 3211-3220.
22. Sa-Ardyen, P.; Vologodskii, A. V.; Seeman, N. C., The flexibility of DNA double crossover molecules. *Biophys. J.* **2003,** *84* (6), 3829-3837.
23. Liu, D.; Park, S. H.; Reif, J. H.; LaBean, T. H., DNA nanotubes self-assembled from triple-crossover tiles as templates for conductive nanowires. *Proc. Natl. Acad. Sci. U. S. A.* **2004,** *101* (3), 717-722.
24. Winfree, E.; Liu, F.; Wenzler, L. A.; Seeman, N. C., Design and self-assembly of two-dimensional DNA crystals. *Nature* **1998,** *394* (6693), 539-44.
25. Lin, C.; Liu, Y.; Rinker, S.; Yan, H., DNA tile based self-assembly: building complex nanoarchitectures. *ChemPhysChem* **2006,** *7* (8), 1641-7.
26. Zhang, F.; Jiang, S.; Li, W.; Hunt, A.; Liu, Y.; Yan, H., Self-Assembly of Complex DNA Tessellations by Using Low-Symmetry Multi-arm DNA Tiles. *Angew. Chem. Int. Ed. Engl.* **2016,** *55* (31), 8860-3.
27. Park, S. H.; Barish, R.; Li, H.; Reif, J. H.; Finkelstein, G.; Yan, H.; Labean, T. H., Three-helix bundle DNA tiles self-assemble into 2D lattice or 1D templates for silver nanowires. *Nano Lett.* **2005,** *5* (4), 693-6.
28. Wei, B.; Mi, Y., A New Triple Crossover Triangle (TXT) Motif for DNA Self-Assembly. *Biomacromolecules* **2005,** *6* (5), 2528-2532.
29. Mathieu, F.; Liao, S.; Kopatsch, J.; Wang, T.; Mao, C.; Seeman, N. C., Six-helix bundles designed from DNA. *Nano Lett.* **2005,** *5* (4), 661-5.
30. Liu, D.; Wang, M.; Deng, Z.; Walulu, R.; Mao, C., Tensegrity: construction of rigid DNA triangles with flexible four-arm DNA junctions. *J. Am. Chem. Soc.* **2004,** *126* (8), 2324-5.
31. Yan, H.; Park, S. H.; Finkelstein, G.; Reif, J. H.; LaBean, T. H., DNA-templated self-assembly of protein arrays and highly conductive nanowires. *Science* **2003,** *301* (5641), 1882-4.
32. He, Y.; Chen, Y.; Liu, H.; Ribbe, A. E.; Mao, C., Self-assembly of hexagonal DNA two-dimensional (2D) arrays. *J. Am. Chem. Soc.* **2005,** *127* (35), 12202-3.
33. He, Y.; Tian, Y.; Chen, Y.; Deng, Z.; Ribbe, A. E.; Mao, C., Sequence symmetry as a tool for designing DNA nanostructures. *Angew. Chem. Int. Ed. Engl.* **2005,** *44* (41), 6694-6.
34. Liu, H.; Chen, Y.; He, Y.; Ribbe, A. E.; Mao, C., Approaching the limit: can one DNA oligonucleotide assemble into large nanostructures? *Angew. Chem. Int. Ed. Engl.* **2006,** *45* (12), 1942-5.
35. Liu, H.; He, Y.; Ribbe, A. E.; Mao, C., Two-dimensional (2D) DNA crystals assembled from two DNA strands. *Biomacromolecules* **2005,** *6* (6), 2943-5.

36. Park, S. H.; Pistol, C.; Ahn, S. J.; Reif, J. H.; Lebeck, A. R.; Dwyer, C.; LaBean, T. H., Finite-Size, Fully Addressable DNA Tile Lattices Formed by Hierarchical Assembly Procedures. *Angew. Chem. Int. Ed.* **2006,** *45* (5), 735-739.
37. Liu, Y.; Ke, Y.; Yan, H., Self-assembly of symmetric finite-size DNA nanoarrays. *J. Am. Chem. Soc.* **2005,** *127* (49), 17140-1.
38. Chworos, A.; Severcan, I.; Koyfman, A. Y.; Weinkam, P.; Oroudjev, E.; Hansma, H. G.; Jaeger, L., Building Programmable Jigsaw Puzzles with RNA. *Science* **2004,** *306* (5704), 2068-2072.
39. Winfree, E., Algorithmic Self-Assembly of DNA: Theoretical Motivations and 2D Assembly Experiments. *J. Biomol. Struct. Dyn.* **2000,** *17* (sup1), 263-270.
40. Mao, C.; LaBean, T. H.; Relf, J. H.; Seeman, N. C., Logical computation using algorithmic self-assembly of DNA triple-crossover molecules. *Nature* **2000,** *407* (6803), 493-6.
41. Rothemund, P. W. K.; Papadakis, N.; Winfree, E., Algorithmic Self-Assembly of DNA Sierpinski Triangles. *PLoS Biol.* **2004,** *2* (12), e424.
42. Barish, R. D.; Rothemund, P. W. K.; Winfree, E., Two Computational Primitives for Algorithmic Self-Assembly: Copying and Counting. *Nano Lett.* **2005,** *5* (12), 2586-2592.
43. Lau, K. L.; Sleiman, H. F., Minimalist Approach to Complexity: Templating the Assembly of DNA Tile Structures with Sequentially Grown Input Strands. *ACS Nano* **2016,** *10* (7), 6542-51.
44. Yan, H.; LaBean, T. H.; Feng, L.; Reif, J. H., Directed nucleation assembly of DNA tile complexes for barcode-patterned lattices. *Proceedings of the National Academy of Sciences* **2003,** *100* (14), 8103-8108.
45. Wilner, O. I.; Orbach, R.; Henning, A.; Teller, C.; Yehezkeli, O.; Mertig, M.; Harries, D.; Willner, I., Self-assembly of DNA nanotubes with controllable diameters. *Nature Communications* **2011,** *2* (1), 540.
46. Wang, W.; Lin, T.; Zhang, S.; Bai, T.; Mi, Y.; Wei, B., Self-assembly of fully addressable DNA nanostructures from double crossover tiles. *Nucleic Acids Res.* **2016,** *44* (16), 7989-7996.
47. Rus, D.; Tolley, M. T., Design, fabrication and control of origami robots. *Nature Reviews Materials* **2018,** *3* (6), 101-112.
48. Liu, Y.; Park, J.; Lang, R. J.; Emami-Neyestanak, A.; Pellegrino, S.; Humayun, M. S.; Tai, Y. In *Parylene origami structure for intraocular implantation*, 2013 Transducers & Eurosensors XXVII: The 17th International Conference on Solid-State Sensors, Actuators and Microsystems (TRANSDUCERS & EUROSENSORS XXVII), 16-20 June 2013; 2013; pp 1549-1552.
49. Rothemund, P. W. K., Folding DNA to create nanoscale shapes and patterns. *Nature* **2006,** *440* (7082), 297-302.
50. Saccà, B.; Niemeyer, C. M., DNA origami: the art of folding DNA. *Angew. Chem. Int. Ed. Engl.* **2012,** *51* (1), 58-66.
51. Douglas, S. M.; Marblestone, A. H.; Teerapittayanon, S.; Vazquez, A.; Church, G. M.; Shih, W. M., Rapid prototyping of 3D DNA-origami shapes with caDNAno. *Nucleic Acids Res.* **2009,** *37* (15), 5001-6.
52. Jabbari, H.; Aminpour, M.; Montemagno, C., Computational Approaches to Nucleic Acid Origami. *ACS Combinatorial Science* **2015,** *17* (10), 535-547.
53. Benson, E.; Mohammed, A.; Gardell, J.; Masich, S.; Czeizler, E.; Orponen, P.; Högberg, B., DNA rendering of polyhedral meshes at the nanoscale. *Nature* **2015,** *523* (7561), 441-4.
54. Castro, C. E.; Kilchherr, F.; Kim, D. N.; Shiao, E. L.; Wauer, T.; Wortmann, P.; Bathe, M.; Dietz, H., A primer to scaffolded DNA origami. *Nat. Methods* **2011,** *8* (3), 221-9.
55. Ke, Y.; Douglas, S. M.; Liu, M.; Sharma, J.; Cheng, A.; Leung, A.; Liu, Y.; Shih, W. M.; Yan, H., Multilayer DNA origami packed on a square lattice. *J. Am. Chem. Soc.* **2009,** *131* (43), 15903-8.

56. Douglas, S. M.; Dietz, H.; Liedl, T.; Högberg, B.; Graf, F.; Shih, W. M., Self-assembly of DNA into nanoscale three-dimensional shapes. *Nature* **2009,** *459* (7245), 414-8.
57. Dietz, H.; Douglas, S. M.; Shih, W. M., Folding DNA into twisted and curved nanoscale shapes. *Science (New York, N.Y.)* **2009,** *325* (5941), 725-730.
58. Liedl, T.; Högberg, B.; Tytell, J.; Ingber, D. E.; Shih, W. M., Self-assembly of three-dimensional prestressed tensegrity structures from DNA. *Nat Nanotechnol* **2010,** *5* (7), 520-4.
59. Han, D.; Pal, S.; Nangreave, J.; Deng, Z.; Liu, Y.; Yan, H., DNA origami with complex curvatures in three-dimensional space. *Science (New York, N.Y.)* **2011,** *332* (6027), 342-6.
60. Han, D.; Pal, S.; Liu, Y.; Yan, H., Folding and cutting DNA into reconfigurable topological nanostructures. *Nature nanotechnology* **2010,** *5* (10), 712-7.
61. Zhang, F.; Jiang, S.; Wu, S.; Li, Y.; Mao, C.; Liu, Y.; Yan, H., Complex wireframe DNA origami nanostructures with multi-arm junction vertices. *Nature nanotechnology* **2015,** *10* (9), 779-84.
62. Ke, Y.; Sharma, J.; Liu, M.; Jahn, K.; Liu, Y.; Yan, H., Scaffolded DNA origami of a DNA tetrahedron molecular container. *Nano Lett* **2009,** *9* (6), 2445-7.
63. Andersen, E. S.; Dong, M.; Nielsen, M. M.; Jahn, K.; Subramani, R.; Mamdouh, W.; Golas, M. M.; Sander, B.; Stark, H.; Oliveira, C. L.; Pedersen, J. S.; Birkedal, V.; Besenbacher, F.; Gothelf, K. V.; Kjems, J., Self-assembly of a nanoscale DNA box with a controllable lid. *Nature* **2009,** *459* (7243), 73-6.
64. Wei, B.; Dai, M.; Yin, P., Complex shapes self-assembled from single-stranded DNA tiles. *Nature* **2012,** *485* (7400), 623-6.
65. Ke, Y.; Ong, L. L.; Shih, W. M.; Yin, P., Three-dimensional structures self-assembled from DNA bricks. *Science (New York, N.Y.)* **2012,** *338* (6111), 1177-83.
66. Ong, L. L.; Hanikel, N.; Yaghi, O. K.; Grun, C.; Strauss, M. T.; Bron, P.; Lai-Kee-Him, J.; Schueder, F.; Wang, B.; Wang, P.; Kishi, J. Y.; Myhrvold, C.; Zhu, A.; Jungmann, R.; Bellot, G.; Ke, Y.; Yin, P., Programmable self-assembly of three-dimensional nanostructures from 10,000 unique components. *Nature* **2017,** *552* (7683), 72-77.
67. Tikhomirov, G.; Petersen, P.; Qian, L., Fractal assembly of micrometre-scale DNA origami arrays with arbitrary patterns. *Nature* **2017,** *552* (7683), 67-71.
68. Dunn, K. E.; Dannenberg, F.; Ouldridge, T. E.; Kwiatkowska, M.; Turberfield, A. J.; Bath, J., Guiding the folding pathway of DNA origami. *Nature* **2015,** *525* (7567), 82-6.
69. Niekamp, S.; Blumer, K.; Nafisi, P. M.; Tsui, K.; Garbutt, J.; Douglas, S. M., Folding complex DNA nanostructures from limited sets of reusable sequences. *Nucleic acids research* **2016,** *44* (11), e102.
70. Praetorius, F.; Kick, B.; Behler, K. L.; Honemann, M. N.; Weuster-Botz, D.; Dietz, H., Biotechnological mass production of DNA origami. *Nature* **2017,** *552* (7683), 84-87.
71. Han, D.; Qi, X.; Myhrvold, C.; Wang, B.; Dai, M.; Jiang, S.; Bates, M.; Liu, Y.; An, B.; Zhang, F.; Yan, H.; Yin, P., Single-stranded DNA and RNA origami. *Science (New York, N.Y.)* **2017,** *358* (6369).
72. Goodman, R. P.; Berry, R. M.; Turberfield, A. J., The single-step synthesis of a DNA tetrahedron. *Chemical Communications* **2004,** (12), 1372-1373.
73. Aldaye, F. A.; Sleiman, H. F., Modular access to structurally switchable 3D discrete DNA assemblies. *Journal of the American Chemical Society* **2007,** *129* (44), 13376-7.
74. Aldaye, F. A.; Lo, P. K.; Karam, P.; McLaughlin, C. K.; Cosa, G.; Sleiman, H. F., Modular construction of DNA nanotubes of tunable geometry and single- or double-stranded character. *Nature nanotechnology* **2009,** *4* (6), 349-52.

75. Hariri, A. A.; Hamblin, G. D.; Gidi, Y.; Sleiman, H. F.; Cosa, G., Stepwise growth of surface-grafted DNA nanotubes visualized at the single-molecule level. *Nature chemistry* **2015,** *7* (4), 295-300.
76. Hotchkiss, R. D., The quantitative separation of purines, pyrimidines, and nucleosides by paper chromatography. *J. Biol. Chem.* **1948,** *175* (1), 315-32.
77. Holliday, R.; Pugh, J. E., DNA Modification Mechanisms and Gene Activity during Development. *Science* **1975,** *187* (4173), 226-232.
78. Compere, S. J.; Palmiter, R. D., DNA methylation controls the inducibility of the mouse metallothionein-I gene lymphoid cells. *Cell* **1981,** *25* (1), 233-40.
79. Michelson, A. M.; Todd, A. R., Nucleotides part XXXII. Synthesis of a dithymidine dinucleotide containing a 3′: 5′-internucleotidic linkage. *Journal of the Chemical Society (Resumed)* **1955,** (0), 2632-2638.
80. Smith, M.; Rammler, D. H.; Goldberg, I. H.; Khorana, H. G., Studies on Polynucleotides. XIV.1 Specific Synthesis of the C3″-C5″ Interribonucleotide Linkage. Syntheses of Uridylyl-(3″→5″)-Uridine and Uridylyl-(3″→5″)-Adenosine2. *Journal of the American Chemical Society* **1962,** *84* (3), 430-440.
81. Schaller, H.; Weimann, G.; Lerch, B.; Khorana, H. G., Studies on Polynucleotides. XXIV.1 The Stepwise Synthesis of Specific Deoxyribopolynucleotides (4).2 Protected Derivatives of Deoxyribonucleosides and New Syntheses of Deoxyribonucleoside-3″ Phosphates3. *Journal of the American Chemical Society* **1963,** *85* (23), 3821-3827.
82. Khorana, H. G., Tener, G. M. Moffatt, J. G. and Pol, E. H., A new approach to the synthesis of polynucleotides. *Chem. and Ind. London* **1956** 1523.
83. Agarwal, K. L.; BÜChi, H.; Caruthers, M. H.; Gupta, N.; Khorana, H. G.; Kleppe, K.; Kumar, A.; Ohtsuka, E.; Rajbhandary, U. L.; Van De Sande, J. H.; Sgaramella, V.; Weber, H.; Yamada , T., Total Synthesis of the Gene for an Alanine Transfer Ribonucleic Acid from Yeast *Nature* **1970,** *227* (5253), 27-34.
84. Letsinger, R. L.; Mahadevan, V., Oligonucleotide Synthesis on a Polymer Support1,2. *Journal of the American Chemical Society* **1965,** *87* (15), 3526-3527.
85. Letsinger, R. L.; Ogilvie, K. K., Nucleotide chemistry. XIII. Synthesis of oligothymidylates via phosphotriester intermediates. *Journal of the American Chemical Society* **1969,** *91* (12), 3350-3355.
86. Letsinger, R. L.; Lunsford, W. B., Synthesis of thymidine oligonucleotides by phosphite triester intermediates. *Journal of the American Chemical Society* **1976,** *98* (12), 3655-3661.
87. Beaucage, S. L.; Caruthers, M. H., Deoxynucleoside phosphoramidites—A new class of key intermediates for deoxypolynucleotide synthesis. *Tetrahedron Letters* **1981,** *22* (20), 1859-1862.
88. Alvarado-Urbina, G.; Sathe, G. M.; Liu, W. C.; Gillen, M. F.; Duck, P. D.; Bender, R.; Ogilvie, K. K., Automated synthesis of gene fragments. *Science (New York, N.Y.)* **1981,** *214* (4518), 270-4.
89. Goodchild, J., Conjugates of oligonucleotides and modified oligonucleotides: a review of their synthesis and properties. *Bioconjugate Chemistry* **1990,** *1* (3), 165-187.
90. Madsen, M.; Gothelf, K. V., Chemistries for DNA Nanotechnology. *Chemical Reviews* **2019,** *119* (10), 6384-6458.
91. Gillet, L. C. J.; Alzeer, J.; Schärer, O. D., Site-specific incorporation of N -(deoxyguanosin-8-yl)-2-acetylaminofluorene (dG-AAF) into oligonucleotides using modified ‘ultra-mild’ DNA synthesis. *Nucleic Acids Res.* **2005,** *33* (6), 1961-1969.

92. Schulhof, J. C.; Molko, D.; Teoule, R., The final deprotection step in oligonucleotide synthesis is reduced to a mild and rapid ammonia treatment by using labile base-protecting groups. *Nucleic Acids Res.* **1987,** *15* (2), 397-416.
93. Sinha, N. D.; Davis, P.; Usman, N.; Pérez, J.; Hodge, R.; Kremsky, J.; Casale, R., Labile exocyclic amine protection of nucleosides in DNA, RNA and oligonucleotide analog synthesis facililating N-deacylation, minimizing depurination and chain degradation. *Biochimie* **1993,** *75* (1), 13-23.
94. Schwechheimer, C.; Doll, L.; Wagenknecht, H.-A., Synthesis of Dye-Modified Oligonucleotides via Copper(I)-Catalyzed Alkyne Azide Cycloaddition Using On- and Off-Bead Approaches. *Current Protocols in Nucleic Acid Chemistry* **2018,** *72* (1), 4.80.1-4.80.13.
95. Kenney, M.; Ray, S.; Boles, T. C., Mutation Typing Using Electrophoresis and Gel-Immobilized AcryditeTM Probes. *BioTechniques* **1998,** *25* (3), 516-521.
96. Allabush, F.; Mendes, P. M.; Tucker, J. H. R., Acrylamide-dT: a polymerisable nucleoside for DNA incorporation. *RSC Advances* **2019,** *9* (54), 31511-31516.
97. UltraMild Base Protection Phosphoramidites and Supports. https://www.glenresearch.com/browse/ultramild-base-protection-phosphoramidites-and-supports.
98. Srivastava, S. C.; Pandey, D.; Srivastava, N. P.; Bajpai, S. P., RNA Synthesis: Phosphoramidites for RNA synthesis in the reverse direction. Highly efficient synthesis and application to convenient introduction of ligands, chromophores and modifications of synthetic RNA at the 3’- end. *Nucleic Acids Symp. Ser.* **2008,** *52* (1), 103-104.
99. Claeboe, C. D.; Gao, R.; Hecht, S. M., 3'-modified oligonucleotides by reverse DNA synthesis. *Nucleic Acids Res.* **2003,** *31* (19), 5685-5691.
100. Koga, M.; Moore, M. F.; Beaucage, S. L., Alternating .alpha.,.beta.-oligothymidylates with alternating (3'.fwdarw.3')- and (5'.fwdarw.5')-internucleotidic phosphodiester linkages as models for antisense oligodeoxyribonucleotides. *The Journal of Organic Chemistry* **1991,** *56* (12), 3757-3759.
101. Koga, M.; Wilk, A.; Moore, M. F.; Scremin, C. L.; Zhou, L.; Beaucage, S. L., Synthesis and Physicochemical Properties of Alternating .alpha.,.beta.-Oligodeoxyribonucleotides with Alternating (3'.fwdarw.3')- and (5'.fwdarw.5')-Internucleotidic Phosphodiester Linkages. *The Journal of Organic Chemistry* **1995,** *60* (6), 1520-1530.
102. Ortigão, J. F.; Rösch, H.; Selter, H.; Fröhlich, A.; Lorenz, A.; Montenarh, M.; Seliger, H., Antisense effect of oligodeoxynucleotides with inverted terminal internucleotidic linkages: a minimal modification protecting against nucleolytic degradation. *Antisense research and development* **1992,** *2* (2), 129-46.
103. Seliger, H.; Fröhlich, A.; Montenarh, M.; Ortigao, J. F. R.; Rösch, H., Oligonucleotide Analogues with Terminal 3’-3’- and 5’-5’-Internucleotidic Linkages as Antisense Inhibitors of Viral Gene Expression. *Nucleosides and Nucleotides* **1991,** *10* (1-3), 469-475.
104. van de Sande, J.; Ramsing, N.; Germann, M.; Elhorst, W.; Kalisch, B.; von Kitzing, E.; Pon, R.; Clegg, R.; Jovin, T., Parallel stranded DNA. *Science (New York, N.Y.)* **1988,** *241* (4865), 551-557.
105. Durand, M.; Peloille, S.; Thuong, N. T.; Maurizot, J. C., Triple-helix formation by an oligonucleotide containing one (dA)12 and two (dT)12 sequences bridged by two hexaethylene glycol chains. *Biochemistry* **1992,** *31* (38), 9197-9204.
106. Hölz, K.; Hoi, J. K.; Schaudy, E.; Somoza, V.; Lietard, J.; Somoza, M. M., High-Efficiency Reverse (5’→3’) Synthesis of Complex DNA Microarrays. *Scientific Reports* **2018,** *8* (1), 15099.

107. Wagner, T.; Pfleiderer, W., Nucleotides, Part LXV , Synthesis of 2'-Deoxyribonucleoside 5'-Phosphoramidites: New Building Blocks for the Inverse (5'-3')-Oligonucleotide Approach. *Helvetica Chimica Acta* **2000,** *83* (8), 2023-2035.
108. Defrancq, E.; Singh, Y.; Spinelli, N., Chemical Strategies for Oligonucleotide-Conjugates Synthesis. *Current Organic Chemistry* **2008,** *12* (4), 263-290.
109. Lönnberg, H., Solid-Phase Synthesis of Oligonucleotide Conjugates Useful for Delivery and Targeting of Potential Nucleic Acid Therapeutics. *Bioconjugate Chemistry* **2009,** *20* (6), 1065-1094.
110. Zatsepin, T. S.; Oretskaya, T. S., Synthesis and Applications of Oligonucleotide□Carbohydrate Conjugates. *Chemistry & Biodiversity* **2004,** *1* (10), 1401-1417.
111. Singh, Y.; Murat, P.; Defrancq, E., Recent developments in oligonucleotide conjugation. *Chemical Society Reviews* **2010,** *39* (6), 2054-2070.
112. Lu, K.; Duan, Q.-P.; Ma, L.; Zhao, D.-X., Chemical Strategies for the Synthesis of Peptide−Oligonucleotide Conjugates. *Bioconjugate Chemistry* **2010,** *21* (2), 187-202.
113. Robles, J.; Pedroso, E.; Grandas, A., Stepwise Solid-Phase Synthesis of the Nucleopeptide Phac-Phe-Val-Ser(p3'ACT)-Gly-OH. *The Journal of Organic Chemistry* **1994,** *59* (9), 2482-2486.
114. Juby, C. D.; Richardson, C. D.; Brousseau, R., Facile preparation of 3'oligonucleotide-peptide conjugates. *Tetrahedron Letters* **1991,** *32* (7), 879-882.
115. Marchán, V.; Rodríguez-Tanty, C.; Estrada, M.; Pedroso, E.; Grandas, A., Alternative Procedures for the Synthesis of Methionine-Containing Peptide−Oligonucleotide Hybrids. *European Journal of Organic Chemistry* **2000,** *2000* (13), 2495-2500.
116. Truffert, J.-C.; Lorthioir, O.; Asseline, U.; Thuong, N. T.; Brack, A., On-line solid phase synthesis of oligonucleotide-peptide hybrids using silica supports. *Tetrahedron Letters* **1994,** *35* (15), 2353-2356.
117. Robles, J.; Pedroso, E.; Grandas, A., Solid phase synthesis of a model nucleopeptide with a phosphodiester bond between the 5' end of a trinucleotide and a serine residue. *Tetrahedron Letters* **1991,** *32* (34), 4389-4392.
118. De Napoli, L.; Messere, A.; Montesarchio, D.; Piccialli, G.; Benedetti, E.; Bucci, E.; Rossi, F., A new solid-phase synthesis of oligonucleotides 3'-conjugated with peptides. *Bioorganic & Medicinal Chemistry* **1999,** *7* (2), 395-400.
119. de Champdoré, M.; De Napoli, L.; Di Fabio, G.; Messere, A.; Montesarchio, D.; Piccialli, G., New nucleoside based solid supports. Synthesis of 5',3'-derivatized thymidine analogues. *Chemical Communications* **2001,** (24), 2598-2599.
120. Bergmann, F.; Bannwarth, W., Solid phase synthesis of directly linked peptide-oligodeoxynucleotide hybrids using standard synthesis protocols. *Tetrahedron Letters* **1995,** *36* (11), 1839-1842.
121. Agrawal, S.; Christodoulou, C.; Gait, M. J., Efficient methods for attaching non-radioactive labels to the 5' ends of synthetic oligodeoxyribonucleotides. *Nucleic acids research* **1986,** *14* (15), 6227-6245.
122. Huisgen, R., 1,3-Dipolar Cycloadditions. Past and Future. *Angewandte Chemie International Edition in English* **1963,** *2* (10), 565-598.
123. Tornøe, C. W.; Christensen, C.; Meldal, M., Peptidotriazoles on Solid Phase: [1,2,3]-Triazoles by Regiospecific Copper(I)-Catalyzed 1,3-Dipolar Cycloadditions of Terminal Alkynes to Azides. *The Journal of Organic Chemistry* **2002,** *67* (9), 3057-3064.

124. Wenska, M.; Alvira, M.; Steunenberg, P.; Stenberg, Å.; Murtola, M.; Strömberg, R., An activated triple bond linker enables 'click' attachment of peptides to oligonucleotides on solid support. *Nucleic acids research* **2011,** *39* (20), 9047-9059.
125. Gierlich, J.; Burley, G. A.; Gramlich, P. M. E.; Hammond, D. M.; Carell, T., Click Chemistry as a Reliable Method for the High-Density Postsynthetic Functionalization of Alkyne-Modified DNA. *Organic Letters* **2006,** *8* (17), 3639-3642.
126. Fantoni, N. Z.; El-Sagheer, A. H.; Brown, T., A Hitchhiker's Guide to Click-Chemistry with Nucleic Acids. *Chemical Reviews* **2021,** *121* (12), 7122-7154.
127. Gramlich, P. M. E.; Warncke, S.; Gierlich, J.; Carell, T., Click–Click–Click: Single to Triple Modification of DNA. *Angew. Chem. Int. Ed.* **2008,** *47* (18), 3442-3444.
128. Jawalekar, A. M.; Malik, S.; Verkade, J. M. M.; Gibson, B.; Barta, N. S.; Hodges, J. C.; Rowan, A.; Van Delft, F. L., Oligonucleotide Tagging for Copper-Free Click Conjugation. *Molecules* **2013,** *18* (7), 7346-7363.
129. van Delft, P.; Meeuwenoord, N. J.; Hoogendoorn, S.; Dinkelaar, J.; Overkleeft, H. S.; van der Marel, G. A.; Filippov, D. V., Synthesis of oligoribonucleic acid conjugates using a cyclooctyne phosphoramidite. *Org Lett* **2010,** *12* (23), 5486-9.
130. Marks, I. S.; Kang, J. S.; Jones, B. T.; Landmark, K. J.; Cleland, A. J.; Taton, T. A., Strain-promoted "click" chemistry for terminal labeling of DNA. *Bioconjugate chemistry* **2011,** *22* (7), 1259-1263.
131. Glen Report 27.17: Technical Brief - DBCO-dT - An Unusual Case of Iodine Sensitivity. https://www.glenresearch.com/reports/gr27-17.
132. Sletten, E. M.; Nakamura, H.; Jewett, J. C.; Bertozzi, C. R., Difluorobenzocyclooctyne: Synthesis, Reactivity, and Stabilization by β-Cyclodextrin. *Journal of the American Chemical Society* **2010,** *132* (33), 11799-11805.
133. Stenzel, M. H., Bioconjugation Using Thiols: Old Chemistry Rediscovered to Connect Polymers with Nature's Building Blocks. *ACS Macro Letters* **2013,** *2* (1), 14-18.
134. Connolly, B. A.; Rider, P., Chemical synthesis of oligonucleotides containing a free sulphydryl group and subsequent attachment of thiol specific probes. *Nucleic acids research* **1985,** *13* (12), 4485-4502.
135. Stasińska, A. R.; Putaj, P.; Chmielewski, M. K., Disulfide bridge as a linker in nucleic acids' bioconjugation. Part I: An overview of synthetic strategies. *Bioorganic Chemistry* **2019,** *92*, 103223.
136. Stasińska, A. R.; Putaj, P.; Chmielewski, M. K., Disulfide bridge as a linker in nucleic acids' bioconjugation. Part II: A summary of practical applications. *Bioorganic Chemistry* **2020,** *95*, 103518.
137. Fontaine, S. D.; Reid, R.; Robinson, L.; Ashley, G. W.; Santi, D. V., Long-Term Stabilization of Maleimide–Thiol Conjugates. *Bioconjugate Chemistry* **2015,** *26* (1), 145-152.
138. Dougan, J. A.; Karlsson, C.; Smith, W. E.; Graham, D., Enhanced oligonucleotide–nanoparticle conjugate stability using thioctic acid modified oligonucleotides. *Nucleic acids research* **2007,** *35* (11), 3668-3675.
139. Sharma, J.; Chhabra, R.; Andersen, C. S.; Gothelf, K. V.; Yan, H.; Liu, Y., Toward Reliable Gold Nanoparticle Patterning On Self-Assembled DNA Nanoscaffold. *Journal of the American Chemical Society* **2008,** *130* (25), 7820-7821.
140. Wada, T.; Mochizuki, A.; Higashiya, S.; Tsuruoka, H.; Kawahara, S.-i.; Ishikawa, M.; Sekine, M., Synthesis and properties of 2-azidodeoxyadenosine and its incorporation into oligodeoxynucleotides. *Tetrahedron Letters* **2001,** *42* (52), 9215-9219.

141. Kiviniemi, A.; Virta, P.; Lönnberg, H., Utilization of Intrachain 4'-C-Azidomethylthymidine for Preparation of Oligodeoxyribonucleotide Conjugates by Click Chemistry in Solution and on a Solid Support. *Bioconjugate Chemistry* **2008,** *19* (8), 1726-1734.
142. Santner, T.; Hartl, M.; Bister, K.; Micura, R., Efficient Access to 3'-Terminal Azide-Modified RNA for Inverse Click-Labeling Patterns. *Bioconjugate Chem.* **2014,** *25* (1), 188-195.
143. Fomich, M. A.; Kvach, M. V.; Navakouski, M. J.; Weise, C.; Baranovsky, A. V.; Korshun, V. A.; Shmanai, V. V., Azide Phosphoramidite in Direct Synthesis of Azide-Modified Oligonucleotides. *Org. Lett.* **2014,** *16* (17), 4590-4593.
144. Lingala, S.; Nordstrøm, L. U.; Mallikaratchy, P. R., Synthesis of stable azide and alkyne functionalized phosphoramidite nucleosides. *Tetrahedron Lett.* **2019,** *60* (3), 211-213.
145. El-Sagheer, A. H.; Brown, T., New strategy for the synthesis of chemically modified RNA constructs exemplified by hairpin and hammerhead ribozymes. *Proceedings of the National Academy of Sciences* **2010,** *107* (35), 15329-15334.
146. Miller, G. P.; Kool, E. T., A Simple Method for Electrophilic Functionalization of DNA. *Organic Letters* **2002,** *4* (21), 3599-3601.
147. Kukwikila, M.; Gale, N.; El-Sagheer, A. H.; Brown, T.; Tavassoli, A., Assembly of a biocompatible triazole-linked gene by one-pot click-DNA ligation. *Nature chemistry* **2017,** *9* (11), 1089-1098.
148. Lartia, R.; Murat, P.; Dumy, P.; Defrancq, E., Versatile Introduction of Azido Moiety into Oligonucleotides through Diazo Transfer Reaction. *Organic Letters* **2011,** *13* (20), 5672-5675.
149. Sánchez, A.; Pedroso, E.; Grandas, A., Maleimide-Dimethylfuran exo Adducts: Effective Maleimide Protection in the Synthesis of Oligonucleotide Conjugates. *Organic Letters* **2011,** *13* (16), 4364-4367.
150. Okamoto, A.; Tainaka, K.; Saito, I., A facile incorporation of the aldehyde function into DNA: 3-formylindole nucleoside as an aldehyde-containing universal nucleoside. *Tetrahedron Letters* **2002,** *43* (26), 4581-4583.
151. Glen Report 23.16: Technical Brief - Labelling Carboxy-Modifiers with Multiple Reporter Molecules. https://www.glenresearch.com/reports/gr23-16.
152. Diala, I.; Osada, A.; Maruoka, S.; Imanisi, T.; Murao, S.; Ato, T.; Ohba, H.; Fujii, M., Synthesis of phosphorothioate oligonucleotide–peptide conjugates by solid phase fragment condensation. *Bioorganic & Medicinal Chemistry Letters* **2007,** *17* (23), 6576-6578.
153. Hill, K. W.; Taunton-Rigby, J.; Carter, J. D.; Kropp, E.; Vagle, K.; Pieken, W.; McGee, D. P. C.; Husar, G. M.; Leuck, M.; Anziano, D. J.; Sebesta, D. P., Diels−Alder Bioconjugation of Diene-Modified Oligonucleotides. *The Journal of Organic Chemistry* **2001,** *66* (16), 5352-5358.
154. Anderson, E.; Picken, D., The synthesis of diene-containing nucleoside phosphoramidites and their use in the labeling of oligonucleotides. *Nucleosides, nucleotides & nucleic acids* **2005,** *24* (5-7), 761-5.
155. Schoch, J.; Staudt, M.; Samanta, A.; Wiessler, M.; Jäschke, A., Site-Specific One-Pot Dual Labeling of DNA by Orthogonal Cycloaddition Chemistry. *Bioconjugate Chemistry* **2012,** *23* (7), 1382-1386.
156. Antsypovich, S. I.; von Kiedrowski, G., A novel versatile phosphoramidite building block for the synthesis of 5'- and 3'-hydrazide modified oligonucleotides. *Nucleosides, nucleotides & nucleic acids* **2005,** *24* (3), 211-26.
157. Raddatz, S.; Mueller-Ibeler, J.; Kluge, J.; Wäss, L.; Burdinski, G.; Havens, J. R.; Onofrey, T. J.; Wang, D.; Schweitzer, M., Hydrazide oligonucleotides: new chemical modification for chip array attachment and conjugation. *Nucleic acids research* **2002,** *30* (21), 4793-4802.

158. Defrancq, E.; Lhomme, J., Use of an aminooxy linker for the functionalization of oligodeoxyribonucleotides. *Bioorganic & Medicinal Chemistry Letters* **2001,** *11* (7), 931-933.
159. Salo, H.; Virta, P.; Hakala, H.; Prakash, T. P.; Kawasaki, A. M.; Manoharan, M.; Lönnberg, H., Aminooxy Functionalized Oligonucleotides: Preparation, On-Support Derivatization, and Postsynthetic Attachment to Polymer Support. *Bioconjugate Chemistry* **1999,** *10* (5), 815-823.
160. Omumi, A.; Beach, D. G.; Baker, M.; Gabryelski, W.; Manderville, R. A., Postsynthetic Guanine Arylation of DNA by Suzuki−Miyaura Cross-Coupling. *Journal of the American Chemical Society* **2011,** *133* (1), 42-50.
161. Lercher, L.; McGouran, J. F.; Kessler, B. M.; Schofield, C. J.; Davis, B. G., DNA Modification under Mild Conditions by Suzuki–Miyaura Cross-Coupling for the Generation of Functional Probes. *Angewandte Chemie International Edition* **2013,** *52* (40), 10553-10558.
162. Kottysch, T.; Ahlborn, C.; Brotzel, F.; Richert, C., Stabilizing or destabilizing oligodeoxynucleotide duplexes containing single 2'-deoxyuridine residues with 5-alkynyl substituents. *Chemistry (Weinheim an der Bergstrasse, Germany)* **2004,** *10* (16), 4017-28.
163. Krause, A.; Hertl, A.; Muttach, F.; Jäschke, A., Phosphine-free Stille-Migita chemistry for the mild and orthogonal modification of DNA and RNA. *Chemistry (Weinheim an der Bergstrasse, Germany)* **2014,** *20* (50), 16613-9.
164. Wang, J.; Shang, J.; Xiang, Y.; Tong, A., General Method for Post-Synthetic Modification of Oligonucleotides Based on Oxidative Amination of 4-Thio-2'-deoxyuridine. *Bioconjugate Chemistry* **2021,** *32* (4), 721-728.
165. Alves, A. M.; Holland, D.; Edge, M. D., A chemical method of labelling oligodeoxyribonucleotides with biotin: A single step procedure using a solid phase methodology. *Tetrahedron Letters* **1989,** *30* (23), 3089-3092.
166. Pieles, U.; Sproat, B. S.; Lamm, G. M., A protected biotin containing deoxycytidine building block for solid phase synthesis of biotinylated oligonucleotides. *Nucleic acids research* **1990,** *18* (15), 4355-60.
167. Fu, A.; Micheel, C. M.; Cha, J.; Chang, H.; Yang, H.; Alivisatos, A. P., Discrete Nanostructures of Quantum Dots/Au with DNA. *Journal of the American Chemical Society* **2004,** *126* (35), 10832-10833.
168. Nakata, E.; Liew, F. F.; Uwatoko, C.; Kiyonaka, S.; Mori, Y.; Katsuda, Y.; Endo, M.; Sugiyama, H.; Morii, T., Zinc-Finger Proteins for Site-Specific Protein Positioning on DNA-Origami Structures. *Angewandte Chemie International Edition* **2012,** *51* (10), 2421-2424.
169. Eskelinen, A.-P.; Kuzyk, A.; Kaltiaisenaho, T. K.; Timmermans, M. Y.; Nasibulin, A. G.; Kauppinen, E. I.; Törmä, P., Assembly of Single-Walled Carbon Nanotubes on DNA-Origami Templates through Streptavidin–Biotin Interaction. *Small* **2011,** *7* (6), 746-750.
170. Fairhead, M.; Krndija, D.; Lowe, E. D.; Howarth, M., Plug-and-play pairing via defined divalent streptavidins. *J Mol Biol* **2014,** *426* (1), 199-214.
171. Los, G. V.; Encell, L. P.; McDougall, M. G.; Hartzell, D. D.; Karassina, N.; Zimprich, C.; Wood, M. G.; Learish, R.; Ohana, R. F.; Urh, M.; Simpson, D.; Mendez, J.; Zimmerman, K.; Otto, P.; Vidugiris, G.; Zhu, J.; Darzins, A.; Klaubert, D. H.; Bulleit, R. F.; Wood, K. V., HaloTag: A Novel Protein Labeling Technology for Cell Imaging and Protein Analysis. *ACS Chemical Biology* **2008,** *3* (6), 373-382.
172. Keppler, A.; Gendreizig, S.; Gronemeyer, T.; Pick, H.; Vogel, H.; Johnsson, K., A general method for the covalent labeling of fusion proteins with small molecules in vivo. *Nature Biotechnology* **2003,** *21* (1), 86-89.

173. Gautier, A.; Juillerat, A.; Heinis, C.; Corrêa, I. R., Jr.; Kindermann, M.; Beaufils, F.; Johnsson, K., An engineered protein tag for multiprotein labeling in living cells. *Chemistry & biology* **2008,** *15* (2), 128-36.
174. Derr, N. D.; Goodman, B. S.; Jungmann, R.; Leschziner, A. E.; Shih, W. M.; Reck-Peterson, S. L., Tug-of-War in Motor Protein Ensembles Revealed with a Programmable DNA Origami Scaffold. *Science (New York, N.Y.)* **2012,** *338* (6107), 662-665.
175. Tan, D. J. Y.; Cheong, V. V.; Lim, K. W.; Phan, A. T., A modular approach to enzymatic ligation of peptides and proteins with oligonucleotides. *Chemical Communications* **2021,** *57* (45), 5507-5510.
176. Meschaninova, M. I.; Novopashina, D. S.; Semikolenova, O. A.; Silnikov, V. N.; Venyaminova, A. G., Novel Convenient Approach to the Solid-Phase Synthesis of Oligonucleotide Conjugates. *Molecules* **2019,** *24* (23), 4266.
177. Meschaninova, M. I.; Entelis, N. S.; Chernolovskaya, E. L.; Venyaminova, A. G., A Versatile Solid-Phase Approach to the Synthesis of Oligonucleotide Conjugates with Biodegradable Hydrazone Linker. *Molecules* **2021,** *26* (8), 2119.
178. Milesi, D.; Kutyavin, I.; Lukhtanov, E. A.; Gorn, V. V.; Reed, M. W., Synthesis of oligonucleotide conjugates in anhydrous dimethyl sulfoxide. In *Methods in Enzymology*, Academic Press: 2000; Vol. 313, pp 164-173.
179. Trinh, T.; Chidchob, P.; Bazzi, H. S.; Sleiman, H. F., DNA micelles as nanoreactors: efficient DNA functionalization with hydrophobic organic molecules. *Chem. Commun.* **2016,** *52* (72), 10914-10917.
180. Dore, M. D.; Fakhoury, J. J.; Lacroix, A.; Sleiman, H. F., Templated synthesis of spherical RNA nanoparticles with gene silencing activity. *Chemical Communications* **2018,** *54* (80), 11296-11299.
181. Shivalingam, A.; Brown, T., Synthesis of chemically modified DNA. *Biochemical Society Transactions* **2016,** *44* (3), 709-715.
182. Klöcker, N.; Weissenboeck, F. P.; Rentmeister, A., Covalent labeling of nucleic acids. *Chemical Society Reviews* **2020,** *49* (23), 8749-8773.
183. Saiki, R.; Scharf, S.; Faloona, F.; Mullis, K.; Horn, G.; Erlich, H.; Arnheim, N., Enzymatic amplification of beta-globin genomic sequences and restriction site analysis for diagnosis of sickle cell anemia. *Science (New York, N.Y.)* **1985,** *230* (4732), 1350-1354.
184. Alemdaroglu, F. E.; Zhuang, W.; Zöphel, L.; Wang, J.; Berger, R.; Rabe, J. P.; Herrmann, A., Generation of Multiblock Copolymers by PCR: Synthesis, Visualization and Nanomechanical Properties. *Nano Letters* **2009,** *9* (10), 3658-3662.
185. Lee, J. K.; Jung, Y. H.; Tok, J. B. H.; Bao, Z., Syntheses of Organic Molecule−DNA Hybrid Structures. *ACS Nano* **2011,** *5* (3), 2067-2074.
186. Trinh, T.; Saliba, D.; Liao, C.; de Rochambeau, D.; Prinzen, A. L.; Li, J.; Sleiman, H. F., "Printing" DNA Strand Patterns on Small Molecules with Control of Valency, Directionality, and Sequence. *Angew. Chem. Int. Ed.* **2019,** *58* (10), 3042-3047.
187. Leconte, A. M.; Hwang, G. T.; Matsuda, S.; Capek, P.; Hari, Y.; Romesberg, F. E., Discovery, Characterization, and Optimization of an Unnatural Base Pair for Expansion of the Genetic Alphabet. *J. Am. Chem. Soc.* **2008,** *130* (7), 2336-2343.
188. Krömer, M.; Bártová, K.; Raindlová, V.; Hocek, M., Synthesis of Dihydroxyalkynyl and Dihydroxyalkyl Nucleotides as Building Blocks or Precursors for Introduction of Diol or Aldehyde Groups to DNA for Bioconjugations. *Chemistry – A European Journal* **2018,** *24* (46), 11890-11894.
189. Paredes, E.; Das, S. R., Click Chemistry for Rapid Labeling and Ligation of RNA. *ChemBioChem* **2011,** *12* (1), 125-131.

190. Guo, C.; Watkins, C. P.; Hili, R., Sequence-Defined Scaffolding of Peptides on Nucleic Acid Polymers. *J. Am. Chem. Soc.* **2015,** *137* (34), 11191-11196.
191. Hili, R.; Niu, J.; Liu, D. R., DNA Ligase-Mediated Translation of DNA Into Densely Functionalized Nucleic Acid Polymers. *J. Am. Chem. Soc.* **2013,** *135* (1), 98-101.
192. Kong, D.; Lei, Y.; Yeung, W.; Hili, R., Enzymatic Synthesis of Sequence-Defined Synthetic Nucleic Acid Polymers with Diverse Functional Groups. *Angew. Chem. Int. Ed.* **2016,** *55* (42), 13164-13168.
193. Lei, Y.; Kong, D.; Hili, R., A High-Fidelity Codon Set for the T4 DNA Ligase-Catalyzed Polymerization of Modified Oligonucleotides. *ACS Combinatorial Science* **2015,** *17* (12), 716-721.
194. Lei, Y.; Washington, J.; Hili, R., Efficiency and fidelity of T3 DNA ligase in ligase-catalysed oligonucleotide polymerisations. *Org. Biomol. Chem.* **2019,** *17* (7), 1962-1965.
195. Pljevaljcic, G.; Pignot, M.; Weinhold, E., Design of a New Fluorescent Cofactor for DNA Methyltransferases and Sequence-Specific Labeling of DNA. *Journal of the American Chemical Society* **2003,** *125* (12), 3486-3492.
196. Peters, W.; Willnow, S.; Duisken, M.; Kleine, H.; Macherey, T.; Duncan, K. E.; Litchfield, D. W.; Lüscher, B.; Weinhold, E., Enzymatic Site-Specific Functionalization of Protein Methyltransferase Substrates with Alkynes for Click Labeling. *Angewandte Chemie International Edition* **2010,** *49* (30), 5170-5173.
197. Dai, N.; Bitinaite, J.; Chin, H.-G.; Pradhan, S.; Corrêa Jr., I. R., Evaluation of UDP-GlcN Derivatives for Selective Labeling of 5-(Hydroxymethyl)cytosine. *ChemBioChem* **2013,** *14* (16), 2144-2152.
198. Li, F.; Dong, J.; Hu, X.; Gong, W.; Li, J.; Shen, J.; Tian, H.; Wang, J., A Covalent Approach for Site-Specific RNA Labeling in Mammalian Cells. *Angewandte Chemie International Edition* **2015,** *54* (15), 4597-4602.
199. Ehret, F.; Zhou, C. Y.; Alexander, S. C.; Zhang, D.; Devaraj, N. K., Site-Specific Covalent Conjugation of Modified mRNA by tRNA Guanine Transglycosylase. *Molecular Pharmaceutics* **2018,** *15* (3), 737-742.
200. Liu, W.; Tagawa, M.; Xin, H. L.; Wang, T.; Emamy, H.; Li, H.; Yager, K. G.; Starr, F. W.; Tkachenko, A. V.; Gang, O., Diamond family of nanoparticle superlattices. *Science (New York, N.Y.)* **2016,** *351* (6273), 582-586.
201. Acuna, G. P.; Möller, F. M.; Holzmeister, P.; Beater, S.; Lalkens, B.; Tinnefeld, P., Fluorescence Enhancement at Docking Sites of DNA-Directed Self-Assembled Nanoantennas. *Science (New York, N.Y.)* **2012,** *338* (6106), 506-510.
202. Kuzyk, A.; Schreiber, R.; Fan, Z.; Pardatscher, G.; Roller, E.-M.; Högele, A.; Simmel, F. C.; Govorov, A. O.; Liedl, T., DNA-based self-assembly of chiral plasmonic nanostructures with tailored optical response. *Nature* **2012,** *483* (7389), 311-314.
203. Kuzyk, A.; Schreiber, R.; Zhang, H.; Govorov, A. O.; Liedl, T.; Liu, N., Reconfigurable 3D plasmonic metamolecules. *Nature Materials* **2014,** *13* (9), 862-866.
204. Edwardson, T. G. W.; Lau, K. L.; Bousmail, D.; Serpell, C. J.; Sleiman, H. F., Transfer of molecular recognition information from DNA nanostructures to gold nanoparticles. *Nature chemistry* **2016,** *8* (2), 162-170.
205. Luo, X.; Chidchob, P.; Rahbani, J. F.; Sleiman, H. F., Encapsulation of Gold Nanoparticles into DNA Minimal Cages for 3D-Anisotropic Functionalization and Assembly. *Small* **2018,** *14* (5), 1702660.
206. Fu, J.; Liu, M.; Liu, Y.; Woodbury, N. W.; Yan, H., Interenzyme Substrate Diffusion for an Enzyme Cascade Organized on Spatially Addressable DNA Nanostructures. *Journal of the American Chemical Society* **2012,** *134* (12), 5516-5519.

207. Stein, I. H.; Steinhauer, C.; Tinnefeld, P., Single-Molecule Four-Color FRET Visualizes Energy-Transfer Paths on DNA Origami. *Journal of the American Chemical Society* **2011,** *133* (12), 4193-4195.
208. Heilemann, M.; Tinnefeld, P.; Sanchez Mosteiro, G.; Garcia Parajo, M.; Van Hulst, N. F.; Sauer, M., Multistep Energy Transfer in Single Molecular Photonic Wires. *Journal of the American Chemical Society* **2004,** *126* (21), 6514-6515.
209. Turek, V. A.; Chikkaraddy, R.; Cormier, S.; Stockham, B.; Ding, T.; Keyser, U. F.; Baumberg, J. J., Thermo-Responsive Actuation of a DNA Origami Flexor. *Advanced Functional Materials* **2018,** *28* (25), 1706410.
210. Mai, Y.; Eisenberg, A., Self-assembly of block copolymers. *Chemical Society Reviews* **2012,** *41* (18), 5969-5985.
211. Li, Z.; Zhang, Y.; Fullhart, P.; Mirkin, C. A., Reversible and Chemically Programmable Micelle Assembly with DNA Block-Copolymer Amphiphiles. *Nano Letters* **2004,** *4* (6), 1055-1058.
212. Gissot, A.; Di Primo, C.; Bestel, I.; Giannone, G.; Chapuis, H.; Barthélémy, P., Sensitive liposomes encoded with oligonucleotide amphiphiles: a biocompatible switch. *Chemical Communications* **2008,** (43), 5550-5552.
213. Jia, F.; Lu, X.; Tan, X.; Zhang, K., Facile synthesis of nucleic acid–polymer amphiphiles and their self-assembly. *Chemical Communications* **2015,** *51* (37), 7843-7846.
214. Liu, K.; Zheng, L.; Liu, Q.; de Vries, J. W.; Gerasimov, J. Y.; Herrmann, A., Nucleic Acid Chemistry in the Organic Phase: From Functionalized Oligonucleotides to DNA Side Chain Polymers. *Journal of the American Chemical Society* **2014,** *136* (40), 14255-14262.
215. Edwardson, T. G. W.; Carneiro, K. M. M.; Serpell, C. J.; Sleiman, H. F., An Efficient and Modular Route to Sequence-Defined Polymers Appended to DNA. *Angewandte Chemie International Edition* **2014,** *53* (18), 4567-4571.
216. Bousmail, D.; Amrein, L.; Fakhoury, J. J.; Fakih, H. H.; Hsu, J. C. C.; Panasci, L.; Sleiman, H. F., Precision spherical nucleic acids for delivery of anticancer drugs. *Chemical science* **2017,** *8* (9), 6218-6229.
217. Serpell, C. J.; Edwardson, T. G. W.; Chidchob, P.; Carneiro, K. M. M.; Sleiman, H. F., Precision Polymers and 3D DNA Nanostructures: Emergent Assemblies from New Parameter Space. *Journal of the American Chemical Society* **2014,** *136* (44), 15767-15774.
218. Chidchob, P.; Edwardson, T. G. W.; Serpell, C. J.; Sleiman, H. F., Synergy of Two Assembly Languages in DNA Nanostructures: Self-Assembly of Sequence-Defined Polymers on DNA Cages. *Journal of the American Chemical Society* **2016,** *138* (13), 4416-4425.
219. Schnitzler, T.; Herrmann, A., DNA Block Copolymers: Functional Materials for Nanoscience and Biomedicine. *Accounts of Chemical Research* **2012,** *45* (9), 1419-1430.
220. Liu, H.; Zhu, Z.; Kang, H.; Wu, Y.; Sefan, K.; Tan, W., DNA-Based Micelles: Synthesis, Micellar Properties and Size-Dependent Cell Permeability. *Chemistry – A European Journal* **2010,** *16* (12), 3791-3797.
221. Ding, K.; Alemdaroglu, F. E.; Börsch, M.; Berger, R.; Herrmann, A., Engineering the structural properties of DNA block copolymer micelles by molecular recognition. *Angewandte Chemie (International ed. in English)* **2007,** *46* (7), 1172-5.
222. Edwardson, T. G.; Carneiro, K. M.; McLaughlin, C. K.; Serpell, C. J.; Sleiman, H. F., Site-specific positioning of dendritic alkyl chains on DNA cages enables their geometry-dependent self-assembly. *Nature chemistry* **2013,** *5* (10), 868-75.

223. Trinh, T.; Liao, C.; Toader, V.; Barłóg, M.; Bazzi, H. S.; Li, J.; Sleiman, H. F., DNA-imprinted polymer nanoparticles with monodispersity and prescribed DNA-strand patterns. *Nature chemistry* **2018,** *10* (2), 184-192.
224. Vyborna, Y.; Vybornyi, M.; Rudnev, A. V.; Häner, R., DNA-Grafted Supramolecular Polymers: Helical Ribbon Structures Formed by Self-Assembly of Pyrene-DNA Chimeric Oligomers. *Angewandte Chemie (International ed. in English)* **2015,** *54* (27), 7934-8.
225. Kamps, A. C.; Cativo, M. H. M.; Chen, X.-J.; Park, S.-J., Self-Assembly of DNA-Coupled Semiconducting Block Copolymers. *Macromolecules* **2014,** *47* (11), 3720-3726.
226. Bousmail, D.; Chidchob, P.; Sleiman, H. F., Cyanine-Mediated DNA Nanofiber Growth with Controlled Dimensionality. *Journal of the American Chemical Society* **2018,** *140* (30), 9518-9530.
227. Patwa, A.; Gissot, A.; Bestel, I.; Barthélémy, P., Hybrid lipid oligonucleotide conjugates: synthesis, self-assemblies and biomedical applications. *Chemical Society Reviews* **2011,** *40* (12), 5844-5854.
228. Pfeiffer, I.; Höök, F., Bivalent Cholesterol-Based Coupling of Oligonucletides to Lipid Membrane Assemblies. *Journal of the American Chemical Society* **2004,** *126* (33), 10224-10225.
229. Sun, L.; Gao, Y.; Xu, Y.; Chao, J.; Liu, H.; Wang, L.; Li, D.; Fan, C., Real-Time Imaging of Single-Molecule Enzyme Cascade Using a DNA Origami Raft. *Journal of the American Chemical Society* **2017,** *139* (48), 17525-17532.
230. Langecker, M.; Arnaut, V.; Martin, T. G.; List, J.; Renner, S.; Mayer, M.; Dietz, H.; Simmel, F. C., Synthetic Lipid Membrane Channels Formed by Designed DNA Nanostructures. *Science (New York, N.Y.)* **2012,** *338* (6109), 932-936.
231. Chidchob, P.; Offenbartl-Stiegert, D.; McCarthy, D.; Luo, X.; Li, J.; Howorka, S.; Sleiman, H. F., Spatial Presentation of Cholesterol Units on a DNA Cube as a Determinant of Membrane Protein-Mimicking Functions. *Journal of the American Chemical Society* **2019,** *141* (2), 1100-1108.
232. Perrault, S. D.; Shih, W. M., Virus-Inspired Membrane Encapsulation of DNA Nanostructures To Achieve In Vivo Stability. *ACS Nano* **2014,** *8* (5), 5132-5140.
233. Yang, Y.; Wang, J.; Shigematsu, H.; Xu, W.; Shih, W. M.; Rothman, J. E.; Lin, C., Self-assembly of size-controlled liposomes on DNA nanotemplates. *Nature chemistry* **2016,** *8* (5), 476-483.
234. Shi, J.; Bergstrom, D. E., Assembly of Novel DNA Cycles with Rigid Tetrahedral Linkers. *Angewandte Chemie International Edition in English* **1997,** *36* (1-2), 111-113.
235. Ahmed, M. U.; Yoshimura, Y.; Mosharraf Hossain, M.; Tamiya, E.; Fujimoto, K., Construction of branched DNA for SNP determination on glass-chip using photochemical ligation. *BioChip Journal* **2011,** *5* (3), 206.
236. Thaner, R. V.; Eryazici, I.; Farha, O. K.; Mirkin, C. A.; Nguyen, S. T., Facile one-step solid-phase synthesis of multitopic organic–DNA hybrids via “click” chemistry. *Chemical Science* **2014,** *5* (3), 1091-1096.
237. Aldaye, F. A.; Sleiman, H. F., Sequential self-assembly of a DNA hexagon as a template for the organization of gold nanoparticles. *Angewandte Chemie (International ed. in English)* **2006,** *45* (14), 2204-9.
238. Aldaye, F. A.; Sleiman, H. F., Dynamic DNA templates for discrete gold nanoparticle assemblies: control of geometry, modularity, write/erase and structural switching. *Journal of the American Chemical Society* **2007,** *129* (14), 4130-1.

239. Aldaye, F. A.; Lo, P. K.; Karam, P.; McLaughlin, C. K.; Cosa, G.; Sleiman, H. F., Modular construction of DNA nanotubes of tunable geometry and single- or double-stranded character. *Nature nanotechnology* **2009,** *4* (6), 349-352.
240. Lo, P. K.; Karam, P.; Aldaye, F. A.; McLaughlin, C. K.; Hamblin, G. D.; Cosa, G.; Sleiman, H. F., Loading and selective release of cargo in DNA nanotubes with longitudinal variation. *Nature chemistry* **2010,** *2* (4), 319-328.
241. Takezawa, Y.; Shionoya, M., Metal-Mediated DNA Base Pairing: Alternatives to Hydrogen-Bonded Watson–Crick Base Pairs. *Accounts of Chemical Research* **2012,** *45* (12), 2066-2076.
242. Yang, H.; Metera, K.; Sleiman, H., DNA modified with metal complexes: Applications in the construction of higher order metal DNA nanostructures. *Coordination Chemistry Reviews* **2010,** *254*, 2403-2415.
243. Mitra, D.; Di Cesare, N.; Sleiman, H. F., Self-Assembly of Cyclic Metal–DNA Nanostructures using Ruthenium Tris(bipyridine)-Branched Oligonucleotides. *Angewandte Chemie International Edition* **2004,** *43* (43), 5804-5808.
244. Choi, J. S.; Kang, C. W.; Jung, K.; Yang, J. W.; Kim, Y.-G.; Han, H., Synthesis of DNA triangles with vertexes of bis(terpyridine)iron(II) complexes. *Journal of the American Chemical Society* **2004,** *126* (28), 8606-8607.
245. Yang, H.; McLaughlin, C. K.; Aldaye, F. A.; Hamblin, G. D.; Rys, A. Z.; Rouiller, I.; Sleiman, H. F., Metal–nucleic acid cages. *Nature chemistry* **2009,** *1* (5), 390-396.
246. Yang, H.; Altvater, F.; de Bruijn, A. D.; McLaughlin, C. K.; Lo, P. K.; Sleiman, H. F., Chiral Metal–DNA Four-Arm Junctions and Metalated Nanotubular Structures. *Angewandte Chemie International Edition* **2011,** *50* (20), 4620-4623.
247. Rousina-Webb, A.; Lachance-Brais, C.; Rizzuto, F. J.; Askari, M. S.; Sleiman, H. F., Transition-Metal-Functionalized DNA Double-Crossover Tiles: Enhanced Stability and Chirality Transfer to Metal Centers. *Angew. Chem. Int. Ed.* **2020,** *59* (10), 4091-4098.
248. Yang, H.; Rys, A. Z.; McLaughlin, C. K.; Sleiman, H. F., Templated ligand environments for the selective incorporation of different metals into DNA. *Angewandte Chemie (International ed. in English)* **2009,** *48* (52), 9919-23.
249. Dauphin-Ducharme, P.; Rosati, F.; Greschner, A.; De Bruijn, A. D.; Salvatore, D.; Toader, V.; Lau, K. L.; Mauzeroll, J.; Sleiman, H., Modulation of Charge Transport Across Double-Stranded DNA by the Site-Specific Incorporation of Copper Bis-Phenanthroline Complexes. *Langmuir* **2015,** *31* (5), 1850-1854.
250. Askari, M. S.; Lachance-Brais, C.; Rizzuto, F. J.; Toader, V.; Sleiman, H., Remote control of charge transport and chiral induction along a DNA-metallohelicate. *Nanoscale* **2019,** *11* (24), 11879-11884.
251. Kulkarni, J. A.; Witzigmann, D.; Thomson, S. B.; Chen, S.; Leavitt, B. R.; Cullis, P. R.; van der Meel, R., The current landscape of nucleic acid therapeutics. *Nature nanotechnology* **2021,** *16* (6), 630-643.
252. Ke, Y.; Castro, C.; Choi, J. H., Structural DNA Nanotechnology: Artificial Nanostructures for Biomedical Research. *Annual Review of Biomedical Engineering* **2018,** *20* (1), 375-401.
253. Hu, Q.; Li, H.; Wang, L.; Gu, H.; Fan, C., DNA Nanotechnology-Enabled Drug Delivery Systems. *Chemical Reviews* **2019,** *119* (10), 6459-6506.
254. Bujold, K. E.; Lacroix, A.; Sleiman, H. F., DNA Nanostructures at the Interface with Biology. *Chem* **2018,** *4* (3), 495-521.
255. Jiang, S.; Ge, Z.; Mou, S.; Yan, H.; Fan, C., Designer DNA nanostructures for therapeutics. *Chem* **2021,** *7* (5), 1156-1179.

256. Stephenson, M. L.; Zamecnik, P. C., Inhibition of Rous sarcoma viral RNA translation by a specific oligodeoxyribonucleotide. *Proc Natl Acad Sci U S A* **1978,** *75* (1), 285-288.
257. Zamecnik, P. C.; Stephenson, M. L., Inhibition of Rous sarcoma virus replication and cell transformation by a specific oligodeoxynucleotide. *Proc Natl Acad Sci U S A* **1978,** *75* (1), 280-284.
258. Dang, C. V.; Reddy, E. P.; Shokat, K. M.; Soucek, L., Drugging the 'undruggable' cancer targets. *Nature reviews. Cancer* **2017,** *17* (8), 502-508.
259. Neklesa, T. K.; Winkler, J. D.; Crews, C. M., Targeted protein degradation by PROTACs. *Pharmacology & therapeutics* **2017,** *174*, 138-144.
260. Yamamoto, T.; Nakatani, M.; Narukawa, K.; Obika, S., Antisense drug discovery and development. *Future medicinal chemistry* **2011,** *3* (3), 339-65.
261. Burnett, J. C.; Rossi, J. J., RNA-based therapeutics: current progress and future prospects. *Chemistry & biology* **2012,** *19* (1), 60-71.
262. Fire, A.; Xu, S.; Montgomery, M. K.; Kostas, S. A.; Driver, S. E.; Mello, C. C., Potent and specific genetic interference by double-stranded RNA in Caenorhabditis elegans. *Nature* **1998,** *391* (6669), 806-11.
263. Mulhbacher, J.; St-Pierre, P.; Lafontaine, D. A., Therapeutic applications of ribozymes and riboswitches. *Current opinion in pharmacology* **2010,** *10* (5), 551-6.
264. Chan, C. W.; Khachigian, L. M., DNAzymes and their therapeutic possibilities. *Internal medicine journal* **2009,** *39* (4), 249-51.
265. Roberts, T. C.; Langer, R.; Wood, M. J. A., Advances in oligonucleotide drug delivery. *Nature Reviews Drug Discovery* **2020,** *19* (10), 673-694.
266. Crooke, S. T., Molecular Mechanisms of Antisense Oligonucleotides. *Nucleic acid therapeutics* **2017,** *27* (2), 70-77.
267. Lieberman, J., Tapping the RNA world for therapeutics. *Nature Structural & Molecular Biology* **2018,** *25* (5), 357-364.
268. Stein, C. A.; Castanotto, D., FDA-Approved Oligonucleotide Therapies in 2017. *Molecular therapy : the journal of the American Society of Gene Therapy* **2017,** *25* (5), 1069-1075.
269. Deleavey, Glen F.; Damha, Masad J., Designing Chemically Modified Oligonucleotides for Targeted Gene Silencing. *Chemistry & biology* **2012,** *19* (8), 937-954.
270. Watts, J. K.; Katolik, A.; Viladoms, J.; Damha, M. J., Studies on the hydrolytic stability of 2'-fluoroarabinonucleic acid (2'F-ANA). *Organic & Biomolecular Chemistry* **2009,** *7* (9), 1904-1910.
271. Crooke, S. T.; Wang, S.; Vickers, T. A.; Shen, W.; Liang, X.-h., Cellular uptake and trafficking of antisense oligonucleotides. *Nature Biotechnology* **2017,** *35* (3), 230-237.
272. Juliano, R. L., Intracellular Trafficking and Endosomal Release of Oligonucleotides: What We Know and What We Don't. *Nucleic acid therapeutics* **2018,** *28* (3), 166-177.
273. Juliano, R. L., The delivery of therapeutic oligonucleotides. *Nucleic acids research* **2016,** *44* (14), 6518-48.
274. Geary, R. S.; Norris, D.; Yu, R.; Bennett, C. F., Pharmacokinetics, biodistribution and cell uptake of antisense oligonucleotides. *Advanced Drug Delivery Reviews* **2015,** *87*, 46-51.
275. Daneman, R.; Prat, A., The blood-brain barrier. *Cold Spring Harb Perspect Biol* **2015,** *7* (1), a020412-a020412.
276. Takakura, K.; Kawamura, A.; Torisu, Y.; Koido, S.; Yahagi, N.; Saruta, M., The Clinical Potential of Oligonucleotide Therapeutics against Pancreatic Cancer. *Int J Mol Sci* **2019,** *20* (13), 3331.

277. Xiong, H.; Veedu, R. N.; Diermeier, S. D., Recent Advances in Oligonucleotide Therapeutics in Oncology. *Int J Mol Sci* **2021,** *22* (7).
278. Shi, Y.; van der Meel, R.; Chen, X.; Lammers, T., The EPR effect and beyond: Strategies to improve tumor targeting and cancer nanomedicine treatment efficacy. *Theranostics* **2020,** *10* (17), 7921-7924.
279. Nakamura, Y.; Mochida, A.; Choyke, P. L.; Kobayashi, H., Nanodrug Delivery: Is the Enhanced Permeability and Retention Effect Sufficient for Curing Cancer? *Bioconjug Chem* **2016,** *27* (10), 2225-2238.
280. The cost of getting personal. *Nature Medicine* **2019,** *25* (12), 1797-1797.
281. Min, H. S.; Kim, H. J.; Naito, M.; Ogura, S.; Toh, K.; Hayashi, K.; Kim, B. S.; Fukushima, S.; Anraku, Y.; Miyata, K.; Kataoka, K., Systemic Brain Delivery of Antisense Oligonucleotides across the Blood–Brain Barrier with a Glucose-Coated Polymeric Nanocarrier. *Angewandte Chemie International Edition* **2020,** *59* (21), 8173-8180.
282. Yu, B.; Zhao, X.; Lee, L. J.; Lee, R. J., Targeted delivery systems for oligonucleotide therapeutics. *AAPS J* **2009,** *11* (1), 195-203.
283. Falzarano, M. S.; Passarelli, C.; Ferlini, A., Nanoparticle delivery of antisense oligonucleotides and their application in the exon skipping strategy for Duchenne muscular dystrophy. *Nucleic acid therapeutics* **2014,** *24* (1), 87-100.
284. Eckstein, F., Phosphorothioates, essential components of therapeutic oligonucleotides. *Nucleic acid therapeutics* **2014,** *24* (6), 374-87.
285. Iyer, R. P.; Egan, W.; Regan, J. B.; Beaucage, S. L., 3H-1,2-Benzodithiole-3-one 1,1-dioxide as an improved sulfurizing reagent in the solid-phase synthesis of oligodeoxyribonucleoside phosphorothioates. *Journal of the American Chemical Society* **1990,** *112* (3), 1253-1254.
286. Stein, C. A.; Subasinghe, C.; Shinozuka, K.; Cohen, J. S., Physicochemical properties of phosphorothioate oligodeoxynucleotides. *Nucleic acids research* **1988,** *16* (8), 3209-3221.
287. Iwamoto, N.; Butler, D. C. D.; Svrzikapa, N.; Mohapatra, S.; Zlatev, I.; Sah, D. W. Y.; Meena; Standley, S. M.; Lu, G.; Apponi, L. H.; Frank-Kamenetsky, M.; Zhang, J. J.; Vargeese, C.; Verdine, G. L., Control of phosphorothioate stereochemistry substantially increases the efficacy of antisense oligonucleotides. *Nature Biotechnology* **2017,** *35* (9), 845-851.
288. Knouse, K. W.; deGruyter, J. N.; Schmidt, M. A.; Zheng, B.; Vantourout, J. C.; Kingston, C.; Mercer, S. E.; Mcdonald, I. M.; Olson, R. E.; Zhu, Y.; Hang, C.; Zhu, J.; Yuan, C.; Wang, Q.; Park, P.; Eastgate, M. D.; Baran, P. S., Unlocking P(V): Reagents for chiral phosphorothioate synthesis. *Science (New York, N.Y.)* **2018,** *361* (6408), 1234-1238.
289. Østergaard, M. E.; De Hoyos, C. L.; Wan, W. B.; Shen, W.; Low, A.; Berdeja, A.; Vasquez, G.; Murray, S.; Migawa, M. T.; Liang, X.-h.; Swayze, E. E.; Crooke, S. T.; Seth, P. P., Understanding the effect of controlling phosphorothioate chirality in the DNA gap on the potency and safety of gapmer antisense oligonucleotides. *Nucleic acids research* **2020,** *48* (4), 1691-1700.
290. Khvorova, A.; Watts, J. K., The chemical evolution of oligonucleotide therapies of clinical utility. *Nature Biotechnology* **2017,** *35* (3), 238-248.
291. Enmark, M.; Rova, M.; Samuelsson, J.; Örnskov, E.; Schweikart, F.; Fornstedt, T., Investigation of factors influencing the separation of diastereomers of phosphorothioated oligonucleotides. *Anal Bioanal Chem* **2019,** *411* (15), 3383-3394.
292. Pinheiro, V. B.; Holliger, P., Towards XNA nanotechnology: new materials from synthetic genetic polymers. *Trends in Biotechnology* **2014,** *32* (6), 321-328.

293. Duffy, K.; Arangundy-Franklin, S.; Holliger, P., Modified nucleic acids: replication, evolution, and next-generation therapeutics. *BMC Biology* **2020,** *18* (1), 112.
294. Obika, S.; Nanbu, D.; Hari, Y.; Andoh, J.-i.; Morio, K.-i.; Doi, T.; Imanishi, T., Stability and structural features of the duplexes containing nucleoside analogues with a fixed N-type conformation, 2′-O,4′-C-methyleneribonucleosides. *Tetrahedron Letters* **1998,** *39* (30), 5401-5404.
295. Koshkin, A. A.; Singh, S. K.; Nielsen, P.; Rajwanshi, V. K.; Kumar, R.; Meldgaard, M.; Olsen, C. E.; Wengel, J., LNA (Locked Nucleic Acids): Synthesis of the adenine, cytosine, guanine, 5-methylcytosine, thymine and uracil bicyclonucleoside monomers, oligomerisation, and unprecedented nucleic acid recognition. *Tetrahedron* **1998,** *54* (14), 3607-3630.
296. Corey, D. R., Chemical modification: the key to clinical application of RNA interference? *The Journal of clinical investigation* **2007,** *117* (12), 3615-22.
297. Watts, J. K.; Sadalapure, K.; Choubdar, N.; Pinto, B. M.; Damha, M. J., Synthesis and Conformational Analysis of 2‘-Fluoro-5-methyl-4‘-thioarabinouridine (4‘S-FMAU). *The Journal of Organic Chemistry* **2006,** *71* (3), 921-925.
298. Damha, M. J.; Wilds, C. J.; Noronha, A.; Brukner, I.; Borkow, G.; Arion, D.; Parniak, M. A., Hybrids of RNA and Arabinonucleic Acids (ANA and 2‘F-ANA) Are Substrates of Ribonuclease H. *Journal of the American Chemical Society* **1998,** *120* (49), 12976-12977.
299. Souleimanian, N.; Deleavey, G. F.; Soifer, H.; Wang, S.; Tiemann, K.; Damha, M. J.; Stein, C. A., Antisense 2'-Deoxy, 2'-Fluroarabino Nucleic Acids (2'F-ANAs) Oligonucleotides: In Vitro Gymnotic Silencers of Gene Expression Whose Potency Is Enhanced by Fatty Acids. *Mol Ther Nucleic Acids* **2012,** *1* (10), e43-e43.
300. Deleavey, G. F.; Watts, J. K.; Alain, T.; Robert, F.; Kalota, A.; Aishwarya, V.; Pelletier, J.; Gewirtz, A. M.; Sonenberg, N.; Damha, M. J., Synergistic effects between analogs of DNA and RNA improve the potency of siRNA-mediated gene silencing. *Nucleic acids research* **2010,** *38* (13), 4547-4557.
301. Nielsen, P. E.; Egholm, M.; Berg, R. H.; Buchardt, O., Sequence-selective recognition of DNA by strand displacement with a thymine-substituted polyamide. *Science (New York, N.Y.)* **1991,** *254* (5037), 1497-500.
302. Egholm, M.; Buchardt, O.; Christensen, L.; Behrens, C.; Freier, S. M.; Driver, D. A.; Berg, R. H.; Kim, S. K.; Norden, B.; Nielsen, P. E., PNA hybridizes to complementary oligonucleotides obeying the Watson–Crick hydrogen-bonding rules. *Nature* **1993,** *365* (6446), 566-568.
303. Huang, Y.-C.; Cao, C.; Tan, X.-L.; Li, X.; Liu, L., Facile solid-phase synthesis of PNA–peptide conjugates using pNZ-protected PNA monomers. *Organic Chemistry Frontiers* **2014,** *1* (9), 1050-1054.
304. de Koning, M. C.; van der Marel, G. A.; Overhand, M., Synthetic developments towards PNA-peptide conjugates. *Current opinion in chemical biology* **2003,** *7* (6), 734-40.
305. Mier, W.; Eritja, R.; Mohammed, A.; Haberkorn, U.; Eisenhut, M., Peptide–PNA Conjugates: Targeted Transport of Antisense Therapeutics into Tumors. *Angew. Chem. Int. Ed.* **2003,** *42* (17), 1968-1971.
306. Benizri, S.; Gissot, A.; Martin, A.; Vialet, B.; Grinstaff, M. W.; Barthélémy, P., Bioconjugated Oligonucleotides: Recent Developments and Therapeutic Applications. *Bioconjugate chemistry* **2019,** *30* (2), 366-383.
307. Winkler, J., Oligonucleotide conjugates for therapeutic applications. *Ther Deliv* **2013,** *4* (7), 791-809.

308. Soutschek, J.; Akinc, A.; Bramlage, B.; Charisse, K.; Constien, R.; Donoghue, M.; Elbashir, S.; Geick, A.; Hadwiger, P.; Harborth, J.; John, M.; Kesavan, V.; Lavine, G.; Pandey, R. K.; Racie, T.; Rajeev, K. G.; Röhl, I.; Toudjarska, I.; Wang, G.; Wuschko, S.; Bumcrot, D.; Koteliansky, V.; Limmer, S.; Manoharan, M.; Vornlocher, H. P., Therapeutic silencing of an endogenous gene by systemic administration of modified siRNAs. *Nature* **2004,** *432* (7014), 173-8.
309. Wolfrum, C.; Shi, S.; Jayaprakash, K. N.; Jayaraman, M.; Wang, G.; Pandey, R. K.; Rajeev, K. G.; Nakayama, T.; Charrise, K.; Ndungo, E. M.; Zimmermann, T.; Koteliansky, V.; Manoharan, M.; Stoffel, M., Mechanisms and optimization of in vivo delivery of lipophilic siRNAs. *Nature Biotechnology* **2007,** *25* (10), 1149-1157.
310. Nishina, K.; Unno, T.; Uno, Y.; Kubodera, T.; Kanouchi, T.; Mizusawa, H.; Yokota, T., Efficient in vivo delivery of siRNA to the liver by conjugation of alpha-tocopherol. *Molecular therapy : the journal of the American Society of Gene Therapy* **2008,** *16* (4), 734-40.
311. Osborn, M. F.; Coles, A. H.; Biscans, A.; Haraszti, R. A.; Roux, L.; Davis, S.; Ly, S.; Echeverria, D.; Hassler, M. R.; Godinho, B. M. D. C.; Nikan, M.; Khvorova, A., Hydrophobicity drives the systemic distribution of lipid-conjugated siRNAs via lipid transport pathways. *Nucleic Acids Res.* **2018,** *47* (3), 1070-1081.
312. Lacroix, A.; Edwardson, T. G. W.; Hancock, M. A.; Dore, M. D.; Sleiman, H. F., Development of DNA Nanostructures for High-Affinity Binding to Human Serum Albumin. *Journal of the American Chemical Society* **2017,** *139* (21), 7355-7362.
313. Lacroix, A.; Fakih, H. H.; Sleiman, H. F., Detailed cellular assessment of albumin-bound oligonucleotides: Increased stability and lower non-specific cell uptake. *Journal of Controlled Release* **2020,** *324*, 34-46.
314. Xie, J.; Bi, Y.; Zhang, H.; Dong, S.; Teng, L.; Lee, R. J.; Yang, Z., Cell-Penetrating Peptides in Diagnosis and Treatment of Human Diseases: From Preclinical Research to Clinical Application. *Frontiers in Pharmacology* **2020,** *11* (697).
315. Lindberg, S.; Copolovici, D. M.; Langel, U., Therapeutic delivery opportunities, obstacles and applications for cell-penetrating peptides. *Ther Deliv* **2011,** *2* (1), 71-82.
316. Gump, J. M.; June, R. K.; Dowdy, S. F., Revised role of glycosaminoglycans in TAT protein transduction domain-mediated cellular transduction. *The Journal of biological chemistry* **2010,** *285* (2), 1500-7.
317. Voirin, E.; Behr, J.-P.; Kotera, M., Versatile synthesis of oligodeoxyribonucleotide–oligospermine conjugates. *Nat. Protoc.* **2007,** *2* (6), 1360-1367.
318. Nothisen, M.; Bagilet, J.; Behr, J.-P.; Remy, J.-S.; Kotera, M., Structure Tuning of Cationic Oligospermine–siRNA Conjugates for Carrier-Free Gene Silencing. *Mol. Pharm.* **2016,** *13* (8), 2718-2728.
319. Nothisen, M.; Kotera, M.; Voirin, E.; Remy, J.-S.; Behr, J.-P., Cationic siRNAs Provide Carrier-Free Gene Silencing in Animal Cells. *J. Am. Chem. Soc.* **2009,** *131* (49), 17730-17731.
320. Nothisen, M.; Perche-Létuvée, P.; Behr, J.-P.; Remy, J.-S.; Kotera, M., Cationic Oligospermine-Oligonucleotide Conjugates Provide Carrier-free Splice Switching in Monolayer Cells and Spheroids. *Molecular Therapy - Nucleic Acids* **2018,** *13*, 483-492.
321. Ng, E. W. M.; Shima, D. T.; Calias, P.; Cunningham, E. T.; Guyer, D. R.; Adamis, A. P., Pegaptanib, a targeted anti-VEGF aptamer for ocular vascular disease. *Nat. Rev. Drug Discovery* **2006,** *5* (2), 123-132.
322. Rosina, C.; Bottoni, F.; Staurenghi, G., Clinical experience with pegaptanib sodium. *Clin Ophthalmol* **2008,** *2* (3), 485-488.

323. Shu, Z.; Tanaka, I.; Ota, A.; Fushihara, D.; Abe, N.; Kawaguchi, S.; Nakamoto, K.; Tomoike, F.; Tada, S.; Ito, Y.; Kimura, Y.; Abe, H., Disulfide-Unit Conjugation Enables Ultrafast Cytosolic Internalization of Antisense DNA and siRNA. *Angew. Chem. Int. Ed.* **2019,** *58* (20), 6611-6615.
324. Shu, Z.; Ota, A.; Takayama, Y.; Katsurada, Y.; Kusamori, K.; Abe, N.; Nakamoto, K.; Tomoike, F.; Tada, S.; Ito, Y.; Nishikawa, M.; Kimura, Y.; Abe, H., Intracellular Delivery of Antisense DNA and siRNA with Amino Groups Masked with Disulfide Units. *Chemical and Pharmaceutical Bulletin* **2020,** *68* (2), 129-132.
325. Low, P. S.; Henne, W. A.; Doorneweerd, D. D., Discovery and development of folic-acid-based receptor targeting for imaging and therapy of cancer and inflammatory diseases. *Acc. Chem. Res.* **2008,** *41* (1), 120-9.
326. Dohmen, C.; Fröhlich, T.; Lächelt, U.; Röhl, I.; Vornlocher, H.-P.; Hadwiger, P.; Wagner, E., Defined Folate-PEG-siRNA Conjugates for Receptor-specific Gene Silencing. *Mol Ther Nucleic Acids* **2012,** *1* (1), e7-e7.
327. Orellana, E. A.; Tenneti, S.; Rangasamy, L.; Lyle, L. T.; Low, P. S.; Kasinski, A. L., FolamiRs: Ligand-targeted, vehicle-free delivery of microRNAs for the treatment of cancer. *Science Translational Medicine* **2017,** *9* (401), eaam9327.
328. Nair, J. K.; Willoughby, J. L. S.; Chan, A.; Charisse, K.; Alam, M. R.; Wang, Q.; Hoekstra, M.; Kandasamy, P.; Kel'in, A. V.; Milstein, S.; Taneja, N.; O'Shea, J.; Shaikh, S.; Zhang, L.; van der Sluis, R. J.; Jung, M. E.; Akinc, A.; Hutabarat, R.; Kuchimanchi, S.; Fitzgerald, K.; Zimmermann, T.; van Berkel, T. J. C.; Maier, M. A.; Rajeev, K. G.; Manoharan, M., Multivalent N-Acetylgalactosamine-Conjugated siRNA Localizes in Hepatocytes and Elicits Robust RNAi-Mediated Gene Silencing. *J. Am. Chem. Soc.* **2014,** *136* (49), 16958-16961.
329. Prakash, T. P.; Brad Wan, W.; Low, A.; Yu, J.; Chappell, A. E.; Gaus, H.; Kinberger, G. A.; Østergaard, M. E.; Migawa, M. T.; Swayze, E. E.; Seth, P. P., Solid-phase synthesis of 5'-triantennary N-acetylgalactosamine conjugated antisense oligonucleotides using phosphoramidite chemistry. *Bioorg. Med. Chem. Lett.* **2015,** *25* (19), 4127-4130.
330. Matsuda, S.; Keiser, K.; Nair, J. K.; Charisse, K.; Manoharan, R. M.; Kretschmer, P.; Peng, C. G.; V. Kel'in, A.; Kandasamy, P.; Willoughby, J. L. S.; Liebow, A.; Querbes, W.; Yucius, K.; Nguyen, T.; Milstein, S.; Maier, M. A.; Rajeev, K. G.; Manoharan, M., siRNA Conjugates Carrying Sequentially Assembled Trivalent N-Acetylgalactosamine Linked Through Nucleosides Elicit Robust Gene Silencing In Vivo in Hepatocytes. *ACS Chem. Biol.* **2015,** *10* (5), 1181-1187.
331. Cuellar, T. L.; Barnes, D.; Nelson, C.; Tanguay, J.; Yu, S.-F.; Wen, X.; Scales, S. J.; Gesch, J.; Davis, D.; van Brabant Smith, A.; Leake, D.; Vandlen, R.; Siebel, C. W., Systematic evaluation of antibody-mediated siRNA delivery using an industrial platform of THIOMAB–siRNA conjugates. *Nucleic Acids Res.* **2014,** *43* (2), 1189-1203.
332. Dovgan, I.; Koniev, O.; Kolodych, S.; Wagner, A., Antibody–Oligonucleotide Conjugates as Therapeutic, Imaging, and Detection Agents. *Bioconjugate Chem.* **2019,** *30* (10), 2483-2501.
333. Dugal-Tessier, J.; Thirumalairajan, S.; Jain, N., Antibody-Oligonucleotide Conjugates: A Twist to Antibody-Drug Conjugates. *J Clin Med* **2021,** *10* (4), 838.
334. Tan, M.; Vernes, J.-M.; Chan, J.; Cuellar, T. L.; Asundi, A.; Nelson, C.; Yip, V.; Shen, B.; Vandlen, R.; Siebel, C.; Meng, Y. G., Real-time quantification of antibody–short interfering RNA conjugate in serum by antigen capture reverse transcription–polymerase chain reaction. *Anal. Biochem.* **2012,** *430* (2), 171-178.

335. Gordon, M. R.; Canakci, M.; Li, L.; Zhuang, J.; Osborne, B.; Thayumanavan, S., Field Guide to Challenges and Opportunities in Antibody-Drug Conjugates for Chemists. *Bioconjugate Chem.* **2015,** *26* (11), 2198-2215.
336. Goldmacher, V. S.; Amphlett, G.; Wang, L.; Lazar, A. C., Statistics of the Distribution of the Abundance of Molecules with Various Drug Loads in Maytansinoid Antibody–Drug Conjugates. *Mol. Pharm.* **2015,** *12* (6), 1738-1744.
337. Nielsen, T. B.; Thomsen, R. P.; Mortensen, M. R.; Kjems, J.; Nielsen, P. F.; Nielsen, T. E.; Kodal, A. L. B.; Cló, E.; Gothelf, K. V., Peptide-Directed DNA-Templated Protein Labelling for The Assembly of a Pseudo-IgM. *Angew. Chem. Int. Ed.* **2019,** *58* (27), 9068-9072.
338. Skovsgaard, M. B.; Mortensen, M. R.; Palmfeldt, J.; Gothelf, K. V., Aptamer-Directed Conjugation of DNA to Therapeutic Antibodies. *Bioconjugate Chem.* **2019,** *30* (8), 2127-2135.
339. Ye, J.; Liu, E.; Gong, J.; Wang, J.; Huang, Y.; He, H.; Yang, V. C., High-Yield Synthesis of Monomeric LMWP(CPP)-siRNA Covalent Conjugate for Effective Cytosolic Delivery of siRNA. *Theranostics* **2017,** *7* (9), 2495-2508.
340. Yang, J.; Chen, C.; Tang, X., Cholesterol-Modified Caged siRNAs for Photoregulating Exogenous and Endogenous Gene Expression. *Bioconjugate Chem.* **2018,** *29* (4), 1010-1015.
341. Skakuj, K.; Wang, S.; Qin, L.; Lee, A.; Zhang, B.; Mirkin, C. A., Conjugation Chemistry-Dependent T-Cell Activation with Spherical Nucleic Acids. *J. Am. Chem. Soc.* **2018,** *140* (4), 1227-1230.
342. Cutler, J. I.; Auyeung, E.; Mirkin, C. A., Spherical nucleic acids. *J. Am. Chem. Soc.* **2012,** *134* (3), 1376-91.
343. Zhang, K.; Hao, L.; Hurst, S. J.; Mirkin, C. A., Antibody-Linked Spherical Nucleic Acids for Cellular Targeting. *J. Am. Chem. Soc.* **2012,** *134* (40), 16488-16491.
344. Fakhoury, J. J.; Edwardson, T. G.; Conway, J. W.; Trinh, T.; Khan, F.; Barłóg, M.; Bazzi, H. S.; Sleiman, H. F., Antisense precision polymer micelles require less poly(ethylenimine) for efficient gene knockdown. *Nanoscale* **2015,** *7* (48), 20625-20634.
345. Fakih, H. H.; Katolik, A.; Malek-Adamian, E.; Fakhoury, J. J.; Kaviani, S.; Damha, M. J.; Sleiman, H. F., Design and enhanced gene silencing activity of spherical 2'-fluoroarabinose nucleic acids (FANA-SNAs). *Chemical Science* **2021,** *12* (8), 2993-3003.
346. Fakhoury, J. J.; McLaughlin, C. K.; Edwardson, T. W.; Conway, J. W.; Sleiman, H. F., Development and Characterization of Gene Silencing DNA Cages. *Biomacromolecules* **2014,** *15* (1), 276-282.
347. Ren, K.; Liu, Y.; Wu, J.; Zhang, Y.; Zhu, J.; Yang, M.; Ju, H., A DNA dual lock-and-key strategy for cell-subtype-specific siRNA delivery. *Nature Communications* **2016,** *7* (1), 13580.
348. Kanasty, R.; Dorkin, J. R.; Vegas, A.; Anderson, D., Delivery materials for siRNA therapeutics. *Nat. Mater.* **2013,** *12* (11), 967-977.
349. Lee, H.; Lytton-Jean, A. K. R.; Chen, Y.; Love, K. T.; Park, A. I.; Karagiannis, E. D.; Sehgal, A.; Querbes, W.; Zurenko, C. S.; Jayaraman, M.; Peng, C. G.; Charisse, K.; Borodovsky, A.; Manoharan, M.; Donahoe, J. S.; Truelove, J.; Nahrendorf, M.; Langer, R.; Anderson, D. G., Molecularly self-assembled nucleic acid nanoparticles for targeted in vivo siRNA delivery. *Nat. Nanotechnol.* **2012,** *7* (6), 389-393.
350. Rahman, M. A.; Wang, P.; Zhao, Z.; Wang, D.; Nannapaneni, S.; Zhang, C.; Chen, Z.; Griffith, C. C.; Hurwitz, S. J.; Chen, Z. G.; Ke, Y.; Shin, D. M., Systemic Delivery of Bc12-Targeting siRNA by DNA Nanoparticles Suppresses Cancer Cell Growth. *Angew. Chem. Int. Ed. Engl.* **2017,** *56* (50), 16023-16027.

351. Lin, Q.-Y.; Mason, J. A.; Li, Z.; Zhou, W.; O'Brien, M. N.; Brown, K. A.; Jones, M. R.; Butun, S.; Lee, B.; Dravid, V. P.; Aydin, K.; Mirkin, C. A., Building superlattices from individual nanoparticles via template-confined DNA-mediated assembly. **2018,** *359* (6376), 669-672.
352. Ponnuswamy, N.; Bastings, M. M. C.; Nathwani, B.; Ryu, J. H.; Chou, L. Y. T.; Vinther, M.; Li, W. A.; Anastassacos, F. M.; Mooney, D. J.; Shih, W. M., Oligolysine-based coating protects DNA nanostructures from low-salt denaturation and nuclease degradation. *Nature Communications* **2017,** *8* (1), 15654.
353. Pedersen, R. O.; Kong, J.; Achim, C.; LaBean, T. H., Comparative Incorporation of PNA into DNA Nanostructures. **2015,** *20* (9), 17645-17658.
354. Flory, J. D.; Shinde, S.; Lin, S.; Liu, Y.; Yan, H.; Ghirlanda, G.; Fromme, P., PNA-Peptide Assembly in a 3D DNA Nanocage at Room Temperature. *J. Am. Chem. Soc.* **2013,** *135* (18), 6985-6993.
355. Tuerk, C.; Gold, L., Systematic evolution of ligands by exponential enrichment: RNA ligands to bacteriophage T4 DNA polymerase. **1990,** *249* (4968), 505-510.
356. Ellington, A. D.; Szostak, J. W., In vitro selection of RNA molecules that bind specific ligands. *Nature* **1990,** *346* (6287), 818-822.
357. Sefah, K.; Shangguan, D.; Xiong, X.; O'Donoghue, M. B.; Tan, W., Development of DNA aptamers using Cell-SELEX. *Nat. Protoc.* **2010,** *5* (6), 1169-85.
358. Thiel, W. H.; Bair, T.; Peek, A. S.; Liu, X.; Dassie, J.; Stockdale, K. R.; Behlke, M. A.; Miller, F. J., Jr.; Giangrande, P. H., Rapid Identification of Cell-Specific, Internalizing RNA Aptamers with Bioinformatics Analyses of a Cell-Based Aptamer Selection. *PLoS One* **2012,** *7* (9), e43836.
359. Berkhout, B.; Klaver, B., In vivo selection of randomly mutated retroviral genomes. *Nucleic Acids Res.* **1993,** *21* (22), 5020-5024.
360. Kraemer, S.; Vaught, J. D.; Bock, C.; Gold, L.; Katilius, E.; Keeney, T. R.; Kim, N.; Saccomano, N. A.; Wilcox, S. K.; Zichi, D.; Sanders, G. M., From SOMAmer-Based Biomarker Discovery to Diagnostic and Clinical Applications: A SOMAmer-Based, Streamlined Multiplex Proteomic Assay. *PLoS One* **2011,** *6* (10), e26332.
361. Rohloff, J. C.; Gelinas, A. D.; Jarvis, T. C.; Ochsner, U. A.; Schneider, D. J.; Gold, L.; Janjic, N., Nucleic Acid Ligands With Protein-like Side Chains: Modified Aptamers and Their Use as Diagnostic and Therapeutic Agents. *Molecular Therapy - Nucleic Acids* **2014,** *3*, e201.
362. Kong, D.; Yeung, W.; Hili, R., In Vitro Selection of Diversely Functionalized Aptamers. *Journal of the American Chemical Society* **2017,** *139* (40), 13977-13980.
363. O'Reilly, R. K.; Turberfield, A. J.; Wilks, T. R., The Evolution of DNA-Templated Synthesis as a Tool for Materials Discovery. *Acc. Chem. Res.* **2017,** *50* (10), 2496-2509.
364. Li, X.; Liu, D. R., DNA-Templated Organic Synthesis: Nature's Strategy for Controlling Chemical Reactivity Applied to Synthetic Molecules. *Angewandte Chemie International Edition* **2004,** *43* (37), 4848-4870.
365. Gartner, Z. J.; Liu, D. R., The Generality of DNA-Templated Synthesis as a Basis for Evolving Non-Natural Small Molecules. *Journal of the American Chemical Society* **2001,** *123* (28), 6961-6963.
366. Calderone, C. T.; Puckett, J. W.; Gartner, Z. J.; Liu, D. R., Directing Otherwise Incompatible Reactions in a Single Solution by Using DNA-Templated Organic Synthesis. *Angewandte Chemie International Edition* **2002,** *41* (21), 4104-4108.
367. Gartner, Z. J.; Kanan, M. W.; Liu, D. R., Expanding the Reaction Scope of DNA-Templated Synthesis. *Angewandte Chemie International Edition* **2002,** *41* (10), 1796-1800.

368. Gartner, Z. J.; Tse, B. N.; Grubina, R.; Doyon, J. B.; Snyder, T. M.; Liu, D. R., DNA-Templated Organic Synthesis and Selection of a Library of Macrocycles. *Science (New York, N.Y.)* **2004,** *305* (5690), 1601-1605.
369. Usanov, D. L.; Chan, A. I.; Maianti, J. P.; Liu, D. R., Second-generation DNA-templated macrocycle libraries for the discovery of bioactive small molecules. *Nature chemistry* **2018,** *10* (7), 704-714.
370. Gartner, Z. J.; Grubina, R.; Calderone, C. T.; Liu, D. R., Two Enabling Architectures for DNA-Templated Organic Synthesis. *Angewandte Chemie International Edition* **2003,** *42* (12), 1370-1375.
371. Hansen, M. H.; Blakskjær, P.; Petersen, L. K.; Hansen, T. H.; Højfeldt, J. W.; Gothelf, K. V.; Hansen, N. J. V., A Yoctoliter-Scale DNA Reactor for Small-Molecule Evolution. *Journal of the American Chemical Society* **2009,** *131* (3), 1322-1327.
372. Snyder, T. M.; Liu, D. R., Ordered Multistep Synthesis in a Single Solution Directed by DNA Templates. *Angewandte Chemie International Edition* **2005,** *44* (45), 7379-7382.
373. Milnes, P. J.; McKee, M. L.; Bath, J.; Song, L.; Stulz, E.; Turberfield, A. J.; O'Reilly, R. K., Sequence-specific synthesis of macromolecules using DNA-templated chemistry. *Chem. Commun.* **2012,** *48* (45), 5614-5616.
374. He, Y.; Liu, D. R., Autonomous multistep organic synthesis in a single isothermal solution mediated by a DNA walker. *Nature nanotechnology* **2010,** *5* (11), 778-782.
375. Czlapinski, J. L.; Sheppard, T. L., Nucleic acid template-directed assembly of metallosalen-DNA conjugates. *Journal of the American Chemical Society* **2001,** *123* (35), 8618-9.
376. Nielsen, M.; Thomsen, A. H.; Cló, E.; Kirpekar, F.; Gothelf, K. V., Synthesis of Linear and Tripoidal Oligo(phenylene ethynylene)-Based Building Blocks for Application in Modular DNA-Programmed Assembly. *The Journal of Organic Chemistry* **2004,** *69* (7), 2240-2250.
377. Gothelf, K. V.; Thomsen, A.; Nielsen, M.; Cló, E.; Brown, R. S., Modular DNA-Programmed Assembly of Linear and Branched Conjugated Nanostructures. *Journal of the American Chemical Society* **2004,** *126* (4), 1044-1046.
378. Nielsen, M.; Dauksaite, V.; Kjems, J.; Gothelf, K. V., DNA-Directed Coupling of Organic Modules by Multiple Parallel Reductive Aminations and Subsequent Cleavage of Selected DNA Sequences. *Bioconjugate Chemistry* **2005,** *16* (4), 981-985.
379. Lo, P. K.; Sleiman, H. F., Nucleobase-Templated Polymerization: Copying the Chain Length and Polydispersity of Living Polymers into Conjugated Polymers. *J. Am. Chem. Soc.* **2009,** *131* (12), 4182-4183.
380. Nakamura, S.; Ogasawara, S.; Matuda, S.; Saito, I.; Fujimoto, K., Template Directed Reversible Photochemical Ligation of Oligodeoxynucleotides. *Molecules* **2012,** *17* (1), 163-178.
381. Fujimoto, K.; Matsuda, S.; Takahashi, N.; Saito, I., Template-Directed Photoreversible Ligation of Deoxyoligonucleotides via 5-Vinyldeoxyuridine. *Journal of the American Chemical Society* **2000,** *122* (23), 5646-5647.
382. Gerling, T.; Kube, M.; Kick, B.; Dietz, H., Sequence-programmable covalent bonding of designed DNA assemblies. *Science Advances* **2018,** *4* (8), eaau1157.
383. De Stefano, M.; Vesterager Gothelf, K., Dynamic Chemistry of Disulfide Terminated Oligonucleotides in Duplexes and Double-Crossover Tiles. *ChemBioChem* **2016,** *17* (12), 1122-1126.
384. Simmel, F. C.; Yurke, B.; Singh, H. R., Principles and Applications of Nucleic Acid Strand Displacement Reactions. *Chem. Rev.* **2019,** *119* (10), 6326-6369.
385. Seelig, G.; Yurke, B.; Winfree, E., Catalyzed Relaxation of a Metastable DNA Fuel. *J. Am. Chem. Soc.* **2006,** *128* (37), 12211-12220.

386. Olson, X.; Kotani, S.; Yurke, B.; Graugnard, E.; Hughes, W. L., Kinetics of DNA Strand Displacement Systems with Locked Nucleic Acids. *The Journal of Physical Chemistry B* **2017,** *121* (12), 2594-2602.
387. Tan, W.; Wang, K.; Drake, T. J., Molecular beacons. *Curr. Opin. Chem. Biol.* **2004,** *8* (5), 547-553.
388. Rangel, A. E.; Hariri, A. A.; Eisenstein, M.; Soh, H. T., Engineering Aptamer Switches for Multifunctional Stimulus-Responsive Nanosystems. **2020,** *32* (50), 2003704.
389. Zheng, J.; Yang, R.; Shi, M.; Wu, C.; Fang, X.; Li, Y.; Li, J.; Tan, W., Rationally designed molecular beacons for bioanalytical and biomedical applications. *Chem. Soc. Rev.* **2015,** *44* (10), 3036-3055.
390. Okamoto, A.; Tanabe, K.; Inasaki, T.; Saito, I., Phototriggered Drug Release from Functionalized Oligonucleotides by a Molecular Beacon Strategy. *Angew. Chem. Int. Ed.* **2003,** *42* (22), 2502-2504.
391. Song, X.; Reif, J., Nucleic Acid Databases and Molecular-Scale Computing. *ACS Nano* **2019,** *13* (6), 6256-6268.
392. Qian, L.; Winfree, E., Scaling Up Digital Circuit Computation with DNA Strand Displacement Cascades. **2011,** *332* (6034), 1196-1201.
393. Hanewich-Hollatz, M. H.; Chen, Z.; Hochrein, L. M.; Huang, J.; Pierce, N. A., Conditional Guide RNAs: Programmable Conditional Regulation of CRISPR/Cas Function in Bacterial and Mammalian Cells via Dynamic RNA Nanotechnology. *ACS Central Science* **2019,** *5* (7), 1241-1249.
394. Hochrein, L. M.; Li, H.; Pierce, N. A., High-Performance Allosteric Conditional Guide RNAs for Mammalian Cell-Selective Regulation of CRISPR/Cas. *ACS Synthetic Biology* **2021,** *10* (5), 964-971.
395. Rudchenko, M.; Taylor, S.; Pallavi, P.; Dechkovskaia, A.; Khan, S.; Butler Jr, V. P.; Rudchenko, S.; Stojanovic, M. N., Autonomous molecular cascades for evaluation of cell surfaces. *Nat. Nanotechnol.* **2013,** *8* (8), 580-586.
396. Morihiro, K.; Ankenbruck, N.; Lukasak, B.; Deiters, A., Small Molecule Release and Activation through DNA Computing. *J. Am. Chem. Soc.* **2017,** *139* (39), 13909-13915.
397. DeLuca, M.; Shi, Z.; Castro, C. E.; Arya, G., Dynamic DNA nanotechnology: toward functional nanoscale devices. *Nanoscale Horizons* **2020,** *5* (2), 182-201.
398. Yurke, B.; Turberfield, A. J.; Mills, A. P., Jr.; Simmel, F. C.; Neumann, J. L., A DNA-fuelled molecular machine made of DNA. *Nature* **2000,** *406* (6796), 605-8.
399. Shin, J.-S.; Pierce, N. A., A Synthetic DNA Walker for Molecular Transport. *J. Am. Chem. Soc.* **2004,** *126* (35), 10834-10835.
400. Zhang, D. Y.; Seelig, G., Dynamic DNA nanotechnology using strand-displacement reactions. *Nature Chem.* **2011,** *3* (2), 103-113.
401. Albert, S. K.; Hu, X.; Park, S.-J., Dynamic Nanostructures from DNA-Coupled Molecules, Polymers, and Nanoparticles. **2019,** *15* (26), 1900504.
402. Mao, C.; Sun, W.; Shen, Z.; Seeman, N. C., A nanomechanical device based on the B-Z transition of DNA. *Nature* **1999,** *397* (6715), 144-6.
403. Douglas, S. M.; Bachelet, I.; Church, G. M., A Logic-Gated Nanorobot for Targeted Transport of Molecular Payloads. **2012,** *335* (6070), 831-834.
404. Li, S.; Jiang, Q.; Liu, S.; Zhang, Y.; Tian, Y.; Song, C.; Wang, J.; Zou, Y.; Anderson, G. J.; Han, J.-Y.; Chang, Y.; Liu, Y.; Zhang, C.; Chen, L.; Zhou, G.; Nie, G.; Yan, H.; Ding, B.; Zhao, Y., A DNA nanorobot functions as a cancer therapeutic in response to a molecular trigger in vivo. *Nat. Biotechnol.* **2018,** *36* (3), 258-264.
405. Ijäs, H.; Hakaste, I.; Shen, B.; Kostiainen, M. A.; Linko, V., Reconfigurable DNA Origami Nanocapsule for pH-Controlled Encapsulation and Display of Cargo. *ACS Nano* **2019,** *13* (5), 5959-5967.

406. Bujold, K. E.; Fakhoury, J.; Edwardson, T. G. W.; Carneiro, K. M. M.; Briard, J. N.; Godin, A. G.; Amrein, L.; Hamblin, G. D.; Panasci, L. C.; Wiseman, P. W.; Sleiman, H. F., Sequence-responsive unzipping DNA cubes with tunable cellular uptake profiles. *Chemical Science* **2014,** *5* (6), 2449-2455.
407. Bujold, K. E.; Hsu, J. C. C.; Sleiman, H. F., Optimized DNA "Nanosuitcases" for Encapsulation and Conditional Release of siRNA. *Journal of the American Chemical Society* **2016,** *138* (42), 14030-14038.
408. Fakih, H. H.; Fakhoury, J. J.; Bousmail, D.; Sleiman, H. F., Minimalist Design of a Stimuli-Responsive Spherical Nucleic Acid for Conditional Delivery of Oligonucleotide Therapeutics. *ACS Appl. Mater. Interfaces* **2019,** *11* (15), 13912-13920.
409. Liao, W.-C.; Lu, C.-H.; Hartmann, R.; Wang, F.; Sohn, Y. S.; Parak, W. J.; Willner, I., Adenosine Triphosphate-Triggered Release of Macromolecular and Nanoparticle Loads from Aptamer/DNA-Cross-Linked Microcapsules. *ACS Nano* **2015,** *9* (9), 9078-9086.
410. Liu, M.; Fu, J.; Hejesen, C.; Yang, Y.; Woodbury, N. W.; Gothelf, K.; Liu, Y.; Yan, H., A DNA tweezer-actuated enzyme nanoreactor. *Nature Communications* **2013,** *4* (1), 2127.
411. Peng, H.; Newbigging, A. M.; Reid, M. S.; Uppal, J. S.; Xu, J.; Zhang, H.; Le, X. C., Signal Amplification in Living Cells: A Review of microRNA Detection and Imaging. *Anal. Chem.* **2020,** *92* (1), 292-308.
412. Bi, S.; Yue, S.; Zhang, S., Hybridization chain reaction: a versatile molecular tool for biosensing, bioimaging, and biomedicine. *Chem. Soc. Rev.* **2017,** *46* (14), 4281-4298.
413. Dirks, R. M.; Pierce, N. A., Triggered amplification by hybridization chain reaction. *Proc. Natl. Acad. Sci. U. S. A.* **2004,** *101* (43), 15275-15278.
414. Evanko, D., Hybridization chain reaction. *Nat. Methods* **2004,** *1* (3), 186-186.
415. Yang, B.; Zhang, X.-B.; Kang, L.-P.; Shen, G.-L.; Yu, R.-Q.; Tan, W., Target-Triggered Cyclic Assembly of DNA–Protein Hybrid Nanowires for Dual-Amplified Fluorescence Anisotropy Assay of Small Molecules. *Anal. Chem.* **2013,** *85* (23), 11518-11523.
416. Sun, J.; Jiang, W.; Zhu, J.; Li, W.; Wang, L., Label-free fluorescence dual-amplified detection of adenosine based on exonuclease III-assisted DNA cycling and hybridization chain reaction. *Biosens. Bioelectron.* **2015,** *70*, 15-20.
417. Zheng, J.; Hu, Y.; Bai, J.; Ma, C.; Li, J.; Li, Y.; Shi, M.; Tan, W.; Yang, R., Universal Surface-Enhanced Raman Scattering Amplification Detector for Ultrasensitive Detection of Multiple Target Analytes. *Anal. Chem.* **2014,** *86* (4), 2205-2212.
418. Song, W.; Zhu, K.; Cao, Z.; Lau, C.; Lu, J., Hybridization chain reaction-based aptameric system for the highly selective and sensitive detection of protein. *Analyst* **2012,** *137* (6), 1396-1401.
419. Zhang, Y.; Chen, Z.; Tao, Y.; Wang, Z.; Ren, J.; Qu, X., Hybridization chain reaction engineered dsDNA for Cu metallization: an enzyme-free platform for amplified detection of cancer cells and microRNAs. *Chem. Commun.* **2015,** *51* (57), 11496-11499.
420. Bi, S.; Chen, M.; Jia, X.; Dong, Y.; Wang, Z., Hyperbranched Hybridization Chain Reaction for Triggered Signal Amplification and Concatenated Logic Circuits. *Angew. Chem. Int. Ed. Engl.* **2015,** *54* (28), 8144-8.
421. Xuan, F.; Hsing, I. M., Triggering Hairpin-Free Chain-Branching Growth of Fluorescent DNA Dendrimers for Nonlinear Hybridization Chain Reaction. *J. Am. Chem. Soc.* **2014,** *136* (28), 9810-9813.
422. Choi, H. M. T.; Beck, V. A.; Pierce, N. A., Next-Generation in Situ Hybridization Chain Reaction: Higher Gain, Lower Cost, Greater Durability. *ACS Nano* **2014,** *8* (5), 4284-4294.

423. Choi, H. M. T.; Schwarzkopf, M.; Fornace, M. E.; Acharya, A.; Artavanis, G.; Stegmaier, J.; Cunha, A.; Pierce, N. A., Third-generation in situ hybridization chain reaction: multiplexed, quantitative, sensitive, versatile, robust. *Development* **2018,** *145* (12).
424. Ang, Y. S.; Yung, L.-Y. L., Rational design of hybridization chain reaction monomers for robust signal amplification. *Chem. Commun.* **2016,** *52* (22), 4219-4222.
425. Kim, K. T.; Angerani, S.; Winssinger, N., A minimal hybridization chain reaction (HCR) system using peptide nucleic acids. *Chemical Science* **2021,** *12* (23), 8218-8223.
426. Huang, J.; Wang, H.; Yang, X.; Quan, K.; Yang, Y.; Ying, L.; Xie, N.; Ou, M.; Wang, K., Fluorescence resonance energy transfer-based hybridization chain reaction for in situ visualization of tumor-related mRNA. *Chemical Science* **2016,** *7* (6), 3829-3835.
427. Lu, S.; Hu, T.; Wang, S.; Sun, J.; Yang, X., Ultra-Sensitive Colorimetric Assay System Based on the Hybridization Chain Reaction-Triggered Enzyme Cascade Amplification. *ACS Appl. Mater. Interfaces* **2017,** *9* (1), 167-175.
428. Rana, M.; Balcioglu, M.; Kovach, M.; Hizir, M. S.; Robertson, N. M.; Khan, I.; Yigit, M. V., Reprogrammable multiplexed detection of circulating oncomiRs using hybridization chain reaction. *Chem. Commun.* **2016,** *52* (17), 3524-3527.
429. Liu, P.; Yang, X.; Sun, S.; Wang, Q.; Wang, K.; Huang, J.; Liu, J.; He, L., Enzyme-Free Colorimetric Detection of DNA by Using Gold Nanoparticles and Hybridization Chain Reaction Amplification. *Anal. Chem.* **2013,** *85* (16), 7689-7695.
430. Huang, J.; Wu, Y.; Chen, Y.; Zhu, Z.; Yang, X.; Yang, C. J.; Wang, K.; Tan, W., Pyrene-Excimer Probes Based on the Hybridization Chain Reaction for the Detection of Nucleic Acids in Complex Biological Fluids. *Angew. Chem. Int. Ed.* **2011,** *50* (2), 401-404.
431. Yang, L.; Liu, C.; Ren, W.; Li, Z., Graphene Surface-Anchored Fluorescence Sensor for Sensitive Detection of MicroRNA Coupled with Enzyme-Free Signal Amplification of Hybridization Chain Reaction. *ACS Appl. Mater. Interfaces* **2012,** *4* (12), 6450-6453.
432. Shimron, S.; Wang, F.; Orbach, R.; Willner, I., Amplified Detection of DNA through the Enzyme-Free Autonomous Assembly of Hemin/G-Quadruplex DNAzyme Nanowires. *Anal. Chem.* **2012,** *84* (2), 1042-1048.
433. Ren, J.; Wang, J.; Han, L.; Wang, E.; Wang, J., Kinetically grafting G-quadruplexes onto DNA nanostructures for structure and function encoding via a DNA machine. *Chem. Commun.* **2011,** *47* (38), 10563-10565.
434. Yang, H.; Gao, Y.; Wang, S.; Qin, Y.; Xu, L.; Jin, D.; Yang, F.; Zhang, G.-J., In situ hybridization chain reaction mediated ultrasensitive enzyme-free and conjugation-free electrochemcial genosensor for BRCA-1 gene in complex matrices. *Biosens. Bioelectron.* **2016,** *80*, 450-455.
435. Wu, Z.; Liu, G.-Q.; Yang, X.-L.; Jiang, J.-H., Electrostatic Nucleic Acid Nanoassembly Enables Hybridization Chain Reaction in Living Cells for Ultrasensitive mRNA Imaging. *J. Am. Chem. Soc.* **2015,** *137* (21), 6829-6836.
436. Zhu, G.; Zheng, J.; Song, E.; Donovan, M.; Zhang, K.; Liu, C.; Tan, W., Self-assembled, aptamer-tethered DNA nanotrains for targeted transport of molecular drugs in cancer theranostics. *Proceedings of the National Academy of Sciences* **2013,** *110* (20), 7998-8003.
437. Zhang, L.; Wang, S.; Yang, Z.; Hoshika, S.; Xie, S.; Li, J.; Chen, X.; Wan, S.; Li, L.; Benner, S. A.; Tan, W., An Aptamer-Nanotrain Assembled from Six-Letter DNA Delivers Doxorubicin Selectively to Liver Cancer Cells. *Angew. Chem. Int. Ed.* **2020,** *59* (2), 663-668.

438. Wang, Y.-M.; Wu, Z.; Liu, S.-J.; Chu, X., Structure-Switching Aptamer Triggering Hybridization Chain Reaction on the Cell Surface for Activatable Theranostics. *Anal. Chem.* **2015,** *87* (13), 6470-6474.
439. Xiong, M.; Rong, Q.; Kong, G.; Yang, C.; Zhao, Y.; Qu, F.-L.; Zhang, X.-B.; Tan, W., Hybridization chain reaction-based nanoprobe for cancer cell recognition and amplified photodynamic therapy. *Chem. Commun.* **2019,** *55* (21), 3065-3068.
440. Meng, W.; Muscat, R. A.; McKee, M. L.; Milnes, P. J.; El-Sagheer, A. H.; Bath, J.; Davis, B. G.; Brown, T.; O'Reilly, R. K.; Turberfield, A. J., An autonomous molecular assembler for programmable chemical synthesis. *Nature Chem.* **2016,** *8*, 542.
441. Green, S. J.; Lubrich, D.; Turberfield, A. J., DNA hairpins: fuel for autonomous DNA devices. *Biophys. J.* **2006,** *91* (8), 2966-2975.
442. Li, D.; Wu, Y.; Gan, C.; Yuan, R.; Xiang, Y., Bio-cleavable nanoprobes for target-triggered catalytic hairpin assembly amplification detection of microRNAs in live cancer cells. *Nanoscale* **2018,** *10* (37), 17623-17628.
443. Zhu, D.; Huang, J.; Lu, B.; Zhu, Y.; Wei, Y.; Zhang, Q.; Guo, X.; Yuwen, L.; Su, S.; Chao, J.; Wang, L., Intracellular MicroRNA Imaging with MoS2-Supported Nonenzymatic Catassembly of DNA Hairpins. *ACS Appl. Mater. Interfaces* **2019,** *11* (23), 20725-20733.
444. Liao, X.; Li, L.; Pan, J.; Peng, T.; Ge, B.; Tang, Q., In situ biosensor for detection miRNA in living cells based on carbon nitride nanosheets with catalytic hairpin assembly amplification. **2018,** *33* (1), 190-195.
445. Zhang, K.; Song, S.; Huang, S.; Yang, L.; Min, Q.; Wu, X.; Lu, F.; Zhu, J.-J., Lighting Up MicroRNA in Living Cells by the Disassembly of Lock-Like DNA-Programmed UCNPs-AuNPs through the Target Cycling Amplification Strategy. **2018,** *14* (40), 1802292.
446. Zhang, D. Y.; Turberfield, A. J.; Yurke, B.; Winfree, E., Engineering Entropy-Driven Reactions and Networks Catalyzed by DNA. *Science* **2007,** *318* (5853), 1121-1125.
447. He, L.; Lu, D.; Liang, H.; Xie, S.; Zhang, X.; Liu, Q.; Yuan, Q.; Tan, W., mRNA-Initiated, Three-Dimensional DNA Amplifier Able to Function inside Living Cells. *J. Am. Chem. Soc.* **2018,** *140* (1), 258-263.
448. Lu, Y.; Liu, J., Functional DNA nanotechnology: emerging applications of DNAzymes and aptamers. *Curr. Opin. Biotechnol.* **2006,** *17* (6), 580-588.
449. Zhou, W.; Ding, J.; Liu, J., Theranostic DNAzymes. *Theranostics* **2017,** *7* (4), 1010-1025.
450. Willner, I.; Shlyahovsky, B.; Zayats, M.; Willner, B., DNAzymes for sensing, nanobiotechnology and logic gate applications. *Chem. Soc. Rev.* **2008,** *37* (6), 1153-1165.
451. Ma, L.; Liu, J., Catalytic Nucleic Acids: Biochemistry, Chemical Biology, Biosensors, and Nanotechnology. *iScience* **2020,** *23* (1), 100815.
452. Huo, W.; Li, X.; Wang, B.; Zhang, H.; Zhang, J.; Yang, X.; Jin, Y., Recent advances of DNAzyme-based nanotherapeutic platform in cancer gene therapy. *Biophysics Reports* **2020,** *6* (6), 256-265.
453. He, Z.-M.; Zhang, P.-H.; Li, X.; Zhang, J.-R.; Zhu, J.-J., A Targeted DNAzyme-Nanocomposite Probe Equipped with Built-in Zn2+ Arsenal for Combined Treatment of Gene Regulation and Drug Delivery. *Scientific Reports* **2016,** *6* (1), 22737.
454. Zhang, Z.; Balogh, D.; Wang, F.; Willner, I., Smart Mesoporous SiO2 Nanoparticles for the DNAzyme-Induced Multiplexed Release of Substrates. *J. Am. Chem. Soc.* **2013,** *135* (5), 1934-1940.
455. Meng, L.; Ma, W.; Lin, S.; Shi, S.; Li, Y.; Lin, Y., Tetrahedral DNA Nanostructure-Delivered DNAzyme for Gene Silencing to Suppress Cell Growth. *ACS Appl. Mater. Interfaces* **2019,** *11* (7), 6850-6857.
456. He, D.; Hai, L.; Wang, H.; Wu, R.; Li, H.-W., Enzyme-free quantification of exosomal microRNA by the target-triggered assembly of the polymer DNAzyme nanostructure. *Analyst* **2018,** *143* (4), 813-816.

457. Ma, Z.; Taylor, J.-S., Nucleic acid-triggered catalytic drug release. *Proceedings of the National Academy of Sciences* **2000,** *97* (21), 11159-11163.
458. Cai, J.; Li, X.; Taylor, J. S., Improved Nucleic Acid Triggered Probe Activation through the Use of a 5-Thiomethyluracil Peptide Nucleic Acid Building Block. *Org. Lett.* **2005,** *7* (5), 751-754.
459. Ma, Z.; Taylor, J.-S., PNA-Based RNA-Triggered Drug-Releasing System. *Bioconjugate Chem.* **2003,** *14* (3), 679-683.
460. Di Pisa, M.; Seitz, O., Nucleic Acid Templated Reactions for Chemical Biology. *ChemMedChem* **2017,** *12* (12), 872-882.
461. Seitz, O., Templated chemistry for bioorganic synthesis and chemical biology. *J. Pept. Sci.* **2019,** *25* (7), e3198.
462. Ma, Z.; Taylor, J.-S., Nucleic acid triggered catalytic drug and probe release: A new concept for the design of chemotherapeutic and diagnostic agents. *Bioorg. Med. Chem.* **2001,** *9* (9), 2501-2510.
463. Gorska, K.; Manicardi, A.; Barluenga, S.; Winssinger, N., DNA-templated release of functional molecules with an azide-reduction-triggered immolative linker. *Chem. Commun.* **2011,** *47* (15), 4364-4366.
464. Franzini, R. M.; Kool, E. T., Efficient Nucleic Acid Detection by Templated Reductive Quencher Release. *J. Am. Chem. Soc.* **2009,** *131* (44), 16021-16023.
465. Wu, H.; Cisneros, B. T.; Cole, C. M.; Devaraj, N. K., Bioorthogonal Tetrazine-Mediated Transfer Reactions Facilitate Reaction Turnover in Nucleic Acid-Templated Detection of MicroRNA. *J. Am. Chem. Soc.* **2014,** *136* (52), 17942-17945.
466. Wu, H.; Alexander, S. C.; Jin, S.; Devaraj, N. K., A Bioorthogonal Near-Infrared Fluorogenic Probe for mRNA Detection. *J. Am. Chem. Soc.* **2016,** *138* (36), 11429-11432.
467. Röthlingshöfer, M.; Gorska, K.; Winssinger, N., Nucleic Acid Templated Uncaging of Fluorophores Using Ru-Catalyzed Photoreduction with Visible Light. *Org. Lett.* **2012,** *14* (2), 482-485.
468. Sadhu, K. K.; Winssinger, N., Detection of miRNA in Live Cells by Using Templated RuII-Catalyzed Unmasking of a Fluorophore. *Chemistry – A European Journal* **2013,** *19* (25), 8182-8189.
469. Holtzer, L.; Oleinich, I.; Anzola, M.; Lindberg, E.; Sadhu, K. K.; Gonzalez-Gaitan, M.; Winssinger, N., Nucleic Acid Templated Chemical Reaction in a Live Vertebrate. *ACS Central Science* **2016,** *2* (6), 394-400.
470. Chang, D.; Lindberg, E.; Winssinger, N., Critical Analysis of Rate Constants and Turnover Frequency in Nucleic Acid-Templated Reactions: Reaching Terminal Velocity. *J. Am. Chem. Soc.* **2017,** *139* (4), 1444-1447.
471. Kim, K. T.; Angerani, S.; Chang, D.; Winssinger, N., Coupling of DNA Circuit and Templated Reactions for Quadratic Amplification and Release of Functional Molecules. *J. Am. Chem. Soc.* **2019,** *141* (41), 16288-16295.
472. Lindberg, E.; Angerani, S.; Anzola, M.; Winssinger, N., Luciferase-induced photoreductive uncaging of small-molecule effectors. *Nature Communications* **2018,** *9* (1), 3539.
473. Chen, X.-H.; Roloff, A.; Seitz, O., Consecutive Signal Amplification for DNA Detection Based on De Novo Fluorophore Synthesis and Host–Guest Chemistry. *Angew. Chem. Int. Ed.* **2012,** *51* (18), 4479-4483.
474. Vázquez, O.; Seitz, O., Cytotoxic peptide–PNA conjugates obtained by RNA-programmed peptidyl transfer with turnover. *Chemical Science* **2014,** *5* (7), 2850-2854.
475. Erben, A.; Grossmann, T. N.; Seitz, O., DNA-instructed acyl transfer reactions for the synthesis of bioactive peptides. *Bioorg. Med. Chem. Lett.* **2011,** *21* (17), 4993-4997.
476. Erben, A.; Grossmann, T. N.; Seitz, O., DNA-Triggered Synthesis and Bioactivity of Proapoptotic Peptides. *Angew. Chem. Int. Ed.* **2011,** *50* (12), 2828-2832.

|2|

Amplified self-immolative release of small molecules by spatial isolation of reactive groups on DNA minimal architectures

This chapter is composed mainly of work published as "Amplified Self-Immolative Release of Small Molecules by Spatial Isolation of Reactive Groups on DNA-Minimal Architectures" by Alexander L. Prinzen, Daniel Saliba, Christopher Hennecker, Tuan Trinh, Anthony Mittermaier and Hanadi F. Sleiman. Angewante chemie, 2020, 59, 12900-12908.

Contribution of Authors: Alexander Prinzen helped design and develop the project, primarily contributed to the production of experimental data from small molecule synthesis, DNA synthesis, HPLC purification, mass spectrometry (MS), electrophoresis, dynamic light scattering (DLS), and wrote the paper. **Daniel Saliba** performed the denaturing agarose gels, helped design and assemble the DNA Track nanostructures, synthesized some DNA strands, and aided data interpretation. **Christopher Hennecker** and **Anthony Mittermaier** performed the kinetics analysis of the HCR process and aided with data interpretation. **Tuan Trinh** performed some AFM imaging. **Hanadi F. Sleiman** designed the project, guided interpretation of data, result discussion, co-wrote the paper and provided funding for the project.

2.1. Preface

Triggering the release of small molecules in response to unique biomarkers is important for applications in drug delivery and bio-detection. Due to typically low quantities of biomarker, amplifying release is necessary to gain appreciable responses. As can be seen from Chapter 1, nucleic acids have been used for both their biomarker recognition properties and as stimuli, notably in amplified small molecule release via nucleic acid-templated catalysis (NATC). The multiple components and reversibility of NATC, however, make it difficult to apply *in vivo*. In this chapter, we report the evolution of two different strategies to generate a standalone drug release device which amplifies the release of small molecules, in response to a biological signal in an amplified manner. The first strategy explores the first use the hybridization chain reaction (HCR) for the amplified, conditional release of small molecules from standalone nanodevices. In this strategy, we couple HCR with a DNA-templated reaction resulting in the amplified, immolative release of small molecules. Moreover, we integrate the HCR components into single nanodevices as DNA tracks and spherical nucleic acids, spatially isolating reactive groups until triggering. Overall, this work translates the amplification of HCR into small molecule release without the use of multiple components, and will aid its application to biosensing, imaging and drug delivery. In the second strategy, we explore using molecular beacons and self-immolative polymers for the recognition and amplification components respectively. This strategy uses

molecular beacons in combination with DNA templated reactions to initiate the head-to-toe depolymerization of a self-immolative polymer.

2.2. Introduction

Concealing the activity of functional small molecules, such as fluorescent or therapeutic structures, and triggering their release in active form in response to a biological stimulus has important applications in a variety of different areas including smart therapeutics, biological detection and bio-imaging.[1] Nucleic acids are favorable biological molecules to trigger the release of pro-functional small molecules, because of their protein recognition properties (e.g., aptamers) and unique spatiotemporal expression profiles (e.g., mRNA, miRNA). They have thus been used as both triggers and recognition components in a variety of stimuli-responsive nanodevices.[2-3] However, many of these devices respond to a stoichiometric amount of stimulus, and thus, the typically small amounts of biological targets present in vitro or in vivo would not be sufficient to elicit a sizable response.[4-8]

To address this issue, many amplification methods have been developed.[9-11] Notably, the release of functional small molecules via nucleic acid-templated catalysis has emerged as a powerful tool to amplify nucleic acid signals into detection and drug release responses.[11-15] This approach uses two DNA-small molecule conjugates, which perform a DNA-templated reaction with each other upon binding a nucleic acid target. The reaction releases the small molecule payload from the conjugate, allowing it to elicit its function.[14, 16] While this is a powerful method, it does require separate components that are able to reversibly bind the target template in order to generate turnover, making it primarily feasible *in vitro.*[17] Due to differences in pharmacokinetics and tissue distribution of different components, it would be desirable to combine the amplification system into a single nanodevice for in vivo applications.

Integrating reactive functional groups into a single device, however, poses the significant challenge of preventing the groups from reacting non-specifically until they are triggered. Some natural systems have evolved unique mechanisms to spatially isolate different reactive groups within the same structure.[18] Enzymes such as plasminogen[19] and vascular endothelial growth

factors C & D[20], have precisely placed intramolecular reactive thiol and disulfide moieties, which are brought in close proximity upon allosteric recognition. In DNA nanotechnology, reactive functional groups can be effectively separated for sequential transfer reactions in the form of a DNA walker.[21]

In addition to DNA-templated chemical reactions, other oligonucleotide amplification mechanisms that rely on toehold mediated strand displacement have been extensively investigated.[24] For example, enzyme-free isothermal amplification methods, such as the hybridization chain reaction (HCR)[9, 25] or catalytic hairpin assembly (CHA)[26] rely on metastable hairpins for amplification. Moreover, the different component molecules necessary for these methods have been combined into single metastable nanodevices using DNA nanotechnology approaches.[27-31] HCR in particular has been used for bio-sensing assays[32], bio-imaging[33], bio-medicine[34-35], and small molecule synthesis[36]. While previous HCR-small molecule hybrids have been generated that release through non-specific hydrolysis[35] or diffusion[34, 37], to our knowledge HCR has not been developed for the conditional release of small molecules.

Furthermore, molecular amplification in the form of self-immolative polymers (SIPs) have been thoroughly investigated.[22] These polymers amplify a stimulus from one end of the polymer, degrading the polymer in a head to tail fashion, and have been made responsive to a multitude of different stimuli. Side chains on these polymers have also been developed to release small molecule cargo in an amplified manner.[23] Yet to our knowledge, these types of molecular architectures have not been developed to be responsive to non-enzymatic molecular recognition of a biological stimulus.

In this chapter, we set out to develop a standalone, amplifying drug release device that is responsive to the molecular recognition of biological triggers. We developed two designs based on either SIP's or HCR for the amplification mechanism. The first design described, develops the hybridization chain reaction (HCR) for the conditional, amplified release of pro-functional small molecules. Combining HCR with a DNA-templated reaction and strategically positioning reactive functional groups on each hairpin allows these reactive groups to be kept separated under high dilution conditions. Once polymerization is induced, the reactive groups increase in effective

concentration and can trigger a self-immolative mechanism, releasing functional small molecules in an amplified manner.

Importantly, this method operates using toehold-mediated strand displacement with metastable hairpins, allowing their combination into complex structures. By using different DNA nanostructures, such as polymerizable tracks and spherical nucleic acids, we show that both HCR hairpin components can be integrated into a single structure, while effectively separating reactivity until triggering. Using DNA nanotechnology allows for the organization of different functional components with high precision and structural control.

In this chapter, HCR is the tool used to achieve amplification, but the innovation in our approach lies in the spatial separation of chemically reactive functional groups within the same nanostructure, for triggered amplified release of small molecules. This required careful synthetic and kinetic studies, which will be valuable for the diagnostic and therapeutic communities. We anticipate that the development of these systems can lead to new analytical tools for biosensing and bioimaging as well as stimuli-responsive drug delivery vehicles. This approach is a combination of two areas of research: DNA-templated catalysis and DNA-based amplification methods like HCR. In principle, it can be applied to any DNA based toehold mediated amplification methods such as CHA.[10]

Our second design was a preliminary approach we took before using HCR and it combines SIP's and a molecular beacon integrated into a single device for both amplification and biological responsiveness. In this design, reactive functional groups are kept separated on the 5' and 3' ends of a double stranded molecular beacon. The SIP is connected to the molecular beacon at one of these ends, and once a trigger strand is introduced, the hairpin of the molecular beacon forms, bringing the reactive functional groups into close proximity. These reactive groups then cleave the SIP from the molecular beacon and induce the amplified depolymerization of the SIP. We demonstrate the mechanism for this strand displacement and that by carefully selecting orthogonal protecting groups, release can only occur when the protecting group is removed.

2.3. Results and Discussion

2.3.1. Design # 1, Synthesis and Characterization of HCR.

To use HCR for conditional release, two processes are required, 1) HCR polymerization for amplification and 2) a DNA mediated bond cleavage reaction that occurs after polymerization to liberate the small molecules.

In the simplest version of HCR there are two hairpins (H1 & H2) that are designed to have a toehold domain (T), a stem domain (S) and a loop domain (L). Both the toehold and loop domains on opposite hairpins are complementary to each other but are kinetically trapped and do not hybridize (Figure 2.1a.). The HCR process begins when an initiator strand (I) is introduced, binding to the toehold domain of H1, displacing the stem domain, and revealing the loop domain (Figure 2.1b-i). From here the loop domain of H1 binds to the toehold domain of H2, displacing its stem domain and revealing its loop domain (Figure 2.1b-ii). This process repeats until all H1 and H2 are consumed, generating amplification with long polymers of H1 and H2 (Figure 2.1b-v). To address the second process, each of the hairpins in the HCR process was modified with unique design features. To the stem domain of H1 was added a reactive group (E), connected through a linker group (R) to the small functional molecule (M) (Figure 2.1a.). H2 was modified between the stem and loop domains with another reactive group (N). The groups (E) and (N) serve the purpose of reacting together in a bond cleavage process. After polymerization these groups would be strategically placed in close proximity on each monomer to increase their effective concentration and react as a DNA templated reaction (Figure 2.1b-iii). We chose to use a DNA-templated sulfide nucleophilic attack for the bond cleavage reaction (Figure 2.1b). DNA-templated thiol-disulfide exchange has typically been used as a DNA ligation reaction[39-41], but also in nucleic acid templated catalysis[42]. In our design, the (E) domain of H1 is a disulfide that can be cleaved by the thiol group (N) of H2, releasing the (R) and (M) groups. Interestingly, this DNA-templated reaction is accompanied by covalent bond formation between (E) and (N) in the resulting polymer (Figure 2.1.c). To our knowledge this would be the first time that HCR is accompanied by component ligation. In addition to providing an additional method to monitor

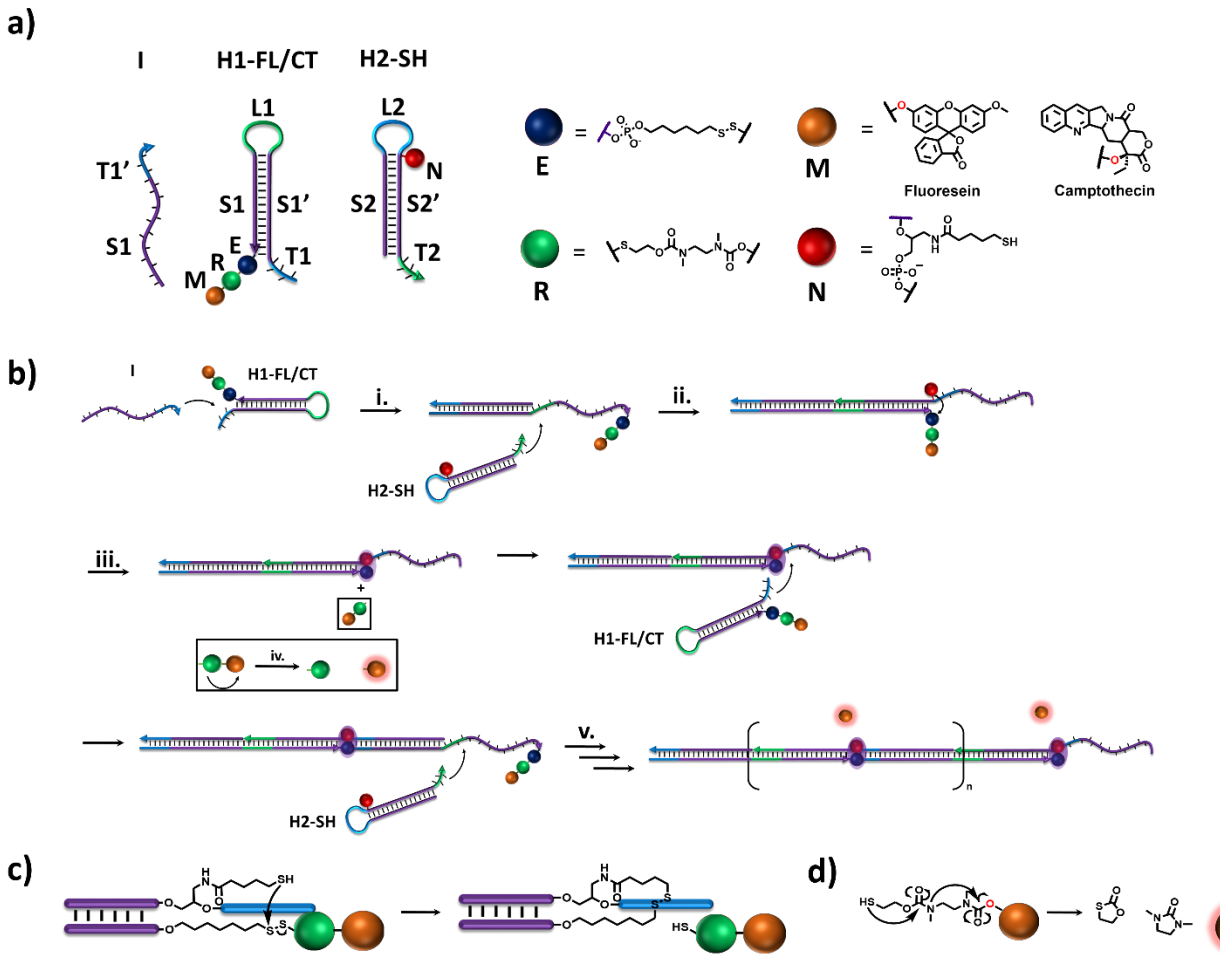

Figure 2. 1-HCR strategy for generating an amplifying nanodevice

(a) Design of H1-Fl/ H1-CT and H2-SH for HCR **(b)** Mechanism of HCR resulting in the release of pro-functional molecules: i. initiator hybridizes to the toehold domain of H1 and performs a toehold mediated strand displacement. ii. Loop domain of H1 hybridizes to the toehold domain of H2 and performs a toehold mediated strand displacement. iii. DNA templated reaction occurs, releasing the pro-functional molecule connected to a biodegradable linker. iv. Immolative linker degrades to release the functional molecule in its active form. v. The HCR process repeats polymerizing H1 and H2, amplifying the release of pro-functional molecule. **(c)** Mechanism of DNA templated disulfide exchange, resulting in the release of the pro-functional molecule. **(d)** Mechanism of immolative linker degradation, resulting in the release of active molecule.

the process using denaturing gel electrophoresis (see below), this results in a more stable, less dynamic polymer which makes it a useful material, rather than only a side-product.

In addition to the bond cleavage reaction, we also required a method to conceal and then recover the activity of the small molecule (M). Therefore, we introduced a self immolative linker

(R) between (E) and (M). Using the self-immolative linker (R) gives us a traceless degradable linker that is triggered by the bond cleavage reaction (Figure 2.1b iv). More specifically, while (M) and (R) are connected to (E) its activity is sequestered until the DNA templated bond cleavage reaction occurs and the self immolative linker undergoes a series of intramolecular cyclization's to release the small molecule (M), recovering its activity (Figure 2.1d). We introduced an extra diethylamine linkage into (R) to form carbamate linkages, as opposed to carbonate linkages, as this had been shown previously to reduce non-specific hydrolysis of the functional molecule from the linker.[43-44] To monitor the extent and rate of small molecule release in real time by fluorescence spectroscopy we initially chose (M) to be a methoxyfluorescein molecule (Figure 2.1a), that is non-emissive when connected to the self immolative linker.[45]

Modified H1 and H2 strands were synthesized and reacted to generate methoxyfluorescein conjugated H1 (H1-FL) and thiol modified H2 (H2-SH). These strands were then characterized by gel electrophoresis and LC/MS (Figure 2.1a, and detailed synthesis and characterization in section 2.5.6.). For H2-SH, it was non-trivial to install an internal thiol modification, as complex synthesis and purification factors must be considered and there are limited commercial reagents available (Figure 2.1a for structure and detailed in Section 2.5.6.5). Briefly, to overcome these challenges we functionalized H2 with a serinol amino modification in the desired location and labelled it on the solid support with an activated ester molecule containing a disulfide, before the final deprotection. Stability of the H1-FL strand was confirmed by fluorescence and high-performance liquid chromatography (HPLC), with no appreciable degradation over 24 hrs (*Experimental* Figure 2.29 and Table 2.3).

We are able to monitor the system using three methods 1) the degree of monomer consumption, as determined by native agarose gel electrophoresis gel electrophoresis (AGE), which informs on the efficiency and rate of the HCR process (Figure 2.2a and Figure 2.2c) 2) the degree of ligation as determined by denaturing AGE, which informs on the yield and kinetics of release of the pro-methoxyfluorescein molecule (Figure 2.2b and Figure 2.2c) and 3) fluorescence intensity increase of the fluorophore, which informs on the yield and rate of the self-immolative cyclization's to produce the active molecule (Figure 2.2c). First, to determine the extent of

amplification, we performed our polymerizations at a constant hairpin concentration of 750nM, while varying the amount of initiator between 0 and 1 equiv. (*Experimental* Figure 2.29, and Table 2.3).

It was found that between 1 and 0.1 equiv. of initiator, our system polymerized to ≈90% (Figure 2.2a). At 0.1 equiv. of initiator the polymerization afforded approx. 640 nM of released methoxyfluorescein which is significantly more than the concentration of initiator (75 nM), indicating amplified release (Figure 2.2c and *Experimental* Figure 2.29). This represents an 85% yield over three steps (Polymerization, ligation & linker degradation) with respect to the concentration of H1-FL (Figure 2.2c). Even at 25nM initiator concentration we were able to release 340 nM of methoxyfluorescein which approaches the concentration of some relevant

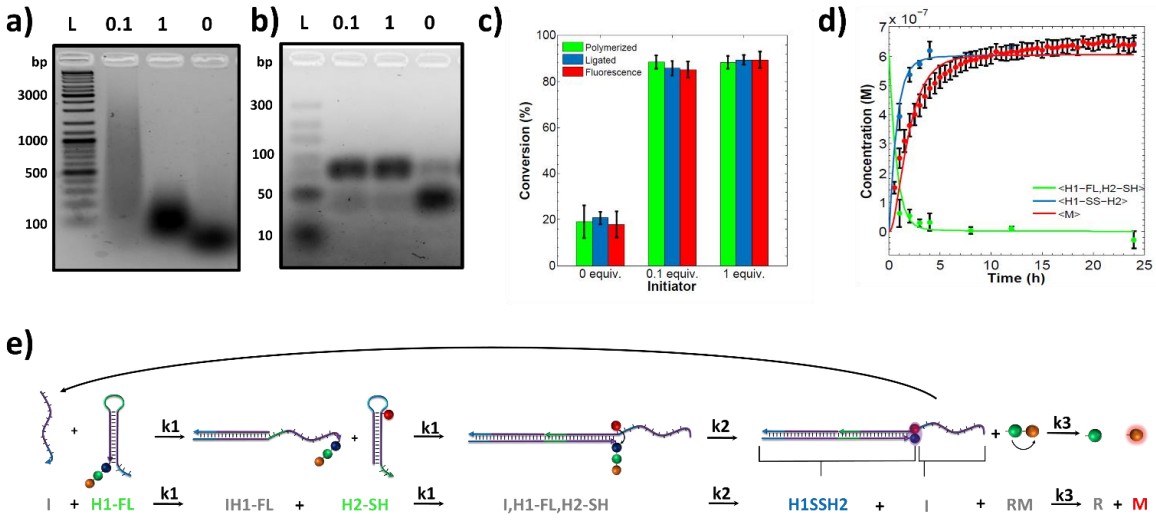

Figure 2. 2 Characterization of HCR between H1-FL and H2-SH after 24hr

(a) Native agarose and **(b)** Denaturing agarose: L: Ladder, Lane 0: H1-FL + H2-SH, Lane 0.1: Lane 0 + 0.1 equiv. I-1, Lane 1: Lane 0 + 1 equiv. I-1. d. **(c)** Degree of monomer consumption, ligation and released methoxyfluorescein after 24 hr of H1-FL and H2-SH with 0, 0.1 and 1 equiv. I-1. **(d)** HCR kinetics, experimental data is represented as circles and simulated kinetics are solid lines. Error bars correspond to the standard deviation of triplicate measurements. Native-AGE (green) is reported as the average value of H1 and H2 strands, denatured-AGE (blue) is reporting on ligated H1H2 complexes, fluorescence measurements (red) report on the completion of immolative cyclization. **(e)** Sequential mechanism of the HCR reaction with ligation and immolative cyclization steps, the colours of each species correspond to their traces in d, species that were not measured are represented in grey (see section 2.5.8.2. *Experimental* Figure 2.33 for more detail.).

biomarkers (*Experimental* Figure 2.29).[46] The ligation product of H1-FL and H2-SH was further confirmed by LC-MS (*Experimental* Figure 2.31). We confirmed that the disulfide exchange reaction was still viable over time and that the overall yield was not reduced due to non-specific thiol oxidation by performing a series of polymerizations initiated at different time points (*Experimental* Figure 2.32).

For the sequences used, circuit leakage at 0 equiv. of initiator was found to be only 5% after 1hr up to a maximum of approx. 20% over 24hrs (Figure 2.2c and *Experimental* Figure 2.29). We determined that circuit leakage was not due to non-specific reactions between H1-FL and H2-SH by exposing H1-FL to a non-hybridizing H2-SH (H2-2-SH), resulting in minimal release (*Experimental* Figure 2.29 and Table 2.3). Therefore, it was determined that leakage is primarily due to spontaneous polymerization between H1-FL and H2-SH when no initiator is present. Leakage was further reduced to <10% over 24hr in the second generation by increasing the stem length of the hairpins from 12 to 18 bases, (see below).

To verify that our system follows the intended HCR mechanism (Figure 2.1b), the kinetics of assembly were analyzed according to the scheme shown in Figure 2.2e. The initiator, I, and polymer I(H1H2)n bind to hairpin H1, and the IH1 dimer and polymer I(H1H2)nH1 bind to H2 according to the second-order rate constant k1. These steps were assumed to have identical kinetics, since the toe-hold and stem loop regions are identical in H1 and H2. The ligation of adjacent H1 and H2 fragments (and concomitant release of the pro-functional molecule) obeyed first-order kinetics with rate constant k2. The immolative cyclization reaction was described with the first-order rate constant k3. Theoretical kinetic traces were obtained by numerically integrating the coupled differential equations (see section 2.5.8.2). The native AGE, denaturing AGE, and fluorescence data were fit to this kinetic scheme by non-linear least squares minimization, yielding the rate constants k1, k2, and k3. In addition, we found it necessary to account for a small amount of unreacted material present at the end of the reactions, which can be attributed to misfolded secondary structures, spurious synthesis errors, and/or stoichiometric concentration differences between the two DNA strands (Figure 2.2a and *Experimental* Figure

2.29).[47-48] We therefore included an adjustable parameter in the fits describing the concentration of inactive or "misfolded" H1 and H2 strands and assumed equal quantities of both.

Kinetics were assessed at 0.1eq of initiator at 25°C, and the calculated curves were in excellent agreement with the experimental data, giving us a high degree of confidence that this system follows an HCR mechanism (Figure 2.2d). The total amount of misfolded material was found to be 144 ± 5 nM, reducing the effective starting concentration of each hairpin from 750 nM to about 606 nM. The association rate constant (k1) was found to be 1·104 ± 1·103 M-1 s-1. This is slightly slower than reported in previous studies of hairpin-hairpin interactions, possibly due to the additional functional groups present in the H1-FL and H2-SH strands (Figure 2.2d and *Experimental* Figure 2.29).[49] We found that the ligation step was much faster than H1/H2 association, meaning that the rate of pro-functional molecule release is governed almost exclusively by k1. It was therefore not possible to extract a precise value for k2, though a lower bound of $\gtrsim$1·10-3 s-1 was obtained. Finally, the rate of the immolative cyclisation's (k3) was found to be 2.1·10-4 ± 3·10-5 s-1, making it the slowest step of the reaction. It is likely also the slowest step in templated HCR, as templation can accelerate HCR by two orders of magnitude.[30]

To showcase the versatility of our system to release different functional molecules we generated another H1 hairpin making (M) a camptothecin prodrug (H1-CT) (Figure 2.1a for structure and detailed synthesis in Section 2.5.6.). The amount of release from H1-CT, was monitored through native/denaturing agarose and HPLC analysis. Release was found to be comparable the H1-FL releasing 80-95% of the camptothecin prodrug (*Experimental* Figure 2.34 and Table 2.6).

Looking towards future applications of our system, we analyzed the release of small molecule from H1-FL in response to biologically relevant reducing conditions. We exposed H1-FL to both extracellular (0.01mM) and intracellular (1mM), levels of free thiols, in the form of DTT.[50] Release was monitored by fluorescence and HPLC analysis. Minimal release was found when H1-FL was exposed to extracellular levels of reducing agent over 24hrs, while intracellular levels of reducing agent cleaved the small molecule from H1-FL (*Experimental* Figure 2.35 and Table 2.7). Given the wealth of HCR sequences which respond to various extracellular signals through the

use of aptamers, we anticipate that our system could operate through extracellular recognition and release events followed by drug internalization.[35, 51-52] This may be a more viable method without the need to internalize the DNA component which is always a challenge for oligonucleotide therapeutics.[53]

2.3.2. Design, Synthesis and Characterization of DNA Templated HCR.

Having shown that we could indeed amplify the release of functional molecules using HCR, we then investigated whether both components could be integrated into a single nanodevice. Localized HCR has been recently shown to accelerate the rate of HCR on single stranded and DNA origami templates.[29-30] This strategy operates by anchoring the hairpins to a single scaffold, increasing their effective concentration. A major advantage of anchoring the hairpins is that a robust nanostructure is formed which is more desired for in vivo applications. However, the hairpins of the circuit in this previous strategy are all unique in sequence and required to be precisely placed on the scaffolds, hindering scalability. Additionally, the extent of polymerization was controlled by the size of the scaffold, and while this may be beneficial for creating defined circuits, limits amplification to the size of the scaffold. Another recent strategy to localize HCR has been to selectively recruit the HCR hairpins with a supramolecular scaffold, using a short reversible hybridization region.[54] In this case, the hairpins no longer needed to be precisely placed and the extent of polymerization was no longer confined to the template, however, this results in a weakly held construct that is more suited to in vitro than in vivo applications

Keeping these two strategies in mind, we developed a design that allows us to generate a robust structure with two hairpins anchored to a short DNA scaffold. This results in a two-hairpin monomer that can polymerize upon analyte recognition (Figure 2.3a). Using a design like this means that 1) HCR is not limited to the size of the scaffold, and 2) only two hairpins need to be precisely placed. To achieve this, our design makes some changes to the sequences of the original HCR system.

First, to avoid circuit leakage, we increased the stem length (S) of the hairpins from a 12 to an 18 b.p. hybridization region. Next we extended the 5' and 3' ends of the H1 and H2 hairpins to provide a hybridization region (A) that could then be used to hybridize to a DNA scaffold (B') via adapter strands S1 & S2 with sequence (A-B) (Figure 2.3a.). Sequence's B1 and B2 were designed to be two turns of DNA, orienting the hairpins on the scaffold in the same direction. Additionally, we added a spacer region (X) next to the loop region (L) of the hairpins as this had

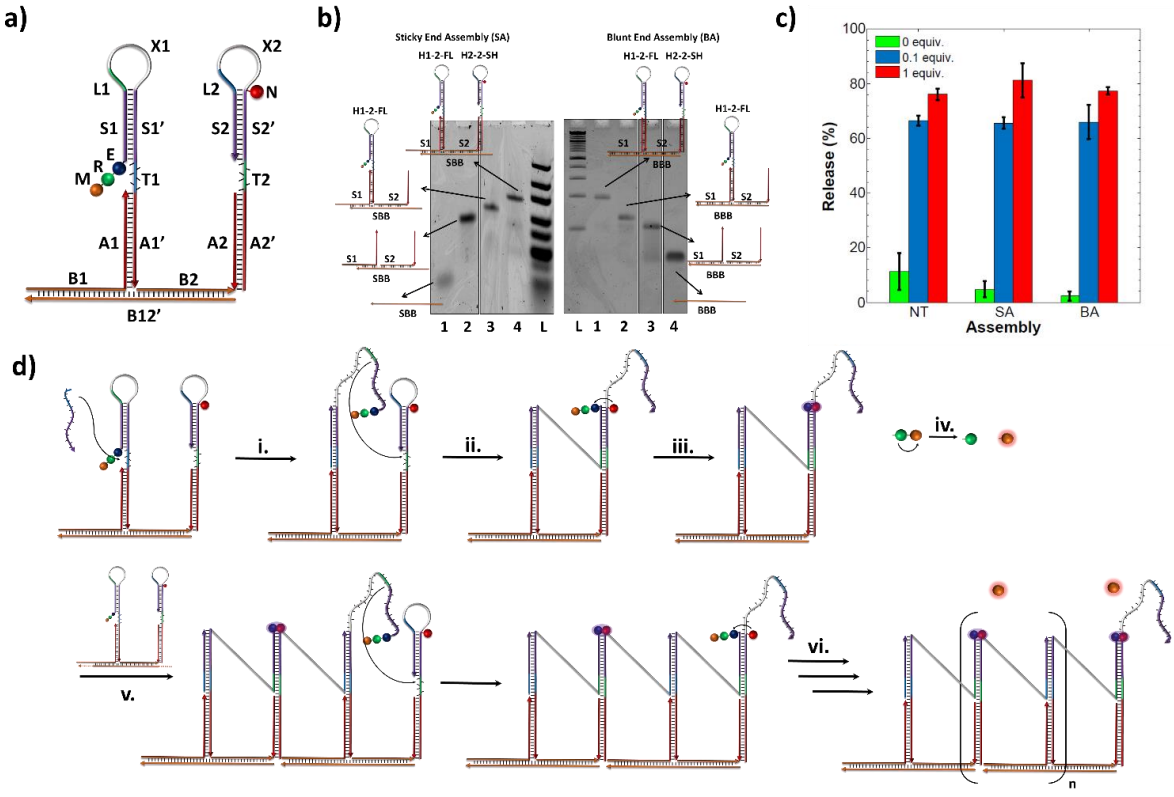

Figure 2. 3 Characterization of templated HCR

(a) Design of Blunt (BA) end assembly with H1-2-FL and H2-2-SH hairpins. (b) Native PAGE of the assembly of BA and SA. **(c)** Release of methoxyfluorescein from the HCR of H1-2-FL and H2-2-SH with 0, 0.1, and 1 equiv. of I-2, on No Template (NT), SA, and BA after 24hr, fluorescence was measured at λ_{ex}= 470 nm, λ_{em}= 515 nm. **(d)** Mechanism of HCR by the BA: i. Initiator hybridizes intermolecularly to T1 of H1-2-FL and performs a strand displacement, exposing the L1 region. ii. L1 hybridizes intramolecularly to T2 on H2-2-SH and performs a strand displacement to expose the L2 region. iii. a DNA templated reaction occurs releasing the pro-functional molecule connected to the immolative linker. iv. Degradation of the immolative linker to release the active functional molecule. v. L2 region hybridizes intermolecularly to the T1 region of another BA unit. vi. Polymerization continues, amplifying the release of active molecule

been shown previously to allow templated HCR to occur without steric constraints.[29] We calculated that, for our system, adding 11 T spacers was sufficient to allow the loop region of one hairpin unit to hybridize with the overhang region of the next hairpin unit, once initiated (Figure 2.3a).

Polymerization of the single unit occurs by an intermolecular initiation of H1 (Figure 2.3d-i) on the template followed by an intramolecular hybridization to H2 (Figure 2.3d-ii). Here, a nucleic acid templated reaction can occur, releasing the cargo (Figure 2.3d-iii). Additionally, H2 is available for an intermolecular hybridization to H1 on another unit, the whole process then repeats growing the polymer (Figure 2.3d-v and Figure 2.3d-vi).

For this design two types of DNA templates were generated for HCR, one with blunt ends on the template (BBB) and the other with short sticky ends (SBB) (Figure 2.3b). Inspired by the supramolecular scaffold method of localized HCR, we hypothesized that the short sticky ends could improve propagation of the HCR unit, by reversibly associating the individual units together, giving overall enhanced kinetics for release.

The modified hairpins were synthesized using the general procedure to generate H1-2-FL and H2-2-SH (Detailed in Section 2.5.6.). Before moving forward with the templated HCR, we first examined the effect of the changes made to H1-FL and H2-SH had on leakage and polymerization without using a template (NT). By increasing the stem (S) of these hairpins from 12 to 18 bps, the resulting leakage was ≤10% over 24hrs. Next, we introduced the hairpins to 1 equiv. (750nM) of initiator strand (I-2) and found that over 24 hrs, approximately 560 nM of the conjugate was released, representing a 75% yield over 3 steps. With 0.1 equiv. of initiator (75 nM) approximately 490 nM of the conjugate was released, indicating that amplification was once again achieved, and representing a 65% yield over 3 steps (Figure 2.3c). Analysis of the native agarose gel reveals that the polymerized species seem to have lower average molecular weight distributions (*Experimental* Figure 2.36a, lane NT-0.1), than the original counterparts (*Experimental* Figure 2.29c. lane 5). We suspect that with the changes made to the hairpins, the propagation rate of polymerization has been slowed down (H1 hybridizing to H2), while the initiator binding step is still rapid (I hybridizing to H1).

Confirming that HCR still works with these changes, we then moved on to generate the sticky (SA) and blunt (BA) ended assemblies. To make the assemblies we pre-annealed each of the hairpins separately for correct folding, and then hybridized them with each template at room temperature (Figure 2.3b, detailed in section 2.5.9.1). Control experiments without initiator showed the absence of non-specific reactivity between the H1-2-FL disulfide and the H2-2-SH thiol, as leakage was comparable to the non-templated hairpins (Figure 2.3c, and *Experimental* Figure 2.36-2.37 and Table 2.8). Upon adding 1 equiv. and 0.1 equiv. of initiator strand (I-2) to each of the assemblies, we found that the yields and amplification were maintained compared to the non-templated hairpins, 75% and 65% respectively, amplifying approximately 6.5x (Figure 2.3c).

Comparing the sticky and blunt ended assemblies when 1 equiv. of initiator is added (*Experimental* Figure 2.36.a. lanes SA-1 & BA-1), the blunt ended assemblies remain more defined and do not appear to polymerize as the sticky ended assemblies. We hypothesize that this is due to a combination of slow propagation and a pre-organization effect with the sticky ended assemblies. If, in solution the sticky ended assemblies are pre-organized, then when initiator is introduced instead of polymerizing uni-directionally, the polymerization can occur in two directions (*Experimental* Figure 2.38.a.). Statistically this can leave un-hybridized hairpins in the middle of the pre-organized polymer, which then can only hybridize intermolecularly. Indeed, when we look at the atomic force microscopy (AFM) of the sticky, and blunt ended assemblies and no template with 0.1equiv of initiator we find that there is more bundling of the sticky ended assemblies, than the blunt ended assemblies and no template, indicating increased intermolecular branching between units (*Experimental* Figure 2.38.b.-d.).

Ultimately, we found that the rate of release between the sticky and blunt ended assemblies and no template remained unchanged (*Experimental* Figure 2.37). This is consistent with remaining intermolecular hybridizations between units, and the slowest step being the immolative cyclization's to activate the fluorophore. Based on the native gel and AFM analysis we can infer that the intramolecular hybridizations do in fact occur faster than intermolecular hybridizations, however more detailed studies on strictly the rate of polymerization would be

needed to confirm. Overall, it was successfully established that we could in fact integrate a set of reactive hairpins into a single nanodevice, and selectively activate the amplified release of pro-functional small molecules in response to a DNA signal. Interestingly, the HCR process also results in a cross-linked and rigid polymeric nanostructure that is partially ligated, and the presence of this structure at e.g., the disease site could possibly contribute a therapeutic effect. This approach would be similar to enzyme-triggered peptide self-assembly, which has been shown to selectively kill cancer cells.[55]

2.3.3. Design, Synthesis and Characterization of Spherical Nucleic acid Templated HCR.

Having shown the integration of a pair of hairpins into a single device, we next wanted to investigate integrating multiple hairpins into a single nanodevice. Spherical nucleic acids have been extensively studied for their cellular uptake and nuclease resistance properties and provide us a 3D platform for templation of the HCR reaction.[56-58]

In our lab we have developed sequence controlled spherical nucleic acids that are made through the introduction of dodecane phosphoramidites, providing a hydrophobic block for self-assembly.[59-61] For our purposes here, we generated two amphiphilic nucleic acids with opposite directionalities using this method. Each of these strands is then able to hybridize to the overhang region (A) on the previously generated H1-2-FL and H2-2-SH hairpins, giving them the correct directionality for the HCR process to occur (Figure 2.4.a.). The assemblies were generated in a stepwise fashion by first generating the spherical nucleic acid and sequentially adding each hairpin (Figure 2.4b, detailed in Section 2.5.10.1). After the assemblies were generated, we found that there was minimal leakage (≤10%) of the system over 24hrs by HPLC, native/denaturing & fluorescence (Figure 2.4c. and *Experimental* Figures 2.39-2.41 and Table 2.9).

The amount of release was then monitored in response to 1 and 0.1equiv of initiator (I-2). Here we found that the yields were slightly improved from 75% to 82% for the 1equiv and from 66% to 74% for 0.1equiv of initiator, over three steps (Figure 2.4c.). Once again, we were able to amplify the signal of 75 nM by releasing 560 nM of methoxyfluorescein, giving us an overall amplification of approximately 7.5x. Additionally, we characterized the HCR polymerization by dynamic light scattering (DLS) and atomic force microscopy (AFM). By both techniques we observed that the particles clustered together when 1 or 0.1 equiv. of initiator

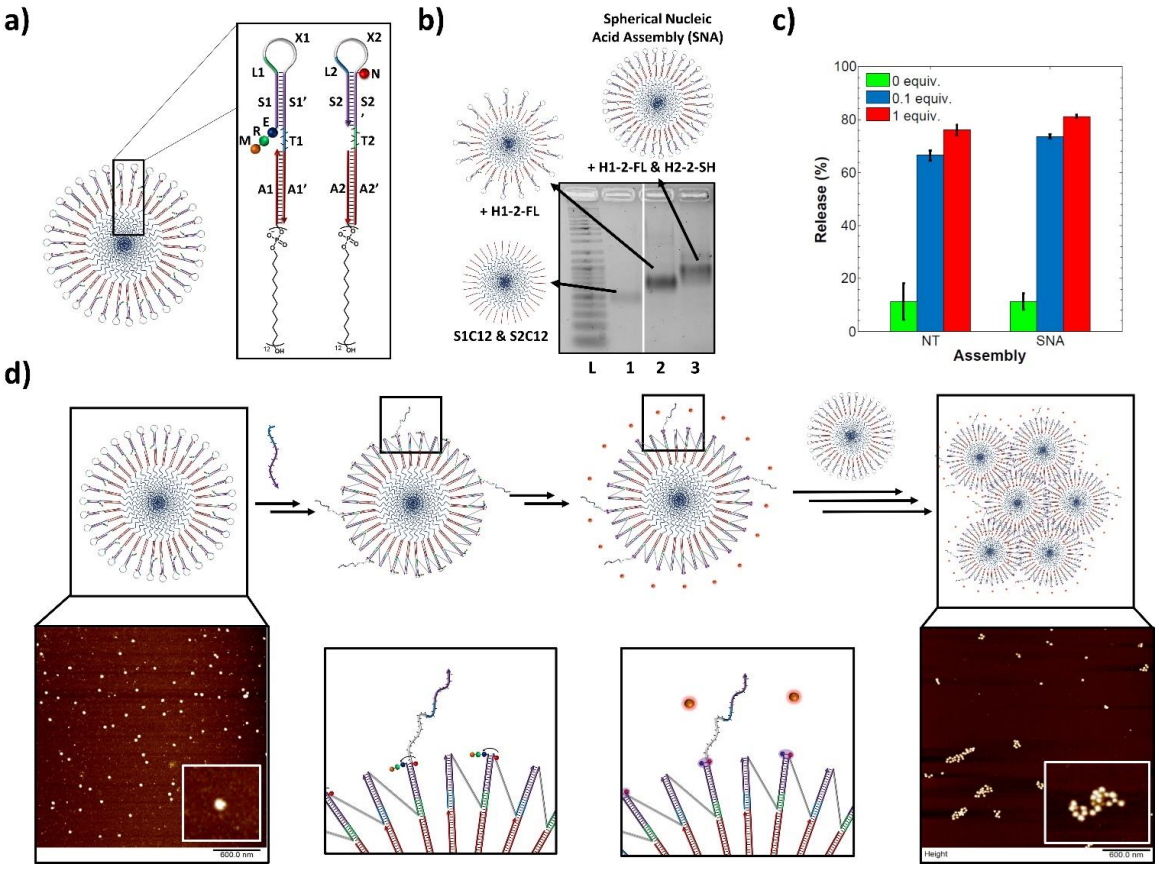

Figure 2. 4 Characterization of SNA templated HCR

(a) Design of Spherical nucleic acid (SNA) assemblies for HCR between H1-2-FL and H2-2-SH. **(b)** Native agarose of the SNA assembly. **(c)** Release of methoxyfluorescein from the HCR of H1-2-FL and H2-2-SH with 0, 0.1, and 1 equiv. of I-2, on No Template (NT) and SNA assembly after 24hr, fluorescence was measured at λ_{ex}= 470 nm, λ_{em}= 515 nm. (d) Mechanism and AFM characterization of the release of functional molecules from the SNA assembly, resulting in clustering of the SNA's.

strand was added, generating large aggregates of SNA's (Figure 2.4d and *Experimental* Figure 2.42). These changes in morphology in response to a low amount of DNA signal may be of further interest for future dynamic nanotechnology studies. In contrast to the approach in Fig. 2.3., the SNA carries multiple hairpins, rather than just two, and each SNA nanostructure can release a relatively large number of small molecules. Using spherical nucleic acids as the platform for HCR allows for localization of multiple HCR components in a single device and is more suited for future in vivo studies, where distribution of different components may differ.

2.3.4. Design # 2 Molecular Beacon Triggered SIP.

2.3.4.1. Design and Synthesis

In a traditional molecular beacon, the hairpin starts off with the stem closed, using a fluorophore and quencher in close proximity to each other at the 3' and 5' ends of the hairpin.[38] The fluorophore is non-emissive in this state, but upon recognition of the input strand, the hairpin opens up and these groups are separated, resulting in a fluorescent output. For our purposes, to use molecular beacons for the initiation of a SIP, two processes were required, 1) recognition of a trigger strand to *close* the molecular beacon and 2) a bond cleavage event after the hairpin closes to initiate the SIP.

We can address the first requirement, by reversing the traditional molecular beacon mechanism. Beginning with a double stranded DNA duplex between the molecular beacon (MB) and separating strand (S) which has a short overhang region (H) (Figure 2. 5a. & c.-i.), an input strand (I) can be introduced which hybridizes to (S), leaving a fully double stranded output and a new single stranded (MB) output (Figure 2. 5.c.ii.). (MB) can then rearrange back into a hairpin conformation (Figure 2.5c. iii.). For the second process, (MB) can be chemically modified with the SIP (P) at the 5' connected through a reactive linker (L). On the 3' end of (MB), the complementary reaction partner (T) can be introduced, which cleaves (L) once in close enough proximity after strand displacement (Figure 2. 5c.-iv.), initiating (P) (Figure 2. 5c-v.).

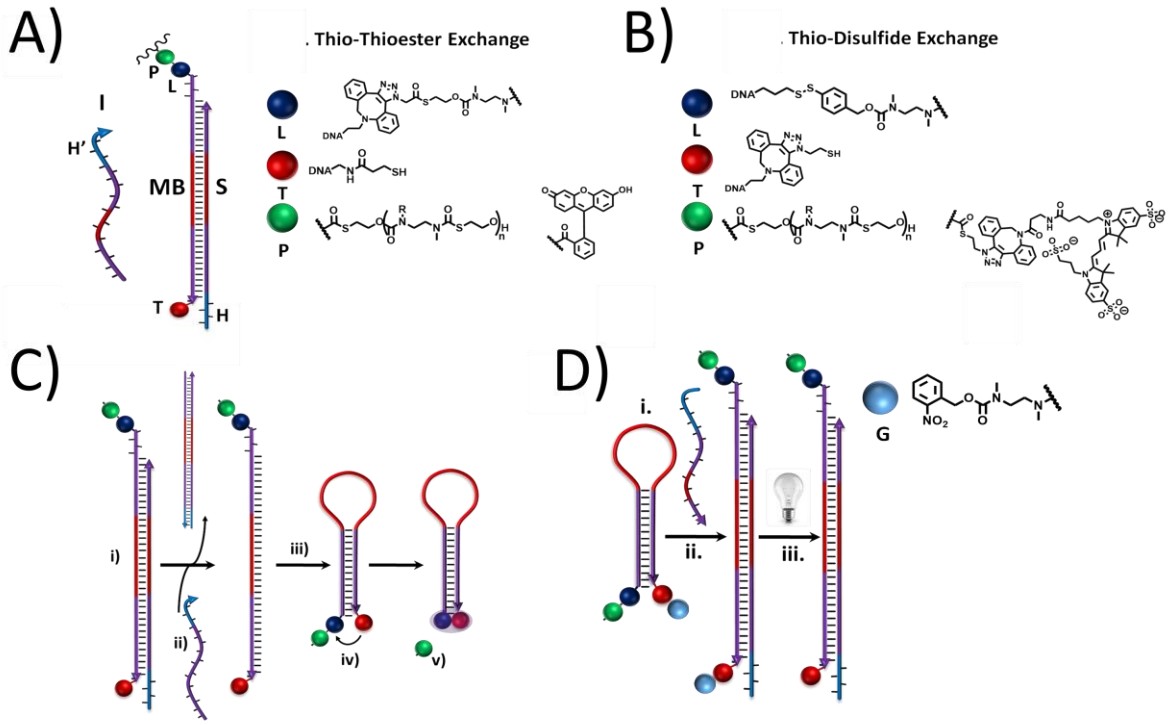

Figure 2. 5-Design and mechanism of strategy 2

(A) Design of the Molecular beacon device using either Thio-thioester exchange or **(B)** Thio-disulfide exchange for the release of the SIP or fluorophore (P) **(C)** Mechanism of the molecular beacon initiated self-immolative polymer i. double stranded molecular beacon keeping reactive groups separated ii. Initiator is introduced and (S) is displaced leaving the single stranded (MB) strand iii. (MB) rearranges back into a hairpin structure iv. DNA templated reaction occurs between (T) and (L) to release (P) v) if (P) is a self-immolative polymer, depolymerization occurs. **(D)** Protecting group strategy i. (T) is introduced into (MB) with the light cleavable protecting group (G) ii. (S) is added to separate reactive groups on (MB) iii. (T) is deprotected by the cleavage of (G) using light

This second requirement however poses a challenge, as reactive functional groups would need to be integrated into (MB) without prematurely reacting with one another. To address this, we devised a protecting group strategy, in which we could introduce (T) into (MB) with an orthogonal protecting group (G) (Figure 2. 5d.-i.). Once (G)(T) and (L)(P) had been introduced into (MB), strand (S) can hybridize and separate the reactive groups from one another (Figure 2. 5d.-ii.). After the reactive groups are separated from each other, (T) can be selectively deprotected, to generate the initial state of the device for the recognition of (I) (Figure 2. 5d.-iii.).

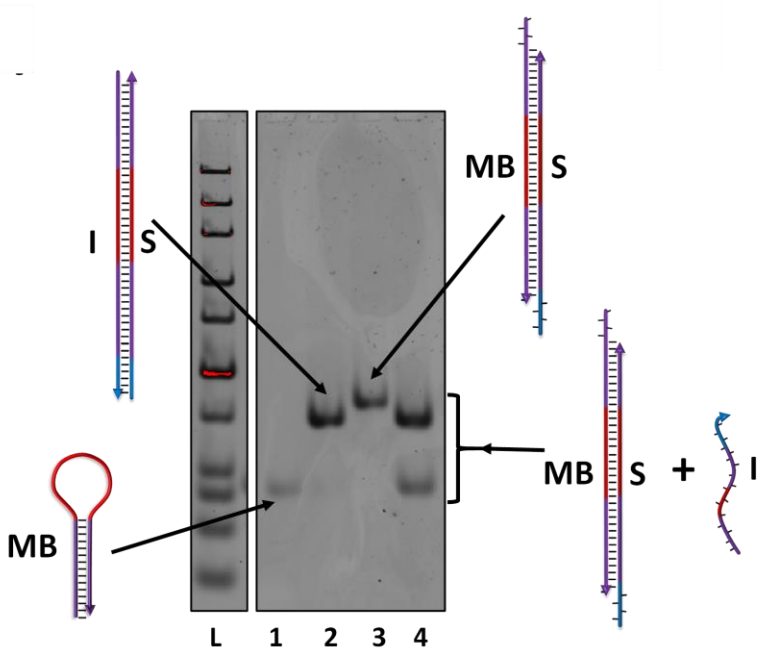

Figure 2. 6 Characterization of molecular beacon strand displacement by Native PAGE

Lane L: Ladder, Lane 1. (MB), Lane 2. (S) + (I), Lane 3. (MB)+(S), Lane 4. (MB)+(S) prehybridized, then (I) is added

As an initial test, we synthesized (MB), (S), and (I) without any modifications, to make sure the strand displacement mechanism would work properly (Figure 2.6). By native PAGE we found that hybridizing (MB) to (S), and then introducing (I), resulted in the proper strand displacement mechanism, releasing (MB) and generating a new (S):(I) duplex (Figure 2.6 lane 4.). Having shown that the strand displacement mechanism worked, we then turned our attention to the bond cleavage reaction.

2.3.4.2. Design # 2, Bond Cleavage Reaction Chemistry.

Initially, for the bond cleavage reaction we chose to use a thio-thioester exchange reaction (Figure 2. 5a.). Thio-thioester exchanges are well known for their use in native chemical ligation and have been used previously in DNA templated transfer reactions. Additionally, many orthogonal protecting groups exist for thiols, which was necessary so we could select the proper protecting group (G). Molecules (**4**) and (**10**) were designed to fit our purpose (Figure 2.7a.). (**4**) was designed to be the thiol functionality and was protected using a photo-labile protecting

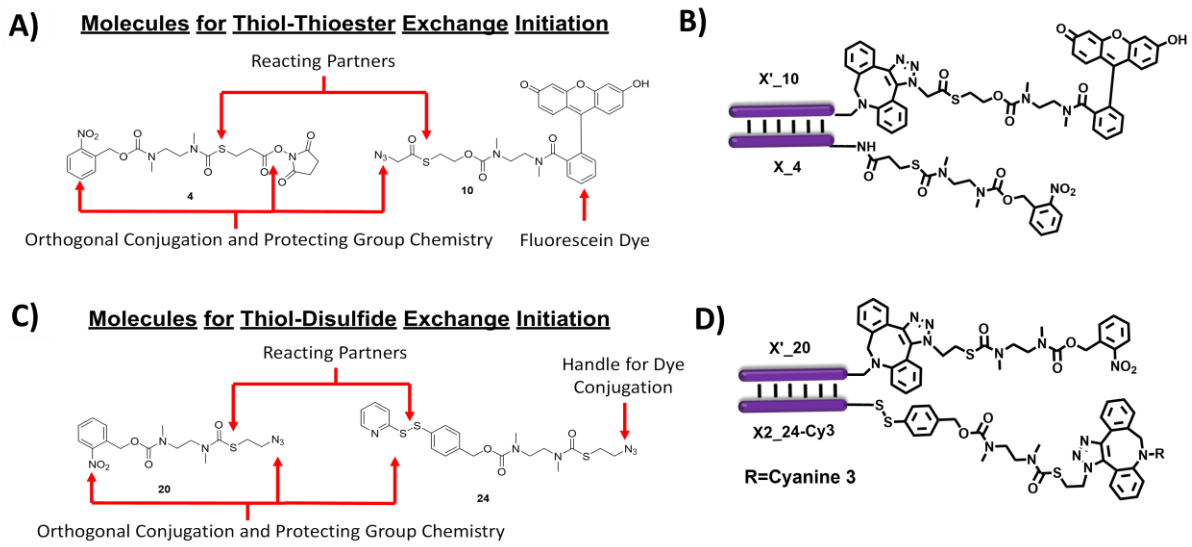

Figure 2. 7 Designs of the small molecules for conjugation to the molecular beacon and small molecule release.

A) & **B)** thiol-thioester approach. **C)** & **D)** Thiol-disulfide approach

group connected to a thiol using a carbamate linkage to mitigate hydrolytic cleavage. (**10**) was designed to have the thioester functionality to react with (**4**). For proof-of-principle, instead of synthesizing (**10**) as a SIP, we conjugated a fluorescent dye to the end of (**10**) to monitor release. Furthermore, to conjugate both (**4**) and (**10**) to (MB) these molecules had to have orthogonal conjugation chemistries. Therefore (**4**) was designed to react with (MB) through an NHS ester chemistry and (**10**) had an azide functionality incorporated to react in a SPAAC reaction. Both (**4**) and (**10**) were synthesized according to *Experimental* Figure 2.10 and Figure 2.11.

To only test the bond cleavage reaction, we first synthesized two separate strands (X) and (X'), with an amine on the 3' end of (X) and a DBCO modification on the 5' end of (X') (Table 2.1 for sequences). (**4**) and (**10**) were reacted with (X) and (X') to generate strands (X_4) and (X'_10) respectively. (Figure 2.7.b.) Products were analyzed by LC-MS (*Experimental* Figure 2.22). Unfortunately, the reaction yield for (X_4) was less than 15% presumably due to hydrolytic cleavage of the NHS ester. Moreover, while (X'_10) was generated, the thioester rapidly degraded (*Experimental* Figure 2.43). Some attempts were made to optimize these reactions,

however hydrolytic cleavage remained a persistent issue for both the NHS ester and thioester, and it was ultimately decided to modify the design of the small molecules.

Moving forward, (**20**) and (**24**) were designed to overcome some of the hydrolytic challenges associated with (**4**) and (**10**) (Figure 2.7c.). Instead of using a thioester exchange reaction, we decided to use a thiol-disulfide exchange for bond cleavage (Figure 2.12b.). In our new design (L) is a disulfide, which connects (P) to the molecular beacon, and (T) remains a thiol, which can react with (L), once in close proximity (Figure 2.12c.). The design of (**20**) remained relatively the same, still using a photo-labile group for protecting the thiol. To mitigate hydrolysis and improve yield, the conjugation chemistry of (**20**) was switched from an NHS-ester to an azide functionality. Switching the conjugation chemistry in (**20**) meant, that (**24**) could not use the same conjugation chemistry, and therefore its conjugation chemistry also had to be changed. (**24**) was designed to have a disulfide functionality, that would react with a thiol and release the SIP. We reasoned that since we had changed the bond cleavage chemistry to a thio-disulfide exchange, we could conjugate the (**24**) using the same type of chemistry to (MB), providing us with an orthogonal conjugation chemistry. Instead of directly integrating a dye into (**24**) to monitor bond cleavage, an azide functionality was installed to conjugate a dye in a second post-synthesis reaction. Both (**20**) and (**24**) were synthesized according to *Experimental* Figures 2.12 and Figure 2.13.

Again, to test only the bond cleavage reaction, two complementary, but separate strands were synthesized (X2) and (X') (Figure 2.7.d). (X2) had a disulfide modification at the 3' end, and there were no changes to (X'). (X2) was reacted with (**24**) in a disulfide exchange reaction, and (**20**) with (X') in a SPAAC reaction to make (X'_20) and (X2_24). Products of both reactions proceeded with good yields (80% & 90%) and were characterized by LC-MS (Figure 2.18). (X2_24) was then reacted with a DBCO-Cy3 small molecule, on the azide to generate (X2_24-Cy3) (Figure 2.7.d and Section 2.5.6.2 for conjugation procedure). Following the synthesis of these two strands, the DNA templated disulfide exchange was tested, to make sure the photo-labile group (G) could be removed and free the thiol. Since, in this initial test two separate strands were used, the templated reaction will result in a ligation product as well as cleavage of the dye from the

strand (Figure 2.8a.). Therefore, the reaction was monitored by denaturing PAGE and imaged under both the gel red and cy3 channels (Figure 2.8b.). Irradiating the strands with UV light for 60min resulted in a ligated product that was not fluorescent (35% yield) (Figure 2.8b. Lane 6). Since the ligated product is not fluorescent this indicates that the dye has been cleaved and that the ligated product is not due to non-specific thymine dimer formation.

To improve the yield of this reaction, the deprotection of the thiol using UV light was probed further. (X'_20) was exposed to UV light for different amounts of time and the products from the reaction were analyzed by HPLC and LC-MS (*Experimental* Figure 2.44). By these methods, 60min was enough time to fully cleave the photo-labile group (*Experimental* Figure 2.44). LC-MS analysis revealed the presence of the product expected from the cleavage of the

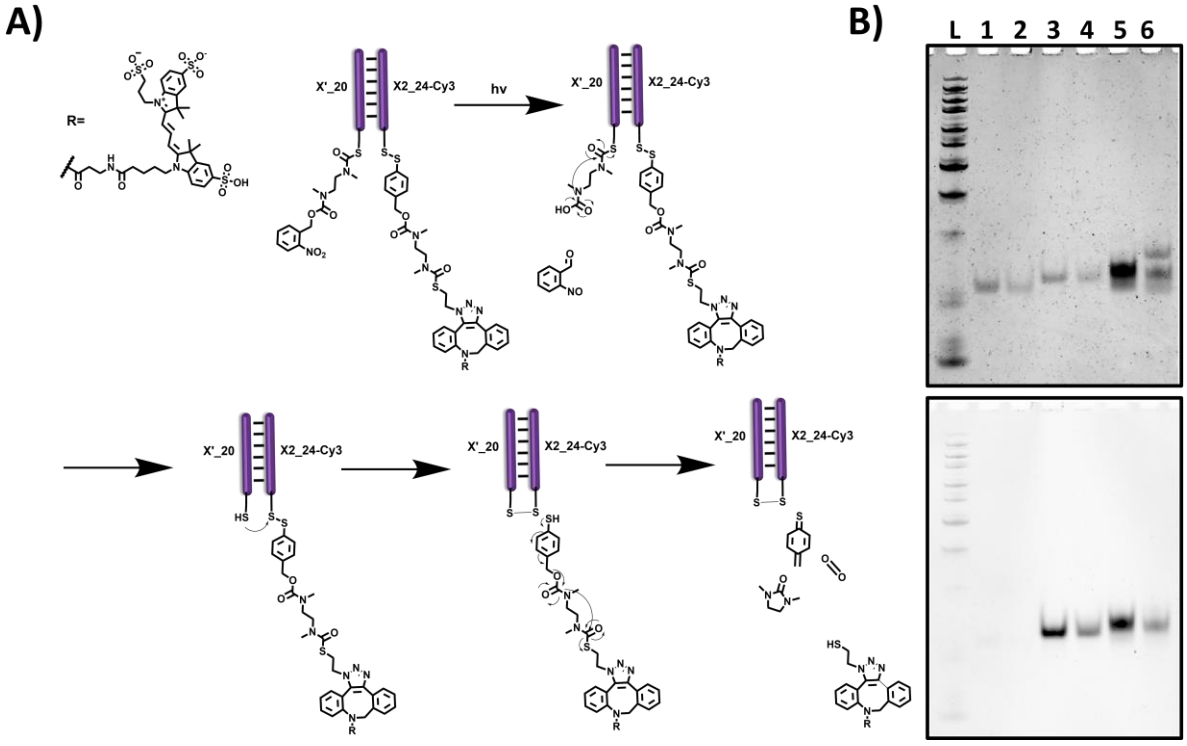

Figure 2. 8 Characterization of fluorophore release and ligation of X'_20 and X2_24-Cy3

(A) mechanism of release and ligation. i) light responsive protecting group is removed revealing a free thiol ii. DNA templated thio-diulfide exchange iii. (P) is released and if it is a SIP can depolymerize. **(B)** denaturing PAGE gel red channel (top) cy3 channel (bottom). Irradiation was done for 60min at 320nm (50uL 3uM) and denoted as "hv". Lane L. Ladder, Lane 1: X2_20, Lane 2: X2_20 + hv, Lane 3: X'_24-Cy3, Lane 4: X'_24-Cy3 + hv, Lane 5: X2_20 + X'_24-Cy3, Lane 6: X2_20 + X'_24-Cy3 + hv

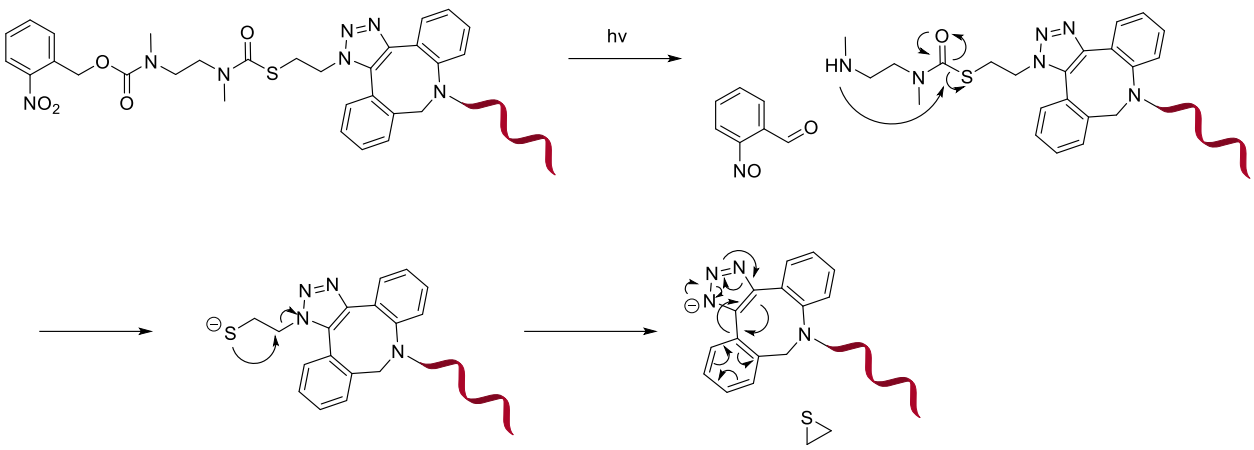

Figure 2. 9 Proposed mechanism for the degradation and loss of ethylene sulfide.

photo-labile group; however, the thiol product was not observed, and a further degradation product was also revealed (*Experimental* Figure 2.45). This degradation product is in line with the loss of ethylene sulfide after the cleavage of the photo-labile group the immolative cyclizations occur. Here, the triazole linkage formed from the SPAAC reaction, acts as a leaving group in the formation of ethylene sulfide (Figure 2.9). It is suspected that the formation of ethylene sulfide is fast, and once formed there is no thiol available to react with the disulfide on the other strand, which effects the overall yield.

To continue using the molecular beacon approach in generating a standalone amplifying, drug release device, the conjugation chemistry of (**20**) would have to be changed, to avoid the ethylene sulfide formation. Although, as conjugation of each small molecule species needs to remain orthogonal, the options are limited for changes to the design.

2.4. Conclusion

In this chapter we have developed a new standalone drug release device which responds to molecular recognition of biological stimuli and amplifies small molecule release. The first approach described demonstrates, that by rationally placing disulfide and thiol functionalities on opposite hairpins of HCR we can amplify a DNA signal to selectively release small molecules. This is the first time HCR has been used for the triggered release of small molecules which can be

monitored in three ways 1) by the degree of monomer consumption, 2) by the degree of ligation and 3) by fluorescence intensity. Unlike previous HCR methods where small molecule cleavage is non-specific, our construct is built to only carry out reactions in the presence of an initiator, significantly decreasing non-specific cargo release. Our synthetic approach can also be applied to other DNA toehold-mediated amplification processes, such as CHA. Additionally, we were able to take advantage of the metastability of the HCR hairpins and integrate both reactive hairpins into single unit nanodevices. We used both DNA and SNA assemblies which, importantly, were able to separate reactive functional groups and isolate reactivity, preventing release, and amplify release when triggered. The nanostructures not only release small molecules, but in addition conditionally generate a partially ligated, crosslinked DNA polymer, which could have added therapeutic effects, in analogy to enzyme-driven peptide assembly. Given the abundance of DNA templated reactions and different HCR sequences, future work will focus on increasing sensitivity and accelerating the kinetics and adapting this method for in vitro/vivo release applications. Our second approach was to use a molecular beacon coupled to a self-immolative polymer to build this device. This approach is quite synthetic challenging, integrating reactive species onto a single oligonucleotide is non-trivial. However, carefully re-designing the conjugation and protecting group chemistry should allow this approach to be used to its full potential.

This chapter looked at oligonucleotide conjugates for conditional small molecule delivery. The molecular recognition properties of oligonucleotides were taken advantage of to selectively release fluorophore and drug molecules upon recognition of the correct DNA sequence. Moreover, using oligonucleotides as a structural building material allowed for us to spatially isolate reactive functional groups on DNA templates and SNA's, integrating all components into a single device. Chemically modifying oligonucleotides was key to generating the small molecule output upon recognition as well as generating the structural templates for component integration. In the next chapter we will explore using chemically modified oligonucleotides as therapeutics and structural building blocks, in the form of stimuli responsive SNAs for antisense oligonucleotide delivery.

2.5. Experimental Section

2.5.1. General

Unless otherwise stated, all commercial reagents and solvents were used without additional purification. Magnesium sulfate hexahydrate (MgSO4·6H2O), tris(hydroxymethyl)aminomethane (Tris), urea, chloroform (CHCl3), hexane (Hex), tetrahydrofurane (THF), dimethyl sulfoxide (DMSO), hydrochloric acid (HCl), sodium hydroxide (NaOH), dichloromethane (CH_2Cl_2), ethyl acetate (ETOAc), ethanol (EtOH), fluorescein, methyl iodide, sodium bicarbonate ($NaHCO_3$), sodium chloride (NaCl), triphosgene, triethylamine, trifluoroacetic acid (TFA), 4-nitrophenyl chloroformate, camptothecin, dimethyl amino pyridine (DMAP), 2, 2'-dithiodipyridine, 1-hexanethiol, N-hydroxysuccinimide, tosyl chloride, 2-Nitrobenzyl alcohol, 4-mercaptobenzoic acid and N,N'-Dicycolhexylcarbodiimide were used as purchased from Sigma-Aldrich. Acetic acid and boric acid were purchased from Fisher Scientific and used without further purification. GelRed™ nucleic acid stain and Sybr Gold were purchased from Biotium Inc. Acetone ACS reagent grade was purchased from Fisher. 5K dialysis tubing was purchased from Fischer Scientific. Acrylamide/Bis-acrylamide (40% 19:1 solution), ammonium persulfate and tetramethylenediamine were obtained from Bioshop Canada Inc. and used as supplied. 1 μmol Universal 1000Å LCAACPG supports and standard reagents used for automated DNA synthesis were purchased through Bioautomation. Sephadex G-25 (super fine, DNA grade) was purchased from Glen Research. Analytical thin layer chromatography (TLC) was performed on TLC plates purchased from Sigma-Aldrich. 1xTAMg buffer is composed of 45 mM Tris and 12.5 mM MgCl2.6H2O with the pH adjusted to 8.0 using glacial acetic acid. TBE buffer is 90 mM Tris, 90 mM boric acid and 2 mM EDTA with a pH of 8.0. TEAA mobile phase is 50 mM triethylammonium acetate with the pH adjusted to 8.0 using glacial acetic acid. 1xPBS buffer is 137 mM NaCl, 2.7 mM KCl, 8 mM Na_2HPO_4, and 2 mM KH_2PO_4 adjusted to pH 8.0 with NaOH. 50x ALK buffer is composed of 1.5M NaOH and 50mM EDTA.

2.5.2. Instrumentation

Standard oligonucleotide synthesis was performed on solid supports using a Mermade MM6 synthesizer from Bioautomation. HPLC purification was carried out on an Agilent Infinity 1260. UV absorbance DNA quantification measurements were performed with a NanoDrop Lite spectrophotometer from Thermo Scientific. For structure assembly, Eppendorf Mastercycler 96-well thermocycler and Bio-Rad T100TM thermal cycler were used to anneal all structures and hairpins. Polyacrylamide gel electrophoresis (PAGE) was performed using 20x20 cm vertical Hoefer 600 electrophoresis units. Agarose Gel Electrophoresis (AGE) was performed on Owl Mini and Owl EasyCast horizontal gel systems. Gels were imaged by a BioRad ChemiDoc MP system. Fluorescence data were measured by a BioTek Cytation 5 imaging reader Reader. Multimode 8 scanning probe microscope and Nanoscope V controller (Bruker, Santa Barbara, CA) was used to acquire AFM images. DynaPro (model MS) molecularsizing instrument was used to measure the particle size distributions. Liquid Chromatography Electrospray Ionization Mass Spectrometry (LC-ESI-MS) was carried out using a Bruker MaXis Impact™. Column chromatography to purify organic compounds was performed on a CombiFlash® Rf + system with RediSep® Silica columns (230-400 mesh) using a proper eluent system. 1H NMR and 13C was recorded on 500 MHz AV500 equipped with a 60 position SampleXpress sample changer (Bruker) and 300 MHz Varian Mercury equipped with an SMS-100 sample changer (Agilent). Visualization of TLC was achieved by UV light (254 nm). Chemical shifts were quoted in parts per million (ppM) referenced to the appropriate residual solvent peak or 0.0 ppm for tetramethylsilane. Abbreviations for 1H NMR: s = singlet, d = doublet, t = triplet, q = quartet, quint = quintet, m = multiplet. High-resolution mass spectra were obtained from Exactive Plus Orbitrap Mass Spectrometer (Thermo Scientific).

2.5.3. Solid Phase Synthesis & Purification of DNA

2.5.3.1. Synthesis

DNA synthesis was performed on a 1 µmole scale, starting from the required nucleotide modified 1000 Å LCAA-CPG solid-support. Coupling efficiency was monitored after removal of the dimethoxytrityl (DMT) 5'-OH protecting groups. DMT-dodecane-diol (cat.# CLP-1114), Fmoc-

Amino-DMT C-3 CED phosphoramidites (cat.# CLP-1661), and dC (cat.# ANP-4675), dT (cat.# ANP-4674), and dA (cat.# ANP-4671) reverse phosphoramidites were purchased from ChemGenes. Thiol modifier C6 SS phosphoramidites (cat. # 148254-21-1) were purchased from Glen Research. Coupling efficiency was monitored by the removal of DMT group on 5'-OH groups. In a glove box under nitrogen atmosphere, DMT-dodecane-diol, Thiol modifier C6 SS, 5'-DBCO-TEG phosphoramidite and Fmoc-Amino-DMT C-3 CED were dissolved in acetonitrile and shaken for 10 mins to achieve final concentration of 0.1 M. The DMT-dodecanediol amidite was activated with 0.25M 5-(ethylthio)tetrazole in anhydrous acetonitrile and the extended coupling times of 5 minutes were used. The amino modifier amidite, DBCO amidite and disulfide amidite were activated by 0.25M 5-(ethylthio)tetrazole in anhydrous acetonitrile but the coupling was performed manually inside the glove box. 3% dichloroacetic acid in dichloromethane was used to remove DMT protecting group on the DNA synthesizer. The reverse phosphoramidites for strand S2 were loaded onto a Mermade MM6 synthesizer from Bioautomation for its synthesis.

2.5.3.2. Deprotection

For unmodified DNA, DNA modified with dodecanediol, and DNA modified with reverse phosphoramidites, after the synthesis was complete the CPG was treated with 28% aqueous ammonium hydroxide solution for 16-18 hours at 60^{o}C in water bath. For disulfide modified DNA, the CPG was treated with 28% aqueous ammonium hydroxide solution for 36-48 hours at r.t. H2 and H2-2 Fmoc-amino modified DNA was not deprotected right away and reacted following procedure (SI-VI b.).

2.5.3.3. Purification

The crude mixtures were then concentrated under reduced pressure at 60^{o}C, suspended 1:1 8 M urea before loading to polyacrylamide/urea gel (12% or 15% denaturing PAGE). The gel was run at 250 V for 30 minutes followed by 500 V for 45-60 minutes in 1x TBE as the running buffer. The gel was then imaged and excised on TLC plate under a UV lamp. The solution was dried to

approximately 1 mL before loading to Sephadex G-25 column. The purified DNA was quantified by the absorbance at 260 nm.

2.5.4. DNA Sequences

Table 2. 1 Sequences used for DNA Conjugates.

(D =DMT-dodecane-diol), (Bold represents reverse phosphoramidites), (FmocNH = Fmoc-Amino-DMT C-3 CED phosphoramidite), (SS = Thiol modifier C6 SS phosphoramidite), (DBCO = 5'-DBCO-TEG Phosphoramidite).

Name	Sequences (From 5' to 3')
MB	TCT TGG ACA CAG TAA AGA GAG GTG CGC CCA TTG TGT CCA AGA
S	GTT TAA CCT CTT GGA CAC AAT GGG CGC ACC TCT CTT T
I-0	AAA GAG AGG TGC GCC CAT TGT GTC CAA GAA GTT AAA C
X	TAT ATG GTC AAC TGA AAA A **(FmocNH)**
X'	**(DBCO)** TTT TTC AGT TGA CCA TAT A
X2	TAT ATG GTC AAC TGA AAA A-**SS**
H1	GGA ATT GGG AGT AAG GGC TGT GAT GCC CTT ACT CCC-**SS**
H2[a]	GCC CTT ACT CCC AAT TCC **(FmocNH)** GGG AGT AAG GGC ATC ACA
I-1	GCC CTT ACT CCC AAT TCC
H1-2	**SS**-AGT CTA GGA TTC GGC GTG GGT TAA TTT TTT TTT TTC ACG CCG AAT CCT AGA CTA CTT TGG GAG GAG GAG AAG GAG AGG AGA GA
H2-2[a]	GAA GTG AAG AAG AAG AAA GAG AAG TTA ACC CAC GCC GAA TCC TAG ACT **(FmocNH)** TTT TTT TTT TTC AAA GTA GTC TAG GAT TCG GCG TG
I-2	TTA ACC CAC GCC GAA TCC TAG ACT

S1	CGC CGC ACT GCG GTC CGA TAG TCT CTC CTC TCC TTC TCC TCC TCC
S2	GCG GAT TGC ATC AAT GTT TAG **CTT CAC TTC TTC TTC TTT CTC TTC**
BBB	CTA AAC ATT GAT GCA ATC CGC TCT ATC GGA CCG CAG TGC GGC G
SBB	TGC GGC GTC TAA ACA TTG ATG CAA TCC GCT CTA TCG GAC CGC AG
S1C12	DDD DDD DDD DDD TCT CTC CTC TCC TTC TCC TCC TCC
S2C12	CTT CTC TTT CTT CTT CTT CAC TTC DDD DDD DDD DDD
H1-C	**SS**-GGG AGT AAG GGC ATC ACA GCC CTT ACT CCC AAT TCC

[a] Not cleaved from the solid support and reacted following procedure (SI-VI b.)

2.5.5. Small Molecule Synthesis & Characterization

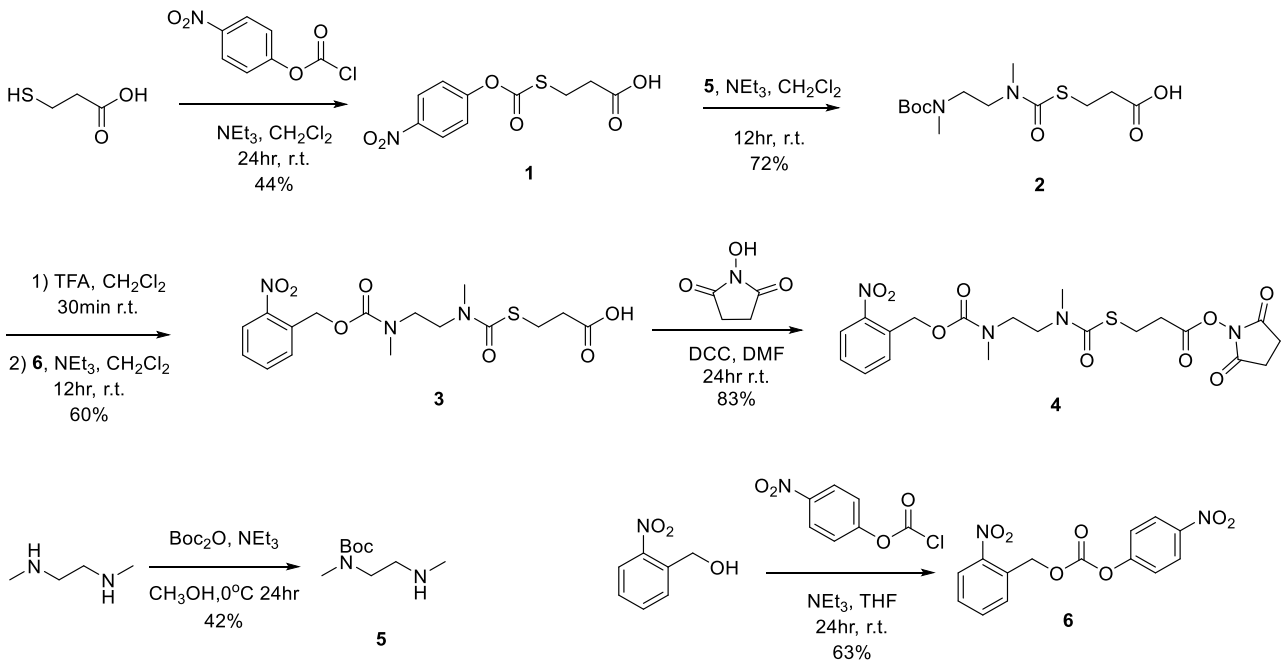

Compound's **5**[62] and **6**[63] were synthesized according to literature protocols.

Figure 2. 10 Synthetic route to generate compound 4

Synthesis of Compound 1

3-mercaptopropionic acid (4g, 38mmol) was dissolved in CH_2Cl_2 (50mL) and NEt_3 (8.2g, 45mmol) was then added. The solution was then cooled to 0°C and p-nitrophenylchloroformate (9.1g, 45mmol) was added and the solution was allowed to react for 24hr at room temperature. Following this, the reaction was extracted with 3 x 1M HCl (75mL) and brine (75mL). The organic phase was dried with $MgSO_4$, filtered and concentrated *in vacuo.* The crude mixture was then adsorbed to celite for purification by column chromatography (3 column volumes 100% EtOAc with 1%NEt_3, then 5:3:2 Hex/Tol/EtOAc with 1%AA) providing compound **1**, as a clear oil (4.5g, 44% yield). %). ^{1}H NMR (500MHz, $CDCl_3$): δ = 2.85 (t, 2H), 3.20 (t, 2H), 7.34 (m, 2H), 8.30 (m, 2H). HRMS (EI): calc. for $[C_{10}H_9O_6NS]^+$ $[M]^+$: 271.02, found 272.0243.

Synthesis of Compound 2

To a solution of compound **1** (3.5g, 13mmol), in CH_2Cl_2 (40mL), a mixture of **5** (2.6g, 13.5mmol)**,** and NEt_3 (2.6g, 14.2mmol) in CH_2Cl_2 (40mL), was added dropwise over 30min at room temperature. The mixture was stirred overnight and then extracted with 3 x 1M HCl (50mL) and the organic phase dried with $MgSO_4$, filtered and concentrated *in vacuo*. The resulting powder was then purified by column chromatography (Hex/EtOAc 8:2 with 1% AA) to provide compound **2** (3g, 72% yield) as a white powder. ^{1}H NMR (500MHz, $CDCl_3$): δ = 1.44 (s, 9H), 2.75 (m, 2H), 2.85 (m, 3H), 2.95 (m, 3H), 3.13 (m, 2H), 3.50 (m, 4H), 10.50 (BS, 1H). HRMS (EI): calc. for $[C_{13}H_{24}O_5N_2S]^+$ $[M]^+$: 320.14, found 320.1456.

Synthesis of Compound 3

First, to a solution of **2** (906mg, 2.83mmol) in CH_2Cl_2 (15mL) was the dropwise addition of TFA (5mL). The reaction mixture was stirred for 30 min and the CH_2Cl_2 was then evaporated. The solution was re-suspended in CH_2Cl_2 (20mL) and evaporated twice more, to remove any TFA, leaving Compound **2** as the TFA salt, which was redisolve in DMF (10mL) and used directly. Next, a solution of **6** (1g, 3.14mmol) and NEt_3 (3.4g, 18.8mmol) was prepared in DMF (10mL). To this, the solution of **2** was added and the resulting mixture was reacted overnight at room temperature. The mixture was then diluted with EtOAc (50mL) and washed with 2 x 1M HCl

(50mL) and brine (50mL). The organic phase was then dried on $MgSO_4$, filtered and concentrated *in vacuo* to give the crude mixture. The crude mixture was then purified by column chromatography (1:1 Hex/EtOAc 1%AA) to give the pure compound **3** as a white solid (752mg, 60% yield) ^{1}H NMR (500MHz, $CDCl_3$): δ = 2.50 (m, 2H), 2.75 (m, 6H), 2.84 (m, 2H), 3.24 (m, 4H), 5.31 (s, 2H), 7.35 (m, 3H), 7.84 (m, 1H), 10.36 (bs, 1H). HRMS (EI): calc. for $[C_{16}H_{21}O_7N_3S]^+$ $[M]^+$: 399.11, found 399.1202.

Synthesis of Compound 4

Compound **3** (520mg, 1.30mmol), and N-hydroxysuccinimide (165mg, 1.43mmol), were first dissolved in CH_2Cl_2 (20mL). To this was added EDC·HCl (275mg, 1.43mmol) and the resultant mixture was allowed to react for 24hr at room temperature. The mixture was then washed with saturated $NaHCO_3$ (50 mL), and saturated NaCl (50 mL). The organic phase was dried on $MgSO_4$, filtered, concentrated *in vacuo* and the crude product was purified by column chromatography (7:3 EtOAc/Hex) to give compound **4** (534mg, 83% yield) as a white solid. ^{1}H NMR (500MHz, $CDCl_3$): δ = 2.87 (s, 4H), 2.98 (m, 8H), 3.15 (m, 2H), 3.5 (m, 4H), 5.50 (s, 2H), 7.56 (m, 3H), 8.11 (m, 1H). HRMS (EI): calc. for $[C_{20}H_{24}O_9N_4S]^+$ $[M]^+$: 496.49, found 497.4972.

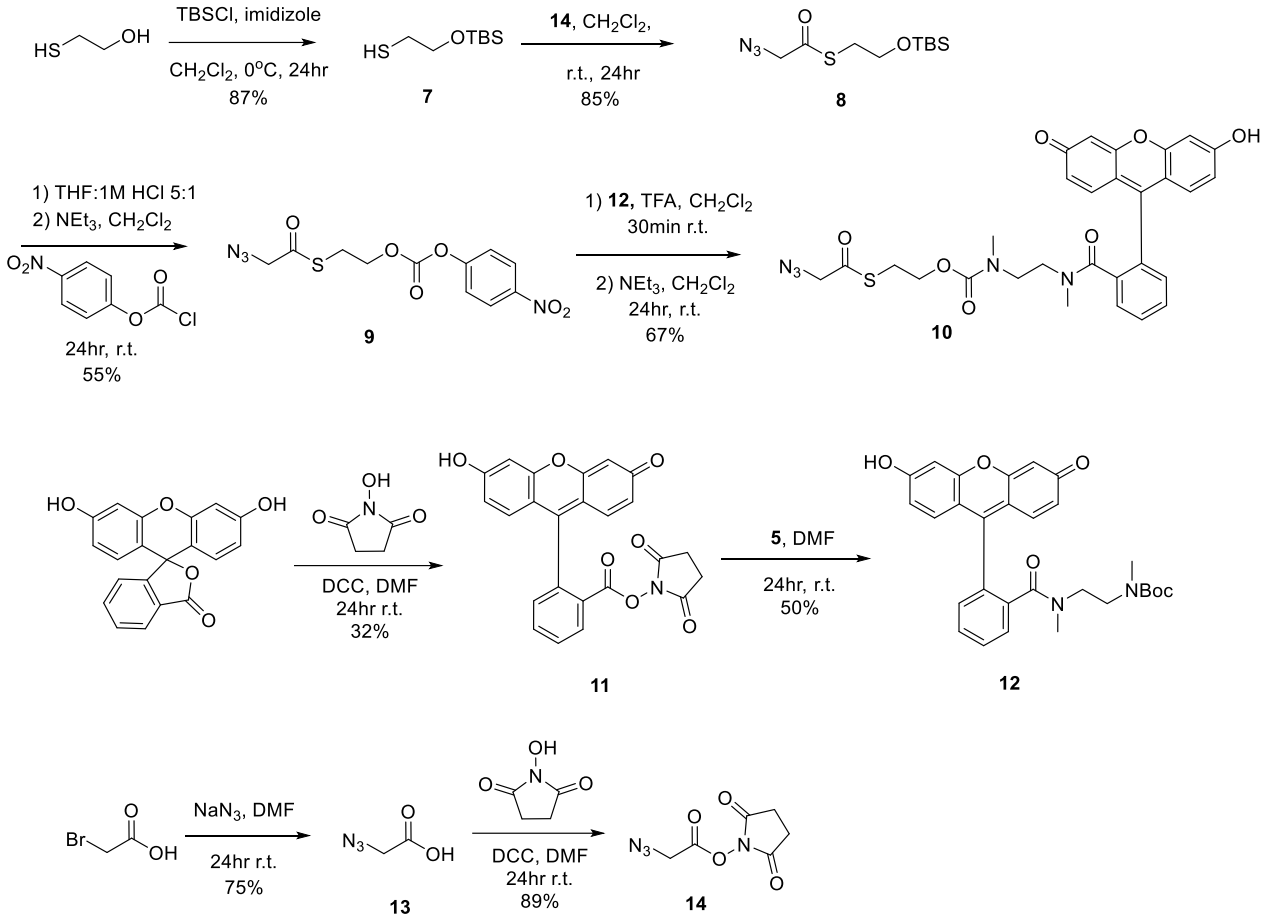

Compounds **7**[64]**, 11**[65]**, 13** and **14**[66] were synthesized according to literature protocols.

Figure 2. 11 Synthetic route to generate compound 10

Synthesis of Compound 8

Compound **7** (1g, 5.2mmol) was dissolved in CH_2Cl_2 (25mL). To this, compound **14** (1.13g, 5.7mmol) was added, and the mixture allowed to react for 24hr at room temperature. After reacting, the solution was washed with 1M HCl (50mL), saturated $NaHCO_3$ (50 mL), and saturated NaCl (50 mL). The organic phase was dried on $MgSO_4$, filtered and concentrated *in vacuo.* The crude material was purified by column chromatography (100% Hex) to give compound **8** (1.2g, 85% yield) ^{1}H NMR (500MHz, $CDCl_3$): δ = 0.08 (s, 6H), 0.90 (s, 9H), 3.13 (t, 2H), 3.76 (t, 2H), 4.02 (s, 2H). HRMS (EI): calc. for $[C_{10}H_{21}O_2N_3SSi]^+$ $[M]^+$: 275.11, found 275.1276.

Synthesis of Compound 9

In a first step compound **8** (1g, 3.63mmol), was dissolved in THF (25mL) and 1M HCl (5mL) was added. The reaction mixture was monitored by TLC, until all starting material had been deprotected (approx. 2hr). The mixture was then diluted with CH_2Cl_2 (50mL) and H_2O (50mL) and extracted 3x with CH_2Cl_2 (20mL). The organic phase was combined and concentrated down to 20mL to give the alcohol of compound **8**, which was used directly. In a separate round bottom flask, p-nitrophenylchloroformate (1.54g, 9.62mmol) and NEt_3 (1.74g, 9.62mmol) were dissolved in CH_2Cl_2 (50mL), and the solution of compound **8,** was added to this. The mixture was allowed to react 24hr at room temperature followed by washing it with 1M HCl (50mL), saturated $NaHCO_3$ (50 mL), and saturated NaCl (50 mL). The organic phase was then dried on $MgSO_4$, filtered and concentrated *in vacuo*. The crude product was then purified by column chromatography (9:1 Hex/EtOAc) to give the pure compound **9** (652mg, 55% yield over 2 steps). ^{1}H NMR (500MHz, $CDCl_3$): δ = 3.24 (t, 2H), 4.04 (s, 2H), 4.42 (t, 2H), 7.34 (m, 2H), 8.27 (m, 2H). HRMS (EI): calc. for $[C_{11}H_{10}O_6N_4S]^+$ $[M]^+$: 326.03, found 326.0342.

Synthesis of Compound 10

First, to a solution of **12** (340mg, 0.67mmol) in CH_2Cl_2 (10mL) was the dropwise addition of TFA (10mL). The reaction mixture was stirred for 30 min and the CH_2Cl_2 was then evaporated. The solution was re-suspended in CH_2Cl_2 (20mL) and evaporated twice more, to remove any TFA, leaving Compound **12** as the TFA salt, which was redisolve in CH_2Cl_2 (10mL) and used directly. Next, a solution of **9** (220mg, 0.67mmol) and NEt_3 (728mg, 4.02mmol) was prepared in CH_2Cl_2 (10mL). To this, the solution of **12** was added and the resulting mixture was reacted overnight at room temperature. The crude mixture was concentrated *in vacuo* and purified directly by column chromatography (from 100% EtOAc, to 9:1 EtOAc/MeOH to 6:4 EtOAc/MeOH) to give the pure compound **10** (265mg, 67% yield) ^{1}H NMR (500MHz, DMSO D_6): δ = 2.62 (m, 4H), 2.79 (m, 2H), 2.85 (m, 3H), 3.14 (m, 3H), 4.12 (s, 2H), 4.24 (t, 2H), 6.51 (m, 4H), 6.90 (m, 2H), 7.43 (m, 2H), 7.67 (m, 2H). HRMS (EI): calc. for $[C_{29}H_{27}O_7N_5S]^+$ $[M]^+$: 589.16, found 587.1705.

Synthesis of Compound 12

Compound **11** (2.3g, 5.23mmol), was dissolved in DMF (15mL). Compound **5** (1.2g, 6.30mmol) was then added to this mixture and allowed to react overnight at room temperature. The crude mixture was then concentrated in vacuo and purified by column chromatography (9:1 EtOAc/MeOH) to give compound **12** as an orange solid (1.3g, 50% yield). ^{1}H NMR (500MHz, DMSO D_6): δ = 1.29 (s, 9H), 2.48 (m, 4H), 2.71 (m, 3H), 3.24 (m, 3H), 6.50 (m, 4H), 6.94 (m, 2H), 7.47 (m, 2H), 7.67 (m,2H). HRMS (EI): calc. for $[C_{29}H_{30}O_6N_2S]^+$ $[M]^+$: 502.21, found 503.2204.

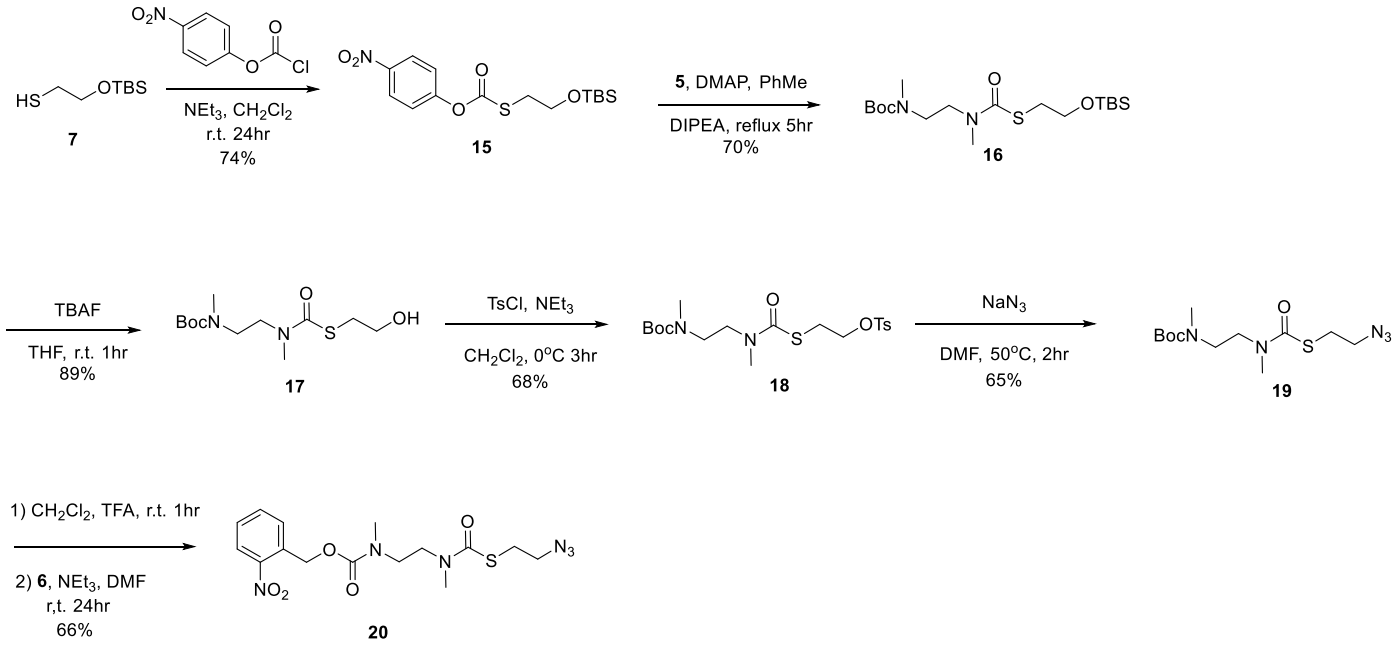

Figure 2. 12 Synthetic route to generate compound 20

Synthesis of Compound 15

To a solution of **7** (10g, 52mmol), in CH_2Cl_2 (150mL) was added NEt_3 (18g, 104mmol) and para-nitro phenyl chloroformate (21g, 104mmol). The reaction was allowed to proceed for 24hr at room temperature. The reaction was then washed with 3 x 1M HCl (100mL), the organic phase dried on $MgSO_4$, filtered and concentrated *in vacuo*. The crude mixture was purified by column chromatography (7:3 Hex/CH_2Cl_2) to give the pure compound **15** (13.8g, 74% yield). ^{1}H NMR (500MHz, $CDCl_3$): δ = 0.08 (s, 6H), 0.89 (s, 9H), 3.11 (t, 2H), 3.83 (t, =2H), 7.32 (m, 2H), 8.27 (m, 2H). HRMS (EI): calc. for $[C_{15}H_{23}O_5NSSi]^+$ $[M]^+$: 357.11, found 358.1114.

Synthesis of Compound 16

Compound **15** (2.2g, 6.12mmol), was dissolved in toluene (50mL). To this solution DMAP (75mg, 0.61mmol), DIPEA (1.58g, 12.4mmol) and compound **5** (1.73g 9.19mmol) were added sequentially. The mixture was then refluxed for 5hr, and then cooled to room temperature. Following this, the solution was washed with 1M HCl (50mL), saturated $NaCO_3$ (50mL) and saturated NaCl (50mL). The organic phase was dried with $MgSO_4$, filtered and concentrated *in vacuo*. This produced compound **16** (1.7g, 70% yield) without any further purification required. ^{1}H NMR (500MHz, $CDCl_3$): δ = 0.05 (s, 6H), 0.89 (s, 9H), 1.44 (s, 9H), 2.86 (s, 3H), 3.02 (m, 5H), 3.33 (m, 2H), 3.48 (m, 2H), 3.72 (t,2H). HRMS (EI): calc. for $[C_{18}H_{38}O_4N_2SSi]^+$ $[M]^+$: 406.23, found 407.2307.

Synthesis of Compound 17

To a solution of compound **16** (1.3g, 3.2mmol) in THF (20mL) was added 1M Tetra-n-butylammonium fluoride in THF (8.6mL). The reaction was complete after 1hr, at which point the solvent was evaporated *in vacuo* and the crude mixture purified by column chromatography (6:4 Hex/EtOAc) to give the pure compound **17** (833mg, 89% yield). ^{1}H NMR (500MHz, $CDCl_3$): δ = 1.45 (s, 9H), 2.86 (m, 3H), 3.02 (s, 3H), 3.10 (t, 2H), 3.34 (m, 2H), 3.48 (m, 2H), 3.74 (m,2H). HRMS (EI): calc. for $[C_{12}H_{24}O_4N_2S]^+$ $[M]^+$: 292.15, found 293.1543.

Synthesis of Compound 18

A mixture of compound **17** (1.1g, 3.76mml), and TsCl (1.43g, 7.52mmol) was dissolved in CH_2Cl_2 (20mL) and cooled to 0^{o}C. To this solution NEt_3 (1.7g, 9.4mmol) was added dropwise. The reaction was complete after 3hr, at which point the solution was washed with 3 x 1M HCl (50mL), dried on $MgSO_4$, filtered and concentrated *in vacuo*. The crude material was purified by column chromatography (6:4 Hex/EtOAc) to afford compound **18** (1.1g, 68% yield). ^{1}H NMR (500MHz, $CDCl_3$): δ = 1.43 (s, 9H), 2.44 (s, 3H), 2.86 (m, 3H), 3.02 (s, 3H), 3.12 (m, 2H), 3.35 (m, 4H), 4.07 (m, 2H), 7.32 (m, 2H), 7.80 (m, 2H). HRMS (EI): calc. for $[C_{19}H_{30}O_6N_2S_2]^+$ $[M]^+$: 446.15, found 447.1594.

Synthesis of Compound 19

Compound **18** (827mg, 1.85mmol) was dissolved in DMF (5mL). NaN_3 (157mg, 2.41mmol) was then added to this solution and heated to 50°C. The reaction was complete after 2hr, at which point the solution was diluted with EtOAc (50mL). The organic phase was washed with 3 x saturated NaCl (50mL), dried on $MgSO_4$, filtered and concentrated *in vacuo*, to give compound **19** (382mg, 65% yield), which required no further purification. ^{1}H NMR (500MHz, $CDCl_3$): δ = 1.45 (s, 9H), 2.86 (m, 3H), 3.01 (s, 3H), 3.07 (m, 2H), 3.37 (m, 2H), 3.48 (m, 4H). HRMS (EI): calc. for $[C_{12}H_{23}O_3N_5S]^+$ $[M]^+$: 317.15, found 318.1602.

Synthesis of Compound 20

First, to a solution of compound **19** (300mg, 0.95mmol) in CH_2Cl_2 (10mL) was added TFA (5mL) dropwise. The reaction mixture was stirred for 30 min and the CH_2Cl_2 was then evaporated. The solution was re-suspended in CH_2Cl_2 (20mL) and evaporated twice more, to remove any TFA, leaving Compound **19** as the TFA salt, which was redisolve in DMF (10mL) and used directly. Separately, compound **6** (363mg, 1.14mmol) was dissolved in DMF (10mL), and added to the first solution. NEt_3 (870mg, 4.8mmol) was then added to the solution and the reaction proceeded for 24hr at room temperature. The solution was then diluted with EtOAc (75mL) and washed with 1M HCl (50mL), and 3 x saturated NaCl (50mL). The organic phase was dried on $MgSO_4$, filtered and concentrated *in vacuo.* To purify, column chromatography was performed (1:1 Hex/EtOAc), affording compound **20** (250mg, 66% yield). ^{1}H NMR (500MHz, $CDCl_3$): δ = 3.08 (m, 8H), 3.54 (m,6H), 5.52 (s, 2H), 7.62 (m, 3H), 8.06 (m, 1H). HRMS (EI): calc. for $[C_{33}H_{33}O_7N_5S_2]^+$ $[M]^+$: 396.12, found 397.1269.

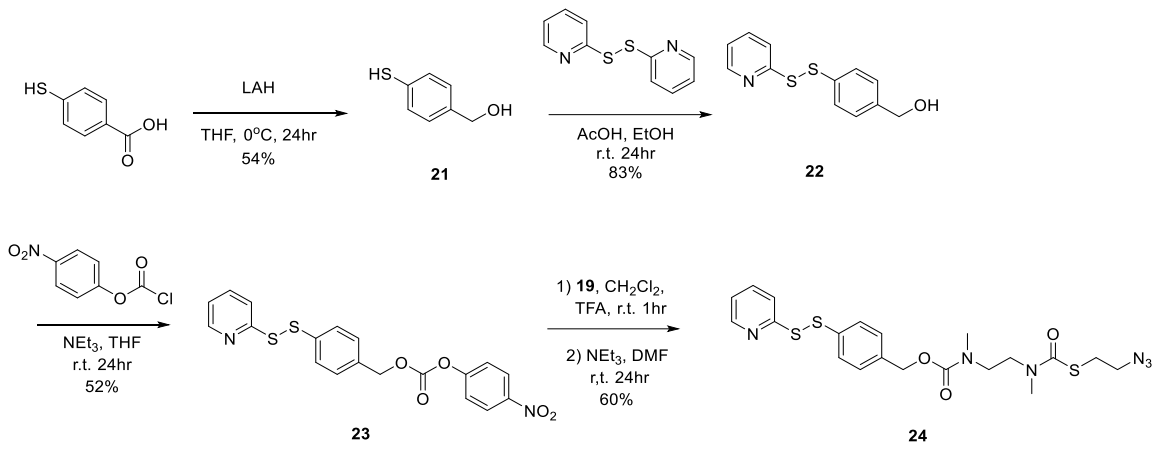

Compound's **21**, **22** and **23** were synthesized according to literature protocols.[67]

Figure 2. 13 Synthetic route to generate Compound 24

Synthesis of Compound 24

Compound **19** (200mg, 0.63mmol) was dissolved in CH_2Cl_2 (10mL), and TFA (5mL) was added dropwise. The reaction mixture was stirred for 30 min and the CH_2Cl_2 was then evaporated. The solution was re-suspended in CH_2Cl_2 (20mL) and evaporated twice more, to remove any TFA, leaving Compound **19** as the TFA salt, which was redisolve in DMF (10mL) and used directly. Separately, a mixture of Compound **23** (290mg, 0.69mmol), in DMF. NEt_3 (570mg, 3.2mmol) was then added to the solution and the reaction proceeded for 24hr at room temperature. The solution was then diluted with EtOAc (75mL) and washed with 1M HCl (50mL), and 3 x saturated NaCl (50mL). The organic phase was dried on $MgSO_4$, filtered and concentrated *in vacuo.* To purify, column chromatography was performed (8:2 to 1:1 Hex/EtOAc), affording compound **24** (186mg, 60% yield). ^{1}H NMR (500MHz, $CDCl_3$): δ = 3.02 (m, 8H), 3.43 (m,6H), 5.07 (s, 2H), 7.10 (m, 1H), 7.26 (m, 2H), 7.48 (m, 2H), 7.61 (m, 2H), 8.47 (m, 1H). HRMS (EI): calc. for $[C_{20}H_{25}O_3N_6S_3]^+$ $[M]^+$: 493.11, found 493.1127.

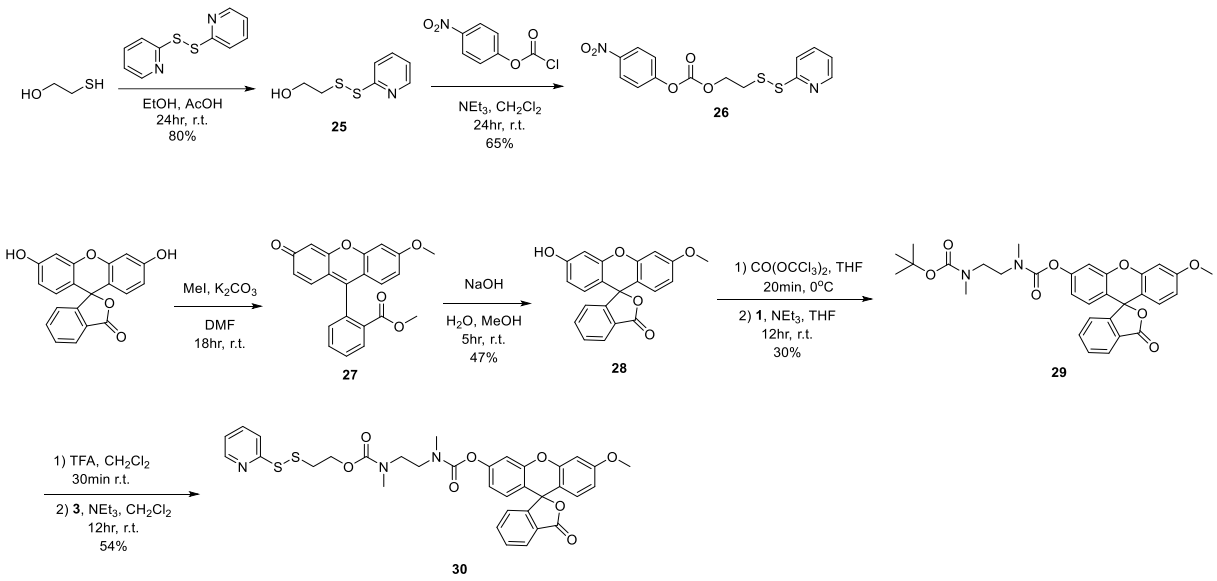

Compound's **25**[68]**, 26**[69] **and 27**[70] were synthesized according to the literature procedures.

Figure 2. 14 Synthetic route to generate pro-methoxyfluorescein.

Synthesis of Compound 28

Compound **28** was synthesized with a slight deviation from the literature procedure.[70] Briefly, to a mixture of fluorescein (6.64g, 20mmol) and K_2CO_3 (4.14g, 30mmol) in 50ml of DMF was added methyl iodide (4.26g, 30mmol) and the reaction proceeded overnight at room temperature. The solution was then diluted with H2O (100 mL) and extracted with ethyl acetate (3 × 100 mL). The organic phase was washed with saturated $NaHCO_3$ (200 mL), and saturated NaCl (200 mL), and then dried on $MgSO_4$, filtered and concentrated *in vacuo*. The collected solid was then purified by column chromatography (100% EtOAc) to provide Compound **28** and used directly in the next step, to generate **5** (3.23g, 47% yield over 2 steps). Characterization was in accordance with what was reported in literature.[70]

Synthesis of Compound 29

In a flame dried round bottom flask, triphosgene (1.37g, 4.62mmol) was dissolved in dry THF (25ml), and cooled to 0 °C. Compound **28** (1.60g, 4.62mmol), with triethylamine (1.20mL,

4.62mmol), was dissolved separately in dry THF and transferred by cannula into the solution of triphosgene. The reaction mixture was stirred for 1 hour, and then nitrogen was passed over the solution to evaporate the THF. Fresh, dry THF (25ml) was added to the reaction mixture, followed by the addition of Compound **5** (700mg, 3.72mmol), separately dissolved in dry THF (25mL) with triethylamine (1.20mL, 4.62mmol). The solution was reacted for an additional 24hrs and then concentrated *in vacuo.* The solution was then re-dissolved in CH_2Cl_2 (100 mL) and washed with 1M HCl (200mL), saturated $NaHCO_3$ (200 mL), and saturated NaCl (200 mL), and then dried on $MgSO_4$, filtered and concentrated *in vacuo*. The crude product was then purified by column chromatography (EtOAc/Hex 1:1) to provide Compound **29** (740mg, 30%). ^{1}H NMR (500MHz, $CDCl_3$): δ = 1.46 (s, 9H), 2.93 (m, 3H), 3.07 (m, 3H), 3.47 (m, 4H), 3.83 (s, 3H), 6.79 (m, 5H), 7.18 (m, 2H), 7.62 (m, 2H), 8.03 (m, 1H). ^{13}C NMR (125MHz, $CDCl_3$): δ = 28.43, 34.53, 35.28, 46.86, 53.50, 55.58, 82.61, 100.87, 110.25, 110.52, 110.95, 111.84, 117.56, 124.06, 124.09, 125.00, 126.50, 128.82, 128.99, 129.84, 135.11, 151.80, 151.85, 152.34, 153.02, 153.90, 161.43, 169.33. HRMS (EI): calc. for $[C_{31}H_{32}O_8N_2]^+$ $[M]^+$: 561.22, found 562.2225.

Synthesis of Compound 30

Compound **29** (500mg, 0.89mmol) was dissolved in CH_2Cl_2 (10 mL) at room temperature. TFA (10 mL) was then added and the reaction mixture was stirred for 2 hours. The CH_2Cl_2 was then evaporated. The solution was re-suspended in CH_2Cl_2 (20mL) and evaporated twice more, to remove any TFA, leaving Compound **29** as the TFA salt in CH_2Cl_2 (20mL), which was used directly. Compound **26** (376mg, 1.07mmol) was dissolved separately in CH_2Cl_2 (20mL) with triethylamine (1mL, mmol) and added to the solution of Compound **29**. This mixture was then reacted overnight and then diluted with CH_2Cl_2 (60mL) and washed with 1M HCl (200mL), saturated $NaHCO_3$ (200 mL), and saturated NaCl (200 mL), and then dried on $MgSO_4$, filtered and concentrated *in vacuo*. The crude product was then purified by column chromatography (EtOAc/Hex 1:1) to provide Compound **30** (326mg, 54%). ^{1}H NMR (500MHz, $CDCl_3$): δ = 3.03 (m, 8H), 3.50 (m, 4H), 3.83 (s, 3H), 4.35 (m, 2H), 6.72 (m, 5H), 7.11 (m, 3H), 7.63 (m, 4H), 8.00 (m, 1H), 8.45 (m, 1H). ^{13}C NMR (125MHz, $CDCl_3$): δ = 35.36, 37.90, 46.35, 46.85, 47.12, 55.59, 63.15, 63.30, 82.57, 100.83, 110.23, 110.47, 110.93, 111.89, 117.48, 117.68, 119.68, 120.82, 124.06, 125.03, 126.50, 128.99, 129.80,

135.07, 137.05, 149.69, 151.79, 152.31, 153.09, 161.41, 169.33. HRMS (EI): calc. for $[C_{34}H_{32}O_8N_3S_2]^+$ $[M]^+$: 673.16, found 674.1624.

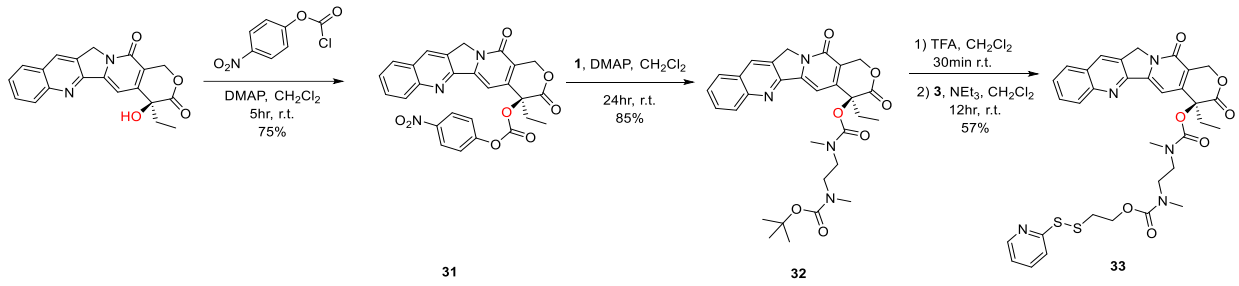

Figure 2. 15 Synthetic route for pro-camptothecin.

Synthesis of Compound 31

Compound **31** was synthesized according to a modified literature procedure.[71] Under dry conditions, Camptothecin (100 mg, 0.29mmol) was dissolved in CH_2Cl_2 (25 mL) and DMAP (71mg 0.58mmol) was added to this solution and stirred for 10 min. 4-Nitrophenyl Chloroformate (117mg, 0.58 mmol) was then added to this solution and the mixture was allowed to stir for 5 hours. The solution was then diluted with CH_2Cl_2 (75 mL) and extracted with 1M HCl (100 mL) and saturated NaCl (100 mL). The organic phase was then dried on $MgSO_4$, filtered and concentrated *in vacuo*. The collected solid was then purified by column chromatography (EtOAc/CH_2Cl_2 1:1) to give Compound **31** (112mg, 75%). Characterization was in accordance with what was reported in the literature.[71]

Synthesis of Compound 32

Compound **31** (100 mg, 0.20 mmol) was dissolved in CH_2Cl_2 (10 mL). To this solution, Compound **5** (75mg, 0.40 mmol) and DMAP (49mg, 0.40 mmol) were added sequentially. The resulting mixture was then stirred for 24 hours. After this the solution was diluted with CH_2Cl_2 (20 mL) and extracted with 1M HCl (20 mL), saturated $NaHCO_3$ (20 mL) and saturated NaCl (20 mL). The organic phase was then dried on $MgSO_4$, filtered and concentrated *in vacuo*. The collected solid was then purified by column chromatography (EtOAc/Hex 1:1) to give Compound **32** (96mg,

85%). ^{1}H NMR (500MHz, $CDCl_3$): δ = 1.05 (m, 3H), 1.46 (m, 9H), 2.16-2.29 (m, 2H), 2.85-2.91 (m, 3H), 3.06-3.19 (m, 3H), 3.32 (m, 2H), 3.43-3.82 (m, 2H), 5.24-5.34 (m, 2H), 5.39-5.44 (m, 1H), 5.68-5.72 (m, 1H), 7.27 (m, 1H), 7.69 (m, 1H), 7.85 (m, 1H), 7.95 (m, 1H), 8.22 (m, 1H), 8.41 (s, 1H). ^{13}C NMR (125MHz, $CDCl_3$): δ = 7.77, 14.21, 21.06, 28.49, 32.01, 32.19, 35.71, 47.61, 49.86, 60.39, 67.17, 120.00, 127.98, 128.16, 128.24, 128.53, 128.55, 129.55, 129.59, 130.65, 131.16, 131.18, 148.86, 152.60, 157.42, 157.45, 171.14. HRMS (EI): calc. for $[C_{30}H_{34}O_7N_4]^+$ $[M]^+$: 562.24, found 563.2493.

Synthesis of Compound 33

Compound **32** (60mg, 0.11mmol) was dissolved in CH_2Cl_2 (10 mL) at room temperature. TFA (10 mL) was then added and the reaction mixture was stirred for 2 hours. The CH_2Cl_2 was then evaporated. The solution was re-suspended in CH_2Cl_2 (20ml) and evaporated twice more, to remove any TFA, leaving compound **32** as the TFA salt in CH_2Cl_2 (20ml), which was used directly. Compound **26** (45mg, 0.13mmol) was dissolved separately in CH_2Cl_2 (20ml) with triethylamine (18µL, 0.13mmol) and added to the solution of compound **32**. This mixture was then reacted 12 hours and then diluted with CH_2Cl_2 (60ml) and washed with 1M HCl (200ml), saturated $NaHCO_3$ (200 mL), and saturated NaCl (200 mL), and then dried on $MgSO_4$, filtered and concentrated *in vacuo*. The crude product was then purified by column chromatography (EtOAc/Hex 1:1) to provide Compound **33** (42mg, 57%). ^{1}H NMR (500MHz, $CDCl_3$): δ = 1.02 (m, 3H), 2.13-2.31 (m, 2H), 2.95 (m, 3H), 3.04 (m, 1H), 3.13 (m, 2H), 3.20 (s, 2H), 3.25-3.82 (m, 5H), 4.27-4.46 (m, 2H), 5.28-5.34 (m, 2H), 5.38-5.44 (m, 1H), 5.68-5.72 (m, 1H), 7.11 (m, 1H), 7.25 (m, 1H), 7.64-7.69 (m, 3H), 7.85 (m, 1H), 7.95 (m, 1H), 8.22 (m, 1H), 8.41 (s, 1H), 8.48 (s, 1H). ^{13}C NMR (125MHz, $CDCl_3$): δ = 7.78, 14.21, 21.07, 32.00, 32.19, 37.87, 47.92, 49.88, 60.40, 63.09, 63.29, 67.18, 96.28, 119.60, 119.76, 119.99, 120.70, 127.99, 128.16, 128.17, 128.26, 128.53, 129.53, 130.67, 131.17, 131.21, 137.03, 148.86, 149.69, 152.60, 156.05, 157.42. HRMS (EI): calc. for $[C_{33}H_{33}O_7N_5S_2]^+$ $[M]^+$: 675.18, found 676.1894.

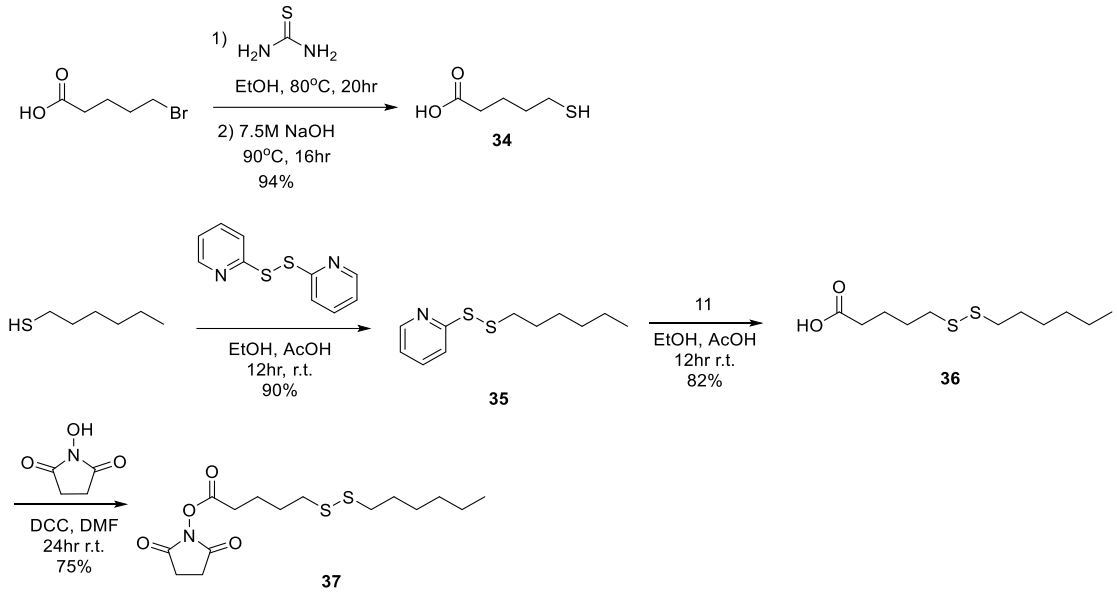

Compound **34** was synthesized according to the literature procedure.[72]

Figure 2. 16 Synthetic route for NHS ester disulfide molecule.

Synthesis of Compound 35

2,2'-Dithiodipyridine (3.73g, 16.91mmol) was dissolved in ethanol (50ml) with acetic acid (5ml). To this 1-Hexanethiol (1.00g, 8.46mmol) was added dropwise and the solution was allowed to react at room temperature for 12 hours. The solution was then concentrated *in vacuo* and the crude material purified by column chromatography (EtOAC/Hex 5:95) to provide Compound **35** (1.73g, 90%). ^{1}H NMR (500MHz, $CDCl_3$): δ = 0.86 (t, J = 6.9Hz, 3H), 1.25 (m, 4H), 1.36 (m, 2H), 1.67 (m, 2H), 2.78 (m, 2H), 7.05 (m, 1H), 7.62 (m, 1H), 7.72 (m, 1H), 8.44 (m, 1H) . ^{13}C NMR (125MHz, $CDCl_3$): δ = 9.26, 17.75, 23.41, 24.14, 26.60, 34.28, 114.75, 115.69, 132.18, 144.78, 155.97. HRMS (EI): calc. for $[C_{11}H_{17}NS_2]^+$ $[M]^+$: 227.08, found 228.0883.

Synthesis of Compound 36

Compound **34** (1.50g, 6.60mmol), was dissolved in ethanol (50ml) with acetic acid (5ml). To this Compound **35** (855mg, 6.60mmol) was added dropwise and the solution was allowed to react at room temperature for 12 hours. The solution was then concentrated *in vacuo* and the crude

material purified by column chromatography (EtOAC/Hex/Acetic Acid 5:94:1) to provide Compound **36** (1.40g, 82%). ^{1}H NMR (500 MHz, $CDCl_3$): δ = 0.90 (t, J = 6.9Hz, 3H), 1.27-1.41 (m, 6H), 1.64-1.77 (m, 6H), 2.37-2.42 (m, 2H), 2.65-2.72 (m, 4H). ^{13}C NMR (125MHz, $CDCl_3$): δ = 14.04, 22.55, 23.46, 28.20, 28.48, 29.20, 31.44, 33.59, 38.46, 39.17, 179.75. HRMS (EI): calc. for $[C_{11}H_{22}O_sS_2]^+$ $[M]^+$: 250.11, found 249.0986.

Synthesis of Compound 37

Compound **36** (690mg, 2.76mmol) and N-hydroxysuccinimide (350mg, 3.31mmol) were dissolved in DMF (20 ml). To this was added N,N'-Dicycolhexylcarbodiimide (625mg, 3.31mmol) and the mixture was reacted for 24 hours. The solution was then filtered to remove the insoluble urea and diluted with H_2O (100 mL) and extracted with ethyl acetate (3 × 100 mL). The organic phase was washed with saturated $NaHCO_3$ (200 mL), and saturated NaCl (200 mL), and then dried on $MgSO_4$, filtered and concentrated *in vacuo*. The crude material was then purified by column chromatography (CH_2Cl_2/Hex 7:3) to provide Compound **37** as a colourless oil (719mg, 75%). ^{1}H NMR (500MHz, $CDCl_3$): δ = 0.88 (t, J = 6.9Hz, 3H), 1.25-1.39 (m, 6H), 1.60-1.68 (m, 2H), 1.79-1.86 (m, 4H), 2.60-2.71 (m, 6H), 2.81 (s, 4H). ^{13}C NMR (125MHz, $CDCl_3$): δ = 14.04, 22.54, 23.34, 25.60, 28.23, 29.19, 30.55, 31.43, 38.15, 39.12, 39.22, 168.32, 169.16. HRMS (EI): calc. for $[C_{15}H_{25}O_4NS_2]^+$ $[M]^+$: 347.12, found $[Na^+]$ 370.1120.

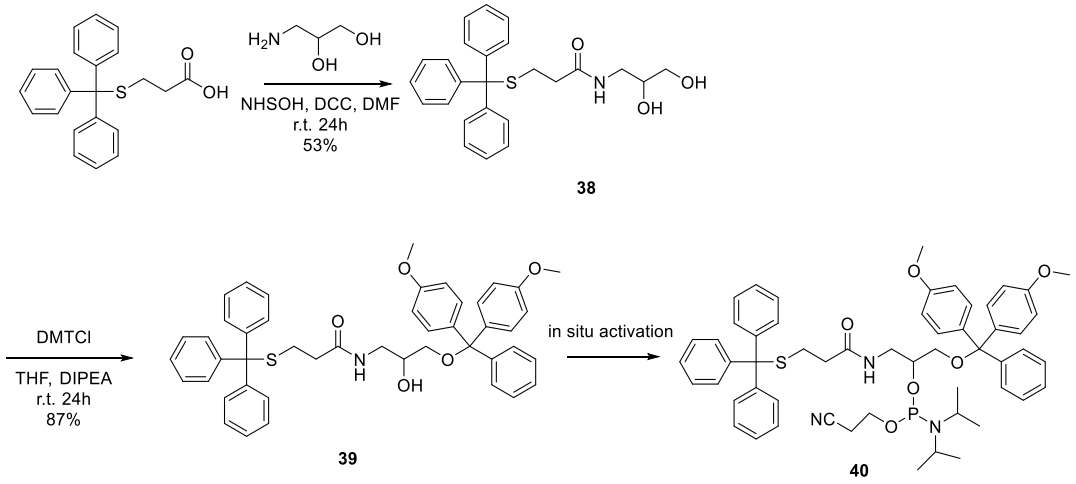

Figure 2. 17 . Synthesis of N-(3-(bis(4-methoxyphenyl)(phenyl)methoxy)-2-hydroxypropyl)-3-(tritylthio)propenamide (Compound 39)

Compound 38:

3-(Tritylthio)propanoic acid (7.43g, 21mmol), 3-Amino-1,2-propandiol (2.04g, 22mmol), and N-hydroxysuccinimide (2.58g, 22mmol) were all dissolved in DMF (50 ml). To this mixture, N,N'-Dicycolhexylcarbodiimide (4.62g, 22mmol) and the mixture was reacted for 24 hours. The solution was then filtered to remove the insoluble urea and diluted with H_2O (100 mL) and extracted with ethyl acetate (3 × 100mL). The organic phase was washed with saturated $NaHCO_3$ (100mL), and saturated NaCl (100 mL), and then dried on $MgSO_4$, filtered and concentrated *in vacuo*. The crude material was then purified by column chromatography (7:3 EtOAc/Hex) to provide Compound **38** (4.67g, 53%). ^{1}H NMR (500MHz, $CDCl_3$): δ = 2.03 (m, 2H), 2.47 (m, 2H), 3.25 (m, 2H), 3.48 (m, 3H), 3.67 (m, 1H), 2.27 (m, 9H), 7.40 (m, 6H). HRMS (EI): calc. for $[C_{25}H_{28}NO_3S]^+$ $[M]^+$: 422.17, found 422.1812.

Compound 39:

Compound **38** (4.67g, 11mmol) was dissolved in THF (50mL). To this was added diisopropylethylamine (613mg, 22mmol) followed by 4, 4' dimethoxytrityl chloride (3.75g, 11mmol) 1/3 every hour over 3 hrs. The mixture was allowed to react for an additional 24hr. The solution was directly concentrated *in vacuo* and purified directly by column chromatography (1:1 Hex/EtOAc) to provide compound **39** (6.93g, 87%). ^{1}H NMR (500MHz, $CDCl_3$): δ = 2.05 (m, 2H), 2.51 (m, 2H), 3.11 (m, 1H), 3.33 (m, 1H), 3.52 (m, 2H), 3.78 (m, 7H), 6.84 (m, 4H), 7.32 (m, 17H), 7.44 (m, 7H). HRMS (EI): calc. for $[C_{46}H_{46}NO_5S]^+$ $[M]^+$: 724.30, found 724.3201.

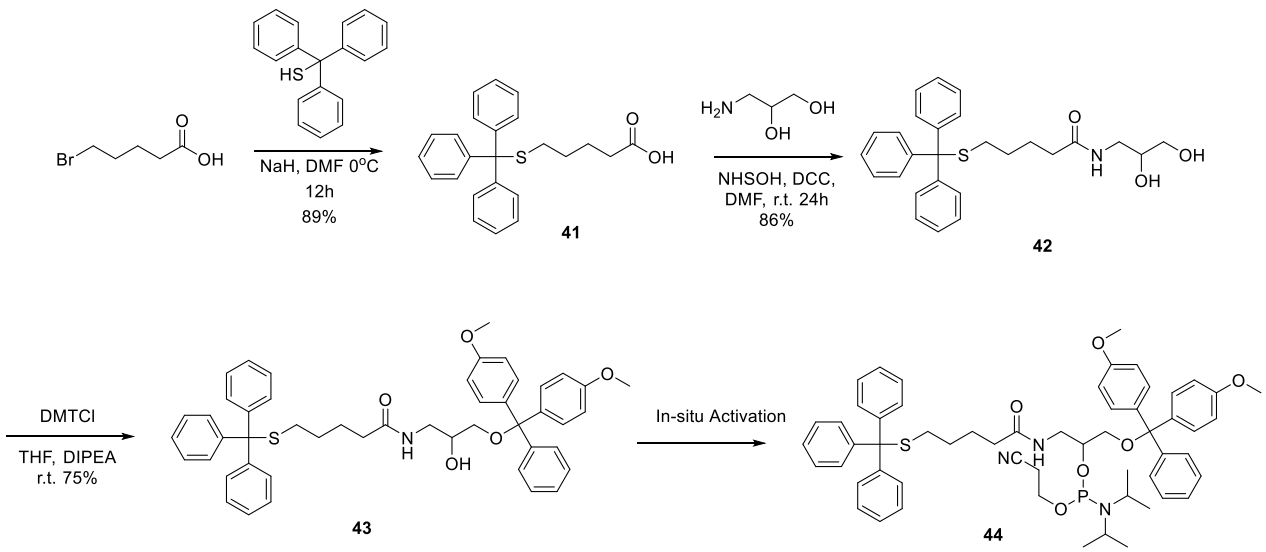

Figure 2. 18 Synthesis N-(3-(bis(4-methoxyphenyl)(phenyl)methoxy)-2-hydroxypropyl)-5-(tritylthio)pentanamide (compound 43)

Compound 41:

Trityl mercaptan (1.00g, 3.62mmol) was added stepwise to a suspension of NaH (360mg, 7.96mmol) in DMF (10mL) under inert conditions at 0°C. The reaction mixture was then stirred for 30min, and a solution of 5-bromopentanoic acid (655mg, 3.62mmol) in DMF (10mL) was added slowly. The reaction mixture was allowed to warm to room temperature and was then stirred overnight. Following this, chloroform (75mL) was added to the reaction mixture and the organic phase was washed with 1M HCl (4 x 100mL) and brine (3 x 100mL). The organic layer was then dried on $MgSO_4$, filtered, and concentrated *in vacuo*. The crude mixture was then purified by column chromatography (7:3 Hex/EtOAc 1% AA) to give compound **41** (1.21g, 89%) ^{1}H NMR (500MHz, $CDCl_3$): δ = 1.42 (m, 2H), 1.58 (m, 2H), 2.25 (m, 4H), 7.22 (m, 3H), 7.32 (m, 7H), 7.46 (m, 5H). HRMS (EI): calc. for $[C_{24}H_{25}O_2S]^+$ $[M]^+$: 377.15, found 377.9816.

Compound 42:

Compound **41** (3.2g, 8.50mmol), 3-Amino-1,2-propandiol (852mg, 9.35mmol), and N-hydroxysuccinimide (1.08g, 9.35mmol) were all dissolved in DMF (20 ml). To this mixture, N,N'-Dicycolhexylcarbodiimide (1.93g, 9.35mmol) and the mixture was reacted for 24 hours. The solution was then filtered to remove the insoluble urea and diluted with H_2O (100 mL) and extracted with ethyl acetate (3 × 50mL). The organic phase was washed with saturated $NaHCO_3$

(50mL), and saturated NaCl (50 mL), and then dried on $MgSO_4$, filtered and concentrated *in vacuo*. The crude material was then purified by column chromatography (6:4 EtOAc/Hex to 100% EtOAc) to provide Compound **42** (3.3g, 86%). ^{1}H NMR (500MHz, $CDCl_3$): δ = 1.32 (m, 2H), 1.47 (m, 2H), 2.07 (m, 4H), 3.28 (m, 2H), 3.49 (m, 2H), 3.73 (m, 1H), 6.81 (m, 1H), 7.25 (m, 15H), 7.95 (s, 1H). HRMS (EI): calc. for $[C_{27}H_{32}NO_2S]^+$ $[M]^+$: 449.20, found 449.2134.

Compound 43:

Compound **42** (700mg, 1.56mmol) was dissolved in THF (20mL). To this was added diisopropylethylamine (693mg, 6.24mmol) followed by 4, 4' dimethoxytrityl chloride (454mg, 1.56mmol) 1/3 every hour over 3 hrs. The mixture was allowed to react for an additional 24hr. The solution was directly concentrated *in vacuo* and purified directly by column chromatography (6:4 Hex/EtOAc) to provide compound **43** (880mg, 75%). ^{1}H NMR (500MHz, $CDCl_3$): δ = 1.28 (m, 2H), 1.52 (m, 2H), 1.96 (m, 2H), 2.15 (m, 2H), 3.04 (m, 1H), 3.19 (m, 3H), 3.52 (m, 1H), 3.80 (s, 6H), 3.87 (m, 1H), 6.84 (m, 4H), 7.25 (m, 3H), 7.30 (m, 14H), 7.44 (m, 7H). HRMS (EI): calc. for $[C_{48}H_{50}NO_5S]^+$ $[M]^+$: 751.33, found 751.3256.

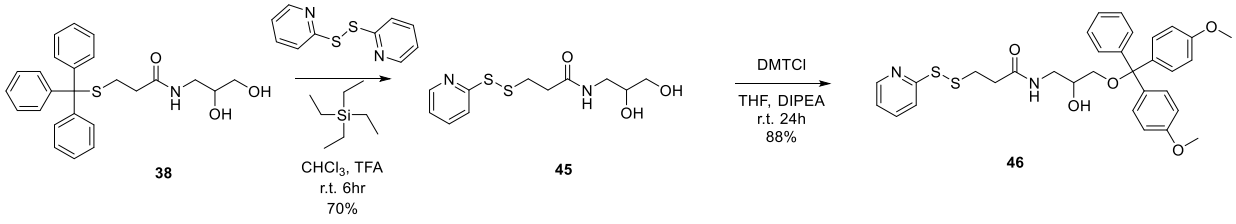

Figure 2. 19 of N-(3-(bis(4-methoxyphenyl)(phenyl)methoxy)-2-hydroxypropyl)-3-(pyridin-2-yldisulfaneyl)propenamide (Compound 46)

Compound 45:

Compound **38** (1.91g, 4.53mmol), was dissolved in $CHCl_3$ (50mL), with tetraethyl-silane (790mg, 4.98mmol), and 2,2',dipyripyldisulfide (2.00g, 9.06mmol). To this solution was added TFA (7mL) and reacted for 6hr at room temperature. Upon completion, the solution was evaporated in vacuo, and then co-evaporated with toluene (3 x 50mL) to remove any residual TFA. The crude mixture was then purified by column chromatography (100% CH_2Cl_2 to 5% MeOH in CH_2Cl_2) to afford compound **45** (914mg, 70%). ^{1}H NMR (500MHz, $CDCl_3$): δ = 2.66 (m, 2H), 3.04 (m, 2H), 3.42

(m, 2H), 4.07 (m, 1H), 4.35 (m, 2H), 6.79 (s, 2H), 7.21 (m, 1H), 7.30 (m, 1H), 7.49 (m, 1H), 7.75 (m, 4H). HRMS (EI): calc. for $[C_{11}H_{16}N_2O_3S_2]^+$ $[M]^+$: 289.06, found 289.0719.

Compound 46:

Compound **45** (800mg, 2.77mmol) was dissolved in THF (20mL). To this was added diisopropylethylamine (1.40g, 11mmol) followed by 4, 4' dimethoxytrityl chloride (940mg, 2.77mmol) 1/3 every hour over 3 hrs. The mixture was allowed to react for an additional 24hr. The solution was directly concentrated *in vacuo* and purified directly by column chromatography (1:1 Hex/EtOAc) to provide compound **46** (1.44g, 88%). ^{1}H NMR (500MHz, $CDCl_3$): δ = 2.57 (m, 2H), 3.05 (m, 2H), 3.21 (m, 2H), 3.30 (m, 2H), 3.61 (m, 1H), 3.82 (s, 6H), 3.96 (m, 1H), 6.85 (m, 5H), 7.07 (m, 1H), 7.26 (m, 6H), 7.43 (m, 2H), 7.63 (m, 2H), 8.49 (m, 1H). HRMS (EI): calc. for $[C_{32}H_{35}N_2O_5S_2]^+$ $[M]^+$: 591.19, found 591.1903.

2.5.6. DNA-Small Molecule Conjugation and Characterization

2.5.6.1. Disulfide Conjugation

First, to a solution of X2, H1 or H1-2 Disulfide (100µL, 18µM) in 1xPBS pH 8.0, was added DTT (1µL, 1.0M) in 1xPBS pH 8.0. The solution was allowed to react for 12 hours, at which point it was then filtered through microcon© 10k filters 6 times with 350µL, 1xPBS pH 8 to remove the excess DTT. After filtration the volume of the solution was re-adjusted to 100µL with 1xPBS pH 8, and DMSO (150µL) was added to the solution. Next, either Compound **24** (6.2mg, 13nmol), Compound **30** (8.75mg, 13nmol) or Compound **33** (8.40mg, 13nmol) was dissolved separately in DMSO (5mL) to give a 2.5 mM solution. 100µL of this solution was then added to the reaction solution, bringing the total volume to 350µL, and the reaction was left for 24 hours at room temperature. After this H_2O (650µL) was added to the reaction solution and the precipitate filtered through InnoSep™ Spin Filters. The solution was then dialyzed with 5K dialysis tubing in H_2O (500mL) for 24 hours. The crude mixture was then dried and purified by RP-HPLC (3-30% ACN in 50 mins) and finally analyzed by LC-MS to give X2 conjugated to compound **24** (X2_24,

88%), H1 conjugated pro-meythoxyfluorescein (H1-FL, 82%), H1 conjugated pro-camptothecin (H1-CT, 86%), and H1-2 conjugated pro-methoxyfluorescein (H1-2-FL, 76%).

2.5.6.2. DBCO Conjugation

X' was first adjusted to (50uL, 25uM) in 1xPBS pH 7.2. Compound 10 (7.4mg, 13nmol) or compound 20 (4.5mg, 13nmol) was then dissolved in DMSO (5mL) to give a 2.5mM solution. 50uL of this solution was then added to the reaction solution bringing the reaction volume to 100uL, and the reaction was left for 24 hours at room temperature. After this H_2O (900µL) was added to the reaction solution and the precipitate filtered through InnoSep™ Spin Filters. The solution was then dialyzed with 5K dialysis tubing in H_2O (500mL) for 24 hours. The crude mixture was then dried and purified by RP-HPLC (3-30% ACN in 50 mins) and finally analyzed by LC-MS to give X' conjugated to compounds 10 and 20, to generate (X'_10, (thioester degraded so no yield was calculated)) and (X'_20, 94%).

To generate (X2_24-Cy3), (X2-24) was first adjusted to (50uL, 25uM) in 1x PBS pH 8. DBCO-Cy3 () (Sigma cat number 777366) was then dissolved in H_2O (680uL) to make a 1.25mM solution and 50uL was added to the solution. After 24hr the reaction mixture was purified directly by RP-HPLC (3-30% ACN in 50 mins) and finally analyzed by LC-MS to give (X2_24-Cy3, 85%).

2.5.6.3. NHS Conjugation

First, a solution of strand X was adjusted to (100uL, 25uM) in 1xPBS pH 7.2. Separately compound **4** (6.21mg, 13nmol) was dissolved in THF (5mL) to make a 2.5mM solution. 100uL of this solution was then added to strand X bringing the final volume to 200uL and the mixture was left overnight to react. The crude mixture was then dried, re-dissolved in 100uL H_2O and purified by RP-HPLC (3-30% ACN in 50 mins) and finally analyzed by LC-MS to give (X_4, 15%).

2.5.6.4. Solid support NHS Ester Conjugation

The Fmoc amino DNA connected to the solid support was first treated with 10% diethylamine in CH_3CN (1.00mL) for 10min to remove the cyanoethyl protecting group. Next, the solid support

was treated with 20% piperidine in DMF (1.0mL) for 10min to remove the Fmoc protecting group from the amine and then washed with CH_3CN (500µL x 3). Separately, Compound **37** (1.00mg, 2.87µmol) was dissolved in DMSO (500µL) and the solid support was added to this solution, followed by DIPEA (25µL, 0.14mmol) and reacted for 24 hours. After this, the solution was centrifuged and the DMSO supernatant removed. The solid support was then washed with CH_3CN (500µL), and centrifuged. The CH_3CN was removed and NH_4OH (1.00mL) was added to the solid support at room temperature for 48 hours, to perform the final cleavage of the DNA from the solid support. NH_4OH was then evaporated and the mixture was re-suspended in H_2O (700µL). The solution was then filtered to remove the solid support and the resulting DNA was purified, first by denaturing PAGE, followed by RP-HPLC (3-30% ACN in 50 mins), and finally analyzed by LC-MS to give H2 conjugated disulfide (H2-SS, 89%) and H2-2 conjugated disulfide (H2-2-SS, 92%).

2.5.6.5. Note on the synthesis and design of H2 disulfide conjugates.

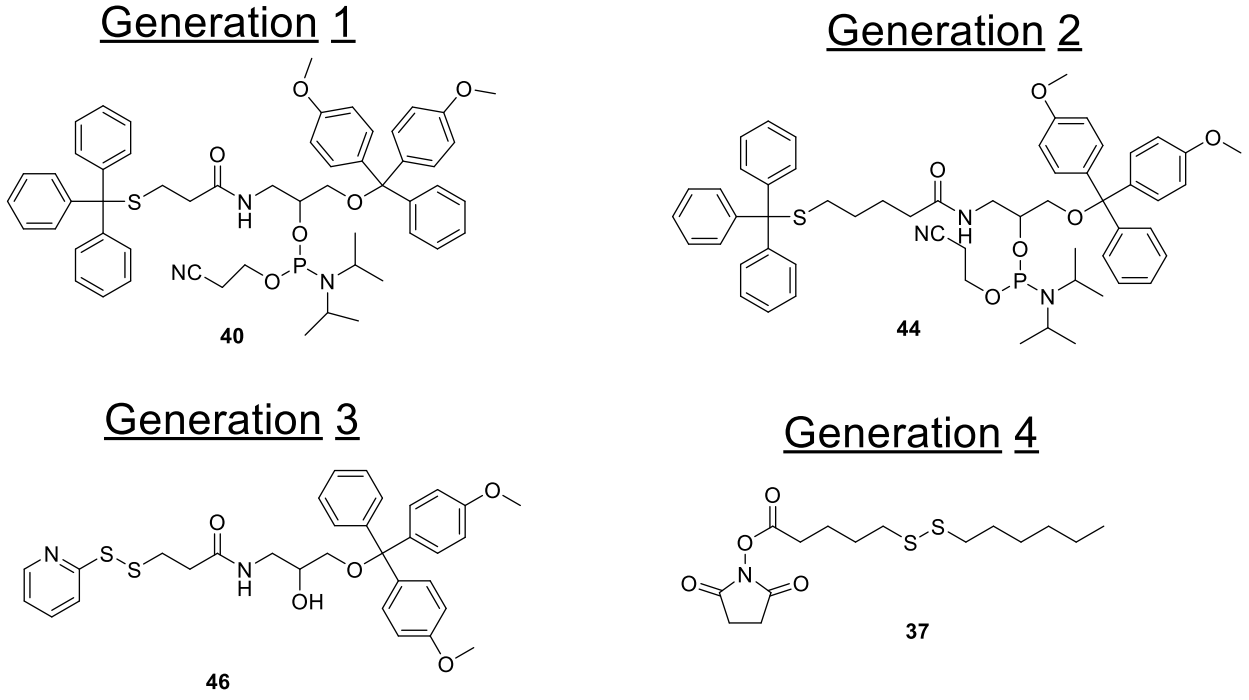

Figure 2. 20 Generations of internal disulfide functionalization methods

Integrating internal modifications to DNA is a non-trivial process and requires that the modification be compatible with both the DNA cycle and deprotection conditions as well as

purification techniques. We found that the commercially available side chain, internal thiol modifications were not 100% compatible with PAGE purification of the strand, as a certain amount reacts with acrylamide in solution capping the thiol. While this is acceptable if further conjugation to the strand is desired, it is not acceptable if this is to be the final product. Additionally, purifying the strand by RP HPLC would not remove (n-1,2,3 etc) oligonucleotides which cause the HCR process to occur sub-optimally. To circumvent these problems, we started off designing new disulfide phosphoramidites described in Figures 2.17, 2.18 and 2.19. Briefly, in the generation 1 design in Figure 2.20 (Compound **40**), we were able to add this molecule to an oligonucleotide chain, however $AgNO_3$ was necessary for deprotecting the trityl protecting group on the thiol. Still, we were able to isolate some product but found that the HCR release mechanism did not occur. We theorized this was due to the length of the alkyl chain connecting the thiol to the DNA and therefore made the generation 2 design (Compound **44)** synthesis in Figure 2.19. Again, the release mechanism did not occur, and therefore decided to change the trityl protecting group as we suspected residual $AgNO_3$ was interfering with the reaction. We then synthesized compound **46** (Figure 2.20) but found that the disulfide cleaved readily upon addition of N,N-diisopropylamino cyanoethyl phosphoramidic chloride. Therefore, we decided to generate the strand using an amine labelling technique in generation 4. We designed a molecule with both an NHS ester functionality and a thiol protected as the disulfide (Figure 2.20). Furthermore, the protecting group was designed to have a long aliphatic chain to ease future purification by RP HPLC and avoid reduction. These modified oligonucleotides were made according to the procedure in section 2.5.4.6). This process gave us strictly full-length nucleic acids, with the desired disulfide functionality.

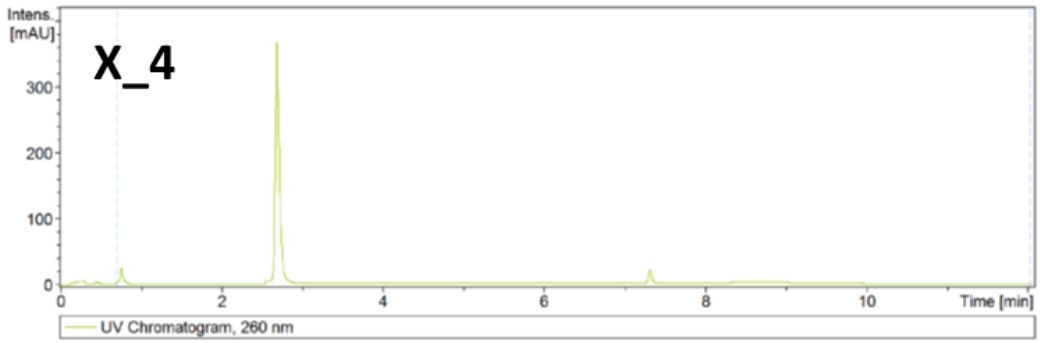
Intens.
[mAU]
X_4
300
200
100
0
0
2
4
6
8
10
Time [min]
UV Chromatogram, 260 nm

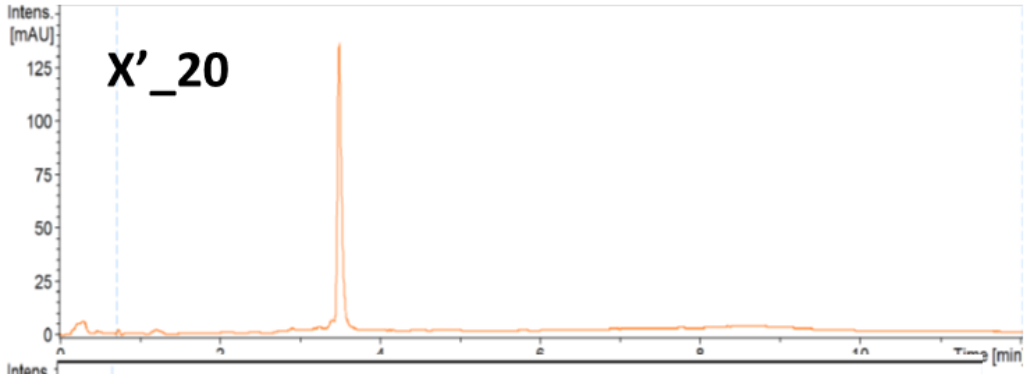
Intens.
[mAU]
X'_20
125
100
75
50
25
0

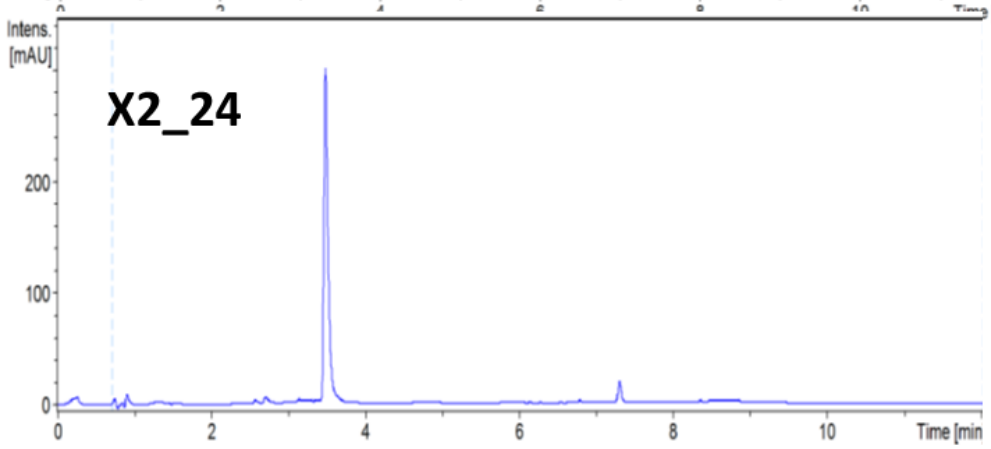
Intens.
[mAU]
X2_24
200
100
0
0
2
4
6
8
10
Time [min

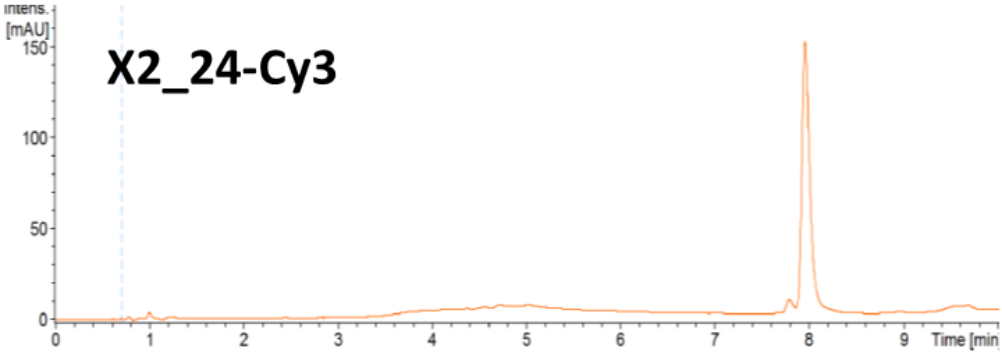
Intens.
[mAU]
X2_24-Cy3
150
100
50
0
0
1
2
3
4
5
6
7
8
9
Time [min

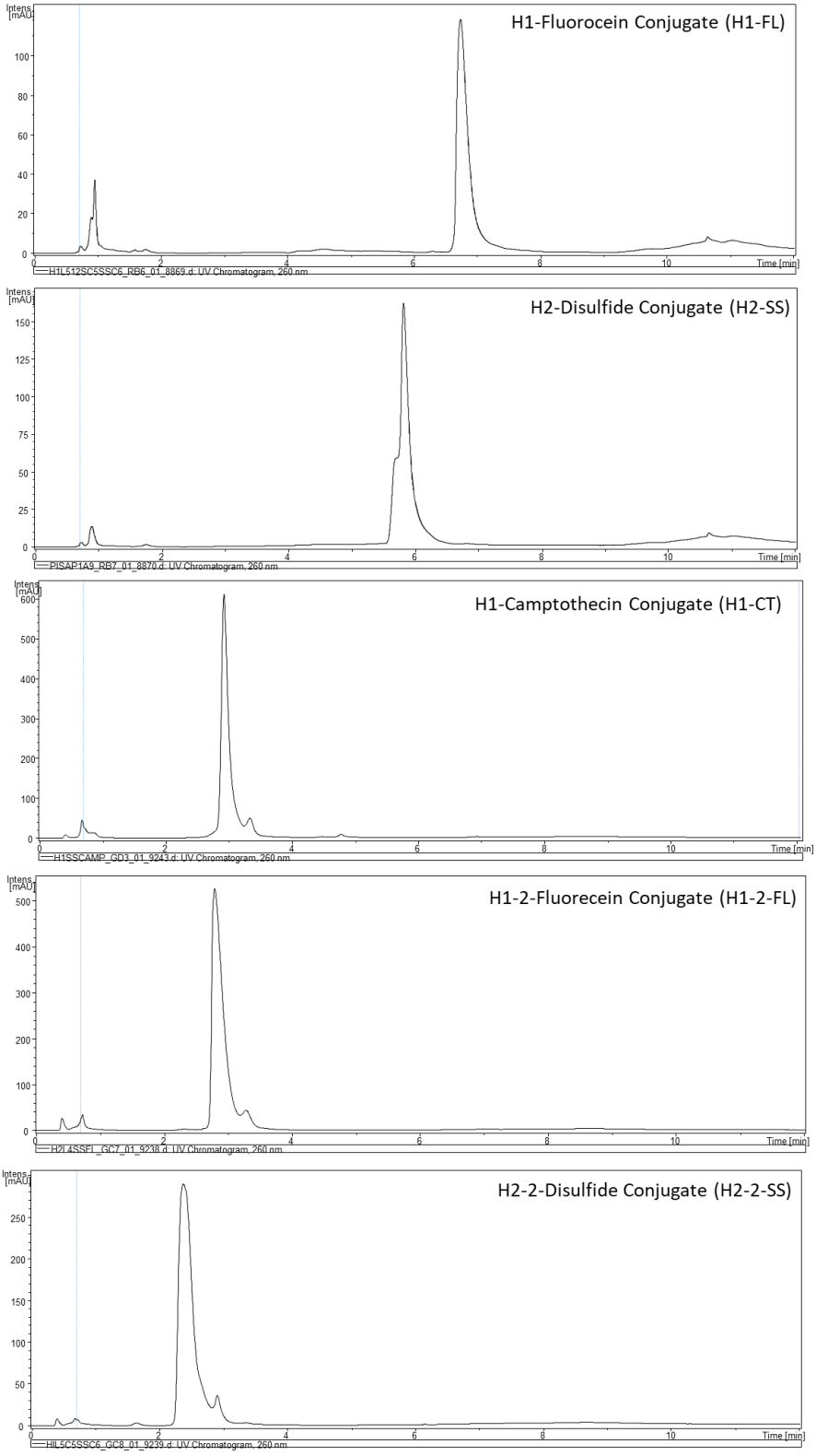

Figure 2. 21 HPLC traces of each of the modified oligonucleotide conjugates

Table 2. 2 LC-ESI-MS data. Calculated and experimental m/z values for synthesized DNA conjugates.

Name	Calculated m/z	Found m/z
X_4	6325.16	6325.09
X'_20	6417.73	6417.91
X2_24	6731.33	6731.25
X2_24-Cy3	7400.54	7400.31
H1-FL	11891.03	11890.35
H2-SS	11375.64	11374.74
H1-CT + [K^+]	11932.05	11930.75
H1-2-FL	26644.57	26643.75
H2-2-SS	26424.41	26424.37

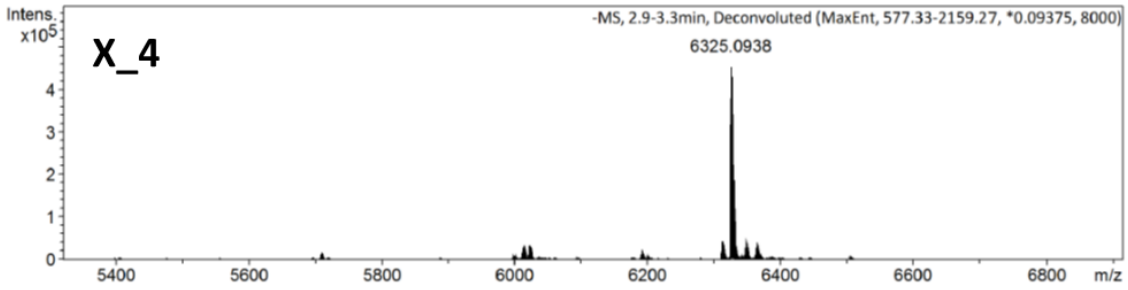
X_4
-MS, 2.9-3.3min, Deconvoluted (MaxEnt, 577.33-2159.27, *0.09375, 8000)
6325.0938
Intens.
x10^5
m/z

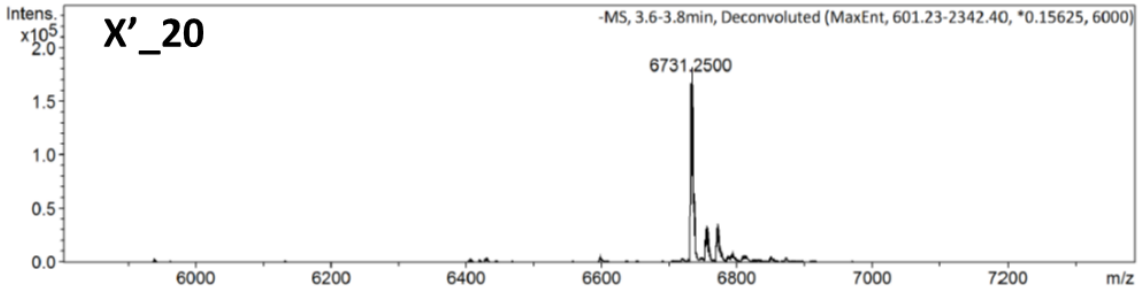
X'_20
-MS, 3.6-3.8min, Deconvoluted (MaxEnt, 601.23-2342.40, *0.15625, 6000)
6731.2500
Intens.
x10^5
m/z

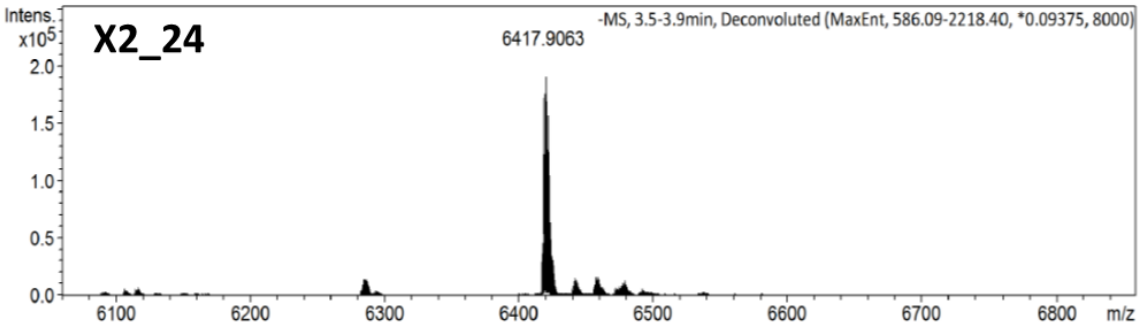
X2_24
-MS, 3.5-3.9min, Deconvoluted (MaxEnt, 586.09-2218.40, *0.09375, 8000)
6417.9063
Intens.
x10^5
m/z

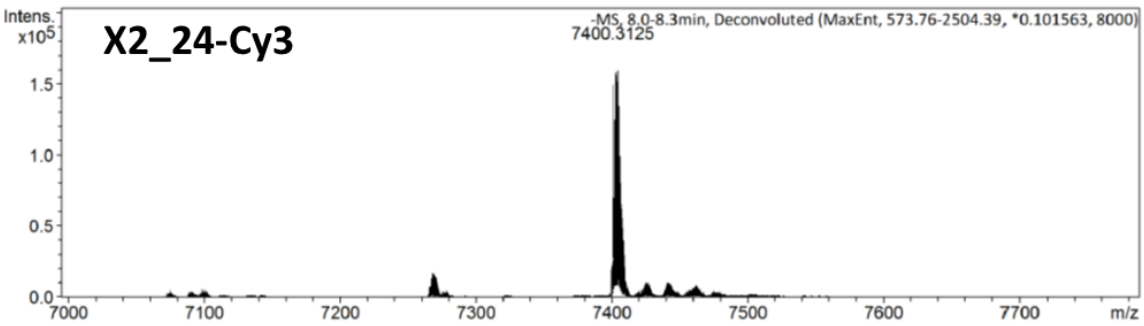
X2_24-Cy3
-MS, 8.0-8.3min, Deconvoluted (MaxEnt, 573.76-2504.39, *0.101563, 8000)
7400.3125
Intens.
x10^5
m/z

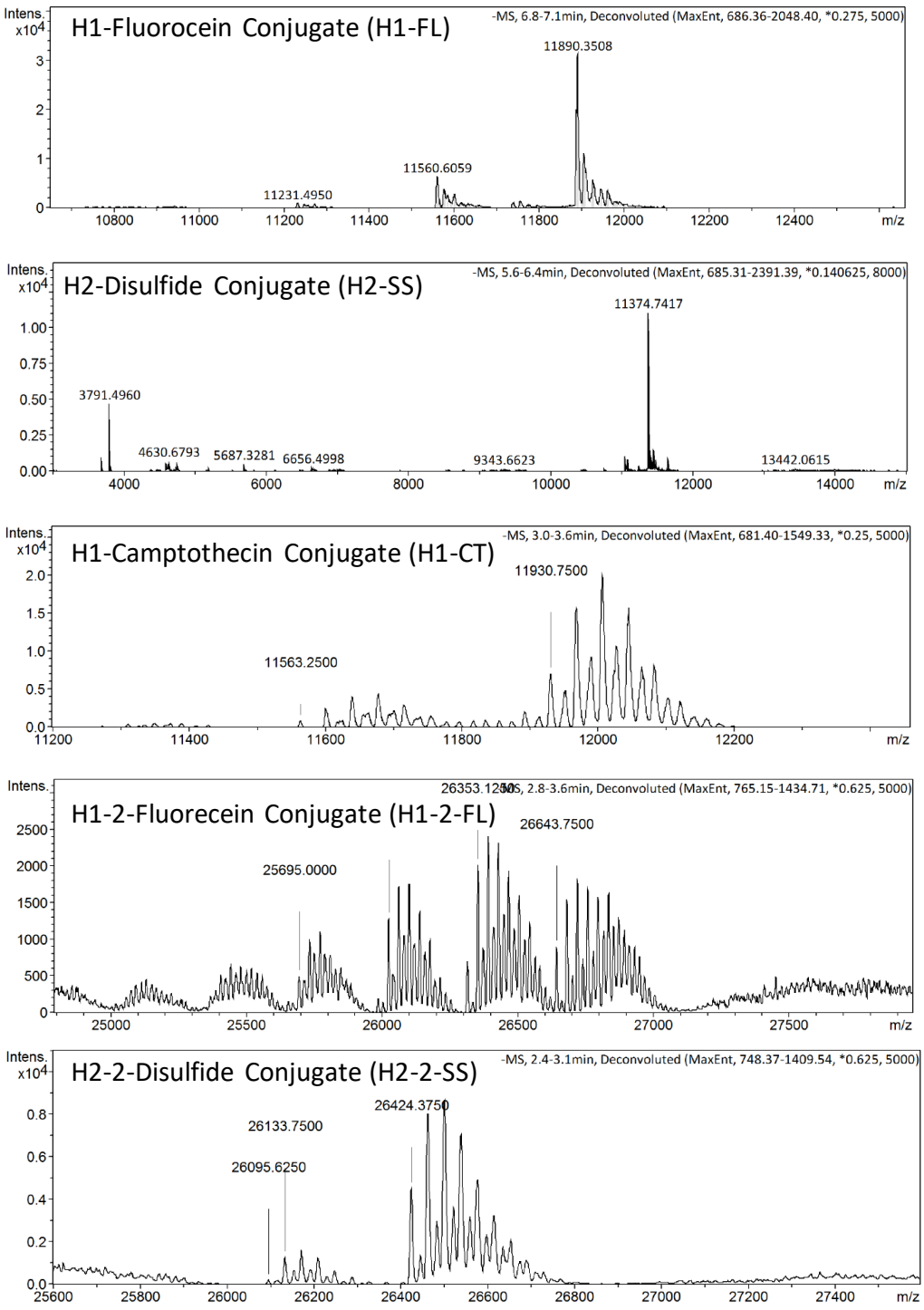

Figure 2. 22 MS characterization of modified oligonucleotide strands

2.5.6.6. H2 Disulfide Reduction Procedure

A solution of H2-SS in 1xPBS pH 8 or H2-2-SS in 1x TAMg pH 8 (100µL, 30µM) was first thermocycled from 95°-10 over 4hr. Following thermocycling, DTT (1µL, 1M) in 1xPBS pH 8 for H2-SS or 1xTAMg pH 8 for H2-2-SS, was added and allowed to react for 12 hours. The solution was then filtered through microcon© 10k filters 6 times with 1xPBS pH 8 for H2-SS or 1xTAMg pH 8 for H2-2-SS to remove the excess DTT to give either the reduced H2-SS (H2-SH) or the reduced H2-2-SS (H2-2-SH). After filtration, the DNA was re-quantified, adjusted to the desired concentration in their respective buffers for the HCR experiments and used without any further purification. Full reduction of the disulfide was confirmed by HPLC analysis (Figure 2.15).

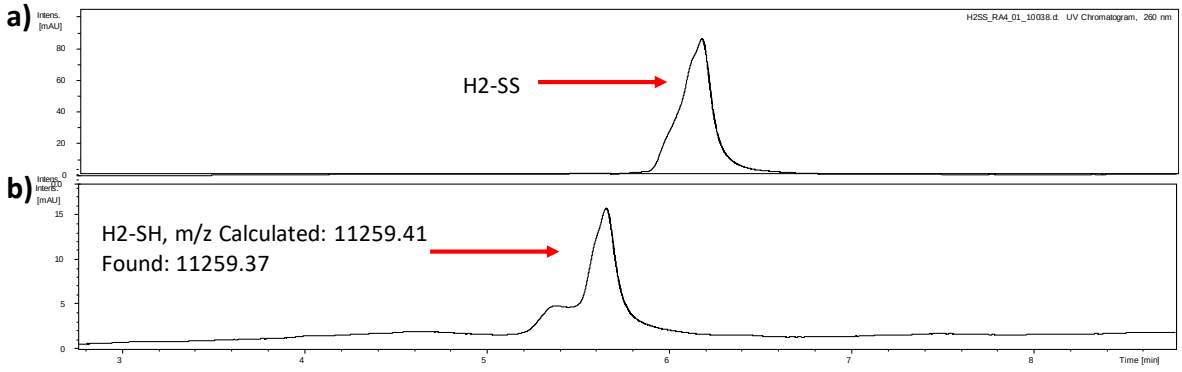

Figure 2. 23 HPLC of (a) H2-SS (b) H2-SS after 24hr of reacting with 100mM DTT to produce H2-SH.

2.5.7. Characterization of HCR; Strategy 2

2.5.7.1. Gel Characterization-Native AGE

Native agarose gel electrophoresis was used to characterize the degree of monomer consumption of the HCR products. In each case, 2.5% AGE was carried out at 4°C for 2.0 hours at a constant voltage of 100 V. Typical sample loading is 3.5 picomoles with respect to the DNA per lane (4.5 µL of 0.75 µM DNA). The gels were stained with GelRed DNA stain and imaged under a DNA-selective channel. Band intensities were quantified using Image lab 5.2 software and the hairpin consumption was calculated using a densitometry analysis of the non-polymerized hairpin bands, compared to a control hairpin band of H1-FL and H2-SS at T=0, using the ladder as an internal standard.[73]

2.5.7.2. Gel Characterization- Denaturing AGE

Denaturing agarose gel electrophoresis was used to characterize the degree of ligation of the HCR products. In each case, a 4.2% denaturing AGE was prepared with 50xALK stock solution diluted to 1xALK with miiliQ H_2O. The gel was carried out at 4°C for 2.25 hours at a constant voltage of 55 V. Typical sample loading is 5.4 picomoles with respect to the DNA per lane (7.0 µL of 0.75 µM DNA). The gels were stained with Sybr Gold DNA stain and imaged under a DNA-selective channel. Band intensities were quantified by Image lab 5.2 software; however, Sybr Gold does not stain with a linear intensity. Therefore, a calibration curves were generated to quantify the yield of ligation. The calibration curves were calculated by using the ladder as an internal standard and generating a ratio between the 150 b.p marker of the ladder and the intensity of H1-FL & H2-SS (Figure S7) and H1-2-FL & H2-2-SS (Figure S8).

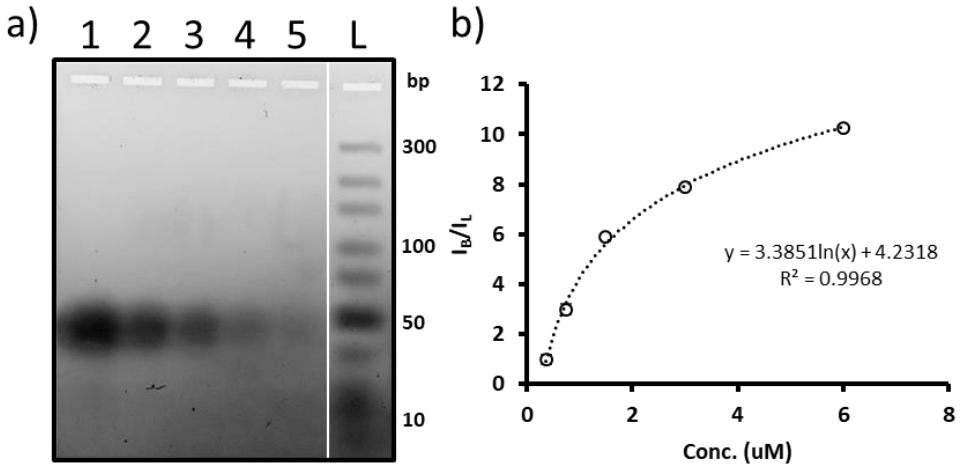

Figure 2. 24 Denaturing Calibration curve for H1-FL and H2-SS

(a) Denaturing agarose gel of H1-FL & H2-SS for calibration curve **L**: Ladder, **Lane 1**: 6µM, **Lane 2**: 3µM, **Lane 3:** 1.5µM**, Lane 4:** 0.75µM, **Lane 5**: 0.375µM, concentration is reported as total hairpin concentration (H1-FL + H2-SS) **(b)** non-linear calibration curve of the ratio between the band intensity and ladder intensity (I_B/I_L) and concentration of H1-FL + H2-SS (µM).

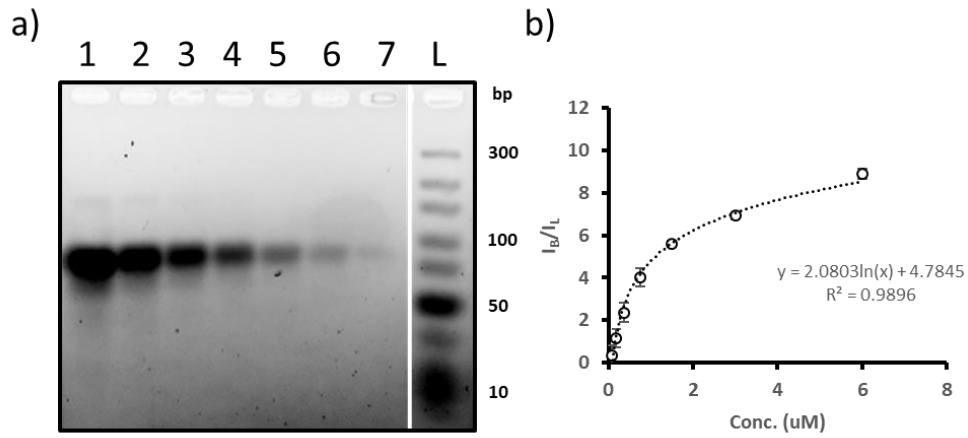

Figure 2. 25 Denaturing Calibration curve for H1-2-FL and H2-2-SS

(a) Denaturing agarose gel of H1-2-FL & H2-2-SS for calibration curve **L**: Ladder, **Lane 1**: 6µM, **Lane 2**: 3µM, **Lane 3:** 1.5µM**, Lane 4:** 0.75µM, **Lane 5**: 0.375µM, **Lane 6**: 0.188µM, **Lane 7**: 0.094µM, concentration is reported as total hairpin concentration (H1-2-FL + H2-2-SS) **(b)** non-linear calibration curve of the ratio between the band intensity and ladder intensity (I_B/I_L) and concentration of H1-2-FL + H2-2-SS (µM).

2.5.7.3. HPLC Characterization

HPLC was used to confirm the release of the linker and small molecule from H1-FL and H1-2-FL. For H1-FL and H1-2-FL, calibration curves were produced through dilution of H1-FL (Figure S9) and H1-2-FL (Figure S10), and yields were calculated based on the consumption of the H1-FL or H1-2-FL peaks. Unless otherwise stated, 5µL of 750 nM samples were injected and samples were run through a Phenomenex Luna C18(2)-HST column (2.5 µM 120A 2.1 x 50 mm) using a gradient of 98% mobile phase A (100 mM HFIP and 5 mM TEA in H_2O) and 2% mobile phase B (MeOH) to 40% mobile phase A and 60% mobile phase B in 8 minutes.

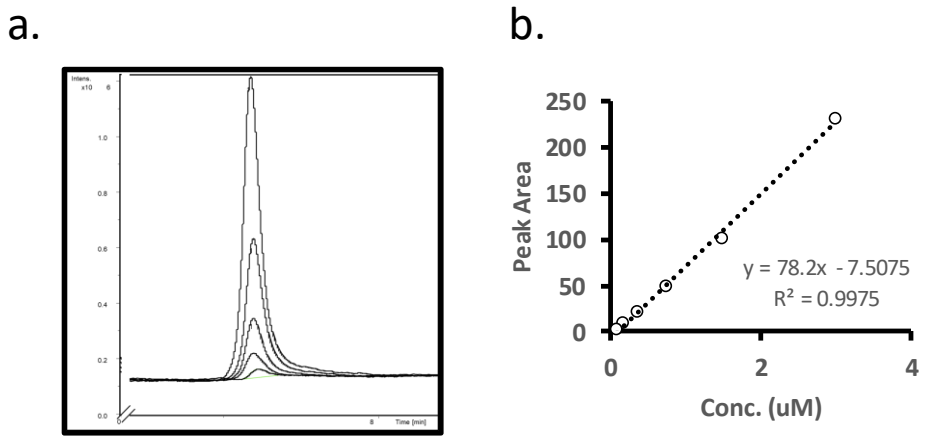

Figure 2. 26 HPLC Calibration curve for H1-FL

(a) HPLC traces of H1-FL at 3µM, 1.5µM, 0.75µM, 0.375µM, 0.188µM and 0.094µM **(b)** HPLC Calibration Curve of H1-FL

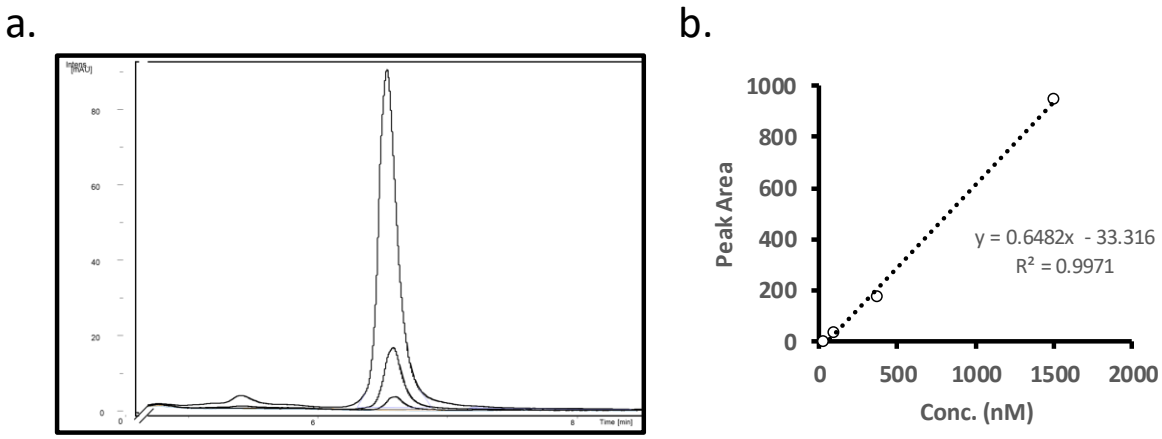

Figure 2. 27 HPLC Calibration curve for H1-2-FL

(a) HPLC traces of H1-2-FL at 1500nM, 375nM, 94nM and 6nM **(b)** HPLC Calibration Curve of H1-2-FL

2.5.7.4. Fluorescence Characterization

Fluorescence scans were performed on a BioTek Cytation 5 imaging reader. For fluorescence measurements, each sample (60 µL at 0.75 µM DNA concentration) was assembled in either 1 x PBS buffer for original HCR or 1xTAMg for templated HCR. The conversion of a given reaction was calculated by first correcting for background fluorescence and then by comparing the fluorescence level to a control reaction of H1-FL with 3x excess of a thiolated version of its full

complement (H1-C-SH). Here, H1-FL and H1-C-SH were thermally annealed at 750nM from 95-5^{o}C over 6hr and then incubated for a further 24hr in both 1xPBS pH 8 or 1xTAMg pH 8. H1-C-SH was prepared using the general H2 reduction procedure starting from H1-C (SI-VI c). We assumed that the immolative cyclizations achieved 100% conversion to generate methoxyfluorescein. HPLC analysis of the reaction confirmed that the complete cleavage of pro-methoxyfluorescein from H1-FL was achieved under these conditions (Figure S11).

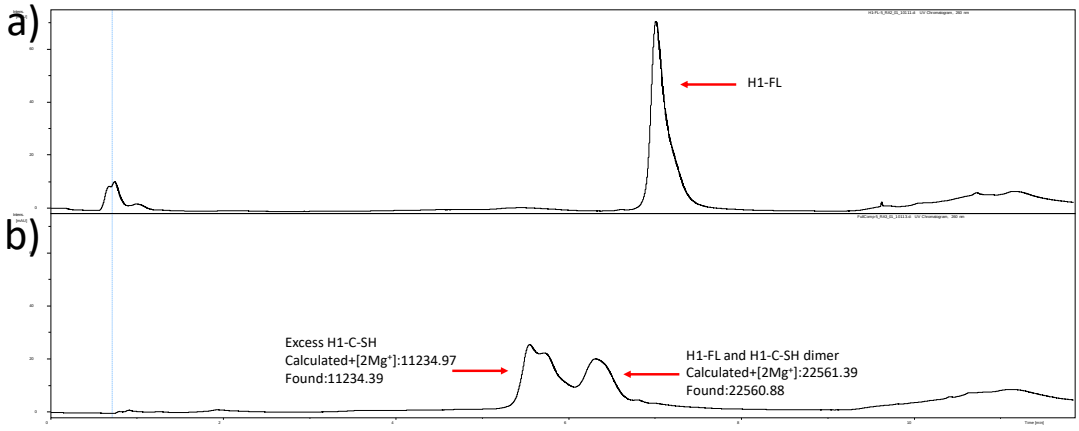

Figure 2. 28 HPLC's indicating the cleavage of the small molecule from the H1-FL hairpin

by hybridizing H1-FL with its complement H1-C-SH in 1xTAMg pH 8 for 24 hr. **(a)** H1-FL **(b)** H1-FL after hybridization with H1-C-SH.

2.5.7.5. Gel Characterization- Native PAGE

The blunt (BA) and sticky (SA) assemblies were examined by Native PAGE assays (5-6%) by mixing with 2 µL of glycerol mix (7:1 glycerol/H2O) and loaded on to the gel with 1xTAMg as the running buffer. The gel was run at 250 V for 2.5 hours, stained with GelRed and imaged.

2.5.7.6. AFM Characterization

Dry AFM was carried out using a MultiMode8™ SPM connected to a Nanoscope™ V controller (Bruker, Santa Barbara, CA). All images were obtained using ScanAsyst mode in air with AC160TS cantilevers (Nominal values: Tip radius – 2 nm, Resonant frequency – 300 kHz, Spring constant – 42 N/m) from Bruker. 5 µL of each sample prepared at 5 µM in TAMg buffer was deposited on a

freshly cleaved mica surface (ca. 7 x 7 mm) and allowed to adsorb for 2-5 seconds. Then 50 µL of 0.22 µm filtered Millipore water was dropped on the surface and instantly removed with filter paper. The surface was then washed with a further 100 µL of water (2 x 50 µL), wicked with a filter paper, and the excess removed with a flow of nitrogen (or air). Samples were dried under vacuum for at least 3 hours prior to imaging

2.5.7.7. DLS Characterization

Dynamic light scattering (DLS) experiments were carried out using a DynaPro™ S10 Instrument from Wyatt Technology. A cumulants fit model was used to confirm the presence and determine the size the SNA's and clusters of SNA's. Sterile water and 1xTAMg buffer were filtered using a 0.45 µm nylon syringe filter before use in DLS sample preparation. 20 µL of sample (concentration: 0.75 µM) was used in each measurement. All measurements were carried out in triplicate at 25 °C.

2.5.8. Original HCR

2.5.8.1. HCR Assembly and initiation Procedure

For all experiments, hairpins H1-FL or H1-CT and I-1 were first prepared separately as 3µM solutions in 1xPBS pH 8. H1-FL or H1-CT were thermocycled from 95^{o}C to 4^{o}C over 4hr. H2-SH was prepared as a 3µM solution in 1xPBS pH 8 following the H2 disulfide reduction procedure (SI-VI c.). I-1 was diluted to 0.300µM (0.1eq), 0.225µM (0.075eq), 0.150µM (0.050eq), and 0.075µM (0.025eq) samples in 1xPBS pH 8. Experiments were then performed by first mixing 25µL of H1-FL or H1-CT, with H2-SH, then diluting with 25µL 1xPBS pH 8. 25µL of initiator was then added according to the specific initiator equivalency, to give 100µL of 750nM final concentrations of each hairpin. For samples with no initiator 25µL of 1xPBS pH 8 was added instead.

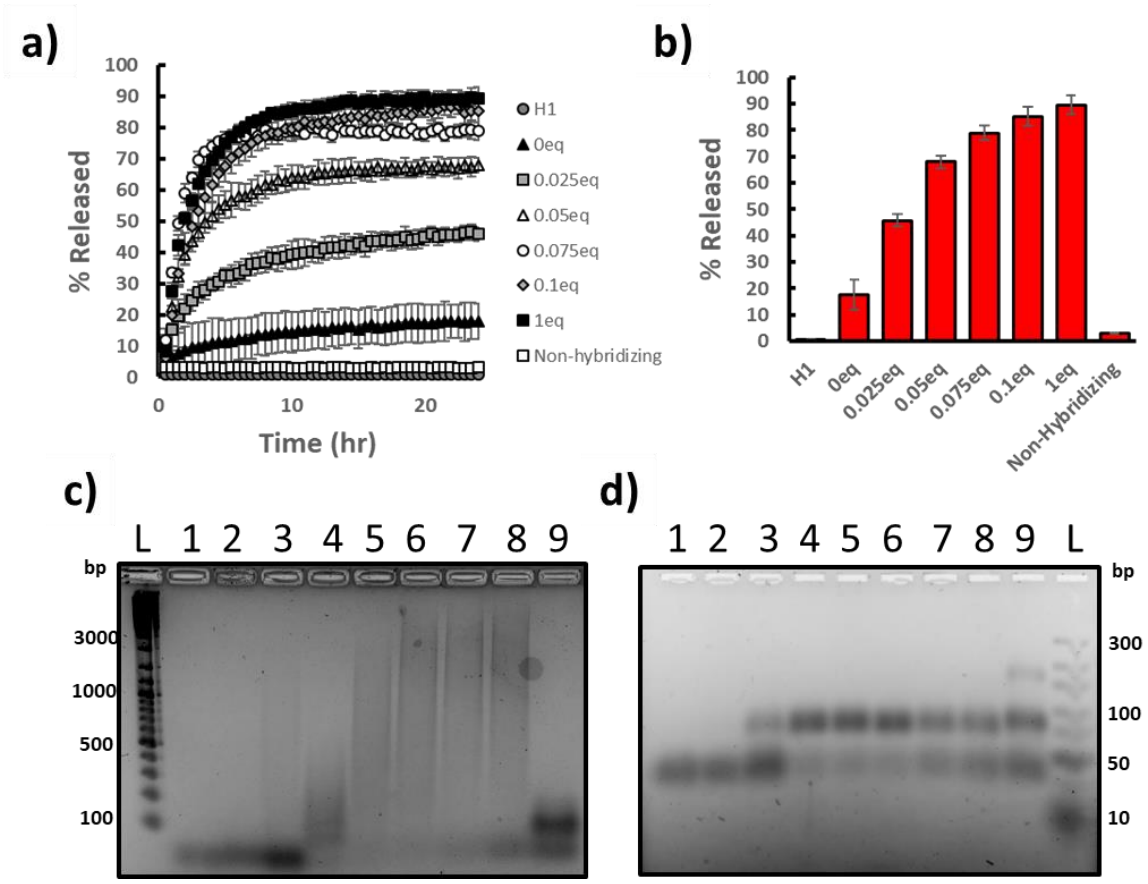

Figure 2. 29 Original HCR characterization

(a) HCR between H1-FL and H2-SH with different initiator equivalence, over 24hr, resulting in the release of methoxyfluorescein. **(b)** Overall released methoxyfluorescein after 24hr. All experiments were run in triplicate and fluorescence was measured at λ_{ex}= 470 nm, λ_{em}= 515 nm. **(c)** Native agarose and **(d)** Denaturing agarose. **L**: Ladder, **Lane 1**: H1-FL, **Lane 2**: H2-SH, **Lane 3**: Lane 1 + Lane 2, **Lane 4**: Lane 3 + 1 equiv. I-1, **Lane 5**: Lane 3 + 0.1 equiv. I-1, **Lane 6**: Lane 3 + 0.075 equiv. I-1, **Lane 7**: Lane 3 + 0.050 equiv. I-1, **Lane 8**: Lane 3 + 0.025 equiv. I-1, **Lane 9**: Lane 1 + H2-2-SH. All experiments were run in triplicate.

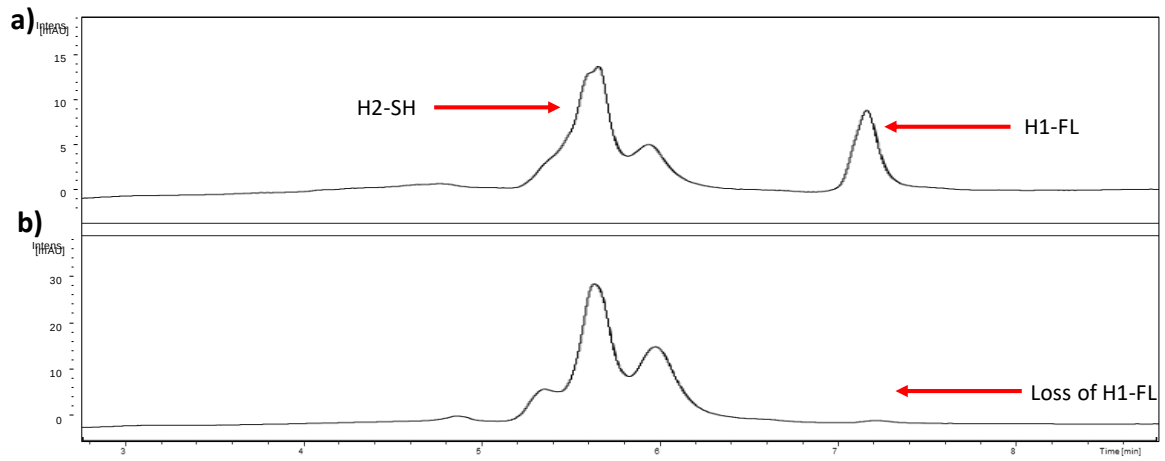

Figure 2. 30 Representative HPLC of Original HCR

(a) H1-FL and H2-SH with no initiator, over 24 hr, **(b)** H1-FL and H2-SH with 1 equiv. I-1, over 24 hr.

Table 2. 3 HPLC Characterization of HCR between H1-FL and H2-SH over 24hr.

Ret. Time, area, height, and amount are based on the H1-FL peak and run in triplicate.

Experiment	Ret. time, min	Area mAU*min	Height, mAU	Amount, nM	Yield,%	Std dev., %
H1-FL	7.2	50.68	12.4	744	99.2	5.5
H2-SH	-	-	-	-	-	-
H1-FL + H2-SH	7.2	37.18	9.2	571	76.1	5.0
H1-FL + H2-SH + 1 equiv. I-1	-	-	-	-	-	-
H1-FL + H2-SH + 0.1 equiv. I-1	7.2	2.35	1.3	126	16.8	1.2
H1-FL + H2-SH + 0.075 equiv. I-1	7.2	4.70	1.8	156	20.8	0.8

H1-FL + H2-SH + 0.05 equiv. I-1	7.2	10.77	4.2	234	31.2	2.0
H1-FL + H2-SH + 0.025 equiv. I-1	7.2	24.43	6.8	408	54.4	1.8
H1-FL + H2-2-SH	7.2	49.38	10.3	727	96.9	2.3

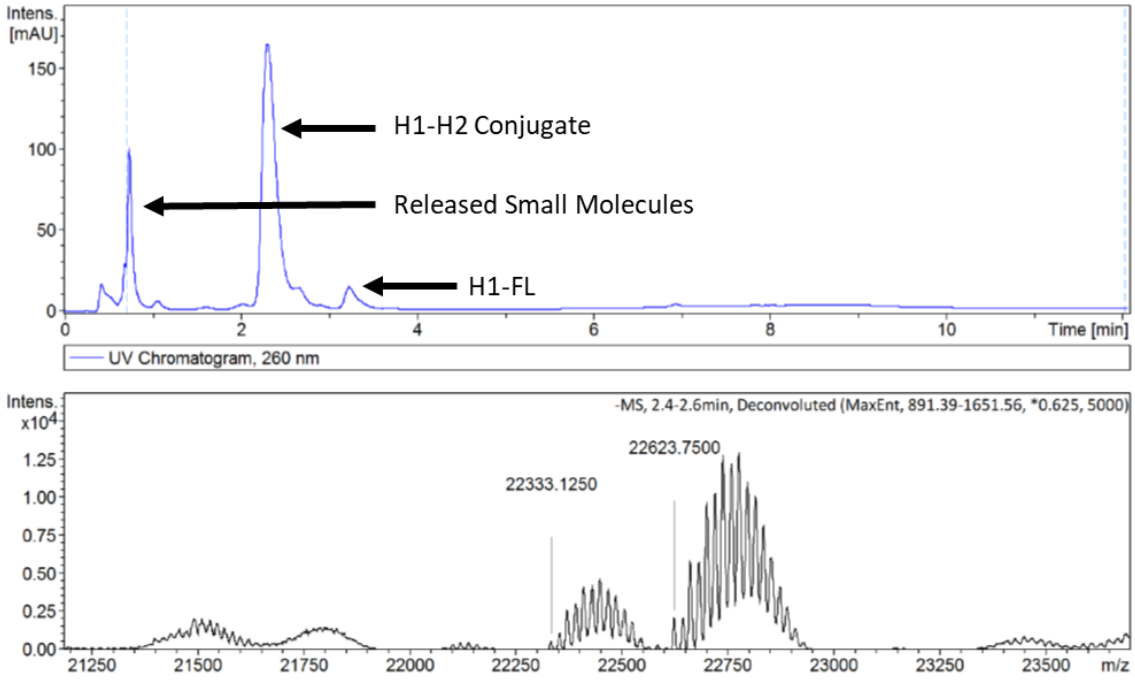

Figure 2. 31 LC-MS of the H1-H2 conjugate produced after HCR polymerization

with 1 equiv. of initiator strand. Calculated [K^+]: 22,624.83 Found: 22,623.75.

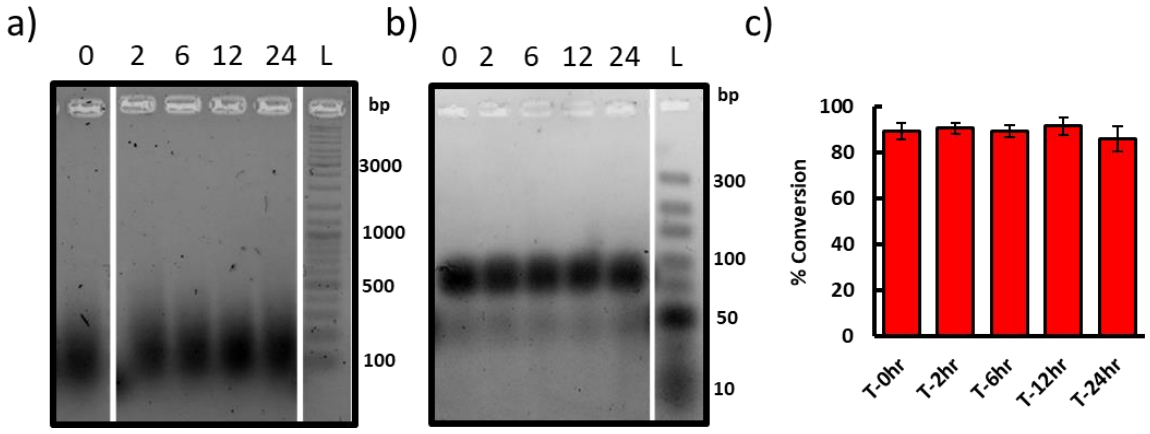

Figure 2. 32 Viability of the HCR reaction over time.

H1-FL and H2-SH were prepared and then mixed together and initiated with 1 equiv. I-1 after 0hr, 2hr, 6hr, 12hr and 24hr. Once a sample was initiated HCR was allowed to proceed for 24hr, at which point the sample was flash frozen, and characterized by **(a)** Native Agarose **(b)** Denaturing agarose: **L:** ladder, **Lane 2**: HCR initiated after 2hr, **Lane 6:** HCR initiated after 6hr, **Lane 12**: HCR initiated after 12hr, **Lane 24:** HCR initiated after 24hr, and **(c)** Overall released methoxyfluorescein after 24hr. All experiments were run in triplicate and fluorescence was measured at λ_{ex}=470 nm, λ_{em}= 515 nm.

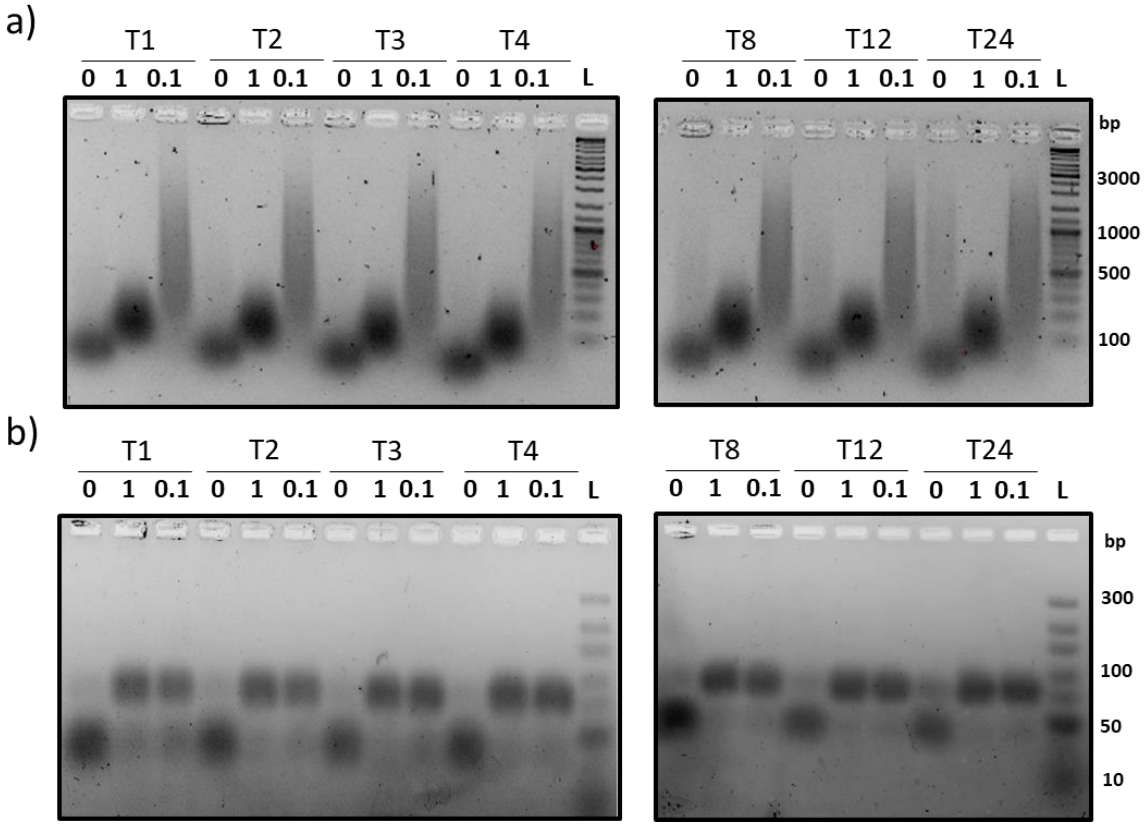

Figure 2. 33 Kinetics of HCR between H1-FL and H2-SH with 0, 1 and 0.1 equiv.

I-1. Aliquots of each sample were taken after 1hr, 2hr, 3hr, 4hr, 8hr, 12hr and 24hr, and flash frozen to be then characterized by **(a)** Native agarose **(b)** Denaturing agarose. **Lanes 0**: H1-FL and H2-SH, **Lanes 1**: H1-FL, H2-SH and 1 equiv. I, **Lanes 0.1**: H1-FL, H2-SH and 0.1 equiv. I. **Lanes T1**: HCR after 1hr, **Lanes T2**: HCR after 2hr, **Lanes T3**: HCR after 3hr, **Lanes T4**: HCR after 4hr, **Lanes T8**: HCR after 8hr, **Lanes T12**: HCR after 12hr, and **Lanes T24**: HCR after 24hr. All experiments were run in triplicate.

2.5.8.2. Kinetics analysis of HCR profiles

The HCR profiles were fit to a model which proceeds through **(i)** a set of repeating, sequential, non-reversible biomolecular reactions to describe the HCR reaction, where addition of the second hairpin (H2) both leads to a species that can then ligate and a sticky end which is the initiator for H1. There was no leakage pathway in this model, thus the concentration of growing polymers remained constant during the entire reaction ($[I] + [IH1] = [I]_0$). We assumed sequential addition of H1 and H2 strands leading to a non-negligible accumulation of partially-extended polymers containing one more H1 than H2 fragments. Thus depletion of H2 strands was slightly

delayed when compared to H1 strands.[29] A model with simultaneous addition of H1 and H2 strands was also tested but found to have ~5% higher RSS and ~5% slower k_1. The rate constant (k_1) was assumed to be equal for both H1 and H2 addition, as the hairpins' stem and toehold regions are the same **(ii)** An effectively unimolecular ligation reaction between hybridized H1 and H2 strands. The fits were insensitive to the exact value of this rate constant; however, a lower bound could be determined. Fits were performed with k_2 fixed at values varying over several orders of magnitude. The RSS was essentially identical for $k_2 \geq$ 1e-3 s^{-1} but increased for slower k_2 (Table S2), identifying 1e-3 s^{-1} as the lower bound. This shows that step (i) is rate-determining for pro-functional molecule release and that ligation is effectively instantaneous compared to the addition of H1 and H2 strands. **(iii)** A unimolecular reaction which describes the immolative cyclization.

The set of Eqs. 1:8 were numerically integrated using the ordinary differential equation (ODE) solvers in MATLAB to obtain the concentrations of <H1, H2>, H1H2, FL, as a function of time.

$$\frac{d[H1]}{dt} = -k_1[I][H1] \text{ (1)}$$

$$\frac{d[H2]}{dt} = -k_1[IH1][H2] \text{ (2)}$$

$$\frac{d[I]}{dt} = -k_1[I][H1] + k_1[IH1][H2] \text{ (3)}$$

$$\frac{d[IH1]}{dt} = k_1[I][H1] - k_1[IH1][H2] \text{ (4)}$$

$$\frac{d[IH1H2]}{dt} = k_1[IH1][H2] - k_2[IH1H2] \text{ (5)}$$

$$\frac{d[H1H2]}{dt} = k_2[IH1H2] \text{ (6)}$$

$$\frac{d[FL]}{dt} = k_2[IH1H2] - k_3[FL] \text{ (7)}$$

$$\frac{d[FL^*]}{dt} = k_3[FL] \text{ (8)}$$

The sets of concentration profiles were fit by varying the kinetic parameters to minimize the RSS between the experimental and fitted absorbance data according to

$$RSS = \sum_{X=(<H1,H2>,\ H1H2,\ FL^*)} \sum_{k=1}^{N} \left(\frac{[X]^{exp}(t_k) - [X]^{sim}(t_k, \varepsilon)}{N * \sigma_{X,k}} \right)^2 \quad (9)$$

Where $[X]^{exp}(t_k)$ and $[X]^{sim}(t_k, \varepsilon)$ are the experimental and fitted concentration profiles respectively for the k[th] time point in the reaction, $\varepsilon = [k_1, k_2, k_3, [Misfolded]]$ are the rate constants of each individual reaction step - optimized parameters can be found in table S1.

2.5.8.3. Statistical Analysis of Errors for Kinetic Fitting

Errors in the fit parameters for HCR parameters were calculated using the variance-covariance matrix[74] given by

$$V = \frac{RSS}{DF} * (X\ W\ X')^{-1} \quad (10)$$

Where *RSS* is the residual sum of squared differences between experimental and fitted data points*, DF* is the degrees of freedom of the fit (*N* data points minus *Φ* parameters of the fit) and *W* is a diagonal matrix of fitting weights, in this case all taken to be identically 1. *X* is a matrix of the first derivatives of the differences between the experimental and calculated data points (A^{exp} and A^{calc}), with respect to increments in each of the adjustable parameters (Φ_i). The element corresponding to the i^{th} adjustable parameter and j^{th} data point is thus

$$X_{ij} = \frac{\partial\left(A_j^{exp} - A_j^{calc}\right)}{\partial \Phi_i} \equiv \frac{\partial \alpha_j}{\partial \Phi_i} \quad (11)$$

where A_j^{calc} is evaluated at the optimized set of parameters, Φ. The elements were evaluated numerically according to

$$X_{ij} = \frac{\partial\left(A_j^{calc}(-\Delta) - A_j^{calc}(+\Delta)\right)}{2\Delta} \quad (12)$$

Where $A_j^{calc}(\pm\Delta)$ is the j^{th} data point calculated with all adjustable parameters set to their optimized values except, for the i^{th} parameter, which is incremented by $\pm\Delta$. For a fit with *N* data points and *M* adjustable parameters this gives

$$X = \begin{bmatrix} \frac{\partial \alpha_1}{\partial \Phi_1} & \cdots & \frac{\partial \alpha_N}{\partial \Phi_1} \\ \vdots & \ddots & \vdots \\ \frac{\partial \alpha_1}{\partial \Phi_M} & \cdots & \frac{\partial \alpha_N}{\partial \Phi_M} \end{bmatrix} \qquad (13)$$

The diagonal elements in *V* are the variances of the optimized fit parameters, while the off-diagonal elements are the covariances between the errors of the optimized parameters. Errors in fitted parameters were taken as the square root of the variances.

2.5.8.4. HCR Kinetic Parameters

Table 2. 4 Optimized Kinetic Parameters

k_1	1e4 ± 1e3 M^{-1} s^{-1}
k_2	$\gtrsim$ 1e-3 s^{-1}
k_3	2.1e-4 ± 2e-5 s^{-1}
[Misfolded]	1.44e-7 ± 5e-9 M
RSS	3.92

Table 2. 5 Varying Ligation Rate

k_1 (M^{-1} s^{-1})	**k_2 (s^{-1})**	**k_3 (s^{-1})**	**[Misfolded] (M)**	**RSS**
1.0e4 ± 1e3	1e3	2.1e-4 ± 2e-5	1.44e-7 ± 5e-9	3.92
1.0e4 ± 1e3	1e2	2.1e-4 ± 2e-5	1.44e-7 ± 5e-9	3.92
1.0e4 ± 1e3	1	2.1e-4 ± 2e-5	1.44e-7 ± 5e-9	3.92

1.0e4 ± 1e3	1e-1	2.1e-4 ± 2e-5	1.44e-7 ± 5e-9	3.92
1.0e4 ± 1e3	1e-2	2.2e-4 ± 2e-5	1.44e-7 ± 5e-9	3.96
1.3e4 ± 2e3	1e-3	2.3e-4 ± 3e-5	1.46e-7 ± 6e-9	4.26
2.9e7 ± 1e6	1e-4	1.0 ± 0.1	1.43e-7 ± 6e-9	14.1
6.7e7 ± 3e6	1e-5	0.5 ± 31	1.1e-7 ± 6e-8	325

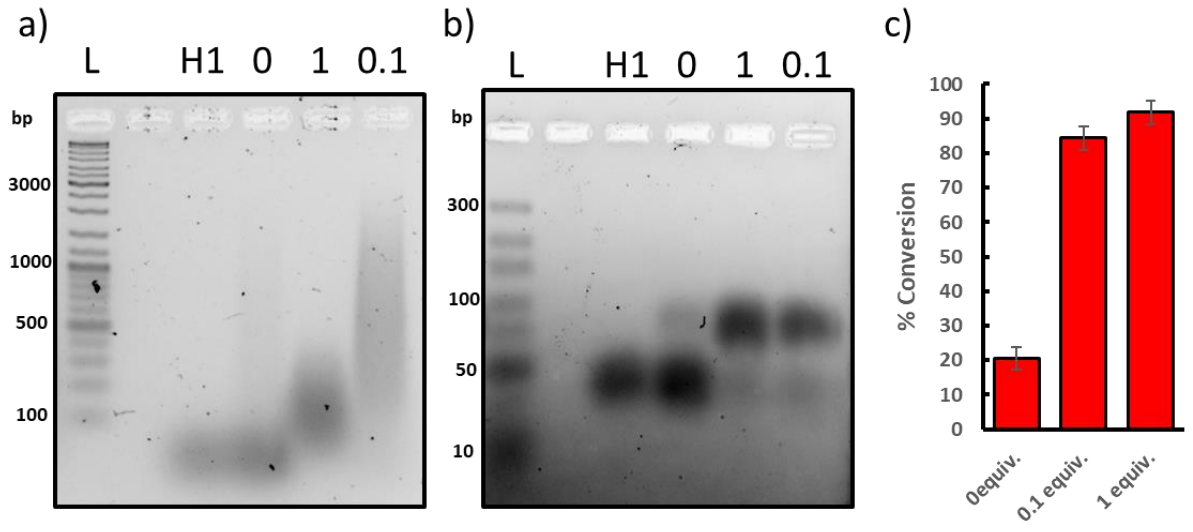

Figure 2. 34 Characterization of HCR with camptothecin conjugated H1

(a) Native agarose **(b)** Denaturing agarose; **Lane 0:** H1-CT + H2-SH, **Lane 1:** Lane 0 + 1 equiv. I-1**, Lane 0.1:** Lane 0 + 0.01 equiv. I-1, and **(c)** Denaturing agarose band intensity analysis. All experiments were run in triplicate.

Table 2. 6 HPLC Characterization of HCR between H1-CT and H2-SH over 24hr.

Ret. Time, area, height, and amount are based on the H1-CT peak and ran in triplicate. *Note that a calibration curve was not made for H1-CT and instead yield and amount are based on the area of the H1-CT peak in each experiment over the area of the H1-CT peak alone, assumed to be 750nM. All runs were performed in triplicate.

Experiment	Ret. time, min	Area mAU*min	Height, mAU	Amount, nM	Yield,%	Std dev., %
H1-CT*	6.6	109.8	28.6	750	-	-
H1-CT + H2-SH	6.6	89.5	24.8	611	81.5	5.6
H1-CT + H2-SH + 1 equiv. I	6.6	9.2	3.0	62.9	8.4	3.2
H1-CT + H2-SH + 0.1 equiv. I	6.6	11.2	4.0	76.2	10.2	4.2

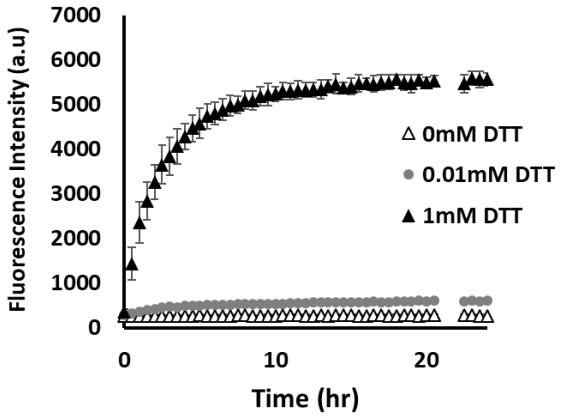

Figure 2. 35 Fluorescence characterization of H1-FL

with 0mM, 0.01mM and 1mM of DTT, over 24hr, resulting in the release of methoxyfluorescein.

Table 2. 7 HPLC Characterization of H1-FL

with 0mM, 0.01mM and 1mM of DTT after 24hr. Ret. Time, area, height, and amount are based on the H1-FL peak and run in triplicate.

Experiment	Ret. time, min	Area mAU*min	Height, mAU	Amount, nM	Yield,%	Std dev., %
H1-FL	7.2	50.68	12.4	744	99.2	5.5
H1-FL + 0.01mM DTT	7.2	47.73	9.9	706	94.1	2.0
H1-FL + 1mM DTT	7.2	2.22	1.2	124	16.5	1.0

2.5.9. Templated HCR

2.5.9.1. Assembly and Initiation Procedure

The blunt (**BA**) and sticky (**SA**) end assemblies were prepared by first combining the two staple strands (S1 & S2) with the desired template (BBB for blunt end assembly or SBB for sticky end assembly) and H1-2-FL in 1xTAMg pH 8, at a final concentration of 1.25µM. For the samples with no template H1-2-FL was diluted to 1.25µM with 1xTAMg pH 8 instead. The mixtures were then annealed from 95°C to 4°C over 8hr. H2-2-SH was prepared separately in 1xTAMg pH 8, as a 5µM solution following the H2 disulfide reduction procedure (SI-VI c.), and added to the mixtures at room temperature for 10 min, bringing the concentration of the mixtures to 1µM. I-2 was prepared separately as 3µM (1equiv.) and 0.3µM (0.1equiv.) solutions in 1xTAMg pH 8. Assemblies were initiated by mixing 75µL of assembly and 25µL initiator according to the specific experimental conditions, and ran at r.t. to give 100µL of 750nM final concentrations of each assembly. For samples with no initiator 25µL of 1xTAMg pH 8 was added instead.

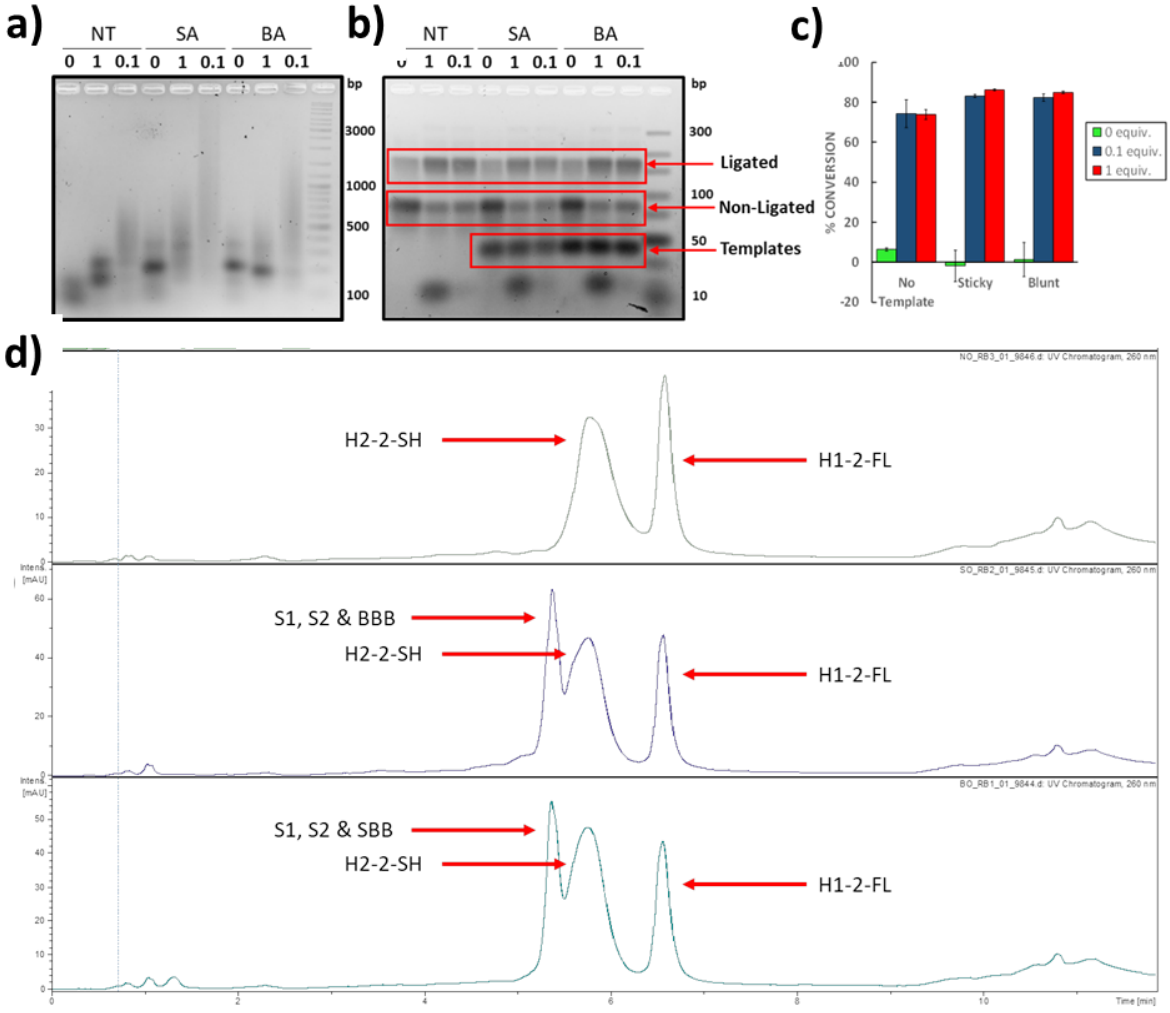

Figure 2. 36 HCR between H1-2-FL and H2-2-SH on blunt and sticky ended assemblies and no template with 0, 1 and 0.1 equiv. I-2 over 24hr,

Characterized by **(a)** Native agarose **(b)** Denaturing agarose. **Lanes 0**: assemblies with 0 equiv. I-2, **Lanes 1**: assemblies with 1 equiv. I-2, **Lanes 0.1**: assemblies with 0.1 equiv. I-2. **Lanes NT**: HCR with no template **Lanes SA**: HCR with sticky end assembly, **Lanes BA**: HCR with blunt end assembly. **(c)** Denaturing agarose analysis using the calibration curve in Figure 2.25. All experiments were run in triplicate. **(d)** HPLC's indicating the stability of H1-2-FL with H2-2-SH after 24hr on No Template (top) Blunt End Template (middle) and Sticky End Template (bottom)

Table 2. 8 HPLC Characterization of HCR between H1-2-FL and H2-2-SH over 24hr.

on No template (NT), Sticky end assembly (SA) and Blunt end assembly (BA) Ret. Time, area, height, and amount are based on the H1-2-FL peak and ran in triplicate.

Experiment	Ret. time, min	Area mAU*min	Height, mAU	Amount, nM	Yield,%	Std dev., %
H1-2-FL	6.7	452.83	47.8	750.0	100.0	0.8
H2-2-SH	-	-	-	-	-	-
H1-2-FL + H2-2-SH	6.7	398.15	45.6	665.6	88.8	6.7
H1-2-FL + H2-2-SH + 1 equiv. I-2	6.7	82.56	9.6	178.8	23.8	1.2
H1-2-FL + H2-2-SH + 0.1 equiv. I-2	6.7	129.41	11.1	251.0	33.5	6.2
SA	6.7	470.90	48.9	777.9	103.7	1.9
SA + 1 equiv. I-2	6.7	57.91	6.2	140.7	18.8	6.3
SA + 0.1 equiv. I-2	6.7	134.10	13.7	258.3	34.4	2.1
BA	6.7	471.33	45.5	778.5	103.8	3.2
BA + 1 equiv. I-2	6.7	76.98	7.4	170.2	22.7	2.1
BA + 0.1 equiv. I-2	6.7	132.19	11.3	255.3	34.0	1.8

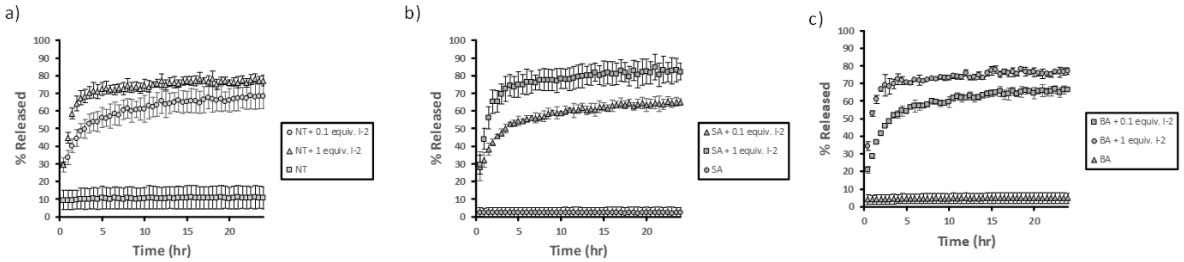

Figure 2. 37 Templated HCR fluorescence characterization of HCR between H1-2-FL and H2-2-SH with 0, 1, and 0.1 equiv. I-2, over 24hr,

on (a) No Template (NT) (b) Sticky End Assembly (SA) and (c) Blunt End Assembly (BA), resulting in the release of methoxyfluorescein. All measurements were made in triplicate and fluorescence was measured at λex= 470 nm, λem= 515 nm.

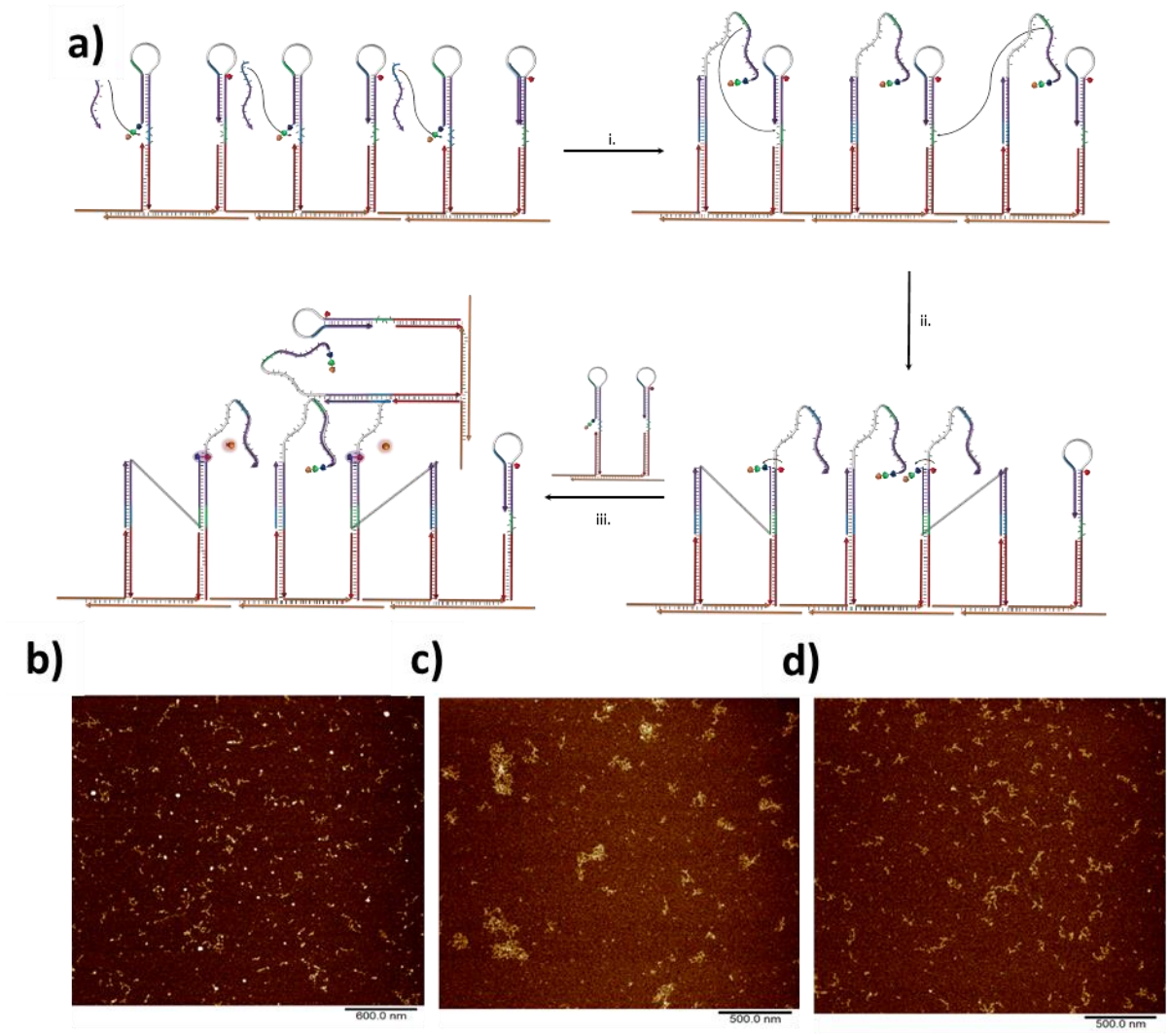

Figure 2. 38 Mechanism and AFM images of templated HCR

(a) Proposed mechanism for the increased amount of clustering for the sticky ended assemblies when initiator I-2 is added. i. H1-2-FL of the pre-organized sticky ended assembly (SA) hybridizes to initiator I-2 at different locations. ii. the polymerization has two directions to hybridize H2-2-SH. iii. Due to the bidirectional polymerization, this leaves un-hybridized, internal hairpins which can only hybridize intermolecularly, increasing the amount of clustering. AFM images of HCR between H1-2-FL and H2-2-SH with 0.1 equiv. I-2 over 24 hr, on **(b)** No Template (NT) **(c)** Sticky end Assembly (SA) and **(d)** Blunt end Assembly (BA). Note: Qualitatively it appears that the SA is more clustered than NT or BA possibly due to more intermolecular hybridizations between units.

2.5.10. SNA HCR

2.5.10.1. Procedure for SNA Assembly and initiation

The spherical nucleic acid (**SNA**) assembly was prepared by first combining the two amphiphilic strands (S1C12 & S2C12) in 1xTAMg pH 8, at a final concentration of 5µM and annealing from 95°C to 4°C over 8hr. H1-2-FL was prepared separately as a 3µM solution in 1xTAMg pH 8 and annealed from 95°C to 4°C over 4hr, before being added to the SNA solution and annealing again from 44°C to 22°C over 4hr, bringing the concentration of the SNA to 2.5µM. H2-2-SH was prepared separately in 1xTAMg pH 8, as a 3uM solution following the H2 disulfide reduction procedure (SI-VI c), and added to the mixture at room temperature for 10 min, bringing the concentration of the SNA to 1.67µM. I-2 was prepared separately as 3µM (1equiv.) and 0.3µM (0.1equiv.) solutions in 1xTAMg pH 8. Assemblies were initiated by mixing 75µL of assembly and 25µL initiator equivalent according to the specific experimental conditions, to give 100µL of 1.25µM final concentrations of SNA and 750nM final concentration of each hairpin. For samples with no initiator 25µL of 1xTAMg pH 8 was added instead.

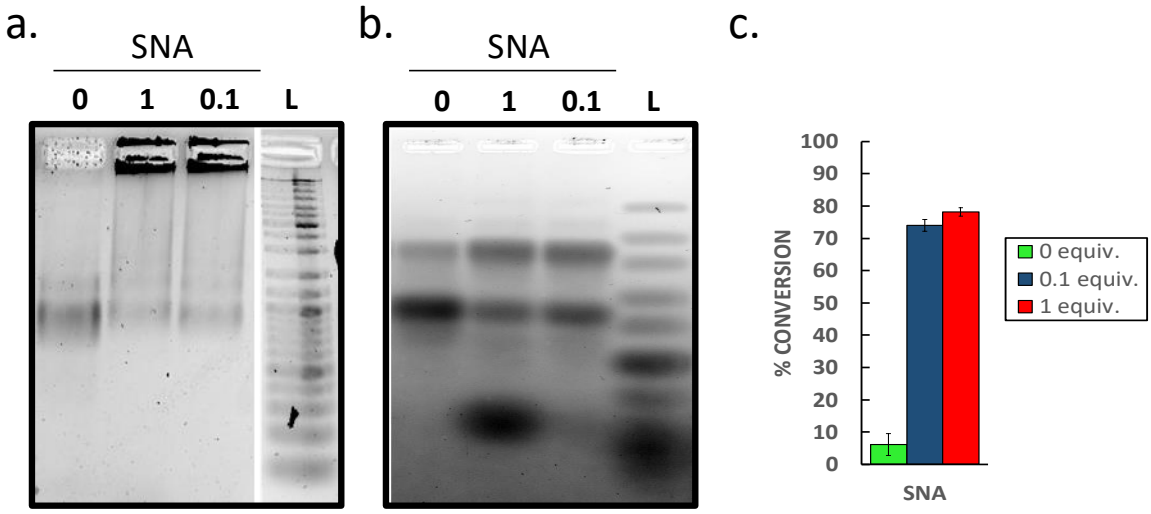

Figure 2. 39 HCR between H1-2-FL and H2-2-SH on a spherical nucleic acid template

with 0, 1 and 0.1 equiv. I-2 over 24hr characterized by (a) Native agarose (b) Denaturing agarose. Lanes 0: assemblies with 0 equiv. I-2, Lanes 1: assemblies with 1 equiv. I-2, Lanes 0.1: assemblies with 0.1 equiv. I-2. (c) Denaturing agarose analysis. All experiments were run in triplicate.

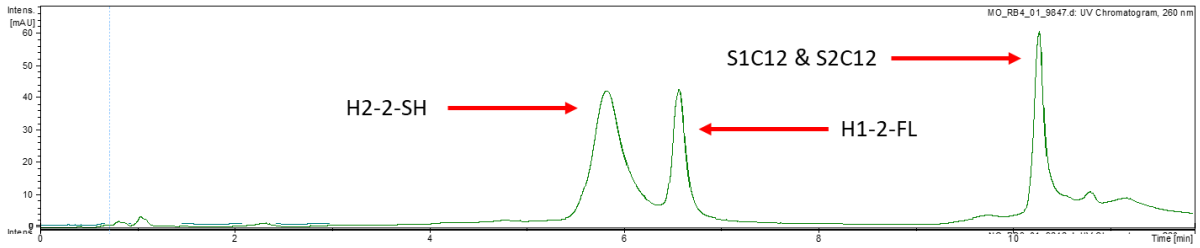

Figure 2. 40 HPLC Trace indicating the stability of H1-2-FL & H2-2-SH after 24hrs on the SNA template.

Table 2. 9 HPLC Characterization of HCR between H1-2-FL and H2-2-SH over 24hr on Spherical nucleic acid assembly (SNA)

Ret. Time, area, height, and amount are based on the H1-2-FL peak and experiments were run in triplicate.

Experiment	Ret. time, min	Area mAU*min	Height, mAU	Amount, nM	Yield,%	Std dev., %
SNA	6.7	387.84	40.3	649.7	86.6	5.1
SNA + 1 equiv. I	6.7	57.53	6.5	140.2	18.7	1.2
SNA + 0.1 equiv. I	6.7	94.67	10.1	197.4	26.3	1.1

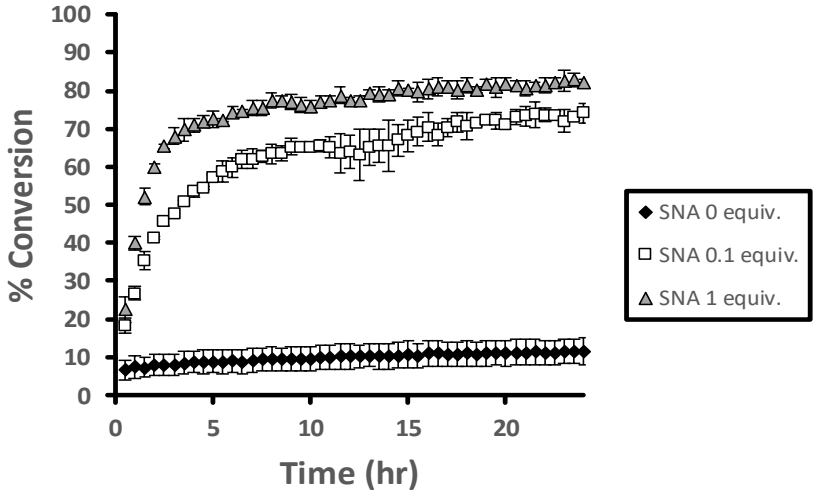

Figure 2. 41 HCR fluorescence characterization of HCR between H1-FL and H2-SH

with 0, 1 and 0.1 equiv. of I-2, over 24hr on a spherical nucleic acid assembly (SNA), resulting in the release of methoxyfluorescein. All experiments were run in triplicate and fluorescence was measured at λex= 470 nm, λem= 515 nm.

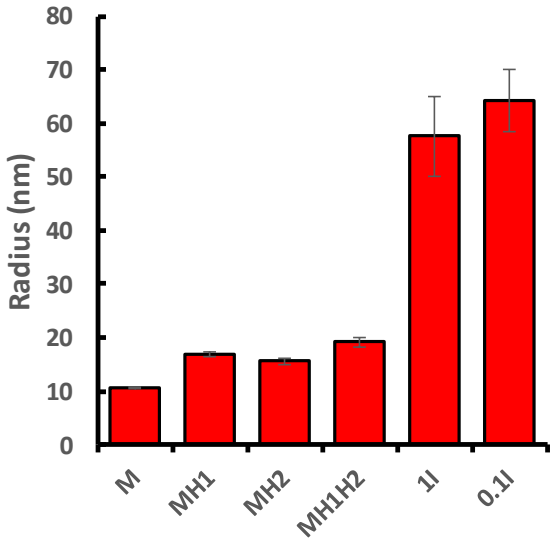

Figure 2. 42 DLS analysis of the average radius of the spherical nucleic acids.

M: S1C12 + S2C12, MH1: S1C12 + S2C12 + H1-2-FL, MH2: S1C12 + S2C12 + H2-2-SH, MH1H2: S1C12 + S2C12 + H1-2-FL + H2-2-SH, 1I: MH1H2+ 1equiv. I-2, 0.1I: MH1H2 + 0.1 equiv. I-2.

2.5.11. Characterization of Molecular Beacon SIP; Strategy 2

2.5.11.1. Gel Characterization- Native PAGE

Strand displacement reaction was monitored using Native PAGE assays (5-6%) by mixing with 2 µL of glycerol mix (7:1 glycerol/H2O) and loaded on to the gel with 1xTAMg as the running buffer. The gel was run at 250 V for 1 hour, stained with GelRed and imaged.

2.5.11.2. Gel Characterization- Denaturing PAGE

Denaturing PAGE was used to analyze the cleavage of the fluorescent dye and subsequent ligation of X2_24-Cy3 to X'_20. Samples were resolved on 20% PAGE (TBE) denaturing gel (20.7 mL H2O, 1.8 mL of 1x TBE, 7.5 mL 40% acrylamide, 8 M urea).

2.5.11.3. Strand displacement procedure

First, separate 10uL solutions of (MB), (S) and (I) were prepared at 9uM in 1x TAMg. Displacement was performed by first mixing 3µL of (MB) and (S), and thermocycling from 95°C to 4°C over 4hr. To the 6uL of (MB:S) duplex, 3uL of (I) was added at room temperature.

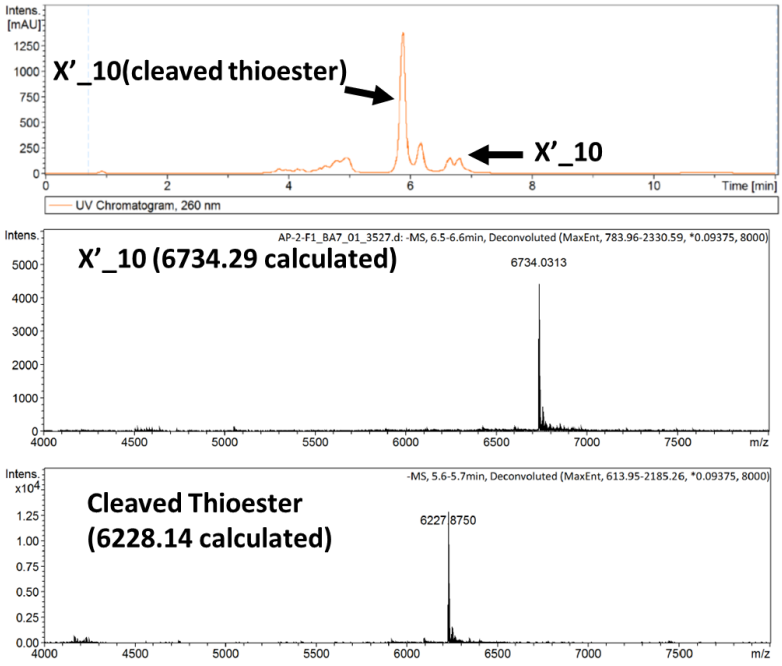

Figure 2. 43 HPLC and MS characterization of X'_10; the thioester readily cleaves to the carboxylic acid product.

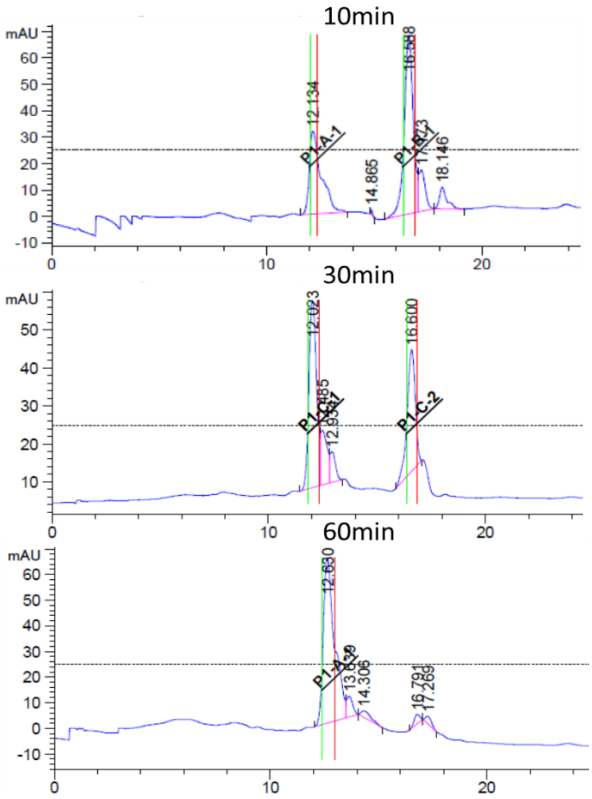

Figure 2. 44 RP-HPLC of X2_20, (3-30% ACN in 50 mins) irradiated at 320nm light

for **(a)** 10min, **(b)** 30min, and **(c)** 60min.

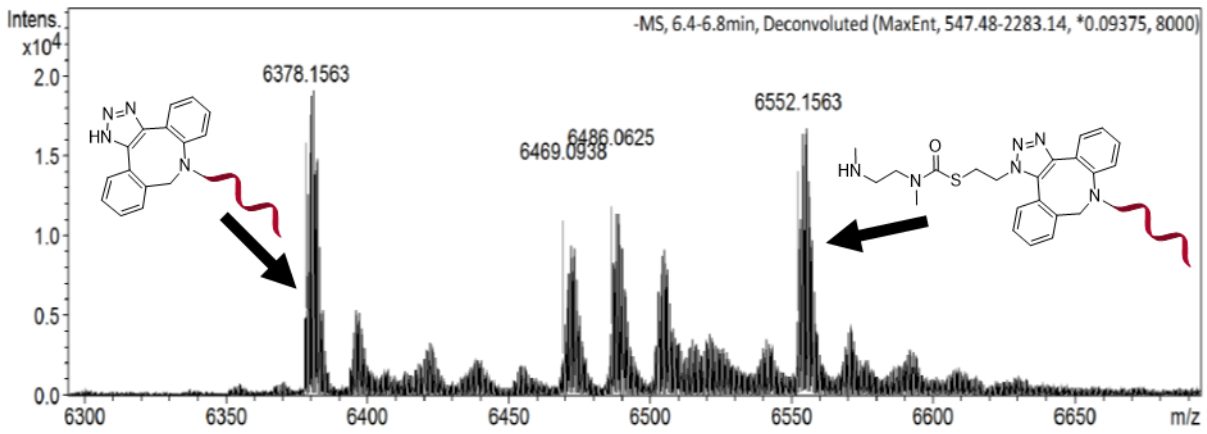

Figure 2. 45 MS Characterization of light cleaved X2_20, after 60min of irradiation.

2.6. References

1. Di Pisa, M.; Seitz, O., Nucleic Acid Templated Reactions for Chemical Biology. *ChemMedChem* **2017,** *12* (12), 872-882.
2. Kolpashchikov, D. M., Evolution of Hybridization Probes to DNA Machines and Robots. *Acc. Chem. Res.* **2019,** *52* (7), 1949-1956.
3. Yu, Y.; Jin, B.; Li, Y.; Deng, Z., Stimuli-Responsive DNA Self-Assembly: From Principles to Applications. *Chemistry – A European Journal* **2019,** *25* (42), 9785-9798.
4. Fakih, H. H.; Fakhoury, J. J.; Bousmail, D.; Sleiman, H. F., Minimalist Design of a Stimuli-Responsive Spherical Nucleic Acid for Conditional Delivery of Oligonucleotide Therapeutics. *ACS Appl. Mater. Interfaces* **2019,** *11* (15), 13912-13920.
5. Bujold, K. E.; Hsu, J. C. C.; Sleiman, H. F., Optimized DNA "Nanosuitcases" for Encapsulation and Conditional Release of siRNA. *J. Am. Chem. Soc.* **2016,** *138* (42), 14030-14038.
6. Nagatsugi, F.; Nakayama, S.; Sasaki, S., Development Of The Novel Drug Releasing System Triggered By Hybridization With Target Sequence. *Nucleosides, Nucleotides Nucleic Acids* **2007,** *26* (6-7), 799-803.
7. Okamoto, A.; Tanabe, K.; Inasaki, T.; Saito, I., Phototriggered Drug Release from Functionalized Oligonucleotides by a Molecular Beacon Strategy. *Angew. Chem. Int. Ed.* **2003,** *42* (22), 2502-2504.
8. Bujold, K. E.; Fakhoury, J.; Edwardson, T. G. W.; Carneiro, K. M. M.; Briard, J. N.; Godin, A. G.; Amrein, L.; Hamblin, G. D.; Panasci, L. C.; Wiseman, P. W.; Sleiman, H. F., Sequence-responsive unzipping DNA cubes with tunable cellular uptake profiles. *Chemical Science* **2014,** *5* (6), 2449-2455.
9. Dirks, R. M.; Pierce, N. A., Triggered amplification by hybridization chain reaction. *Proc. Natl. Acad. Sci. U. S. A.* **2004,** *101* (43), 15275-15278.
10. Yin, P.; Choi, H. M. T.; Calvert, C. R.; Pierce, N. A., Programming biomolecular self-assembly pathways. *Nature* **2008,** *451*, 318.
11. Ma, Z.; Taylor, J.-S., Nucleic acid-triggered catalytic drug release. *Proceedings of the National Academy of Sciences* **2000,** *97* (21), 11159-11163.
12. Gorska, K.; Manicardi, A.; Barluenga, S.; Winssinger, N., DNA-templated release of functional molecules with an azide-reduction-triggered immolative linker. *Chem. Commun.* **2011,** *47* (15), 4364-4366.
13. Chang, D.; Lindberg, E.; Winssinger, N., Critical Analysis of Rate Constants and Turnover Frequency in Nucleic Acid-Templated Reactions: Reaching Terminal Velocity. *J. Am. Chem. Soc.* **2017,** *139* (4), 1444-1447.
14. Sadhu, K. K.; Winssinger, N., Detection of miRNA in Live Cells by Using Templated RuII-Catalyzed Unmasking of a Fluorophore. *Chemistry – A European Journal* **2013,** *19* (25), 8182-8189.
15. Kim, K. T.; Angerani, S.; Chang, D.; Winssinger, N., Coupling of DNA Circuit and Templated Reactions for Quadratic Amplification and Release of Functional Molecules. *J. Am. Chem. Soc.* **2019,** *141* (41), 16288-16295.
16. Ma, Z.; Taylor, J.-S., Nucleic acid triggered catalytic drug and probe release: A new concept for the design of chemotherapeutic and diagnostic agents. *Bioorg. Med. Chem.* **2001,** *9* (9), 2501-2510.
17. Holtzer, L.; Oleinich, I.; Anzola, M.; Lindberg, E.; Sadhu, K. K.; Gonzalez-Gaitan, M.; Winssinger, N., Nucleic Acid Templated Chemical Reaction in a Live Vertebrate. *ACS Central Science* **2016,** *2* (6), 394-400.
18. Chiu, J.; Hogg, P. J., Allosteric disulfides: Sophisticated molecular structures enabling flexible protein regulation. *The Journal of biological chemistry* **2019,** *294* (8), 2949-2960.

19. Butera, D.; Wind, T.; Lay, A. J.; Beck, J.; Castellino, F. J.; Hogg, P. J., Characterization of a reduced form of plasma plasminogen as the precursor for angiostatin formation. *The Journal of biological chemistry* **2014,** *289* (5), 2992-3000.
20. Chiu, J.; Wong, J. W. H.; Gerometta, M.; Hogg, P. J., Mechanism of Dimerization of a Recombinant Mature Vascular Endothelial Growth Factor C. *Biochemistry* **2014,** *53* (1), 7-9.
21. He, Y.; Liu, D. R., Autonomous multistep organic synthesis in a single isothermal solution mediated by a DNA walker. *Nat. Nanotechnol.* **2010,** *5*, 778.
22. Roth, M. E.; Green, O.; Gnaim, S.; Shabat, D., Dendritic, Oligomeric, and Polymeric Self-Immolative Molecular Amplification. *Chem. Rev.* **2016,** *116* (3), 1309-1352.
23. Weinstain, R.; Sagi, A.; Karton, N.; Shabat, D., Self-Immolative Comb-Polymers: Multiple-Release of Side-Reporters by a Single Stimulus Event. **2008,** *14* (23), 6857-6861.
24. Zhang, D. Y.; Seelig, G., Dynamic DNA nanotechnology using strand-displacement reactions. *Nature Chem.* **2011,** *3* (2), 103-113.
25. Choi, H. M. T.; Beck, V. A.; Pierce, N. A., Next-Generation in Situ Hybridization Chain Reaction: Higher Gain, Lower Cost, Greater Durability. *ACS Nano* **2014,** *8* (5), 4284-4294.
26. Yin, P.; Choi, H. M. T.; Calvert, C. R.; Pierce, N. A., Programming biomolecular self-assembly pathways. *Nature* **2008,** *451* (7176), 318-322.
27. Ren, K.; Xu, Y.; Liu, Y.; Yang, M.; Ju, H., A Responsive "Nano String Light" for Highly Efficient mRNA Imaging in Living Cells via Accelerated DNA Cascade Reaction. *ACS Nano* **2018,** *12* (1), 263-271.
28. Chatterjee, G.; Dalchau, N.; Muscat, R. A.; Phillips, A.; Seelig, G., A spatially localized architecture for fast and modular DNA computing. *Nat. Nanotechnol.* **2017,** *12* (9), 920-927.
29. Bui, H.; Miao, V.; Garg, S.; Mokhtar, R.; Song, T.; Reif, J., Design and Analysis of Localized DNA Hybridization Chain Reactions. *Small* **2017,** *13* (12), 1602983.
30. Bui, H.; Shah, S.; Mokhtar, R.; Song, T.; Garg, S.; Reif, J., Localized DNA Hybridization Chain Reactions on DNA Origami. *ACS Nano* **2018,** *12* (2), 1146-1155.
31. Wang, J.; Wang, D.-X.; Ma, J.-Y.; Wang, Y.-X.; Kong, D.-M., Three-dimensional DNA nanostructures to improve the hyperbranched hybridization chain reaction. *Chemical Science* **2019**.
32. Park, C. R.; Park, S. J.; Lee, W. G.; Hwang, B. H., Biosensors Using Hybridization Chain Reaction - Design and Signal Amplification Strategies of Hybridization Chain Reaction. *Biotechnol. Bioprocess Eng.* **2018,** *23* (4), 355-370.
33. Choi, H. M. T.; Chang, J. Y.; Trinh, L. A.; Padilla, J. E.; Fraser, S. E.; Pierce, N. A., Programmable in situ amplification for multiplexed imaging of mRNA expression. *Nat. Biotechnol.* **2010,** *28* (11), 1208-1212.
34. Zhu, G.; Zheng, J.; Song, E.; Donovan, M.; Zhang, K.; Liu, C.; Tan, W., Self-assembled, aptamer-tethered DNA nanotrains for targeted transport of molecular drugs in cancer theranostics. *Proceedings of the National Academy of Sciences* **2013,** *110* (20), 7998-8003.
35. Wang, Y.-M.; Wu, Z.; Liu, S.-J.; Chu, X., Structure-Switching Aptamer Triggering Hybridization Chain Reaction on the Cell Surface for Activatable Theranostics. *Anal. Chem.* **2015,** *87* (13), 6470-6474.
36. Meng, W.; Muscat, R. A.; McKee, M. L.; Milnes, P. J.; El-Sagheer, A. H.; Bath, J.; Davis, B. G.; Brown, T.; O'Reilly, R. K.; Turberfield, A. J., An autonomous molecular assembler for programmable chemical synthesis. *Nature Chem.* **2016,** *8*, 542.
37. Jiang, T.; Zhou, L.; Liu, H.; Zhang, P.; Liu, G.; Gong, P.; Li, C.; Tan, W.; Chen, J.; Cai, L., Monitorable Mitochondria-Targeting DNAtrain for Image-Guided Synergistic Cancer Therapy. *Anal. Chem.* **2019,** *91* (11), 6996-7000.

38. Tan, W.; Wang, K.; Drake, T. J., Molecular beacons. *Curr. Opin. Chem. Biol.* **2004,** *8* (5), 547-553.
39. De Stefano, M.; Vesterager Gothelf, K., Dynamic Chemistry of Disulfide Terminated Oligonucleotides in Duplexes and Double-Crossover Tiles. *ChemBioChem* **2016,** *17* (12), 1122-1126.
40. McKee, M. L.; Evans, A. C.; Gerrard, S. R.; O'Reilly, R. K.; Turberfield, A. J.; Stulz, E., Peptidomimetic bond formation by DNA-templated acyl transfer. *Org. Biomol. Chem.* **2011,** *9* (5), 1661-1666.
41. Li, D.; Wang, X.; Shi, F.; Sha, R.; Seeman, N. C.; Canary, J. W., Templated DNA ligation with thiol chemistry. *Org. Biomol. Chem.* **2014,** *12* (44), 8823-8827.
42. Patzke, V.; McCaskill, J. S.; Kiedrowski, G. v., DNA with 3'-5'-Disulfide Links—Rapid Chemical Ligation through Isosteric Replacement. *Angew. Chem. Int. Ed.* **2014,** *53* (16), 4222-4226.
43. Meyer, Y.; Richard, J.-A.; Massonneau, M.; Renard, P.-Y.; Romieu, A., Development of a New Nonpeptidic Self-Immolative Spacer. Application to the Design of Protease Sensing Fluorogenic Probes. *Org. Lett.* **2008,** *10* (8), 1517-1520.
44. Meyer, Y.; Richard, J.-A.; Delest, B.; Noack, P.; Renard, P.-Y.; Romieu, A., A comparative study of the self-immolation of para-aminobenzylalcohol and hemithioaminal-based linkers in the context of protease-sensitive fluorogenic probes. *Org. Biomol. Chem.* **2010,** *8* (8), 1777-1780.
45. Dan, K.; Veetil, A. T.; Chakraborty, K.; Krishnan, Y., DNA nanodevices map enzymatic activity in organelles. *Nat. Nanotechnol.* **2019,** *14* (3), 252-259.
46. Bosson, Andrew D.; Zamudio, Jesse R.; Sharp, Phillip A., Endogenous miRNA and Target Concentrations Determine Susceptibility to Potential ceRNA Competition. *Mol. Cell* **2014,** *56* (3), 347-359.
47. Chen, X.; Briggs, N.; McLain, J. R.; Ellington, A. D., Stacking nonenzymatic circuits for high signal gain. *Proceedings of the National Academy of Sciences* **2013,** *110* (14), 5386-5391.
48. Zhang, D. Y.; Winfree, E., Robustness and modularity properties of a non-covalent DNA catalytic reaction. *Nucleic Acids Res.* **2010,** *38* (12), 4182-4197.
49. Zhang, D. Y.; Turberfield, A. J.; Yurke, B.; Winfree, E., Engineering Entropy-Driven Reactions and Networks Catalyzed by DNA. *Science* **2007,** *318* (5853), 1121-1125.
50. Mura, S.; Nicolas, J.; Couvreur, P., Stimuli-responsive nanocarriers for drug delivery. *Nat. Mater.* **2013,** *12* (11), 991-1003.
51. Xu, Q.; Zhu, G.; Zhang, C.-y., Homogeneous Bioluminescence Detection of Biomolecules Using Target-Triggered Hybridization Chain Reaction-Mediated Ligation without Luciferase Label. *Anal. Chem.* **2013,** *85* (14), 6915-6921.
52. Wang, L.; Li, W.; Sun, J.; Zhang, S.-Y.; Yang, S.; Li, J.; Li, J.; Yang, H.-H., Imaging of Receptor Dimers in Zebrafish and Living Cells via Aptamer Recognition and Proximity-Induced Hybridization Chain Reaction. *Anal. Chem.* **2018,** *90* (24), 14433-14438.
53. Lacroix, A.; Vengut-Climent, E.; de Rochambeau, D.; Sleiman, H. F., Uptake and Fate of Fluorescently Labeled DNA Nanostructures in Cellular Environments: A Cautionary Tale. *ACS Central Science* **2019,** *5* (5), 882-891.
54. Engelen, W.; Wijnands, S. P. W.; Merkx, M., Accelerating DNA-Based Computing on a Supramolecular Polymer. *J. Am. Chem. Soc.* **2018,** *140* (30), 9758-9767.
55. Zhou, J.; Du, X.; Yamagata, N.; Xu, B., Enzyme-Instructed Self-Assembly of Small d-Peptides as a Multiple-Step Process for Selectively Killing Cancer Cells. *J. Am. Chem. Soc.* **2016,** *138* (11), 3813-3823.
56. Tan, X.; Li, B. B.; Lu, X.; Jia, F.; Santori, C.; Menon, P.; Li, H.; Zhang, B.; Zhao, J. J.; Zhang, K., Light-Triggered, Self-Immolative Nucleic Acid-Drug Nanostructures. *J. Am. Chem. Soc.* **2015,** *137* (19), 6112-6115.

57. Tan, X.; Lu, X.; Jia, F.; Liu, X.; Sun, Y.; Logan, J. K.; Zhang, K., Blurring the Role of Oligonucleotides: Spherical Nucleic Acids as a Drug Delivery Vehicle. *J. Am. Chem. Soc.* **2016,** *138* (34), 10834-10837.
58. Kapadia, C. H.; Melamed, J. R.; Day, E. S., Spherical Nucleic Acid Nanoparticles: Therapeutic Potential. *BioDrugs* **2018,** *32* (4), 297-309.
59. Fakhoury, J. J.; Edwardson, T. G.; Conway, J. W.; Trinh, T.; Khan, F.; Barłóg, M.; Bazzi, H. S.; Sleiman, H. F., Antisense precision polymer micelles require less poly(ethylenimine) for efficient gene knockdown. *Nanoscale* **2015,** *7* (48), 20625-20634.
60. Edwardson, T. G. W.; Carneiro, K. M. M.; Serpell, C. J.; Sleiman, H. F., An Efficient and Modular Route to Sequence-Defined Polymers Appended to DNA. *Angew. Chem. Int. Ed.* **2014,** *53* (18), 4567-4571.
61. Bousmail, D.; Amrein, L.; Fakhoury, J. J.; Fakih, H. H.; Hsu, J. C. C.; Panasci, L.; Sleiman, H. F., Precision spherical nucleic acids for delivery of anticancer drugs. *Chemical Science* **2017,** *8* (9), 6218-6229.
62. Kaufmann, L.; Traulsen, N. L.; Springer, A.; Schröder, H. V.; Mäkelä, T.; Rissanen, K.; Schalley, C. A., Evaluation of multivalency as an organization principle for the efficient synthesis of doubly and triply threaded amide rotaxanes. *Organic Chemistry Frontiers* **2014,** *1* (5), 521-531.
63. Wang, Z.; Gao, M.; Sun, J.; Liang, D.; Jia, X., Photoresponsive Dendronized Copolymers of Styrene and Maleic Anhydride Pendant with Poly(amidoamine) Dendrons as Side Groups. *Macromolecules* **2013,** *46* (5), 1723-1731.
64. Kumazawa, M.; Tejima, M.; Fukuda, M.; Takeda, S.; Suzuki, K.; Mizumoto, Y.; Sato, K.; Waki, M.; Miyachi, H.; Asai, A.; Takikawa, O.; Hashimoto, T.; Ohno, O.; Matsuno, K., Discovery of Carbono(di)thioates as Indoleamine 2,3-Dioxygenase 1 Inhibitors. *ACS Medicinal Chemistry Letters* **2021,** *12* (2), 211-216.
65. Gao, J.; Wang, P.; Giese, R. W., Xanthamide Fluorescent Dyes. *Anal. Chem.* **2002,** *74* (24), 6397-6401.
66. Wang, H.; Zhuang, J.; Thayumanavan, S., Functionalizable Amine-Based Polymer Nanoparticles. *ACS Macro Letters* **2013,** *2* (10), 948-951.
67. Suma, T.; Cui, J.; Müllner, M.; Fu, S.; Tran, J.; Noi, K. F.; Ju, Y.; Caruso, F., Modulated Fragmentation of Proapoptotic Peptide Nanoparticles Regulates Cytotoxicity. *J. Am. Chem. Soc.* **2017,** *139* (11), 4009-4018.
68. Murthy, N.; Campbell, J.; Fausto, N.; Hoffman, A. S.; Stayton, P. S., Bioinspired pH-Responsive Polymers for the Intracellular Delivery of Biomolecular Drugs. *Bioconjugate Chem.* **2003,** *14* (2), 412-419.
69. Dewit, M. A.; Beaton, A.; Gillies, E. R., A reduction sensitive cascade biodegradable linear polymer. *J. Polym. Sci., Part A: Polym. Chem.* **2010,** *48* (18), 3977-3985.
70. Reja, S. I.; Sharma, N.; Gupta, M.; Bajaj, P.; Bhalla, V.; Parihar, R. D.; Ohri, P.; Kaur, G.; Kumar, M., A Highly Selective Fluorescent Probe for Detection of Hydrogen Sulfide in Living Systems: In Vitro and in Vivo Applications. *Chemistry – A European Journal* **2017,** *23* (41), 9872-9878.
71. Cheetham, A. G.; Ou, Y.-C.; Zhang, P.; Cui, H., Linker-determined drug release mechanism of free camptothecin from self-assembling drug amphiphiles. *Chem. Commun.* **2014,** *50* (45), 6039-6042.
72. Rühling, A.; Schaepe, K.; Rakers, L.; Vonhören, B.; Tegeder, P.; Ravoo, B. J.; Glorius, F., Modular Bidentate Hybrid NHC-Thioether Ligands for the Stabilization of Palladium Nanoparticles in Various Solvents. *Angew. Chem. Int. Ed.* **2016,** *55* (19), 5856-5860.
73. Ang, Y. S.; Yung, L.-Y. L., Rational design of hybridization chain reaction monomers for robust signal amplification. *Chem. Commun.* **2016,** *52* (22), 4219-4222.
74. Tellinghuisen, J., Statistical Error Propagation. *The Journal of Physical Chemistry A* **2001,** *105* (15), 3917-3921.

|3|

Investigating the *in vitro* Fate of Disulfide Spherical Nucleic Acids

This chapter is composed mainly of work from the *manuscript in preparation "*Investigating the *in vitro* Fate of Disulfide Spherical Nucleic Acids" by Alexander L. Prinzen, Jathavan Asohan, Violeta Toader, Xin Luo and Hanadi F. Sleiman.

Contribution of Authors: Alexander Prinzen helped design and develop the project, primarily contributed to the production of experimental data from small molecule synthesis, DNA synthesis, HPLC purification, size exclusion chromatography, mass spectrometry (MS), electrophoresis, dynamic light scattering (DLS), nile red assays, binding experiments and wrote the manuscript. **Jathavan Asohan** performed the firefly luciferase gene silencing assays, flow cytometry experiments and fluorescence microscopy experiments. **Alexander Prinzen** and **Jathavan Asohan** both analyzed *in vitro* data. **Violeta Toader** synthesized the final steps for the phosphoramidites. **Xin Luo** performed some AFM imaging. **Hanadi F. Sleiman** designed the project, guided interpretation of data, result discussion, co-wrote the paper and provided funding for the project

3.1 Preface

In Chapter 2 we modified oligonucleotides for the stimuli responsive release of small molecule drugs. While small molecule drugs are the most widely used form of therapeutic, there are many drug targets that are not accessible by small molecules, as most small molecule drugs, must bind to enzyme active sites to generate an effect. Nucleic acid therapeutics (NATs) on the other hand, open many more targets as they act on the post-transcriptional level. However, the delivery of NATs to their intended targets faces many barriers. Spherical nucleic acids (SNAs) are 3D spherical nanostructures consisting of densely packed oligonucleotides. SNAs have been used to improve biodistribution, cellular uptake and stability of NATs, however protein binding, and target accessibility remain limitations of these particles. In this chapter, by introducing biodegradable disulfide bonds into the core of SNAs we sought to improve silencing through selective degradation of the particles under intracellular conditions. However, by testing the stimuli responsiveness under *in vitro* conditions, we serendipitously discovered that these SNAs fall apart to bind serum protein albumin. We found that our strands, when bound to albumin, improved the protein's cellular uptake. Through our carefully designed studies we reasoned that observed silencing patterns were caused by differences in release rate from this protein. With this new mechanistic information, we pursued 3 areas, 1) non transfected silencing, 2) crosslinking of the SNAs and 3) extended silencing of the albumin bound strands. Overall, our study reinforces that accessibility of NATs to bind their targets is important for their efficacy

whether the ASO is in a SNA or bound to albumin. Overall, this chapter provides a holistic study on the fate of our SNAs under *in vitro* conditions, then applies this information to enhance gene silencing.

3.2 Introduction

Oligonucleotide therapeutics have the potential to revolutionize the treatment of various diseases, by providing the ability to treat previously undruggable targets[1-2]. Of the different oligonucleotide therapeutics, antisense oligonucleotides (ASOs) have found widespread use due to notable advantages such as their single stranded nature, high stability, and ease of production through solid phase synthesis.[3] However, the ability for an ASOs to treat a disease depends on a variety of factors including biodistribution, stability, and cellular uptake.[4-5] Due to the repulsion between the negatively charged oligonucleotides, and cellular membranes uptake of nucleic acid material into cells remains challenging. Additionally, nucleases present in blood, can readily degrade single stranded oligonucleotides before ever reaching the intended target. Moreover, most oligonucleotides are directed towards the liver and kidneys and have limited circulation lifetimes.

To address these issues spherical nucleic acids (SNAs) have been developed and found a wide range of applications including diagnostics, drug delivery and gene silencing.[6] These are 3D spherical nanostructures consisting of densely packed oligonucleotides. The high density of strands packed into a spherical shape protects the strands from nuclease degradation.[7-8] SNAs have also been found to have improved cellular uptake, as the highly dense negative charge of these nanostructures most likely results in recognition by scavenger receptors.[9-10] Additionally SNAs have increase circulation times *in vivo,* as their nanometer size avoids renal clearance[11-12].

In the Sleiman lab, we have generated SNAs using sequence defined polymers[13] for both drug delivery[11] and gene silencing[14-16]. Sequence defined SNAs are particles arising from the self-assembly of DNA-polymer strands in aqueous media. These molecules are synthesized via sequence-controlled addition of non-canonical bases to a growing DNA strand on solid support, using automated DNA synthesis, generating a hydrophobic block. Multiple copies of a DNA-

polymer strand than assemble into micellar particles with a narrow dispersity[13]. From a clinical point of view, these particles are advantageous, due to being composed of a single type of molecule that form larger structures with very low polydispersity, easing their FDA approval process.

The accessibility of NATs to bind their intracellular targets is important for their gene silencing abilities[14, 17-19]. While encapsulation of NATs into nanoparticles improves cellular uptake and *in vivo* distribution, this can diminish their accessibility and silencing ability, post internalization[20]. Ideally, an SNA that maintains its shape and then disassembles upon internalization would have increased silencing capability. Previous work has shown that SNAs which disassemble intracellularly have better therapeutic profiles than SNAs that remained intact[14, 20]. Currently, the core of these sequence defined SNAs has been limited to simple hydrophobic modifications, arising from phosphoramidite building blocks. While these amidites have proven useful in assembling SNAs, introducing biodegradable bonds within the core of the SNAs could improve their silencing ability, and has yet to be explored.

Part of the challenge in producing sequence-defined, stimuli responsive SNAs, is the compatibility of the stimuli-responsive component with solid phase oligonucleotide synthesis. Any modification that is introduced must be compatible with the multiple coupling, oxidation, capping, and final deprotection steps, which limits the type of stimuli that can be used for eventual core destabilization. One functionality that is both compatible with the synthesis cycle and is responsive to intracellular reducing conditions is the disulfide bond.

High concentration of glutathione intracellularly provides an excellent stimulus to break disulfide bonds and has been taken advantage of in a multitude of stimuli-responsive devices, which are specifically triggered inside cells[21-23]. Oligonucleotides conjugated with disulfide polymers have been previously used for the delivery of anticancer therapeutics[24] and ASOs[25]. Moreover, disulfides have been used as cleavable linkages between ASOs and uptake enhancing ligands[18]. Different disulfide phosphoramidites have also been conjugated to oligonucleotides and used for the chemical ligation of DNA tiles[26], studying hairpin stem-loop structures[27] as well as providing mechanistic insights into protein binding[28]. Therefore, disulfide phosphoramidites can bridge the

gap, between stimuli-responsiveness and DNA synthesis, selectively dissociating in the presence of glutathione, while having compatibility with the oligonucleotide synthesis cycle.

In this chapter, we begin by developing a hydrophobic disulfide phosphoramidite that can be added sequentially to an ASO using a traditional oligonucleotide synthesizer, to generate sequence-defined, reduction responsive SNAs. We generated a series of SNAs, each with different numbers of disulfide units appended to the ASO. We find that the disulfide SNAs have much better silencing ability than SNAs without any disulfides. Interestingly, from our initial experiments, a silencing pattern emerged depending on how many disulfide units were appended to the ASO. We hypothesized that this silencing pattern was a result of how susceptible the SNAs were to reducing conditions. However, after probing factors such as strand stability, cellular uptake, particle stability and protein binding, we determined that the degree to which SNAs fall apart to bind serum protein albumin plays a direct role in silencing activity.

Albumin is the most abundant protein in the body and due to its size has been used to influence the circulation and stability of ASO therapeutics *in vivo*[29-31]. While binding to albumin improves these factors, it has been shown to also reduce the cellular uptake of these therapeutics[32-33]. Surprisingly, we found that our disulfide ASO/albumin complexes did not diminish the cellular uptake of the ASO but improved the uptake of albumin. Disulfides have been previously shown to promote the cellular uptake of various substrates[34-36] and when appended to ASOs even silence without transfection agents under serum free conditions[37-38]. We determined that our disulfide ASO/albumin complex was promoted through a thiol mediated uptake process.

Using this new mechanistic information, we then further studied three aspects of these SNAs 1) non-transfected silencing of the disulfide DNA, 2) crosslinking ability of the SNAs and 3) prolonged silencing effects of the disulfide ASO/Albumin complex. We found that under conditions with or without serum proteins, meaningful non-transfected silencing could not be produced. Crosslinking our SNAs through disulfide bond formation reduced albumin binding and subsequently increased silencing on shorter time scales. Finally, due to association with albumin, our strands degraded at a slower rate than unmodified strands, and we were able to achieve prolonged silencing over 72hr.

Overall, we begin by providing a systematic study into how our disulfide modified ASO-SNAs behave in biological media, highlighting some of the factors that must be considered when probing the fate of these oligonucleotides. Ultimately, we do find that accessibility of the ASO for its target determines the level of silencing, whether bound to albumin or maintained within an SNA. These new ASO/albumin complexes have the potential to give us both favorable distribution properties of SNAs, without diminishing uptake of the ASO therapeutic by using a disulfide mediated process.

3.3 Results and Discussion

3.3.1 Synthesis and Self-Assembly of Disulfide ASO's

In Chapter 2, we reported a method for the addition of a disulfide functional group as a side chain in the middle of an oligonucleotide, but low yields prevented the synthesis of oligonucleotides with multiple disulfide units[39]. Using this molecule as a starting point, we designed a new disulfide phosphoramidite, which could be installed using standard solid-phase synthesis, allowing for the addition of multiple units in a sequence defined manner (Figure 3 .1a.). The hydrophobic C6 alkyl chain connected to the disulfide functionality can be used to promote the self-assembly of SNAs, when used in tandem with multiple units. Synthesis of our disulfide phosphoramidite was done following Figure 3 .1a. To compare specifically the effect of the disulfide we synthesized another phosphoramidite analogous to our disulfide phosphoramidite but with a carbon-carbon linkage replacing the disulfide (Figure 3 .1b.).

To find the number of units needed for self-assembly of the SNA, we varied the number of hydrophobic monomers from 4 to 6. Ultimately, we synthesized 6 different phosphorothioated (PS) ASO strands that target firefly luciferase, appending 4,5 and 6 of our disulfide units (S4, S5 & S6) and control non-disulfide units (C4, C5, & C6) (Figure 3 .2.a.). Furthermore, to visualize our strands in cells, an additional 6 analogous strands with cyanine 3 (Cy3) dyes at the interface between the ASO and disulfide units were synthesized (see section 4.5.4. for sequences). The placement of the dye at the interface between these two blocks was chosen specifically to ensure the dye does not influence uptake into cells[40], and to prevent degradation of the Cy3. The synthesis of all strands was confirmed by LC-MS (*Experimental* Figure 3 .9).

The self-assembly of S4, S5 and S6 was tested using native PAGE analysis. (Figure 3 .2.b.). We found that in magnesium containing buffer, all strands assembled into higher order structures.

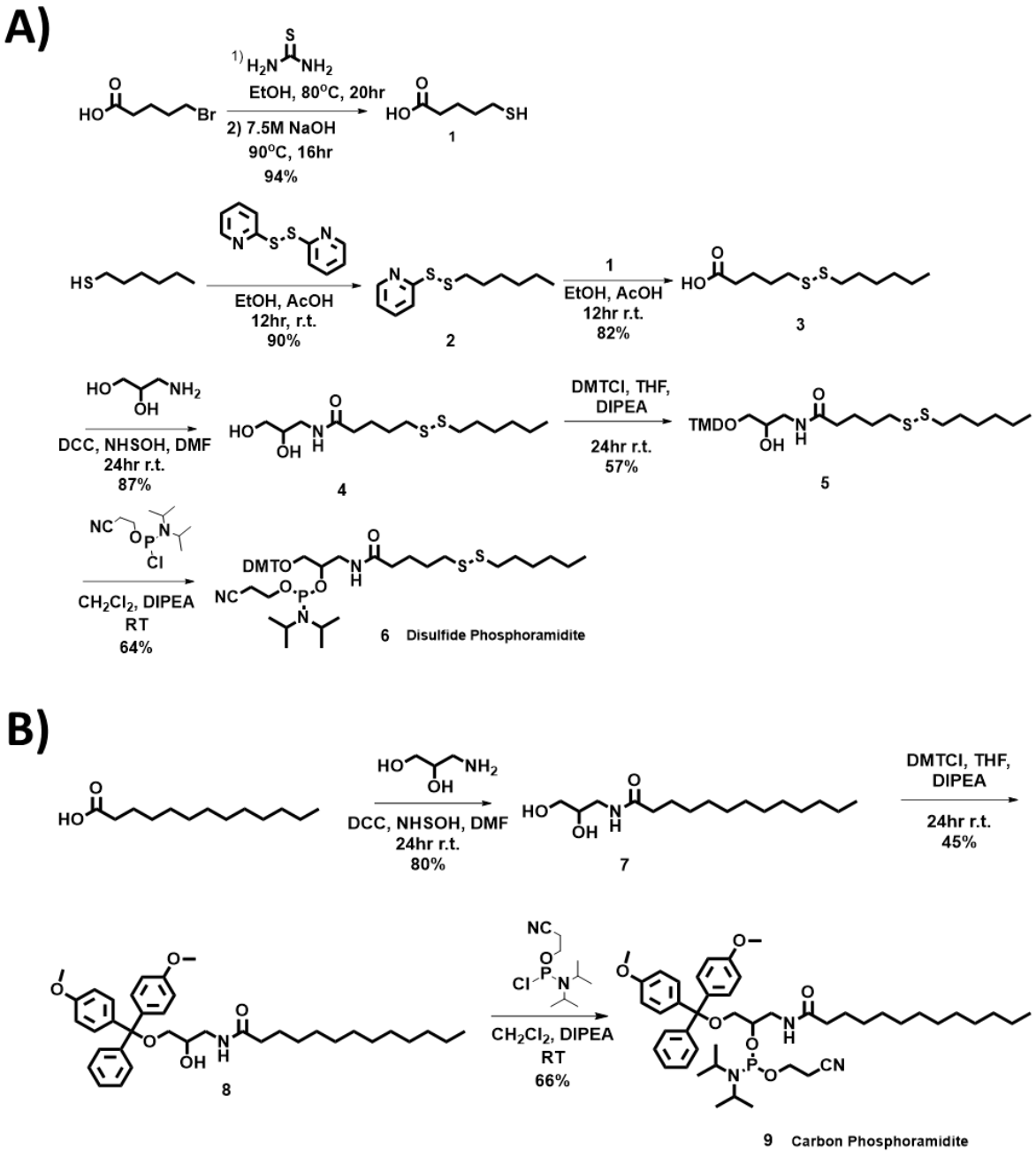

Figure 3. 1 Synthetic schemes for (A). the synthesis of the disulfide phosphoramidite and (B). the carbon phosphoramidite.

Using AFM and DLS these structures were confirmed to be SNAs with diameters of approximately 10nm (*Experimental* Figure 3 .10.- 4.11). In the case of C5 and C6, these SNAs remained stable even under denaturing conditions, highlighting the increased hydrophobicity of the C-C linkage vs the S-S linkage (*Experimental* Figure 3 .12).

3.3.2 Luciferase Assay & Reduction Sensitivity of SNA's

Once SNA formation was confirmed, we then probed the gene silencing. After 24hr we found that our SNAs with disulfide cores silenced more than the SNAs with pure carbon cores. (Figure 3 .2c. & *Experimental* Figure 3 .13 for cell viability assay). Interestingly, we found that, as the number of hydrophobic modifications were decreased, silencing activity increased (Figure 3 .2c.). Another interesting trend we found was that over 48hr the three strands resulted in the same level of silencing, indicating that there was a delayed silencing effect from the S5 and S6 SNAs (Figure 3 .2c.).

We were intrigued by this result and decided to investigate the reason that this silencing pattern emerged. We hypothesized that, due to the differing number of disulfides within the core of the SNAs, the difference in silencing could be due to differences in the rate of disassembly of the SNAs under the intracellular reducing conditions of the cell, with 4 disulfide units disassembling faster than 5, and faster again than 6. To probe this hypothesis, we reduced our SNAs in the presence of dithiothreitol (DTT) and monitored degradation by native/denaturing PAGE, native AGE (Figure 3 .2d. & *Experimental* Figure 3 .14) We also performed a nile red encapsulation and release assay, monitoring the fluorescence of the nile red dye molecule as it is nearly non-emissive in aqueous media but fluorescent in non-polar environments such as the core of our SNAs (*Experimental* Figure 3 .15).

Indeed, we found that the relative stability between the different SNAs was dependent on the number of units present. S4 was completely reduced after 24h with 10mM DTT (Figure 3 .2.d, lane 4) while S5 is only partially reduced (Figure 3 .2.d, lane 5) and S6 remained the most intact (Figure 3 .2d. Lane 6). The control strands showed no responsiveness to reducing conditions, remaining intact after 48 hours even under 100mM DTT (*Experimental* Figure 3 .14 b.). This result

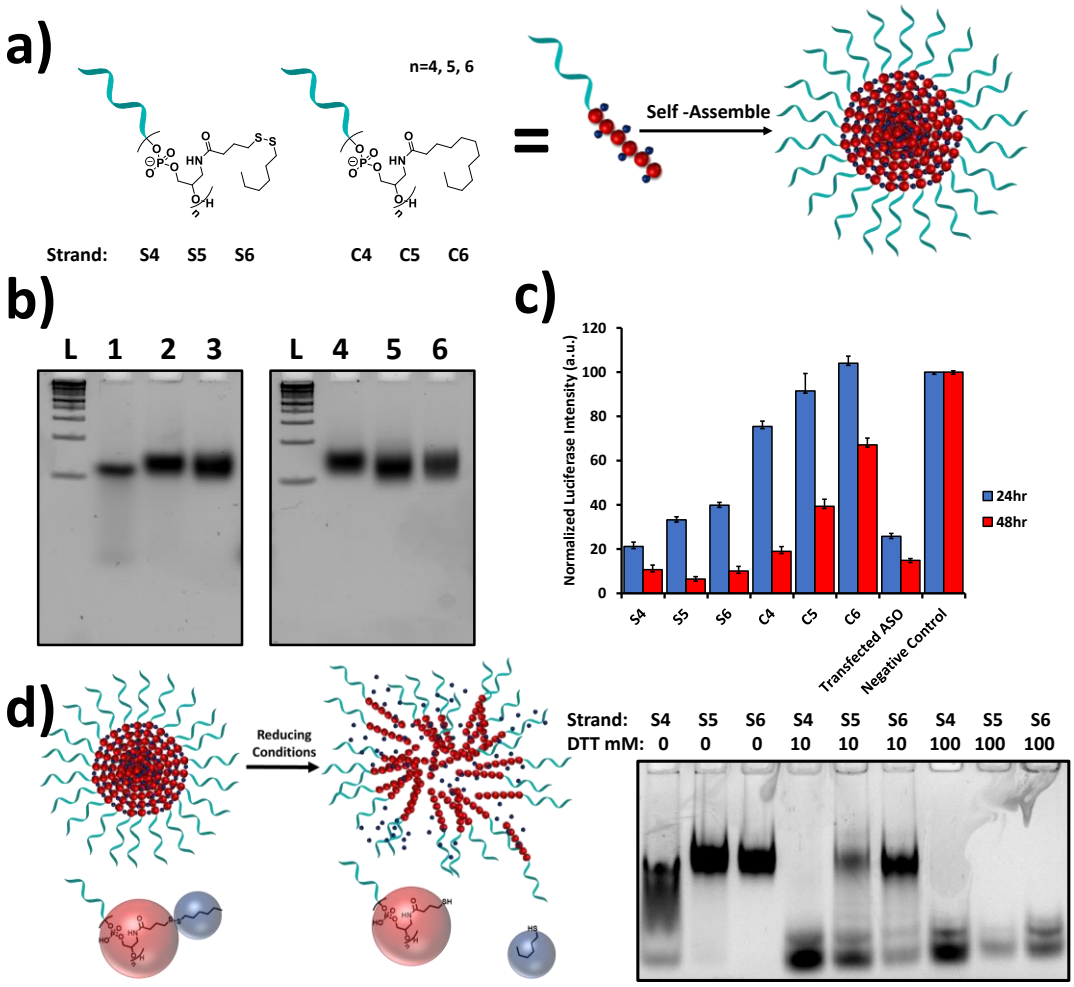

Figure 3. 2 Assembly, luciferase silencing assay and degradation of strands under reducing conditions.

a. schematic of disulfide strands (S4, S5 & S6) and carbon analogues (C4, C5, & C6) strands used in this chapter. **b.** Native PAGE of SNAs formed from each strand Lane 1: S4, Lane 2: S5, Lane 3: S6, Lane 4: C4, Lane 5: C5, Lane 6: C6. **c.** luciferase activity after 24, 48h incubation, and normalized to CellTiter-Blue and negative control (no ASO). Error bars represent SD for 6 replicates of each sample. ASO final concentration is 1uM strands for all samples. **d.** Native PAGE of the reduction of S4, S5, and S6 SNAs with 0, 10, & 100mM DTT.

seemed to be in line with our hypothesis, but then promoted the next question regarding if the structures remain intact in the extracellular medium.

3.3.3 Determination of the Protein Corona & Extracellular Particle Stability

For our disassembly hypothesis to be correct, the particles would have to be intact when entering cells and disassemble when they reach the intracellular reducing environment. It has been

previously shown that there are a multitude of serum proteins that can bind to SNAs[41]. Albumin is the most common protein in serum and has hydrophobic pockets to bind a variety of ligands including PS oligonucleotides[42]. Therefore, we investigated the protein corona of the SNAs to determine whether our structures remain intact, with a particular focus on albumin.

To assess the albumin binding properties of the SNAs we first performed an electrophoretic mobility shift assay (EMSA) using SNAs incubated with serum proteins, and albumin (Figure 3 .3a.). We found that there is a distinct gel mobility shift between our samples in solution (Figure

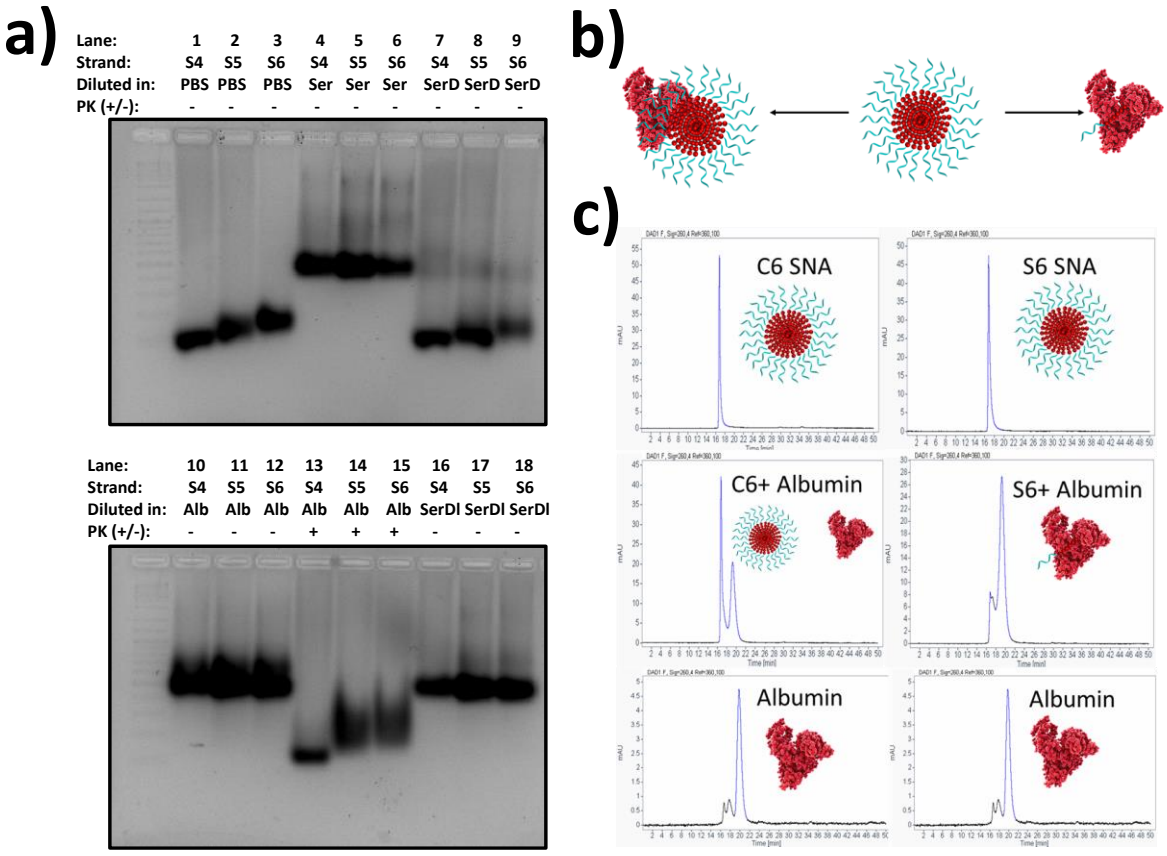

Figure 3. 3 Protein binding analysis of the SNAs.

a. schematic representing the potential ways albumin can bind to the SNA's: albumin either binds to the corona of the SNA or disassembles the SNA to bind the single strand. **b.** EMSA (native AGE) of the binding of S4, S5, and S6 to proteins under different conditions: 1xPBS pH 7.2 (PBS), Serum (Ser), albumin depleted serum (SerD), albumin (Alb), or diluted serum (SerDl) incubated at 37°C for 2hr PK = Proteinase K. **c.** SEC comparing the binding of albumin to C6 and S6: C6 maintains its structure when incubated with albumin, while the S6 SNA is not maintained.

3 .3a. lanes 1-3) and when incubated with serum (Figure 3 .3a. lanes 4-6). Additionally, when incubated with just albumin, the same shift in mobility is observed (Figure 3 .3a. lanes 10-12). When we depleted the serum of albumin, we found that the gel mobility of the initial SNAs was recovered (Figure 3 .3a. lanes 7-9), indicating that albumin is the primary serum protein binding to our SNAs. To ensure this effect was not an artifact caused by dilution, serum was diluted by the same factor as the depleted serum and the shift was retained (Figure 3 .3a. lanes 16-18). We also degraded the albumin using a proteinase K treatment and found that the SNAs were recovered after degradation (Figure 3 .3a. lanes 13-15), suggesting that the SNAs may stay intact or may reassemble. These gel results were similar for the C4, C5, and C6 control strands (*Experimental* Figure 3 .17).

While EMSA is a good indicator to confirm proteins can bind, using it for further qualitative analysis is problematic. The same albumin binding samples run on both PAGE and AGE gave drastically different sizes when compared to the MW marker (*Experimental* Figure 3 .16.). Therefore, gel mobility seems to be dependent more on pore size and only provides information regarding whether the protein binds.

Here it can be seen that in fact albumin does bind to our structures, however the state of the SNAs after binding to albumin was unclear, with two possible options: either the SNA's had fallen apart after binding albumin, or albumin was bound to the outside of the particles creating a protein shell (Figure 3 .3.b.). To assess this, we performed both dynamic light scattering (DLS) and size exclusion chromatography (SEC) studies to probe whether the size of the SNAs increased upon albumin addition (Figure 3 .3c. & *Experimental* Figures 4.18-4.19). By DLS we found that after the addition of albumin the size of the particles decreased to 8nm, the diameter of albumin (*Experimental* Figure 3 .18). This was confirmed by SEC where we found that the peak corresponding to the particles disappears when albumin is added to the solution and the intensity of the albumin peak at 260nm increases significantly (Figure 3 .3c. & *Experimental* Figure 3 .19). Notably here, control strands C4, C5 and C6 showed an increased resistance to albumin binding with their peaks remaining in the SEC trace after 24hr incubation with serum, (*Experimental* Figure 3 .20). As these strands showed the worst silencing, this added resistance to albumin

binding indicates that these particles may remain intact intracellularly, and this lack of accessibility is what may be affecting their silencing ability.

Given this new information we generated host-guest titration curves, by mixing the Cy3 versions of S4, S5, and S6 with varying amounts of albumin and measuring the fluorescence intensity. All strands fit well to a statistical 2:1 DNA:Albumin curve with variations in equilibrium dissociation constants (Kd) between 300 and 600nM, where C4, C5 and C6 Kd's were too high to be calculated using this method (See section 4.5.14 for details and *Experimental* Table 4.3 for Kd's). Each albumin can bind multiple disulfide ASO's due to 4 hydrophobic binding pockets within its tertiary structure. We have previously reported a hydrophobic ligand which was able to bind all four pockets at once resulting in 1:1 binding, however here it appears that co-operative binding of our different units is not realized.[43] To assess whether Albumin is covalently binding to the disulfide ASO's via its free thiol in position 34 we performed SDS-PAGE. SDS PAGE revealed that there was no difference between any of the strand's, indicating albumin is not covalently linking to the disulfide strands (*Experimental* Figure 3 .21.).

3.3.4 Serum Stability and Cellular Uptake of SNA's

To form a complete picture, we next investigated if there was a difference in degradation between the three strands. We found that the strands did not degrade significantly below 80% over 72hr (*Experimental* Figure 3 .22). This is consistent with the serum stability of other albumin bound ASOs that have been previously reported by our lab[32]. Importantly, serum stability helps us interpret cellular uptake results more easily, ensuring that during cell experiments we can analyze activity of the full oligonucleotide structure, not degraded DNA side products[40].

Fluorescence-activated cell sorting (FACS) and fluorescence microscopy revealed that there was no significant difference in the cellular uptake of the strands over 24 hours (Figure 3 .4.a. and 4.4.b.). There are many factors affecting uptake e.g., protein binding, and possible disulfide-mediated uptake, complicating the reasoning behind the relative uptake. Regardless, there seems to be no difference between the uptake of the disulfide ASO strands and the unmodified ASO over 24hr, therefore uptake seems unlikely to be a contributing factor in the difference in silencing. Surprisingly the C4, C5 and C6 SNAs had the highest uptake but the lowest silencing

(Figure 3 .4.b. and *Experimental* Figure 3 .23.). This enhanced uptake with reduced silencing supports the stability of these particles during the uptake process. Again, highlighting the fact that the biodegradable disulfide bond is very important for gene silencing.

As albumin binding was expected to reduce the uptake of ASOs[32] it was interesting to see that the uptake of the disulfide strands and the unmodified ASO were roughly the same. This could be caused by a combination of two factors, 1) albumin bound disulfide ASO strands have a reduced uptake at earlier timepoints, but slowly dissociate from albumin and by 24hrs have entered cells to the same level as strands unassociated with albumin or 2) the disulfides on the ASOs are promoting the cellular uptake of the entire ASO/albumin complex. Disulfide ASOs have been previously shown to promote cellular uptake and silence without the use of transfection agents under serum free conditions[37]. Moreover, it has been recently suggested that under

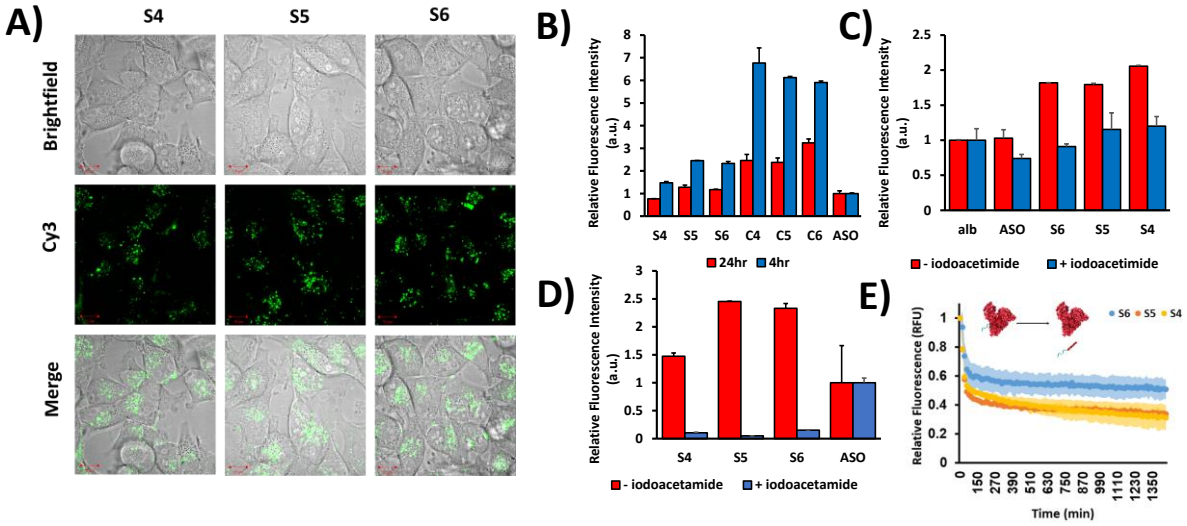

Figure 3. 4 Investigation into the cellular uptake and degradation of the SNAs and albumin bound strands

a. microscopy images of S4, S5, and S6 **b.** FACS of Cy3 labelled strands taken up in cells over 24 and 4 hr. (uptake is relative to the ASO control) **c.** FACS of Alexa 647 labelled albumin up taken over 4hr with and without iodoacetamide **Alb=** albumin alone, **ASO=** Albumin + unmodified ASO, **S6**= albumin + S6**, S5**= albumin + S5, **S4**= albumin + S4 (uptake is relative to the uptake of albumin on its own). **d.** FACS of Cy3 labelled strands up taken over 4hr with and without iodoacetamide (uptake is relative to the ASO control). e. fluorescence intensity of albumin bound S4, S5, and S6 under reducing conditions over 24h λ_{ex}= 561 nm, λ_{em}= 585 nm

serum free conditions, phosphorothioate DNA can contribute to the uptake of these oligonucleotides as well[44].

We found by FACS after 4hrs that there was in fact an increase in uptake between the disulfide strands and the positive ASO control, indicating that the disulfides may be helping to promote the uptake of the ASO/albumin complex, overcoming the reduced uptake from being bound to albumin (Figure 3 .4b.). Cellular uptake of Alexa 647-labelled albumin pre-incubated with S4, S5 and S6 was then monitored by FACS and showed higher albumin uptake than with an unmodified ASO, or no strand added (Figure 3 .4.c.). Additionally, when we blocked the thiol mediated pathway with iodoacetamide, the uptake of albumin bound to S4, S5 and S6 reduced to similar levels as albumin on its own (Figure 3 .4.c.). Moreover, the Cy3 labelled strands decreased in uptake when iodoacetamide was used, providing further evidence the uptake of the albumin/ASO complex is thiol mediated (Figure 3 .4.d.).

3.3.5 Dissociation from Albumin under Reducing Conditions

Hydrophobic groups appended to NATs have been shown to influence binding to lipid membranes and proteins, and affect intracellular trafficking[45]. We theorized that, since the disulfide strands are associated with albumin and possibly other proteins, under intracellular reducing conditions they could shed their hydrophobic groups, changing their association, and become more accessible for silencing. The rate of dissociation from albumin would be dependant on how many units were attached to the ASO, with fewer units reducing faster and silencing quicker. As a model system we looked at the dissociation of our strands from albumin under simulated reducing conditions. We took our fluorescently labeled strands and pre-bound them to albumin, then placed them under reducing conditions using DTT as a reducing agent, at intracellular concentrations of glutathione. We then looked at the relative rate of release from the albumin after binding and reduction by fluorescence and Native AGE (Figure 3 .4.e. and *Experimental* Figures 4.24- 4.25.) The relative fluorescence intensity decreases more rapidly with fewer disulfide modifications, and free ASO can be seen in the Native AGE of the reduced samples. This suggests that once internalized, the amount of association with albumin and other

proteins could determine how accessible the oligonucleotide is for silencing (Figure 3 .4.e. and *Experimental* Figure 3 .24).

In summary a complete picture can be formed for how our SNAs are behaving *in vitro* (*Experimental* Figure 3 .26.). The C4, C5 and C6 strands all remain as SNAs when placed in media, while S4, S5 and S6 fall apart to bind albumin. C4, C5 and C6 are uptaken as SNAs, giving them an enhanced uptake profile, while S4, S5 and S6 are internalized with albumin bound, which is promoted by a disulfide mediated process. Once internalized, the reducing conditions of the cell can slowly dissociate the S4, S5 and S6 strands at different rates depending on how many units are appended. This is in contrast with C4, C5 and C6 which fall apart much more slowly under these conditions, severely diminishing their silencing ability.

3.5.2 Non-Transfected Silencing

Given that uptake of albumin and of S4, S5, S6 was promoted by a disulfide mediated process, attempts were made to see if our strands could silence without the use of transfection agents. Using relevant biological conditions, however, is essential to properly assess how the therapeutic would operate *in vivo*. Previous studies on disulfide mediated uptake have opted to use *in vitro* conditions lacking serum proteins to exemplify the disulfide uptake process[34-35, 44]. While these studies are remarkable, they reflect the operation of the system in an ideal case with no proteins present, not acknowledging the association of proteins in serum which can heavily influence the uptake of different therapeutics[46]. Therefore, we pursued non-transfected silencing both with and without serum proteins.

As a positive control, we synthesized a disulfide phosphoramidite from the literature (Figure 3 .5a) and generated an additional two ASO strands each with 5 of these disulfide units, one with a fluorescent dye (SO & SO-Cy3) (Figure 3 .5 b.). Previous studies have shown that by appending at least 5 of these disulfide units to an ASO, 30-40% silencing could be achieved[37]. We confirmed these strands by LC-MS and probed this strand for albumin binding and release, finding that it too binds to albumin with a nanomolar Kd (Figure 3 .5.c. & d. and *Experimental* Figure 3 .9 (LC-MS), & Table 4.3.(Kd)). Interestingly, this strand dissociates from albumin at a faster rate than S4,

S5, and S6, possibly due to a preferential reaction with the non-tertbutyl thiol due to steric interference and solvent accessibility of the disulfide once bound to the albumin (Figure 3 .5.d.).

To use our strands for non-transfected silencing we wanted to make sure that they would remain single stranded under biologically relevant salt concentrations. Using native PAGE, it was found that S4, S5, and S6 did not assemble into higher order structures under physiologically relevant salt conditions (Figure 3 .5.e.). Additionally, critical micelle concentrations for each strand in PBS

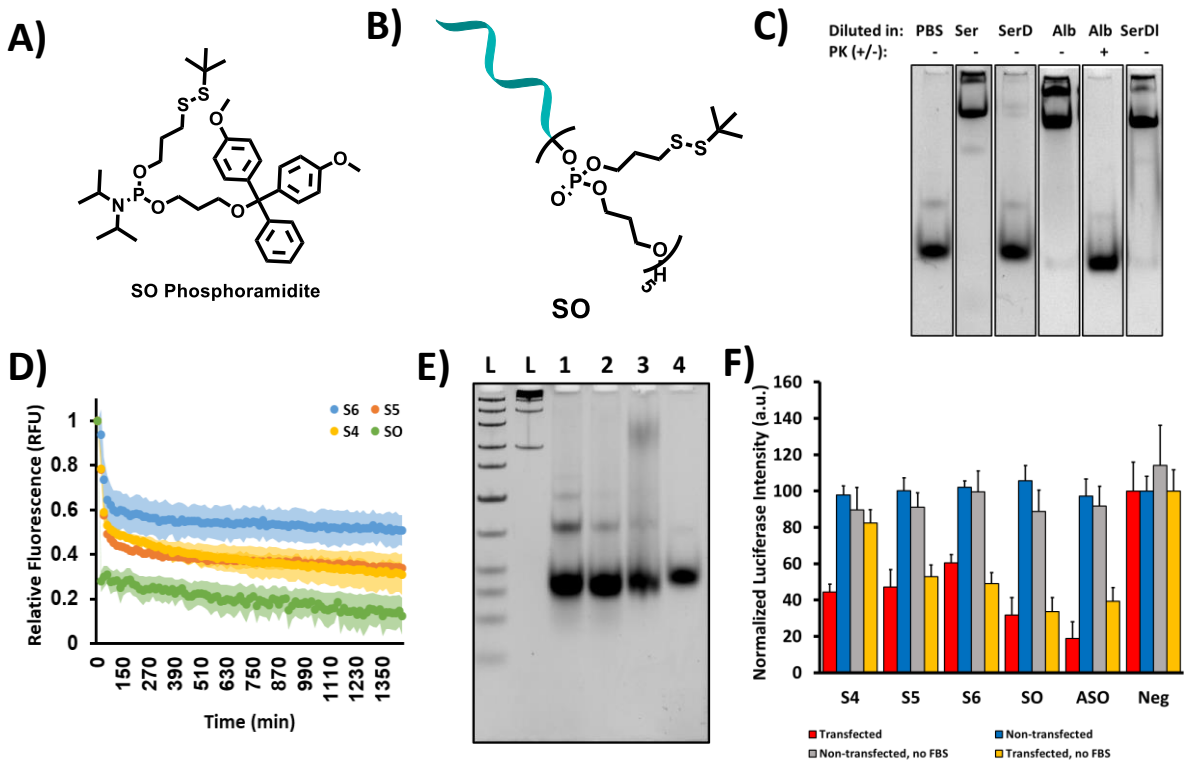

Figure 3. 5 Investigation of luciferase activity without the use of transfection agents

; **a.** Structure of the literature disulfide phosphoramidite **b.** structure of the SO strand **c.** EMSA (Native PAGE) of the binding of SO, to proteins under different conditions: 1xPBS pH 7.2 (PBS), Serum (Ser), albumin depleted serum (SerD), albumin (Alb), or diluted serum (SerDl) incubated at 37°C for 2hr PK = Proteinase K **d.** Plot of the fluorescence of strands including SO, incubated with albumin and the addition of 10mM DTT over 24hr. **e.** Native TBE PAGE of strands assembled in 1xPBS pH 7.2 Lane 1: S4, Lane 2: S5, Lane 3: S6, Lane 4: SO, **f**. luciferase activity after 24h incubation, red: transfected, blue: non-transfected, yellow: transfected without FBS and grey: non-transfected without FBS. Samples are normalized to CellTiter-Blue and negative control (no ASO). Error bars represent SD for 6 replicates of each sample. ASO final concentration is 500 nM strands for all samples.

ranged between 1uM and 2uM (*Experimental* Figure 3 .28 & Table 4.4.) providing further evidence that the strands would remain single stranded in silencing assays.

Confirming that S4, S5, S6 and SO would remain single stranded, we performed a luciferase silencing assay, both in the presence and absence of transfection agents, and with or without serum proteins (Figure 3 .5. f. and *Experimental* Figure 3 .28 for MTT). As expected, transfected silencing, without first preassembling S4, S5, and S6, showed no difference to the silencing of the SNA luciferase assay, as these strands would be bound to albumin either way. SO, when transfected with FBS showed more silencing than S4, S5, and S6, most likely due to the increased dissociation rate from albumin. In our hands however, non-transfected silencing was not realized with or without FBS. Even with the strand from the literature, silencing was only observed when transfection agents were used. This could be due to differences in the way the assay was performed or changes to the target sequence used. Additionally, while the viability of the cells without FBS was still around 80% it was still significantly lower than with FBS (100%) which could affect the overall analysis (*Experimental* Figure 3 .28).

3.3.6 Crosslinking of the SNAs

Finding that our strands disassembled to bind albumin, we sought to stabilize the SNAs towards albumin, through disulfide crosslinking. Disulfide crosslinking of nanoparticles is a well-established method of stabilizing the particles in a reversible manner[47-48] and photo-crosslinking has been previously used to enhance the stability of SNAs[49]. To crosslink the particles, we assembled them in magnesium containing buffer and varied the amount of the reducing agent 2-mercaptoethanol (BME) added to the solution (Figure 3 .6. a.). By titrating the disulfide strands with varying concentrations of BME we looked for the ideal concentration that allowed for the most cross-linked particles, while minimizing complete reduction of the strands caused by an overabundance of BME. Maximum crosslinking was determined by denaturing PAGE as being the concentration of BME which gave the least amount of single stranded product. We found that BME concentrations for S4, S5 and S6 at 60uM to maximize crosslinking were 12.5mM, 25mM, and 50mM respectively (*Experimental* Figure 3 .29 a. & b.).

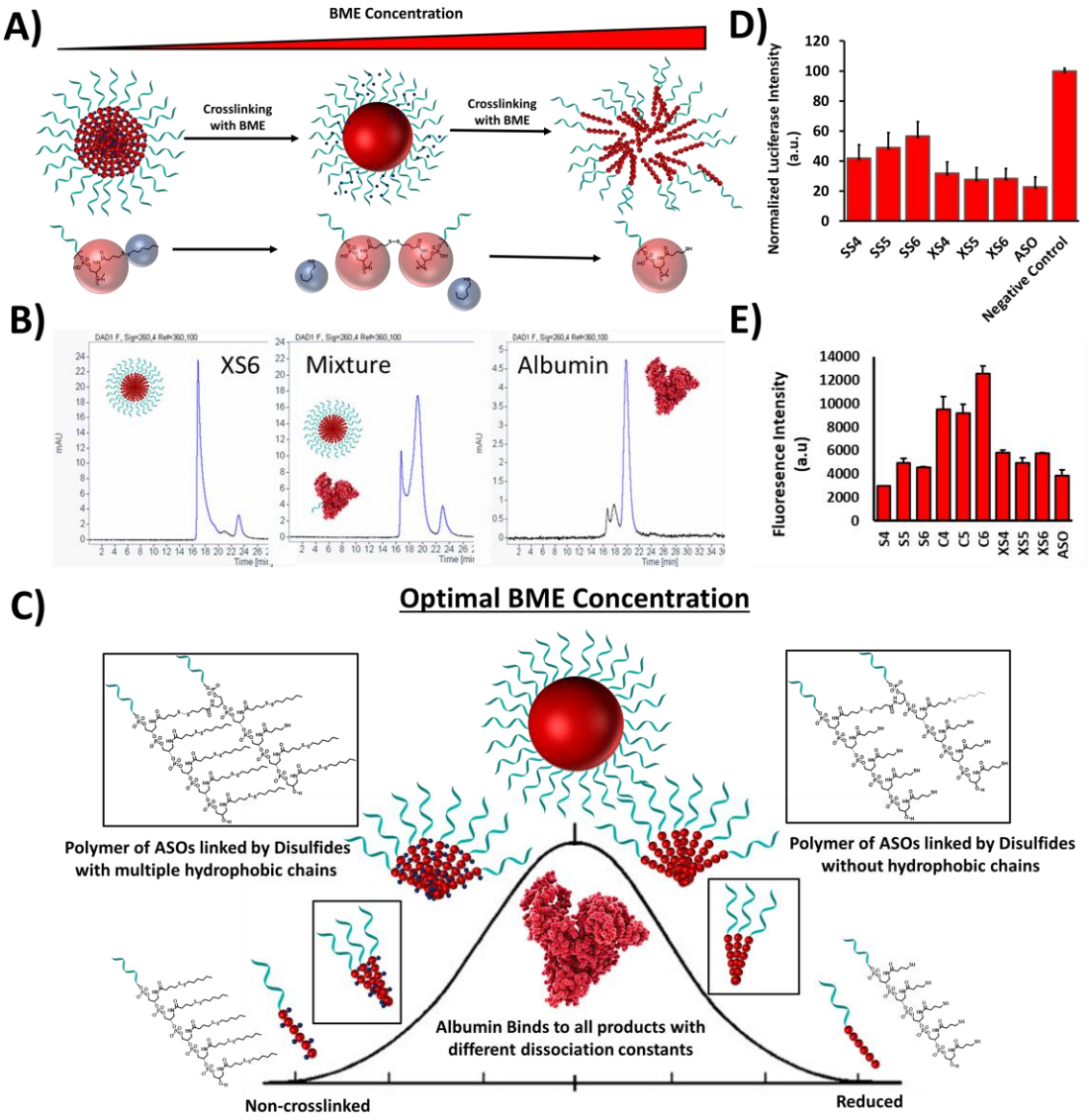

Figure 3. 6 Investigation of the effect of crosslinking of S4, S5 and S6 on luciferase activity

a. scheme of the process crosslinking the SNAs: as BME concentration increases, there is an optimal concentration which gives the most amount of crosslinking without degrading the SNA. **b.** SEC of crosslinked S6 (XS6) incubated with albumin for 2h, showing added stability. **c.** Distribution of different products after the crosslinking process at the optimal BME concentration. Albumin binds to all the different species present after the crosslinking process with different Kds; products in-between the crosslinked SNA (middle) and non-crosslinked strands may have a higher affinity for albumin due to multivalency of the hydrophobic sidechains **d.** luciferase activity of SNAs and crosslinked SNAs after 24h incubation and normalized to CellTiter-Blue and negative control (no ASO). Error bars represent SD for 6 replicates of each sample. ASO final concentration is 500 nM strands for all samples. **e.** FACS of crosslinked Cy3 labelled strands taken up in cells over 24h

Next, we looked at the albumin binding to these crosslinked SNAs. We performed an EMSA

titration curve of albumin binding to the S4, S5 and S6 SNAs crosslinked with differing amounts of BME and found that new bands appeared when the SNA's had been crosslinked (*Experimental* Figure 3 .29.c.). Another EMSA follow up titration experiment where we then varied the amount of albumin and BME showed that these new bands showed up earlier in the titration (lower albumin conc.) as the amount of crosslinking was increased (*Experimental* Figure 3 .30.). EMSA evidence suggests that the particles bind albumin differently than the single-stranded counterparts. Using SEC analysis, we observed that cross-linked SNAs bound to albumin less preferentially, as the SNA peak could still be observed as opposed to the non-crosslinked samples (Figure 3 .6.b. and *Experimental* Figure 3 .31). Binding curves were also made for the crosslinked particles and found to still be within the nanomolar range, indicating that albumin still binds tightly to the particles (*Experimental* Table 4.3.). However, due to the nature of the crosslinking process, many individual products are produced, and this data may be convoluted due to a distribution of species present in solution (Figure 3 .6.c.).

When looking at albumin binding to these crosslinked SNAs, a few factors are at play, the relative stability of the SNA, and how strongly albumin binds to the single strand with or without cleaved hexanethiol. During the crosslinking process, hexanethiol units from the disulfide SNAs are cleaved and released, reducing the hydrophobic content of the particle. This in essence should reduce the overall affinity for albumin, in combination with now being locked into a spherical shape. However, not all hexanethiol gets cleaved from the disulfide ASO during the crosslinking process at the optimal BME concentration (Figure 3 .6.c.). Remaining hexanethiol units on now connected strands could act to counterbalance these effects in a multivalent way and still bind to albumin. While there are some particles that are likely to remain fully crosslinked, there is a distribution of different products, and some particles will lose their shape and bind as a polymer of disulfide linked ASOs. This is most evident in the native AGE of the BME titration of S4, where lower bands can be clearly seen as the degree of crosslinking increases (Figure 3 .29 a. right.). Overall, there may not to be enough crosslinking points to generate a large population of fully stable SNAs and what exists in solution is a mixture of stable SNAs, polymers of disulfide linked

ASOs, strands with fully cleaved hexanethiol sidechains and strands which remain un-crosslinked (Figure 3.6.c.).

A luciferase gene silencing assay was performed on the crosslinked versions of S4, S5 and S6. We found that gene silencing was greatly improved over the non-crosslinked versions over 24h and comparable to the positive control (Figure 3.6. d. & *Experimental* Figure 3 .31 for MTT). By FACS, cellular uptake of the crosslinked S5 and S6 were slightly improved, most likely due to a population of intact SNA's (Figure 3.6. e.). S4 did not show an improved uptake which is in line with the tendency of the S4 SNA to lose its shape. Compared to the C4, C5 and C6 SNA's, the cellular uptake of the crosslinked SNA's was still much lower, which is consistent with being remained bound to albumin and losing their spherical structure.

Taken together, the information points to the fact that the enhanced silencing is most likely due to the decrease of hydrophobic groups and subsequent increase in accessibility, rather than increased uptake as SNA's. Additionally, the fact that a disulfide reduction event can release two ASO strands that have been linked together as opposed to simply disconnecting a hydrophobic subunit in the non-crosslinked version may also be providing increased silencing. In the future increasing the number of disulfide subunits per ASO and crosslinking may provide more robust crosslinked SNA's that are maintained better extracellularly and released intracellularly to improve silencing further. Alternatively, the *in vivo* effects of having multiple ASO copies bound to albumin may also provide some benefit as branched ASOs have been shown to have better distribution in the central nervous system[50].

3.3.7 Extended Luciferase Assay

Modified-release dosage is a method that is used in drug delivery to either delay, extend or target the release of small molecule drugs. Specifically delayed-release dosage can result in extended therapeutic effects, which would be desirable to reduce the number of doses one would take. In fact, the GalNac ligand that is used in some of the most sophisticated siRNA technology to date, operates by providing a depot for ASOs to be slowly released. Inspired by this, we decided to test the silencing effect of all our strands over a longer period[51]. Remarkably, we found that over 72hr our strands maintained their level of silencing 40-60% while the positive control ASO loses

silencing (Figure 3.7. and *Experimental* Figure 3.31. for MTT). Binding to albumin has been shown to protect oligonucleotides from degradation and likely plays a part in the prolonged silencing over 72 hr. Interestingly, silencing seems to start to improve for C5 and C6 over longer timescales as well, indicating that they may eventually fall apart or degrade partially *in vitro*. Tunability in the silencing by appending different number of units could prove useful when sustained silencing is desired and help provide more control over spatio-temporal silencing.

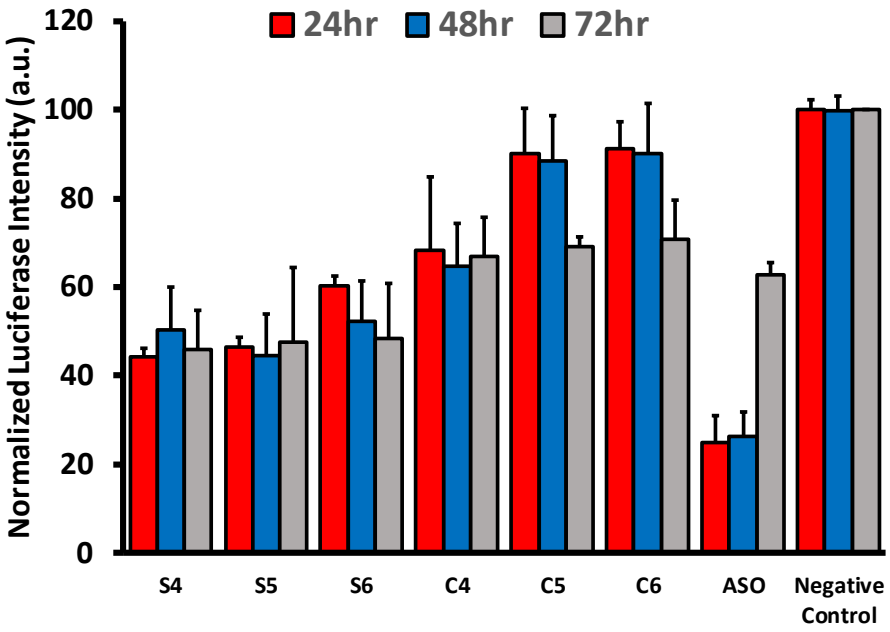

Figure 3. 7 Duration of effect: luciferase activity after 24, 48, or 72 h incubation, and normalized to CellTiter-Blue and negative control (no ASO).

Error bars represent SD for 6 replicates of each sample. ASO final concentration is 500 nM strands for all samples.

3.4 Conclusion

In conclusion, we synthesized a new disulfide phosphoramidite, and appended, multiple units to an ASO, resulting in their self-assembly into SNAs. We found that SNAs with disulfides silenced more than SNAs without and depending on how many disulfide units were appended to the ASO/SNA, the rate of silencing could be modulated. Through our carefully designed studies we determined that the spherical nature of the SNAs is not maintained in serum, and they fall apart to bind albumin. Further studies revealed that the cellular uptake of the disulfide ASO/albumin

complex was promoted through a thiol mediated uptake process. Contrary to our initial hypothesis, this led us to conclude that the differences in silencing are most likely due to the different rates of albumin dissociation under cellular reducing conditions. As a result of these new mechanistic insights, we further pursued three different applications: 1) non-transfected silencing of our disulfide ASOs 2) crosslinking of the disulfide SNAs and 3) prolonged silencing of the disulfide ASO/albumin complex. In our hands we found that non-transfected silencing was not realized, crosslinking the SNAs improved silencing on shorter time scales, and that silencing was maintained for the disulfide ASO/albumin complex over 72hrs. Overall, our initial intention of tuning gene silencing by increasing the accessibility of an ASO to an mRNA target through the introduction of biodegradable bonds into a SNA was realized. These new ASO/albumin complexes have the potential to give us both the favorable distribution properties of albumin, which is the most used protein in drug delivery applications, without diminishing uptake of the ASO therapeutic, by using a disulfide mediated cellular uptake process. Moreover, this study aims to highlight the importance of probing many aspects of a biological system, especially protein binding, before reaching conclusions.

In this chapter we explored how we can use oligonucleotides as both therapeutics and as a structural material. Chemically modifying an ASO with hydrophobic units, allowed for the self-assembly of SNAs and binding to albumin, which would otherwise not be accessible with unmodified oligonucleotides. The structure of these new conjugates provided better uptake and nuclease resistance for the oligonucleotide therapeutic. Moreover, using a disulfide bond within the hydrophobic modification gave these entities stimuli responsive behavior and better uptake via a disulfide mediated process. In the next chapter we will revisit the small molecule-oligonucleotide conjugates from Chapter 2 and demonstrate methods for improving this system for more biologically relevant conditions. We will use more advanced oligonucleotide conjugates for both structural and recognition purposes.

3.5 Experimental Section

3.5.1 General:

Unless otherwise stated, all commercial reagents and solvents were used without additional purification. Magnesium sulfate hexahydrate (MgSO4·6H2O), tris(hydroxymethyl)aminomethane (Tris), urea, chloroform (CHCl3), hexane (Hex), tetrahydrofurane (THF), dimethyl sulfoxide (DMSO), hydrochloric acid (HCl), sodium hydroxide (NaOH), dichloromethane (CH_2Cl_2), ethyl acetate (ETOAc), ethanol (EtOH), fluorescein, methyl iodide, sodium bicarbonate ($NaHCO_3$), sodium chloride (NaCl), triphosgene, triethylamine, trifluoroacetic acid (TFA), 4-nitrophenyl chloroformate, camptothecin, dimethyl amino pyridine (DMAP), 2, 2'-dithiodipyridine, 1-hexanethiol, N-hydroxysuccinimide, and N,N'-Dicycolhexylcarbodiimide were used as purchased from Sigma-Aldrich. Acetic acid and boric acid were purchased from Fisher Scientific and used without further purification. GelRed™ nucleic acid stain and Sybr Gold were purchased from Biotium Inc. Acetone ACS reagent grade was purchased from Fisher. 5K dialysis tubing was purchased from Fischer Scientific. Acrylamide/Bis-acrylamide (40% 19:1 solution), ammonium persulfate and tetramethylenediamine were obtained from Bioshop Canada Inc. and used as supplied. 1 μmol Universal 1000Å LCAACPG supports and standard reagents used for automated DNA synthesis were purchased through Bioautomation. Sephadex G-25 (super fine, DNA grade) was purchased from Glen Research. Analytical thin layer chromatography (TLC) was performed on TLC plates purchased from Sigma-Aldrich. 1xTAMg buffer is composed of 45 mM Tris and 12.5 mM MgCl2.6H2O with the pH adjusted to 8.0 using glacial acetic acid. TBE buffer is 90 mM Tris, 90 mM boric acid and 2 mM EDTA with a pH of 8.0. TEAA mobile phase is 50 mM triethylammonium acetate with the pH adjusted to 8.0 using glacial acetic acid. 1xPBS buffer is 137 mM NaCl, 2.7 mM KCl, 8 mM Na_2HPO_4, and 2 mM KH_2PO_4 adjusted to pH 8.0 with NaOH. 50x ALK buffer is composed of 1.5M NaOH and 50mM EDTA.

3.5.2 Instrumentation:

Standard oligonucleotide synthesis was performed on solid supports using a Mermade MM6 synthesizer from Bioautomation. HPLC purification was carried out on an Agilent Infinity 1260. UV absorbance DNA quantification measurements were performed with a NanoDrop Lite

spectrophotometer from Thermo Scientific. For structure assembly, Eppendorf Mastercycler 96-well thermocycler and Bio-Rad T100TM thermal cycler were used to anneal all structures and hairpins. Polyacrylamide gel electrophoresis (PAGE) was performed using 20x20 cm vertical Hoefer 600 electrophoresis units. Agarose Gel Electrophoresis (AGE) was performed on Owl Mini and Owl EasyCast horizontal gel systems. Gels were imaged by a BioRad ChemiDoc MP system. Fluorescence data were measured by a BioTek Cytation 5 imaging reader Reader. Multimode 8 scanning probe microscope and Nanoscope V controller (Bruker, Santa Barbara, CA) was used to acquire AFM images. DynaPro (model MS) molecularsizing instrument was used to measure the particle size distributions. Liquid Chromatography Electrospray Ionization Mass Spectrometry (LC-ESI-MS) was carried out using a Bruker MaXis Impact™. Column chromatography to purify organic compounds was performed on a CombiFlash® Rf + system with RediSep® Silica columns (230-400 mesh) using a proper eluent system. 1H NMR and 13C was recorded on 500 MHz AV500 equipped with a 60 position SampleXpress sample changer (Bruker) and 300 MHz Varian Mercury equipped with an SMS-100 sample changer (Agilent). Visualization of TLC was achieved by UV light (254 nm). Chemical shifts were quoted in parts per million (ppM) referenced to the appropriate residual solvent peak or 0.0 ppm for tetramethylsilane. Abbreviations for 1H NMR: s = singlet, d = doublet, t = triplet, q = quartet, quint = quintet, m = multiplet. High-resolution mass spectra were obtained from Exactive Plus Orbitrap Mass Spectrometer (Thermo Scientific).

3.5.3 DNA Synthesis

3.5.3.1 Synthesis

DNA synthesis was performed on a 1 µmole scale, starting from the required nucleotide modified 1000 Å LCAA-CPG solid-support. Coupling efficiency was monitored after removal of the dimethoxytrityl (DMT) 5-OH protecting groups. Cyanine 3 phosphoramidite (cat. # 182873-76-3) was purchased from Glen Research. Coupling efficiency was monitored by the removal of DMT group on 5'-OH groups. In a glove box under nitrogen atmosphere, Compounds **6**, Compound 9 and SO phosphoramidite were dissolved in acetonitrile and shaken for 10 mins to achieve final concentration of 0.1 M. The amidites were activated with 0.25M 5-(ethylthio)tetrazole in anhydrous acetonitrile and the extended coupling times of 5 minutes were used. The cyanine 3 phosphoramidite was activated by 0.25M 5-(ethylthio)tetrazole in anhydrous acetonitrile but the

coupling was performed manually inside the glove box. 3% dichloroacetic acid in dichloromethane was used to remove DMT protecting group on the DNA synthesizer.

3.5.3.2 Deprotection

For unmodified DNA, DNA modified with dodecanediol, and DNA modified with reverse phosphoramidites, after the synthesis was complete the CPG was treated with 28% aqueous ammonium hydroxide solution for 16-18 hours at 60^{o}C in water bath. For disulfide modified DNA, the CPG was treated with 28% aqueous ammonium hydroxide solution for 36-48 hours at r.t.

3.5.3.3 Purification

The crude mixtures were then concentrated under reduced pressure at 60^{o}C, suspended 1:1 8 M urea before loading to polyacrylamide/urea gel (12% or 15% denaturing PAGE). The gel was run at 250 V for 30 minutes followed by 500 V for 45-60 minutes in 1x TBE as the running buffer. The gel was then imaged and excised on TLC plate under a UV lamp. The solution was dried to approximately 1 mL before loading to Sephadex G-25 column. The purified DNA was quantified by the absorbance at 260 nm

3.5.4 Oligonucleotide Sequences:

Table 3. 1 Sequences used for DNA Conjugates.

(D =DMT-dodecane-diol), (lower case represents phosphorothioated), (X = Compound 6), (3= cyanine 3 phosphoramidite), (Y = Compound 9), (Z = SO phosphoramidite),

Name	Sequences (From 5’ to 3’)
ASO	atatccttgtcgtatccc
S4	XXXXatatccttgtcgtatccc
S5	XXXXXatatccttgtcgtatccc
S6	XXXXXXatatccttgtcgtatccc
C4	YYYYatatccttgtcgtatccc

C5	YYYYYatatccttgtcgtatccc
C6	YYYYYYatatccttgtcgtatccc
SO	ZZZZZatatccttgtcgtatccc
ASOCy3	3atatccttgtcgtatccc
S4Cy3	XXXX3atatccttgtcgtatccc
S5Cy3	XXXXX3atatccttgtcgtatccc
S6Cy3	XXXXXX3atatccttgtcgtatccc
C4Cy3	YYYY3atatccttgtcgtatccc
C5Cy3	YYYYY3atatccttgtcgtatccc
C6Cy3	YYYYYY3atatccttgtcgtatccc
SOCy3	ZZZZZ3atatccttgtcgtatccc

3.5.5 Small Molecule Synthesis:

Compounds 1,2 and 3 were synthesized according to procedures from Chapter 2.

Compound 4:

Previously reported compound **3** was synthesized according to established protocols. Compound **3** (7g, 28mmol), 3-Amino-1,2-propandiol (1.8g, 29.4mmol), and N-hydroxysuccinimide (2.3g, 29.4mmol) were dissolved in DMF (50 ml). To this was added N,N'-Dicycolhexylcarbodiimide (4.09g, 29.4mmol) and the mixture was reacted for 24 hours. The solution was then filtered to remove the insoluble urea and diluted with H_2O (100 mL) and extracted with ethyl acetate (3 × 50mL). The organic phase was washed with saturated $NaHCO_3$ (50mL), and saturated NaCl (50 mL), and then dried on $MgSO_4$, filtered and concentrated *in vacuo*. The crude material was then purified by column chromatography (3CV's 95:5 EtOAc/Hex, then 5%MeOH in CH_2Cl_2) to provide

Compound **4** as a white solid (7.9g, 87%). ^{1}H NMR (500MHz, $CDCl_3$): δ = 0.86 (t, 3H), 1.26 (m, 18H), 1.47 (m, 2H), 2.07 (m, 2H), 2.98 (m, 1H), 3.15 (m, 1H), 3.27 (m, 2H), 3.46 (m, 1H).). ^{13}C NMR (125MHz, $CDCl_3$): δ = 14.42, 22.57, 25.80, 29.16, 29.29, 29.43, 29.50, 31.33, 33.82, 35.77, 42.51, 64.09, 71.05, 173.16. HRMS (EI): calc. for $[C_{14}H_{29}O_3NNaS_2]^+$ $[M]^+$: 346.16, found 346.1476.

Compound 5:

Compound **4** (2.5g, 7.73mmol) was dissolved in THF (25mL). To this was added diisopropylethylamine (4g, 30.9mmol) followed by 4, 4' dimethoxytrityl chloride (2.62g, 7.73mmol) 1/3 every hour over 3 hrs. The mixture was allowed to react for an additional 24hr. The solution was directly concentrated *in vacuo* and purified directly by column chromatography (3CV's 9:1 Hex/EtOAc, 1:1 Hex/EtOAc) to provide compound **5** (2.76g, 57%). ^{1}H NMR (500MHz, DMSO D_6): δ = 0.86 (t, 3H), 1.24 (m, 18H), 1.40 (m, 2H), 1.99 (m, 2H), 2.86 (m, 2H), 3.00 (m, 1H), 3.26 (m, 1H), 3.69 (m, 1H).), 3.75 (s, 6H), 6.87 (m, 4H), 7.25 (m, 7H), 7.42 (m, 2H), (7.65, 1H). ^{13}C NMR (125MHz, DMSO D_6): δ = 14.42, 22.57, 25.80, 29.16, 29.26, 29.40, 29.50, 31.23, 31.77, 35.81, 36.25, 39.50, 39.67, 39.83, 39.92, 43.04, 55.47, 60.22, 66.22, 69.28, 85.64, 113.53, 127.00, 128.17, 128.24, 130.20, 136.31, 145.59, 158.46, 162.77, 172.84. HRMS (EI): calc. for $[C_{35}H_{47}O_5NNaS_2]^+$ $[M]^+$: 648.29, found 648.2765.

Compound 6:

Compound 5 (2.2 g, 3.51 mmol, 1 eq) was dissolved in 30 mL dry dichloromethane under an inert atmosphere. DIPEA (1.47 mL, 8.45 mmol, 2.4 eq) was added followed by the dropwise addition of N,N-diisopropylamino cyanoethyl phosphoramidic chloride (ChemGenes) (1g, 4.22 mmol, 1.2 eq) . The reaction mixture was stirred for 2.5 h at room temperature protected from light. The solvent was removed under reduced pressure and the redidue was purified by column chromatography: Hexanes : Ethyl acetate : TEA 60 : 40 : 1 (v : v : v). Two fractions were separated (Rf_1 = 0.51 and Rf_2 = 0.43) that corresponded to the two diastereoisomers. 1.87 g in total (64. 3 %). Fraction 1: H NMR (500 MHz, $CDCl_3$) δ 7.48-7.44 (m, 2H, H_{Ar}), 7.37-7.28 (m, 6H, H_{Ar}), 7.23 (t, 1H, *J* = 7.4 Hz, H_{Ar}), 6.85 (d, 4H, *J* = 6.85 Hz, H_{Ar}), 5.80 (t, 1H, *J* = 5.6 Hz, N*H*), 4.05 (hep, 1H, *J* = 5.15 Hz, C*H*OP), 3.81 (s, 6H, OC*H*$_3$), 3.80-3.59 (m, 4H), 3.58-3.45 (m, 2H), 3.30-3.21 (m, 2H), 2.68 (dd, 4H, *J* = 7.35 Hz), 2.47 (t, 2H, *J* = 6.4 Hz), 2.09 (t, 2H, *J* = 6.85 Hz), 1.72-1.63 (m, 6H), 1.44-1.27

(m, 8H), 1.22 (d, 6H, *J* = 1.80 Hz, iPr), 1.20 (d, *J* = 1.85 Hz, 6H, iPr), 0.91 (t, 3H, *J* = 7.0 Hz) C NMR (125.8 MHz, $CDCl_3$) δ 172.42, 158.54, 144.65, 135.85, 135.76, 130.09, 128.19, 127.87, 126.88, 117.71, 113.16, 86.25, 71.66 (d, *J* = 15.09 Hz), 64.47(d, *J* = 3.2 Hz), 58.34 (d, *J* = 18.77 Hz), 55.26, 43.22(d, *J* = 12.35 Hz), 42.26 (d, *J* = 4.57 Hz), 39.10, 38.52, 36.17, 31.44, 29.20, 28.78, 28.21, 24.73, 24.71, 24.67, 24.65, 24.53, 22.55, 21.07, 20.29 (d, *J* = 6.86 Hz), 14.05. ^{31}P NMR (203 MHz, $CDCl_3$) δ 148.78. **HRMS** (ESI) calc for $C_{44}H_{64}N_3O_6PS_2Na$ 848.3866 found 848.3853 Fraction 2 H NMR (500 MHz, $CDCl_3$) δ 7.46 (d, 2H, *J* = 7.0 Hz, H_{Ar}), 7.34 (d, 4H, *J* = 8.85 Hz, H_{Ar}), 7.29 (t, 2H, *J* = 7.35 Hz, H_{Ar}), 7.22 (t, 1H, *J* = 7.35 Hz, H_{Ar}), 6.83 (d, 4H, *J* = 9.0 Hz, H_{Ar}), 6.09 (t, *J* = 5.8 Hz, N*H*), 4.04 (hep, 1H, *J* = 6.85 Hz, C*H*OP), 3.96-3.86 (m, 1H), 3.80 (s, 6H, OC*H*$_3$), 3.83-3.75 (m, 1H), 3.64-3.53 (m, 3H), 3.25-3.08 (m, 2H), 2.75-2.63 (m, 6H), 2.16 (t, 2H, *J* = 7.35 Hz), 1.75-1.63 (m, 7H), 1.44-1.24 (m, 6H), 1.20 (d, 6H, *J* = 6.9 Hz, iPr), 1.13 (d, *J* = 6.9 Hz, 6H, iPr), 0.91 (t, 3H, *J* = 7.15 Hz) C NMR (125.8 MHz, $CDCl_3$) δ 172.55, 158.50, 144.68, 135.91, 135.85, 130.08, 130.05, 128.16, 127.83, 126.80, 117.83, 113.13, 86.18, 76.79, 72.20 (d, *J* = 14.65 Hz), 64.84 (d, *J* = 4.11 Hz), 58.00(d, *J* = 20.14 Hz), 55.24, 53.45, 43.26 (d, *J* = 1.3 Hz), 42.29 (d, *J* = 2.74 Hz), 39.07, 38.54, 36.21, 31.44, 29.19, 28.74, 28.22, 24.72, 24.67, 24.63, 24.57, 22.55, 20.55 (d, *J* = 6.86 Hz), 14.05.^{31}P NMR (203 MHz, $CDCl_3$) δ 149. **HRMS** (ESI) calc for $C_{44}H_{64}N_3O_6PS_2Na$ 848.3866 found 848.3850.

Compound 7:

Tridecanoic acid (3g, 14mmol), 3-Amino-1,2-propandiol (1.34g, 14.7mmol), and N-hydroxysuccinimide (1.7g, 14.7mmol) were dissolved in DMF (60 ml). To this was added N,N'-Dicycolhexylcarbodiimide_(3.03g, 14.7mmol) and the mixture was reacted for 24 hours. The solution was then filtered to remove the insoluble urea and diluted with H_2O (100 mL) and extracted with ethyl acetate (3 × 100 mL). The organic phase was washed with saturated $NaHCO_3$ (200 mL), and saturated NaCl (200 mL), and then dried on $MgSO_4$, filtered and concentrated *in vacuo*. The crude material was then purified by column chromatography (3CV's 95:5 EtOAc/Hex, then 5%MeOH in CH_2Cl_2) to provide Compound **7** as a colourless oil (3.22g, 80%). ^{1}H NMR (500MHz, DMSO D_6): δ = 0.87 (t, 3H), 1.27 (m, 6H), 1.58 (m, 6H), 2.11 (m, 2H), 2.69 (m, 4H), 2.99 (m, 1H), 3.17 (m, 1H), 3.27 (m, 2H).), 3.47 (s, 1H), 7.75 (m, 1H). ^{13}C NMR (125MHz, DMSO D_6): δ

= 14.36, 22.46, 24.58, 27.88, 28.64, 28.96, 31.29, 35.22, 38.02, 38.30, 39.46, 39.63, 39.80, 42.51, 64.10, 71.01, 172.87. HRMS (EI): calc. for $[C_{16}H_{33}O_3NNa]^+$ $[M]^+$: 310.25, found 310.2507.

Compound 8:

Compound **7** (3g, 10.4mmol) was dissolved in THF (50mL). To this was added diisopropylethylamine (5.4g, 41.7mmol) followed by 4, 4' dimethoxytrityl chloride (5.3g, 15.6mmol) 1/3 every hour over 3 hrs. The mixture was allowed to react for an additional 24hr. The solution was directly concentrated in vacuo, and purified directly by column chromatography (9:1 Hex/EtOAc to 1:1 Hex/EtOAc) to provide compound **8** (2.8g, 45%). ^{1}H NMR (500MHz, DMSO D_6): δ = 0.86 (t, 3H), 1.27 (m, 4H), 1.35 (m, 2H), 1.59 (m, 6H), 2.05 (m, 2H), 2.67 (m, 4H), 2.86 (m, 2H), 2.98 (m, 1H), 3.26 (m, 1H).), 3.70 (m, 1H), 3.74 (s, 6H), 6.88 (m, 4H), 7.25 (m, 7H), 7.41 (m, 2H) 7.75 (m, 1H). ^{13}C NMR (125MHz, $CDCl_3$): δ = 14.05, 14.22, 21.07, 22.55, 24.42, 24.47, 28.22, 28.65, 29.20, 31.45, 35.94, 36.00, 38.45, 38.62, 39.10, 39.24, 42.89, 55.25, 60.42, 64.65, 70.28, 70.34, 86.25, 113.17, 126.92, 127.93, 128.08, 130.02, 135.73, 144.61, 158.57, 173.80 HRMS (EI): calc. for $[C_{37}H_{51}O_5NNa]^+$ $[M]^+$: 612.38, found 612.3802.

Compound 9:

Compound **8** (2.284 g, 3.87 mmol, 1 eq) and DMAP (0.214 g, 1.69 mmol, 0.42 eq) were dissolved in 30 mL of dry dichloromethane. To the solution DIPEA (2.94 mL, 16.9 mmol, 4.2 eq) was added followed by dropwise addition of N,N-diisopropylamino cyanoethyl phosphoramidic chloride (ChemGenes) (2g, 8.45 mmol, 2.1 eq). The reaction mixture was stirred at room temperature for 2.5 h. The solvent was removed under reduced pressure and the crude reaction mixture was purified by column chromatography (Hex : Ethyl Acetate : TEA, 60 : 40 : 1) to give 2.029 g of Compound **9** (66. 3 %). Two fractions were separated with R_{f1} = 0.64 and R_{f2} = 0.47. Fraction 1 H NMR (800 MHz, $CDCl_3$) δ 7.43 (d, *J* = 7.36 Hz, 2H, H_{Ar}), 7.32 (d, *J* = 8.96 Hz, 4H, H_{Ar}), 7.28 (t, *J* = 7.36 Hz, 2H, H_{Ar}), 7.21 (t, J = 7.36 Hz, 1H, H_{Ar}), 6.82 (d, *J* = 8.08 Hz, 4H, H_{Ar}), 5.73 (t, *J* = 5.76 Hz, 1H, N*H*), 4.03 (hep, *J* = 5.12 Hz, 1H, C*H*OP), 3.79 (s, 6H, OCH_3), 3.76-3.71 (m, 1H), 3.71-3.65 (m, 1H), 3.65-3.58 (m, 1H), 3.55-3.43 (m, 2H) , 3.27-3.18 (m, 2H), 2.44 (t, *J* = 6.32 Hz, 2H), 2.04 (dt, J_1 = 7.68 Hz, J_2 = 2.16 Hz, 2H), 1.53 (p, *J* = 6.04 Hz, 2H), 1.31-1.21 (m, 18H), 1.19 (d, *J* = 2.16 Hz, 6H, iPr), 1.18 (d, *J* = 2.16 Hz, 6H, iPr), 0.88 (t, *J* = 7.2 Hz, 3H, CH_3). ^{31}P NMR (203 MHz, $CDCl_3$) δ 148.92.

^{13}C NMR (201 MHz, $CDCl_3$) δ 173.06, 158.53, 144.66, 135.87, 135.79, 130.09, 128.20, 127.85, 126.86, 117.65, 113.14, 86.23, 72.05 (d, *J* = 116.2 Hz), 64.50, 64.49, 58.39, 58.29, 55.24, 43.26, 43.20, 42.23, 42.21, 36.84, 31.93, 29.69, 29.66, 29.53, 29.38, 29.37, 25.77, 24.70, 24.66, 22.70, 20.28, 20.25, 14.14. **HRMS** (ESI) calc for $C_{46}H_{68}N_3O_6PNa$ 812.4737, found 812.4722. Fraction 2 H NMR (800 MHz, $CDCl_3$) δ 7.44 (d, *J* = 7.52 Hz, 2H, H_{Ar}), 7.33.-7.31 (d, *J* = 8.16 Hz, 4H, H_{Ar}), 7.26 (t, *J* = 7.12 Hz, 2H, H_{Ar}), 7.18 (t, J = 6.08 Hz, 1H, H_{Ar}), 6.81 (d, *J* = 9.04 Hz, 4H, H_{Ar}), 6.02 (t, *J* = 4.4 Hz, 1H, N*H*), 4.46-3.98 (hep, *J* = 6.4 Hz, 1H, C*H*OP), 3.91-3.84 (m, 1H), 3.78 (s, 6H, OCH_3), 3.68-3.53 (m, 3H), 3.39-3.33 (m, 1H), 3.20-3.16 (m, 1H) , 3.11-3.06 (m, 1H), 2.64 (t, *J* = 6.24 Hz, 2H), 2.09 (t, *J* = 8.96 Hz, 2H), 1.32-1.31 (m, 19H), 1.17 (d, *J* = 6.72 Hz, 6H, iPr), 1.11 (d, *J* = 6.64 Hz, 6H, iPr), 0.87 (t, *J* = 7.44 Hz, 3H, CH_3).^{31}P NMR (203 MHz, $CDCl_3$) δ 149.13. ^{13}C NMR (201 MHz, $CDCl_3$) δ 173.14, 158.49, 144.68, 135.93, 130.08, 130.05, 128.16, 127.82, 126.79, 117.71, 113.13, 86.17, 72.19 (*J* = 14.67 Hz), 64.84, 58.03 (*J* = 20.54 Hz), 55.22, 43.26 (*J* = 12.47 Hz), 42.22, 36.88, 31.93, 29.70, 29.67, 29.66, 29.56, 29.45, 29.41, 29.37, 25.84, 24.70, 24.66, 24.62, 24.58, 22.70, 20.49 (*J* = 6.60 Hz), 14.14. **HRMS** (ESI) calc for $C_{46}H_{68}N_3O_6PNa$ 812.4737, found 812.4723.

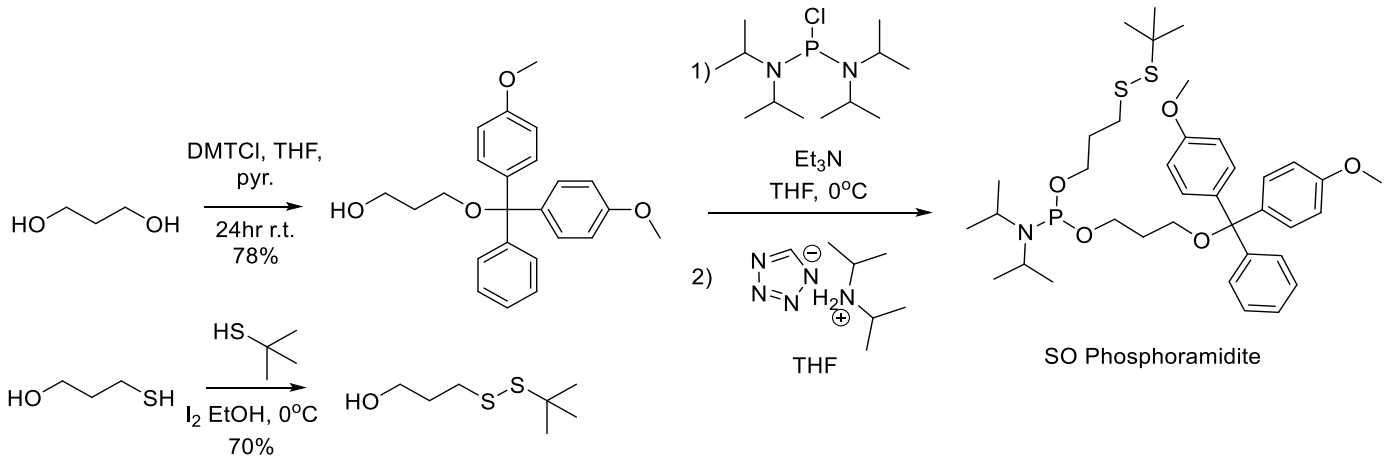

Figure 3. 8 Synthesis of the SO phosphoramidite[37]

3.5.6 Characterization of Oligonucleotide Conjugates

Table 3. 2 LC-ESI-MS data. Calculated and experimental m/z values for synthesized DNA conjugates.

Name:	Calculated	Found
S4	7209.99	7209.61
S5	7595.11	7594.61
S6	7980.22	7979.74
SO	7169.84	7170.66
C4	7066.34	7066.02
C5	7415.54	7415.12
C6	7764.75	7764.22
S4Cy3	7717.23	7715.73
S5Cy3	8102.35	8100.89
S6Cy3	8487.46	8486.91
SOCy3	7573.58	7573.85
C4Cy3	7922.78	7922.17
C5Cy3	8271.99	8271.89
C6Cy3	7677.08	7675.86

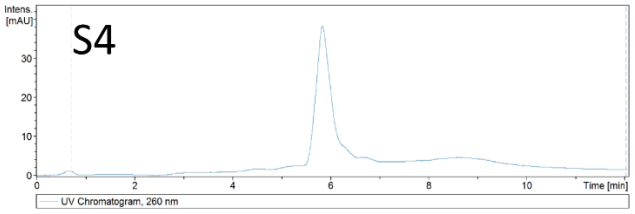
S4
Intens. [mAU]
Time [min]
UV Chromatogram, 260 nm

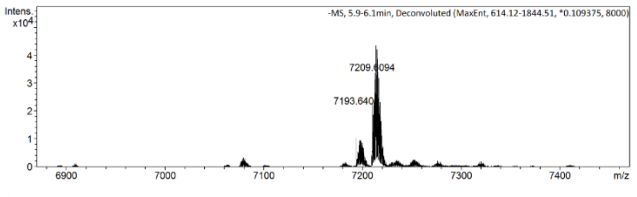
-MS, 5.9-6.1min, Deconvoluted (MaxEnt, 614.12-1844.51, *0.109375, 8000)
Intens. x10^4
7209.6094
7193.6401
m/z

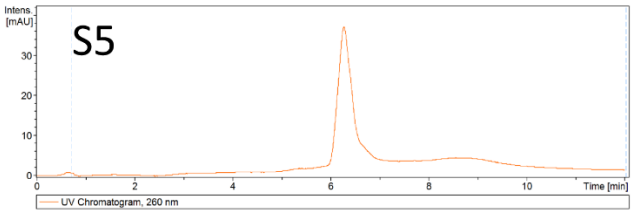
S5
Intens. [mAU]
Time [min]
UV Chromatogram, 260 nm

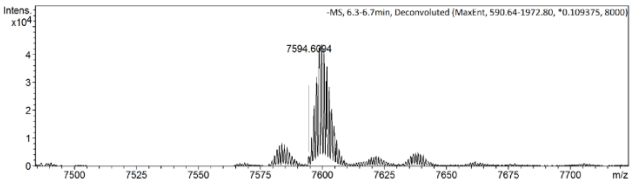
-MS, 6.3-6.7min, Deconvoluted (MaxEnt, 590.64-1972.80, *0.109375, 8000)
Intens. x10^4
7594.6094
m/z

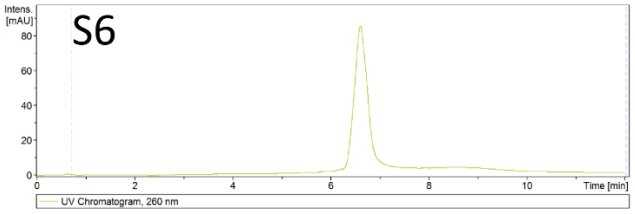
S6
Intens. [mAU]
Time [min]
UV Chromatogram, 260 nm

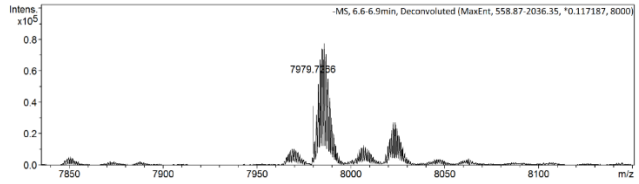
-MS, 6.6-6.9min, Deconvoluted (MaxEnt, 558.87-2036.35, *0.117187, 8000)
Intens. x10^5
7979.7356
m/z

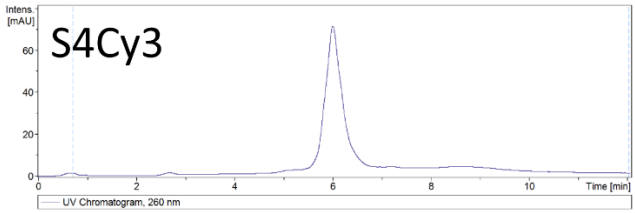
S4Cy3
Intens. [mAU]
Time [min]
UV Chromatogram, 260 nm

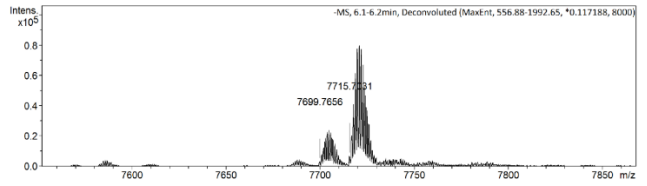
-MS, 6.1-6.2min, Deconvoluted (MaxEnt, 556.88-1992.65, *0.117188, 8000)
Intens. x10^5
7715.7231
7699.7656
m/z

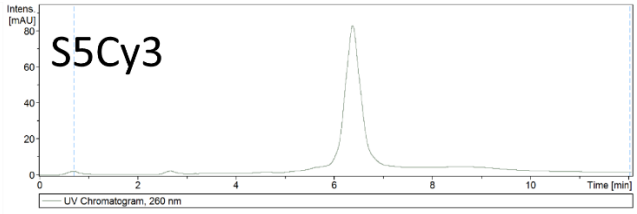
S5Cy3
Intens. [mAU]
Time [min]
UV Chromatogram, 260 nm

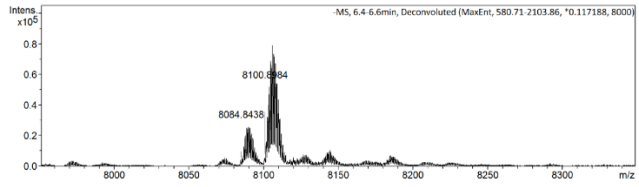
-MS, 6.4-6.6min, Deconvoluted (MaxEnt, 580.71-2103.86, *0.117188, 8000)
Intens. x10^5
8100.8984
8084.8438
m/z

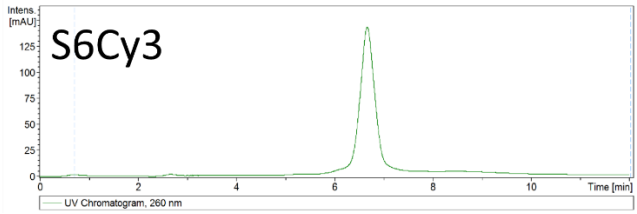
S6Cy3
Intens. [mAU]
Time [min]
UV Chromatogram, 260 nm

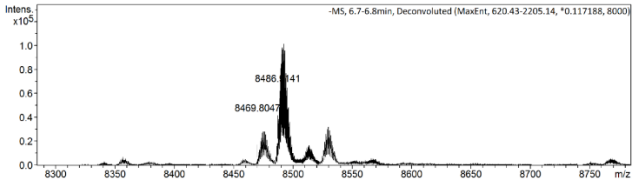
-MS, 6.7-6.8min, Deconvoluted (MaxEnt, 620.43-2205.14, *0.117188, 8000)
Intens. x10^5
8486.8141
8469.8047
m/z

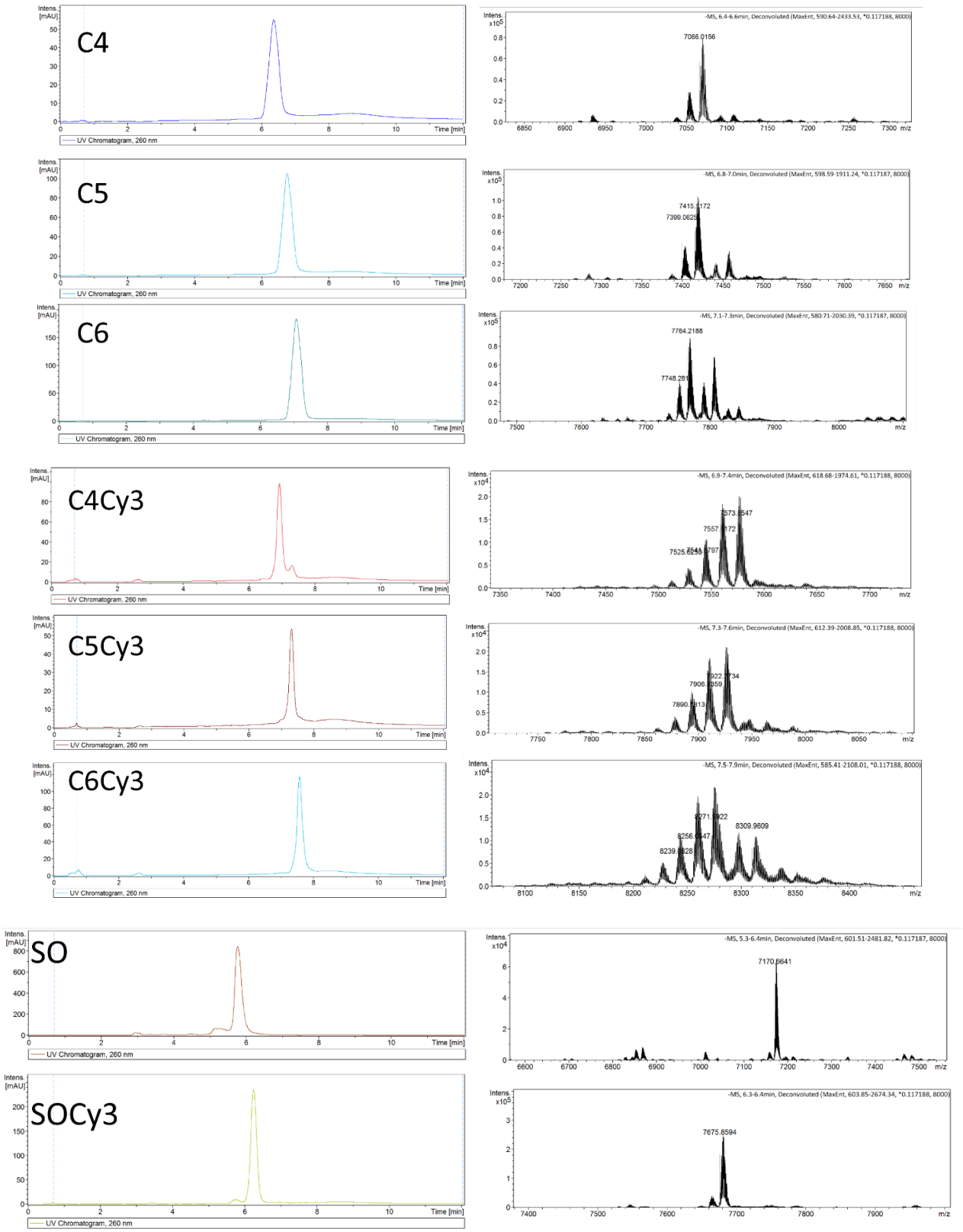

Figure 3. 9 RP-HPLC and MS characterization of modified oligonucleotide strands

3.5.7 Methods

3.5.7.1 Native AGE:

Native agarose gel electrophoresis was used to characterize protein binding and release as well as crosslinking. In each case, 2.5% AGE was carried out at 4°C for 2.0 hours at a constant voltage of 100 V. Typical sample loading is 3.5 picomoles with respect to the DNA per lane (4.5 µL of 0.75 µM DNA). The gels were either stained with GelRed DNA stain and imaged under a DNA-selective channel or cyanine 3 channel. Band intensities were quantified using Image lab 5.2 software

3.5.7.2 Native PAGE:

Native PAGE assays were either run in 1xTAMg (3-6%) (6%: 10.6 mL 1xTAMg, 1.88 mL of 40% acrylamide), or TBE (10%) (10%: 10.0 mL 1xTBE, 2.5 mL of 40% acrylamide),. Samples were prepared by mixing with 2 µL of glycerol mix (7:1 glycerol/H2O) and loaded on to the gel with 1xTAMg or TBE as the running buffer. The gel was run at 250 V for 1 hour, stained with GelRed and imaged.

3.5.7.3 Denaturing PAGE:

Samples were prepared by mixing with 8M urea 1:1 w/w and resolved on 12-20% PAGE (TBE) denaturing gel (20%: 20.7 mL H2O, 1.8 mL of 1x TBE, 7.5 mL 40% acrylamide, 8 M urea).

3.5.7.4 SDS PAGE:

SDS PAGE was carried out by preparing protein samples in LDS sample buffer (4x). Typical sample loading amounts are 5uL of 1mg/mL (coomasie stain). The samples were incubated at 90 °C for 10 min. Samples were then loaded onto a 3-8% Tris-acetate gels and run for 120 min at 100 V with a tris-acetate SDS running buffer at 4^{o}C. Gels were stained for protein with coomasie stain and then visualized with a BioRad ChemiDoc MP system. Image analysis was done in ImageLab.

3.5.7.5 Luciferase Assay:

HeLa cells were maintained in DMEM containing 10% FBS supplemented with antibiotic/antimycotics at 37^{o}C, 5% CO_2. Cells were passed every 3 days in a ratio of 1:5. Luciferase knockdown assays were performed by plating 10000 cells per well in a 96 well plate. Cells were incubated at 37^{o}C, 5% CO_2 to allow for adhesion to the plate. Transfected samples were added to the wells in sextuplicate using Lipofectamine transfection using Optimem as transfection media mix in accordance with vendor procedure. Non transfected samples were

directly added into wells in sextuplicate without any prior dilution. Cells were then incubated for 24-72 hours post addition of DNA.

Cytotoxicity and cell viability was analyzed by incubating cells with using a fluorescent reagent (Celltiter Blue) for 1.5 hours at 37^{o}C, 5% CO_2. Fluorescence from the 96 well plates was then measured Ex. 530nm, Em. 590nm using Biotek Cytation 5 and generation 5 software.

Luciferase assay was performed by first removing media from cells then adding 25 µL of Promega Glo-Lysis Buffer to each well. Luminescence was measured at 528 nm using Biotek citation 5.

3.5.7.6 AFM Characterization:

Dry AFM was carried out using a MultiMode8™ SPM connected to a Nanoscope™ V controller (Bruker, Santa Barbara, CA). All images were obtained using ScanAsyst mode in air with AC160TS cantilevers (Nominal values: Tip radius – 2 nm, Resonant frequency – 300 kHz, Spring constant – 42 N/m) from Bruker. 5 µL of each sample prepared at 5 µM in TAMg buffer was deposited on a freshly cleaved mica surface (ca. 7 x 7 mm) and allowed to adsorb for 2-5 seconds. Then 50 µL of 0.22 µm filtered Millipore water was dropped on the surface and instantly removed with filter paper. The surface was then washed with a further 100 µL of water (2 x 50 µL), wicked with a filter paper, and the excess removed with a flow of nitrogen (or air). Samples were dried under vacuum for at least 3 hours prior to imaging.

3.5.7.7 Dynamic Light Scattering Characterization:

Dynamic light scattering (DLS) experiments were carried out using a DynaPro™ S10 Instrument from Wyatt Technology. A cumulants fit model was used to confirm the presence and determine the size the SNA's and clusters of SNA's. Sterile water, 1x PBS buffer and 1xTAMg buffer were filtered using a 0.45 µm nylon syringe filter before use in DLS sample preparation. 20 µL of sample (concentration: 10 µM) was used in each measurement. All measurements were carried out in triplicate at 25 °C.

3.5.7.8 Size Exclusion:

Unless otherwise stated, 100µL of 3uM samples were injected and samples were run through a Tosoh bioscience, TSKgel G2000SW column (7.5mm I.D x 60cm, 10um) using a mobile phase of 100% 1x PBS pH 7.2. over 50min.

3.5.7.9 Flow Cytometry

HeLa cells were seeded at a density of 1 x 10^6 cells in a 6 well plate. After 24 hours the cells were incubated with the corresponding samples to a final concentration of 1μM for 4 hours. The cells are then detached, washed, and resuspended in 1x PBS and processed using FACS FORTESSA. All measurements were performed in duplicate.

3.5.7.10 FACS with Iodoacetamide

Iodoacetamide was prepared in a 1M stock. HeLa cells were seeded at a density of 1 x 10^6 cells in a 6 well plate. Cells were incubated at 37^{o}C, 5% CO_2 for 24 hours to allow for adhesion to the plate. Cells were incubated with 1.2mM iodoacetamide for 30 minutes. Following this incubation samples were added to a final concentration of 1μM for 4 hours. The cells are then detached, washed and resuspended in 1x PBS and processed using FACS FORTESSA. All measurements were performed in duplicate.

3.5.7.11 Microscopy

For confocal microscopy 5 x 10^5 HeLa cells were plated on a Nunc Lab-Tek Chambered Cover glass (Thermo Scientific 155411) one day before incubation. Oligonucleotides and DNA structures were incubated at a final concentration of 1μM and imaged after 4 hours. Imaging was done under the 63x objective on a Zeiss LSM780 microscope. All images were acquired and were subsequently analyzed using Zen Microscope software.

3.5.8 General Assembly Procedure:

Unless otherwise stated, all experiments were done using a doped system where 15% of the strand was labelled with Cy3 and the remaining 85% was unlabeled. This doped system was used to mitigate any effect the cyanine dye may have when possible. Briefly, unlabeled strand was made to be 51uM and Cy3 labelled strand 9uM in 20uL 1x TAMg pH 8. Strands were then thermocycled from 95^{o}C to 4^{o}C over 12hr. The SNA's were then diluted to desired concentrations and used for further experiments.

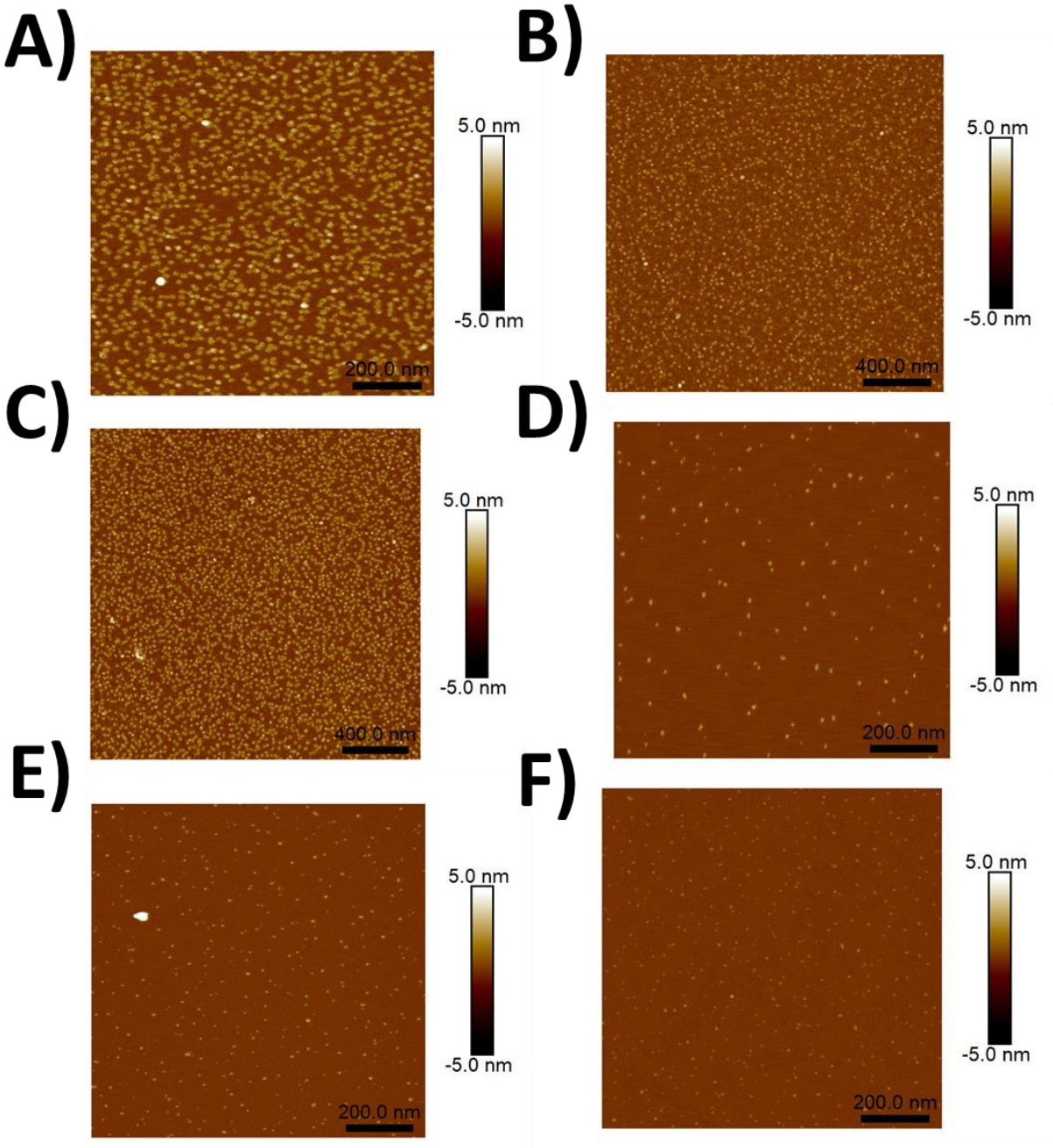

Figure 3. 10 AFM characterization of SNA's a) S6, b) S5, c) S4, d) C6, e) C5, f) C4

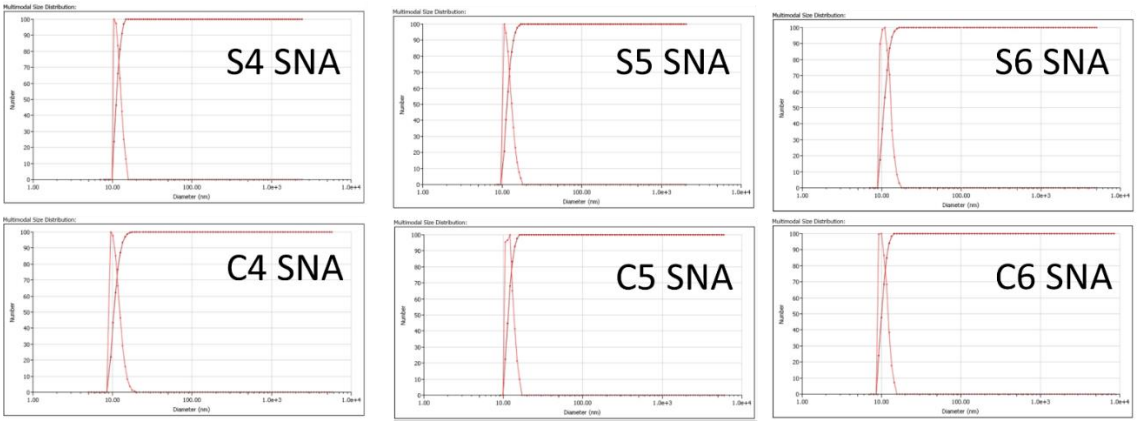

Figure 3. 11. DLS characterization of SNA's

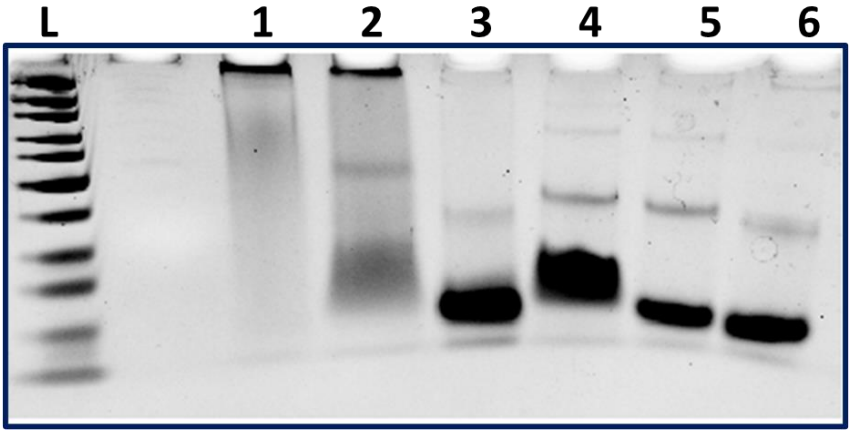

Figure 3. 12. Denaturing gel of strands: Lane 1: C6, Lane 2: C5, Lane 3:C4, Lane 4:S6, Lane 5:S5, Lane 6:S4

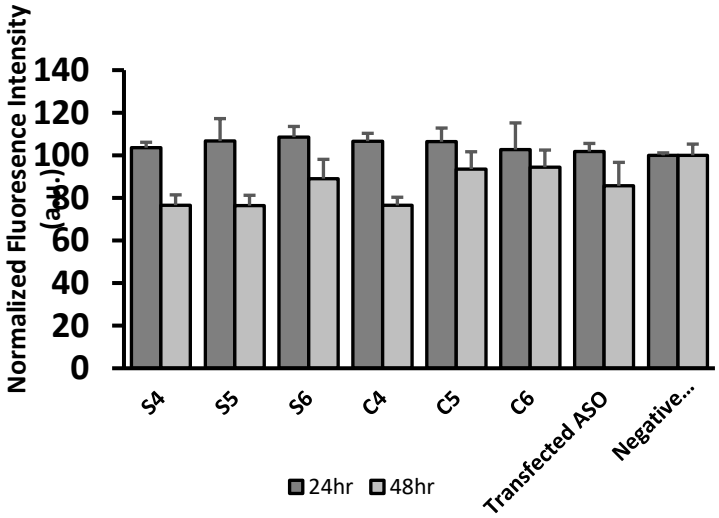

Figure 3. 13. MTT of initial luciferase experiments in Figure 3.1c

3.5.9 Reduction of SNA's:

Strands were first assembled according to 4.5.8. DTT was prepared as 1M and 100mM solutions in 1x PBS pH 7.2. 1uL of each sample was diluted to 18uL by adding 17uL 1xPBS pH 7.2. To reduce the SNA's 2uL of the DTT solutions were added to a final concentration and volume of 3uM, 20uL. For samples where reduction was not done 2uL of 1xPBS pH 7.2 was added instead. Samples where then incubated at 37^{o}C for the desired amount of time and then loaded on Native AGE, Native PAGE and/or Denaturing PAGE.

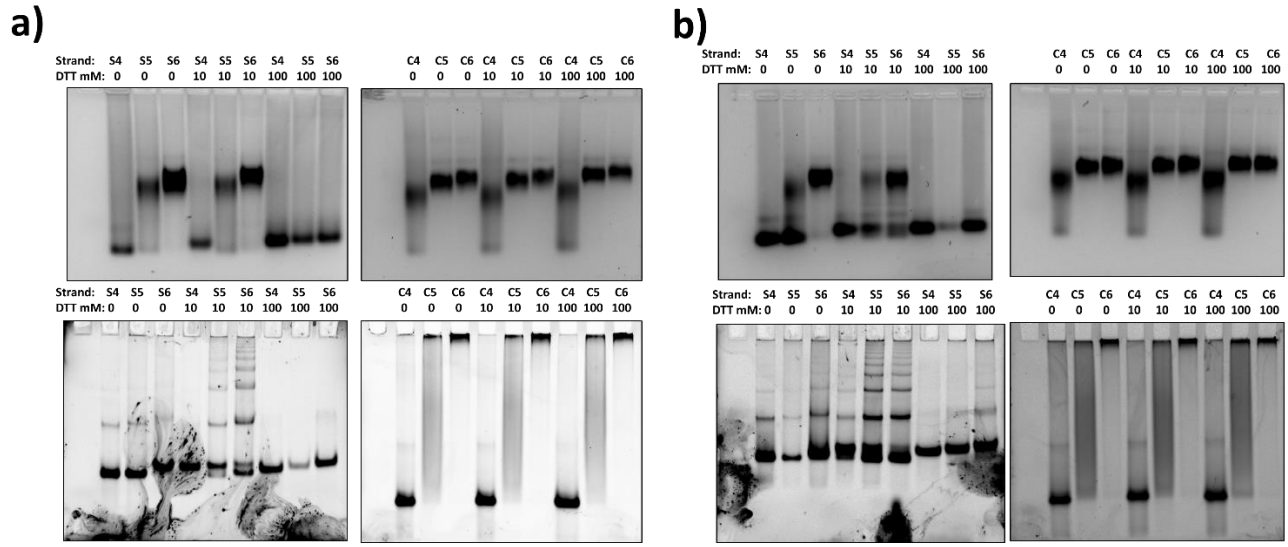

Figure 3. 14. Reduction of S4, S5, S6, C4, C5, and C6 SNA's by DTT over a) 24hr and b) 48hr, by native AGE (Top) and Denaturing PAGE (bottom)

3.5.10 Nile red Encapsulation and Release:

A stock solution of Nile Red 1 mM in acetone was used for all experiments. 6 µL of Nile Red stock in acetone was added to an Eppendorf and briefly incubated at room temperature to allow solvent evaporation. To this, non-labelled S4, S5, S6, C4, C5 and C6 where added as 18uL, 66.67uM in H_2O. The solution was vortexed and then 2uL of 10xTAMg was added to each solution. The mixtures where then thermocycled from 95^{o}C to 4^{o}C over 12hr. Following this, 5uL of each sample was diluted to 90uL by adding 85uL 1xPBS pH 7.2. To reduce the SNA's 10uL of the DTT solutions were added to a final concentration and volume of 3uM, 100uL. For samples where reduction was not done 10uL of 1xPBS pH 7.2 was added instead. Samples where then incubated at 37^{o}C for the desired amount of time, and fluorescence was measured by a Biotek

Cytation 5. Excitation was at 535 nm with a slit-width of 9 nm and emission was monitored between 560 nm and 750 nm.

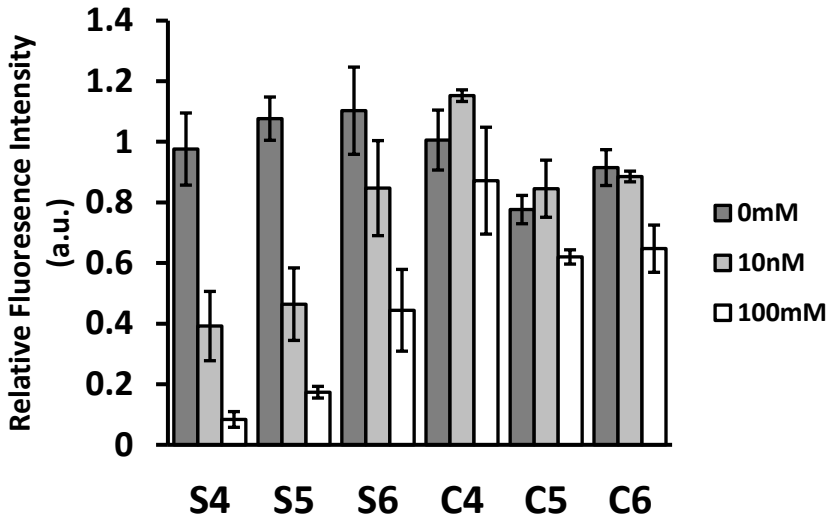

Figure 3. 15. Relative fluorescence intensity of nile red encapsulated

within S4, S5, S6, C4, C5, and C6 SNA's under 0mM DTT, 10 mM DTT and 100mM DTT after 24hr at 37^{o}C. Each sample is relative to itself with 0mM DTT at 0min.

3.5.11 Protein Binding Assays

For protein binding EMSA, samples were first assembled according to 4.5.8. 0.5uL of each sample was then diluted to 10uL with either 1xPBS pH 7.2 (PBS), Serum (Ser), albumin depleted serum (SerD), albumin (Alb), or diluted serum (SerDl) and incubated at 37^{o}C for 2hr. Serum is composed of DMEM containing 10% FBS supplemented with antibiotic/antimycotic. Depletion of albumin from serum was done using the Pierce™ albumin depletion kit (cat # 85160 thermo Fisher) according to the manufacturer's instructions. For the albumin samples a stock 10mg/mL solution of albumin was prepared and 1uL of this solution was added to each SNA sample diluted to 9uL in 1xPBS, to give a final 10uL sample of 3uM SNA and 1mg/mL albumin. Diluted serum was prepared by diluting serum 10x with 1xPBS pH 7.2. For the albumin samples that were treated with Proteinase K (PK), the albumin samples were made up to 9uL and incubated as such. Following incubation 1uL of PK (20mg/mL) was then added to the solution and heated from incubated at 65^{o}C for 30min.

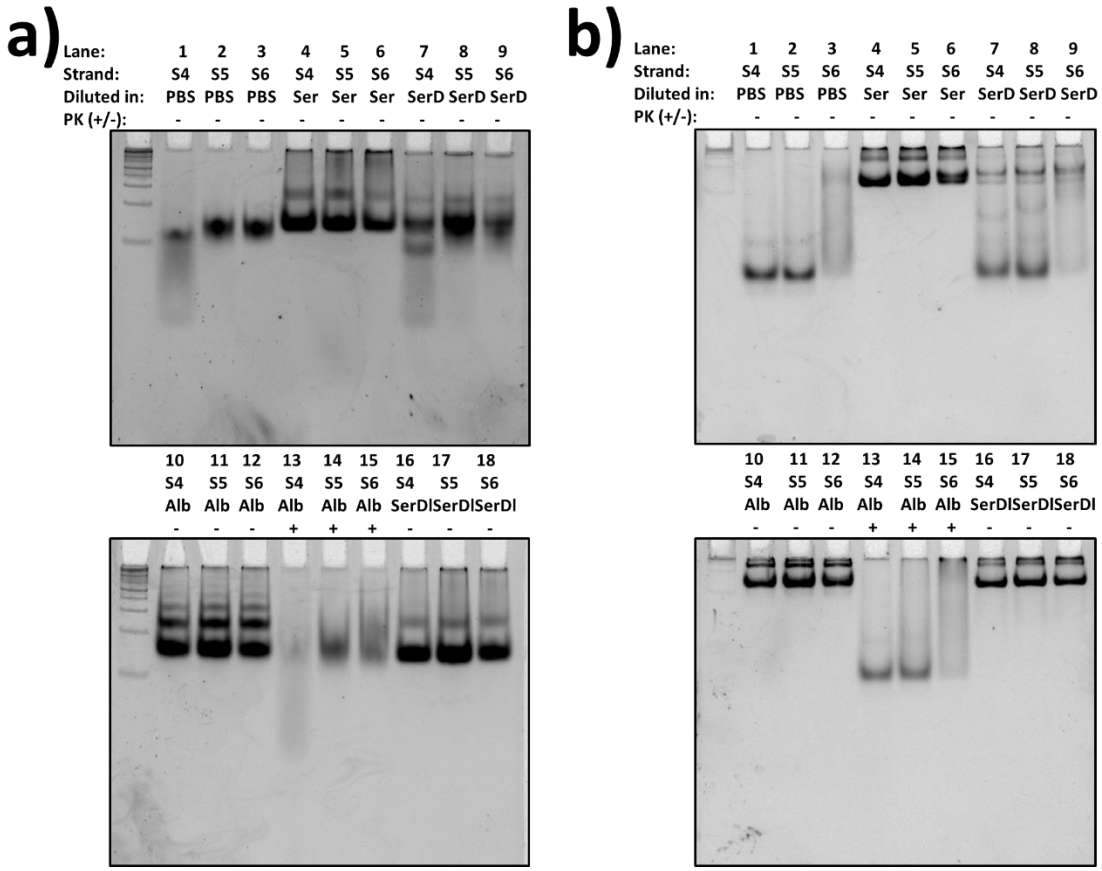

Figure 3. 16. Protein Binding EMSA of S4, S5 and S6 on a) Native 6% TAMg PAGE and b) Native 10% TBE PAGE

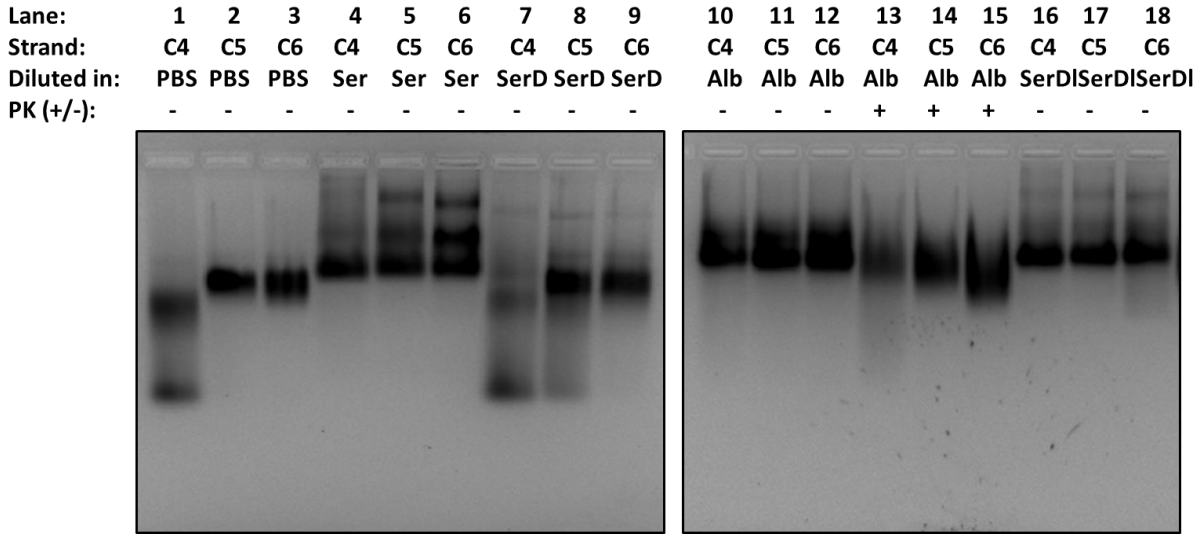

Figure 3. 17. Protein binding EMSA of C4, C5, and C6 on Native AGE

3.5.12 DLS of Albumin bound strands

Samples were first prepared according to 4.5.8. a 10mg/mL solution of albumin was prepared in 1xPBS pH 7.2. 3.33uL of sample was diluted to 18uL in 1xPBS, followed by the addition of 2uL of the 10mg/mL albumin solution. Samples where then incubated for 2hr at 37°C. 20 µL of sample (concentration: 10 µM) was used in each measurement. All measurements were carried out in triplicate at 25 °C.

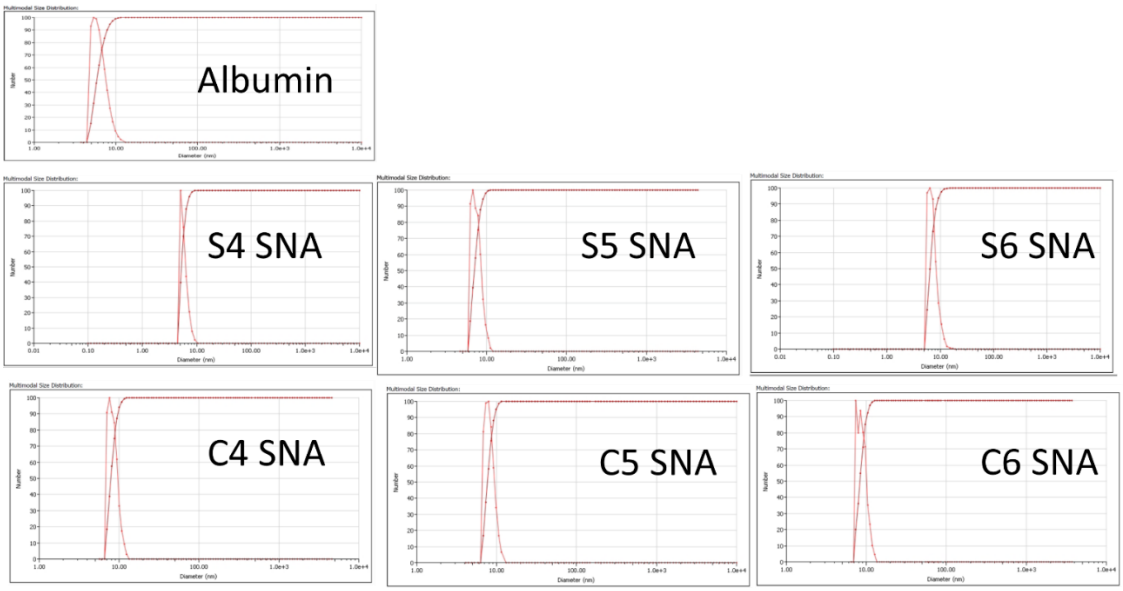

Figure 3. 18 DLS traces for SNA's incubated with albumin at 37°C for 2hr.

3.5.13 Size Exclusion

Samples were first prepared according to 4.5.8. and a 10mg/mL solution of albumin was prepared in 1xPBS pH 7.2. 5uL of each sample was diluted to 90uL in 1xPBS, followed by the addition of 10uL of the 10mg/mL albumin solution. Samples where then incubated for 2hr at 37°C. 100 µL of sample (concentration: 3 µM) was used for each injection. For samples where albumin was not added 10uL of 1xPBS pH 7.2 was added instead. For albumin with no SNA, 10uL of 10mg/mL albumin was diluted to 100uL of 1mg/mL sample. For the samples incubated in serum, 5uL of each sample was diluted to 100uL with serum (composed of DMEM containing 10% FBS supplemented with antibiotic/antimycotic) and injected.

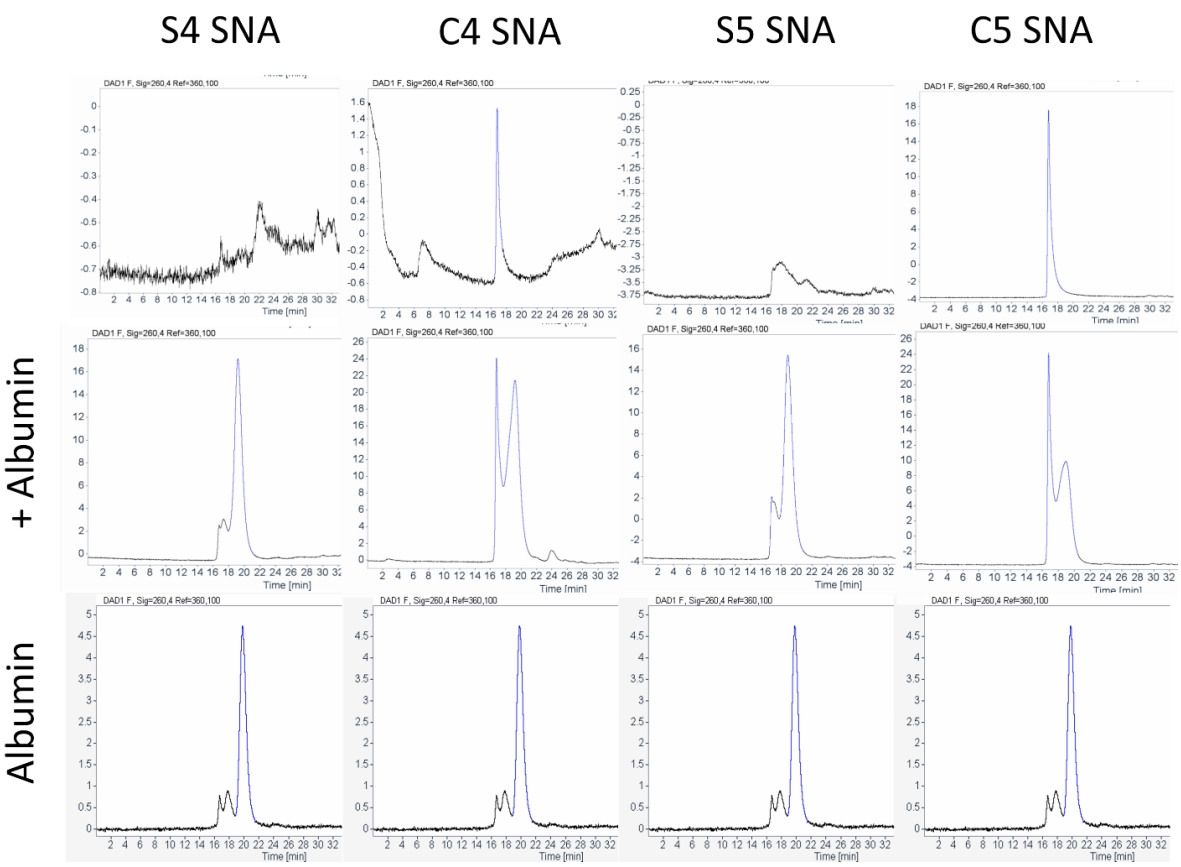

Figure 3. 19 Size exclusion traces of S4, C4, S5, and C5 SNA's with and without incubation with albumin.

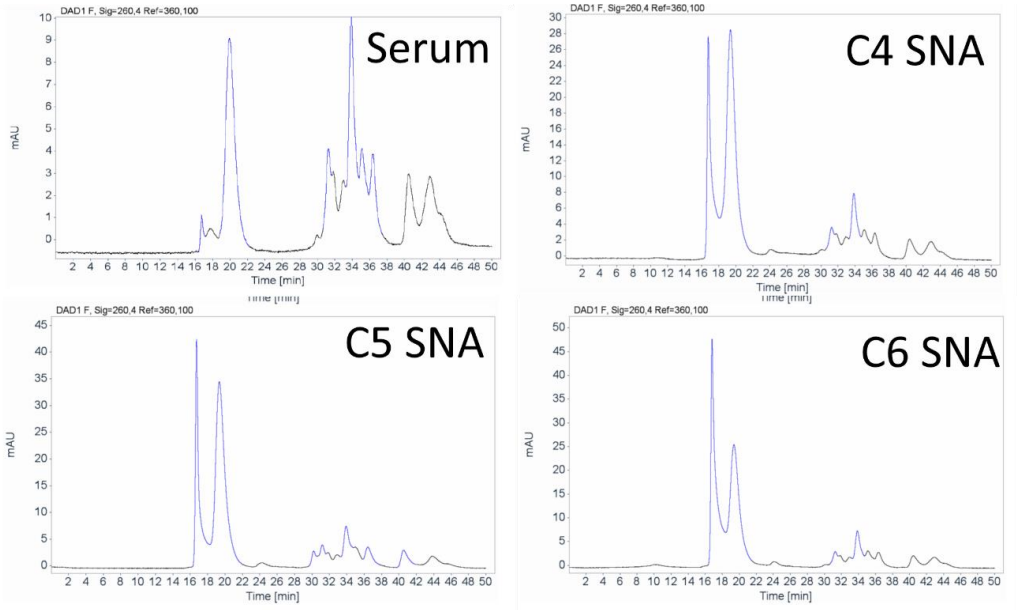

Figure 3. 20 Size Exclusion of C4, C5 and C6 SNA's incubated in serum for 24hr.

3.5.14 Binding Curves:

Binding curves were generated using a fluorescence spectroscopy method. Cyanine 3 labelled samples were first prepared as 20uL 60uM solutions in 1xTAMg. The mixtures where then thermocycled from 95^{o}C to 4^{o}C over 12hr. For crosslinked samples, samples were crosslinked according to section 4.4.20.5 .50uM, 25uM, 12.5uM, 10uM, 7.5uM, 5uM, 4uM, 3uM, 2uM, 1uM, 0.75nM, and 0.50nM solutions of albumin where prepared in 1xPBS pH 7.2. 12 x 0.83uL of each SNA sample was then diluted to 45uL in 1xPBS pH 7.2. To each of these samples, 5uL of each albumin solution was added, and the samples were incubated at 37^{o}C for 2hr. Fluorescence was measured by a Biotek Cytation 5 with an excitation wavelength of 561 nm, and emission of 585 nm. Samples were prepared and measured either 3 or 6 times. Data analysis was performed by Bandfit Host-Guest equilibria software and all data was found to fit well to a statistical 2:1 binding curve, without subtracting initial values[52-54]. *Note:* At high HSA concentration (>5 μM), the protein stick to the wall of the 384-well plate. Therefore, we did not measure binding affinity of the low-affinity constructs, such as ASO, C4, C5 and C6.

Table 3. 3. Calculated dissociation constants of each of the SNA's and strands

DNA strand	Kd (nM)
S4	396 ± 36nM
S5	315 ± 34nM
S6	561 ± 81 nM
C4	-
C5	-
C6	-
SO	610 ± 76nM
XS4	224 ± 19nM
XS5	265 ± 17nM
XS6	172 ± 17nM

3.5.15 SDS PAGE:

Albumin incubated samples were prepared as per section 4.5.11 and loaded on SDS PAGE.

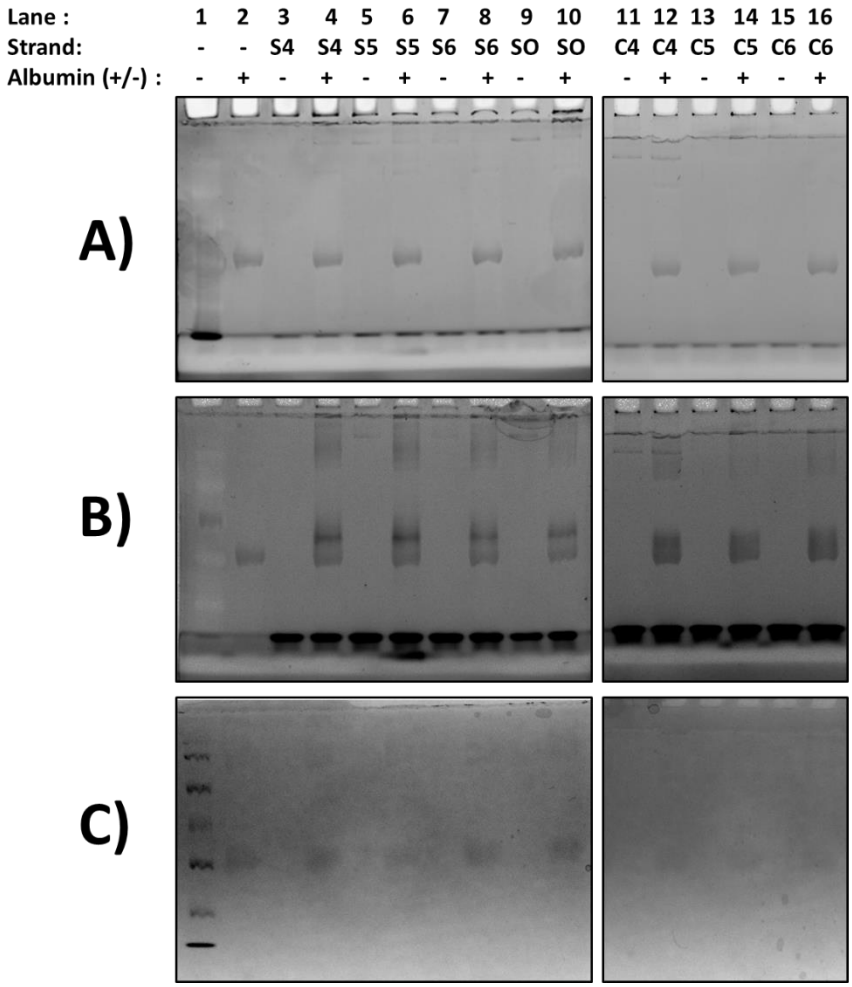

Figure 3. 21 . SDS PAGE of a) Gelred channel, b) Cy3 Channel, c) Coomassie stain

3.5.16 Serum Stability:

Non labelled SNA's were prepared at 60 µM in 1x TAMg pH 8, and thermocycled from 95°C to 4°C over 12hr. Samples were then diluted with cell culture media (DMEM, 10% FBS, 5% AB/AM) to a concentration of 3 µM. Samples were incubated at 37°C, and aliquots were taken at different timepoints and frozen until analysis. Aliquots were then treated with proteinase K and resolved on a 15% denaturing (UREA Polyacrylamide) gel to visualize for stability over time (Figure 3 .21. a., b., &c. (right)). Stability was determined by first producing calibration curves of each strand. Calibration curves were produced by preparing SNA at 60 µM and then diluting with cell culture media (DMEM, 10% FBS, 5% AB/AM) to the desired concentration, treating with proteinase K and

resolving on a 15% denaturing (UREA Polyacrylamide) (Figure 3 .21 a., b. & c. (left)). Calibration curves were plotted by by using the ladder as an internal standard and generating a ratio between the 150 b.p marker of the ladder and the band intensity of each strand at varying concentration (Figure 3 .21 d)). A plot of the relative concentration of each strand over 72hr was then produced using these calibration curves (Figure 3 .21. e.).

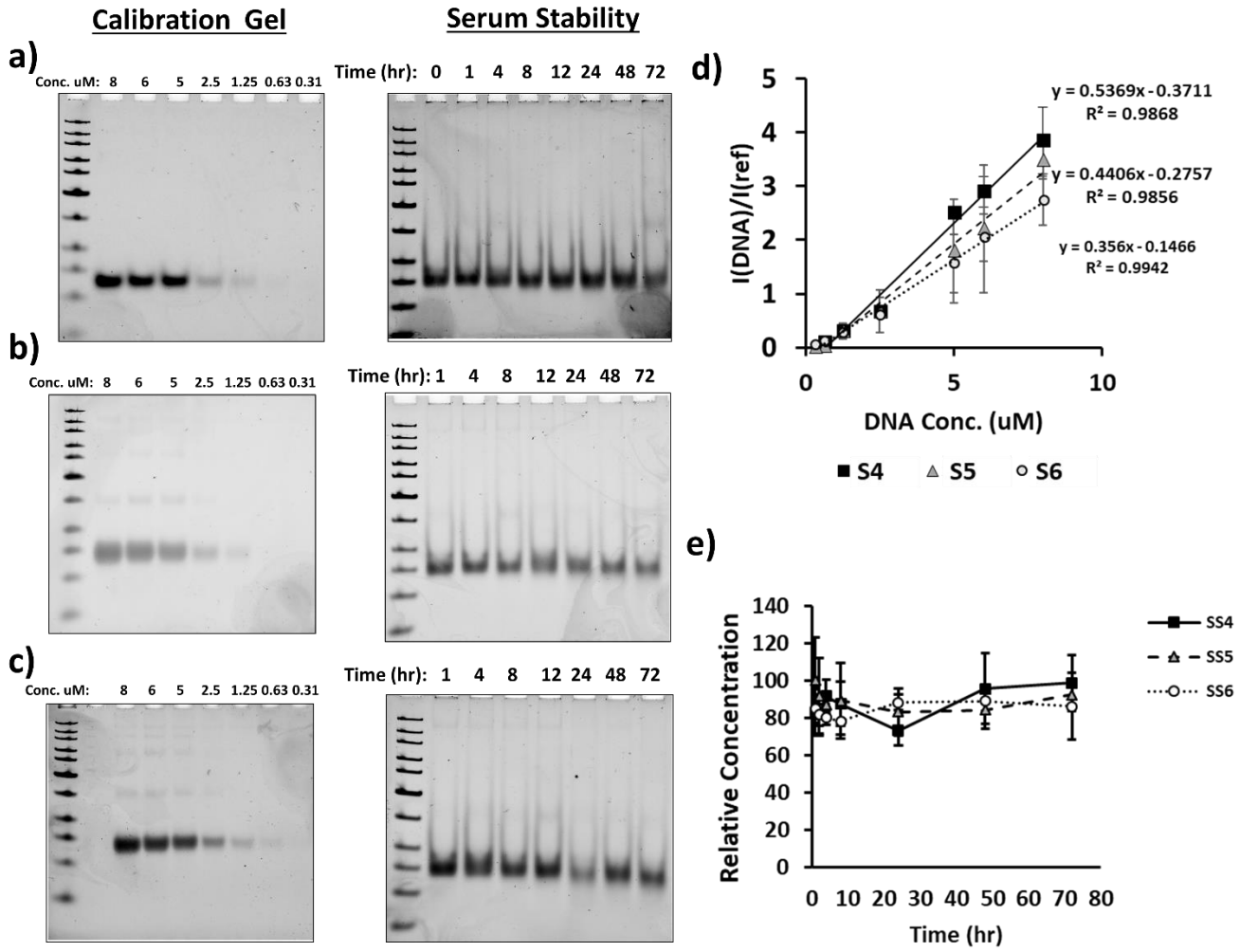

Figure 3. 22 Calibration curves and serum stability of Disulfide SNA's determined by denaturing PAGE.

a) S6, **b)** S5, and **c)** S4, denaturing PAGE of calibration gel (left), denaturing PAGE of SNA's over 72hr (right). **d)** calibration curves of the ratio between the band intensity and ladder intensity (I_B/I_L) and concentration of strands (uM). **e)** Plot of relative concentration for each sample over time.

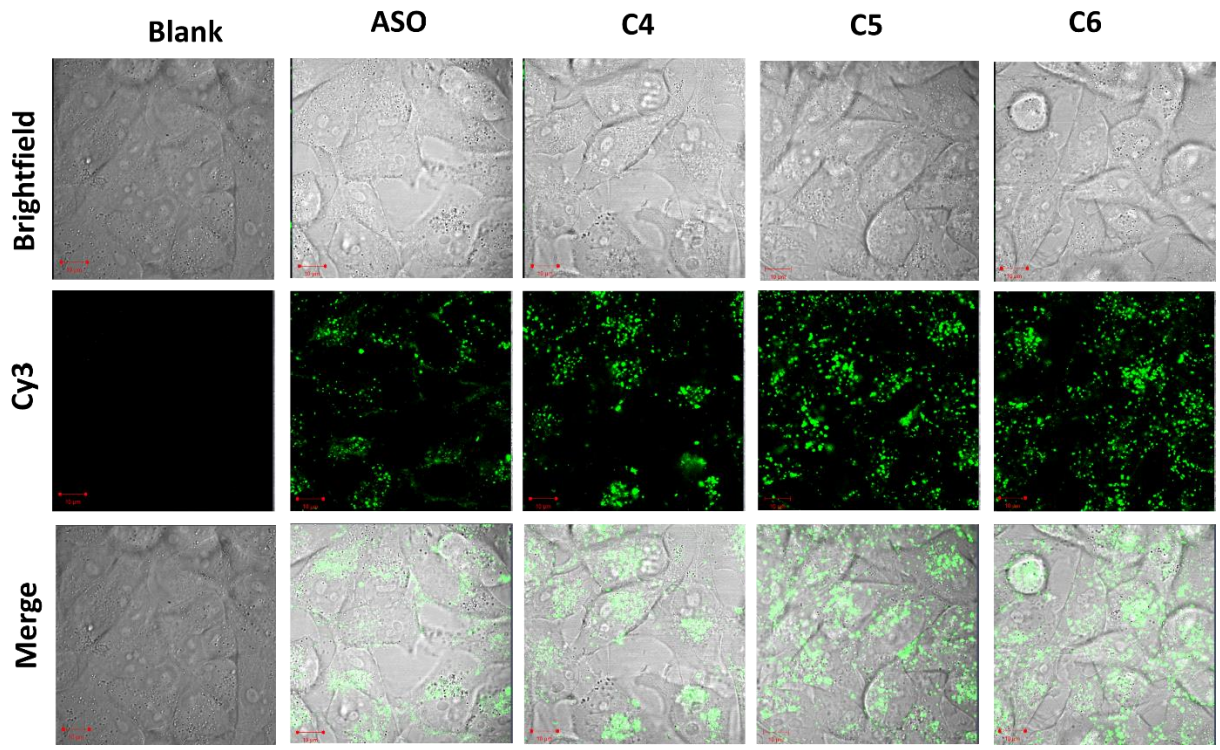

Figure 3. 23 Microscopy images of ASO, C4, C5 and C6 SNA's.

3.5.17 Albumin binding and Reduction Assay:

3.5.17.1 Native AGE

Strands were first assembled according to 4.5.8. DTT was prepared as a 100mM solutions in 1x PBS pH 7.2. Albumin was prepared as a 10mg/mL stock solution on 1xPBS pH 7.2. Samples were prepared by taking 0.5uL of each strand and diluting to 8uL with 1xPBS pH7.2. 1uL of albumin stock was then added and incubated for 2hr at 37°C. For samples with no albumin 1uL of 1xPBS pH 7.2 was added instead. Following incubation, 1uL of the DTT stock was then added and the samples were incubated for a further 24 and 48hr at 37°C. For samples with no albumin 1uL of 1xPBS pH 7.2 was added instead. The samples were then run by native AGE (Figure 3 .23.).

3.5.17.2 Fluorescence Spectroscopy

Cy3 Labelled strands prepared at 60 µM in 1x TAMg pH 8, and thermocycled from 95°C to 4°C over 12hr. DTT was prepared as a 100mM solutions in 1x PBS pH 7.2. Albumin was prepared as a 10mg/mL stock solution on 1xPBS pH 7.2. Samples were prepared by taking 2.5uL of each strand and diluting to 40uL with 1xPBS pH7.2. 5uL of albumin stock was then added and incubated for 2hr at 37°C. For samples with no albumin 5uL of 1xPBS pH 7.2 was added instead. Following

incubation, 5uL of the DTT stock was then added. For samples with no albumin 5uL of 1xPBS pH 7.2 was added instead. The samples were monitored by fluorescence spectroscopy over 24hr at 37^{o}C. Fluorescence was measured by a Biotek Cytation 5 with an excitation wavelength of 561 nm, and emission of 585 nm. Samples were prepared and measured in triplicate. For each sample, florescence was min-max normalized between the fluorescence of each sample with 0mM DTT at 0min (max) and fluorescence of an ASOCy3 control with 10mM DTT after 24hr (min) (Figure 3 .x). Maximum fluorescence of each sample incubated with albumin, with and without 10mM DTT can also be found in Figure 3 .24.

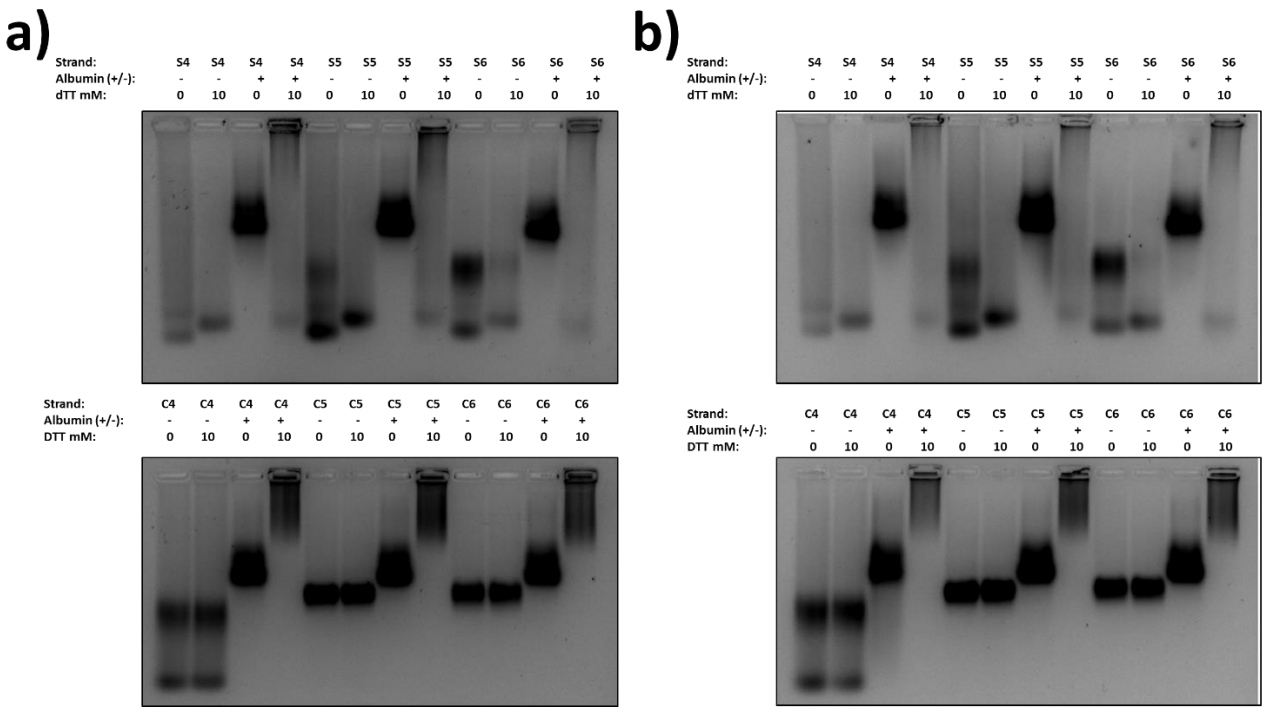

Figure 3. 24. Native AGE of SNA's incubated with albumin and reduced with 10mM DTT. Over a) 24hr and b) 48hr.

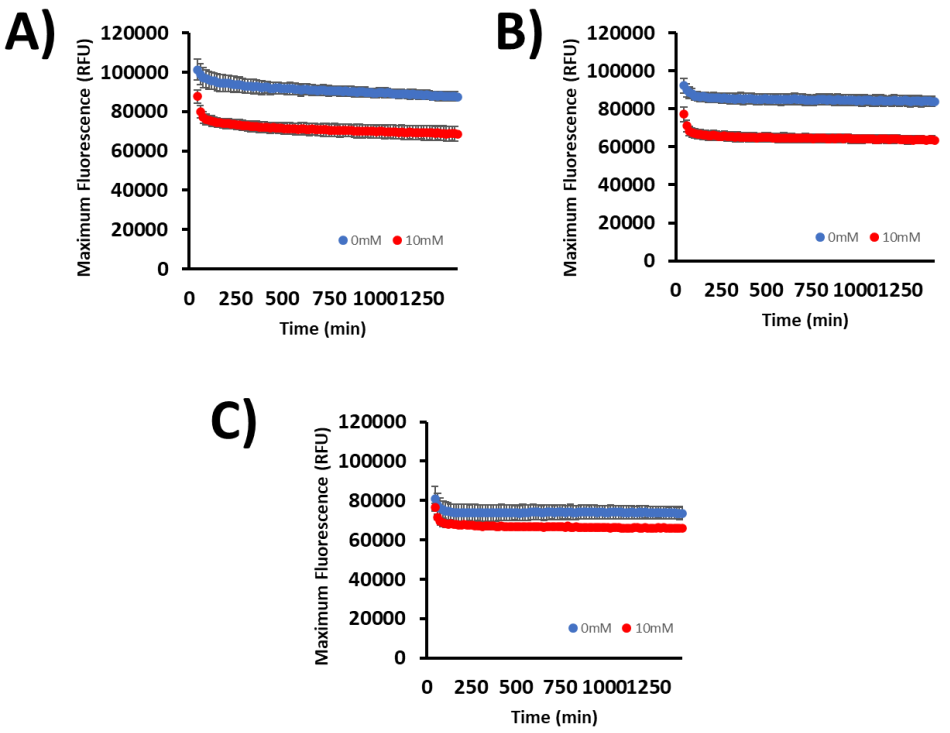

Figure 3. 25. Maximum fluorescence of SNA's incubated with albumin with and without DTT over 24hr at 37°C. a) S4, b) S5 and 6) S6

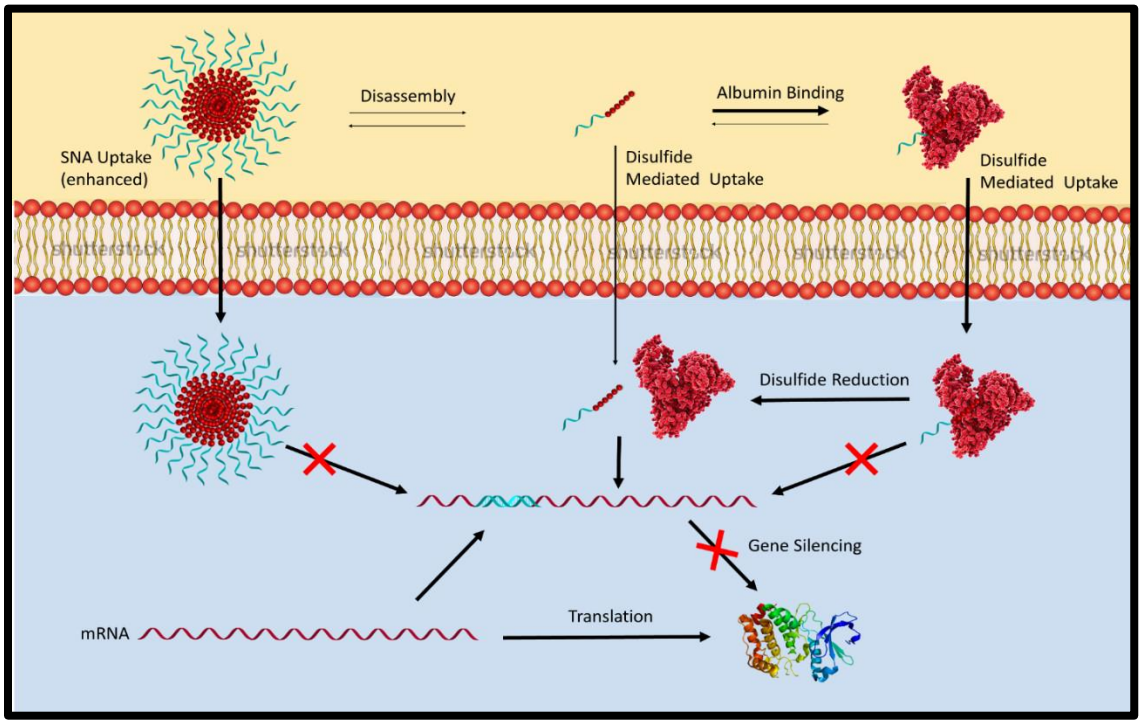

Figure 3. 26 Proposed scheme of uptake and silencing of the SNA and albumin-bound strands.

3.5.18 Critical Micelle Concentration:

To determine the CMC of S4, S5, S6, C4, C5 and C6, fluorescence spectra of 100 µM Nile Red in PBS (1 x PBS) buffer were measured in the presence of increasing concentrations of each strand. A stock solution of Nile Red 1 mM in acetone was used for all experiments. 1 µL of Nile Red stock in acetone was added and briefly incubated at room temperature to allow solvent evaporation. Series dilutions of each strand in 1xPBS (in the range of 50 nM to 10 µM) were made up to a final volume of 100 µL. The mixture was subjected to a heat-cool cycle (95° C - 4° C, over 4 hours). The samples were then transferred to a 96-well top-read microplate, and the plate was read using a Bioteck Synergy wellplate fluorimeter. Excitation was at 535 nm with a slit-width of 9 nm and emission was monitored between 560 nm and 750 nm. The CMC of each strand was investigated using fluorescence emission of a hydrophobic dye, Nile Red. This molecule is almost non-emissive in aqueous media, but when placed in a nonpolar microenvironment like the core of SNAs results in an increased fluorescence signal.

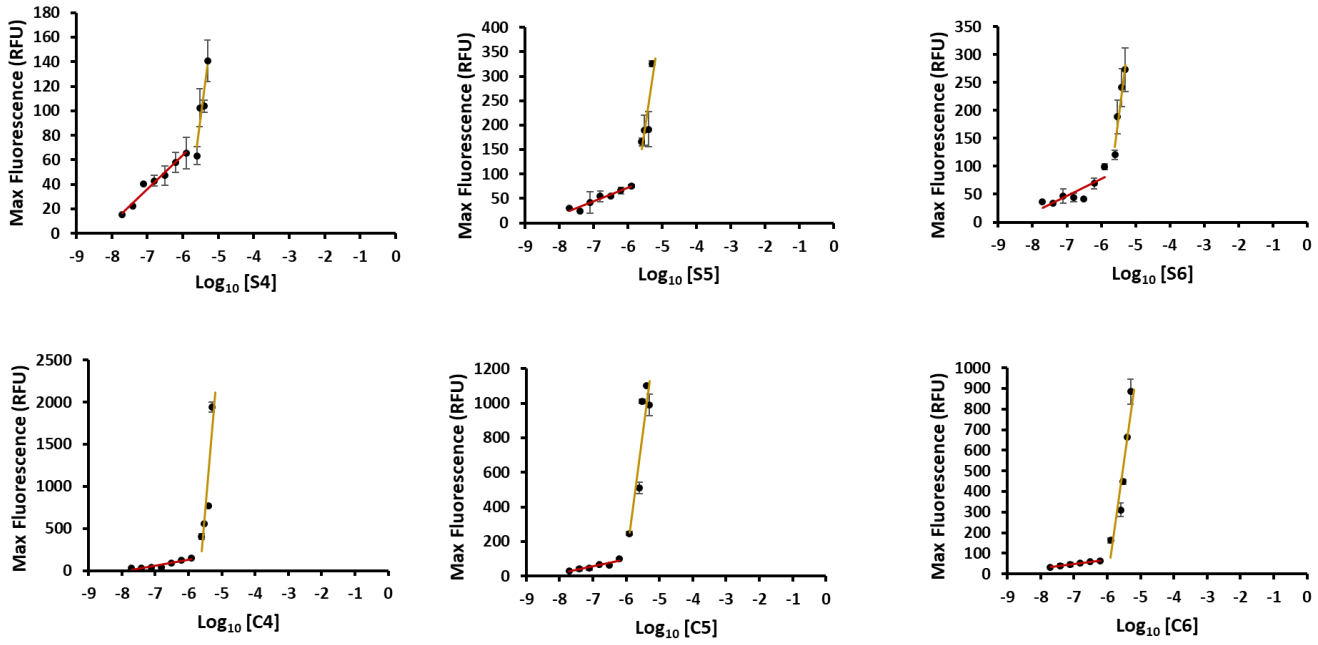

Figure 3. 27. Plot of $\log_{10}$ [SNA] against maximal fluorescence intensity for each SNA in the presence of 100 µM Nile Red.

The CMC was calculated from the intersection of the two linear fits shown on the graph. The measurements were performed in triplicates.

Table 3. 4 Calculated CMCs for each strand in 1xPBS pH 7.2

Strand	CMC (uM)	Stddev (uM)
S4	2.63	0.12
S5	1.74	0.20
S6	1.99	0.23
C4	2.40	0.26
C5	0.98	0.12
C6	1.23	0.11

3.5.19 Non-transfected Silencing Characterization of SO

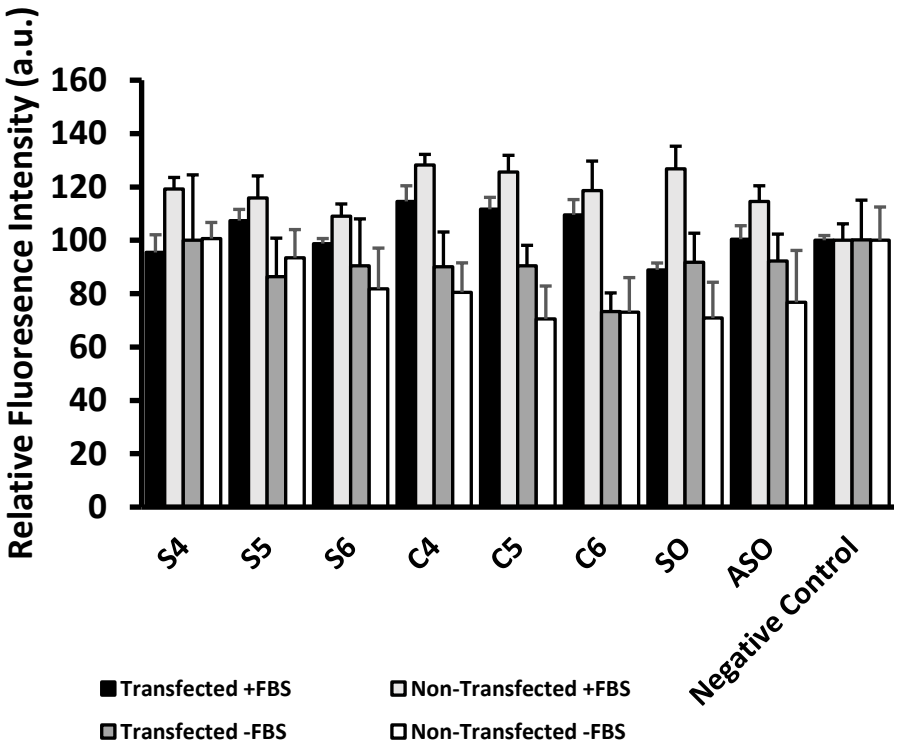

Figure 3. 28 MTT of the non-transfecting silencing experiments in Figure 3 .4b.

3.5.20 Crosslinking:

3.5.20.1 Native AGE & Denaturing PAGE

To crosslink the SNA's, unlabeled strand was made to be 76.5uM and Cy3 labelled strand 13.5uM in 24uL 1x TAMg pH 8. Strands were then thermocycled from 95°C to 4°C over 12hr. BME was prepared as a 1.2M solutions in 1x TAMg pH 8. Iodoacetamide was prepared as 1M solution in 1xPBS pH 7.2. BME was diluted to 600mM, 300mM, 150mM, 75mM, 37.5mM, 18.8mM, 9.4mM and 4.9mM solutions in 1x TAMg pH 8. For the titrations; to 2uL of each SNA was added 1uL of each BME solution. These solutions were then left for 48hr at room temperature. To 1.25uL of each solution was then added 1.25uL of Iodoacetamide and these solutions were left in the dark at room temperature for 1hr. Following this, each sample was further diluted to 25uL with 1xPBS pH 7.2 and ran by native AGE and denaturing PAGE. For samples incubated with albumin, samples were diluted to 22.5uL with 1xPBS pH 7.2 and 2.5uL of a 10mg/ml solution of albumin in 1xPBS pH 7.2 was added and samples incubated for 2hr at 37°C.

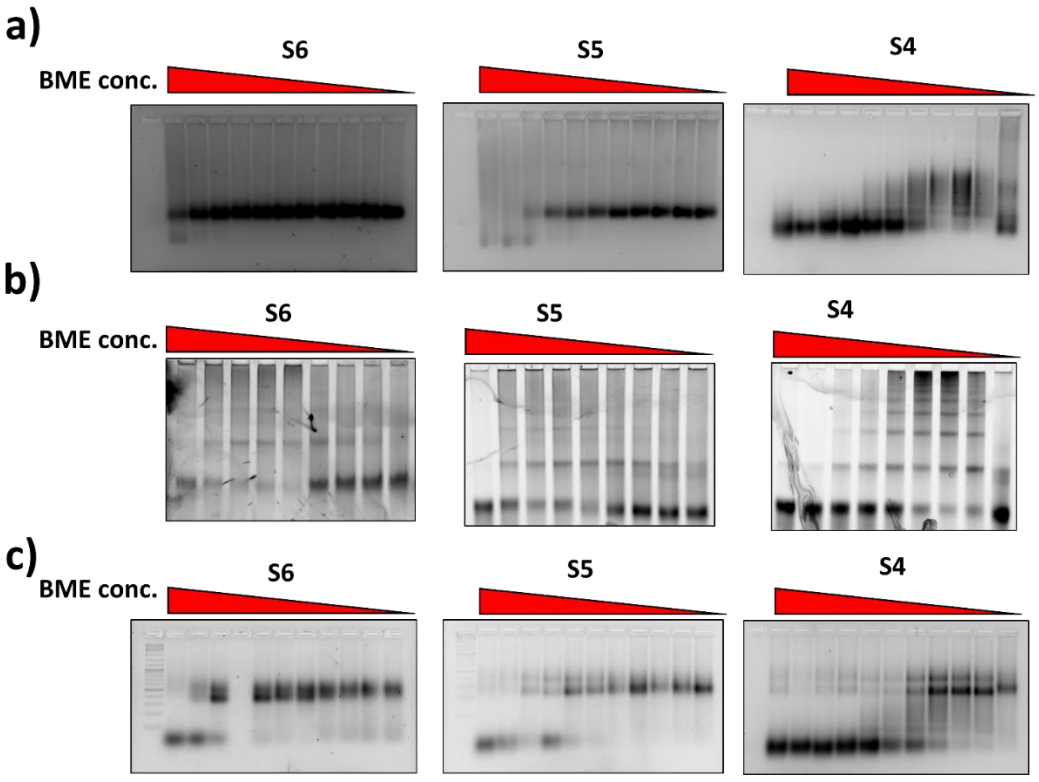

Figure 3. 29 Titration of SNA's crosslinked with varying amounts BME by a) native AGE, b) denaturing PAGE c) native AGE with 1mg/mL albumin added.

3.5.20.2 Crosslinking Albumin Titration:

3.75uM, 1.88uM, 0.94uM, 0.47uM, and 0.23uM solutions of albumin where prepared in 1xPBS pH 7.2. Albumin was added to the crosslinked solutions following 4.x.x. in place of the 10mg/mL solution.

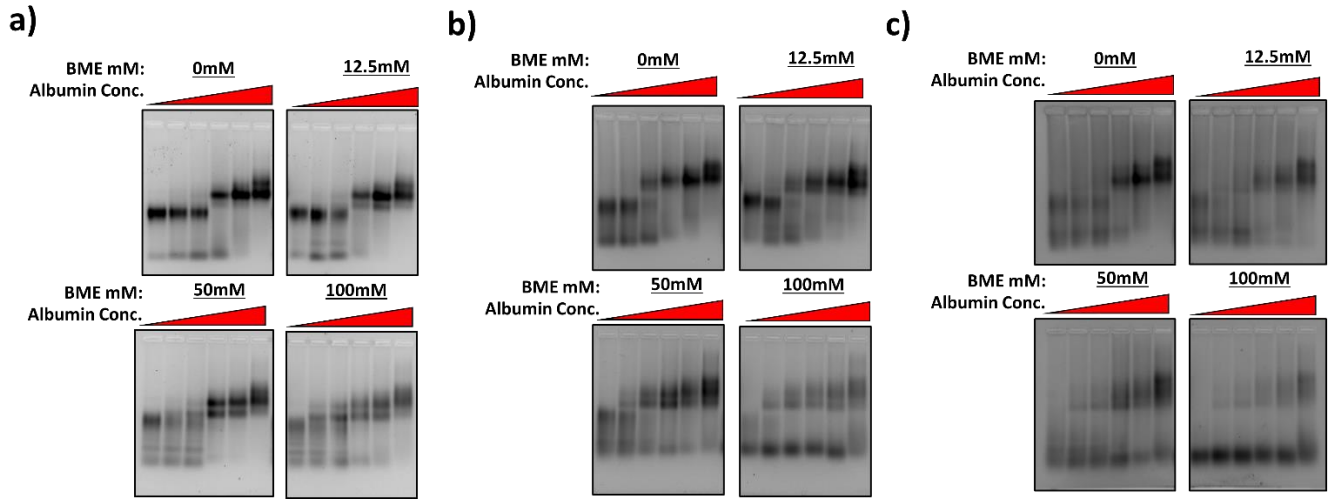

Figure 3. 30. Titration of albumin at different degrees of crosslinking using different BME concentrations by Native AGE. a) S6, b) S5, and c) S4.

3.5.20.3 Size Exclusion

To crosslink the SNA's, unlabeled strand was made to be 90uM and in 24uL 1x TAMg pH 8. Strands were then thermocycled from 95°C to 4°C over 12hr. BME was prepared as a 37.5mM (S4), 75mM (S5), and 150mM (S6) solutions in 1x TAMg pH 8. Iodoacetamide was prepared as 1M solution in 1xPBS pH 7.2. To 24uL of each SNA was added 12uL of each corresponding BME solution. These solutions were then left for 48hr at room temperature. To 10uL of each solution was then added 10uL of Iodoacetamide and these solutions were left in the dark at room temperature for 1hr. Following this, each sample was further diluted to 100uL with 1xPBS pH 7.2 and injected for size exclusion. For samples incubated with albumin, samples were diluted to 90uL with 1xPBS pH 7.2 and 10uL of a 10mg/ml solution of albumin in 1xPBS pH 7.2 was added and samples incubated for 2hr at 37°C, before injecting.

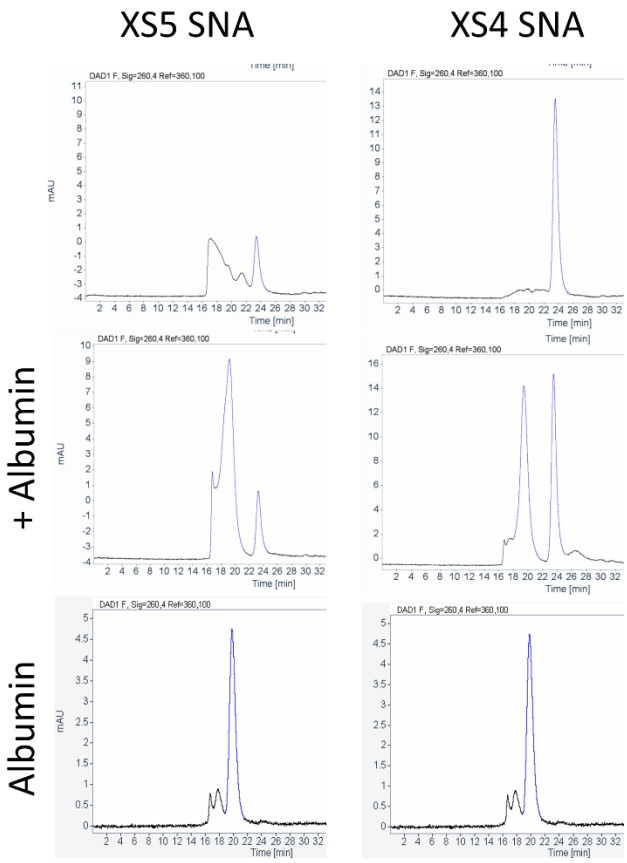

Figure 3. 31. Size exclusion traces of crosslinked S4, and S5 SNA's with and without incubation with albumin.

3.5.20.4 Binding Curves

To crosslink the SNA's, Cy3 labeled strand was made to be 90uM and in 24uL 1x TAMg pH 8. Strands were then thermocycled from 95°C to 4°C over 12hr. BME was prepared as a 37.5mM (S4), 75mM (S5), and 150mM (S6) solutions in 1x TAMg pH 8. Iodoacetamide was prepared as 1M solution in 1xPBS pH 7.2. To 24uL of each SNA was added 12uL of each corresponding BME solution. These solutions were then left for 48hr at room temperature. To 12uL of each solution was then added 12uL of Iodoacetamide and these solutions were left in the dark at room temperature for 1hr. Following this, 12 x 1.66uL of each sample was further diluted to 45uL with 1xPBS pH 7.2 Albumin, samples were prepared as 50uM, 25uM, 12.5uM, 10uM, 7.5uM, 5uM, 4uM, 3uM, 2uM, 1uM, 0.75nM, and 0.50nM solutions in 1xPBS pH 7.2. To each of these samples, 5uL of each albumin solution was added, and the samples were incubated at 37°C for 2hr. (see section 4.5.14 for fluorescencse and analysis protocol).

3.5.20.5 Luciferase Assay & Flow Cytometry

To crosslink the SNA's, unlabeled strand was made to be 90uM and in 24uL 1x TAMg pH 8. Strands were then thermocycled from 95°C to 4°C over 12hr. BME was prepared as a 37.5mM (S4), 75mM (S5), and 150mM (S6) solutions in 1x TAMg pH 8. To 24uL of each SNA was added 12uL of the corresponding BME solution. These solutions were then left for 48hr at room temperature. Following this, the solutions were diluted to 100uL with 1xTAMg pH 8 and dialyzed in 1xTAMG pH 8 using slide-a-lyzer™ mini dialysis devices 3.5K MWCO 0.1mL (cat # 69550 Thermo Fisher) for 8hr, replacing the dialysate every 2hr. Samples were then adjusted to 10uM in 1xTAMg pH 8 for luciferase and flow cytometry experiments.

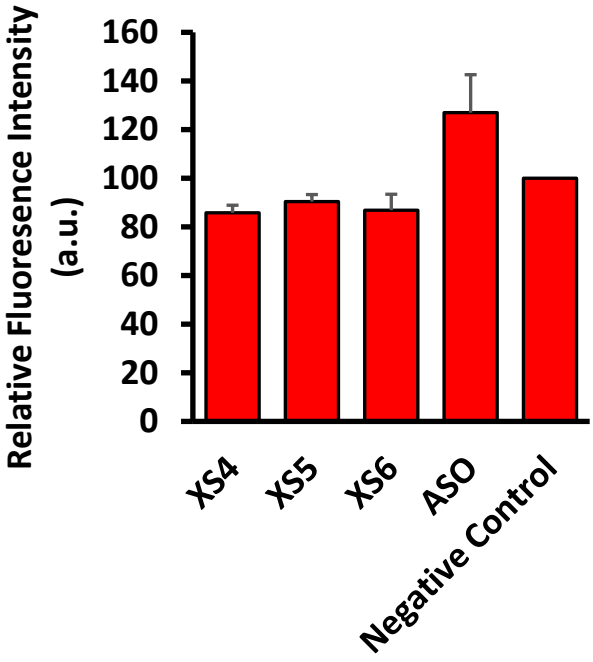

Figure 3. 32. MTT for the crosslinking silencing experiments in Figure 3 .5c.

3.5.21 Extended Silencing

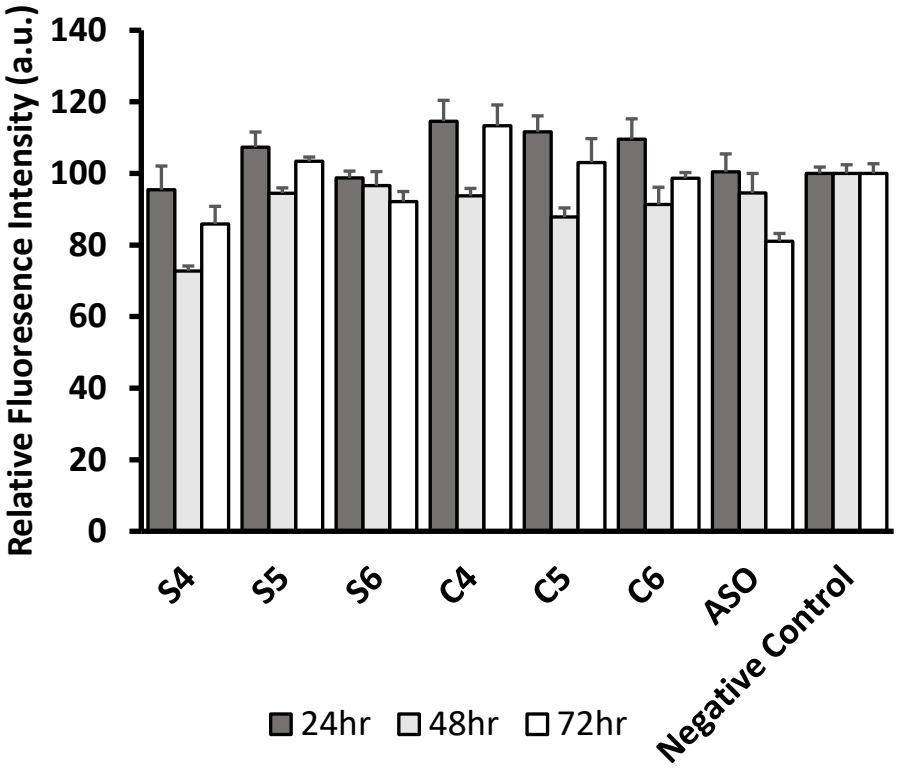

Figure 3. 33. MTT of extended silencing experiments over 72hr in Figure 3 .6.

3.6 References

1. Opalinska, J. B.; Gewirtz, A. M., Nucleic-acid therapeutics: basic principles and recent applications. *Nature Reviews Drug Discovery* **2002,** *1* (7), 503-514.
2. Damha, M. J., Exciting Times in the Field of Nucleic Acid Therapeutics. *Trends in Molecular Medicine* **2019,** *25* (12), 1051-1052.
3. Watts, J. K.; Corey, D. R., Silencing disease genes in the laboratory and the clinic. *J Pathol* **2012,** *226* (2), 365-379.
4. Wang, J.; Lu, Z.; Wientjes, M. G.; Au, J. L. S., Delivery of siRNA therapeutics: barriers and carriers. *AAPS J* **2010,** *12* (4), 492-503.
5. Johannes, L.; Lucchino, M., Current Challenges in Delivery and Cytosolic Translocation of Therapeutic RNAs. *Nucleic acid therapeutics* **2018,** *28* (3), 178-193.
6. Cutler, J. I.; Auyeung, E.; Mirkin, C. A., Spherical Nucleic Acids. *Journal of the American Chemical Society* **2012,** *134* (3), 1376-1391.
7. Seferos, D. S.; Prigodich, A. E.; Giljohann, D. A.; Patel, P. C.; Mirkin, C. A., Polyvalent DNA Nanoparticle Conjugates Stabilize Nucleic Acids. *Nano Letters* **2009,** *9* (1), 308-311.
8. Li, H.; Zhang, B.; Lu, X.; Tan, X.; Jia, F.; Xiao, Y.; Cheng, Z.; Li, Y.; Silva, D. O.; Schrekker, H. S.; Zhang, K.; Mirkin, C. A., Molecular spherical nucleic acids. **2018,** *115* (17), 4340-4344.
9. Patel, P. C.; Giljohann, D. A.; Daniel, W. L.; Zheng, D.; Prigodich, A. E.; Mirkin, C. A., Scavenger Receptors Mediate Cellular Uptake of Polyvalent Oligonucleotide-Functionalized Gold Nanoparticles. *Bioconjugate Chemistry* **2010,** *21* (12), 2250-2256.
10. Choi, C. H. J.; Hao, L.; Narayan, S. P.; Auyeung, E.; Mirkin, C. A., Mechanism for the endocytosis of spherical nucleic acid nanoparticle conjugates. **2013,** *110* (19), 7625-7630.
11. Bousmail, D.; Amrein, L.; Fakhoury, J. J.; Fakih, H. H.; Hsu, J. C. C.; Panasci, L.; Sleiman, H. F., Precision spherical nucleic acids for delivery of anticancer drugs. *Chemical science* **2017,** *8* (9), 6218-6229.
12. Ferrer, J. R.; Sinegra, A. J.; Ivancic, D.; Yeap, X. Y.; Qiu, L.; Wang, J.-J.; Zhang, Z. J.; Wertheim, J. A.; Mirkin, C. A., Structure-Dependent Biodistribution of Liposomal Spherical Nucleic Acids. *ACS nano* **2020,** *14* (2), 1682-1693.
13. Edwardson, T. G. W.; Carneiro, K. M. M.; Serpell, C. J.; Sleiman, H. F., An Efficient and Modular Route to Sequence-Defined Polymers Appended to DNA. *Angewandte Chemie International Edition* **2014,** *53* (18), 4567-4571.
14. Fakih, H. H.; Katolik, A.; Malek-Adamian, E.; Fakhoury, J. J.; Kaviani, S.; Damha, M. J.; Sleiman, H. F., Design and enhanced gene silencing activity of spherical 2'-fluoroarabinose nucleic acids (FANA-SNAs). *Chemical Science* **2021,** *12* (8), 2993-3003.
15. Fakhoury, J. J.; Edwardson, T. G.; Conway, J. W.; Trinh, T.; Khan, F.; Barłóg, M.; Bazzi, H. S.; Sleiman, H. F., Antisense precision polymer micelles require less poly(ethylenimine) for efficient gene knockdown. *Nanoscale* **2015,** *7* (48), 20625-20634.
16. Dore, M. D.; Fakhoury, J. J.; Lacroix, A.; Sleiman, H. F., Templated synthesis of spherical RNA nanoparticles with gene silencing activity. *Chemical Communications* **2018,** *54* (80), 11296-11299.
17. Bujold, K. E.; Hsu, J. C. C.; Sleiman, H. F., Optimized DNA "Nanosuitcases" for Encapsulation and Conditional Release of siRNA. *Journal of the American Chemical Society* **2016,** *138* (42), 14030-14038.
18. Ye, J.; Liu, E.; Gong, J.; Wang, J.; Huang, Y.; He, H.; Yang, V. C., High-Yield Synthesis of Monomeric LMWP(CPP)-siRNA Covalent Conjugate for Effective Cytosolic Delivery of siRNA. *Theranostics* **2017,** *7* (9), 2495-2508.
19. Yang, J.; Chen, C.; Tang, X., Cholesterol-Modified Caged siRNAs for Photoregulating Exogenous and Endogenous Gene Expression. *Bioconjug Chem* **2018,** *29* (4), 1010-1015.

20. Zhang, C.; Hao, L.; Calabrese, C. M.; Zhou, Y.; Choi, C. H. J.; Xing, H.; Mirkin, C. A., Biodegradable DNA-Brush Block Copolymer Spherical Nucleic Acids Enable Transfection Agent-Free Intracellular Gene Regulation. **2015,** *11* (40), 5360-5368.
21. Li, R.; Peng, F.; Cai, J.; Yang, D.; Zhang, P., Redox dual-stimuli responsive drug delivery systems for improving tumor-targeting ability and reducing adverse side effects. *Asian Journal of Pharmaceutical Sciences* **2020,** *15* (3), 311-325.
22. Monteiro, P. F.; Travanut, A.; Conte, C.; Alexander, C., Reduction-responsive polymers for drug delivery in cancer therapy—Is there anything new to discover? **2021,** *13* (2), e1678.
23. Quinn, J. F.; Whittaker, M. R.; Davis, T. P., Glutathione responsive polymers and their application in drug delivery systems. *Polymer Chemistry* **2017,** *8* (1), 97-126.
24. Tan, X.; Lu, X.; Jia, F.; Liu, X.; Sun, Y.; Logan, J. K.; Zhang, K., Blurring the Role of Oligonucleotides: Spherical Nucleic Acids as a Drug Delivery Vehicle. *Journal of the American Chemical Society* **2016,** *138* (34), 10834-10837.
25. Fang, Y.; Lu, X.; Wang, D.; Cai, J.; Wang, Y.; Chen, P.; Ren, M.; Lu, H.; Union, J.; Zhang, L.; Sun, Y.; Jia, F.; Kang, X.; Tan, X.; Zhang, K., Spherical Nucleic Acids for Topical Treatment of Hyperpigmentation. *Journal of the American Chemical Society* **2021,** *143* (3), 1296-1300.
26. De Stefano, M.; Vesterager Gothelf, K., Dynamic Chemistry of Disulfide Terminated Oligonucleotides in Duplexes and Double-Crossover Tiles. *ChemBioChem* **2016,** *17* (12), 1122-1126.
27. Glick, G. D.; Osborne, S. E.; Knitt, D. S.; Marino, J. P., Trapping and isolation of an alternate DNA conformation. *Journal of the American Chemical Society* **1992,** *114* (13), 5447-5448.
28. Wang, L.; Lee, S.-J.; Verdine, G. L., Structural Basis for Avoidance of Promutagenic DNA Repair by MutY Adenine DNA Glycosylase *. *Journal of Biological Chemistry* **2015,** *290* (28), 17096-17105.
29. Sarett, S. M.; Werfel, T. A.; Lee, L.; Jackson, M. A.; Kilchrist, K. V.; Brantley-Sieders, D.; Duvall, C. L., Lipophilic siRNA targets albumin in situ and promotes bioavailability, tumor penetration, and carrier-free gene silencing. **2017,** *114* (32), E6490-E6497.
30. Lau, S.; Graham, B.; Cao, N.; Boyd, B. J.; Pouton, C. W.; White, P. J., Enhanced Extravasation, Stability and in Vivo Cardiac Gene Silencing via in Situ siRNA–Albumin Conjugation. *Molecular Pharmaceutics* **2012,** *9* (1), 71-80.
31. Liu, H.; Moynihan, K. D.; Zheng, Y.; Szeto, G. L.; Li, A. V.; Huang, B.; Van Egeren, D. S.; Park, C.; Irvine, D. J., Structure-based programming of lymph-node targeting in molecular vaccines. *Nature* **2014,** *507* (7493), 519-522.
32. Lacroix, A.; Fakih, H. H.; Sleiman, H. F., Detailed cellular assessment of albumin-bound oligonucleotides: Increased stability and lower non-specific cell uptake. *Journal of Controlled Release* **2020,** *324*, 34-46.
33. Felber, A. E.; Bayó-Puxan, N.; Deleavey, G. F.; Castagner, B.; Damha, M. J.; Leroux, J.-C., The interactions of amphiphilic antisense oligonucleotides with serum proteins and their effects on in vitro silencing activity. *Biomaterials* **2012,** *33* (25), 5955-5965.
34. Gasparini, G.; Bang, E.-K.; Molinard, G.; Tulumello, D. V.; Ward, S.; Kelley, S. O.; Roux, A.; Sakai, N.; Matile, S., Cellular Uptake of Substrate-Initiated Cell-Penetrating Poly(disulfide)s. *Journal of the American Chemical Society* **2014,** *136* (16), 6069-6074.
35. López-Andarias, J.; Saarbach, J.; Moreau, D.; Cheng, Y.; Derivery, E.; Laurent, Q.; González-Gaitán, M.; Winssinger, N.; Sakai, N.; Matile, S., Cell-Penetrating Streptavidin: A General Tool for Bifunctional Delivery with Spatiotemporal Control, Mediated by Transport Systems Such as Adaptive Benzopolysulfane Networks. *Journal of the American Chemical Society* **2020,** *142* (10), 4784-4792.
36. Qian, L.; Fu, J.; Yuan, P.; Du, S.; Huang, W.; Li, L.; Yao, S. Q., Intracellular Delivery of Native Proteins Facilitated by Cell-Penetrating Poly(disulfide)s. **2018,** *57* (6), 1532-1536.

37. Shu, Z.; Tanaka, I.; Ota, A.; Fushihara, D.; Abe, N.; Kawaguchi, S.; Nakamoto, K.; Tomoike, F.; Tada, S.; Ito, Y.; Kimura, Y.; Abe, H., Disulfide-Unit Conjugation Enables Ultrafast Cytosolic Internalization of Antisense DNA and siRNA. **2019,** *58* (20), 6611-6615.
38. Shu, Z.; Ota, A.; Takayama, Y.; Katsurada, Y.; Kusamori, K.; Abe, N.; Nakamoto, K.; Tomoike, F.; Tada, S.; Ito, Y.; Nishikawa, M.; Kimura, Y.; Abe, H., Intracellular Delivery of Antisense DNA and siRNA with Amino Groups Masked with Disulfide Units. *Chemical and Pharmaceutical Bulletin* **2020,** *68* (2), 129-132.
39. Prinzen, A. L.; Saliba, D.; Hennecker, C.; Trinh, T.; Mittermaier, A.; Sleiman, H. F., Amplified Self-Immolative Release of Small Molecules by Spatial Isolation of Reactive Groups on DNA-Minimal Architectures. **2020,** *59* (31), 12900-12908.
40. Lacroix, A.; Vengut-Climent, E.; de Rochambeau, D.; Sleiman, H. F., Uptake and Fate of Fluorescently Labeled DNA Nanostructures in Cellular Environments: A Cautionary Tale. *ACS Central Science* **2019,** *5* (5), 882-891.
41. Zhang, W.; Meckes, B.; Mirkin, C. A., Spherical Nucleic Acids with Tailored and Active Protein Coronae. *ACS Central Science* **2019,** *5* (12), 1983-1990.
42. Crooke, S. T.; Vickers, T. A.; Liang, X.-H., Phosphorothioate modified oligonucleotide-protein interactions. *Nucleic acids research* **2020,** *48* (10), 5235-5253.
43. Lacroix, A.; Edwardson, T. G. W.; Hancock, M. A.; Dore, M. D.; Sleiman, H. F., Development of DNA Nanostructures for High-Affinity Binding to Human Serum Albumin. *Journal of the American Chemical Society* **2017,** *139* (21), 7355-7362.
44. Laurent, Q.; Martinent, R.; Moreau, D.; Winssinger, N.; Sakai, N.; Matile, S., Oligonucleotide Phosphorothioates Enter Cells by Thiol-Mediated Uptake. *n/a* (n/a).
45. Lipid Conjugates Enhance Endosomal Release of Antisense Oligonucleotides Into Cells. **2019,** *29* (5), 245-255.
46. Poulin, P.; Burczynski, F. J.; Haddad, S., The Role of Extracellular Binding Proteins in the Cellular Uptake of Drugs: Impact on Quantitative In Vitro-to-In Vivo Extrapolations of Toxicity and Efficacy in Physiologically Based Pharmacokinetic-Pharmacodynamic Research. *Journal of pharmaceutical sciences* **2016,** *105* (2), 497-508.
47. Fuoco, T.; Pappalardo, D.; Finne-Wistrand, A., Redox-Responsive Disulfide Cross-Linked PLA–PEG Nanoparticles. *Macromolecules* **2017,** *50* (18), 7052-7061.
48. Shao, Y.; Huang, W.; Shi, C.; Atkinson, S. T.; Luo, J., Reversibly crosslinked nanocarriers for on-demand drug delivery in cancer treatment. *Ther Deliv* **2012,** *3* (12), 1409-1427.
49. Banga, R. J.; Meckes, B.; Narayan, S. P.; Sprangers, A. J.; Nguyen, S. T.; Mirkin, C. A., Cross-Linked Micellar Spherical Nucleic Acids from Thermoresponsive Templates. *Journal of the American Chemical Society* **2017,** *139* (12), 4278-4281.
50. Alterman, J. F.; Godinho, B. M. D. C.; Hassler, M. R.; Ferguson, C. M.; Echeverria, D.; Sapp, E.; Haraszti, R. A.; Coles, A. H.; Conroy, F.; Miller, R.; Roux, L.; Yan, P.; Knox, E. G.; Turanov, A. A.; King, R. M.; Gernoux, G.; Mueller, C.; Gray-Edwards, H. L.; Moser, R. P.; Bishop, N. C.; Jaber, S. M.; Gounis, M. J.; Sena-Esteves, M.; Pai, A. A.; DiFiglia, M.; Aronin, N.; Khvorova, A., A divalent siRNA chemical scaffold for potent and sustained modulation of gene expression throughout the central nervous system. *Nature Biotechnology* **2019,** *37* (8), 884-894.
51. Brown, C. R.; Gupta, S.; Qin, J.; Racie, T.; He, G.; Lentini, S.; Malone, R.; Yu, M.; Matsuda, S.; Shulga-Morskaya, S.; Nair, A. V.; Theile, C. S.; Schmidt, K.; Shahraz, A.; Goel, V.; Parmar, R. G.; Zlatev, I.; Schlegel, M. K.; Nair, J. K.; Jayaraman, M.; Manoharan, M.; Brown, D.; Maier, M. A.; Jadhav, V., Investigating the pharmacodynamic durability of GalNAc-siRNA conjugates. *Nucleic acids research* **2020,** *48* (21), 11827-11844.
52. http://supramolecular.org

53. Thordarson, P., Determining association constants from titration experiments in supramolecular chemistry. *Chemical Society Reviews* **2011,** *40* (3), 1305-1323.
54. Brynn Hibbert, D.; Thordarson, P., The death of the Job plot, transparency, open science and online tools, uncertainty estimation methods and other developments in supramolecular chemistry data analysis. *Chemical Communications* **2016,** *52* (87), 12792-12805.

|4|

Development of Stimuli Responsive Oligonucleotide Prodrugs for Enhanced Drug Delivery Applications

This chapter is composed mainly of ongoing work in collaboration with Tyler Brown, Daniel Saliba, Xin Luo and Hanadi F. Sleiman.

Contributions: Alexander Prinzen helped design and develop the projects, primarily contributed to the production of experimental data from small molecule synthesis, DNA synthesis, HPLC purification, mass spectrometry (MS), and gel electrophoresis. **Alexander Prinzen** and **Tyler Brown** performed the SDS PAGE, antibody conjugations and interpretation of results. **Daniel Saliba**, helped design and assemble the templated DNA nanostructures, synthesized some DNA strands, and aided data interpretation. **Xin Luo** performed some AFM imaging and provided the gold nanoparticles. **Hanadi F. Sleiman** designed the project, guided interpretation of data, result discussion, and provided funding for the projects.

4.1. Preface

The oligonucleotide conjugates in chapters 2 and 3 have been used for stimuli responsive release of both small molecule drugs and nucleic acid therapeutics (NATs) using molecular recognition and reducing conditions. However, the ideal stimuli-responsive prodrug is one which only localizes to and is only active in the disease target. Factors such as off-target degradation/activation, delivery to the site of action, rate of metabolism and overall drug specificity, can affect a prodrug's potential to be clinically successful. In this chapter, we describe different strategies to address the above factors and improve our proof-of-concept hybridization chain reaction (HCR) prodrug system from chapter 2. Using different methods, we demonstrate that we can reduce off-target degradation or non-specific activation, generate new conjugates to change the initiation site, as well as modulate HCR rates and increase specificity using new templates. Furthermore, we can increase overall drug specificity by applying the technology to the release of antisense therapeutics. Combining all these methods together within a single DNA nanodevice will help bring to realization the ideal prodrug.

4.2. Introduction

The key challenge for molecules used in chemical biology and medicinal chemistry is specificity. Improving the affinity and specificity of drug binding to reduce off-target effects and increase potency has been at the forefront of drug discovery. However, by virtue of its low surface area and size, a small molecule has few chemical moieties that can engage its target and as such there are limits to how specific they can be.[1] Additionally, this view of drug development

is only concerned with specificity at the molecular level and does not take into consideration targeting beyond the drug/receptor binding interaction.

To address this problem, many prodrugs, polymer-drug conjugates and nanoparticles[2] have been developed.[3] Notably, prodrugs have been traditionally used to improve pharmacokinetic and pharmacodynamic properties of a drug molecule by masking its activity[4]. Early days of prodrug development primarily focused on overcoming physicochemical (e.g., solubility, chemical instability) or biopharmaceutical problems (e.g., bioavailability, toxicity), and as such prodrug activation and distribution were often non-specific. Modern day prodrugs use *selective* targeting and activation to increase therapeutic levels at the site of action and reduce off-target effects, through the conjugation of drugs to targeting moieties using stimuli responsive linkers.[5] Instead of developing new small molecules, these "targeted prodrugs" allow for the repurposing of old drugs by decreasing their toxicity, and this approach has gained a great deal of attention recently, as finding new small molecule drugs becomes more difficult[6].

An ideal prodrug is one which is only directed to and activated at the location of interest. There are many stimuli available to activate prodrugs such as: biological stimuli (i.e., enzyme metabolism), physical stimuli (i.e., light, magnetism, etc.) and chemical stimuli (i.e., pH, redox, etc.). Moreover, both active (using targeting ligand) and passive (using size to avoid clearance) targeting can help to direct prodrugs to desired locations. In terms of specificity; active targeting and biological stimuli, are very attractive as they use molecular recognition of the cells own highly specific proteins.[7] This contrasts with chemical stimuli like pH, and reduction gradients, that can be found in a multitude of different cellular substructures, and physical stimuli, which need an exogenous input to be active.

To this point, the use of DNA nanotechnology to aid in the development of next generation prodrugs and nanoparticles has found distinct advantages.[8-9] The molecular recognition properties of DNA have been used to generate stimuli-responsive devices/prodrugs which operate/metabolize upon molecular recognition of specific biomarkers.[10-12] This type of responsive behaviour is unparalleled by any other type of prodrug or nanoparticle material. However, using the recognition of specific *genetic* markers to generate stimuli-responsive

behaviour poses the challenge of internalizing the DNA device in the first place to recognize such a marker.[13-14] Instead, some devices have opted to use specific extracellular biomarkers to release their cargo or initiate their effect using aptamers and aptamer switches[15-17]. The attachment of aptamers or antibodies to highly potent small molecule drug, in the form of antibody drug conjugates (ADC's) is also used to directly target extracellular biomarkers and has been shown to improve biodistribution and reduce off-target effects[18].

The use of extracellular biomarkers for either direct targeting or inducing stimuli-responsive behaviour does have some limitations, such as 1) the need to target high abundance markers, 2) poor biomarker distribution across the tissue, and 3) non-internalizing biomarkers. To overcome some of these limitations some groups have devised methods such as "click to release" which uses ADCs coupled with a bio-orthogonal reaction[19-20]. In this method, the drug is conjugated to the ADC with the use of a tetrazine responsive linker that can react in a bio-orthogonal tetrazine cyclization reaction to release its payload. In a first step, the ADC is targeted to a high abundance, non-internalizing receptor, and in the second step, the bio-orthogonal tetrazine trigger is introduced, releasing the payload only at the intended site, which can then diffuse into the cell[20]. While methods like "click to release" can address the issues of targeting non-internalizing biomarkers, and poor biomarker distribution, the need to target high abundance markers remains.

Amplifying signals from lower abundant extracellular biomarkers may be a viable way to overcome all three challenges. Indeed, antibodies conjugated with enzymes have been used for antibody-directed enzyme prodrug therapy (ADEPT), to amplify prodrug metabolism at site-specific locations, and have shown great clinical promise[21]. However, issues with the immunogenicity of the enzyme, and clearance of the antibody-enzyme conjugate before prodrug administration remain challenging[22]. Moreover, the exact valency of antibody conjugates has been shown to play a critical role in the therapeutic window and efficacy of these entities[23]. Within DNA nanotechnology, a DNA nanorobot, was designed to site specifically deliver enzymatic cargo only when activated by molecular recognition with nucleolin biomarkers[16].

Overall, even with amplification mechanisms in place, the amount of prodrug that can be ultimately activated or delivered is dependent on the absolute concentration of the biomarker. The prodrug "signal gain" represents the ratio of activated prodrug to biomarker and is important to ensure that enough of a prodrug can be activated to reach the therapeutic window. For example, to increase the gain in prodrugs which are activated by enzymes, self-immolative splitters have been employed[24]. Using these splitters, every prodrug metabolism event resulted in the release of two or more cytotoxic agents, improving the signal gain from the absolute enzyme concentration[25]. Another factor involved with whether prodrug metabolism will result in a therapeutic effect is the rate at which the prodrug is activated. Depending on the effective concentration (EC_{50}) of a drug, rapid metabolism of a prodrug may be necessary to reach this level and have an effect. On the other hand, slower, sustained metabolism may be desired when the EC_{50} is lower.

Generally, binding of small molecules to their protein targets requires binding to a complex 3D tertiary structure. Oligonucleotide therapeutics on the other hand bind using well defined 2D duplex formation to induce their effect. Using oligonucleotide therapeutics adds another layer of specificity and opens more targets than small molecules, as most small molecule targets need active sites to function. However, challenges remain with cellular uptake and the selectivity of oligonucleotide therapeutics for specific cell/tissue types. The generation of oligonucleotide therapeutic prodrugs, which respond to specific biomarkers has the potential to be a solution to increase specificity and reduce off-target effects[26]. However, these are affected by some of the same challenges as small molecule prodrugs such as: signal gain, poor cellular internalization, and release rate.

In this chapter, we demonstrate different strategies to improving our proof-of-principle prodrug system for drug and ASO delivery applications described in Chapter 2. We begin by replacing the disulfide chemistry in the original system, which can be sensitive to off-target reducing conditions, with a bio-orthogonal tetrazine cyclization reaction (Figure 4 .1.a.). Addressing the signal gain and leakage of HCR is then explored. Ligating the stems of the HCR hairpins together using disulfide modifications decreases the leakage of HCR significantly (Figure

4 .1.b.). Strategies to improve the speed and selectivity of HCR are then explored, using new templates, including fully templated amplifiers and logic gates (Figure 4 .1.c.). We further show, by replacing HCR with catalytic hairpin assembly (CHA), we demonstrate the amplified release of ASO strands from a DNA nanoparticle in response to a biological trigger for the selective release of oligonucleotide therapeutics as opposed to small molecules (Figure 4 .1.d.). Finally, we develop DNA-Ab conjugates with controlled valency, using branched DNA. This provides us the potential for an initiator platform that triggers the extracellular release of drugs (Figure 4 .1.e.). Together, these studies demonstrate different strategies towards optimizing and improving the proof of principle prodrug system for real drug delivery applications. Moreover, this work goes over many of the challenges associated with taking the proof of principle design and adopting it for these

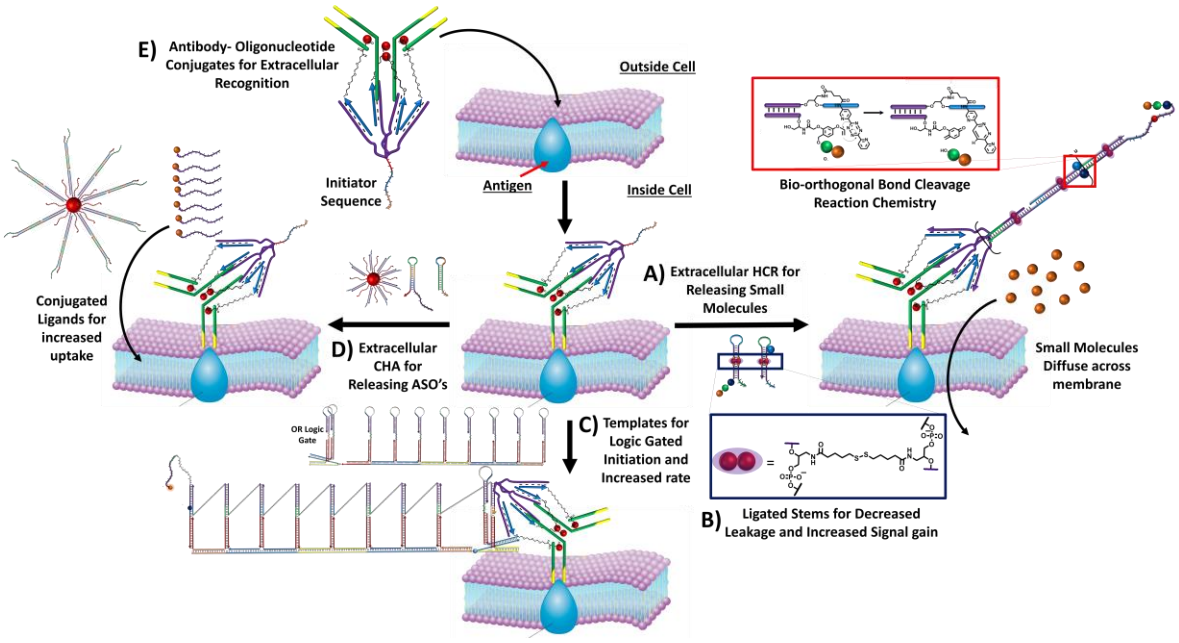

. Figure 4. 1 General scheme displaying the improvements to HCR drug release device from chapter 2

(a) HCR drug release with chemical modifications to release its payload using a bio-orthogonal tetrazine cyclization **(b)** HCR hairpins with ligated stems to improve leakage **(c)** logic gate initiation of HCR templated on a long DNA backbone to improve rate and improve selectivity of HCR. **(d)** extracellular initiation of CHA, for the release of ASO strands which then reveal an uptake enhancing ligand**. (e)** oligonucleotide-antibody conjugates with controlled valency, carrying an initiator sequence can bind to an antigen extracellularly.

applications, as well as the challenges involved with using DNA nanotechnology for biomedical applications in general. The work in this chapter also highlights the tailor ability, that can be achieved when using DNA nanotechnology platforms.

4.3. Results and Discussion

4.3.1. Design and Synthesis of Tetrazine Based Drug Release

To adapt the HCR drug release system for more biologically relevant conditions we decided to use a bio-orthogonal tetrazine cyclization reaction, for bond cleavage. These reactions have been shown to be more stable to biological conditions[27] than other bio-orthogonal reactions *i.e.* Staudinger reductions, and have been performed *in-vivo*[20]. For the tetrazine cyclizations use *in-vivo*, most tetrazine responsive immolative linkers in the literature are based on the strained promoted alkene cyclization[28-29]. These are generally used because they have extremely high-rate constants (2000 $M^{-1} s^{-1}$) and for biological applications a high-rate constant is needed so that species will react at low concentrations. For our purposes however, the reaction is intended to be modulated by the effective concentration on a DNA template. Therefore, a less efficient reaction was needed, so that there would be no unintended reactions off the template. Other DNA templated tetrazine cyclizations have been reported using vinyl groups instead, for the uncaging of fluorophores[30], and seemed to fit our purpose. Additionally, a self-immolative linker which degrades and releases cargo upon a tetrazine cyclization with a vinyl group has been previously reported[31].

Our design places the vinyl capped small molecule on one HCR hairpin and the tetrazine on the other (Figure 4 .2.a.). Once polymerization has occurred, these groups meet and are able to react, resulting in the release of small molecule cargo. For the reaction to generate a release event, (E) was designed so that after the tetrazine cyclization occurred, an immolative 1,6-elimination would happen to release the cargo molecule (M) (Figure 4 .2.b.). To connect (E) to an HCR hairpin the molecular precursor **10** was designed with an NHS ester functionality that would not interfere with the tetrazine cyclization mechanism (Figure 4 .3.).

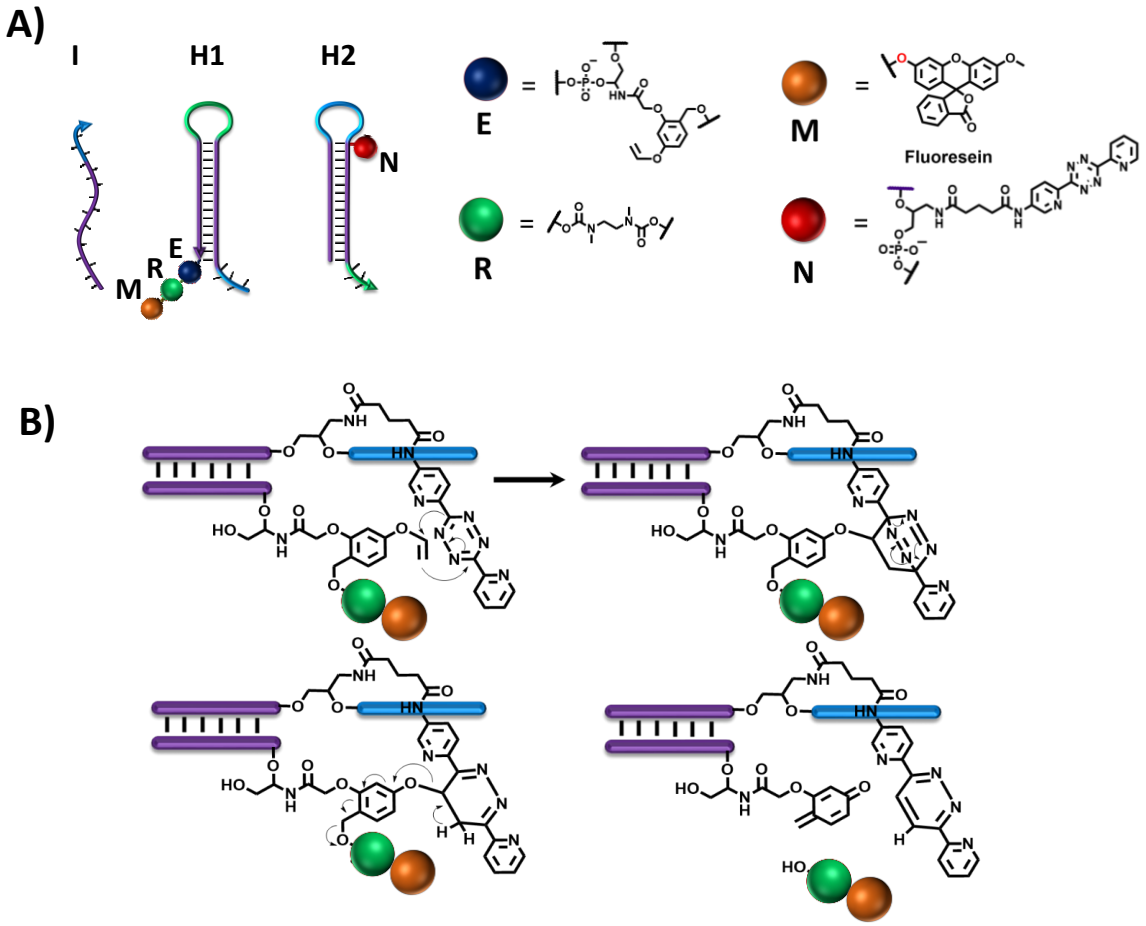

Figure 4. 2Design and mechanism of small molecule release using a DNA templated tetrazine cyclization on HCR hairpins.

(a) HCR hairpin design. (b) tetrazine cyclization reaction resulting in the release of small molecules.

The ongoing synthesis of the (E) precursor **10** was done according to Figure 4 .3. (Section 3.5.5 for detailed procedures). First, 2,4-Dihydoxybenzaldehyde was reacted with 3,4 pyran and p-toluenesulfonic acid, to afford the 4-hydroxyl acetal protected species **1**. **1** was then alkylated with tert-Butyl bromoacetate at the 2-hydroxyl position, affording compound **2**. Using a catalytic amount of p-toluenesulfonic acid, **2** was then deprotected to give the 4-hydroxyl compound **3**. The 4-hydroxyl position of **3** was then alkylated to give the vinyl species **4**. The aldehyde of **4** was then selectively reduced in the presence of the vinyl group using $NaBH_4$ to give compound **5**. A caged fluorophore **8**, was prepared and condensed with **5**, in a sequential 3 step reaction to afford **9**. The preparation of **10** from **9** was met with some difficulty as under the deprotection

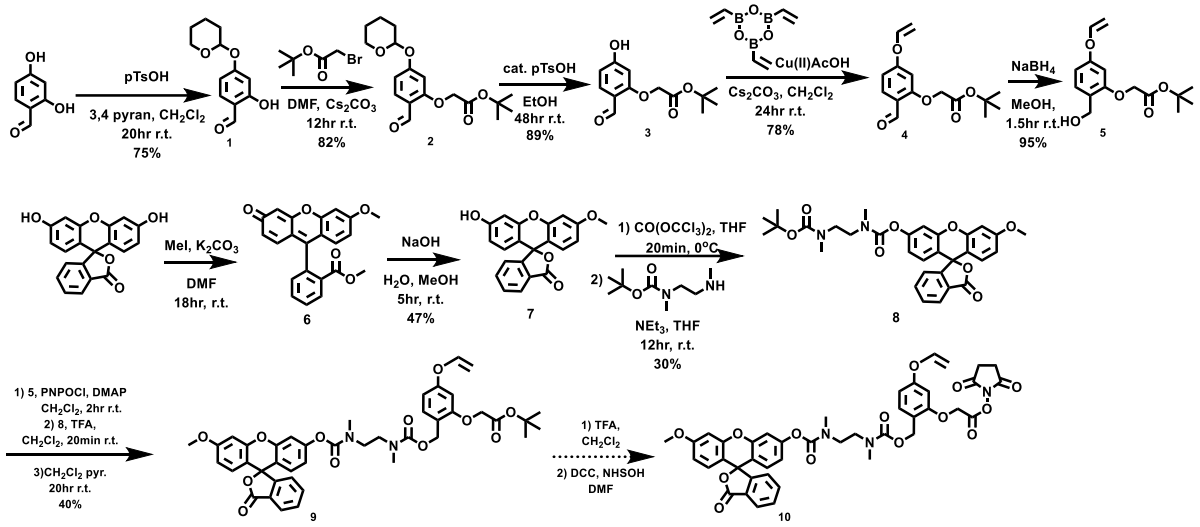

Figure 4. 3 Synthetic scheme for (E)(R)(M) component for bio-orthogonal release.

conditions of the tert-butyl ester, degradation of the vinyl group occurred, prematurely releasing the fluorophore, as apparent by the disappearance of starting material and reformation of compound **7**, with no product isolated. A few different reaction conditions were tested on compound **5** tried to avoid this, however each time degradation occurred (Section 3.5.5 for different reaction conditions). Therefore, moving forward the protecting group chemistry of the side chain would need to be changed.

As a test reaction compound **5** was reacted with tetra-n-butylammonium fluoride (TBAF) and found that degradation did not occur. This indicates that a silyl group may be a promising alternative protecting group. To use a silyl protecting group however, a design change had to be made to **10** installing an alcohol instead of a carboxylic acid (compound **11**). Retro-synthetically, Figure 4 .4. is proposed for this change.

In summary, we have designed a new tetrazine cyclization-based reaction platform for drug release and integration into our HCR system to replace the disulfide reaction chemistry. The synthesis of this version of HCR is ongoing, but we believe that by switching the chemistry to be bio-orthogonal, this will improve the selectivity of the device to only be active when it finds its reaction complement. Future work will focus on completing the synthesis of the HCR hairpins

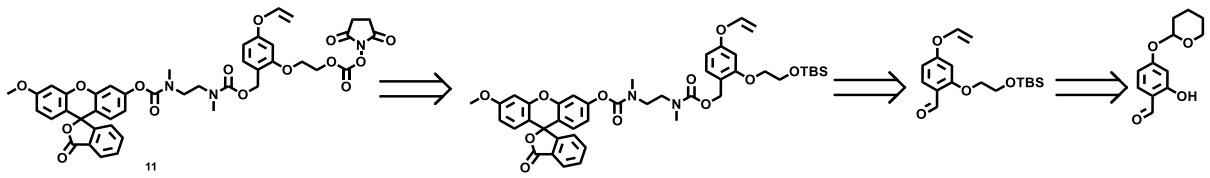

Figure 4. 4. Retrosynthetic scheme of new synthesis for proposed new small molecule component using a silyl protecting group to later install the electrophilic handle for oligonucleotide attachment.

and analyzing prodrug release using this platform. Following some preliminary studies, we plan on testing this device *in-vitro* for releasing anticancer drugs.

4.3.2. Improving Signal Gain and Leakage in HCR

Signal gain in the HCR system is one of the most challenging aspects for its application in drug delivery. The biomarker to release ratio determines whether there is enough signal gain from a biomarker to release enough drug molecule released to elicit a therapeutic response. With traditional sequences of HCR, truncated hairpins are more difficult to be added to the growing polymer and can remain leftover after polymerization, reducing gain (Figure 4 .5.a.). This is because there is only a 6 base toehold region for the strand displacement to occur in the first place and reducing this can significantly slow the strand displacement kinetics. Leakage is also an issue with HCR, where the hairpins in solution together spontaneously polymerize without any initiator present[32]. (Figure 4 .5.b.)

Design parameters surrounding HCR have been well established[33] and improvements to signal gain and leakage have been reported by Pierce *et al*. where they could polymerize all hairpins with 0.01equiv. of initiator strand[34-35]. In these cases, to improve signal gain of HCR, much longer stem and loop regions were used to generate more favorable hybridization kinetics. Moreover, by using longer overhang and loop sequences, truncated hairpins are still able to be integrated into the growing polymer. In these studies, however, post functionalization of the HCR hairpins was not necessary for the application, and therefore the length of the oligonucleotide was less of a concern. For our purposes however, as the length of an oligonucleotide becomes larger, the harder it becomes too post-functionalize it in reasonable yields. Due to this, we took

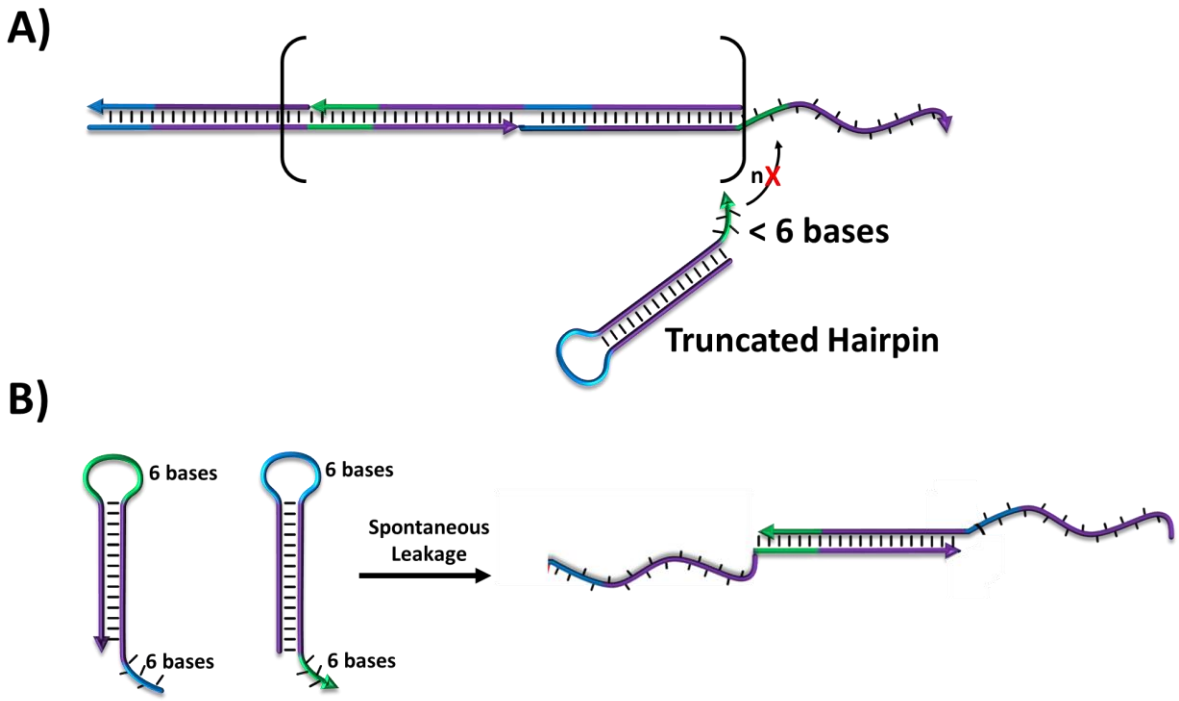

Figure 4. 5. Challenges with the hybridization chain reaction

(a) truncated hairpins reduce signal gain and are not incorporated into the growing polymer **(b)** spontaneous hybridization of the HCR hairpins without initiator results in unintended polymerization

a different approach to improving the signal gain and reducing leakage of shorter HCR hairpins, by introducing in-synthesis chemical modifications to shorter HCR hairpins.

4.5.3.1 Design and Synthesis

We had previously shown in chapter 2 that with the introduction of thiol-disulfide pairs within the HCR hairpins we could ligate the HCR hairpins together. In a reverse manner, our hypothesis was that we could stabilize the hairpin stems of HCR by "pre-ligating" the stems with disulfide bonds that would only break upon recognition of an initiator with active thiol (Figure 4 .6.). The pre-ligated hairpins would inhibit leakage by being unable to spontaneously polymerize. Additionally, we hypothesized that the HCR process could be driven forward by creating an irreversible covalent linkage with each monomer addition, and by using longer overhang and loop sequences mitigate truncated species, thereby improving the signal gain. In designing the hairpins, the placement of the disulfides needs to be carefully selected so that during the

polymerization process, a thiol from one hairpin lines up with the disulfide from another. An example of one of our designs is shown in Figure 4 .6.a. By placing the disulfide in the middle of the stem, thiol-disulfide pairs would line up properly between the two HCR hairpins. The entire process begins with a thiolated initiator (I_M) strand displacing the first part of the stem of the ligated hairpin (H1_M) (Figure 4 .6.b i.). After this, the thiol from (I_M) increases in proximity to

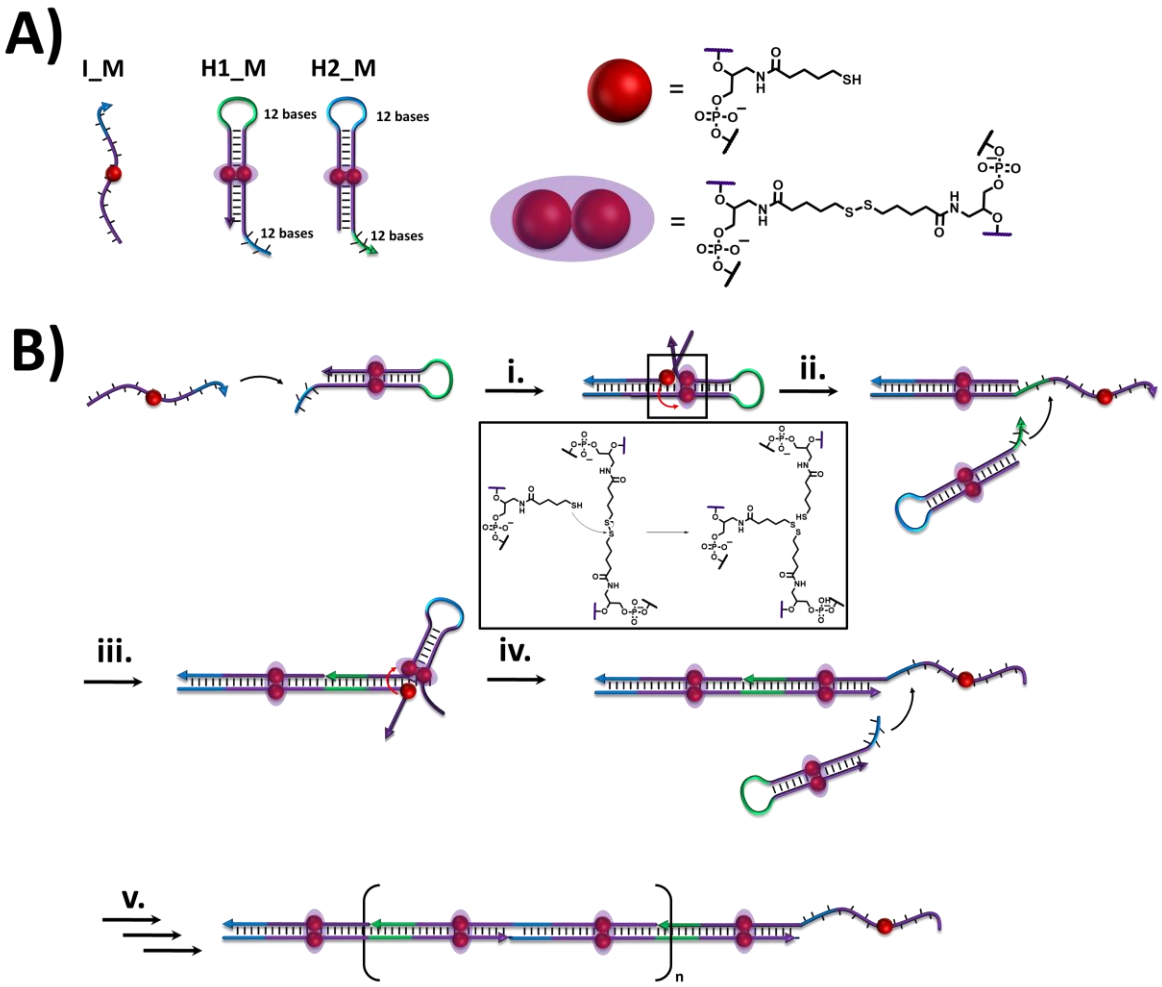

Figure 4. 6. Design example and mechanism of ligated HCR

a) Design of ligated hairpins with the disulfide in the middle of the stem b) mechanism of a ligated HCR polymerization; i. I_M hybridizes to H1_M and displaces the first part of the stem ii. The thiol on I_M increases in local concentration with the disulfide on H1_M and reacts in a disulfide exchange, the finishes displacing the stem of H1_M and generates a ne thiol on H1_M iii. The growing polymer finds an H2_M hairpin and partially displaces the stem iv. The thiol on H1_M reacts with the disulfide on H2_M and finishes displacing the stem of H2_M v. the process repeats growing the polymer.

the disulfide in (H1_M) and can undergo a disulfide exchange (Figure 4 .6.b. ii.). The strand displacement completes, revealing the next sequence for (H2_M) to hybridize to and generates a new thiol on the (H1_M) strand. (H2_M) hybridizes to the initiated polymer (Figure 4 .6.b. iii.) and another templated disulfide exchange occurs between (H1_M) and (H2_M), growing the polymer (Figure 4 .6.b. iv.). This process repeats until all the hairpins are consumed, generating a long fully ligated polymer of (H1_M) and (H2_M) (Figure 4 .6.b. v.).

To synthesize hairpins with multiple disulfides, in defined locations, we used a new disulfide phosphoramidite that we could introduce during the automated solid phase synthesis of DNA (Figure 4 .7.a. & synthesis in chapter 3). The HCR sequences we first chose were based on the improved HCR sequences of Pierce *et al*. with some changes[34]. We chose to use these sequences, as the loops and overhangs of these sequences were 12 base pairs (b.p.) long, giving us a full helical turn for every strand displacement invasion, providing better hybridization kinetics and mitigating truncated species. The disulfide linkages allow us to make hairpins with

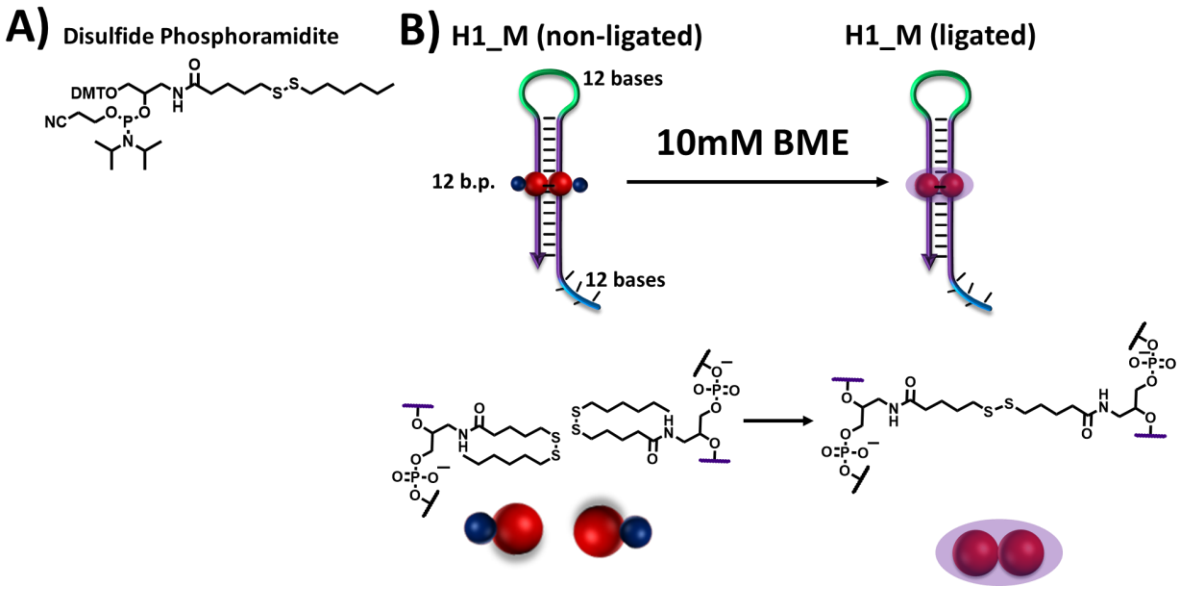

Figure 4. 7. General Ligated Hairpin Synthesis

(a) Structure of the disulfide phosphoramidite used to ligate the HCR hairpins together (b) Ligation of the disulfide functionalized HCR hairpins using 10mM BME. Non-ligated = strands which were not exposed to BME

shorter stems, as they are held by disulfide bonds. Therefore, instead of using a 24 b.p. double stranded region for our stems, we used only a 12 b.p. double stranded region. This gives us enough hybridization stability to ligate our stems together and decrease the overall number of bases by 24. Disulfide strands are ligated together by first pre-annealing the hairpins into the correct hairpin structure followed by the introduction of BME (Figure 4 .7.b.). Non-ligated hairpins are simply HCR hairpins that were not exposed to BME crosslinking but still have disulfide modifications integrated into their structure (Figure 4 .7.b.). Our original design used two disulfides at the top and bottom of each hairpin stem (H1_DD), (H2_DD) and (I_DD) (Figure 4 .8.a.). Synthesis of all strands and ligations are detailed in section 3.5.13 and products confirmed by LC-MS in *Experimental* Figure 4 .30.

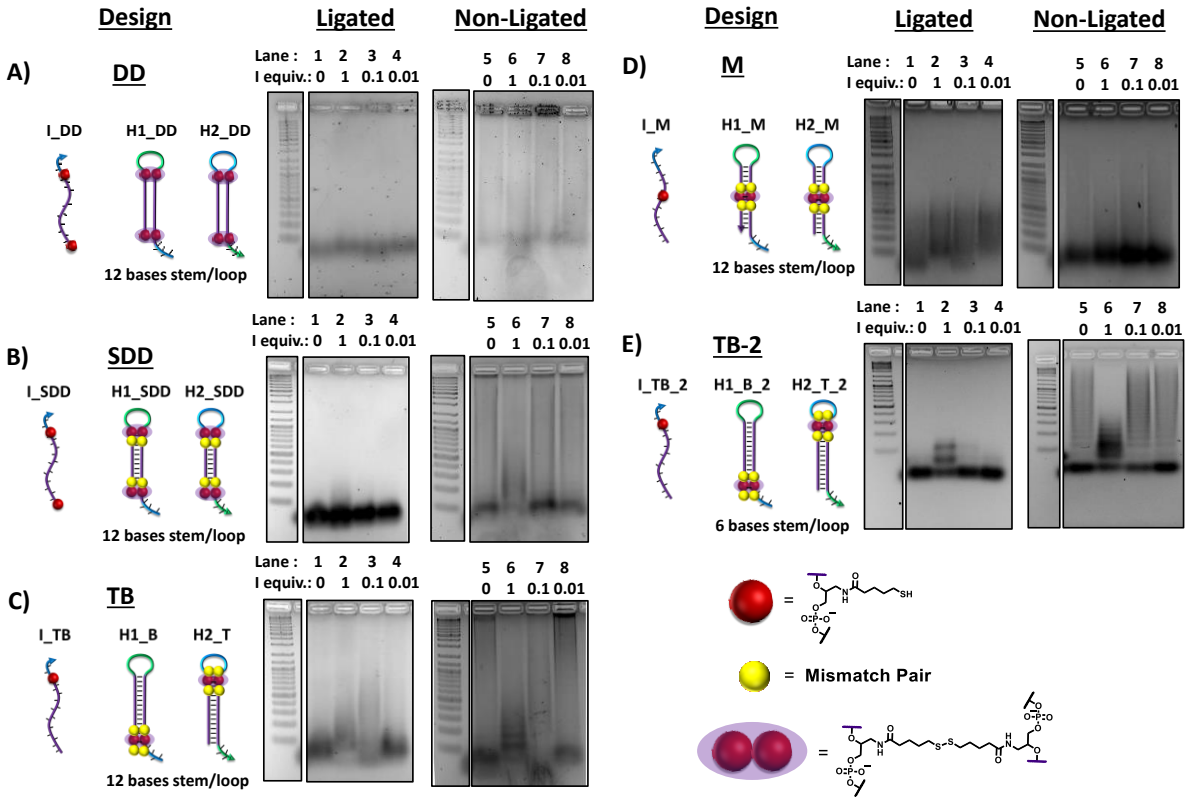

Figure 4. 8. HCR of ligated hairpins. Designs and native agarose

of a) DD, b) SDD c) TB d) M e) TB_2, ligated: Lanes 1-4 & non-ligated: Lanes 5-8. 0 = no initiator, 1 = 1equiv. initiator, 0.1= 0.1equiv. initiator & 0.01=0.01 equiv. initiator.

We then compared the polymerization of the ligated vs. non-ligated hairpins by native AGE introducing 1equiv., 0.1equiv. and 0.01equiv. of initiator strand (Figure 4 .8 a.). By ligating the hairpins together, the leakage of the HCR process was drastically decreased when compared to the non-ligated hairpins (Figure 4 .8 a. lanes 1 & 5). The HCR polymerization process, however, was unable to proceed when the hairpins were pre-ligated (Figure 4 .8 a. lanes 2-4). We hypothesized that this could be due to a high degree of strain on the hairpin stem duplex during the strand displacement step, and as the strand is invading, it is being pushed back by the ligated portion of the stem (Figure 4 .9). For this reason, we then generated a new set of hairpins and initiator, with mismatch spacers right before the disulfide bridge to give some flexibility to the system (H1_SDD), (H2_SDD) and (I_SDD) (Figure 4 .8.b.). Notably, mismatches have been previously shown to increase the hybridization kinetics of HCR to make more monodisperse polymers[36].

The new hairpins were tested against 0, 1, 0.1 and 0.01 equiv. of I and once again leakage was sequestered by the ligated hairpins, as opposed to the non-ligated hairpins (Figure 4 .8.b. lanes 1 &5). Looking at polymerization, it seemed to marginally improve for the 1 equiv. of initiator, however total hairpin consumption was still not realized (figure 4 .8.b. lane 2-4). Overall,

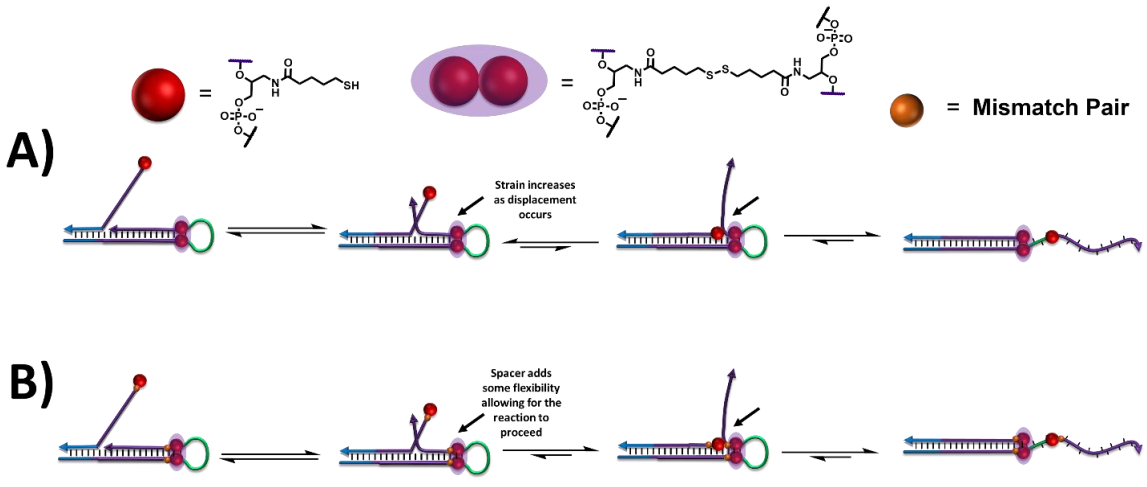

Figure 4. 9. **Schematic of strain during strand displacement of ligated HCR.**

A) without having mismatch pair spacers. **B)** with mismatch pair spacers.

we decided that two disulfides per hairpin may hold the stem together too strongly and decided to reduce the complexity of the system by only using 1 disulfide per hairpin.

We generated two new sets of hairpins and initiators with only 1 disulfide bond, placed either at the top and bottom of corresponding hairpin stems (H1_B, H2_T & I_TB) (Figure 4 .8.c.) or in the middle of the stems (H1_M, H2_M, & I_M) (Figure 4 .8.d). These sets of hairpins were then tested with 0, 1, 0.1 and 0.01 equiv. of (I_M). For (H1_B), and (H2_T), leakage looks like it was still sequestered even when using one disulfide bond in the stem, compared to the non-ligated species (Figure 4 .8.c. lanes 1 & 5). Polymerization of these hairpins seems to be significantly improved, when compared to the "double" disulfide versions, with 1 equiv. of initiator consuming all hairpins (Figure 4 .8.c. lane 2), and some polymerization occurring for 0.1 equiv. of initiator (figure 4 .8.c. lane 3). This polymerization was also done over a longer period (96hrs vs 24hrs), but no further polymerization occurred (*Experimental* Figure 4 .31).

Looking at (H1_M) and (H2_M) (Figure 4 .8.d.), leakage is not as sequestered as the other designs, and in fact looks like it leaks more than the non-ligated hairpins (Figure 4 .8.d. lanes 1 & 5). Additionally, the polymerization lanes did not generate long polymers as would be expected with HCR, in either the ligated or non-ligated samples (figure 4 .8.d. lanes 2-4 & 6-8).

To figure out why we were getting these results, we probed these designs a bit further by looking at them using native PAGE. When we look at the native PAGE of these two sets of hairpins, there is a shift upwards when the ligated hairpins are present together (Figure 4 .10 a. lane 3 & b. Lane 3). This indicates that the hairpins are hybridizing to each other before the initiator is introduced. We hypothesized that this hairpin-hairpin interaction is most likely occurring between the loop of one hairpin and the overhang of the other, somewhat unzipping the two hairpins (Figure 4 .10.). If this was the case, it would prevent the initiator from beginning the HCR process, and each monomer addition would have to compete with this interaction as well. Therefore, we sacrificed our longer hybridization regions and synthesized a new set of hairpins with only 6 bases in the loop and overhang regions to diminish any hairpin-hairpin interactions. This design more closely resembles the original HCR systems, with short loops and longer stems. The disulfides were introduced at the top and bottom of the hairpins, based on

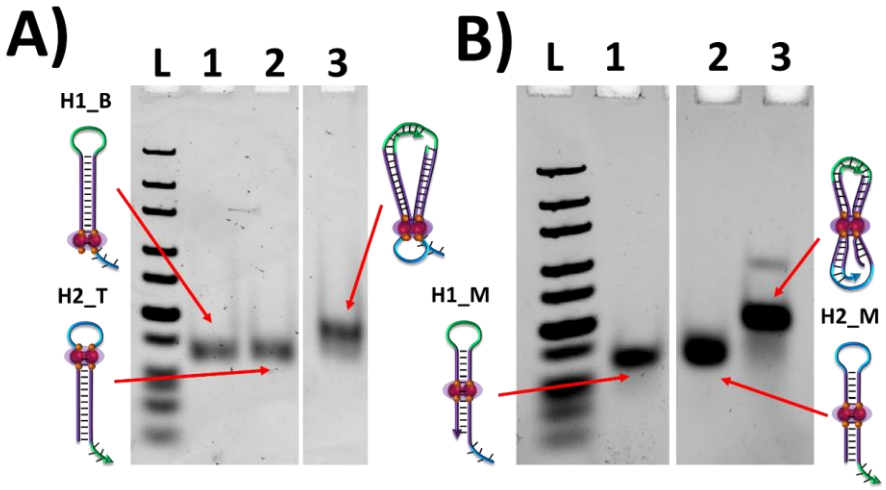

Figure 4. 10. **Native PAGE of hybridizing a) TB design b) M design; lane L: ladder, lane 1: H1, lane 2: H2 and lane 3: H1+H2**

the design that gave us the best previous results (Figure 4 .8.e). We once again polymerized these hairpins and found that leakage was significantly sequestered with the ligated hairpins (figure 4 .8.e. lanes 1 &5). Polymerization with these new hairpins, was still being encumbered however, with only a little bit of polymerization occurring when 1 equiv. of initiator was added (Figure 4 .8. e. lane 2).

Overall, while most of these designs reduced the amount of leakage observed from HCR, the degree of monomer consumption was still lacking in each design. It was hypothesized that this could still be due to opposing strand displacement from the output strand, even with thymine spacers (Figure 4 .9). Indeed, blunt end strand displacement is a known phenomenon that has had to be compensated for in HCR, by adding "clamp" domains to hybridize past the hairpin stem into the loop region[37-38]. To test this hypothesis, we decided to place our designs under "dynamic" conditions, where the disulfide is being constantly formed and broken by the presence of a thiol additive to the solution. This should provide enough flexibility to allow for the strand displacement to optimally occur when the disulfide is in the "broken" state, allowing the polymerization to proceed.

All designs were assessed under “dynamic” conditions with the addition of 10mM BME to the HCR process, mimicking intracellular reducing conditions (Figure 4 .11 & section 3.5.14 for detailed procedure). Generally, dynamic conditions seem to improve the polymerization process of each of the different designs. This provides some evidence that our hypothesis is correct and that by breaking the disulfides under reducing conditions, a higher degree of monomer concumption can occur. Leakage remained more sequestered in the ligated hairpins, when compared to the non-ligated hairpins under dynamic conditions. Interestingly however, when comparing against the same hairpins under non-dynamic conditions, leakage of the ligated hairpins under dynamic conditions increased and leakage of the non-ligated hairpins decreased. This is especially noticeable in the (H1_B_2) and (H2_T_2) polymerizations (Figure 4 .8. e. & Figure 4 .11 d). Considering that the dynamic conditions used are similar conditions to ligate the hairpins in the first place, this can be expected, as the intramolecular disulfide is still more favorable than forming the intermolecular disulfide with BME.

In general, we describe a method for improving the signal gain of HCR using disulfide modifications. Preliminary results show that by ligating the HCR hairpin stems together leakage of the HCR system can be significantly sequestered. Optimization of the polymerization

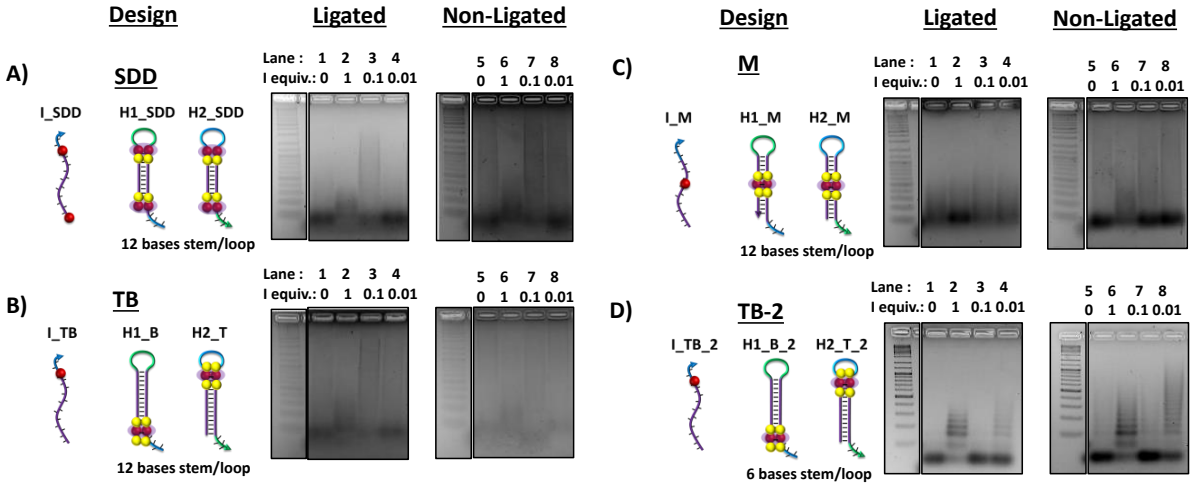

***Figure 4. 11.*. HCR of ligated hairpins performed under dynamic conditions.**

Designs and native agarose of a) SDD, b) TB c) M d) TB_2, ligated: Lanes 1-4 & non-ligated: Lanes 5-8. 0 = no initiator, 1 = 1equiv. initiator, 0.1= 0.1equiv. initiator & 0.01=0.01 equiv. initiator.

conditions have shown that improvements can be made when under dynamic conditions, however the gain still needs to be further improved to rival the optimized sequences reported by Pierce *et al*. which can consume all monomer with 0.01 equiv. of initiator.[34] Moreover, the ideal process would work without the need for dynamic conditions. By adding more spacers in the stem to increase flexibility for the templated disulfide exchange to occur, improvements to polymerization may be realized, however adding too many spacers may result in problems for the initial ligation. In these designs the main purpose of the stem is to provide a template for ligation. Once ligated, there is really no purpose left for the stems in terms of providing stability to the hairpins, as this is now taken over by a covalent bond. Moving forward, reducing the stem length to the minimum length needed just to ligate the stems together, may help to improve the polymerization process, by reducing the number of bases that would need to be displaced by an incoming hairpin or initiator.

4.3.3. Templates for Increased Rate and Selectivity of HCR

The rate of prodrug activation/release is an important factor which determines whether enough drug is activated at any given time, to reach the therapeutic window. Templating HCR on DNA tracks and DNA origami has been previously shown to improve the rate at which the polymerization of the HCR hairpins.[37-38] However, in these studies each hairpin was unique as opposed to the repeatable hairpins normally used for HCR. For our purposes of applying this technology to drug release, having individual unique hairpins does not allow us to scale up the release mechanism as each unique hairpin would have to be chemically modified. Other groups have reduced the number of unique hairpins by templating HCR on long templates with repeating domains, which also increase the rate of HCR[39]. In this method of templation, the template was generated using rolling circle amplification (RCA)[40-41]. The disadvantage of using an RCA template is that there is a lack of control over the length of the template. In our lab we have developed long templates with controlled lengths in the form of temporal growth backbones[42]. These templates can result in unique sequences only at the 5’ and 3’ ends of the strand with repeat sequences up to 2000 bases long in between these two ends and have been used for templating DNA origami[43] as well as DNA tile structures[44].

In chapter 2 we templated our HCR hairpins on small DNA tracks and SNA's but were unable to observe any enhancement in the rate of release. This was due to the rate limiting step being the immolative cyclization, as well as the rate of intermolecular hybridization to find another amplicon. Additionally, it was found that the rate of disulfide exchange was the fastest step in the process. Therefore, while the rate limiting step to produce the active compound are the immolative cyclizations, the detachment of the active compound and linker from the DNA hairpin should be able to be modulated by the rate of HCR.

In this section we have developed new templates to increase the rate of HCR. We use a temporal growth backbone to remove any effect from the intermolecular hybridization of different amplicons. To remove the effect of having the immolative cyclizations as the rate limiting step, we tested our new templates using fluorophore-quencher pairs to generate a fluorescence readout. Moreover, a recent study from our lab has shown the integration of synthetic DNA junctions within these temporal growth backbones, generating trimer and tetramer architectures.[45] Using these architectures, we have also designed and generated localized DNA logic gates for the initiation of HCR. Using logic gates can help to increase the specificity of the device, especially in the case of an AND gate where two inputs would be necessary for initiation. Indeed, DNA logic gates have been previously used to increase specificity and produce small molecule outputs, using non-localized DNA components[46], and design principles for localized DNA computing have been established[47].

4.5.3.1 Design and Synthesis of Temporal growth templated HCR

The design of our HCR amplification system begins with the temporal growth backbone. When generating temporal growth backbones there is a limit to how short the length of each repeat within the backbone, due to the mechanism by which it is made[48]. This limit is about 30 bases, however, to space the repeating hairpins to be close enough to each other to polymerize, the distance between the hairpins needed to be about 20 bases. Therefore, we made a repeat unit on the backbone 42 bases and for every repeat unit on the backbone we engineered one amplicon with two hairpins 20 bases each (Figure 4 .12. a.). Using two staple strands on each repeat sequence of the backbone (BB), we can anchor two alternating hairpins per repeat

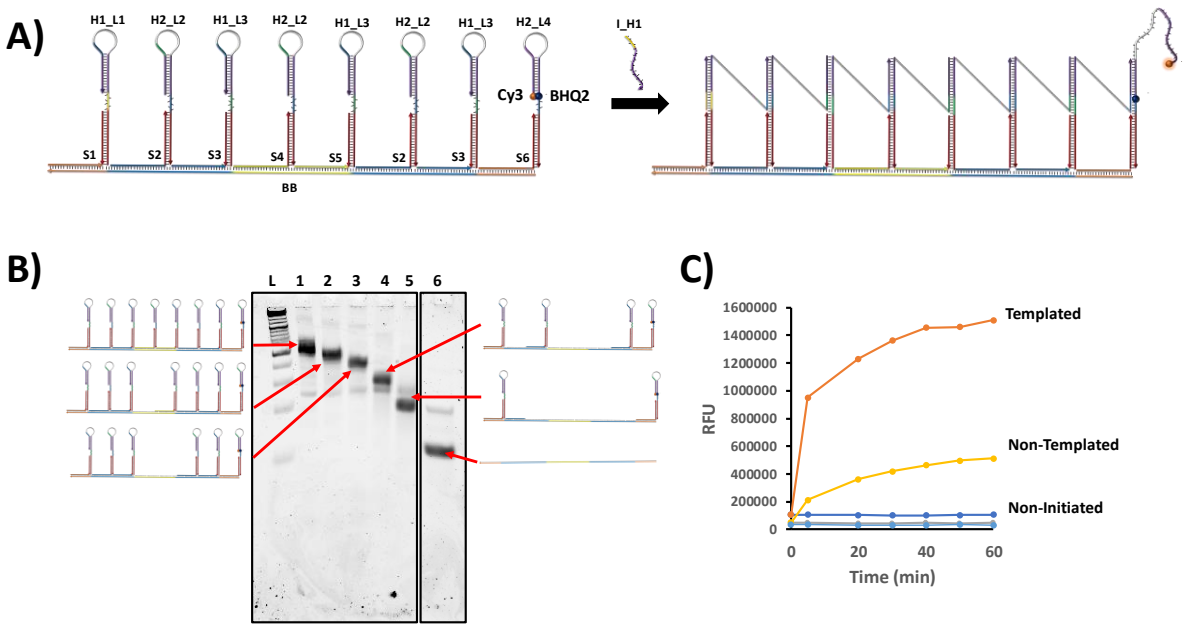

Figure 4. 12.. Hybridization chain reaction templated by a temporal growth backbone.

A) Overall design and mechanism for the temporal growth templated HCR. B) Native PAGE for the assembly of the temporal growth templated HCR. C) Fluorescence output from the opening of H2_L4 in response to no initiator, and I_H1, with and without a template over 60min, fluorescence was measured at λ_{ex}= 561 nm, λ_{em}= 585 nm.

sequence of the backbone with a single base for flexibility in between. The staple strands to connect the hairpins to the backbone, were made using reverse phosphoramidites where necessary to provide the correct directionality for the hairpins to hybridize to one another. We placed a cyanine 3 dye and TBHQ_2 quencher on the final hairpin (H2_L4) to give us our fluorescence readout signal for when the polymerization was complete. H2_L4 was also designed with a unique sequence in the loop of the hairpin, so that polymerization would terminate upon opening. The other unique hairpin on the backbone (H1_L1) has a unique overhang region which only the initiator strand can recognize, to start the polymerization process from one end. Like our originally templated HCR system we used hairpins with 11 T spacers in the loop to reach the next hairpin on the template.

To begin, we decided to use a shorter template with two repeats, to assess whether our hairpins could result in polymerization. The assembly was made in a stepwise manner and

monitored by native PAGE (Figure 4 .12.b. & section 3.5.15 for detailed procedure) Once the assembly was made, we then tested it in response to an equivalent of initiator (I_H1) as well as controls where no template was used, and no initiator. It was found that the rate of polymerization was greatly enhanced for the templated vs non templated HCR and without any initiator present there was no increase in fluorescence (Figure 4 .12.c.). This Indicates that indeed we can use these backbones to template HCR and improve its kinetics.

4.5.3.1 Design and synthesis of a DNA logic gates

Moving on to the DNA logic gates, we designed both an OR and AND gates (Figure 4 .13 & appendix viii.). Previous work in our lab has demonstrated that 3 arm trimers and 4 arm tetramers could be generated with synthetic vertices and each having arms with unique sequences[45]. We reasoned that we could use these as templates for generating logic gated devices.

The design for our OR gate is shown in Figure 4 .13.a. In this design we have 3 hairpins, 2 input hairpins which respond to different initiation sequences (H1_OR_1) and (H1_OR_2) and the third which is the output hairpin with a Cy3, BHQ_2 quenching pair (H2_OR). Each of the input hairpins once initiated by (I_OR_1) or (I_OR_2), can hybridize to the corresponding output hairpin, to give a fluorescence signal. The trimer junction itself, is made with the 5' end of each arm directed toward the center of the junction. Therefore, to get the correct directionality for the hairpins to hybridize properly, we designed two staple strands with half reverse phosphoramidites to hybridize the input hairpins and the template with 2 full helical turns for added stability. Moreover, our hairpins were designed to have 11T spacers so that the sequences could hybridize across the template once initiated. The assembly was made (detailed in section 3.5.16) and monitored by native PAGE (Figure 4 .13.b.). The complete assembly was then evaluated by fluorescence in response to the initiator sequences with or without the template (Figure 4 .13. c.). It was found that without the template even in the presence of initiator, there was no response from the output hairpin and on the template the initiators were necessary to gain a response. This indicates that the OR gate is performing as expected. Interestingly, even

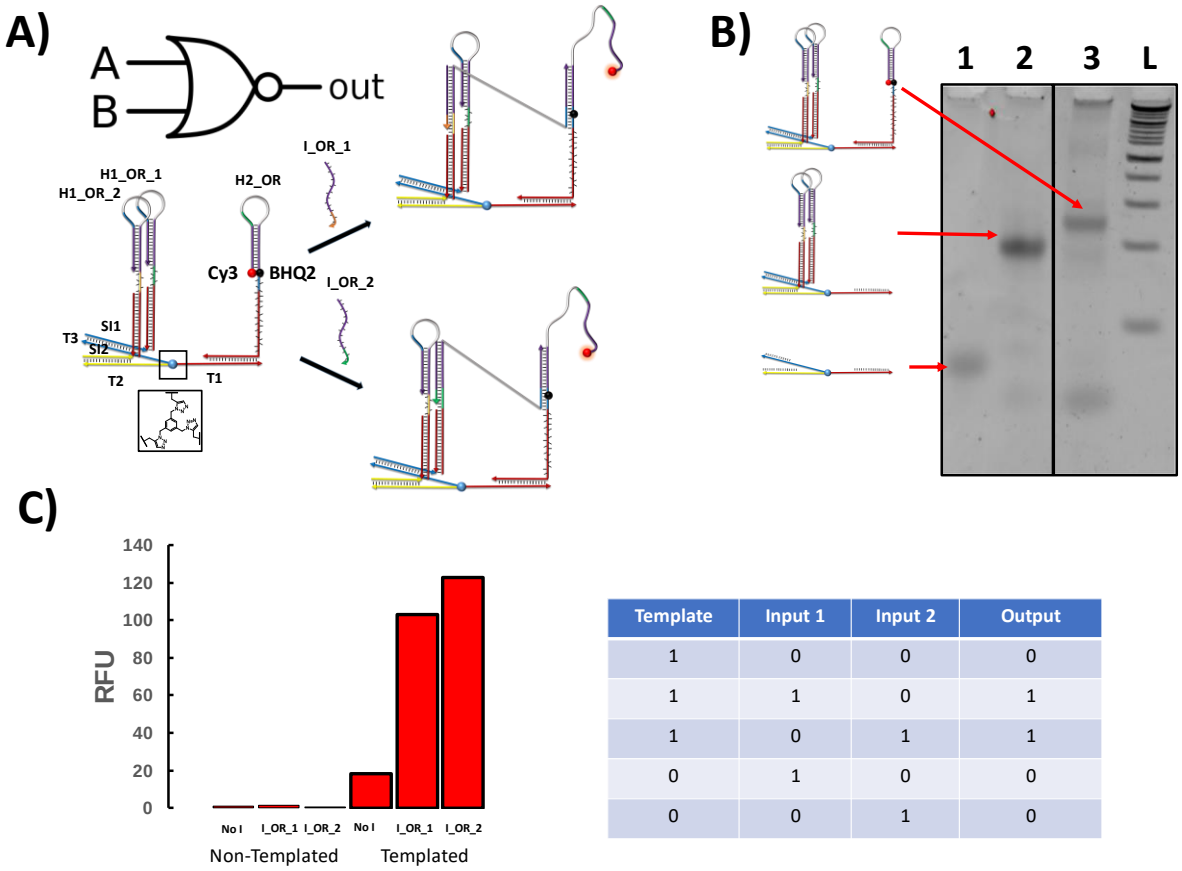

Template	Input 1	Input 2	Output
1	0	0	0
1	1	0	1
1	0	1	1
0	1	0	0
0	0	1	0

Figure 4. 13. **Design and evaluation of a DNA templated OR gate.**

a) Overall design of the DNA templated OR gate. b) Native PAGE of the assembly of the DNA templated OR gate. c) Fluorescence output from the opening of H2_OR in response to no initiator, I_OR_1 and I_OR_2, with and without a template after 24 hr, fluorescence was measured at λ_{ex}= 561 nm, λ_{em}= 585 nm.

though this design was meant to be an OR gate, it might be considered an AND gate because both an initiator and the template itself is necessary to generate a fluorescence output.

Our preliminary results show that we can control HCR rates and initiation using different templates. The next step is to assess a potential "skipping" mechanism in the templated HCR where the enhanced rate could be due to one of the earlier hairpins in the sequence skipping the intermediate hairpins and directly opening the final hairpin, giving us the appearance of an enhanced rate (Figure 4 .14.). If this is the case, we could mitigate this by using more robust backbones such as a DX junction for example. Eventually combing the templates into one large

template could give us a logic gate followed by an amplification step. Expanding to longer backbones, replacing the fluorophore-quencher pairs with chemical modifications for small molecule release and generating DNA AND gates are all more avenues to pursue.

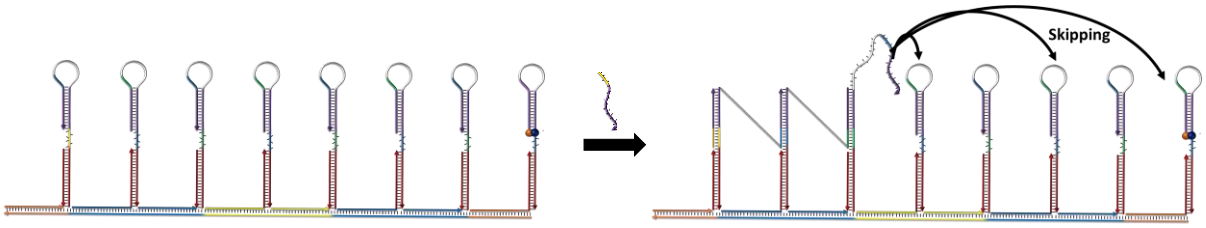

Figure 4. 14. **Mechanism of skipping that can occur on the DNA template.**

4.3.4. Amplified Release of Antisense Oligonucleotides

Small molecule therapeutics have been the cornerstone of modern medicine. While much work has gone into improving their distribution and targeting ability by generating prodrugs and nanoparticles to deliver them to select tissue/cell types, ultimately many diseases are simply untreatable by small molecules. Oligonucleotide therapeutics on the other hand, have the potential to treat previously undruggable disease by targeting messenger RNA transcripts, nuclear DNA as well as other biological targets. However, unless the target itself is unique to the disease state, oligonucleotide therapeutics also lack selective tissue distribution and activation. Therefore, selectively activating oligonucleotide therapeutics at specific locations, using unique biomarkers would be highly advantageous. Previously, our lab has generated logic-gated devices for the selective release of ASO's in response to Bcl-2 and/or Bcl-xL mRNA biomarkers, in the form of a DNA "nanosuitcase"[11] and SNA's[12]. While these devices were able to selectively release their cargo and cause gene silencing, the trigger strands needed to be introduced alongside the devices as these markers were not present in the cells in high enough quantities to release enough ASO to result in silencing. Therefore, an amplification mechanism is required to begin using these types of devices under relevant conditions. In this section, we will go over how we designed and synthesized a device to amplify the release of ASO's from an SNA architecture, as well as how we are adapting it to operate under *in vitro* conditions by increasing nuclease resistance.

4.5.3.1 Design and Synthesis of the release of ASOs using CHA

To apply our amplification technology to selectively releasing ASOs some design changes were required. In HCR the initiator strand is consumed once hybridized to the first hairpin, kick-starting the polymerization process. Other amplification circuits have been produced which recycle the initiator strand to give an amplified strand displacement mechanism without polymerization. Catalytic Hairpin assembly (CHA) is one of these circuits and is used here to amplify the release of ASO strands from an SNA. In a typical CHA circuit there are 4 components: the initiator (I_CHA), two fuel hairpins (H1_CHA) & (H2_CHA), and an output duplex (A:A') (Figure 4 .15.a.). For our purposes we designed (A) to be a luciferase gene silencing sequence (ASO) and added a hydrophobic modification to (A') to make (ASO_C12), so that we could assemble (ASO_C12) into an SNA, which would act as the carrier for the (ASO) (Figure 4 .15.b.). Previous SNA's in our lab have been shown to only be able to hybridize to 50-60% of the complementary strand before becoming too sterically encumbered to hybridize more strands. Adding the strands at a 1:1 ratio would leave both left over strands which are non-hybridized to the SNA and left-over single strands within the SNA. This is problematic because left over single stranded (ASO_C12) within the SNA can act as initiators for the CHA circuit, and leftover (ASO) strands would not be part of the delivery device.

To overcome this, we designed this device with an additional SNA strand (F_C12), which acts as a filler strand within the SNA (Figure 4 .15. b.). Using this strand in combination with (ASO'_C12), at a 1:1 ratio, generates SNA's in which only 50% of the strands are addressable and hybridize to (ASO'_C12). This makes sure that there are no leftover strands and generates defined SNA's. The overall mechanism of our device is as follows, the circuit begins with (I_CHA) hybridizing to (H1_CHA) to expose the (D), (B) & (C) regions (Figure 4 .15 c. i.). (B) and (A) regions on (H1_CHA) then hybridize to the (B') & (A') region on (ASO_C12) (Figure 4 .15. b. ii.) ejecting (ASO) (Figure 4 .15.c.iii.). (H2_CHA) then is used to hybridize to (H1_CHA) and displace (I_CHA) (Figure 4 .15.c. iv.), starting the cycle again (Figure 4 .15.c.v.). Through this process, a small

amount of (I_CHA) results in the amplified output of multiple (ASO) strands (Figure 4 .15.c. vi.). To make sure that the amplification mechanism would work properly, we first synthesized the

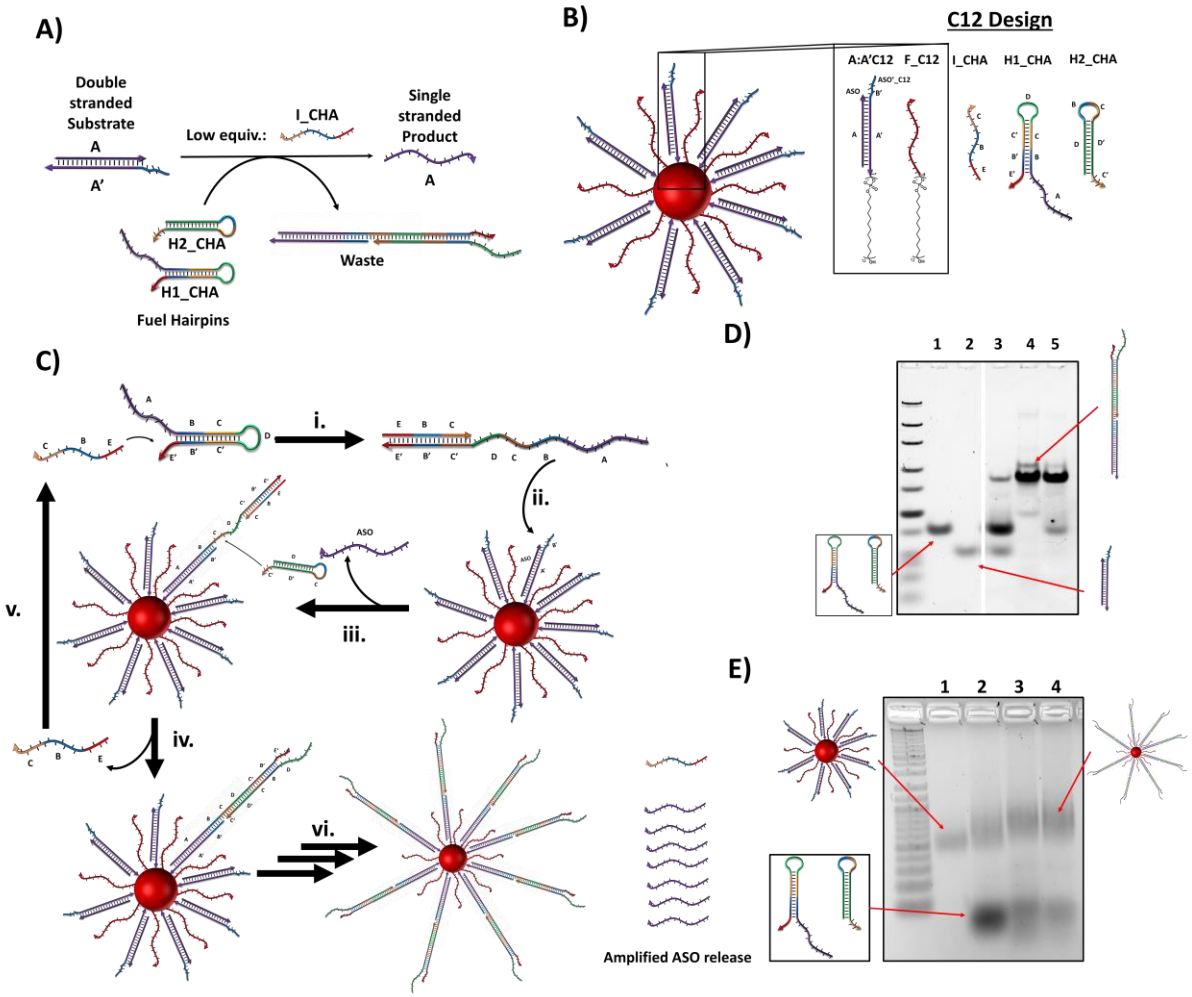

Figure 4. 15. Design and mechanism of the amplified release of antisense oligonucleotides using CHA

a) General CHA scheme resulting in the amplified release of single strand. **b)** Design of the CHA hairpins and SNA **c)** Mechanism of CHA **i.** I_CHA hybridizes to H1_CHA using the E toehold and displaces the stem of H1_CHA **ii.** H1_CHA hybridizes to the hangover B on ASO'_C12 in the SNA **iii.** the ASO strand is displaced from the SNA **iv.** H2_CHA hybridizes to the C region on H1_CHA and displaces I_CHA. **v.** I_CHA is available for another cycle **vi.** the cycle continues until all ASO is displaced from the SNA. **d)** Native PAGE of the CHA mechanism using unmodified strands; **Lane 1**: H1_CHA + H2_CHA, **Lane 2**: ASO: ASO' duplex, **Lane 3:** Lanes 1 + 2, **Lane 4:** Lane 3 +1equiv. I_CHA, **Lane 5:** Lane 3 + 0.1 equiv. I_CHA. **e)** Native AGE of the CHA mechanism using an SNA; **Lane 1**: SNA of ASO + ASO'_C12 + F_C12, **Lane 2**: Lane 1 + H1_CHA + H2_CHA, **Lane 3**: Lane 2 + 1equiv. I_CHA, **Lane 4**: Lane 2 + 0.1equiv. I_CHA.

(A') strand without any hydrophobic component and all other strands. The amplification and release mechanism were monitored by native PAGE (Figure 4 .15.d.).

We confirmed the release mechanism with 1 and 0.1equiv. of (I_CHA) by observing the formation of waste product and consumption of starting duplex (Figure 4 .15.d. lanes 4 & 5) We then synthesized (ASO'_C12) and (F_C12) strands with hydrophobic blocks and assembled them into an SNA (Section 3.5.18 for detailed assembly procedure). The SNA was found to be 10nm diameter by AFM (Figure 4 .32.) and the release mechanism was monitored by native AGE (Figure 4 .15.e.). The SNA assembled as we expected (Figure 4 .15.e. lane 1), with no left-over strands observed in the gel. When we mixed the fuel hairpins (H1_CHA & H2_CHA) and the SNA together, we found that there was minimal leakage of the circuit observed (Figure 4 .15.e. lane 2). Adding (I_CHA) in 1equiv. (Figure 4 .15.e. lane 3) and 0.1equiv. (Figure 4 .15.e. lane 4), the SNA increased in size with a new band forming in both cases with similar intensities, indirectly indicating amplified ejection of the ASO strand.

4.5.3.1 Improving Nuclease Resistance

Our initial tests with this system were accomplished using a phosphodiester backbone DNA, and hence not resistant to biological conditions. Therefore, having found that the mechanism was working properly, we then sought to increase the nuclease resistance of all the strands by introducing PS linkages into the system (Figure 4 .16.a.). PS-PS and PS-PO duplexes have been shown to have reduced affinity for one another, which could affect the leakage and gain of the CHA system. Due to this, we decided to selectively phosphorothioate only the ends of the CHA hairpins and (I_CHA), to maintain PO-PO hybridization within the stems of the hairpins and prevent leaking (H1PS_CHA & H2PS_CHA & I_CHA). Additionally, (ASO'_C12) and (F_C12) were only phosphorothioated at one terminus, as the other ends of these strands already had hydrophobic blocks, making them inaccessible to nucleases in solution (ASO'PS_C12 and FPS_C12). (ASO) was fully phosphorothioated and labelled with a cyanine 3 dye (ASOPS_Cy3), as this would be the active agent after the CHA mechanism and would hybridize to the A' region of (ASO'PS_C12), leaving at least a semi-stable PO-PS duplex.

These new strands were synthesized and the assembly of (ASO'PS_C12), (FPS_C12), and (ASOPS_Cy3), checked. The assembly of these three strands together, however, did not result in similar SNA structures as observed before and were instead large aggregates, which started to

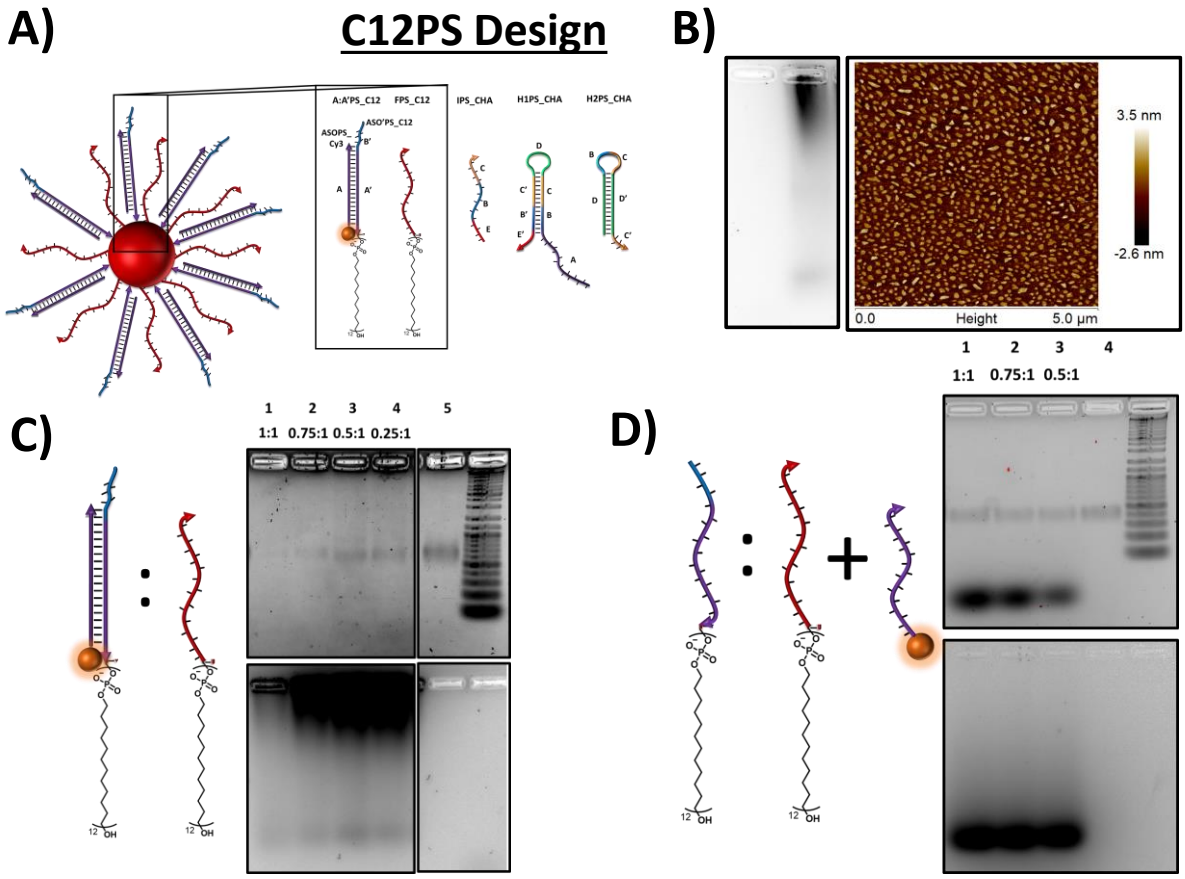

Figure 4. 16. **Design and assembly of changing to PS DNA to increase nuclease resistance of the CHA system.**

a) Overall C12PS Design **b)** Native AGE and AFM of ASO'PS_C12 + ASOPS_Cy3 + FPS_C12 showing aggregation of the particles. **c)** Titration of the assembly of C12PS SNA changing the ratio between the ASOPS_Cy3: ASO'PS_C12 duplex (A: A') and FPS_C12 (F); all strands were assembled together in one pot, imaged under gel red (top) and cy3 (bottom). Lane 1: 1:1 ratio (A:A'): (F), Lane 2: 0.75:1 ratio (A:A'): (F), Lane 3: 0.5:1 ratio (A:A'): (F), Lane 4: 0.25:1 ratio (A:A'): (F), Lane 5: 1:1 ratio ASO'PS_C12: FPS_C12 with no ASOPS_Cy3. Aggregation occurs at all ratios. **d)** Titration of the assembly of C12PS SNA changing the ratio between the ASOPS_Cy3: ASO'PS_C12 duplex (A: A') and FPS_C12 (F); ASO'PS_C12 and FPS_C12 were preassembled before the addition of ASOPS_Cy3, imaged under gel red (top) and cy3 (bottom). Lane 1: 1:1 ratio (A:A'): (F), Lane 2: 0.75:1 ratio (A:A'): (F), Lane 3: 0.5:1 ratio (A:A'): (F), Lane 4: 1:1 ratio ASO'PS_C12: FPS_C12 with no ASOPS_Cy3. ASOPs_Cy3 does not hybridize when preassembled.

precipitate. Native AGE and AFM confirmed that these were in fact aggregates in solution and not SNA's (Figure 4 .16.b.). To get SNA's, we tried different ratios of assembly between (ASO'PS_C12) and (FPS_C12) (Figure 4 .16.c. and d.). We tried adding either (ASOPS_Cy3) directly (Figure 4 .16.c.) or after preassembling the (ASO'PS_C12) and (FPS_C12) (Figure 4 .16. d.). We found that without the addition of (ASOPS_Cy3) SNA's could be formed (Figure 4 .16.c. lane 5 and Figure 4 .16.d. lane 4), however if it was added the new aggregate structures were formed at all ratios (Figure 4 .16.c. lanes 1-4). Additionally, if we preassembled the SNA's and then added (ASOPS_Cy3), heating from 44°C to 20°C, the strand remained unhybridized to the SNA at all ratios (Figure 4 .16.d. lanes 1-3)

It was hypothesized that the core of these structures did not have strong enough interaction to prevent rearrangement of the structure, when (ASOPS_Cy3) was added. Therefore,

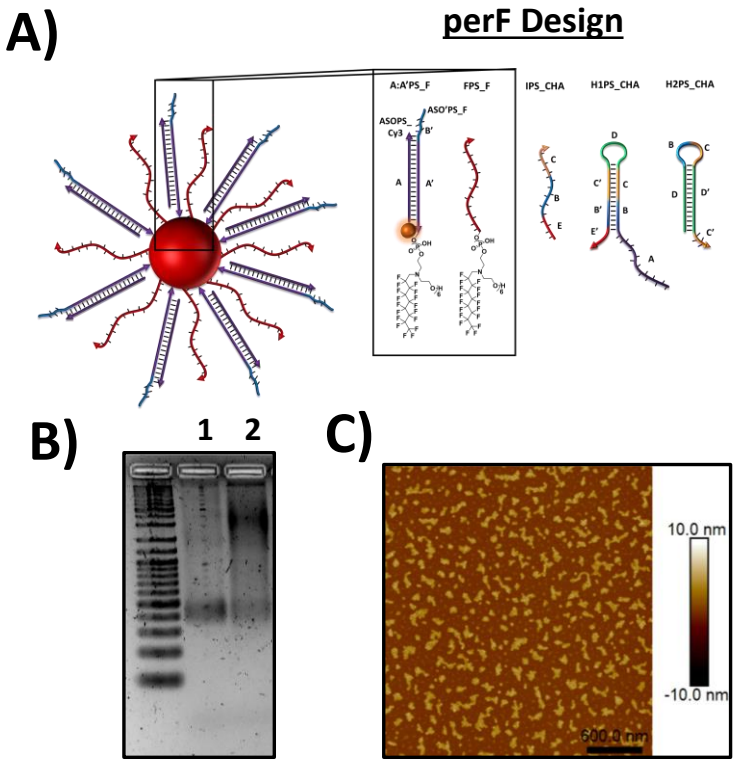

Figure 4. 17. **Design and assembly of SNA's with a perfluoro core.**

a) Overall design of the CHA design using a per-fluorinated core for the SNA. b) Native AGE of the assembly of the per-fluorinated SNA. Lane 1: ASO'PS_F + FPS_F, Lane 2: Lane 1+ ASOPS_Cy3. c) AFM of Lane 2 from b) showing the aggregation of particles upon ASOPS_Cy3 addition.

we decided to replace the hydrophobic C12 block with a much stronger block based on fluorine interactions (Figure 4 .17.a.). Previous studies in the lab had shown that "DNA Teflon" was able to resist denaturation conditions and provide a much stronger interaction than the more common hydrophobic interaction[49]. A previously reported fluorine phosphoramidite was synthesized according to *Experimental* Figure. 3.26, and strands (ASO'PS_F) and (FPS_F) were then synthesized with 6 fluorine modifications each. These strands were assembled and monitored by native AGE and AFM (Figure 4 .17. b. and c.). However once again, as the (ASOPS_Cy3) strand was added to the SNA's, aggregation occurred destroying the SNA's (Figure 4 .17. b. lane 2 and c.).

Another attempt to replace the core of these SNA's was done using gold nanoparticles, as they exist as solid particles, which cannot rearrange. Some design consideration needed to be made when using these particles, as it is not easy to control the exact number of strands connected to a gold particle. Additionally, due to the absorbance of the gold particle, it is difficult to ascertain the concentration of DNA in solution. These are both important for the CHA mechanism where stoichiometry is extremely important, to not cause undesired leakage of the

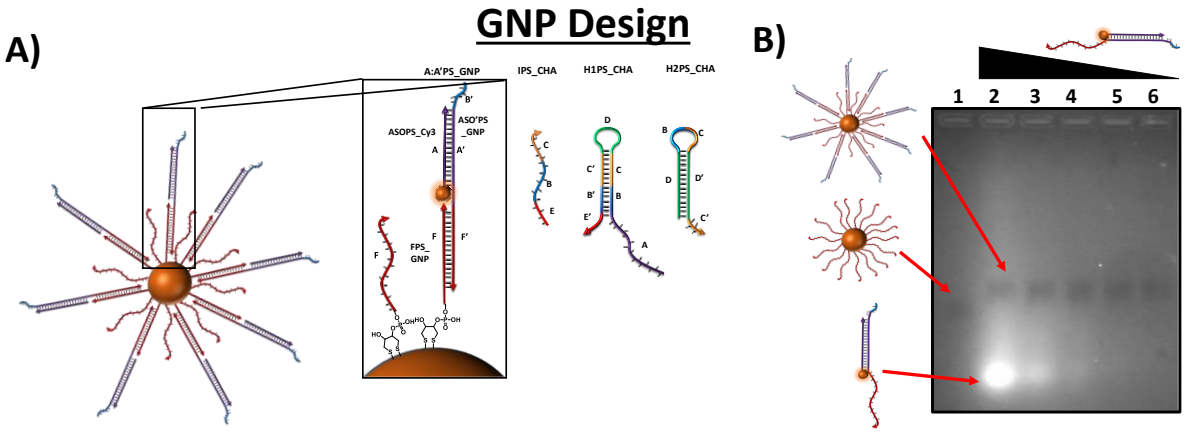

Figure 4. 18. **Design and assembly of the gold nanoparticle design.**

A) Overall design of the gold nanoparticle. B) Native AGE of the titration between FPS_GNP functionalized gold nanoparticle and the ASOPS_Cy3: ASO'PS_GNP duplex (A: A'). Lane 1: GNP, Lane 2: 1+ 100equiv. (A: A')., Lane 3: 1+ 50equiv. (A: A')., Lane 4: 1+ 25equiv. (A: A')., Lane 5: 1+ 12.5equiv. (A: A')., Lane 6: 1+ 6.25equiv. (A: A').

mechanism. To circumvent this, we changed the design so that (ASO'PS) would instead have a hybridization handle (F'), that could be added to functionalized gold particles (ASO'PS_GNP), in known amounts, instead of functionalizing the gold particle directly (Figure 4 .18.a.). A pre-hybridized (ASO'PS_GNP) with (ASOPS_Cy3), would then be able to be added to the functionalized gold particles. We performed a titration of the (A):(A'PS_GNP) duplex to functionalized gold nanoparticles with (FPS_GNP) to assess how many duplexes could be hybridized per gold particle (Figure 4 .18.b.). It was found that the ratio between the gold nanoparticle and the (A):(A'PS_GNP) duplex needed to make sure there were no left-over duplexes, was 1:12.5 of gold particle to DNA duplex. To achieve concentration high enough for *in vitro* gene silencing, and for the CHA mechanism to optimally operate (1uM), this ratio was much too low as a typical gold nanoparticle synthesis only gives a 0.4uM, 25uL solution. This means that each synthesis would only give an approximate 5uM, 25uL solution of ASO functionalized nanoparticle. Considering that solutions required for *in vitro* assays require 15uL of a 20x concentrated stock solution when being introduced to cells, each synthesis would only be able to test one condition at 250nM final concentration.

Re-assessing, it seemed that only the combination of all 3 PS strands was contributing to the aggregation. The primary goal of increased nuclease resistance can be achieved in different ways. Therefore, instead of using PS at the ends of (ASO'_C12) and (F_C12), it was reasoned that we could instead gain nuclease resistance by adding a hexa-ethylene glycol (HEG) modification to the end of the strands, blocking 3' degradation (Figure 4 .19.a.). Adding HEG to the end of the strands might have the added benefit of mitigating protein binding during any i*n vitro* studies. Strand (HEG_ASO'_C12) and (HEG_F_C12), were synthesized accordingly and assembled with (ASOPS_Cy3) to generate well defined SNA's by AFM and native AGE (Figure 4 .19.b. Lane 1 & *Experimental* Figure 4 .33.). The CHA mechanism of these strands was then assessed by native AGE with the (H1PS_CHA), (H2PS_CHA) and (IPS_CHA) sequences (Figure 4 .19.b. lanes 2-4). Like the original PO mechanism, the (ASOPS_Cy3) strand was ejected from the SNA in an amplified manner with only 0.1 equiv. of (IPS_CHA).

Overall, we were able to take a different DNA amplification circuit than HCR (CHA) and apply it to the amplified release of ASO oligonucleotides from SNA's. Careful design considerations needed to be made to avoid spontaneous leakage of the ASO from the

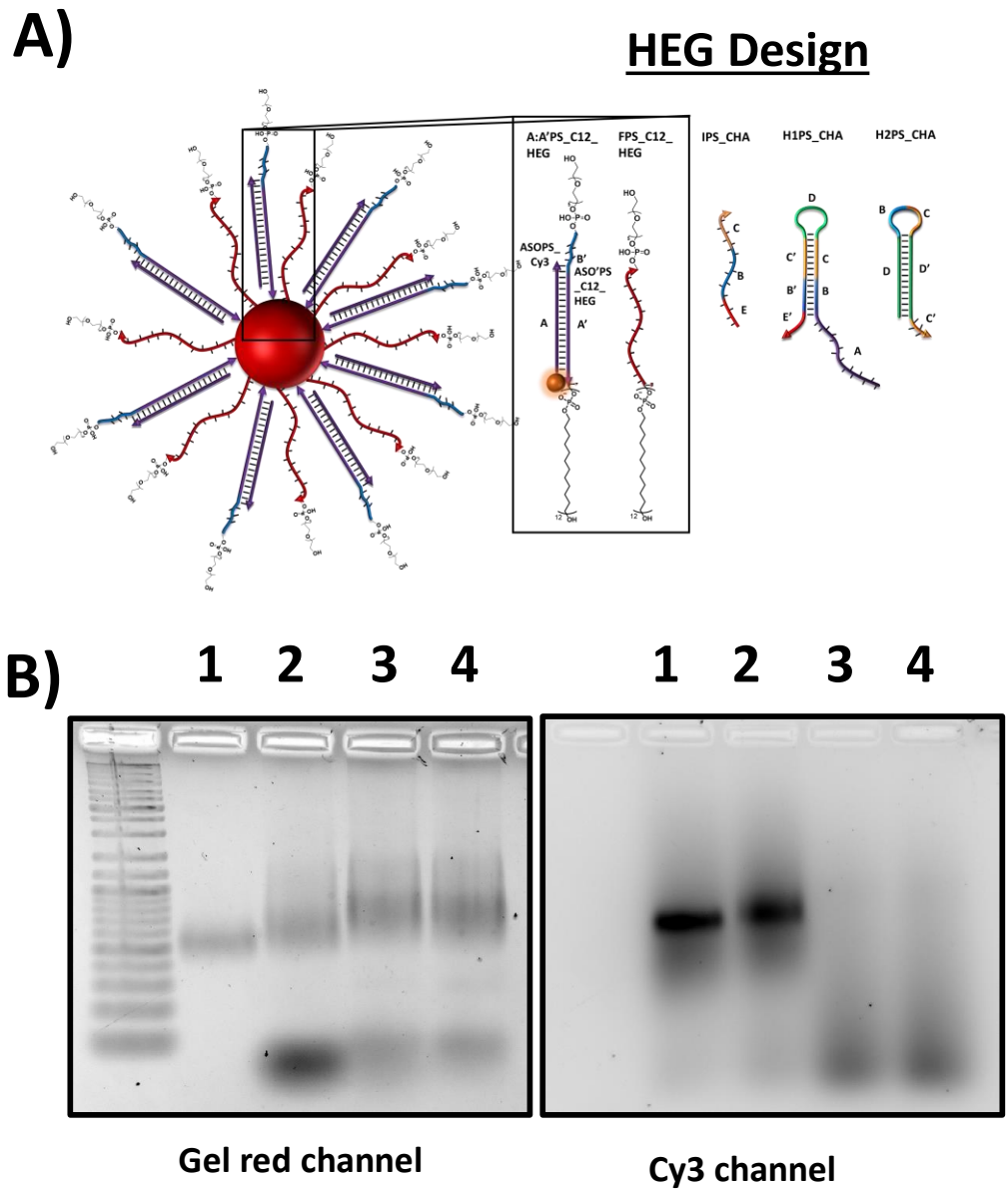

Figure 4. 19. **Design, assembly, and initiation of CHA using the HEG design.**

a) Overall design of the HEG SNA. b) Native PAGE of the assembly and CHA of the HEG SNA's imaged under gel red and cy3. Lane 1: HEG SNA, Lane 2: HEG SNA + H1PS_CHA + H2PS_CHA, Lane 3: Lane 2+ 1equiv. IPS_CHA, Lane 4: Lane2 + 0.1 equiv. IPS_CHA. The ASOPS_Cy3 strand gets ejected in the presence of 1 or 0.1equiv. of initiator.

nanostructure, and it was found to release the ASO strands in an amplified manner. When adapting the system for more *in vitro* conditions, by imparting nuclease resistance to the strands in the form of PS DNA, the assemblies were found to aggregate. Two different SNA cores were tried to avoid this aggregation, however, replacing the PS regions with a HEG modification, ultimately allowed us to regain the assembly and amplification mechanism. Direct future work will focus on the exact nuclease resistance these strands have in serum and testing whether the CHA mechanism can operate under *in-vitro* conditions. Moving forward, modifying the (ASOPS_Cy3) strand with a cellular uptake enhancing modification (i.e., folate), may be an interesting avenue to pursue. Hiding this uptake enhancing modification within the core of the SNA, and only revealing it when the CHA mechanism has occurred, would act as a method to selectively change the uptake profile of the ASO strand.

4.3.5. Antibody-DNA Conjugates with Controlled Valency

Due to the large size and negatively charged nature of DNA, uptake of DNA nanodevices into cells can be quite difficult without the use of a transfection agent[13]. Therefore, efforts have been made to generate devices that work extracellularly[16]. For our device to be active in the extracellular medium, we have pursued the use of Antibody-Oligonucleotide conjugates (AOC's) to initiate the HCR process. This would give us the excellent recognition ability of an antibody to an extracellular biomarker, as well as an oligonucleotide to initiate the HCR process. With this process, the need to internalize the HCR components would not be necessary. Antibody oligonucleotide conjugates have been previously developed to initiate HCR through the integrated into enzyme-linked immunoassays (ELISA)[50-51] and many methods exist for functionalizing antibodies with oligonucleotides[52-53].

One of the most important characteristics of an AOC, however, is the degree of conjugation (DoC). The degree of conjugation of an AOC is of the utmost importance for the conjugate's solubility, function, potency, and toxicity[53]. While there are some methods that exist to give perfect control over the degree of conjugation of an antibody conjugate, these methods typically are done *in-vitro* and are not accessible to non-experts[26, 54]. Current chemical methods for AOC generation by conjugating to free lysine residues on an antibody, using succinimidyl 4-

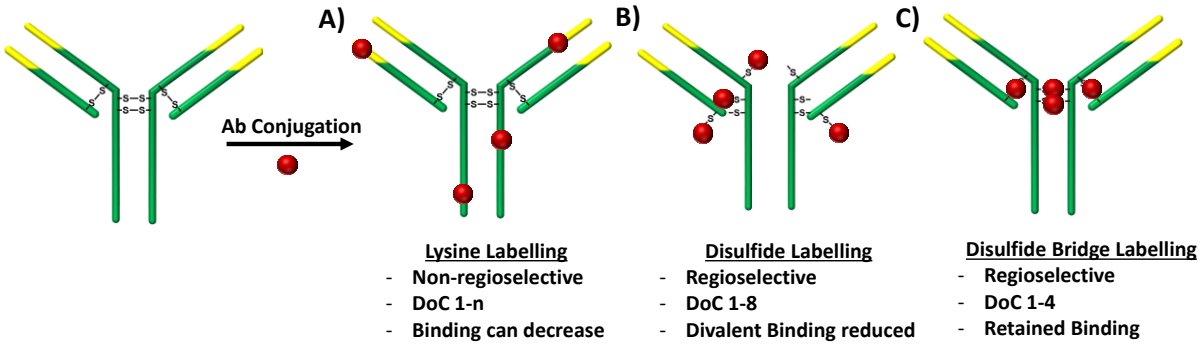

Figure 4. 20. **Different antibody chemical conjugation strategies and there resulting products.**

A) lysine labelling, B) disulfide labelling C) disulfide labelling with bridging linker

(N-maleimidomethyl)cyclohexane-1-carboxylate (SMCC) linkers, result in AOC's with high DoC's at non-regioselective positions, which can interfere with antibody binding[55-57](Figure 4 .20.a.). Degree of conjugation in chemical conjugation can be somewhat controlled, by selecting a ratio between reacting species that centers the Poisson distribution of products around the desired DoC[58]. However, this is at the expense of overall yield and purification techniques must be employed to separate, the unreacted and functionalized antibodies.

Alternatively, conjugation of oligonucleotides through disulfide bridges in antibodies has been established[59-61](Figure 4 .20.b.). While this does give regioselective conjugation, the degree of conjugation is still not controlled resulting in antibodies with DoC's between 1-8. Moreover, breaking the disulfide bonds within antibodies, have been shown to reduce divalent binding of the Ab to its target. To address this second factor, researchers have developed "bridging" disulfide linkers, to stitch the free thiols back together within the antibody[62-63] (Figure 4 .20.c.). The use of these linkers has been shown to re-establish divalent binding, and results in antibody conjugates with DoC's of exactly 4. In our lab we have produced a 1:1 protein: oligonucleotide conjugate between albumin and DNA using 4 hydrophobic dendritic arms attached to the DNA (D-DNA)[64]. These DNA conjugates formed a 1:1 complex with albumin due to the co-operative binding between each of the 4 arms of the conjugate to each of the 4 hydrophobic pockets of albumin.

With all this in mind, we sought to first develop new antibody-oligonucleotide conjugates which we could control the valency of the DNA using a chemical conjugation method. In this section, we generate AOCs by addressing the conserved disulfide bridges, common within a host of antibodies, with a dibromomaleimide-azide (DBM-N3) bridging linker giving us 4 oligonucleotide addressable positions. We react these 4 positions selectively with a short dibenzocyclooctyne (DBCO) conjugated oligonucleotide, giving us antibodies with a DoC of 4 oligonucleotides. Then using different branched oligonucleotides (1B, 2B, 4B) we funnel these hybridization regions into a single focal point with a unique oligonucleotide sequence. Overall, we provide an easy and scalable method to functionalize a host of different Ab with a resultant monovalent oligonucleotide sequence, which gives us complete control over the valency of AOCs for the initiation of HCR.

4.3.5.1. Design

Our system can be split into three different components, 1) The small molecule modified Ab (Ab_N3), 2) the linking Oligonucleotide (L) and 3) the branched oligonucleotide (4B) (Figure 4 .21.). Careful design consideration had to be made for each of these three components to work synergistically with one another. The design of our system began with selecting the conjugation chemistry between the antibody and (L). We chose to use a strain promoted alkyne-azide cycloaddition reaction (SPAAC) to connect (L) to (Ab_N3) as these reactions are: high yielding, the DBCO modification for oligonucleotides is commercially available, no copper is required and this reaction has been used previously to make antibody oligonucleotide conjugates[58]. Since the strained alkyne moiety was going to be on the oligonucleotide portion of the conjugate, this meant that we needed to functionalize our antibody with an azide functional handle at the disulfide bridges. Therefore, the small molecule we chose to use was dibromomaleimide azide (DBM-N3) (Figure 4 .21). This small molecule has previously been used for the functionalization

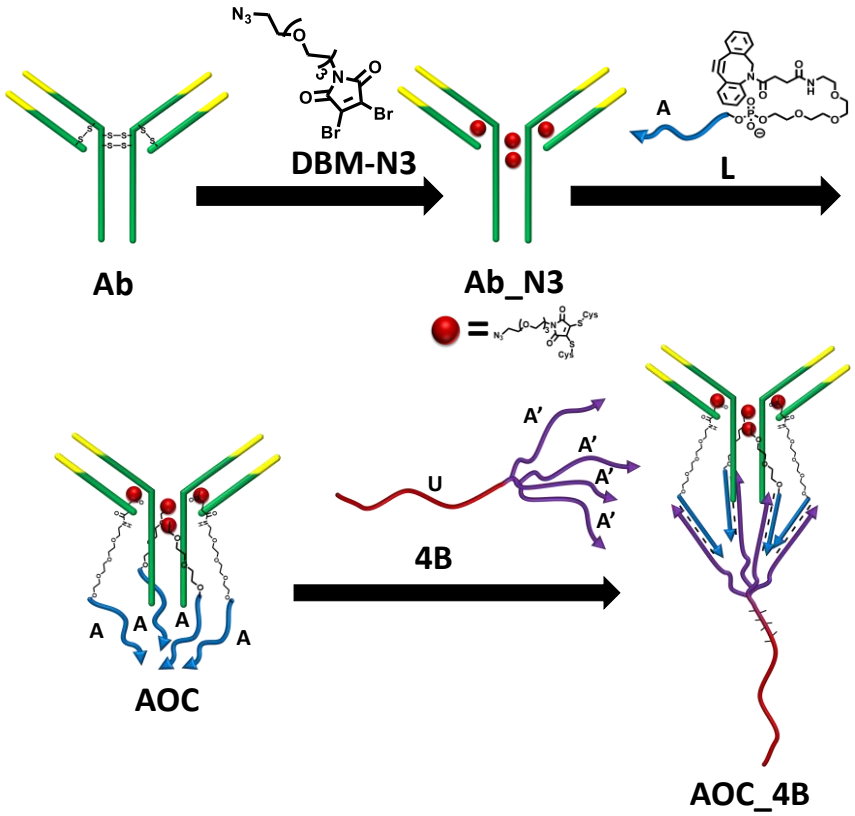

Figure 4. 21. Scheme for generating antibodies with one functional DNA handle (U).

of other proteins at disulfide locations[65] and provided us with both the bridging ability and azide handle to conjugate (L).

4.3.5.2. Synthesis of Ab_N3

To generate (Ab_N3) we first synthesized the small molecule (DBM_N3) following *Experimental* Figure 4 .25. Next, we needed to optimize the conditions to react (DBM_N3) with an antibody to make (Ab_N3). There are two steps to generate (Ab_N3) starting from an unfunctionalized antibody (Ab); reduction and re-ligation (Figure 4 .22.a. i. & ii). As the small molecule had an azide functional group, we would have to remove any reducing agent used in the first step of the (Ab_N3) synthesis, otherwise the azide would be reduced to an amine in a Staudinger reduction. We tried both TCEP (tris(2-carboxyethyl) phosphine) and BME (2-mercaptoethanol), as reducing agents but found that with TCEP the pH had to be carefully adjusted, after dissolution to avoid precipitation of the antibody (data not shown). Therefore, we

decided to use BME as our reducing agent, and performed a titration with different concentrations of BME with antibody to find the optimal BME concentration to reduce all antibody. Reduction of the antibody was monitored by denaturing, non-reducing sodium dodecyl sulphate–polyacrylamide ***gel*** electrophoresis (SDS PAGE) (Figure 4 .22.b. lane 2 and *Experimental* Figure 4 .27). We found that using 100mM BME for 2hr at 37°C was enough to reduce the antibody into 50kDa and 25kDa fractions (Figure 4 .22.b. lane 2). Using this concentration of

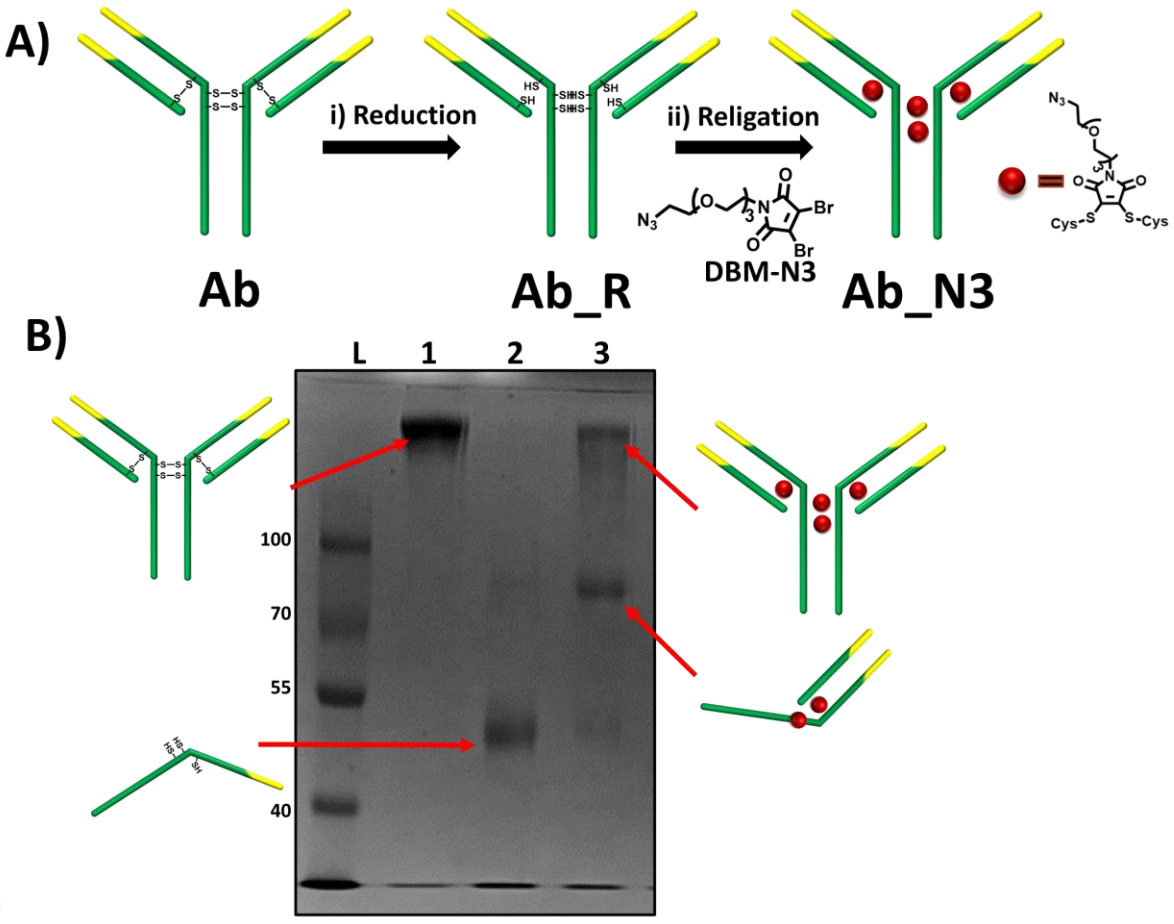

Figure 4. 22.. Synthesis of azide functionalized antibody (Ab_N3)

A) Reaction scheme representing the two steps involved with generating Ab_N3 **i**. reduction with BME and **ii.** religation with the DBM small molecule. **B)** denaturing, non-reducing SDS PAGE of each reaction step with optimized conditions. **Lane 1:** Ab (untreated), **Lane 2:** Ab +100mM BME, **Lane 3:** Ab_R + DBM at a ratio of 1:100 Ab_R: DBM

reducing agent we then moved to reacting the reduced antibody with the (DBM_N3) small molecule.

To remove the BME reducing agent, the mixture was filtered through Zeba® 7K centrifugal filters. We did another titration between (Ab_R) and (DBM_N3) to determine the optimal amount of small molecule to ligate the antibody back together (Figure 4 .22.b. lane 2 and *Experimental* Figure 4 .28). For this reaction we added 10% DMSO to the solution to keep (DBM_N3) soluble. Monitored by non-reducing SDS-PAGE, we found using a ratio of 1:100 (antibody) to (DBM_N3) gave us 75kDa and 150kDa bands, indicating religation (Figure 4 .22.b. lane 3). Notably, we generate 75kDa bands after this reaction as there are two ways that the disulfides in the FC region can ligate back together. Either two heavy chains can be ligated back together (to give 150kDa) or ligation can occur within one heavy chain (75kDa). For antibody binding purposes it is more important that the Fab region disulfides are ligated properly, which in both cases they are. Overall, we generated (Ab_N3) following the reaction scheme in Figure 4 .22.a. and a denaturing, non-reducing SDS PAGE of our optimized conditions is in Figure 4 .22.b. Procedures are detailed in section 3.5.9 and 3.5.10.

4.3.5.3. Design and Synthesis of AOC

In general, to generate (AOC) we needed to react (Ab_N3) with (L) in a SPAAC reaction (Figure 4 .23.a.). First however, some additional design considerations were made regarding (L). We were interested in keeping the oligonucleotide far enough from the antibody so as not to interfere with its binding, but not so far as to eliminate the multivalency of 4 oligonucleotides in proximity. Therefore, added a triethylene glycol spacer between the DBCO functional group and the (L) sequence (Figure 4 .23.c.). Additionally, the sequence of (L) was carefully selected to be only 18 bases long, to maintain hybridization stability with (4B) by having at least 1 helical turn. It was important to also not make (L) too long, as we were limited to using short arm lengths on the complementary (4B), to maintain good yields of this component. Moreover, we synthesized (L) using reverse phosphoramidites, so that we could functionalize the sequence with the DBCO modifier at the end of the synthesis, as well as generate the correct directionality for hybridizing with (4B). With all these design considerations made, we synthesized (L) (Figure 4 .23.c. for

structure and *Experimental* Table 3.1. for sequence). For our initial tests we synthesized a longer version of the linking oligonucleotide (L2) labelled with a cyanine 3 dye (Cy3) so that we could visualize its conjugation by SDS PAGE and have a greater mobility of the conjugate through the gel (*Experimental* Table 3.1. for sequence).

A benefit of our method is that, instead of manipulating the Poisson distribution to generate AOCs with lower degrees of conjugation, (needing complicated purification afterwards) our method intentionally reacts the antibody to completion. Therefore, the ratio between (L2) and (Ab_N3) during the conjugation can be kept high and excess removed by simple filtration. (L2) was synthesized and then reacted with (Ab_N3) in 1xPBS buffer, at a ratio of 1:100 (Ab_N3) to (L2) (Figure 4 .23.a. & section 3.5.11 for procedure). Excess (L2) was then removed with 50KDa Amicon™ ultracentrifugation filters using an optimized procedure with a surfactant (tween 20) to maximize yield. The conjugation was monitored by non-reducing SDS PAGE under native

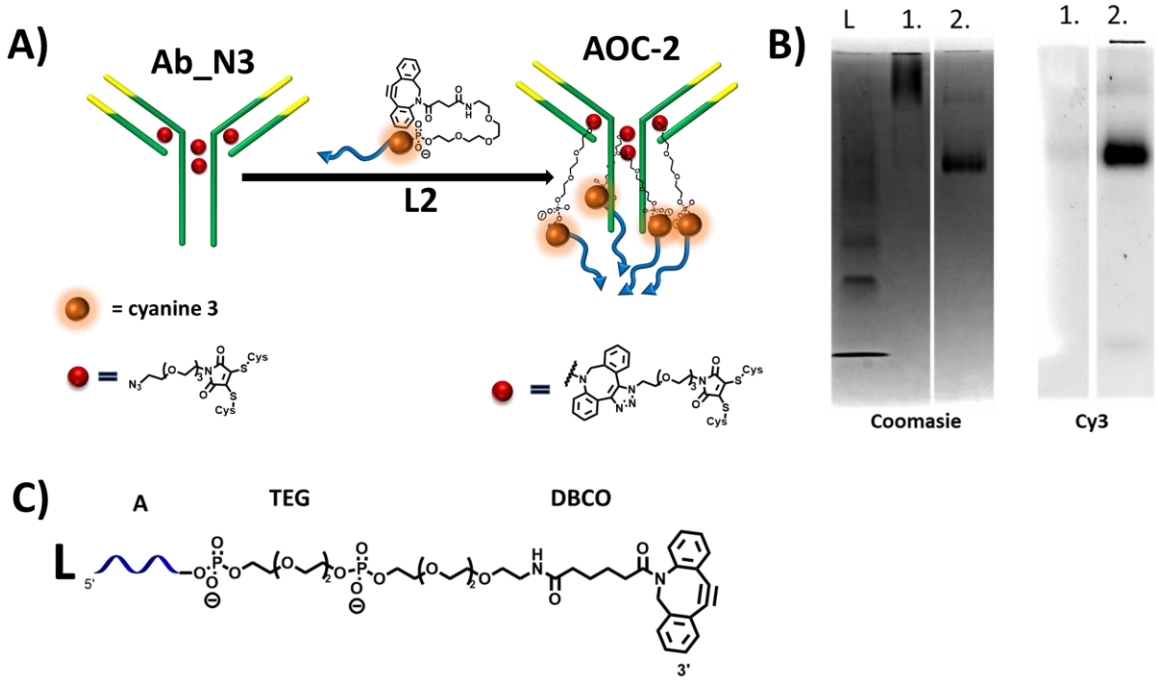

Figure 4. 23. Synthesis of DNA functionalized antibody (AOC)

a) reaction scheme b) native, non-reducing SDS PAGE of reaction under gel red and Cy3 channels; lane 1: Ab_N3 lane 2: Ab_N3 conjugated with L2. c) Structure of the linking strand (L). A= hybridization sequence A TEG= triethylene glycol unit, DBCO= di benzocyclooctyne phosphoramidite

conditions (Figure 4 .23.b.). Before conjugation of (L2) to (Ab_N3), (Ab_N3) does not penetrate the gel and is non fluorescent (figure 4 .23.b. lane 1,). After conjugation there is a single product that penetrates the gel and is fluorescent under the cy3 channel and co-localizes with protein (AOC-2) (Figure 4 .23.b.lane 2.), indicating that conjugation has occurred. Following this, we produced (AOC) using the non-fluorescent (L) with the proper sequence for hybridizing to (4B), monitored by native SDS PAGE (*Experimental* Figure 4 .29).

4.3.5.4. Design and Synthesis of AOC_4B, AOC_2B & AOC_1B

Having produced AOC, we then moved on to the hybridization of the branched DNA to this conjugate. Before doing so, some extra design considerations were made for the dendritic (4B) strand. As previously indicated, the arms of (4B) were kept short to maximize the yield of this component. During DNA synthesis, the branching portion of (4B) is made last, and all 4 arms are made in parallel with the same sequence. Therefore, every base coupling at this stage is 4 base couplings, where each arm has the potential to be capped and terminate the oligonucleotide, reducing yield. Additionally, we designed (4B) to have a triethylene glycol spacer between the unique sequence and the branched sequence, so that the unique sequence would not be sterically encumbered when connected to the antibody and retain its ability to hybridize (Figure 4 .24.a.).

To synthesize (4B) we used commercially available branching units (Figure 4 .24.a. and *Experimental* Table 3.1. for sequence). We also synthesized two other branching sequences with either 2 branches (2B) or 1 branch (1B) for comparing hybridization and gel mobility. We then hybridized (4B), (2B) and (1B) to (AOC) to generate (AOC_4B), (AOC_2B) and (AOC_1B) each in a 4:1 ratio between the branched oligonucleotide and (AOC) respectively and observed the products by Native PAGE (Figure 4 .24.b.). In our preliminary gel, as the number of branching arms decreases the antibody penetrates further into the gel. This indicates that there is more DNA hybridized to (AOC) when there is a lower number of branches. This makes sense as there would be 4 longer unique sequences hybridized in (AOC_1B) as opposed to only 1 unique sequence in (AOC_4B). Additionally, we can observe excess (4B) and no intermediate structures, indicating that there is some co-operativity occurring with the hybridization of this strand (Figure

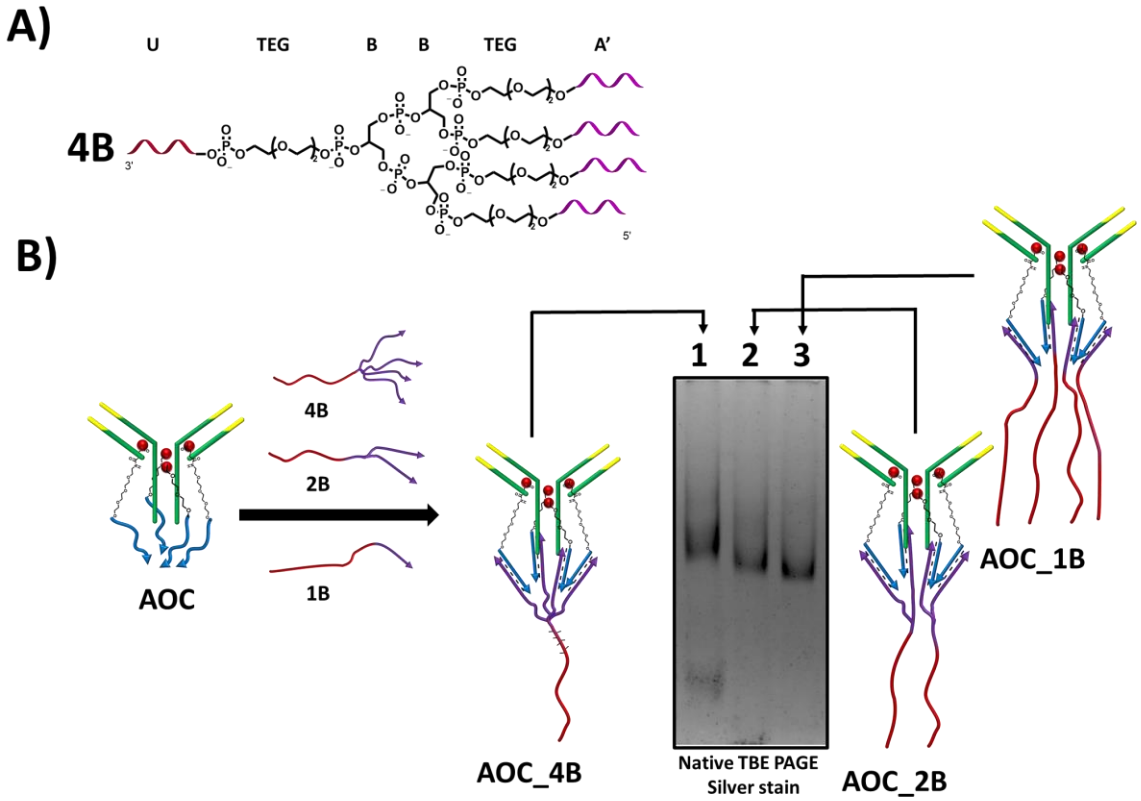

Figure 4. 24. Hybridization of branched oligonucleotides to AOC

(a) Structure of the branched oligonucleotide strand 4B A' = complementary sequence to A, U = unique oligonucleotide sequence, TEG= triethylene glycol unit, B= branching phosphoramidite **(b)** Native TBE PAGE of the hybridization of 4B, 2B and 1B to AOC to generate AOC_4B (lane 1), AOC_2B (lane 2) and AOC_1B (lane 3) respectively.

4 .24.b. lane 2). Moving forward we would only add 1 equiv. of (4B) as hybridization of each branched oligonucleotide is quantitative, removing the need for purification at this step.

Overall, we have produced AOC's with controlled valency using branched DNA hybridization. Future work will focus on fully characterizing the AOC by mass spectrometry, performing an ELISA assay on the AOC to make sure binding is retained, and further characterizing the number of unique sequences per antibody. Moreover, direct future work will focus on testing the HCR polymerization in response to our AOC's as an initiator sequence. We envisage that this method of generating AOC's will go beyond its intended purpose for HCR

initiation and be applicable to other areas where control over the valency of an AOC is important, such as in the development of AOC's for oligonucleotide therapeutics.

4.4. Conclusion

In conclusion, many different approaches have been taken to improve the HCR release system from Chapter 2. By changing the release chemistry, initiating extracellularly, improving the signal gain, using new templates, and changing to oligonucleotide therapeutics. While this work is on-going, important milestones have been reached within each of these areas. Progress towards synthesizing an HCR release system operating with a tetrazine cyclization for bio-orthogonal release has been established. It was shown that by using branched DNA we could make AOC's, that had controlled valency. We further conducted some preliminary studies on the effect of ligating the HCR stems together with disulfide bridges. It was found that by ligating the stems together, the leakage of the HCR system could be significantly reduced. By introducing a longer DNA template, we showed that our method has the potential to increase the rate at which release could occur. Moreover, by using more specialized templates we demonstrated that we could generate devices that operate using "OR" logic. Additionally, we were able to adapt the amplified release method to selectively release ASO strands in response to a low amount of initiator sequence. To increase nuclease resistance in this device, we added HEG modifiers to the periphery of the SNA, and importantly this addition did not change the SNA morphology or encumber the amplification mechanism.

Overall, these changes/improvements to the HCR system will help to adapt the device to operate under more biologically relevant conditions and eventually bring it to the clinic. Avoiding undesired leakage of the device by switching the release chemistry will make sure that it only operates at the desired location without side effects. Improving the signal gain and leakage of the device, will make sure that 1) the device only operates where desired and 2) that there is enough drug molecule released per recognition event to elicit a therapeutic response. Using new templates to increase the rate of release will make sure enough drug is released at one time to generate a therapeutic response. Furthermore, using DNA logic gates will increase the selectivity of the device and mitigate off target effects even further. By moving towards using antisense

oligonucleotides as the output instead of small molecule therapeutics, more disease targets become accessible for the device to generate a response, simply by changing the output sequence. Finally, using extracellular signals to initiate the device, avoids the requirement to internalize DNA into the cell for the device to recognize a target and initiate.

4.5. Experimental Section

4.5.1. General.

Unless otherwise stated, all commercial reagents and solvents were used without additional purification. Magnesium sulfate hexahydrate (MgSO4·6H2O), tris(hydroxymethyl)aminomethane (Tris), urea, chloroform (CHCl3), hexane (Hex), tetrahydrofurane (THF), dimethyl sulfoxide (DMSO), hydrochloric acid (HCl), sodium hydroxide (NaOH), dichloromethane (CH_2Cl_2), ethyl acetate (ETOAc), ethanol (EtOH), fluorescein, methyl iodide, sodium bicarbonate ($NaHCO_3$), sodium chloride (NaCl), triphosgene, triethylamine, trifluoroacetic acid (TFA), 4-nitrophenyl chloroformate, camptothecin, dimethyl amino pyridine (DMAP), 2, 2'-dithiodipyridine, 1-hexanethiol, N-hydroxysuccinimide, and N,N'-Dicycolhexylcarbodiimide were used as purchased from Sigma-Aldrich. Acetic acid and boric acid were purchased from Fisher Scientific and used without further purification. GelRed™ nucleic acid stain and Sybr Gold were purchased from Biotium Inc. Acetone ACS reagent grade was purchased from Fisher. 5K dialysis tubing was purchased from Fischer Scientific. Acrylamide/Bis-acrylamide (40% 19:1 solution), ammonium persulfate and tetramethylenediamine were obtained from Bioshop Canada Inc. and used as supplied. 1 μmol Universal 1000Å LCAACPG supports and standard reagents used for automated DNA synthesis were purchased through Bioautomation. Sephadex G-25 (super fine, DNA grade) was purchased from Glen Research. Analytical thin layer chromatography (TLC) was performed on TLC plates purchased from Sigma-Aldrich. 1xTAMg buffer is composed of 45 mM Tris and 12.5 mM MgCl2.6H2O with the pH adjusted to 8.0 using glacial acetic acid. TBE buffer is 90 mM Tris, 90 mM boric acid and 2 mM EDTA with a pH of 8.0. TEAA mobile phase is 50 mM triethylammonium acetate with the pH adjusted to 8.0 using glacial acetic acid. 1xPBS buffer is 137 mM NaCl, 2.7 mM KCl, 8 mM

Na_2HPO_4, and 2 mM KH_2PO_4 adjusted to pH 8.0 with NaOH. 50x ALK buffer is composed of 1.5M NaOH and 50mM EDTA.

4.5.2. Instrumentation

Standard oligonucleotide synthesis was performed on solid supports using a Mermade MM6 synthesizer from Bioautomation. HPLC purification was carried out on an Agilent Infinity 1260. UV absorbance DNA quantification measurements were performed with a NanoDrop Lite spectrophotometer from Thermo Scientific. For structure assembly, Eppendorf Mastercycler 96-well thermocycler and Bio-Rad T100TM thermal cycler were used to anneal all structures and hairpins. Polyacrylamide gel electrophoresis (PAGE) was performed using 20x20 cm vertical Hoefer 600 electrophoresis units. Agarose Gel Electrophoresis (AGE) was performed on Owl Mini and Owl EasyCast horizontal gel systems. Gels were imaged by a BioRad ChemiDoc MP system. Fluorescence data were measured by a BioTek Cytation 5 imaging reader Reader. Multimode 8 scanning probe microscope and Nanoscope V controller (Bruker, Santa Barbara, CA) was used to acquire AFM images. DynaPro (model MS) molecularsizing instrument was used to measure the particle size distributions. Liquid Chromatography Electrospray Ionization Mass Spectrometry (LC-ESI-MS) was carried out using a Bruker MaXis Impact™. Column chromatography to purify organic compounds was performed on a CombiFlash® Rf + system with RediSep® Silica columns (230-400 mesh) using a proper eluent system. 1H NMR and 13C was recorded on 500 MHz AV500 equipped with a 60 position SampleXpress sample changer (Bruker) and 300 MHz Varian Mercury equipped with an SMS-100 sample changer (Agilent). Visualization of TLC was achieved by UV light (254 nm). Chemical shifts were quoted in parts per million (ppM) referenced to the appropriate residual solvent peak or 0.0 ppm for tetramethylsilane. Abbreviations for 1H NMR: s = singlet, d = doublet, t = triplet, q = quartet, quint = quintet, m = multiplet. High-resolution mass spectra were obtained from Exactive Plus Orbitrap Mass Spectrometer (Thermo Scientific).

4.5.3. Solid Phase Synthesis & Purification of DNA

4.5.3.1. Synthesis

DNA synthesis was performed on a 1 µmole scale, starting from the required nucleotide modified 1000 Å LCAA-CPG solid-support. Coupling efficiency was monitored after removal of the dimethoxytrityl (DMT) 5-OH protecting groups. DMT-dodecane-diol (cat.# CLP-1114), Fmoc-Amino-DMT C-3 CED phosphoramidites (cat.# CLP-1661), and dC (cat.# ANP-4675), dT (cat.# ANP-4674), and dA (cat.# ANP-4671) reverse phosphoramidites were purchased from ChemGenes. Thiol modifier C6 SS phosphoramidites (cat. # 148254-21-1) were purchased from Glen Research. Coupling efficiency was monitored by the removal of DMT group on 5'-OH groups. In a glove box under nitrogen atmosphere, DMT-dodecane-diol, Thiol modifier C6 SS and Fmoc-Amino-DMT C-3 CED were dissolved in acetonitrile and shaken for 10 mins to achieve final concentration of 0.1 M. The DMT-dodecanediol amidite was activated with 0.25M 5-(ethylthio)tetrazole in anhydrous acetonitrile and the extended coupling times of 5 minutes were used. The amino modifier amidite and disulfide amidite were activated by 0.25M 5-(ethylthio)tetrazole in anhydrous acetonitrile but the coupling was performed manually inside the glove box. 3% dichloroacetic acid in dichloromethane was used to remove DMT protecting group on the DNA synthesizer. The reverse phosphoramidites for strand S2 were loaded onto a Mermade MM6 synthesizer from Bioautomation for its synthesis.

4.5.3.2. Deprotection

For unmodified DNA, DNA modified with dodecanediol, and DNA modified with reverse phosphoramidites, after the synthesis was complete the CPG was treated with 28% aqueous ammonium hydroxide solution for 16-18 hours at 60^{o}C in water bath. For disulfide modified DNA, the CPG was treated with 28% aqueous ammonium hydroxide solution for 36-48 hours at r.t.

4.5.3.3. Purification

The crude mixtures were then concentrated under reduced pressure at 60^{o}C, suspended 1:1 8 M urea before loading to polyacrylamide/urea gel (12% or 15% denaturing PAGE). The gel was run at 250 V for 30 minutes followed by 500 V for 45-60 minutes in 1x TBE as the running buffer. The gel was then imaged and excised on TLC plate under a UV lamp. The solution was dried to

approximately 1 mL before loading to Sephadex G-25 column. The purified DNA was quantified by the absorbance at 260 nm.

4.5.4. DNA Sequences

Table 4. 1 Sequences used for DNA Conjugates.

(D =DMT-dodecane-diol), (Bold represents reverse phosphoramidites), (lower case represents phosphorothioated), , (SS = Internal Disulfide phosphoramidite), (DBCO = 5'-DBCO-TEG Phosphoramidite), (TEG= triethylene glycol Phosphoramidite), (Cy3= cyanine 3 phosphoramidite), (B= branching phosphoramidite), (TBHQ2= Thymine modified black hole quencher 2 phosphoramidite) (X= dodecane diol phosphoramidite), (F= perfluoro phosphoramidite), (HEG=Hexaethylene glycol phosphoramidite), (DTPA= dithiol phosphoramidite).

Name	Sequences (From 5' to 3')
L	**GAG AGA AAG GGA GAG GAG** (TEG) (DBCO)
L2	(DBCO) (TEG) (Cy3) CTC ATT CGC CAT AAA CTC TCA ATA ACC
1B	CTC CTC TCC CTT TCT CTC (TEG) (TEG) CTC ATT CGC CAT AAA CTC TCA ATA ACC
2B	CTC CTC TCC CTT TCT CTC (TEG) (B) (TEG) CTC ATT CGC CAT AAA CTC TCA ATA ACC
4B	CTC CTC TCC CTT TCT CTC (TEG) (B) (B) (TEG) CTC ATT CGC CAT AAA CTC TCA ATA ACC
I_DD	(SS)GT CCC TGC CTC T(SS)A ACT TTA ACC CG
H1_DD	CGG GTT AAA GTT (SS)AG AGG CAG GGA C(SS)A AAG TCT AAT CC(SS) GTC CCT GCC TCT (SS)
H2_DD	(SS)GT CCC TGC CTC T(SS)A ACT TTA ACC CG(SS) AGA GGC AGG GAC (SS)GG ATT AGA CTT T
I_SDD	(SS)TG TCC CTG CCT CTT (SS)AA CTT TAA CCC G

H1_SDD	CGG GTT AAA GTT (SS)AA GAG GCA GGG ACA (SS)AA AGT CTA ATC C(SS)A GTC CCT GCC TCT A(SS)
H2_SDD	(SS)TG TCC CTG CCT CTT (SS)AA CTT TAA CCC G(SS)T AGA GGC AGG GAC T(SS)G GAT TAG ACT TT
I_TB	T(SS)T GTC CCT GCC TCT AAC TTT AAC CCG
H1_B	CGG GTT AAA GTT AGA GGC AGG GAC T(SS)T AAA GTC TAA TCC T(SS)T GTC CCT GCC TCT
H2_T	T(SS)T GTC CCT GCC TCT AAC TTT AAC CCG AGA GGC AGG GAC T(SS)T GGA TTA GAC TTT
I_M	GTC CCT T(SS)T GCC TCT AAC TTT AAC CCG
H1_M	CGG GTT AAA GTT AGA GGC T(SS)T AGG GAC AAA GTC TAA TCC GTC CCT T(SS)T GCC TCT
H2_M	GTC CCT A(SS)A GCC TCT AAC TTT AAC CCG AGA GGC A(SS)A AGG GAC GGA TTA GAC TTT
I_TB_2	(SS)AG CCC TTA CTC CCA ATT CC
H1_B_2	GGA ATT GGG AGT AAG GGC T(SS)T GTG AT(SS) TGC CCT TAC TCC C
H2_T_2	(SS)AG CCC TTA CTC CCA ATT CCG GGA GTA AGG GCA (SS)AT CAC A
I_CHA	CGA CAT CTA ACC TAG CTC ACT GAC
H1_CHA	GTC AGT GAG CTA GGT TAG ATG TCG CCA TGT GTA GAC GAC ATC TAA CCT AGC ATA TCC TTG TCG TAT CCC
H2_CHA	AGA TGT CGT CTA CAC ATG GCG ACA TCT AAC CTA GCC CAT GTG TAG A

ASO	ATA TCC TTG TCG TAT CCC
ASO'	GGG ATA CGA CAA GGA TAT GCT AGG TT
F_C12	CTTCTCTTTCTTCTTCTTCACTTC XXXXXXXXXXXX
ASO'_C12	XXX XXX XXX XXX TTT TTG GGA TAC GAC AAG GAT ATG CTA GGT T
ASO'PS_GNP	GAA GTG AAG AAG AAG AAA GAG AAG TTT TTG GGA TAC GAC AAG GAT ATG CTa ggt t
FPS_GNP	CTT CTC TTT CTT CTT CTT CAC TTC (DTPA)
H1PS_CHA	gtc agT GAG CTA GGT TAG ATG TCG CCA TGT GTA GAC GAC ATC TAA CCT AGC ATA TCC TTG TCG Tat ccc
H2PS_CHA	aga tgT CGT CTA CAC ATG GCG ACA TCT AAC CTA GCC CAT GTg tag a
IPS_CHA	cgacaTCTAACCTAGCTCActgac
ASO'PS_C12	XXX XXX XXX XXX TTT TTG GGA TAC GAC AAG GAT ATG CTa ggt t
ASOPS_Cy3	atatccttgtcgtatccc (Cy3)
FPS_C12	ctt ctC TTT CTT CTT CTT CAC TTC XXX XXX XXX XXX
ASO'PS_F	FFF FFF TTT TTG GGA TAC GAC AAG GAT ATG CTa ggt t
FPS_F	ctt ctC TTT CTT CTT CTT CAC TTC FFF FFF
HEG_ASO'_C12	XXX XXX XXX XXX TTT TTG GGA TAC GAC AAG GAT ATG CTA GGT T (HEG)
HEG_F_C12	(HEG) CTT CTC TTT CTT CTT CTT CAC TTC XXX XXX XXX XXX
H1_L1	TTG GTG TGG TGT GGT GTG GTG GTG GGA AGA CAC GCC GAA TCC TAG ACT TTT TTT TTT TTC AAA GTA GTC TAG GAT TCG GCG TG

H2_L2	AGT CTA GGA TTC GGC GTG TGA ATG TTT TTT TTT TTC ACG CCG AAT CCT AGA CTA CTT TGG AAG AAA GAA GAA GAA GAG AGA AA
H1_L3	GAA GTG AAG AAG AAG AAA GAG AAG TTA ACC CAC GCC GAA TCC TAG ACT TTT TTT TTT TTC AAA GTA GTC TAG GAT TCG GCG TG
H2_L4	(Cy3) AGT CTA GGA TTC GGC GTG GGT TAA TTT TTT TTT TTC ACG CCG AAT CCT AGA C (TBHQ) A CTT TGG GAG GAG GAG AAG GAG AGG AGA GA
S1	ACC AGT CTA GAT GTG CTA TT**G AGG AGG AGA GGA GAG GAG AGG AA**
S2	TCC TAA AGC ATG ACC TTC CGC CTC TCC TCT CCT TCT CCT CCT CC
S3	TGT TTC AAG CGC AGC CAG AT**C TTC TCT TTC TTC TTC TTC ACT TC**
S4	TCT TCT GAT CCT TAA CGG CCC CTC TCC TCT CCT TCT CCT CCT CC
S5	GTT GCT GAA CTT TGG TTT GA**C TTC TCT TTC TTC TTC TTC ACT TC**
S6	TCT TCT GAT CGC CAC TAA CCT TTT CTC TCT TCT TCT TCT TTC TTC
I_H1	AGT CTA GGA TTC GGC GTG TCT TCC
BB	AGG TTA GTG GCG ATC AGA AGA AAT CTG GCT GCG CTT GAA ACA ACG GAA GGT CAT GCT TTA GGA ATC AAA CCA AAG TTC AGC AAC AGG CCG TTA AGG ATC AGA AGA AAT CTG GCT GCG CTT GAA ACA ACG GAA GGT CAT GCT TTA GGA GAA TAG CAC ATC TAG ACT GGT
H1_OR_1	TTC CTC TCC TCT CCT CTC CTC CTC AGG AAA CAC GCC GAA TCC TAG AGT TTT TTT TTT TTG ACC TGA CTC TAG GAT TCG GCG TG
H1_OR_2	GAA GTG AAG AAG AAG AAA GAG AAG GAA AGA CAC GCC GAA TCC TAG ACT TTT TTT TTT TTG ACC TGA CTC TAG GAT TCG GCG TG

H2_OR	(Cy3) ACT CTA GGA TTC GGC GTG GGT TAA TTT TTT TTT TTC ACG CCG AAT CCT AGA C (TBHQ) CAG GTC TTT TTT TTT ATA TGG TCA AGT GAA AAG CGG
ST_1	CCT TGG TCC ATA AAA CCG CAC **AAG GAG AGG AGA GGA GAG GAG GAG**
ST_2	TCT ATA CTG GCA AAA CGC TGT **CTT CAC TTC TTC TTC TTT CTC TTC**
I_OR_1	AGT CTA GGA TTC GGC GTG TTT CCT
I_OR_2	AGT CTA GGA TTC GGC GTG TCT TTC
T_1	(Alk) GCC CGC TTT TCA GTT GAC CAT ATA AGG TTA GTG GCG ATC AGA
T_2	(Alk) GTG CGG TTT TAT GGA CCA AGG CCA CAC AGC CGC GAA GAT
T_3	(Alk) ACA GCG TTT TGC CAG TAT AGA AGA AAT TAA GAT AGG CGC GGC

4.5.5. Small Molecule Synthesis & Characterization

Synthesis of Compound 2

Compound **1** (11.80g, 53.0mmol), was first dissolved in DMF (50mL). To this solution, tert-butyl-bromoacetate (11.40g, 58.0mmol) and Cs_2CO_3 (22.50g, 69.0mmol) were sequentially added and the reaction was left overnight to react. Next, the reaction was diluted with EtOAc (100mL) and H_2O (100mL). The organic phase was extracted 3 x with H_2O (100mL), then dried on $MgSO_4$, filtered and concentrated *in vacuo*. The crude mixture was then purified by column chromatography (9:1 Hex/EtOAc) to give compound **2** (14.6g, 82%). ^{1}H NMR (500MHz, $CDCl_3$): δ = 1.50 (s, 9H), 1.61 (m, 1H), 1.73 (m, 2H), 1.88 (m, 2H), 2.00 (m, 2H), 3.75 (m, 2H), 4.63 (s, 2H), 5.50 (s, 1H), 6.53 (s, 1H), 6.74 (m, 1H), 7.82 (m, 1H), 10.42 (s, 1H). ^{13}C NMR (125MHz, $CDCl_3$): 14.21, 18.33, 24.99, 28.03, 30.03, 61.96, 65.96, 82.82, 96.30, 100.43, 109.77, 130.25, 161.92, 163.54, 167.15, 188.34, 188.36. HRMS (EI): calc. for $[C_{18}H_{24}O_6Na]^+$ $[M]^+$: 359.16, found 359.1461.

Synthesis of Compound 3

To a solution of compound **2** (12.0g, 36.0mmol) in EtOH (100mL) was added p-toluenesulfonic acid (1.30g, 5.35mmol). The mixture reacted for 48hr at room temperature, at which point the reaction was complete by TLC. The solvent was evaporated *in vacuo* and the solution diluted with EtOAc (100mL) and H_2O (100mL). The aqueous phase was extracted 3 x with EtOAc (100mL) and then the combined organic phase was washed with saturated NaCl (100mL). The organic phase was then dried on $MgSO_4$, filtered and concentrated *in vacuo*, to then be purified by column chromatography (8:2 Hex/EtOAc). This resulted in the pure compound **3** (8.10g, 89%). ^{1}H NMR (500MHz, $CDCl_3$): δ = 1.51 (s, 9H), 4.62 (s, 2H), 6.34 (s, 1H), 6.54 (m, 1H), 7.76 (m, 1H), 10.33 (s, 1H). ^{13}C NMR (125MHz, $CDCl_3$): 28.04, 65.82, 83.28, 99.63, 109.60, 118.51, 131.08, 161.63, 164.17, 167.48, 189.19. HRMS (EI): calc. for $[C_{13}H_{16}O_5Na]^+$ $[M]^+$: 275.10, found 275.0956.

Synthesis of Compound 4

Compound **3** (5.30g, 20.8mmol) was first dissolved in CH_2Cl_2 (50mL) and 2,4,6-trivinylcyclotriboroxane-pyridine (5.00g, 20.8mmol), cesium carbonate (10.7g, 62.5mmol) and copper (II) acetate (6.03g, 62.5mmol) were added. The reaction was stirred for 24hr at room temperature. NH_4OAc buffer (3M, 100mL) was added and the solution left for an additional 30min. The mixture was then extracted 3 x with EtOAc (75mL), and the combined organic layers were washed with saturated NaCl (100mL), dried on $MgSO_4$, filtered and concentrated *in vacuo*. The crude product was then purified by column chromatography (8:2 Hex/EtOAc), to give compound **4** (5.80g, 78%). ^{1}H NMR (500MHz, $CDCl_3$): δ = 1.52 (s, 9H), 4.65 (m, 3H), 4.95 (m, 1H), 6.44 (s, 1H), 6.70 (m, 2H), 7.89 (m, 1H), 10.45 (s, 1H). ^{13}C NMR (125MHz, $CDCl_3$): 28.05, 66.00, 83.07, 98.48, 100.92, 109.28, 120.86, 130.62, 146.11, 161.84, 162.75, 166.93, 188.22. HRMS (EI): calc. for $[C_{15}H_{18}O_5Na]^+$ $[M]^+$: 301.12, found 301.1346.

Synthesis of Compound 5

Compound **4** (800mg, 2.87mmol) was dissolved in MeOH (20mL) and $NaBH_4$ (326mg, 8.61mmol) was added. The reaction proceeded for 90min at room temperature. The reaction was quenched with H_2O and then extracted with CH_2Cl_2 (3 x 50mL). The organic layers were dried on $MgSO_4$,

filtered and concentrated *in vacuo*. The crude mixture was then purified by column chromatography (9:1 Hex/EtOAc) to give compound **5** (764mg, 95%). ^{1}H NMR (500MHz, $CDCl_3$): δ = 1.51 (s, 9H), 4.47 (m, 1H), 4.60 (s, 2H), 4.69 (s, 2H) 4.80 (m, 1H), 6.49 (s, 1H), 6.62 (m, 2H), 7.23 (m, 1H). ^{13}C NMR (125MHz, $CDCl_3$): 28.06, 61.66, 66.04, 83.14, 95.61, 102.21, 109.43, 125.31, 130.26, 147.92, 157.19, 157.50, 168.09. HRMS (EI): calc. for $[C_{15}H_{20}O_5Na]^+$ $[M]^+$: 303.13, found 303.1296.

Synthesis of Compound 9

First, compound **8** (130mg, 0.23mmol) was dissolved in CH_2Cl_2 (5mL) and TFA (5mL) was added dropwise to the solution. This mixture reacted for 20min and the CH_2Cl_2 was then evaporated. The solution was re-suspended in CH_2Cl_2 (2x10mL) and evaporated twice more, to remove any TFA, leaving compound **8** as the TFA salt, which was redisolve in CH_2Cl_2 (5mL) and used directly. Separately, compound **5** (69.0mg, 0.25mmol) was first dissolved in CH_2Cl_2 (5mL), followed by the addition of p-nitrophenylchloroformate (47mg, 0.23mmol) and pyridine (0.10mL, 1.23mmol), in that order. This reaction was reacted for 2hr at room temperature until all the p-nitrophenylchloroformate was consumed and was also used directly. After this, the solution with the TFA salt of compound **8**, was added to the solution with compound **5** as well as DMAP (150mg, 1.23mmol). This mixture was left to react 12hr and then was washed with NH_4OAc buffer (3M, 20mL), saturated $NaHCO_3$ (20mL) and saturated NaCl (20mL). The organic layer was dried on $MgSO_4$, filtered and concentrated *in vacuo*. The crude product was then purified by column chromatography (1:1 Hex/EtOAc) to give compound **9** (70.0mg, 40%). ^{1}H NMR (500MHz, $CDCl_3$): δ = 1.49 (s, 9H), 3.01 (m, 6H), 3.55 (m, 4H), 3.86 (s, 3H), 4.46 (m, 1H), 4.54 (m, 2H), 4.79 (s, 1H) 5.23 (m, 2H), 6.42 (m, 1H), 6.59 (m, 2H), 6.64 (m, 1H), 6.71 (m, 1H), 6.78 (m, 3H), 7.15 (m, 2H), 7.32 (m, 1H), 7.65 (m, 2H), 8.05 (m, 1H). ^{13}C NMR (125MHz, $CDCl_3$): 14.21, 21.07, 28.04, 35.24, 35.37, 46.83, 55.60, 60.41, 82.44, 82.61, 95.74, 100.88, 101.55, 110.27, 110.98, 111.87, 117.57, 124.09, 125.05, 126.54, 128.89, 129.02, 129.79, 135.06, 147.64, 147.76, 151.83, 152.35, 153.10, 161.43, 169.35. HRMS (EI): calc. for $[C_{42}H_{42}O_{12}N_2Na]^+$ $[M]^+$: 789.27, found 789.2598.

Synthesis Conditions tried to make Compound 10

i) Compound **9** (100mg, 0.13mmol) was dissolved in CH_2Cl_2 (5mL) and TFA (5mL) was added dropwise to the solution. This mixture reacted for 20min and the CH_2Cl_2 was then evaporated. The solution was re-suspended in CH_2Cl_2 (2x10mL) and evaporated twice more, to remove any TFA. NMR and TLC confirmed reformation of compound **7**.

ii) Compound **5** (250mg, 0.89mmol), and KOH (200mg, 3.56mmol), were dissolved in H_2O:EtOH 1:1 (10mL), and refluxed for 3hr. Following this the solution was cooled to room temperature and acidified to pH 5 with acetic acid. The aqueous phase was then diluted with H_2O (40mL), extracted with CH_2Cl_2 (3 x 50mL) dried on $MgSO_4$, filtered and concentrated in vacuo. Crude NMR showed formation of 2-(5-hydroxy-2-(hydroxymethyl)phenoxy)acetic acid.

iii) To a solution of compound **5** (100mg, 0.36mmol), in 4mL of CH_2Cl_2 was added zinc bromide (240mg, 1.07mmol) and the solution was stirred for 24hr. At this time, 40mL of H_2O was added and the mixture was stirred for 2hr. The layers were separated, and the aqueous layer was extracted 3x40mL CH_2Cl_2. The combined organic fractions were then dried on $MgSO_4$, filtered and concentrated in vacuo.[66] Crude NMR showed formation of 2-(5-hydroxy-2-(hydroxymethyl)phenoxy)acetic acid.

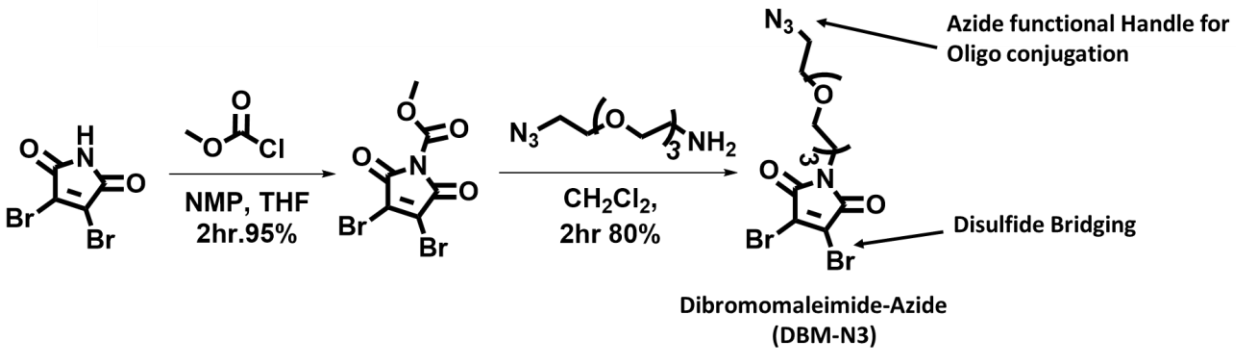

Figure 4. 25 Synthetic scheme for the generation of the small molecule DBM[67].

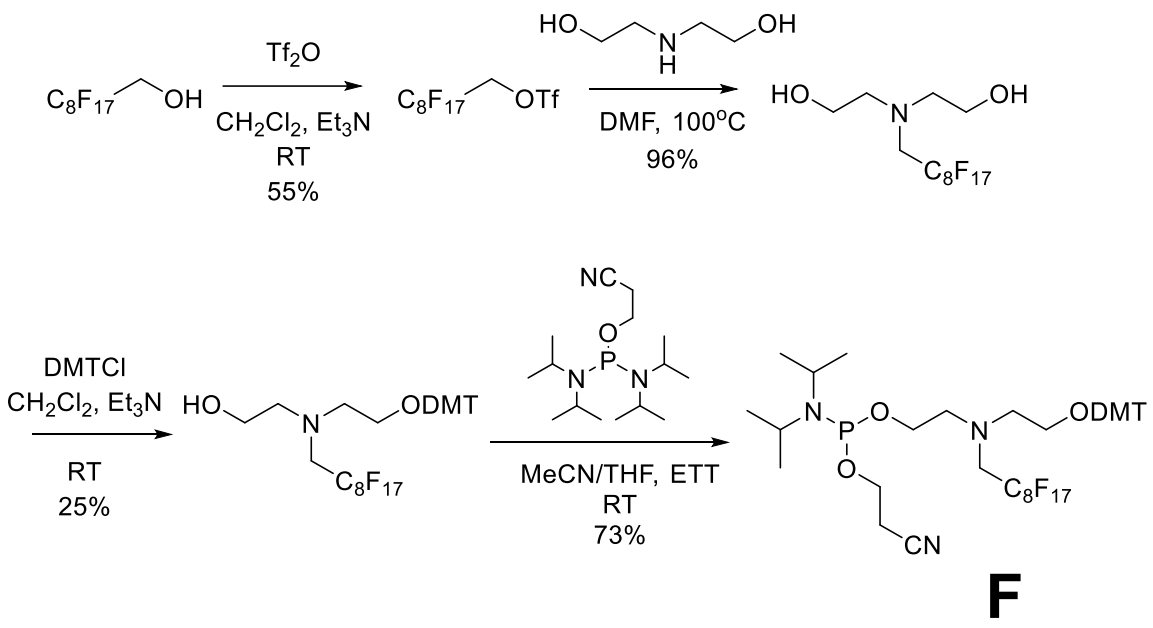

Figure 4. 26. Synthetic scheme for the synthesis of the per fluorinated phosphoramidite (F)[49].

4.5.6. Native AGE:

Native agarose gel electrophoresis was used to characterize ligated HCR, as well as SNA formation. In each case, 2.5% AGE was carried out at 4°C for 2.0 hours at a constant voltage of 100 V. Typical sample loading is 3.5 picomoles with respect to the DNA per lane (4.5 µL of 0.75 µM DNA). The gels were either stained with GelRed DNA stain and imaged under a DNA-selective channel or cyanine 3 channel. Band intensities were quantified using Image lab 5.2 software

4.5.7. Native PAGE:

Native PAGE assays (5-6%) by mixing with 1 µL of glycerol mix and loaded on to the gel with 1xTAMg as the running buffer. Typical sample loading is 3.5 picomoles with respect to the DNA per lane (4.5 µL of 0.75 µM DNA). The gel was run at 250 V for 1 hour, imaged in the cy3 channel and/or stained with GelRed and imaged.

4.5.8. SDS PAGE:

SDS PAGE was carried out by preparing protein samples in LDS sample buffer (4x). Typical sample loading amounts are 5uL of 1mg/mL (coomasie stain) and 1uL of 0.1mg/mL (silver stain). For non-

reducing, denaturing samples, the samples were incubated at 90 °C for 10 min. For non-reducing native samples, no heat shock was used. Samples were then loaded onto a 3-8% Tris-acetate gels and run for 120 min at 100 V with a tris-acetate SDS running buffer at 4°C. Gels were stained for protein with either coomasie stain or Pierce® silver staining kit and then visualized with a BioRad ChemiDoc MP system. Image analysis was carried out in ImageLab.

4.5.9. Reduction of antibodies with BME Procedure

Lyophilized Antibody (Ab) was first prepared and stored as a 9.09mg/mL solution in 1xPBS pH 7.2. Separately, a 10x (10M in optimized conditions) BME concentrated solution of BME in H_2O was made. 11uL of stock Ab was then diluted with 76uL H_2O, and 10uL of 10xPBS pH 7.2. 2uL of a 100mM EDTA solution was then added, followed by 1uL of the 10x BME solution. This gave a final Ab volume and concentration of 100uL, 1mg/mL. This solution was then held at 37°C for 2hr. The mixture was then cooled to room temperature and filtered twice through 7K Zeba® centrifugation filters according to the manufacture's directions to give (Ab_R) (85% yield).

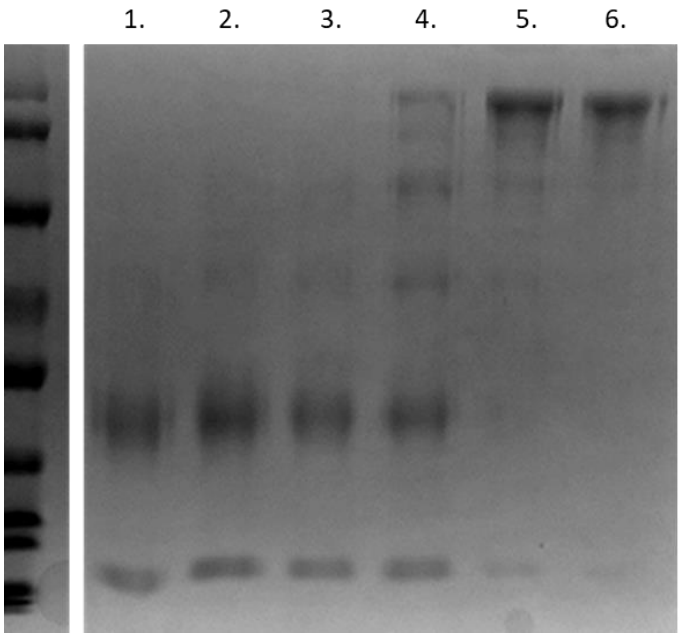

Figure 4. 27. non-reducing, denaturing, SDS PAGE of the titration of antibody with BME;

lane 1: Ab+100mM BME, lane 2: Ab+50mM BME, lane 3: Ab+25mM BME, lane 4: Ab+10mM BME, lane 5: Ab+1mM BME, lane 6: Ab

4.5.10. Optimized procedure for generation of Ab_N3

To a solution of (Ab_R) (100uL, 0.85mg/mL), was added 11.11uL of a 40mM solution of DBM in DMSO at 4°C. Bringing the final concentration of (DBM_N3) to 4mM and the volume and concentration of (Ab_R) to 111.11uL, 0.765mg/mL. This solution was left for 2hr at 4°C, at which point the solution was filtered twice through 7K Zeba® centrifugation filters according to the manufacture's directions to give (Ab_N3) (97.5% yield)

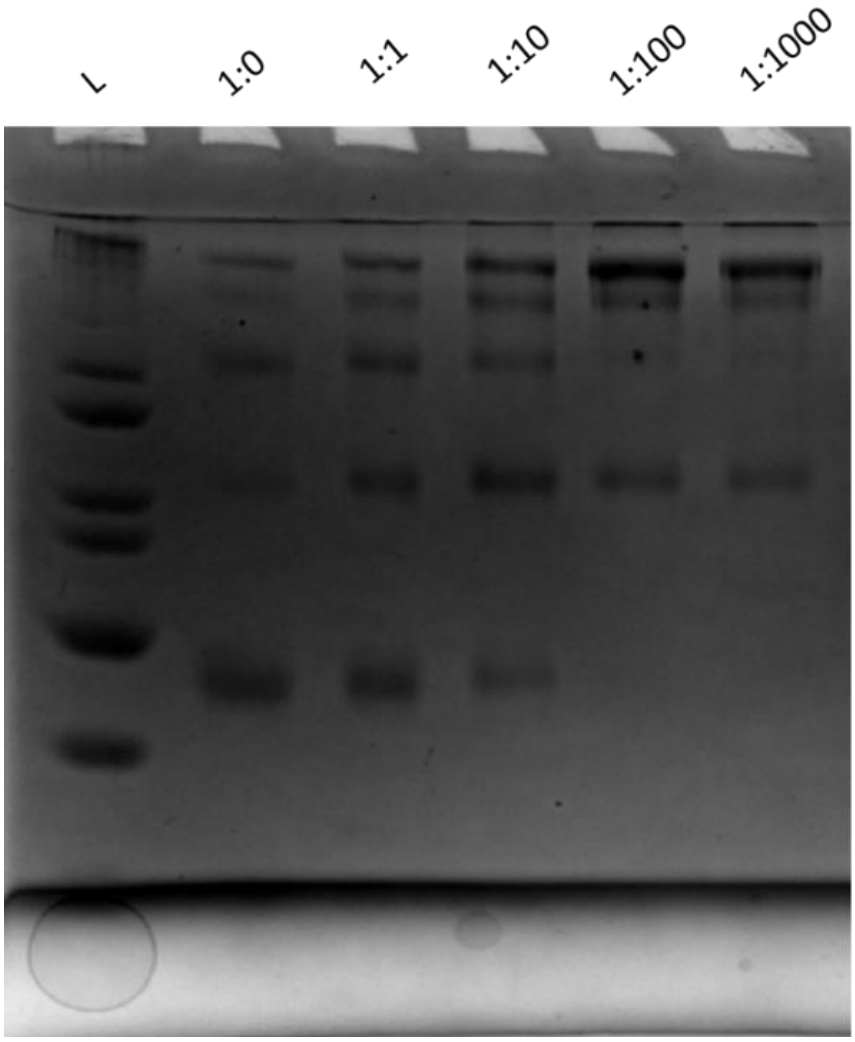

Figure 4. 28. non-reducing, denaturing, SDS PAGE of the titration of titration of Ab_R with DBM

Lane 1: Ladder, Lane 2: Ab_N3, Lane 3: Ab_N3+6uM DBM, Lane 4: Ab_N3+60uM DBM, Lane 5: Ab_N3+0.6mM DBM, lane 6: Ab_N3+ 6mM DBM.

4.5.11. DNA conjugation procedure

Crude DNA; (L) or L(2) were stored in H_2O and prepared for conjugation by diluting to 303uM in 1xPBS pH 7.2. Next, to (Ab_N3) (13.40uL, 0.746mg/ml), was added 6.60uL of either (L) or (L2), bringing the final concentrations of (L) or (L2) to 100uM and the (Ab_N3) to 20uL, 0.5mg/mL, at 4^{o}C for 12hr. Upon completion, the solution was diluted to 0.1mg/ml, 100uL with 1xPBS containing 0.1% tween, and filtered through amicon® ultracentrifugation filters 6x with 1xPBS containing 0.1% tween, to give (AOC) (40uL, 0.22mg/mL, 88% yield).

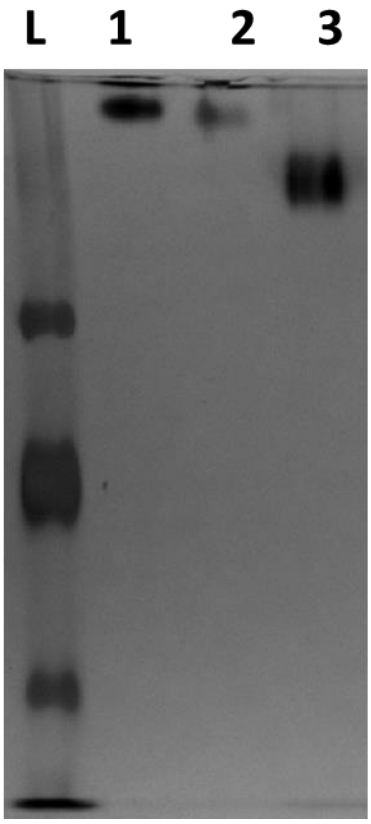

Figure 4. 29. Characterization of the generation of AOC by Native SDS PAGE; lane 1: Ab lane 2: Ab_N3, lane 3: AOC

4.5.12. Hybridization to antibody procedure

First, 4B, 2B and 1B were prepared as 1uM solutions in 1xPBS. To a solution of AOC, (5uL, 0.15mg/mL) in 1xPBS was added 5uL of either 4B, 2B or 1B, and left to hybridize at room temperature for 30min. Mixtures were then run by native TBE PAGE.

4.5.13. Hairpin Ligation procedure

Ligated HCR hairpins were generated by first preparing a 350mM solution of BME in 1xTAMg pH 8. All hairpins were first prepared as 20.51uM in 97.5uL in 1x TAMg pH 8 and thermocycled from 95^{o}C to 4^{o}C over 12hr. Following this 2.5uL of the BME solution was added to each of the hairpin solutions bring the final volume to 100uL and concentration to 20uM with 8.75mM BME. These solutions were left for 48 hr and then purified directly by RP-HPLC (3-50% ACN in 50 mins) and finally analyzed by LC-MS to give ligated hairpins.

Table 4. 2 Predicted and found masses of ligated HCR hairpins:

Name:	Calculated	Found
H1_DD_lig	15865.59	15864.87
H2_DD_lig	15816.55	15815.87
H1_SDD_lig[Na^+]	17157.43	17155.64
H2_SDD_lig[Na^+]	17072.33	17070.71
H1_B_lig	15343.13	15280.55
H2_T_lig	16496.84	16496.28
H1_M_lig	15343.13	15432.47
H2_M_lig	16496.84	16496.42
H1_B_2_lig	12511.57	12511.34
H2_T_2_lig	12387.53	12387.19

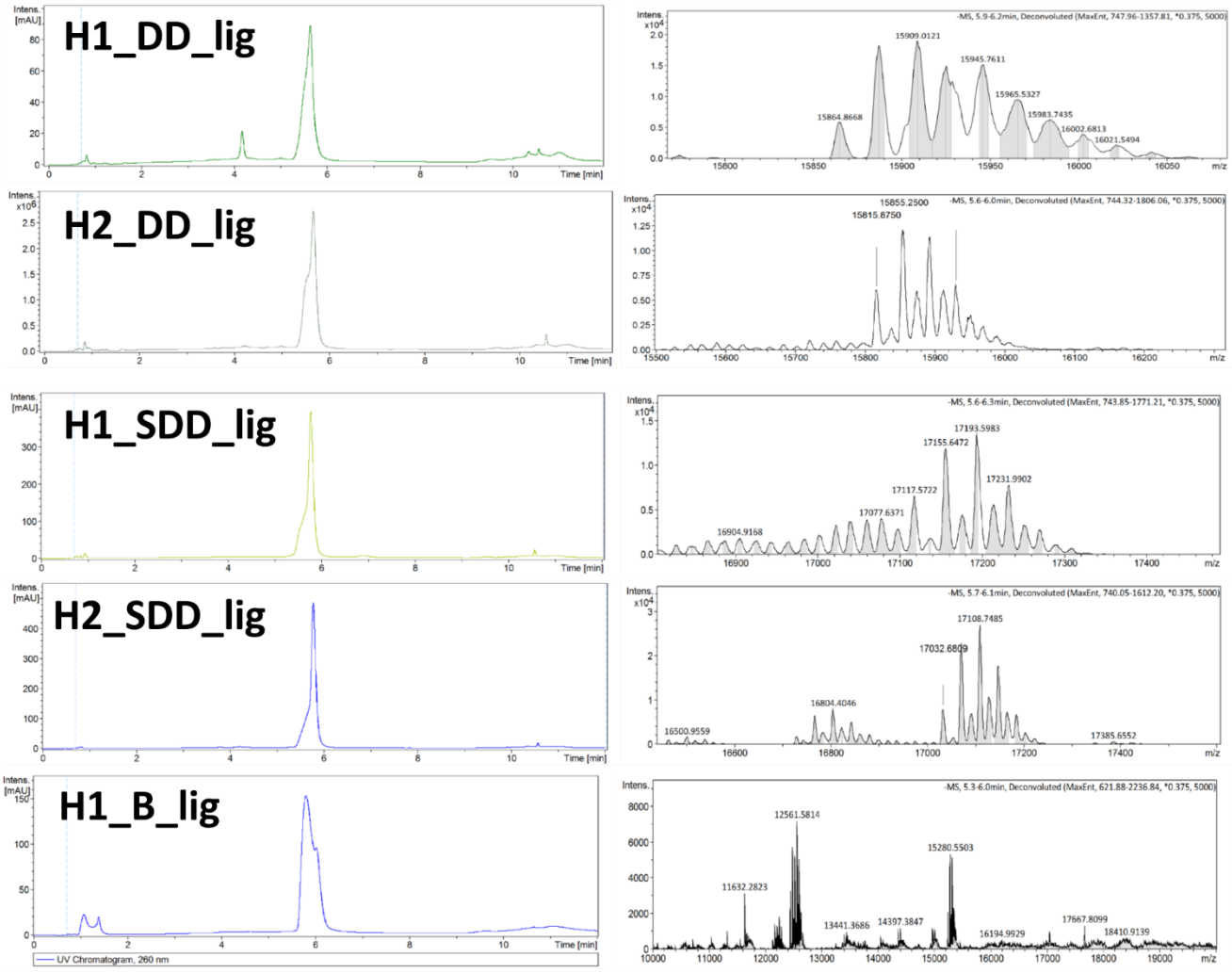
H1_DD_lig
H2_DD_lig
H1_SDD_lig
H2_SDD_lig
H1_B_lig
Intens. [mAU]
Time [min]
UV Chromatogram, 260 nm
-MS, 5.9-6.2min, Deconvoluted (MaxEnt, 747.96-1357.81, *0.375, 5000)
15909.0121
15945.7611
15965.5327
15983.7435
16002.6813
16021.5494
15864.8668
-MS, 5.6-6.0min, Deconvoluted (MaxEnt, 744.32-1806.06, *0.375, 5000)
15855.2500
15815.8750
-MS, 5.6-6.3min, Deconvoluted (MaxEnt, 743.85-1771.21, *0.375, 5000)
17193.5983
17155.6472
17231.9902
17117.5722
17077.6371
16904.9168
-MS, 5.7-6.1min, Deconvoluted (MaxEnt, 740.05-1612.20, *0.375, 5000)
17108.7485
17032.6809
16804.4046
16500.9559
17385.6552
-MS, 5.3-6.0min, Deconvoluted (MaxEnt, 621.88-2236.84, *0.375, 5000)
12561.5814
15280.5503
11632.2823
13441.3686
14397.3847
16194.9929
17667.8099
18410.9139
m/z

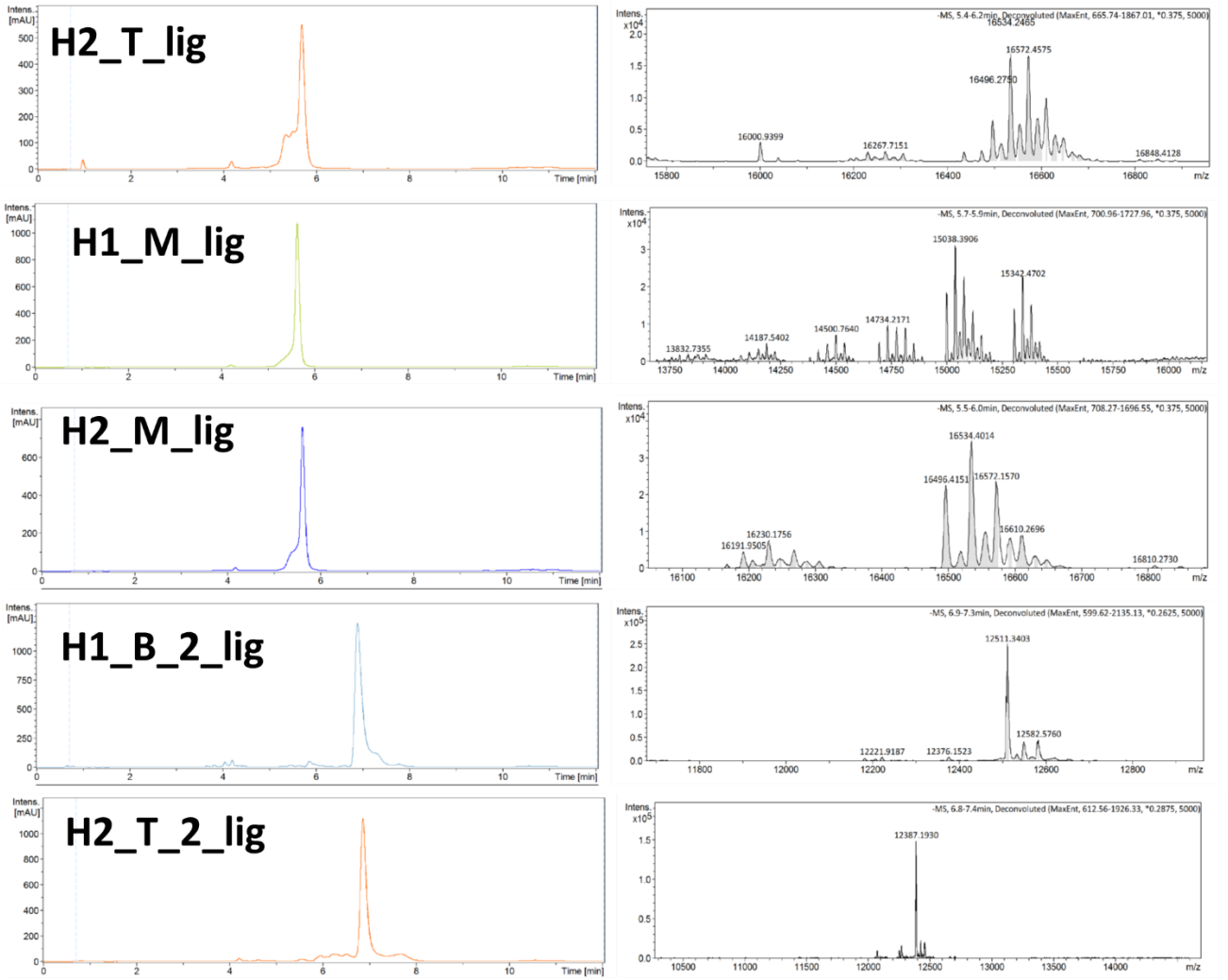

Figure 4. 30. RP_HPLC traces and LC-MS of ligated strands

4.5.14. Ligated HCR polymerization Procedure

For each design, to a solution of I (100uL, 30uM) in 1xPBS pH 8, was added DTT (1µL, 1M) in 1xPBS pH 8 and allowed to react for 12 hours. The solution was then filtered through microcon© 10k filters 6 times with 1xPBS pH 8 to remove the excess DTT to give reduced I strands. After filtration, the DNA was re-quantified, adjusted to 3uM and used without any further purification. H1 and H2 were then prepared separately as 3µM solutions in 1xPBS pH 8. Non-ligated H1 and H2 were thermocycled from 95°C to 4°C over 4hr. I was diluted to 0.300µM (0.1eq), and 0.03µM (0.01eq), in 1xPBS pH 8. Experiments were then performed by first mixing 25µL of H1 and H2, then diluting with 25µL 1xPBS pH 8. For dynamic conditions the mixture was diluted with 25uL of a 40mM

solution of BME in 1xPBS pH 8. 25µL of initiator was then added according to the specific initiator equivalency, to give 100µL of 750nM final concentrations of each hairpin. For samples with no initiator 25µL of 1xPBS pH 8 was added instead.

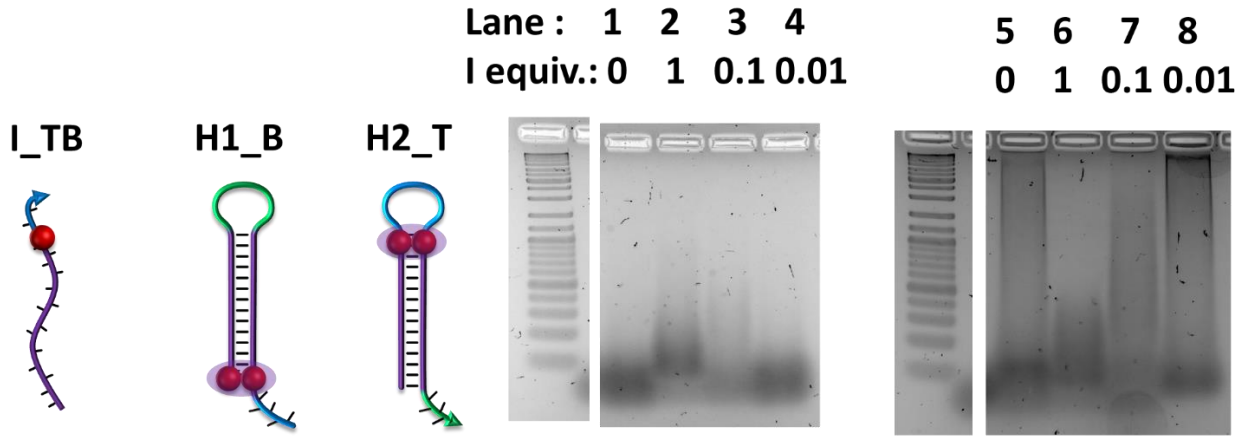

Figure 4. 31. Native AGE of TB design, ligated HCR over 96hr.

4.5.15. Temporal growth Assembly and initiation procedure

Strands; H1_L1, H2_L2, H1_L3, H2_L4, S1, S2, S3, S4, S5 and S6 were all first prepared as 35uL, 2.0uM solutions in 1xTAMg. BB and I_H1 were prepared as 15uL, 1uM solutions in 1xTAMg. Sperate solutions of (H1_L1 and S1), (H2_L2 and S2), (H1_L3 and S3), (H2_L2 and S4), (H1_L3 and S5) and (H2_L4 and S6) were prepared by mixing 15uL of each strand. These 6 mixtures were then thermocycled from 95°C to 4°C over 12hr. Following this, 10uL of BB, 10uL of (H1_L1 and S1), 20uL of), (H2_L2 and S2), 20uL of (H1_L3 and S3), 10uL of (H2_L2 and S4), 10uL of (H1_L3 and S5), and 10uL of (H2_L4 and S6) were mixed, to have a final volume and concentration of 90uL, 111nM and then thermocycled from 44°C to 20°C over 4hr. When no template was used, 10uL of 1xTAMg was used instead. To initiate the HCR process, 10uL of I_H1 was added to the solution at room temperature and monitored by fluorescence. When no initiator was used 10uL of 1xTAMg was used instead.

4.5.16. Preparation of trimer template

The preparation of the trimer template was done following the previously established protocols using T1, T2, and T3 as the templated alkyne strands.[45]

4.5.17. Trimer assembly and OR initiation procedure

First, the DNA trimer, H2_OR, I_OR_1, and I_OR_2 were all made as 5uL, 250nM solutions in 1xTAMg. H1_OR_1, H1_OR_2, ST_1 and ST_2 were prepared as 5uL, 500nM solutions in 1xTAMg. 5uL of trimer and 2.5uL of H1_OR_1, H1_OR_2, ST_1 and ST_2 were then mixed and thermocycled from 95^{o}C to 4^{o}C over 12hr. When no template was used, 5uL of 1xTAMg was used instead. H2_OR was separately thermocycled from 95^{o}C to 4^{o}C over 12hr. Following this, 5uL of H2_OR was added to the trimer mixture and the mixture was thermocycled from 44^{o}C to 20^{o}C over 4hr. To initiate, either 5uL of I_OR_1 *or* I_OR_2 was added to the solution at room temperature and left for 24hr. When no initiator was used 10uL of 1xTAMg was used instead.

4.5.18. CHA SNA Assembly procedures

i) For the C12, PSC12, perF and HEG designs; ASO', ASO and F were all prepared initially as 9uM solutions in 1xTAMg. Equal volumes of each strand were then mixed together to give a final concentration of 3uM of each strand and thermocycled from 95^{o}C to 4^{o}C over 12hr.

ii) For the titration of the PSC12 design in figure 4 .14 c) ASO'PS_C12 and ASOPS_Cy3 were first prepared as 9uM solutions in 1xTAMg. FPS_C12, was prepared as 9uM (1:1), 12.0uM (0.75:1), 18uM (0.5:1) and 36uM (0.25:1) in 1xTAMg. For each ratio, an equal volume of ASO'PS_C12, ASOPS_Cy3 and FPS_C12 were mixed together to always give a final concentration of 3uM with respect to the ASOPS_Cy3 strand. The mixtures were then thermocycled from 95^{o}C to 4^{o}C over 12hr.

iii) For the titration of the PSC12 design in figure 4 .14 d) ASO'PS_C12 and ASOPS_Cy3 were first prepared as 9uM solutions in 1xTAMg. FPS_C12, was prepared as 9uM (1:1), 12.0uM (0.75:1), 18uM (0.5:1) and 36uM (0.25:1) in 1xTAMg. An equal volume of FPS_C12 and ASO'PS_C12 were mixed together and thermocycled from 95^{o}C to 4^{o}C over 12hr. Following this, ASOPS_Cy3 was then added to the mixture in an equal volume and the mixture was thermocycled from 44^{o}C to 20^{o}C over 4hr.

4.5.19. CHA initiation procedure

For each design assessed, H1, H2 and I were prepared separately as 3µM solutions in 1xPBS pH 8 and thermocycled from 95°C to 4°C over 4hr. 10uL of I was diluted 10x to 0.300µM (0.1eq) in 1xPBS pH 8. The SNA assemblies were prepared following 3.x. Experiments were then performed by first mixing 25µL of H1 and H2, and the SNA. 25µL of initiator was then added according to the specific initiator equivalency, to give 100µL of 750nM final concentrations of each mixture. For samples with no initiator or no hairpins, 25µL or 75uL of 1xPBS pH 8 was added respectively.

4.5.20. Gold nanoparticle conjugation

AuNPs functionalized with FPS_GNP strands were prepared by heating purified 12 nm AuNPs (20 to 50 pmol) with 100 equiv. FPS_GNP strands in 1×HEPESNa buffer (total volume 50 to 100 µL) to 50 °C for 1 hr and cooling down to 20 °C over 30 min in a thermal cycler. Then, 40,000 equiv. OEG ligand was added to the solution and incubated for 30 min at room temperature to further passivate the unprotected surface of the AuNP. Next, the poly-conjugated AuNP seeds were washed 5 times with fresh 1×HEPESNa buffer in an 100 kDa Amicon Ultra 0.5 mL centrifugal filter Unit to remove the DNA strands and OEG in excess and then re-quantified on the plate reader based on the absorbance at 450 nm.

4.5.21. Gold nanoparticle assembly

ASO'PS_GNP and ASOPS_Cy3 were prepared initially as 12uM solutions in 1xTAMg pH 8. Equal volumes of each strand (10uL) were then mixed together to give a final concentration of 6uM (20uL) of each strand and thermocycled from 95°C to 4°C over 12hr. A serial dilution was then performed on this solution with 1xTAMg to give solutions with concentrations of 6uM, 3uM, 1.50uM, 0.75uM and 0.375uM 10uL each. The gold nanoparticle functionalized with FPS_GNP was prepared as a 0.06uM solution in 1x TAMg pH 8. Equal volumes (5uL) of each the GNP and ASO duplex were mixed and thermocycled from 44°C to 20°C over 4hr and analyzed by native AGE.

4.5.22. AFM procedure

AFM and TEM sample preparation Samples for AFM imaging were prepared by depositing 5 µL of the sample (5 nM origami) onto a freshly cleaved mica surface for 30 seconds, followed by three times washing with 50 µL of Millipore water. Excess liquid was blown off and dried by a stream of compressed air for 30 seconds. The sample was then put under vacuum for at least 2 hrs prior to imaging. AFM images were acquired in ScanAsyst mode under dry conditions using ScanAsyst-Air silicon tip on nitride lever (tip radius = 2 nm, k = 0.4 N/m, fo = 70 kHz; Bruker).

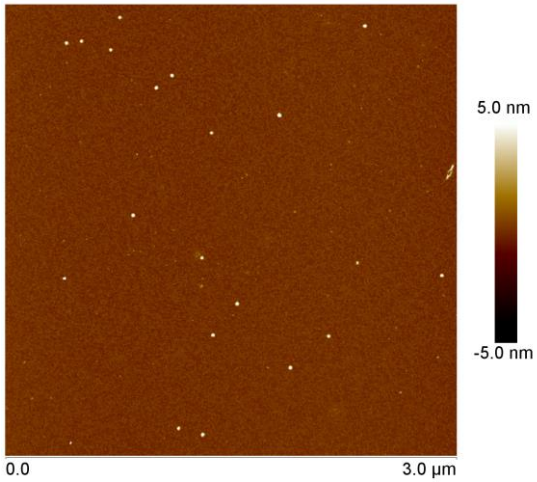

Figure 4. 32. AFM of the SNA's formed with ASO'_C12, F_C12 and ASO

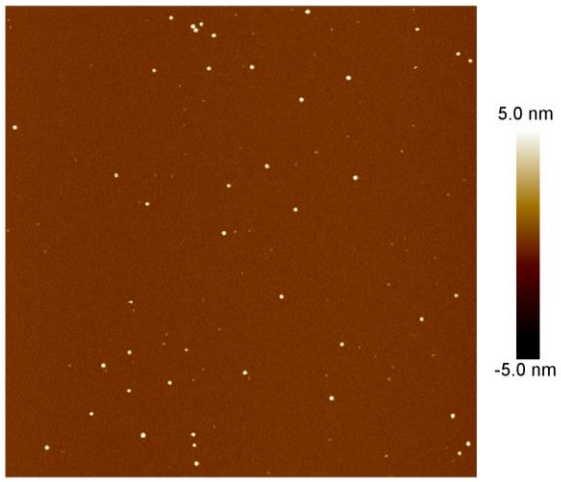

Figure 4. 33.. AFM of the SNA's formed with HEG_ASO'PS_C12 & HEG_FPS_C12 & ASOPS_Cy3

4.6. References

1. Gurevich, E. V.; Gurevich, V. V., Therapeutic potential of small molecules and engineered proteins. *Handb. Exp. Pharmacol.* **2014,** *219*, 1-12.
2. AlSawaftah, N.; Pitt, W. G.; Husseini, G. A., Dual-Targeting and Stimuli-Triggered Liposomal Drug Delivery in Cancer Treatment. *ACS Pharmacology & Translational Science* **2021,** *4* (3), 1028-1049.
3. Xie, A.; Hanif, S.; Ouyang, J.; Tang, Z.; Kong, N.; Kim, N. Y.; Qi, B.; Patel, D.; Shi, B.; Tao, W., Stimuli-responsive prodrug-based cancer nanomedicine. *EBioMedicine* **2020,** *56*, 102821.
4. Jana, S.; Mandlekar, S.; Marathe, P., Prodrug Design to Improve Pharmacokinetic and Drug Delivery Properties: Challenges to the Discovery Scientists. *Curr. Med. Chem.* **2010,** *17* (32), 3874-3908.
5. Taresco, V.; Alexander, C.; Singh, N.; Pearce, A. K., Stimuli-Responsive Prodrug Chemistries for Drug Delivery. **2018,** *1* (4), 1800030.
6. Zhang, Y.; Cui, H.; Zhang, R.; Zhang, H.; Huang, W., Nanoparticulation of Prodrug into Medicines for Cancer Therapy. *n/a* (n/a), 2101454.
7. Francis, R.; Gopalan, G. P.; Sivadas, A.; Joy, N., Properties of Stimuli-Responsive Polymers. In *Biomedical Applications of Polymeric Materials and Composites*, 2016; pp 187-231.
8. Singh, U.; Morya, V.; Datta, B.; Ghoroi, C.; Bhatia, D., Stimuli Responsive, Programmable DNA Nanodevices for Biomedical Applications. **2021,** *9* (514).
9. Yu, Y.; Jin, B.; Li, Y.; Deng, Z., Stimuli-Responsive DNA Self-Assembly: From Principles to Applications. *Chemistry – A European Journal* **2019,** *25* (42), 9785-9798.
10. Wang, H.; Luo, D.; Wang, H.; Wang, F.; Liu, X., Construction of Smart Stimuli-Responsive DNA Nanostructures for Biomedical Applications. **2021,** *27* (12), 3929-3943.
11. Bujold, K. E.; Hsu, J. C. C.; Sleiman, H. F., Optimized DNA "Nanosuitcases" for Encapsulation and Conditional Release of siRNA. *Journal of the American Chemical Society* **2016,** *138* (42), 14030-14038.
12. Fakih, H. H.; Fakhoury, J. J.; Bousmail, D.; Sleiman, H. F., Minimalist Design of a Stimuli-Responsive Spherical Nucleic Acid for Conditional Delivery of Oligonucleotide Therapeutics. *ACS Appl. Mater. Interfaces* **2019,** *11* (15), 13912-13920.
13. Lacroix, A.; Vengut-Climent, E.; de Rochambeau, D.; Sleiman, H. F., Uptake and Fate of Fluorescently Labeled DNA Nanostructures in Cellular Environments: A Cautionary Tale. *ACS Central Science* **2019,** *5* (5), 882-891.
14. Lacroix, A.; Sleiman, H. F., DNA Nanostructures: Current Challenges and Opportunities for Cellular Delivery. *ACS Nano* **2021,** *15* (3), 3631-3645.
15. Ren, K.; Liu, Y.; Wu, J.; Zhang, Y.; Zhu, J.; Yang, M.; Ju, H., A DNA dual lock-and-key strategy for cell-subtype-specific siRNA delivery. *Nature Communications* **2016,** *7* (1), 13580.
16. Li, S.; Jiang, Q.; Liu, S.; Zhang, Y.; Tian, Y.; Song, C.; Wang, J.; Zou, Y.; Anderson, G. J.; Han, J.-Y.; Chang, Y.; Liu, Y.; Zhang, C.; Chen, L.; Zhou, G.; Nie, G.; Yan, H.; Ding, B.; Zhao, Y., A DNA nanorobot functions as a cancer therapeutic in response to a molecular trigger in vivo. *Nat. Biotechnol.* **2018,** *36* (3), 258-264.
17. Zhu, G.; Zheng, J.; Song, E.; Donovan, M.; Zhang, K.; Liu, C.; Tan, W., Self-assembled, aptamer-tethered DNA nanotrains for targeted transport of molecular drugs in cancer theranostics. *Proceedings of the National Academy of Sciences* **2013,** *110* (20), 7998-8003.
18. Nejadmoghaddam, M.-R.; Minai-Tehrani, A.; Ghahremanzadeh, R.; Mahmoudi, M.; Dinarvand, R.; Zarnani, A.-H., Antibody-Drug Conjugates: Possibilities and Challenges. *Avicenna J Med Biotechnol* **2019,** *11* (1), 3-23.
19. Ji, X.; Pan, Z.; Yu, B.; De La Cruz, L. K.; Zheng, Y.; Ke, B.; Wang, B., Click and release: bioorthogonal approaches to "on-demand" activation of prodrugs. *Chem. Soc. Rev.* **2019,** *48* (4), 1077-1094.

20. Rossin, R.; Versteegen, R. M.; Wu, J.; Khasanov, A.; Wessels, H. J.; Steenbergen, E. J.; ten Hoeve, W.; Janssen, H. M.; van Onzen, A. H. A. M.; Hudson, P. J.; Robillard, M. S., Chemically triggered drug release from an antibody-drug conjugate leads to potent antitumour activity in mice. *Nature Communications* **2018,** *9* (1), 1484.
21. Bagshawe, K. D.; Sharma, S. K.; Begent, R. H. J., Antibody-directed enzyme prodrug therapy (ADEPT) for cancer. *Expert Opinion on Biological Therapy* **2004,** *4* (11), 1777-1789.
22. Sharma, S. K.; Bagshawe, K. D., Antibody Directed Enzyme Prodrug Therapy (ADEPT): Trials and tribulations. *Adv. Drug Delivery Rev.* **2017,** *118*, 2-7.
23. Beck, A.; Goetsch, L.; Dumontet, C.; Corvaïa, N., Strategies and challenges for the next generation of antibody–drug conjugates. *Nat. Rev. Drug Discovery* **2017,** *16* (5), 315-337.
24. Gonzaga, R. V.; do Nascimento, L. A.; Santos, S. S.; Machado Sanches, B. A.; Giarolla, J.; Ferreira, E. I., Perspectives About Self-Immolative Drug Delivery Systems. *J. Pharm. Sci.* **2020,** *109* (11), 3262-3281.
25. Grinda, M.; Legigan, T.; Clarhaut, J.; Peraudeau, E.; Tranoy-Opalinski, I.; Renoux, B.; Thomas, M.; Guilhot, F.; Papot, S., An enzyme-responsive system programmed for the double release of bioactive molecules through an intracellular chemical amplification process. *Org. Biomol. Chem.* **2013,** *11* (41), 7129-7133.
26. Cuellar, T. L.; Barnes, D.; Nelson, C.; Tanguay, J.; Yu, S.-F.; Wen, X.; Scales, S. J.; Gesch, J.; Davis, D.; van Brabant Smith, A.; Leake, D.; Vandlen, R.; Siebel, C. W., Systematic evaluation of antibody-mediated siRNA delivery using an industrial platform of THIOMAB–siRNA conjugates. *Nucleic Acids Res.* **2014,** *43* (2), 1189-1203.
27. Karver, M. R.; Weissleder, R.; Hilderbrand, S. A., Synthesis and Evaluation of a Series of 1,2,4,5-Tetrazines for Bioorthogonal Conjugation. *Bioconjugate Chem.* **2011,** *22* (11), 2263-2270.
28. Carlson, J. C. T.; Mikula, H.; Weissleder, R., Unraveling Tetrazine-Triggered Bioorthogonal Elimination Enables Chemical Tools for Ultrafast Release and Universal Cleavage. *J. Am. Chem. Soc.* **2018,** *140* (10), 3603-3612.
29. Versteegen, R. M.; Rossin, R.; ten Hoeve, W.; Janssen, H. M.; Robillard, M. S., Click to Release: Instantaneous Doxorubicin Elimination upon Tetrazine Ligation. **2013,** *52* (52), 14112-14116.
30. Wu, H.; Alexander, S. C.; Jin, S.; Devaraj, N. K., A Bioorthogonal Near-Infrared Fluorogenic Probe for mRNA Detection. *J. Am. Chem. Soc.* **2016,** *138* (36), 11429-11432.
31. Neumann, K.; Jain, S.; Gambardella, A.; Walker, S. E.; Valero, E.; Lilienkampf, A.; Bradley, M., Tetrazine-Responsive Self-immolative Linkers. **2017,** *18* (1), 91-95.
32. Li, S.; Li, P.; Ge, M.; Wang, H.; Cheng, Y.; Li, G.; Huang, Q.; He, H.; Cao, C.; Lin, D.; Yang, L., Elucidation of leak-resistance DNA hybridization chain reaction with universality and extensibility. *Nucleic Acids Res.* **2020,** *48* (5), 2220-2231.
33. Ang, Y. S.; Yung, L.-Y. L., Rational design of hybridization chain reaction monomers for robust signal amplification. *Chem. Commun.* **2016,** *52* (22), 4219-4222.
34. Choi, H. M. T.; Beck, V. A.; Pierce, N. A., Next-Generation in Situ Hybridization Chain Reaction: Higher Gain, Lower Cost, Greater Durability. *ACS Nano* **2014,** *8* (5), 4284-4294.
35. Choi, H. M. T.; Schwarzkopf, M.; Fornace, M. E.; Acharya, A.; Artavanis, G.; Stegmaier, J.; Cunha, A.; Pierce, N. A., Third-generation in situ hybridization chain reaction: multiplexed, quantitative, sensitive, versatile, robust. *Development* **2018,** *145* (12).
36. Figg, C. A.; Winegar, P. H.; Hayes, O. G.; Mirkin, C. A., Controlling the DNA Hybridization Chain Reaction. *J. Am. Chem. Soc.* **2020,** *142* (19), 8596-8601.
37. Bui, H.; Miao, V.; Garg, S.; Mokhtar, R.; Song, T.; Reif, J., Design and Analysis of Localized DNA Hybridization Chain Reactions. *Small* **2017,** *13* (12), 1602983.
38. Bui, H.; Shah, S.; Mokhtar, R.; Song, T.; Garg, S.; Reif, J., Localized DNA Hybridization Chain Reactions on DNA Origami. *ACS Nano* **2018,** *12* (2), 1146-1155.

39. Ren, K.; Xu, Y.; Liu, Y.; Yang, M.; Ju, H., A Responsive "Nano String Light" for Highly Efficient mRNA Imaging in Living Cells via Accelerated DNA Cascade Reaction. *ACS Nano* **2018,** *12* (1), 263-271.
40. Amiram, M.; Quiroz, F. G.; Callahan, D. J.; Chilkoti, A., A highly parallel method for synthesizing DNA repeats enables the discovery of 'smart' protein polymers. *Nat. Mater.* **2011,** *10* (2), 141-148.
41. Liu, D.; Daubendiek, S. L.; Zillman, M. A.; Ryan, K.; Kool, E. T., Rolling Circle DNA Synthesis: Small Circular Oligonucleotides as Efficient Templates for DNA Polymerases. *J. Am. Chem. Soc.* **1996,** *118* (7), 1587-1594.
42. Hamblin, G. D.; Rahbani, J. F.; Sleiman, H. F., Sequential growth of long DNA strands with user-defined patterns for nanostructures and scaffolds. *Nature Communications* **2015,** *6* (1), 7065.
43. Rahbani, J. F.; Hsu, J. C. C.; Chidchob, P.; Sleiman, H. F., Single-stranded templates as railroad tracks for hierarchical assembly of DNA origami. *Nanoscale* **2018,** *10* (29), 13994-13999.
44. Lau, K. L.; Sleiman, H. F., Minimalist Approach to Complexity: Templating the Assembly of DNA Tile Structures with Sequentially Grown Input Strands. *ACS Nano* **2016,** *10* (7), 6542-51.
45. Trinh, T.; Saliba, D.; Liao, C.; de Rochambeau, D.; Prinzen, A. L.; Li, J.; Sleiman, H. F., "Printing" DNA Strand Patterns on Small Molecules with Control of Valency, Directionality, and Sequence. *Angew. Chem. Int. Ed.* **2019,** *58* (10), 3042-3047.
46. Morihiro, K.; Ankenbruck, N.; Lukasak, B.; Deiters, A., Small Molecule Release and Activation through DNA Computing. *J. Am. Chem. Soc.* **2017,** *139* (39), 13909-13915.
47. Chatterjee, G.; Dalchau, N.; Muscat, R. A.; Phillips, A.; Seelig, G., A spatially localized architecture for fast and modular DNA computing. *Nat. Nanotechnol.* **2017,** *12*, 920.
48. Hamblin, G. D.; Rahbani, J. F.; Sleiman, H. F., Sequential growth of long DNA strands with user-defined patterns for nanostructures and scaffolds. *Nature Communications* **2015,** *6*, 7065.
49. de Rochambeau, D.; Barłóg, M.; Edwardson, T. G. W.; Fakhoury, J. J.; Stein, R. S.; Bazzi, H. S.; Sleiman, H. F., "DNA–Teflon" sequence-controlled polymers. *Polymer Chemistry* **2016,** *7* (31), 4998-5003.
50. Guo, Q.; Han, J.-J.; Shan, S.; Liu, D.-F.; Wu, S.-S.; Xiong, Y.-H.; Lai, W.-H., DNA-based hybridization chain reaction and biotin–streptavidin signal amplification for sensitive detection of Escherichia coli O157:H7 through ELISA. *Biosens. Bioelectron.* **2016,** *86*, 990-995.
51. Lin, R.; Feng, Q.; Li, P.; Zhou, P.; Wang, R.; Liu, Z.; Wang, Z.; Qi, X.; Tang, N.; Shao, F.; Luo, M., A hybridization-chain-reaction-based method for amplifying immunosignals. *Nat. Methods* **2018,** *15* (4), 275-278.
52. Dugal-Tessier, J.; Thirumalairajan, S.; Jain, N., Antibody-Oligonucleotide Conjugates: A Twist to Antibody-Drug Conjugates. *J Clin Med* **2021,** *10* (4), 838.
53. Dovgan, I.; Koniev, O.; Kolodych, S.; Wagner, A., Antibody–Oligonucleotide Conjugates as Therapeutic, Imaging, and Detection Agents. *Bioconjugate Chem.* **2019,** *30* (10), 2483-2501.
54. Schumacher, F. F.; Nunes, J. P. M.; Maruani, A.; Chudasama, V.; Smith, M. E. B.; Chester, K. A.; Baker, J. R.; Caddick, S., Next generation maleimides enable the controlled assembly of antibody–drug conjugates via native disulfide bond bridging. *Org. Biomol. Chem.* **2014,** *12* (37), 7261-7269.
55. Schweitzer, B.; Wiltshire, S.; Lambert, J.; O'Malley, S.; Kukanskis, K.; Zhu, Z.; Kingsmore, S. F.; Lizardi, P. M.; Ward, D. C., Immunoassays with rolling circle DNA amplification: a versatile platform for ultrasensitive antigen detection. *Proc. Natl. Acad. Sci. U. S. A.* **2000,** *97* (18), 10113-9.
56. Schnitzbauer, J.; Strauss, M. T.; Schlichthaerle, T.; Schueder, F.; Jungmann, R., Super-resolution microscopy with DNA-PAINT. *Nat. Protoc.* **2017,** *12* (6), 1198-1228.
57. Agasti, S. S.; Wang, Y.; Schueder, F.; Sukumar, A.; Jungmann, R.; Yin, P., DNA-barcoded labeling probes for highly multiplexed Exchange-PAINT imaging. *Chemical Science* **2017,** *8* (4), 3080-3091.
58. Wiener, J.; Kokotek, D.; Rosowski, S.; Lickert, H.; Meier, M., Preparation of single- and double-oligonucleotide antibody conjugates and their application for protein analytics. *Scientific Reports* **2020,** *10* (1), 1457.

59. Liu, H.; Chumsae, C.; Gaza-Bulseco, G.; Hurkmans, K.; Radziejewski, C. H., Ranking the susceptibility of disulfide bonds in human IgG1 antibodies by reduction, differential alkylation, and LC-MS analysis. *Anal. Chem.* **2010,** *82* (12), 5219-26.
60. Sugo, T.; Terada, M.; Oikawa, T.; Miyata, K.; Nishimura, S.; Kenjo, E.; Ogasawara-Shimizu, M.; Makita, Y.; Imaichi, S.; Murata, S.; Otake, K.; Kikuchi, K.; Teratani, M.; Masuda, Y.; Kamei, T.; Takagahara, S.; Ikeda, S.; Ohtaki, T.; Matsumoto, H., Development of antibody-siRNA conjugate targeted to cardiac and skeletal muscles. *Journal of controlled release : official journal of the Controlled Release Society* **2016,** *237*, 1-13.
61. Hsu, N.-S.; Lee, C.-C.; Kuo, W.-C.; Chang, Y.-W.; Lo, S.-Y.; Wang, A. H. J., Development of a Versatile and Modular Linker for Antibody–Drug Conjugates Based on Oligonucleotide Strand Pairing. *Bioconjugate Chem.* **2020,** *31* (7), 1804-1811.
62. Walsh, S. J.; Omarjee, S.; Galloway, W. R. J. D.; Kwan, T. T. L.; Sore, H. F.; Parker, J. S.; Hyvönen, M.; Carroll, J. S.; Spring, D. R., A general approach for the site-selective modification of native proteins, enabling the generation of stable and functional antibody–drug conjugates. *Chemical Science* **2019,** *10* (3), 694-700.
63. Morais, M.; Nunes, J. P. M.; Karu, K.; Forte, N.; Benni, I.; Smith, M. E. B.; Caddick, S.; Chudasama, V.; Baker, J. R., Optimisation of the dibromomaleimide (DBM) platform for native antibody conjugation by accelerated post-conjugation hydrolysis. *Org. Biomol. Chem.* **2017,** *15* (14), 2947-2952.
64. Lacroix, A.; Edwardson, T. G. W.; Hancock, M. A.; Dore, M. D.; Sleiman, H. F., Development of DNA Nanostructures for High-Affinity Binding to Human Serum Albumin. *Journal of the American Chemical Society* **2017,** *139* (21), 7355-7362.
65. Wall, A.; Wills, A. G.; Forte, N.; Bahou, C.; Bonin, L.; Nicholls, K.; Ma, M. T.; Chudasama, V.; Baker, J. R., One-pot thiol–amine bioconjugation to maleimides: simultaneous stabilisation and dual functionalisation. *Chemical Science* **2020,** *11* (42), 11455-11460.
66. Wu, Y.-q.; Limburg, D. C.; Wilkinson, D. E.; Vaal, M. J.; Hamilton, G. S., A mild deprotection procedure for tert-butyl esters and tert-butyl ethers using ZnBr2 in methylene chloride. *Tetrahedron Lett.* **2000,** *41* (16), 2847-2849.
67. Castañeda, L.; Wright, Z. V. F.; Marculescu, C.; Tran, T. M.; Chudasama, V.; Maruani, A.; Hull, E. A.; Nunes, J. P. M.; Fitzmaurice, R. J.; Smith, M. E. B.; Jones, L. H.; Caddick, S.; Baker, J. R., A mild synthesis of N-functionalised bromomaleimides, thiomaleimides and bromopyridazinediones. *Tetrahedron Lett.* **2013,** *54* (27), 3493-3495.

|5|

Conclusions and Future Work

5.1. Contributions to Original Knowledge

On the most basic level, the central theme of this thesis has been the design and synthesis of new oligonucleotide conjugates for applications in drug delivery and gene silencing. Strategies to increase the target specificity by making these conjugates stimuli responsive to both biological and chemical stimuli have been demonstrated. Additionally, taking advantage of structural DNA nanotechnology, the potential for these conjugates to operate *in vivo*, has been enhanced by generating well-ordered structures. Overall, this thesis uses knowledge from many different areas; structural DNA nanotechnology, DNA computation, DNA templated reactions and nucleic acid therapeutics to generate new nanodevices for therapeutic applications.

The research presented in chapter 2 represents two strategies towards generating a standalone DNA nanodevice that amplifies the release of small molecule cargo in response to a molecular recognition event. The first strategy was to use the hybridization chain reaction (HCR) as the amplification mechanism. In this method a DNA templated disulfide exchange is combined with HCR to selectively release both caged fluorophores and small molecule drugs. It was shown that this device was able to release cargo molecules with 6-7x amplification, and the kinetics of release were thoroughly investigated. Furthermore, the individual hairpins of this approach were integrated into a standalone nanodevice using a DNA track and spherical nucleic acids. Importantly, once integrated into these architectures, leakage was kept to a minimum, and reactive functional groups were able to be separated. The second strategy employed the use of molecular beacons in combination with self-immolative polymers to achieve such a device. In this device DNA templated reactions are used in a bond cleavage reaction to release cargo. We demonstrated that the strand displacement mechanism of this strategy performed as expected, and that the bond cleavage chemistry worked, albeit at low yield. Overall, this chapter represents a new method to generate stimuli-responsive prodrugs which are uncaged and released upon molecular recognition events and may have profound impact on new drug formulations moving forward.

The work in chapter 3 presents a method for generating reduction sensitive spherical nucleic acids (SNAs) for gene silencing. A new disulfide phosphoramidite was developed to make

sequence defined SNAs that respond to intracellular reducing conditions. With this new phosphoramidite we conjugated multiple units to an ASO. Luciferase gene silencing assays were performed which revealed that the disulfide bond improved silencing when compared to SNAs without disulfides. Additionally, a silencing pattern emerged within the data, leading us to discover that under *in vitro* conditions the SNAs fell apart to bind the serum protein albumin and increase the uptake of this protein via a disulfide mediated mechanism. Taking advantage of this observation, we investigated three further avenues 1) non-transfected silencing 2) crosslinking the SNAs and 3) extended silencing of the albumin bound conjugates. Overall, this chapter re-affirms that accessibility of an ASO to bind its target is of the utmost importance for gene silencing, whether it is encumbered by being part of an SNA or bound to albumin.

Chapter 4 builds on the findings from chapter 2 to improve the drug delivery device for more biologically relevant conditions. Progress towards replacing the disulfide templated reaction chemistry with a bio-orthogonal tetrazine cyclization has been pursued for the bond cleavage reaction in HCR. Improvements to HCR itself were then pursued with the aim of reducing leakage and increasing signal gain of HCR using disulfide ligated stems in the starting hairpins. We found that while leakage of HCR was significantly suppressed, this was at the cost of polymerization of the HCR hairpins. Hairpins with different ligation positions were synthesized, and the process was carried out under dynamic conditions, with some improvement to polymerization. To improve the rate of release in the HCR system and generate greater selectivity, we designed both longer DNA tracks and DNA logic gates to template the HCR process. We found that on the template, HCR proceeded at a faster rate than off the template. Also using a synthetic DNA trimer gave us a platform for an “OR” gate which could be activated by either one of two input strands. Moreover, we developed a method to completely replace the small molecule therapeutic with an antisense oligonucleotide (ASO). Using catalytic hairpin assembly (CHA) as the amplification mechanism, we were able to selectively eject multiple ASO strands in response to a small amount of trigger molecule. Attempts to increase nuclease resistance by introducing phosphorothioate linkages, led to aggregation of the system. Multiple strategies were pursued to circumvent this aggregation, and ultimately using hexa-ethylene glycol modifications achieved this goal. Finally,

the development of antibody-oligonucleotide conjugates (AOC's) was developed for the goal of triggering HCR extracellularly. Our method for antibody functionalization was based on co-operative hybridization of a multi-branched DNA (B-DNA) construct to an antibody with several hybridization handles, giving us control over the degree of conjugation (DoC) of the antibody.

Taken together, this work reflects our efforts towards generating new oligonucleotide conjugates used in combination with DNA nanotechnology for drug delivery and gene silencing applications. The technology developed here is envisioned to inspire future researchers in the development of new small molecule and oligonucleotide prodrugs.

5.2. Future Work

The DNA devices developed in chapters 2 and 4 have the potential to improve the selectivity of prodrugs to a high degree using molecular recognition as the trigger. This also means that targets other than enzymes can metabolize prodrugs into an active form. Using molecular beacons to initiate HCR that are responsive to other stimuli in the form of aptamer switches, can provide a greater number of targets available, as well as better integration into a single device without necessitating DNA -antibody conjugates. Additionally, self-immolative amplification and HCR are not mutually exclusive amplification techniques and could be used in tandem to increase the signal gain from HCR as well. Indeed, biological systems use many layers of amplification in "signal cascades" to generate greater amplification for the cell's various operations. Spatial isolation of reactive functional groups on DNA architectures is an area that has not been fully explored. There are limited examples in the literature of this concept, and future work should focus on some of the fundamental rules for its applicability.

Changing the chemistry of the device to be bio-orthogonal is critical for its translation into a clinical setting. As such future work can focus on other reaction chemistries other than thiol-disulfide or tetrazine. One suggestion may be to look at Staudinger reduction of 4-azidobenzalcohol derivatives as the bond cleavage reaction. Overall, the tetrazine cyclization may prove to be the best option, as it is more resistant to oxidation in-vitro.

The method developed for extracellular initiation of HCR, using antibody-oligonucleotide conjugates, could also be applied for other applications of antibody-oligonucleotide conjugates where the valency is important. For example, generating antibody-ASO conjugates using the branched hybridization method can help define the valency of these therapeutics to the antibody. Furthermore, some recent studies have shown the conjugation of highly toxic drugs to oligonucleotides and hybridizing them to AOC's can improve the therapeutic index of the antibody drug conjugates. Using the dibromomaleimide (DBM) for initial conjugation to the antibody, while it works, the shelf life of the DBM is only about a week. Therefore, new chemical methods for performing the initial antibody oligonucleotide con be pursued using molecules that have longer shelf lives. In appendix ii we designed and synthesized a dialkene phosphoramidite that could be conjugated to DNA using solid phase synthesis.

While the templated "OR" gate is a nice proof-of-concept, generating a templated "AND" gate is more useful for increasing specificity. Designs for the AND gate have been produced and are in appendix viii. An interesting avenue to pursue here is on the actuation side of DNA computing, where a more complicated algorithm could result in an amplified output of small molecules. This could lead to generating feedback loops where the release of a small molecule binds to an aptamer switch and initiates the next computation. Using a small molecule output for generating supramolecular polymers may also be an interesting pursuit.

Future work to improve the leakage and signal gain in HCR, could look at other supramolecular interactions to stabilize the hairpin stems. Dynamic covalently linked stems it seems, are very strong and may be preventing strand displacement from properly occurring. Studying how different interactions effect the HCR kinetics, leakage and signal gain can provide a fundamental understanding and reveal trends of how these modifications effect HCR for more applications beyond drug delivery.

Developing the amplified release of ASO strands, the next step is to test the nuclease resistance of the modified system. Additionally, adding uptake enhancing ligands to the ASO strand and hiding them within the core of the SNA until triggering would be a way to modulate gene expression only in desired cell-types/locations. Considering that tissue specificity is one of the

major challenges in oligonucleotide therapeutics, this ASO prodrug system could help address this problem.

Improving the ASO-disulfide conjugates from chapter 3 by using more sophisticated ASO modifications such as 2′-deoxy-2′-fluoroarabinonucleic acid (2-FANA), which have shown to silence without the use of transfection agents is the next step for the disulfide ASO conjugates. The *in vivo* gene silencing of the disulfide ASOs can be investigated without hesitation as often *in vitro* silencing does not always reflect what ultimately occurs *in vivo*. Increasing the number of disulfide repeat units appended to these ASOs can also be pursued to enhance crosslinking of the SNA's and stabilize them against albumin binding. Additionally, for our studies we used simple hydrophobic disulfides as the side chain of the phosphoramidite. Changing the side chain to functional units such as cholesterol or amino groups could help to enhance the conjugates therapeutic properties as well. In appendix I. the synthesis of a disulfide phosphoramidite with a triethylene glycol sidechain has been pursued to probe the effect of having a hydrophilic as opposed to hydrophobic side chain, on protein binding. Ultimately a library of different disulfide phosphoramidites could be generated and used in different combinations for sequence defined polymers or ligands for ASOs. Using different combinations of different disulfides here is interesting because ultimately the disulfides get cleaved, and the specific combination is lost once entering cells.

A ^{1}H NMR is provided for each of the unreported small molecules synthesized. and ^{13}C NMR are provided for our published compounds and ^{31}P NMR are provided for phosphoramidites.

6. NMR Spectra

6.1. Molecules from Chapter 2

6.1.1. Compound 1

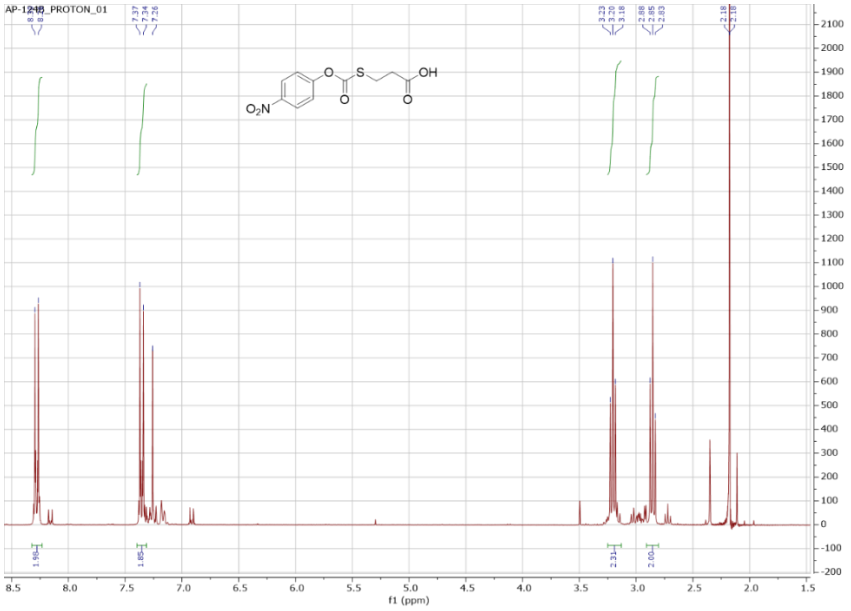

6.1.2. Compound 2

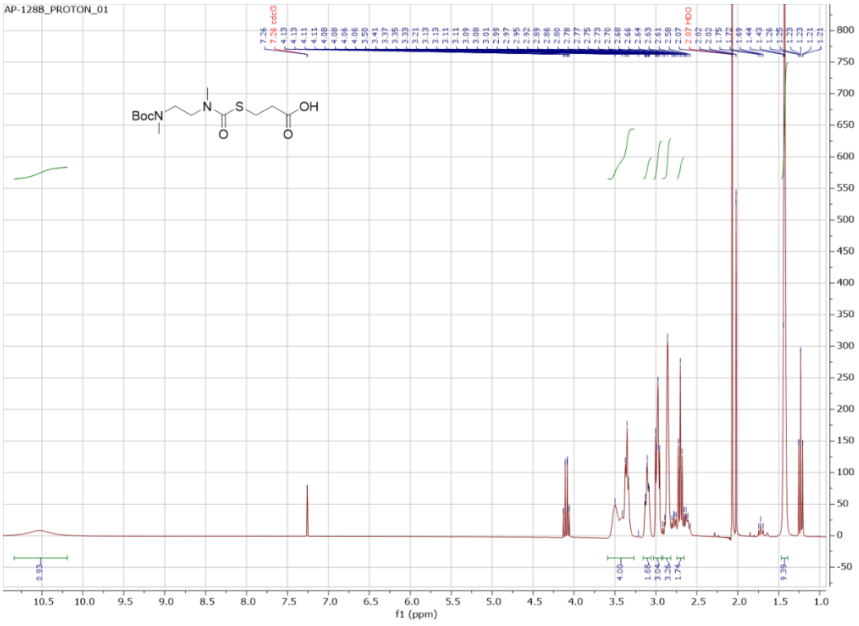

6.1.3. Compound 3

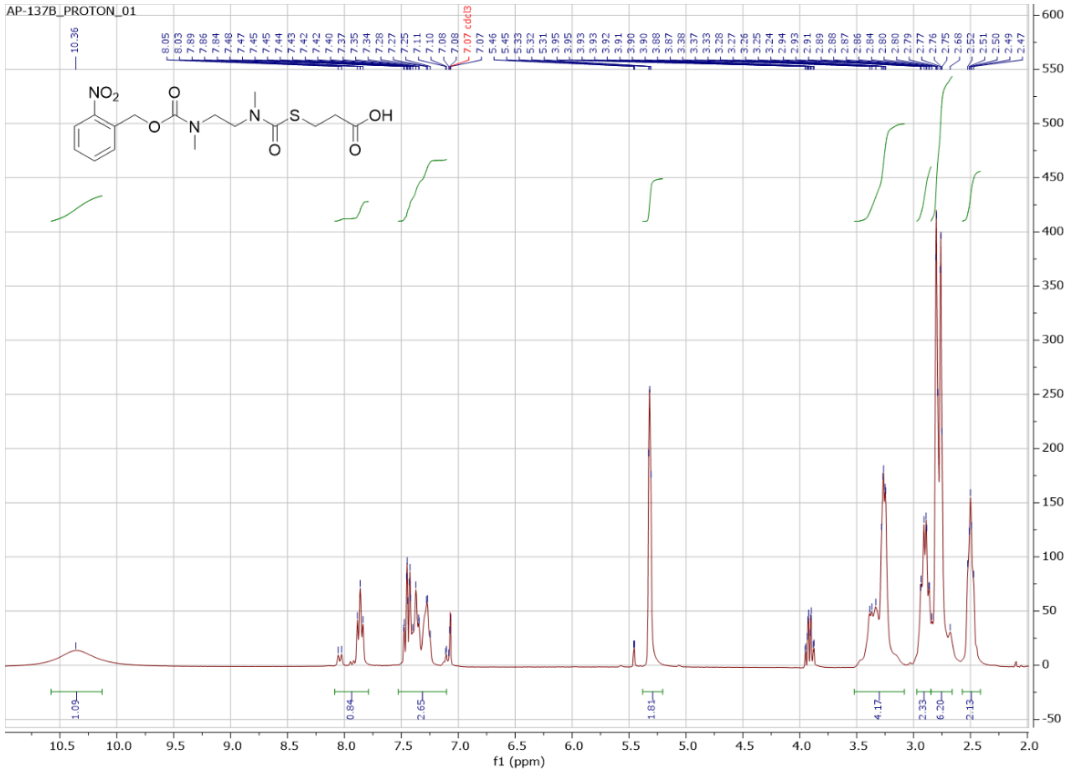

6.1.4. Compound 4

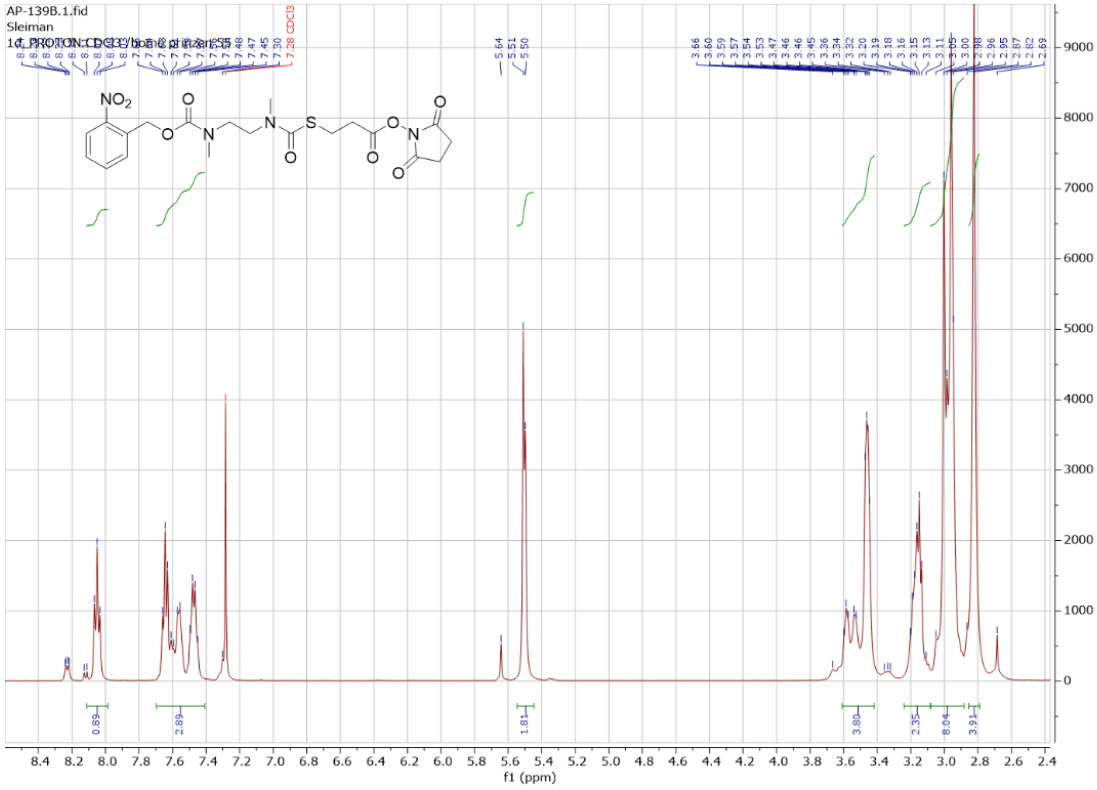

6.1.5. Compound 8

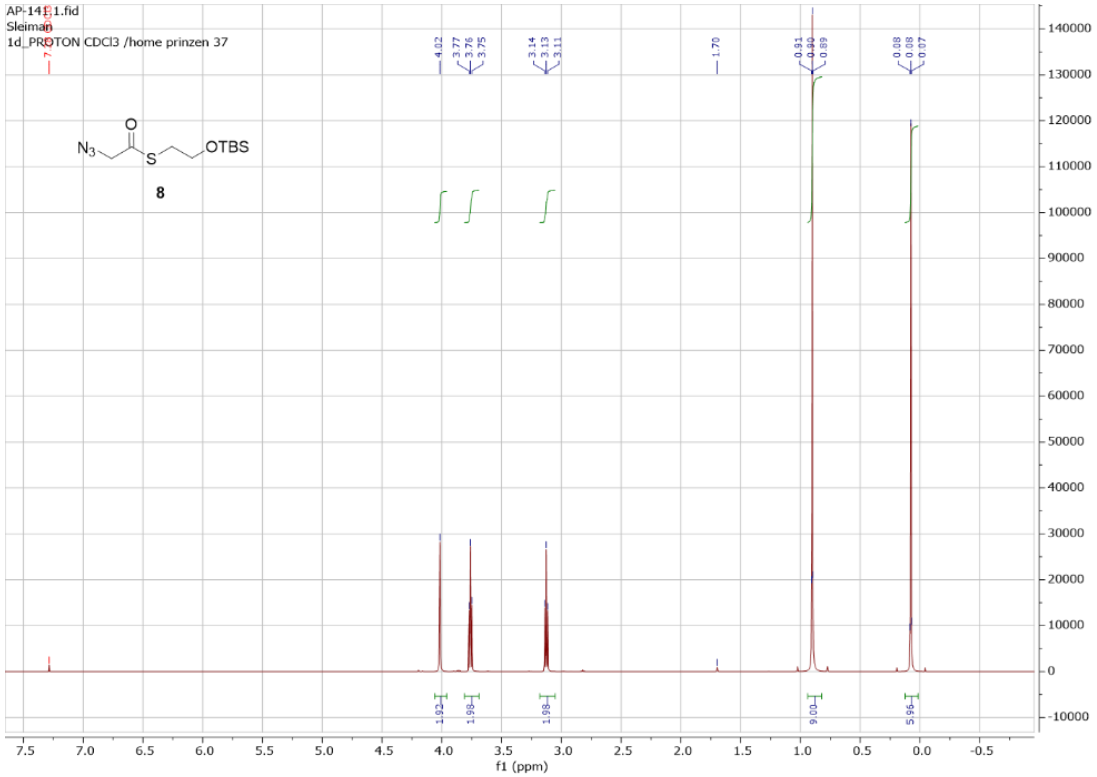

6.1.6. Compound 9

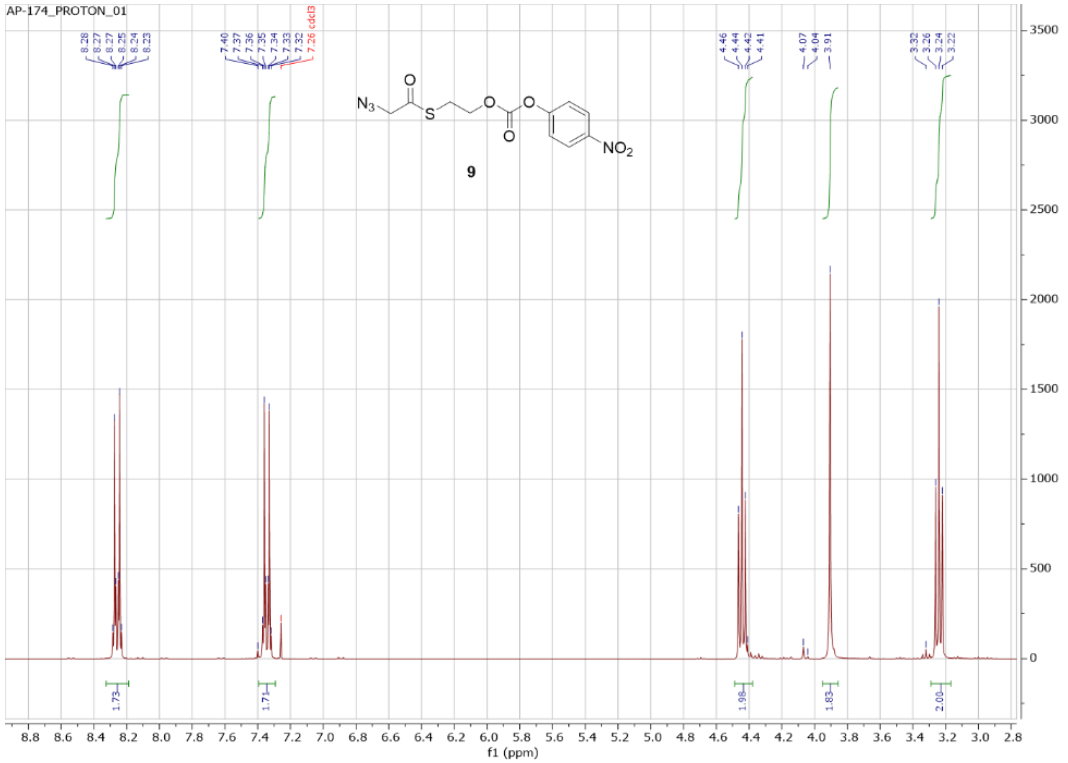

6.1.7. Compound 10

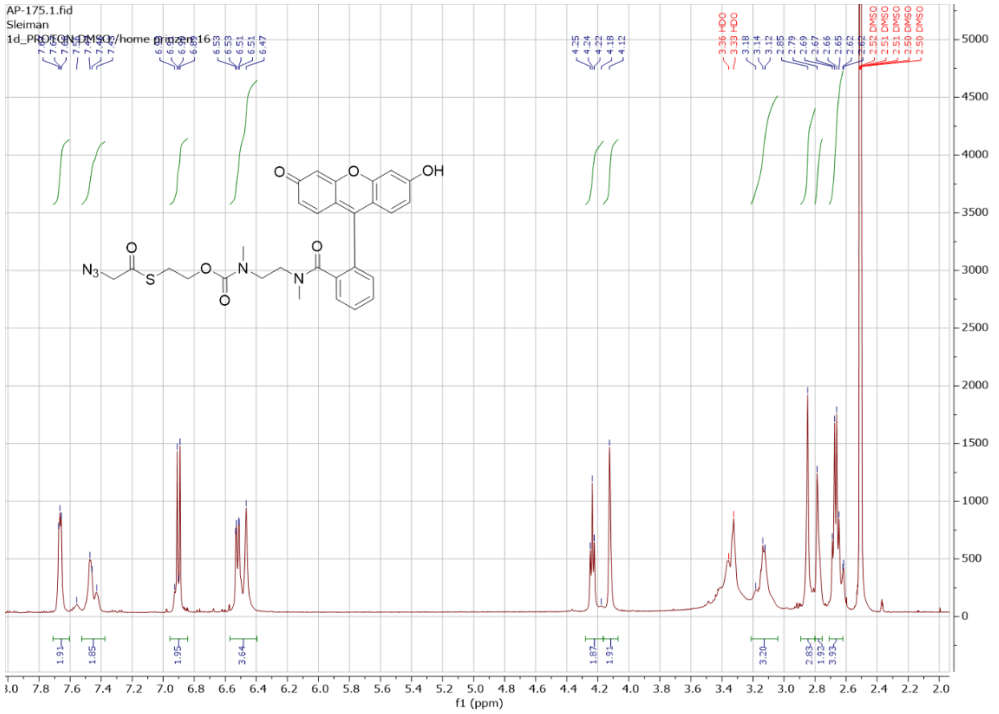

6.1.8. Compound 12

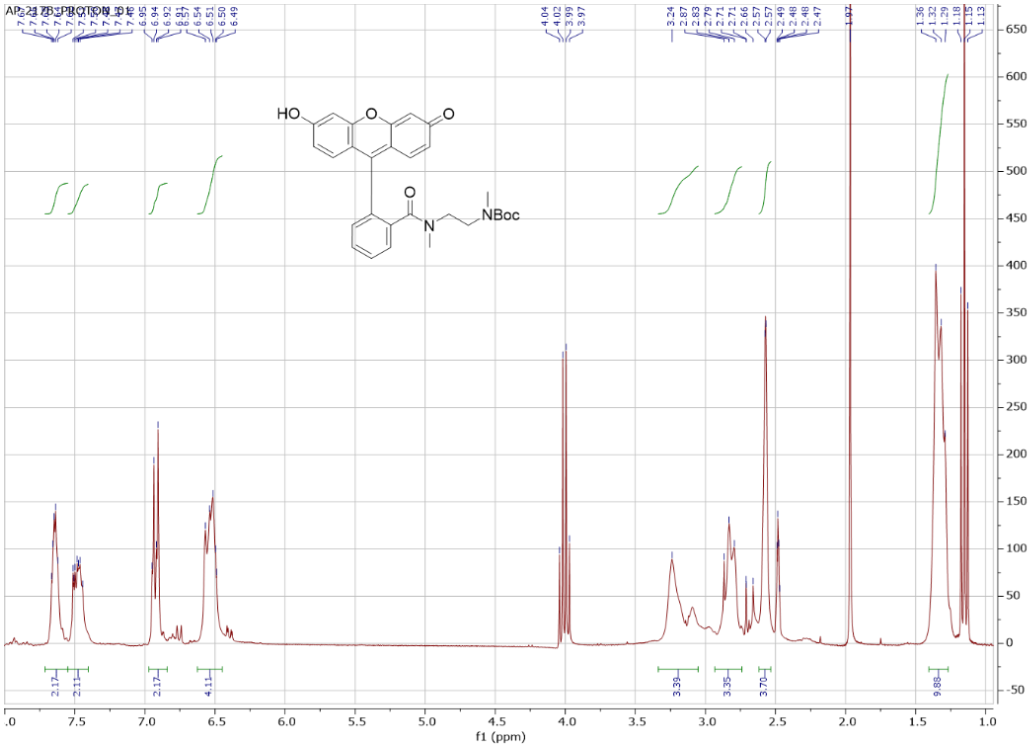

6.1.9. Compound 15

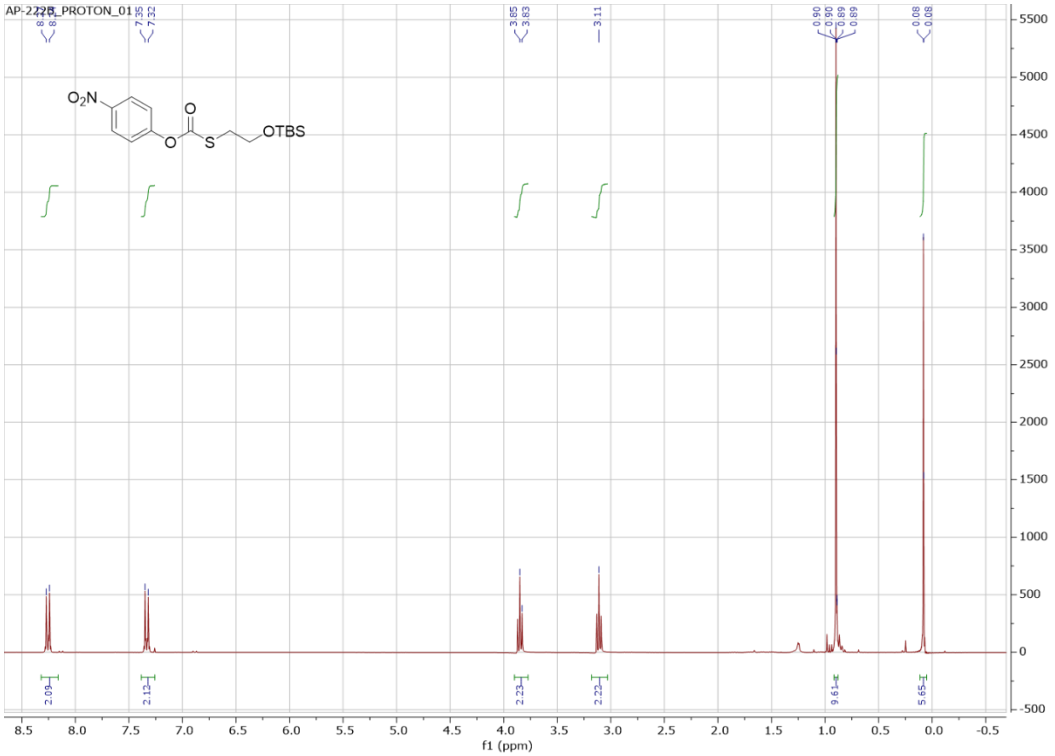

6.1.10. Compound 16

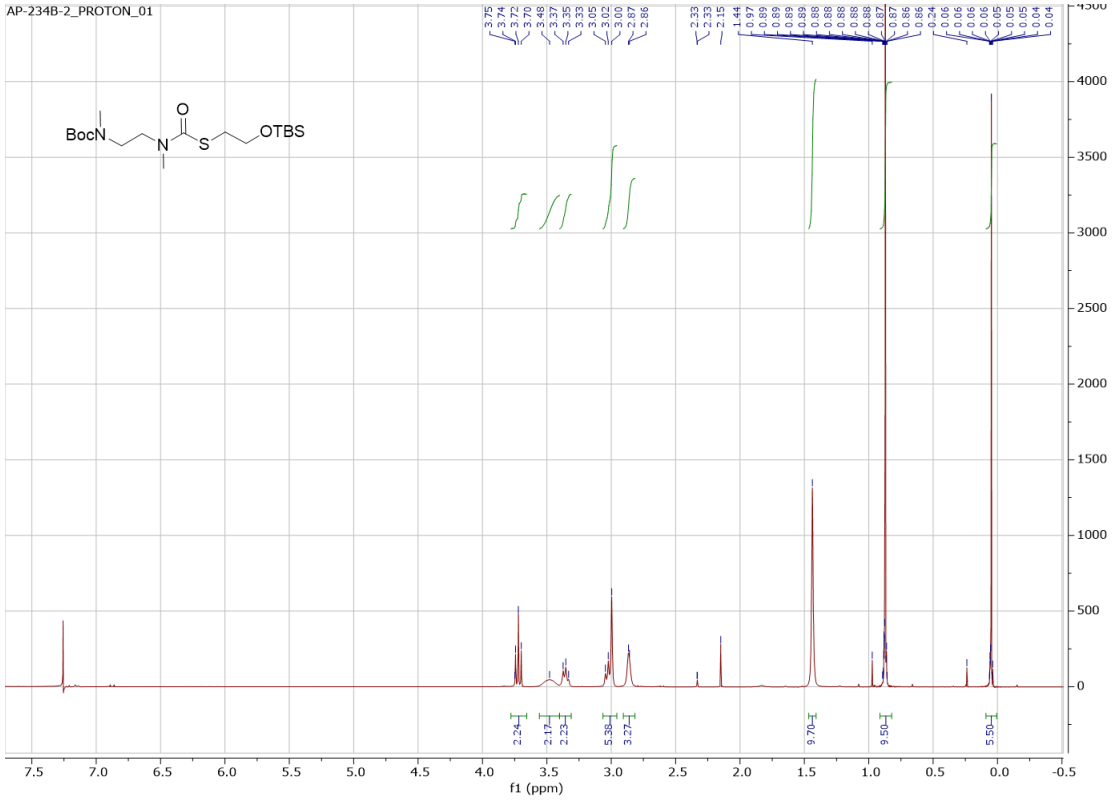

6.1.11. Compound 17

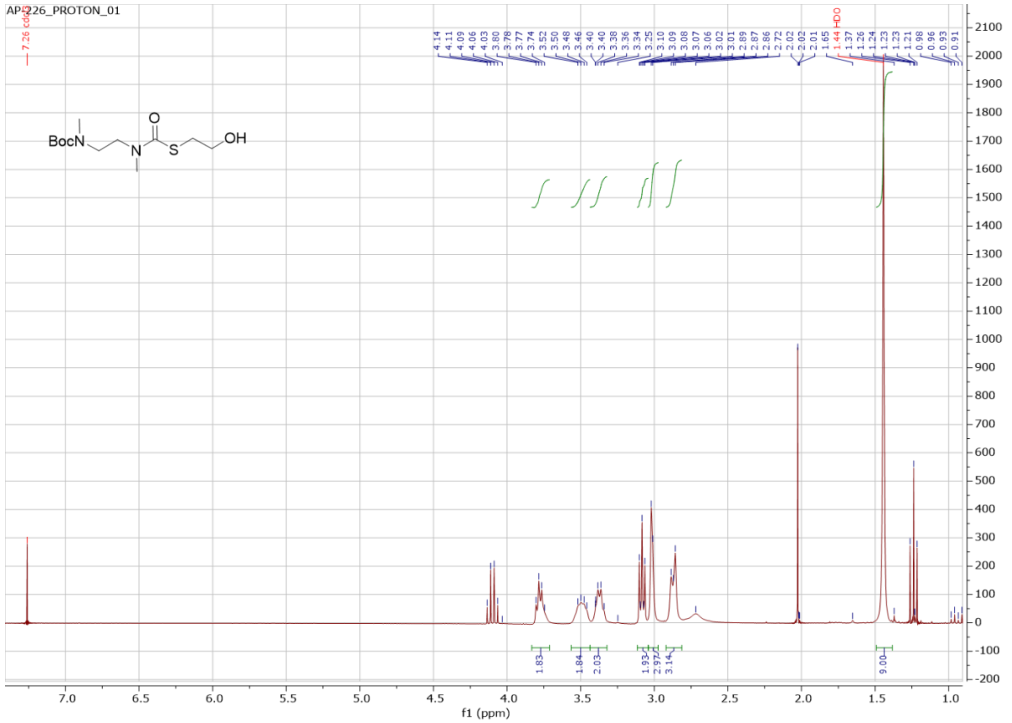

6.1.12. Compound 18

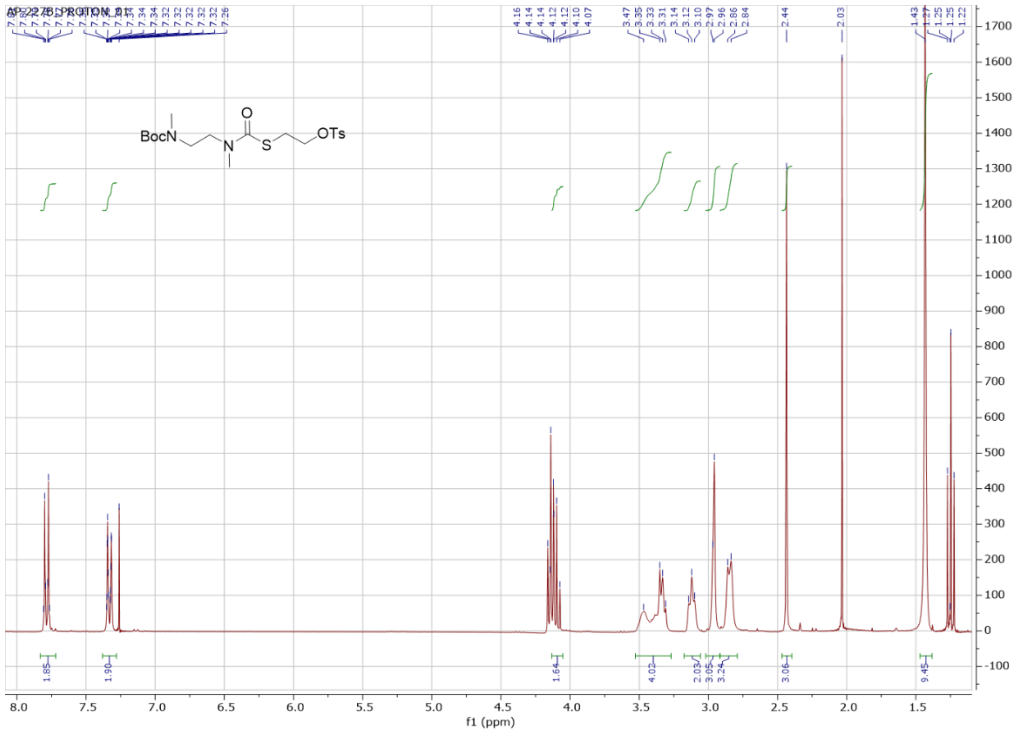

6.1.13. Compound 19

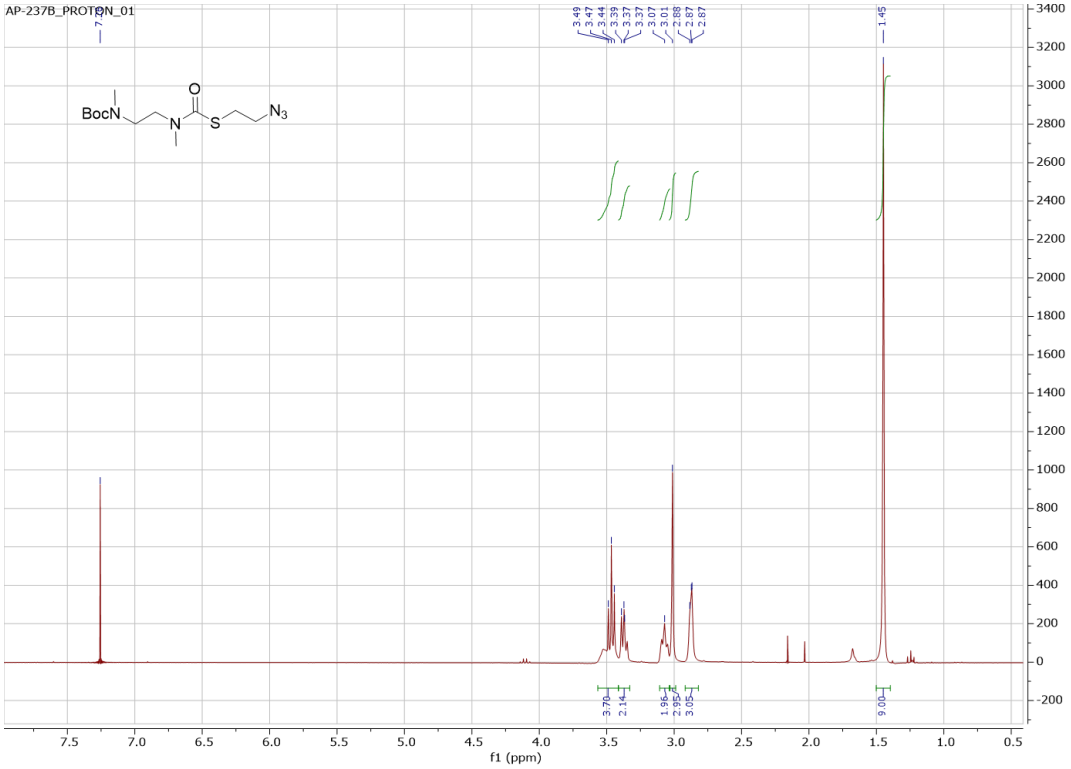

6.1.14. Compound 20

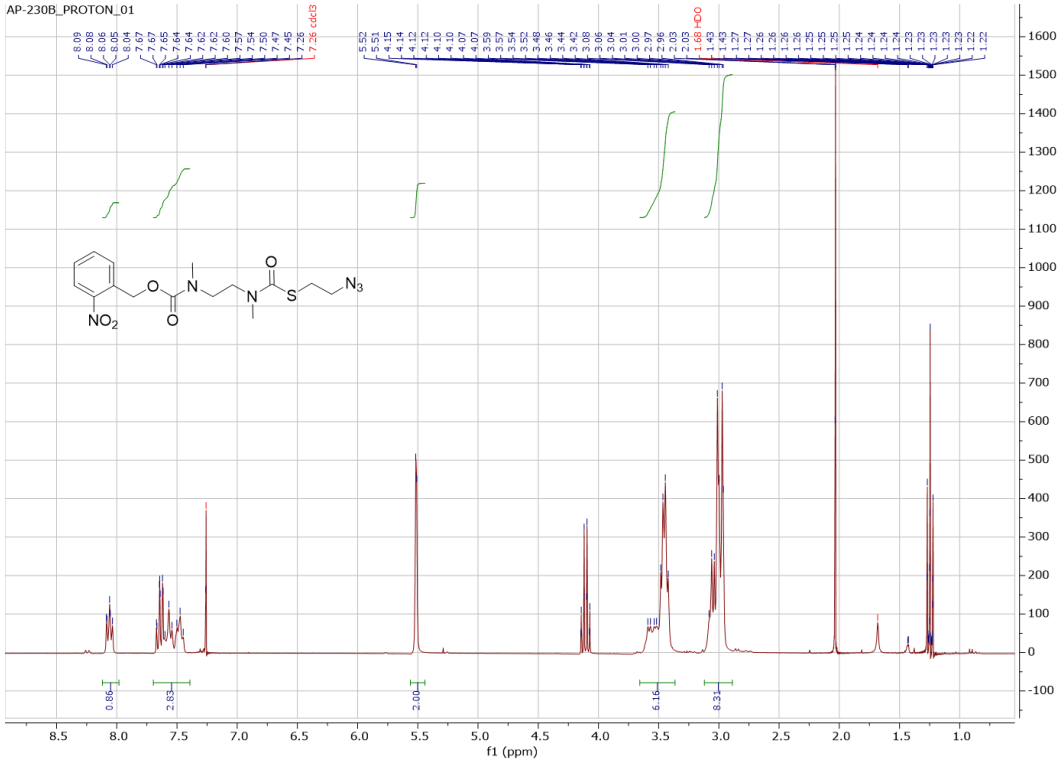

6.1.15. Compound 24

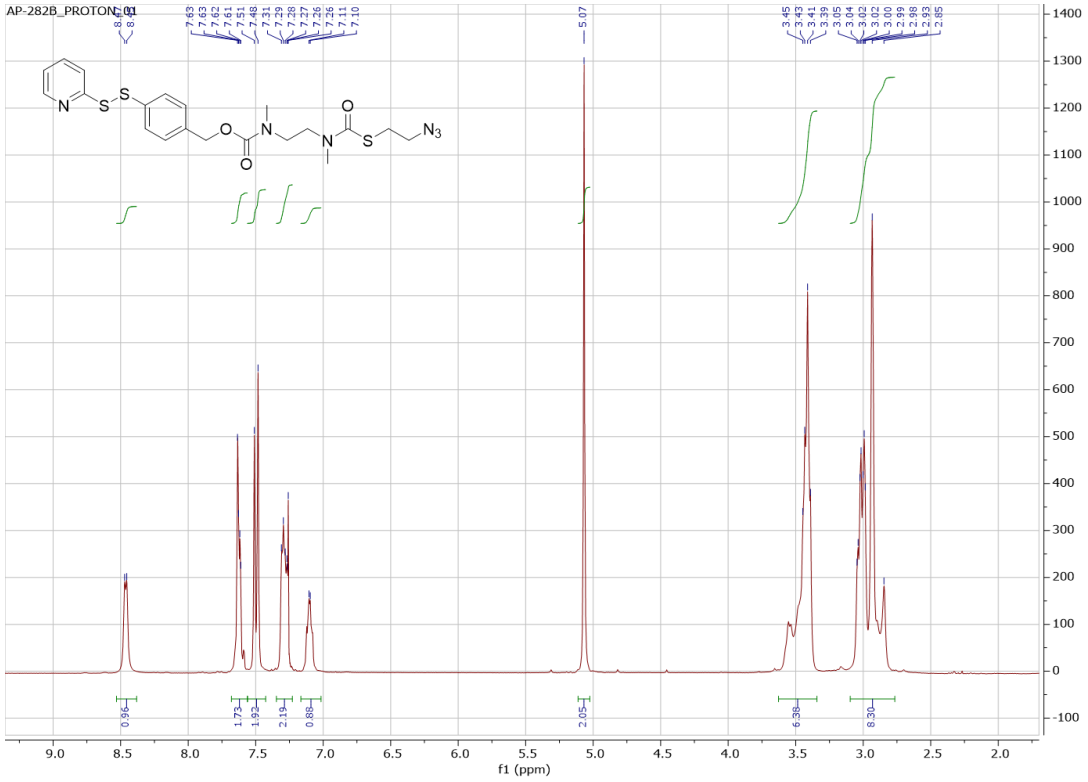

6.1.16. Compound 29

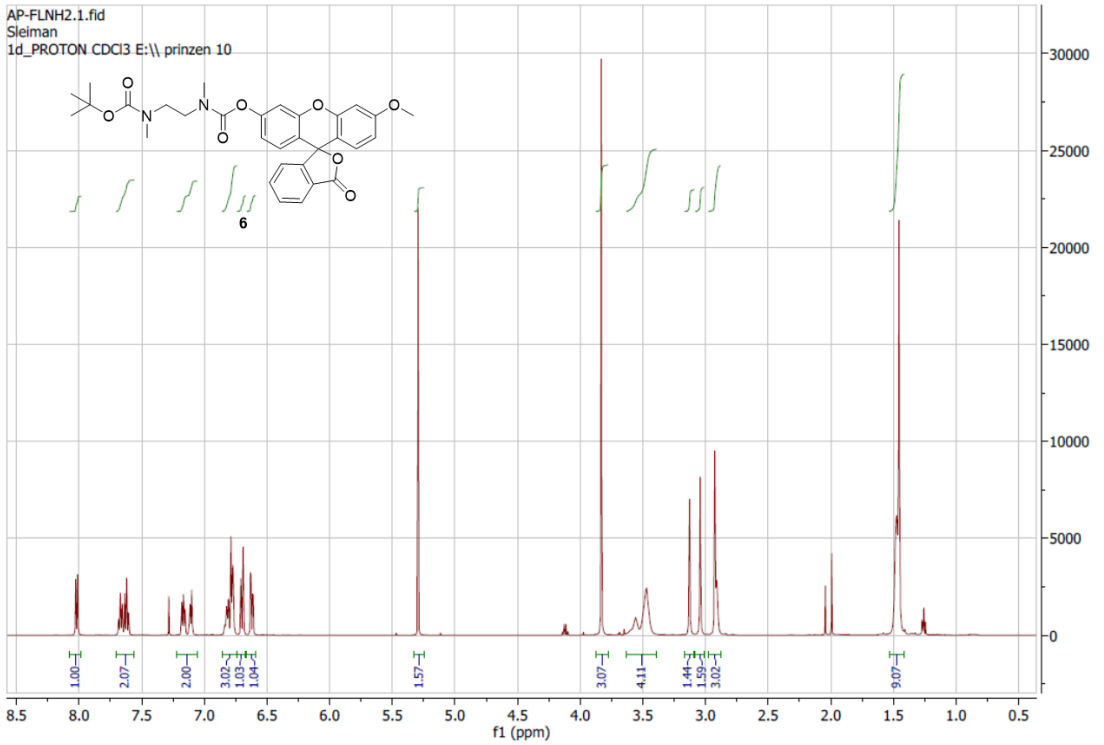

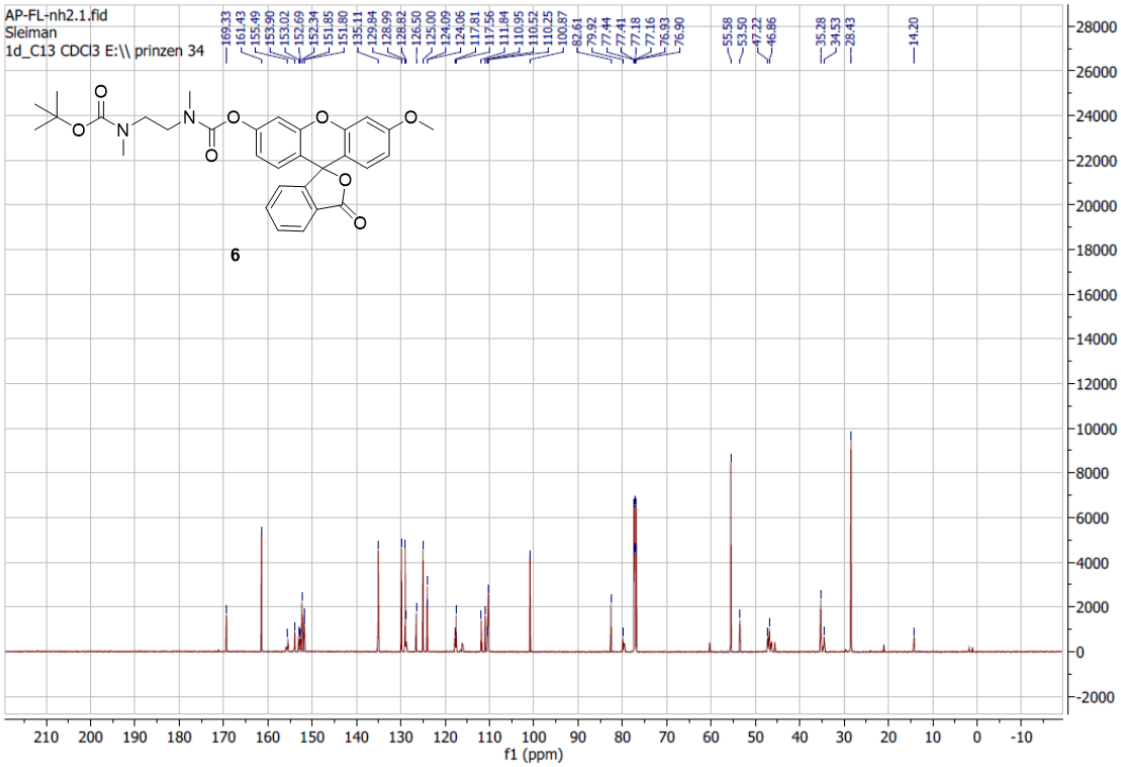

6.1.17. Compound 30

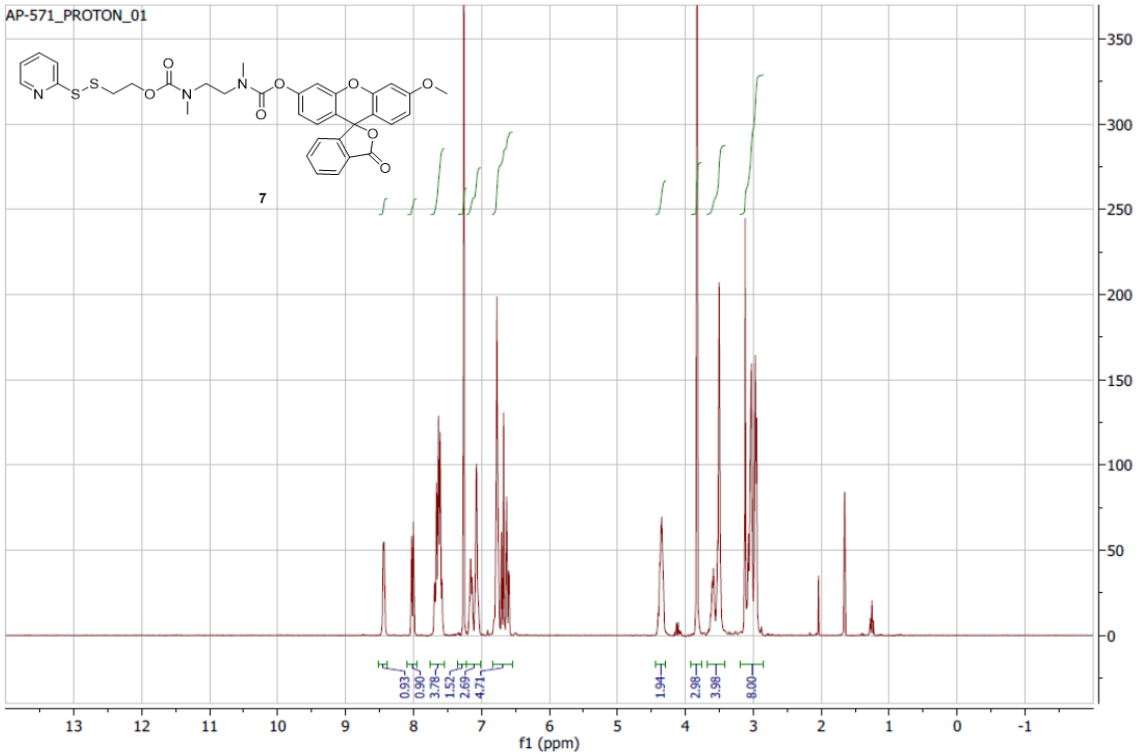

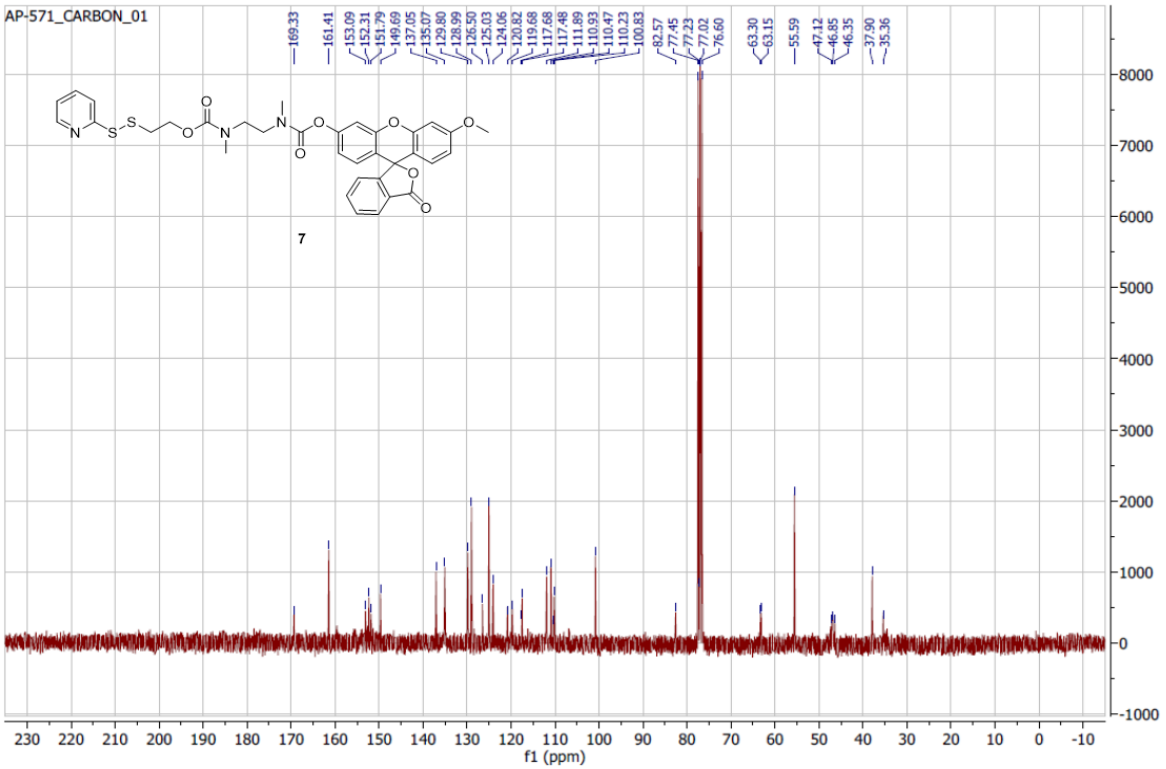

6.1.18. Compound 32

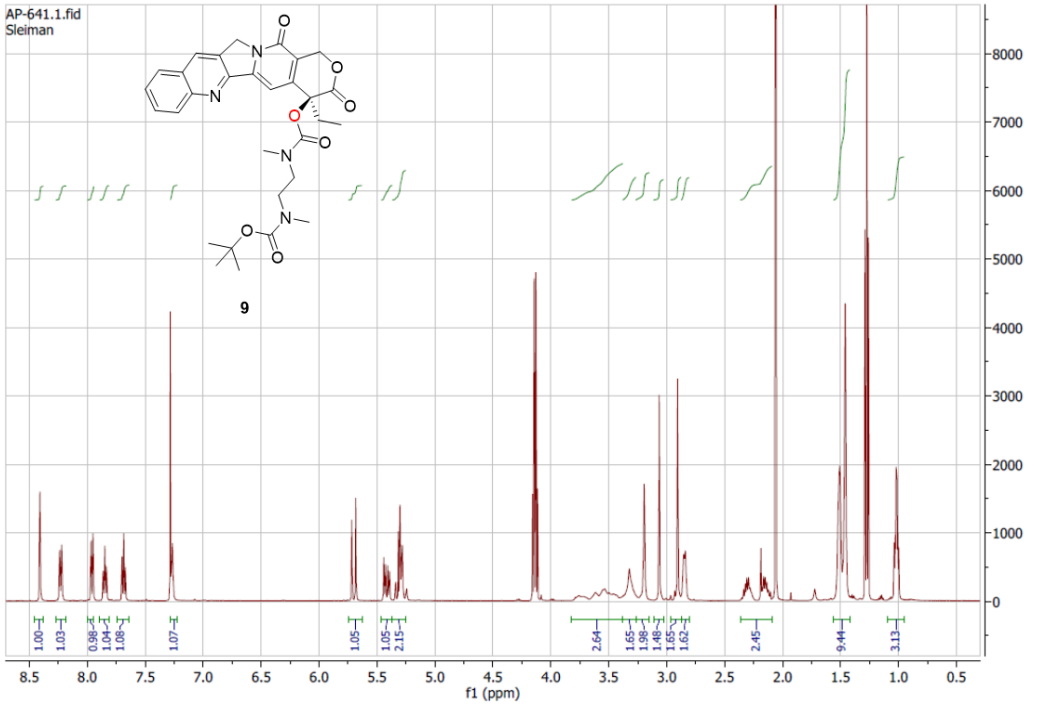

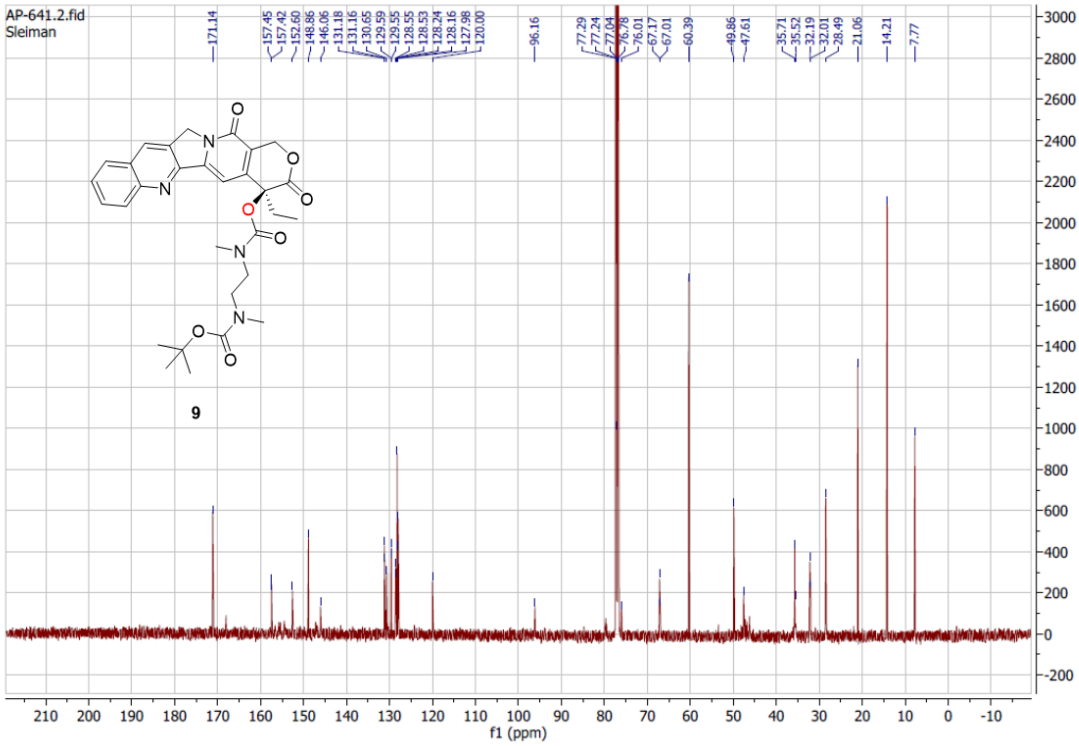

6.1.19. Compound 33

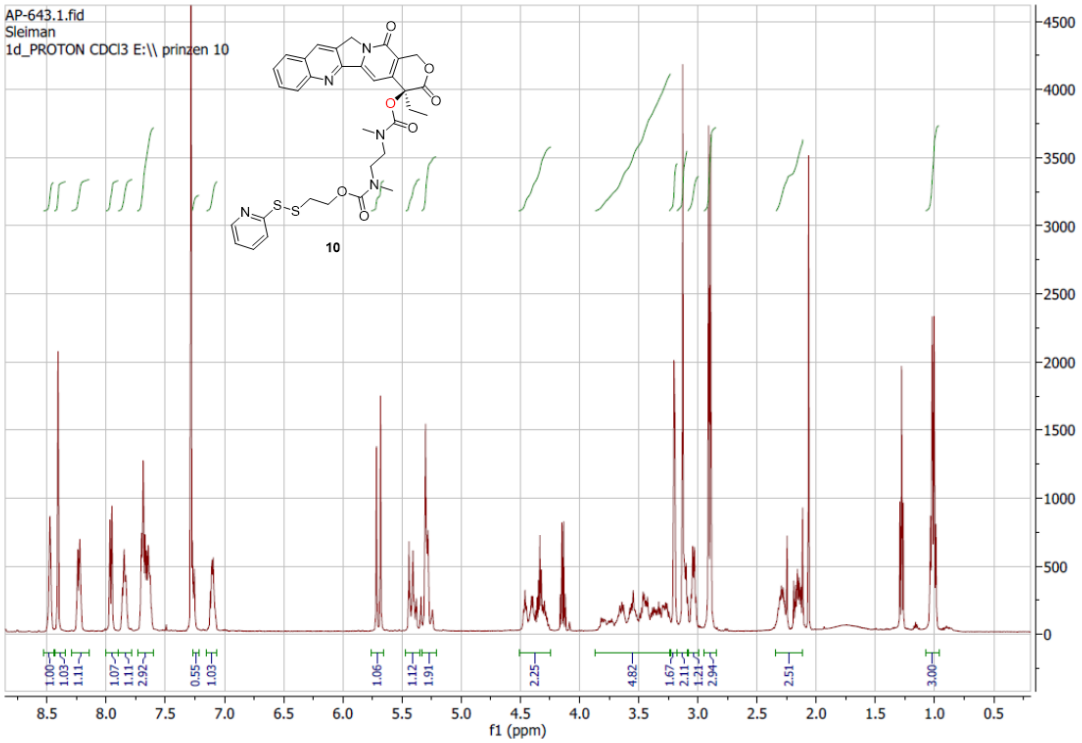

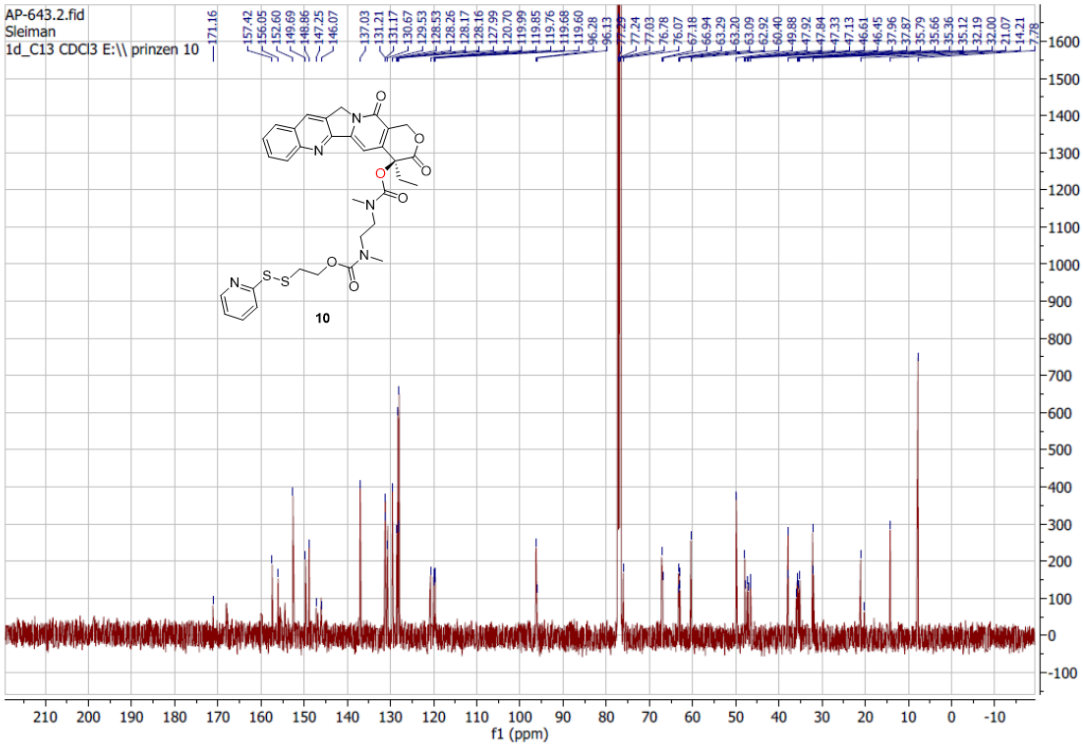

6.1.20. Compound 35

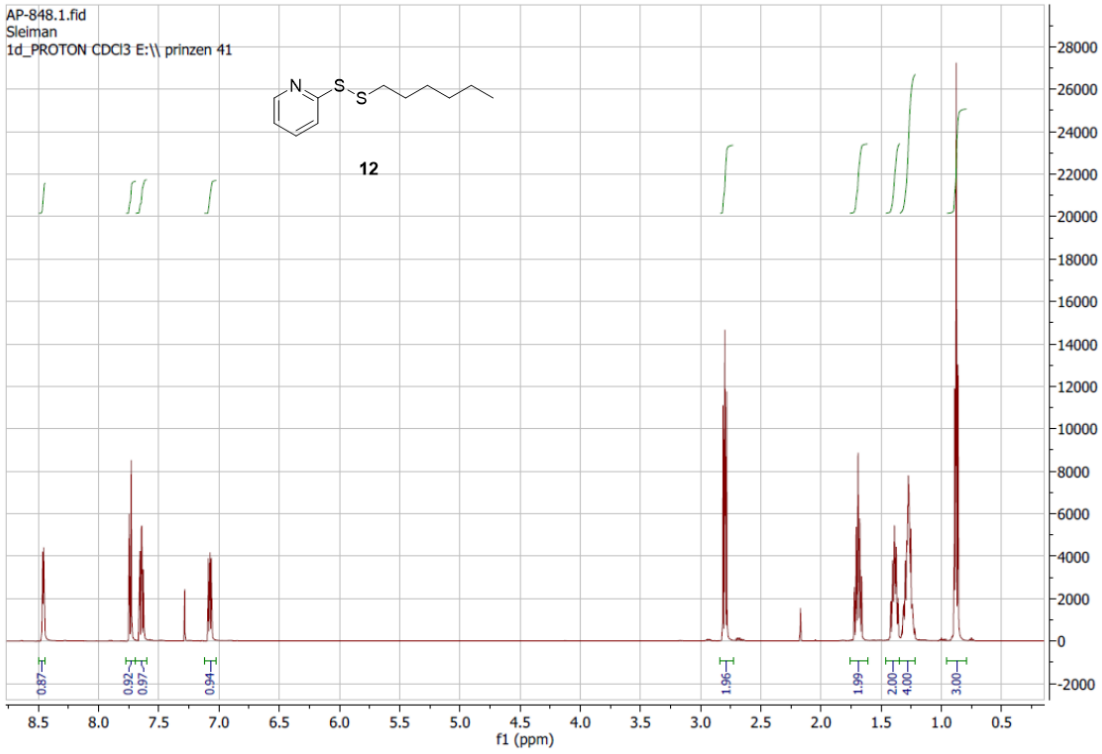

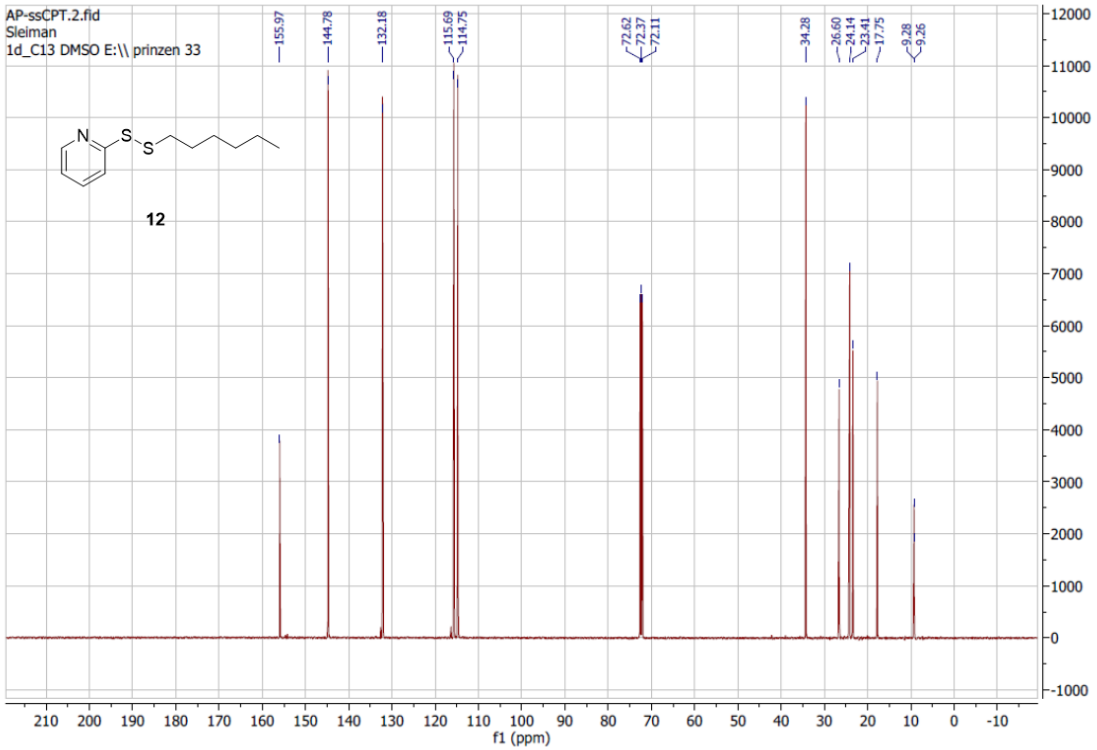

6.1.21. Compound 36

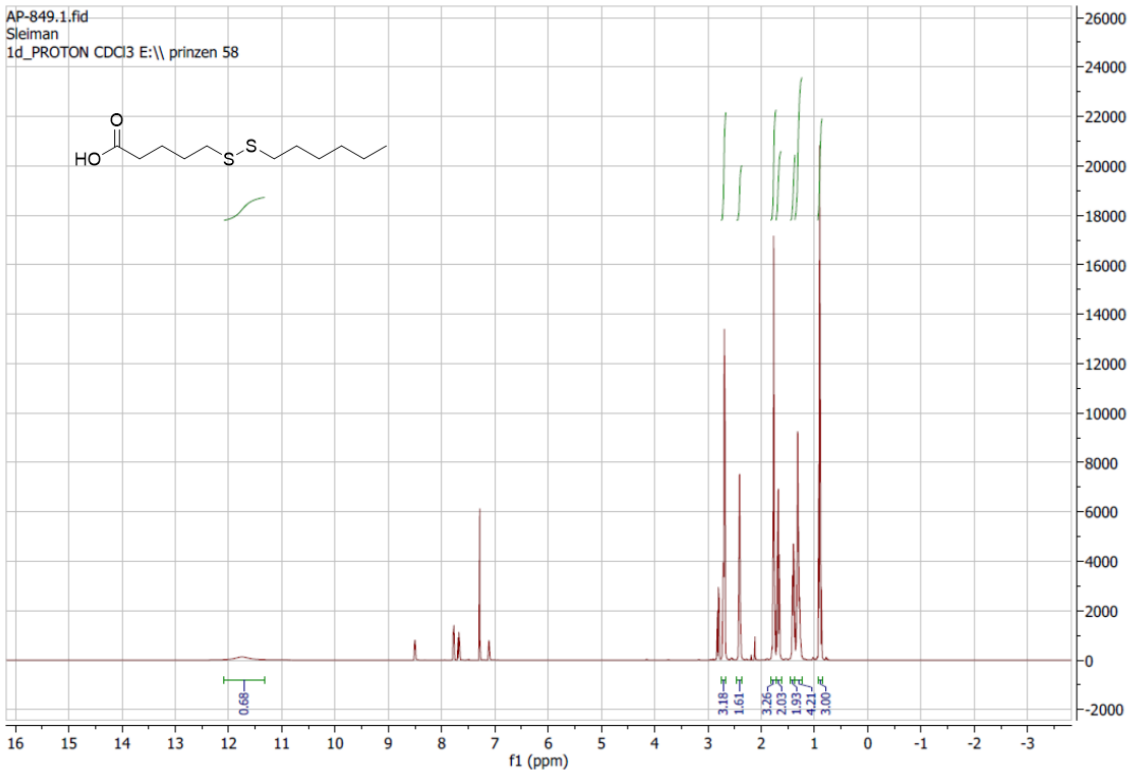

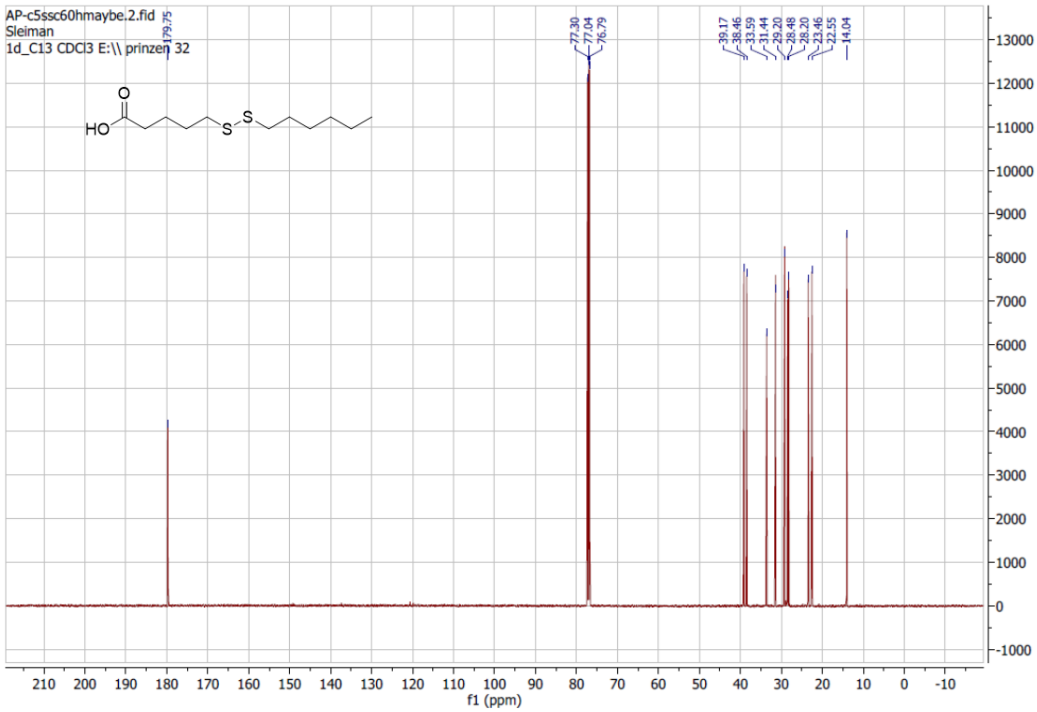

6.1.22. Compound 37

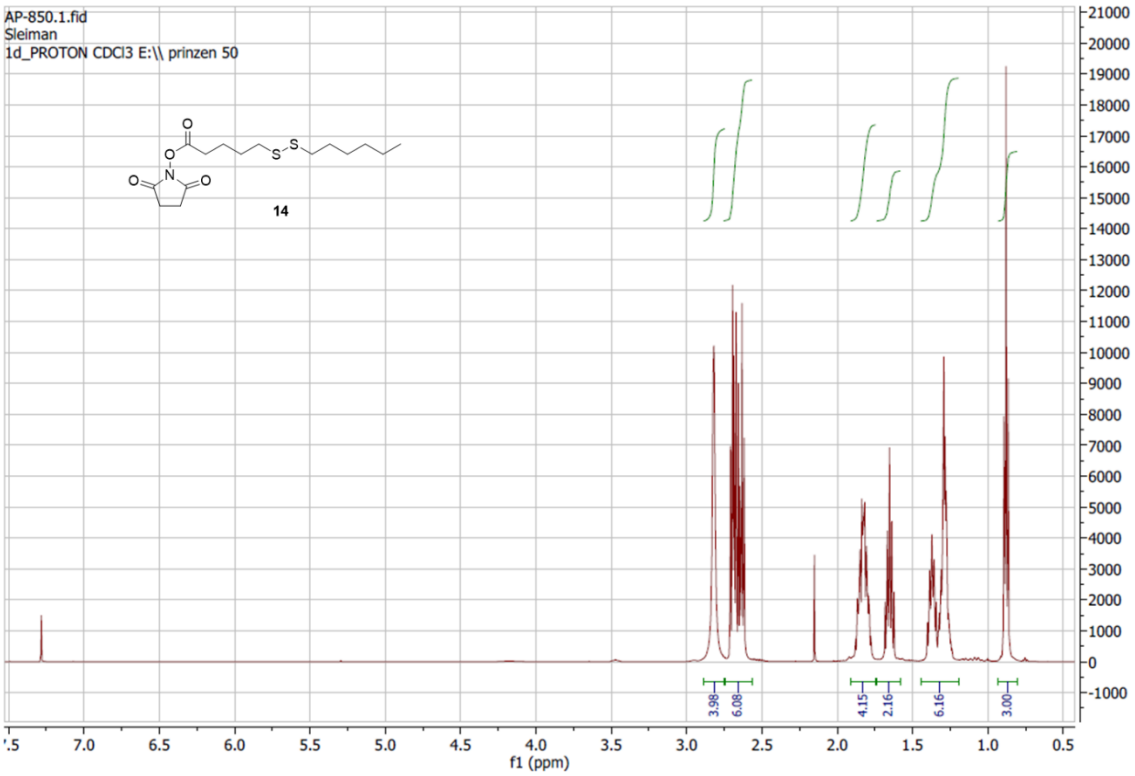

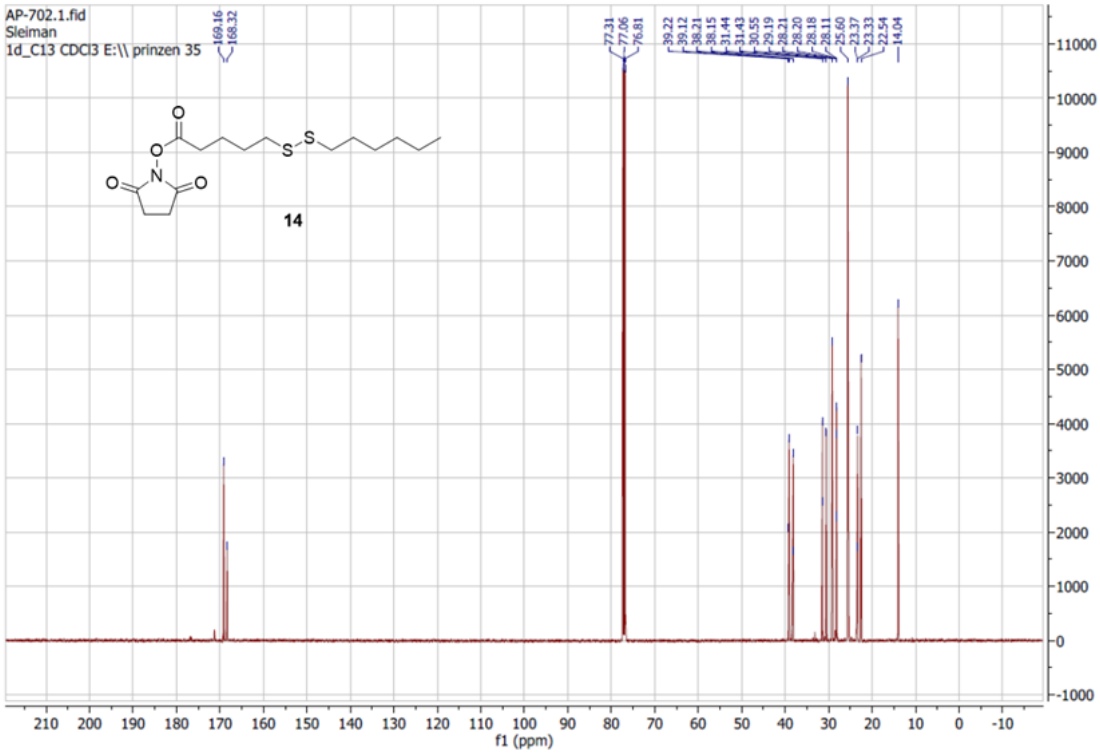

6.1.23. Compound 38

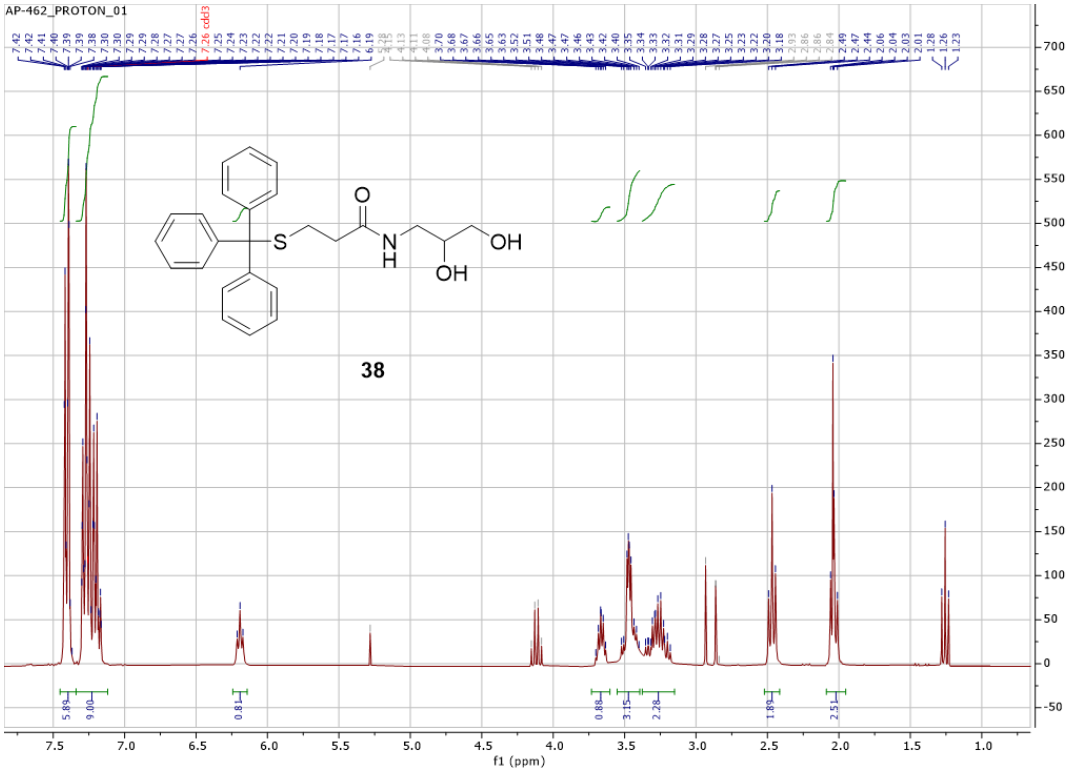

6.1.24. Compound 39

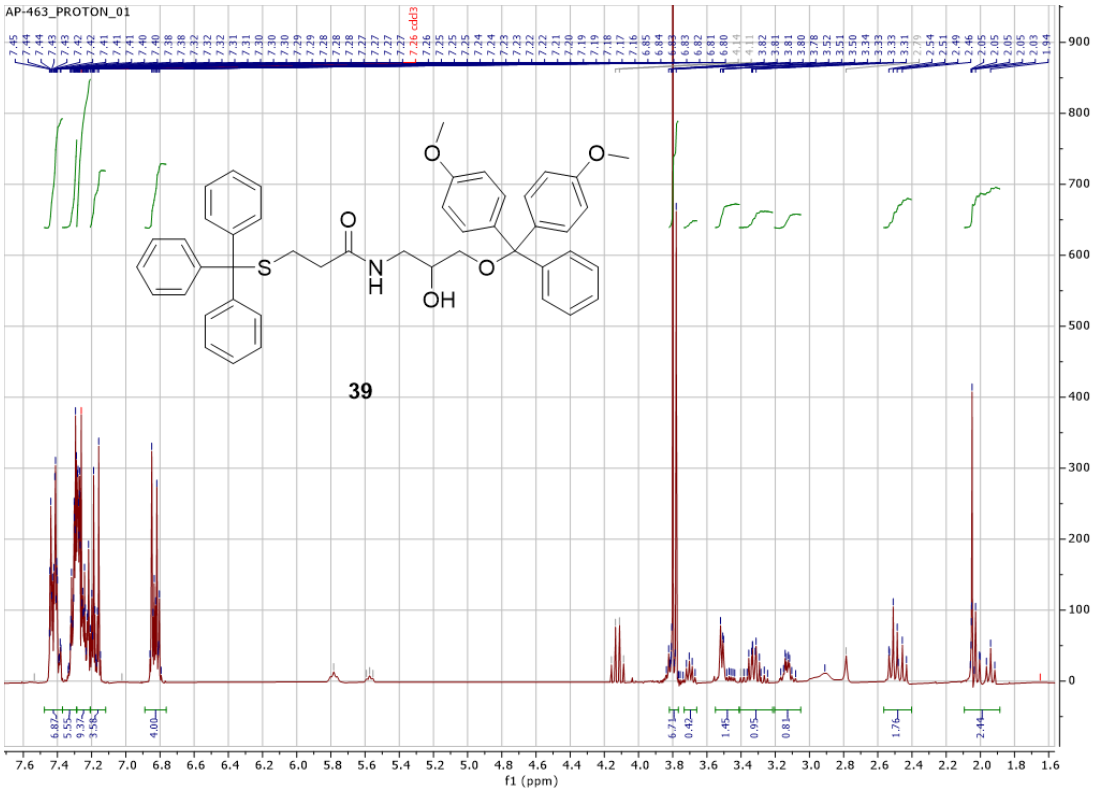

6.1.25. Compound 41

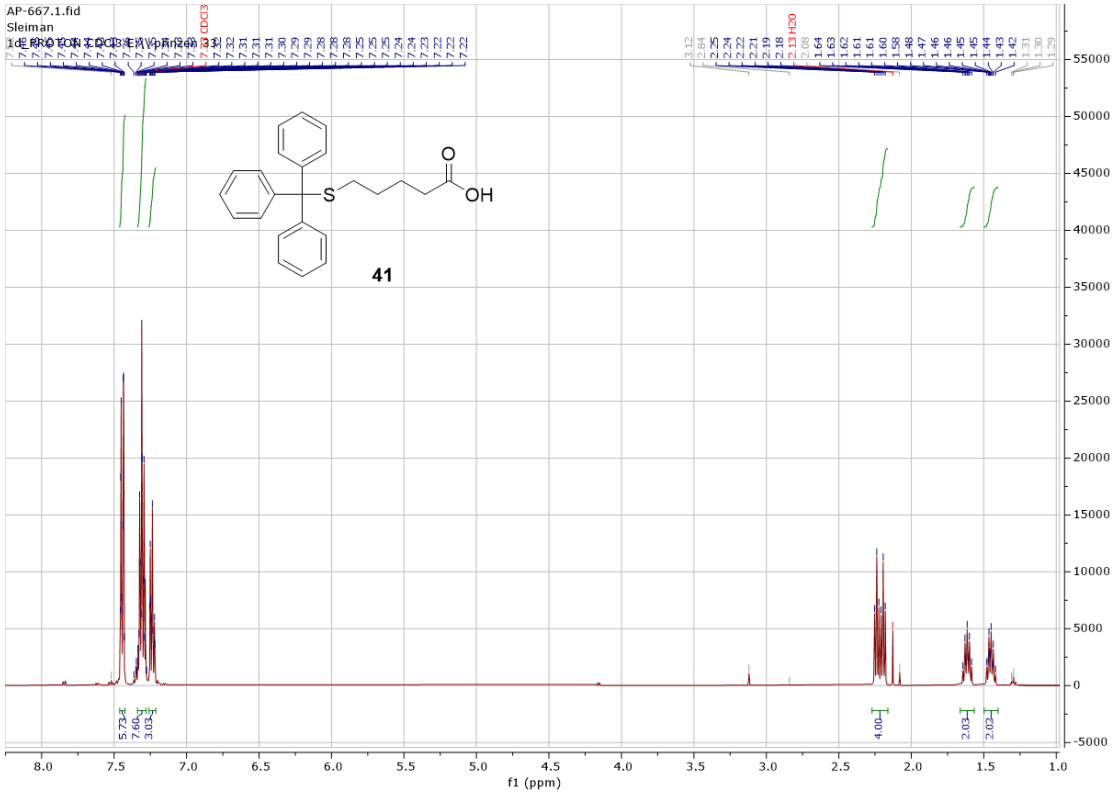

6.1.26. Compound 42

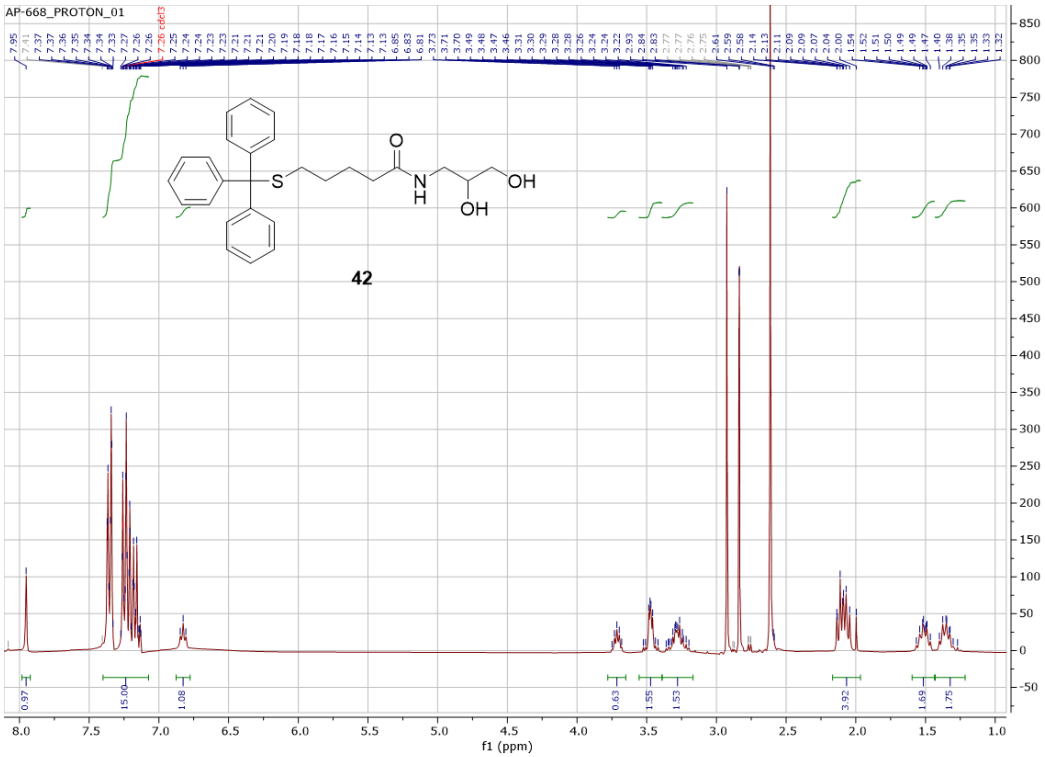

6.1.27. Compound 43

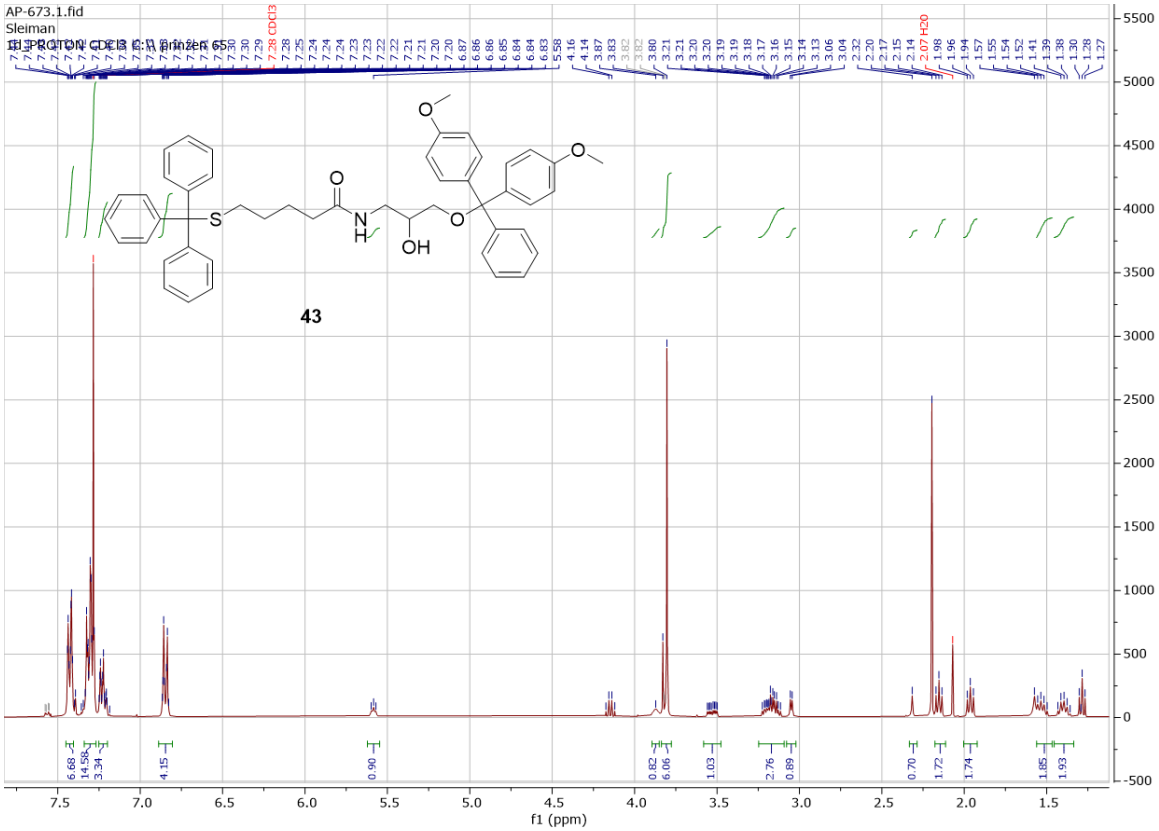

6.1.28. Compound 45

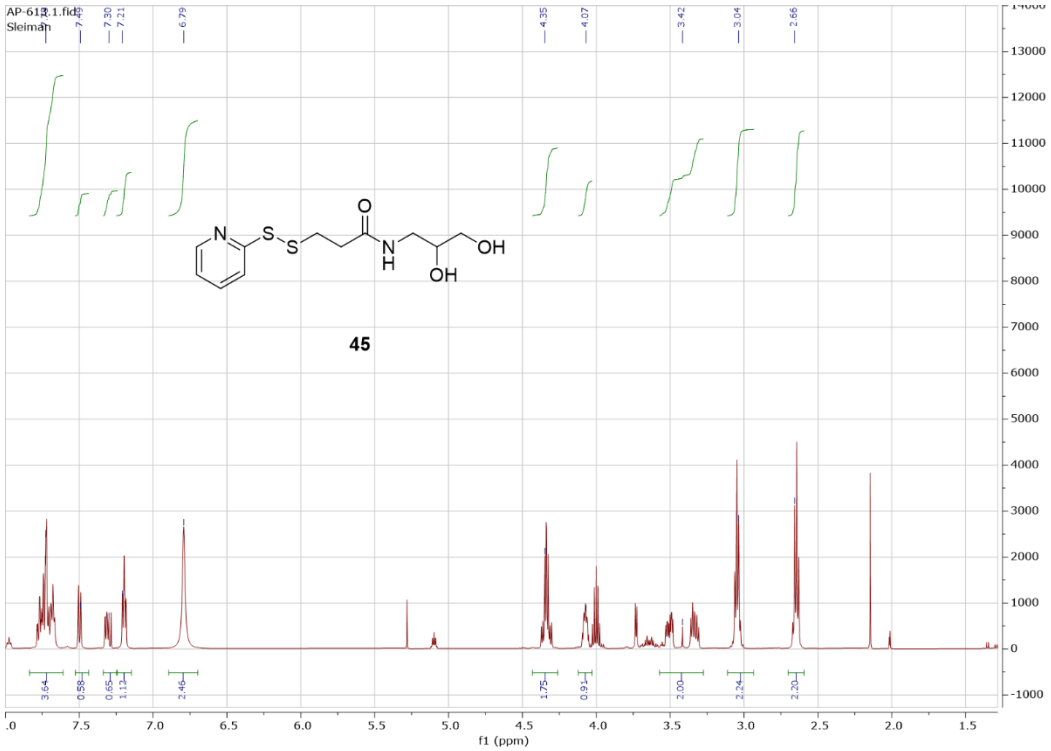

6.1.29. Compound 46

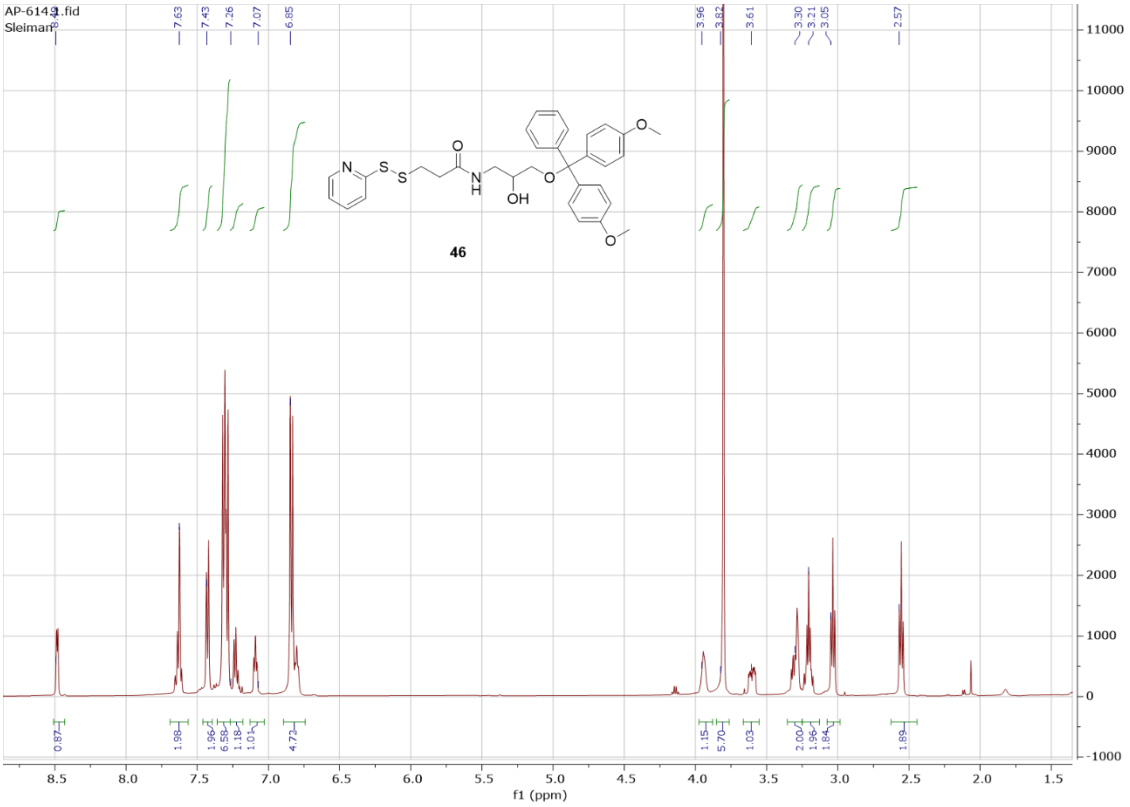

6.2. Molecules from Chapter 3

6.2.1. Compound 4

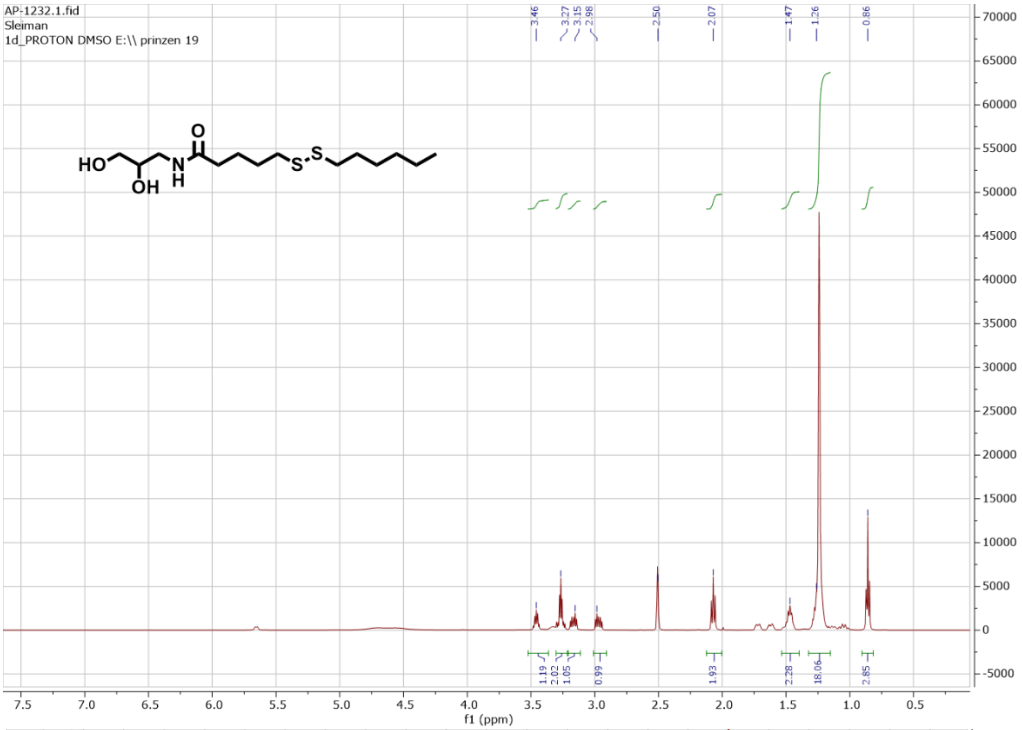

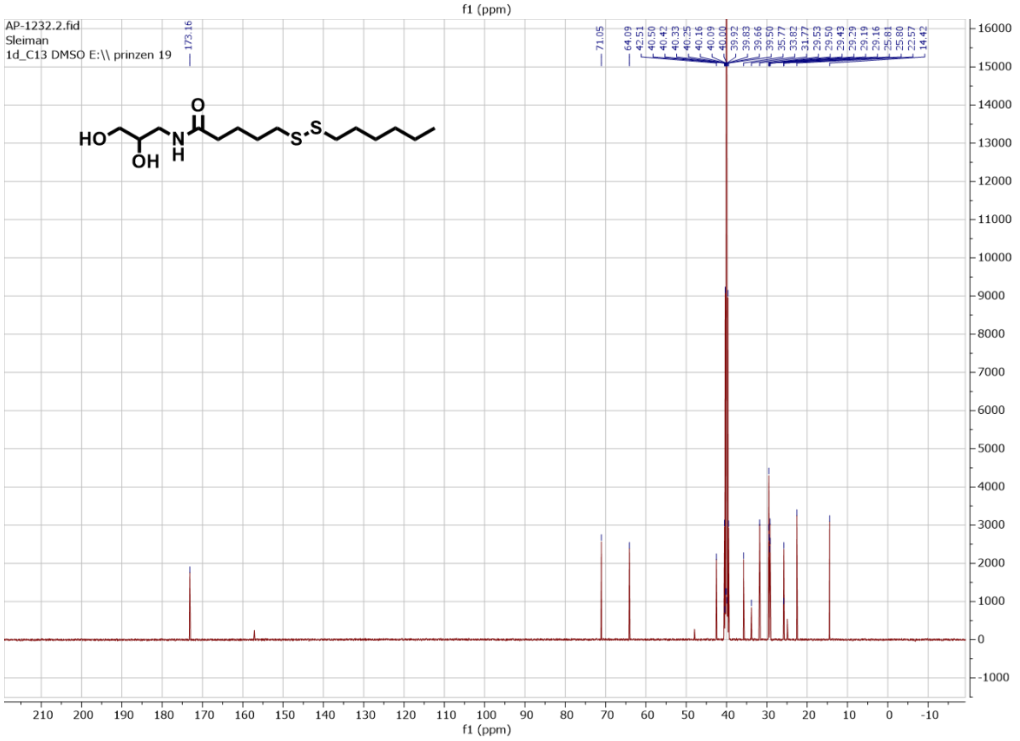

6.2.2. Compound 5

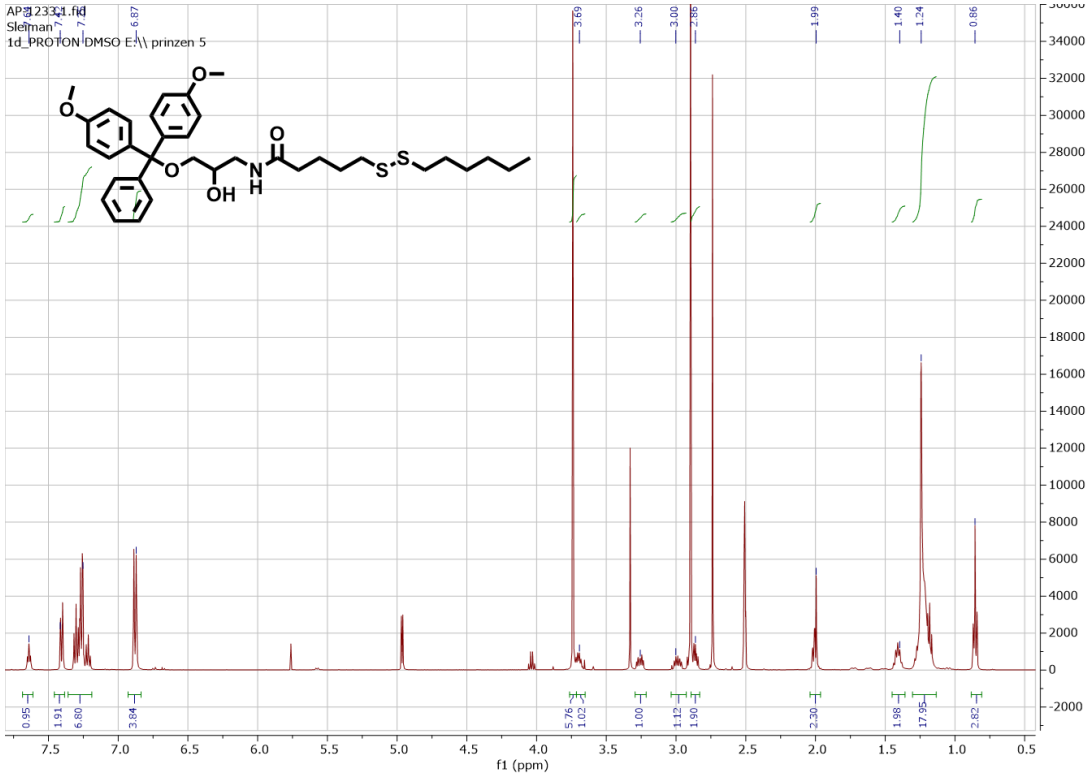

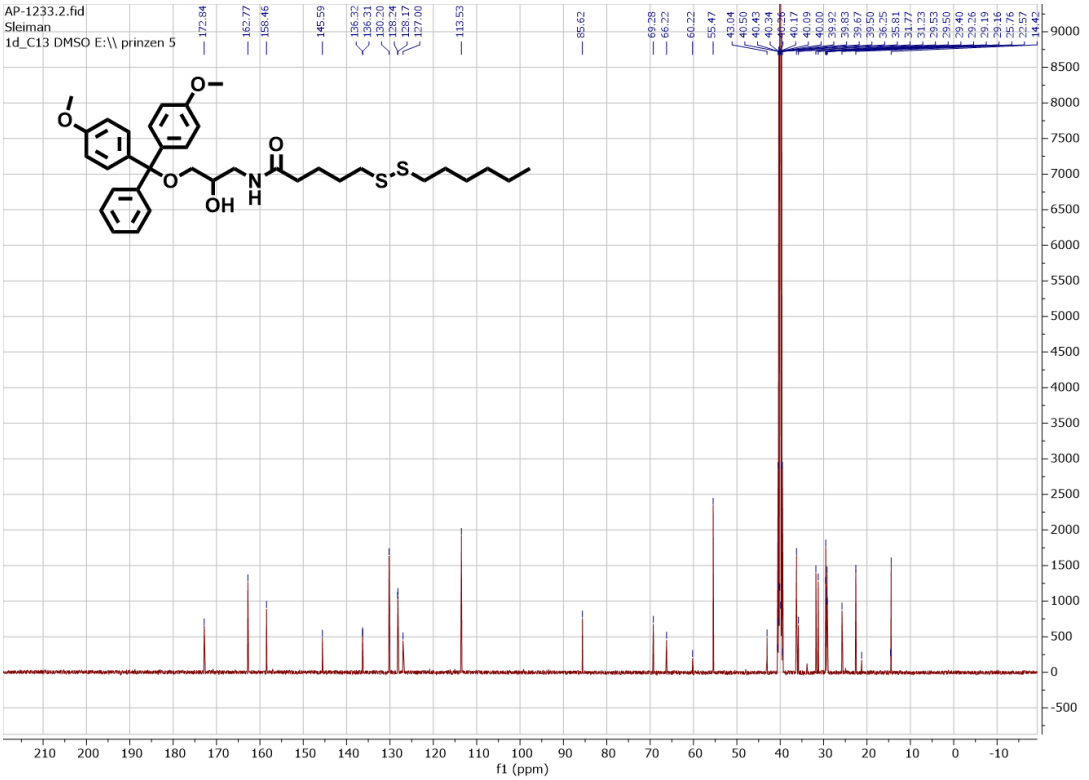

6.2.3. Compound 6

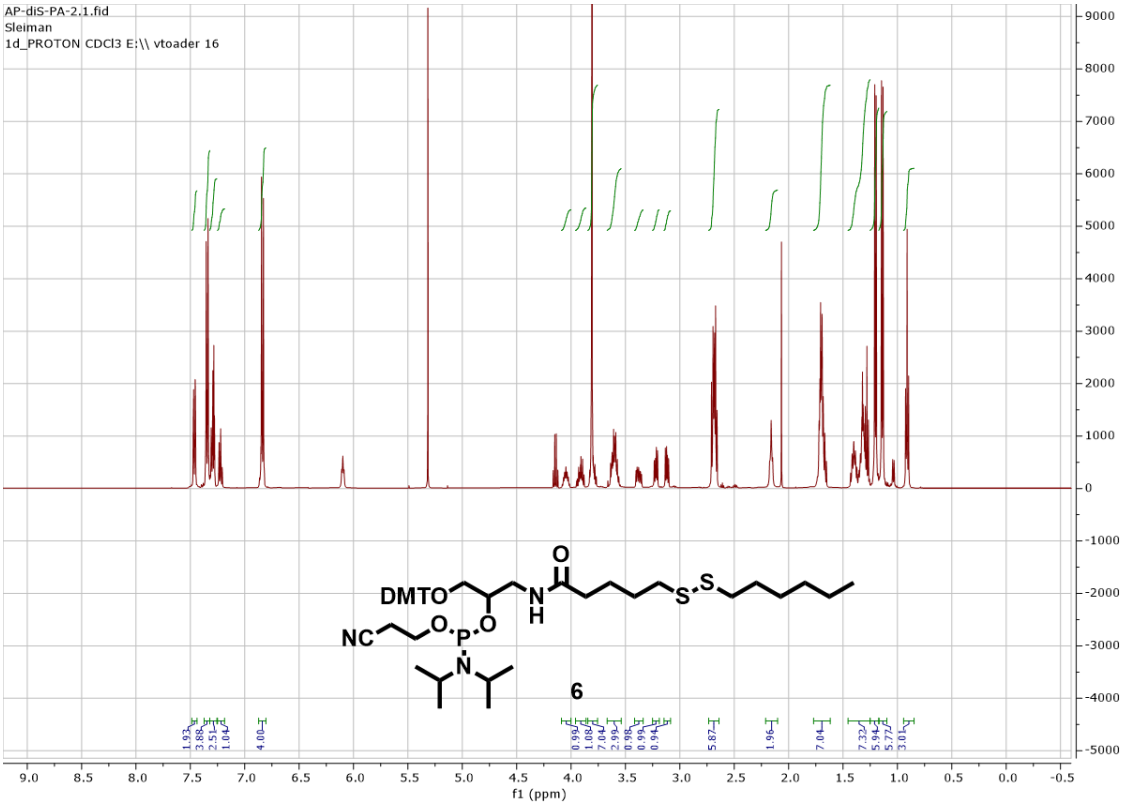

Parameter Value
1Acquisition Date 2021-10-17T00:14:33

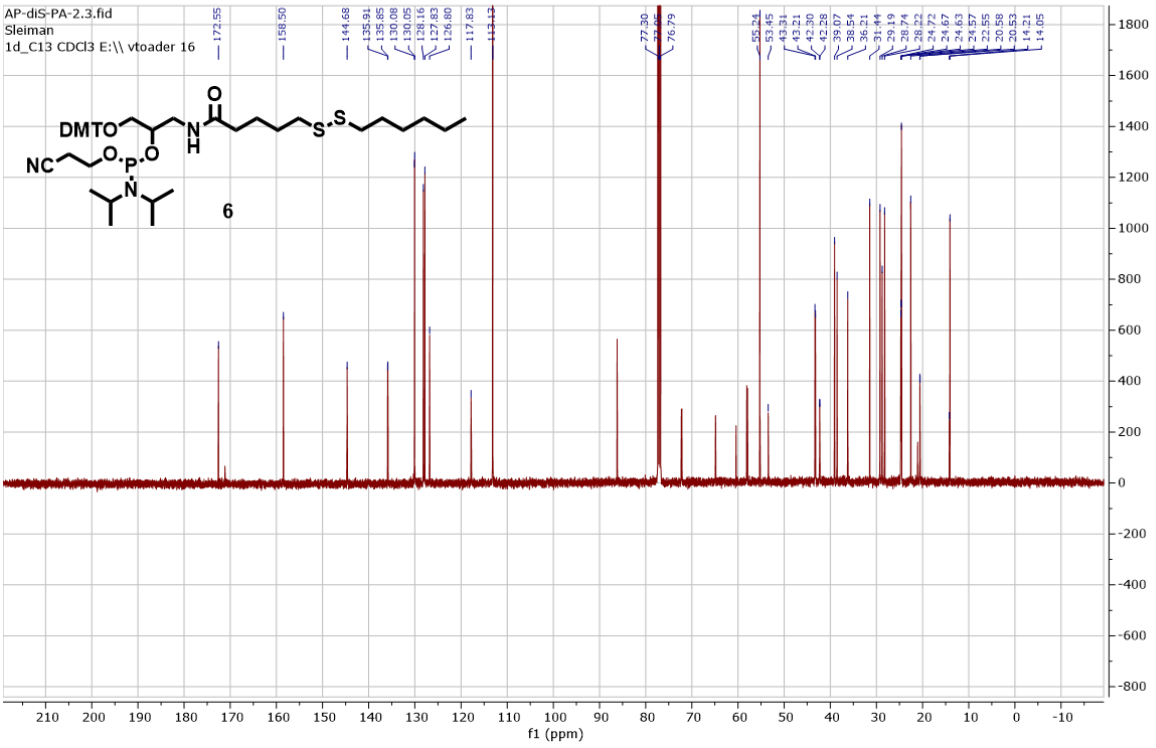

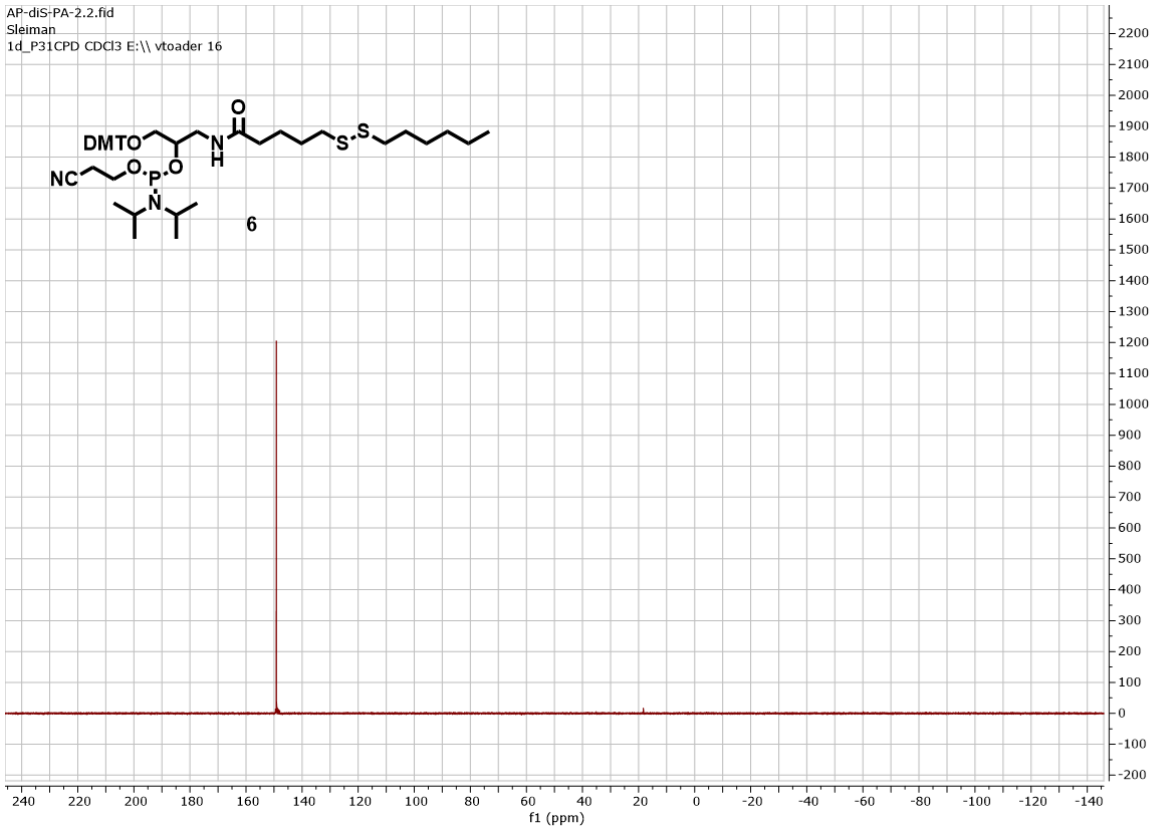
AP-diS-PA-2.2.fid
Sleiman
1d_P31CPD CDCl3 E:\\ vtoader 16
DMTO
NC
O
P
N
H
S
S
6
f1 (ppm)

6.2.4. Compound 7

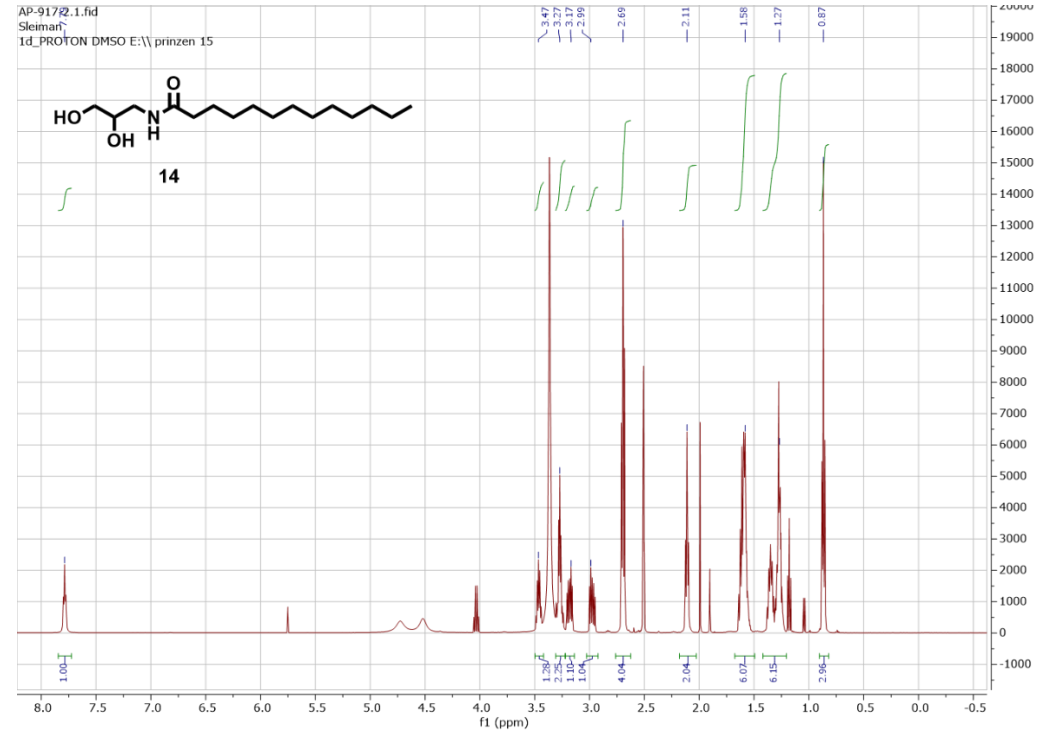

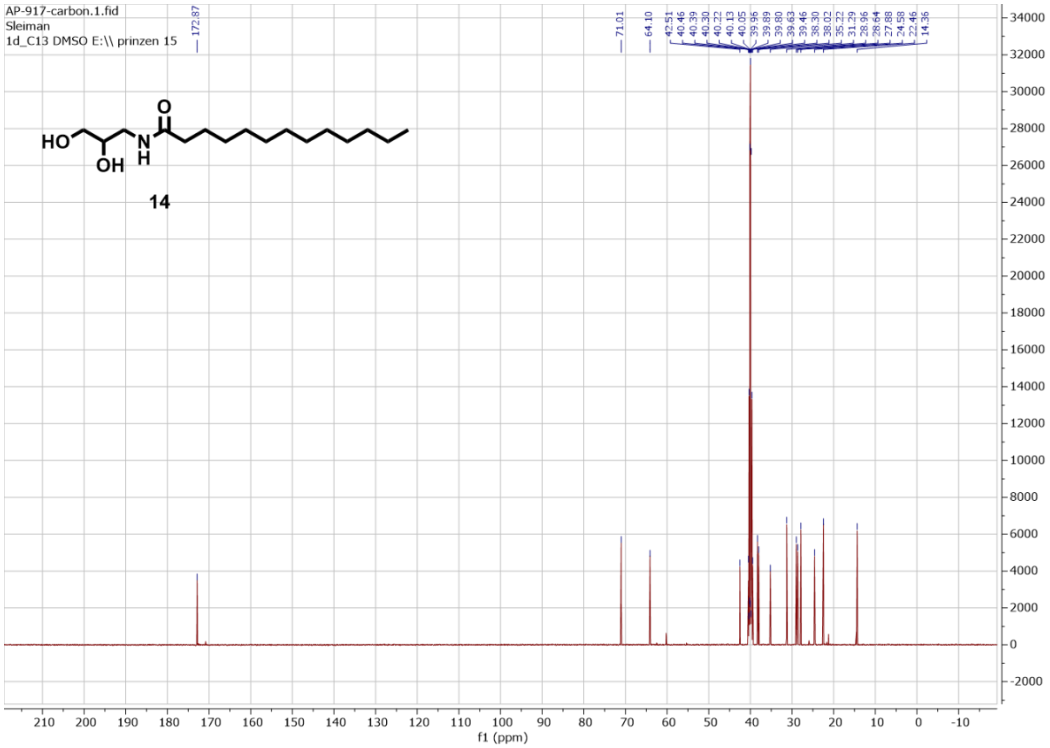

6.2.5. Compound 8

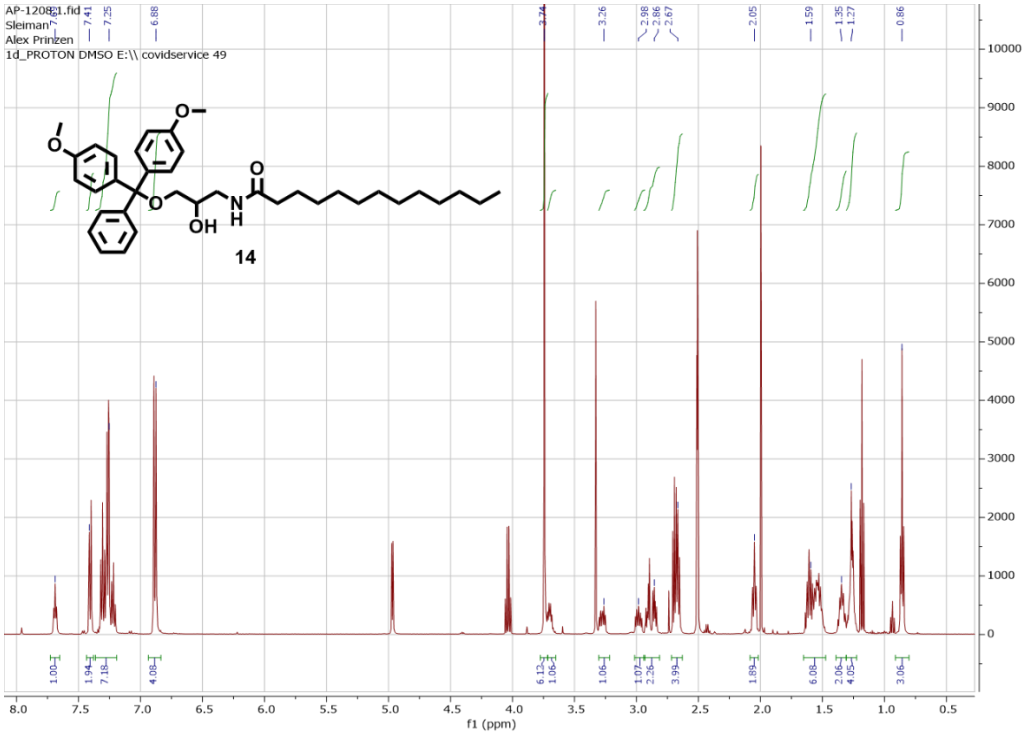

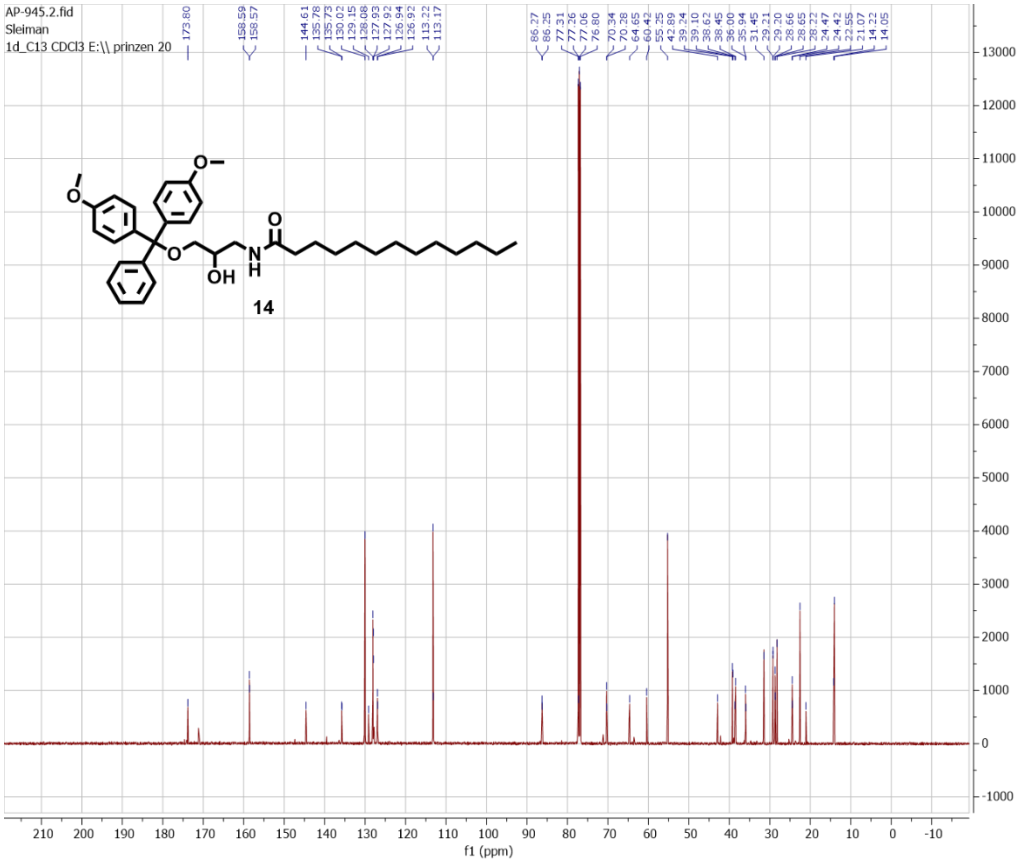

6.2.6. Compound 9

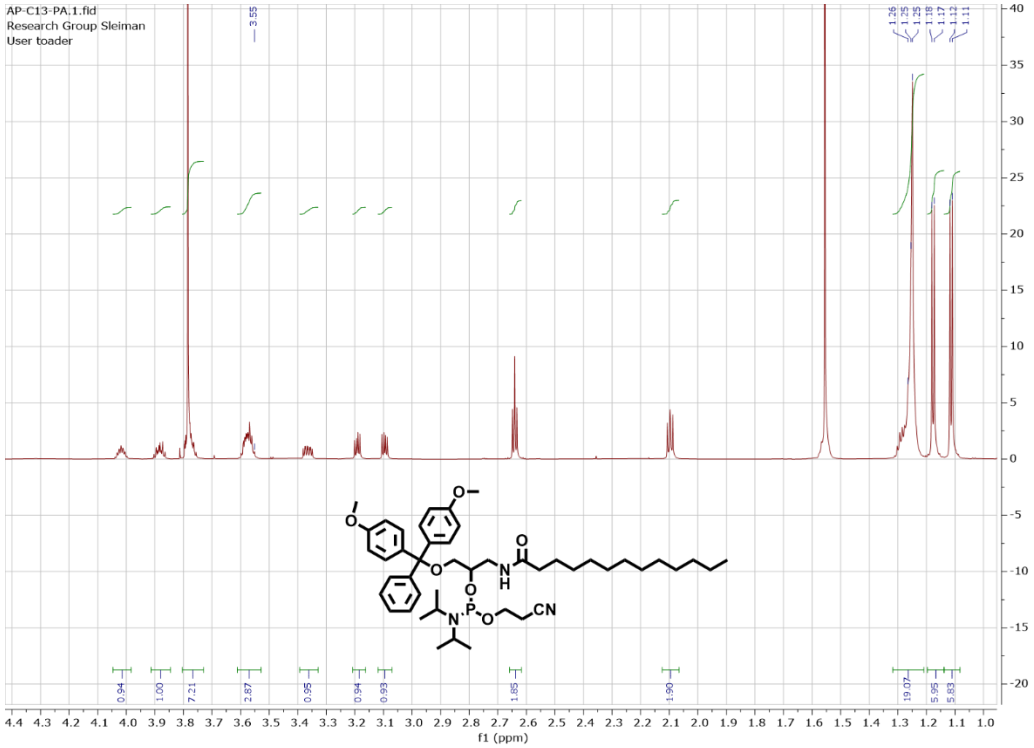

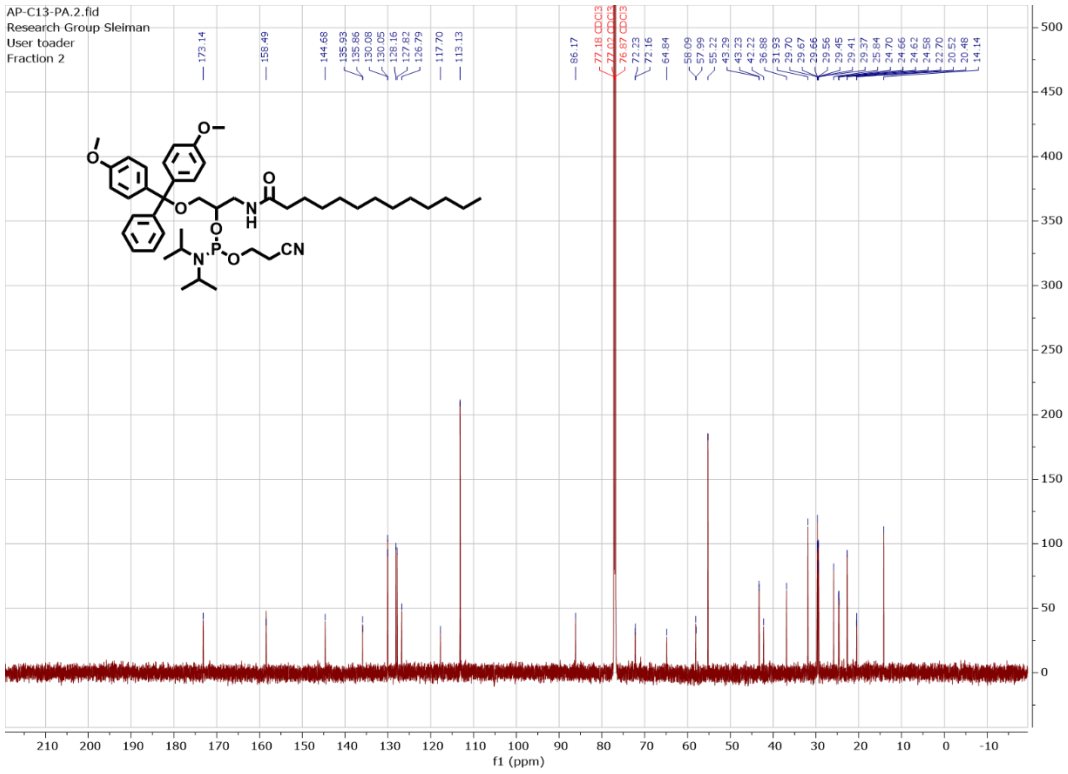

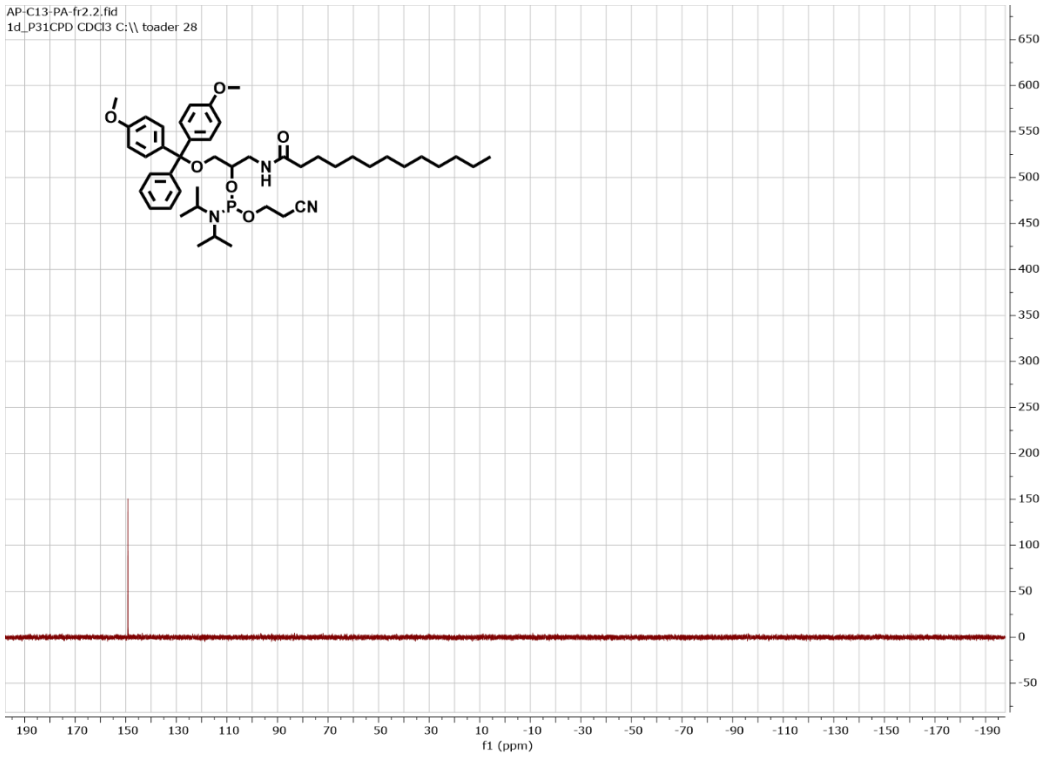
AP-C13-PA-fr2.2.fid
1d_P31CPD CDCl3 C:\\ toader 28
650
600
550
500
450
400
350
300
250
200
150
100
50
0
-50
190 170 150 130 110 90 70 50 30 10 -10 -30 -50 -70 -90 -110 -130 -150 -170 -190
f1 (ppm)

6.3. Molecules from Chapter 4

6.3.1. Compound 2

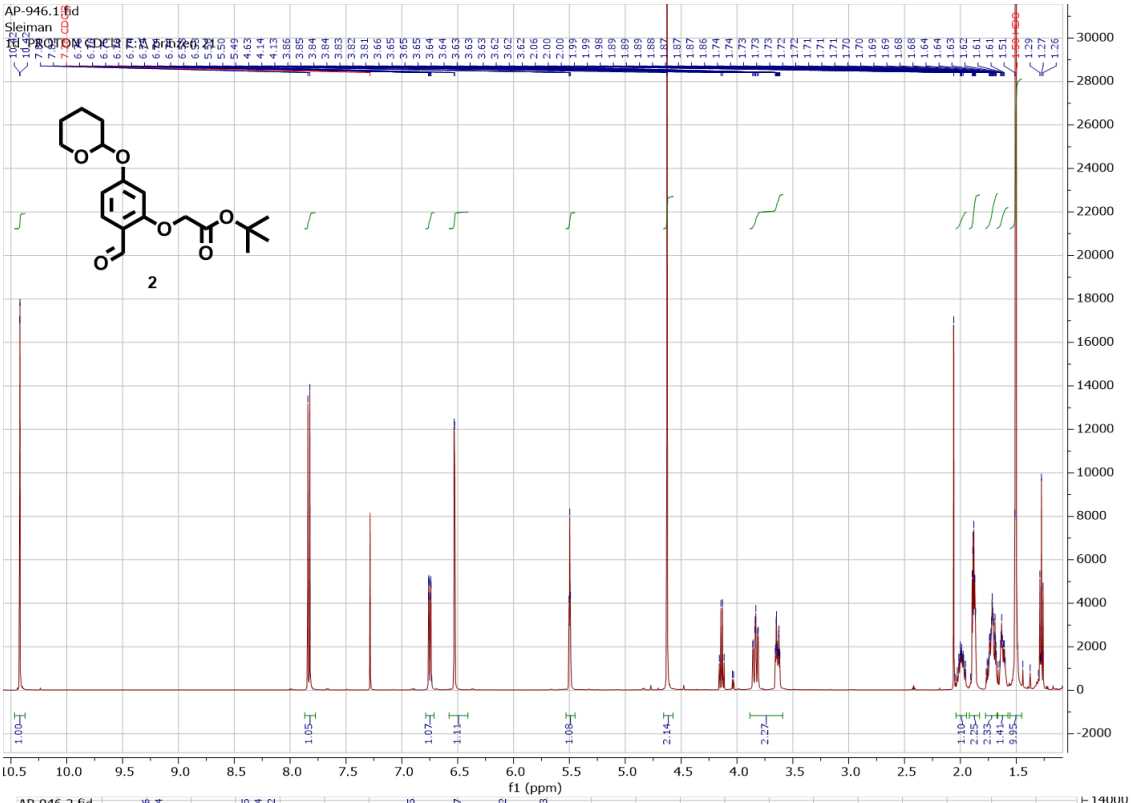

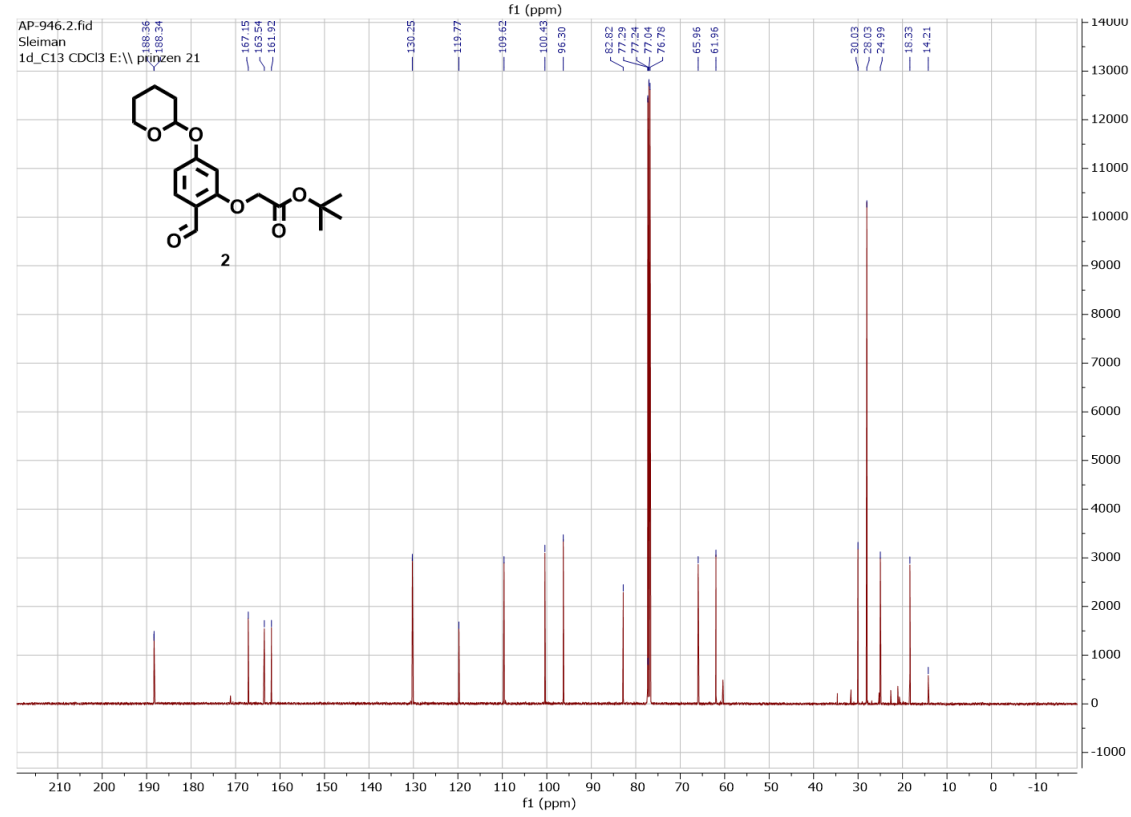

6.3.2. Compound 3

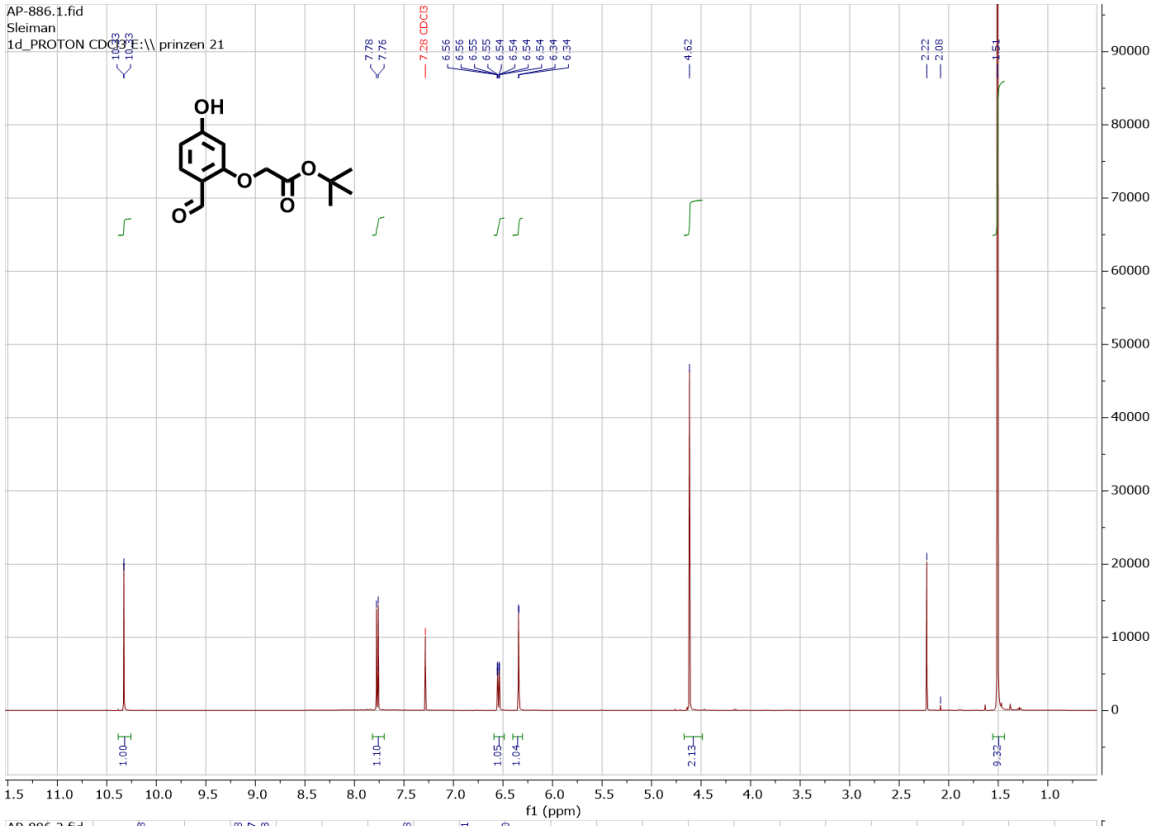

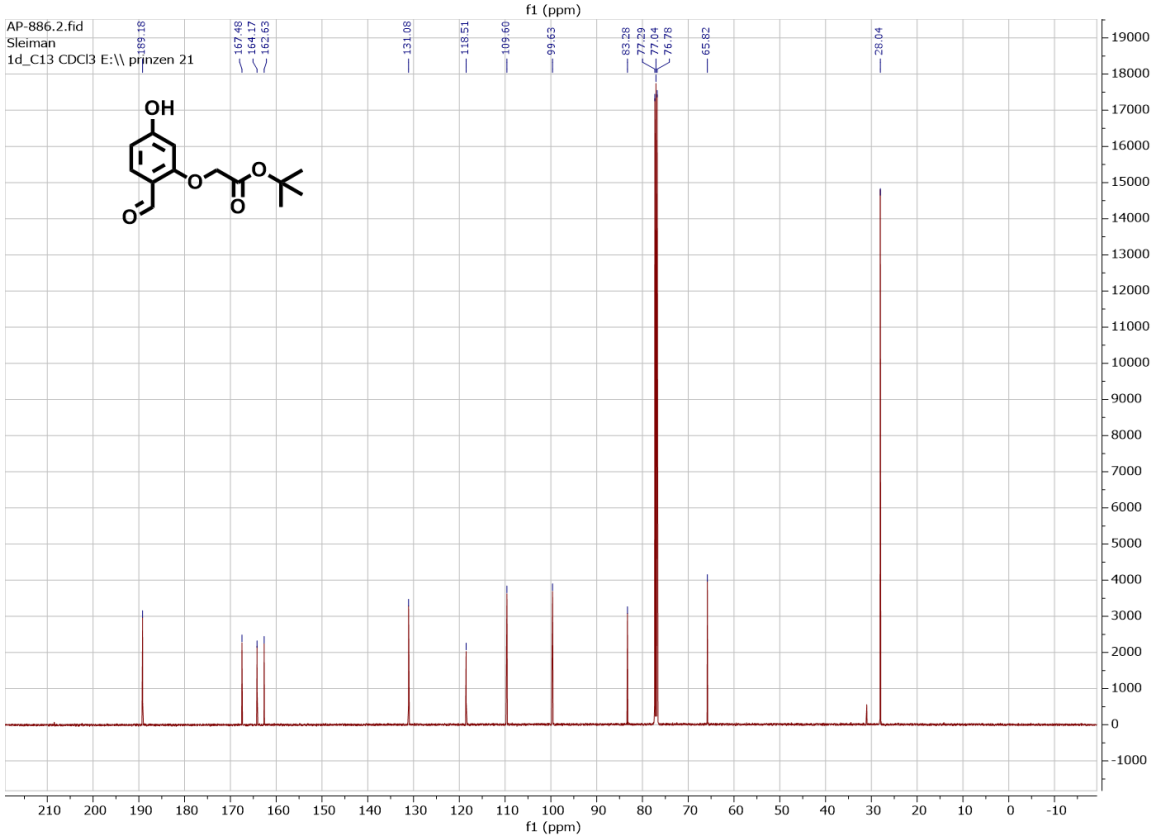

6.3.3. Compound 4

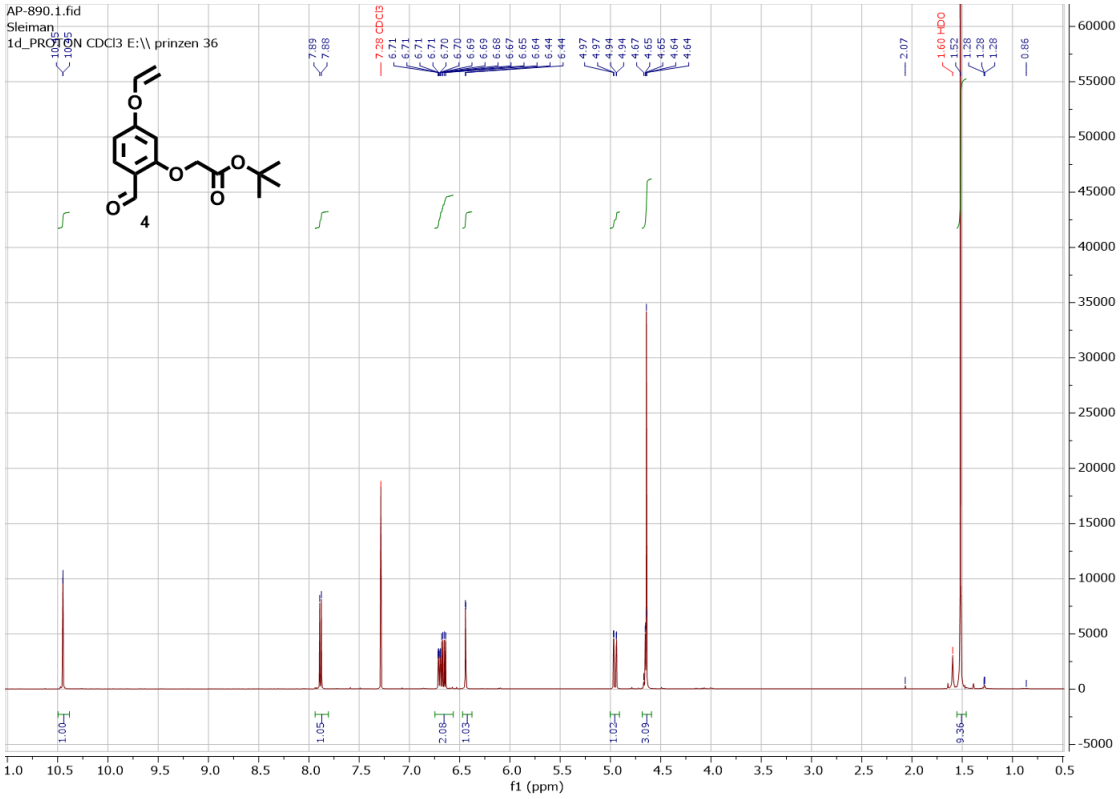

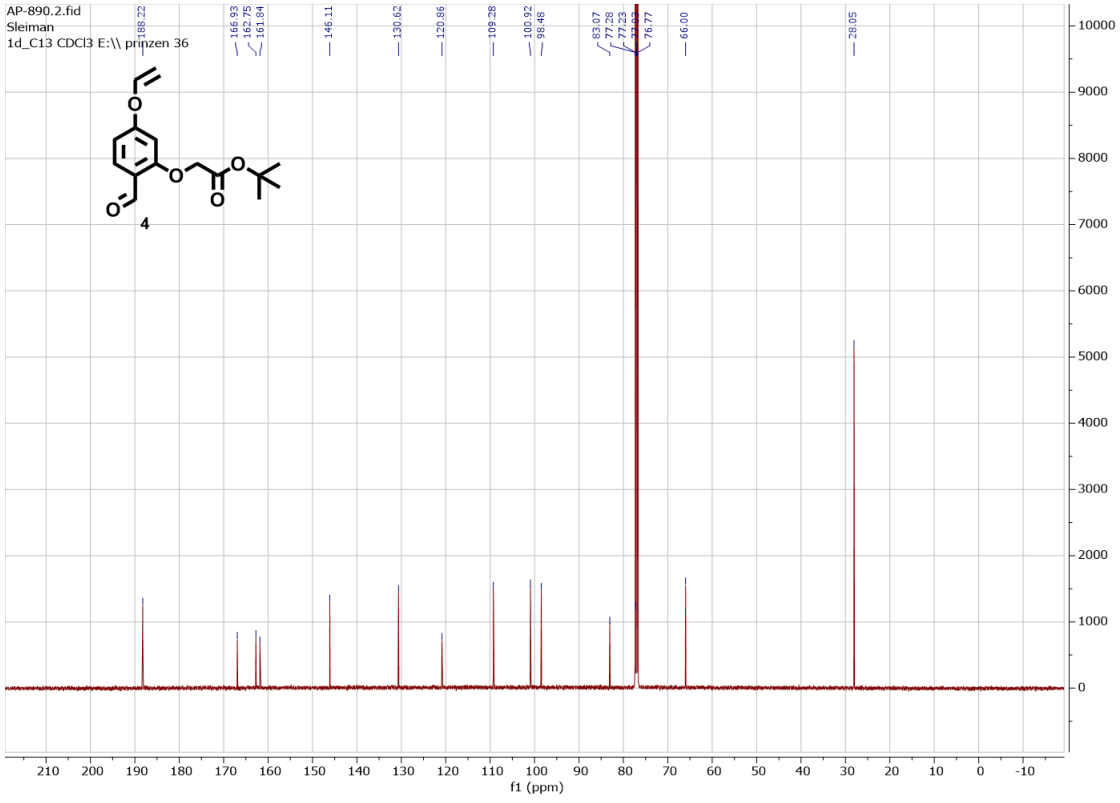

6.3.4. Compound 5

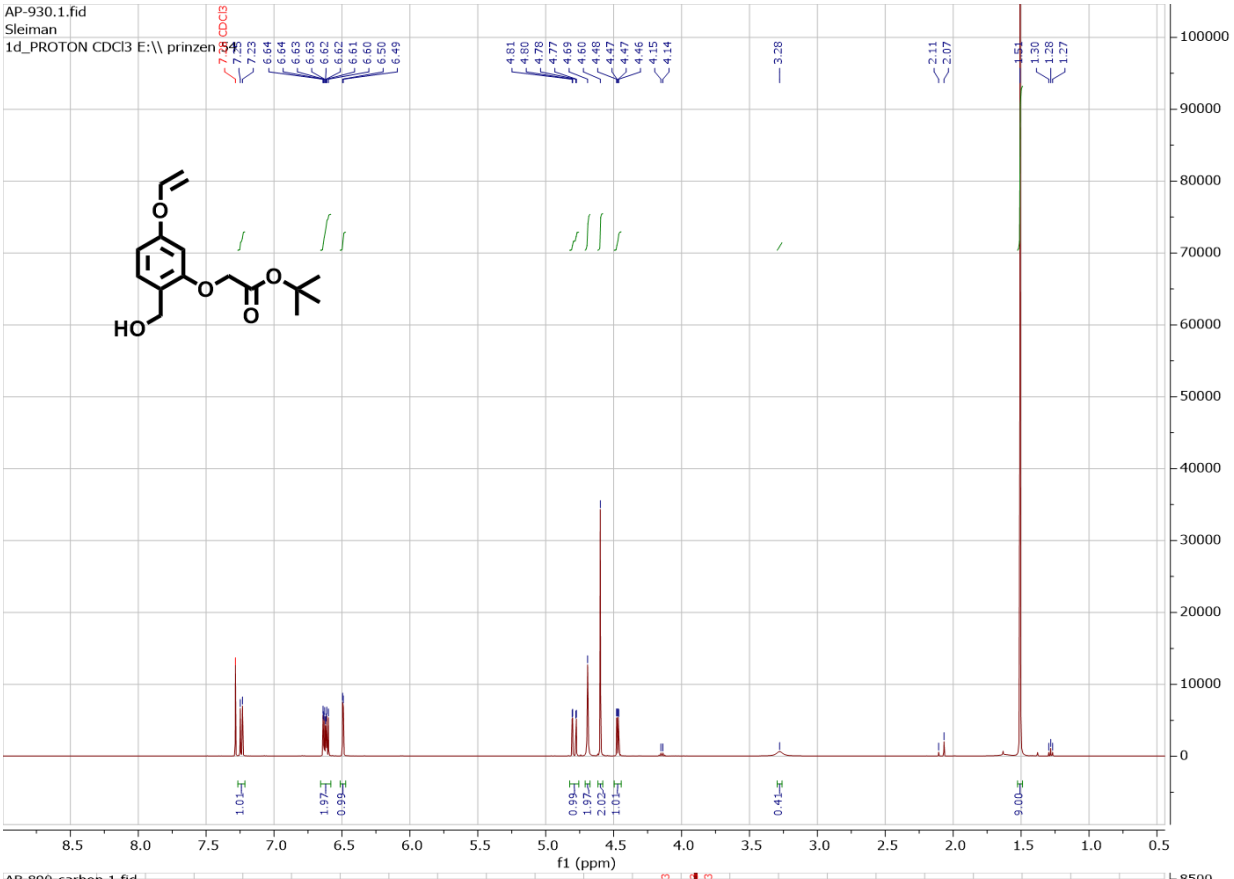

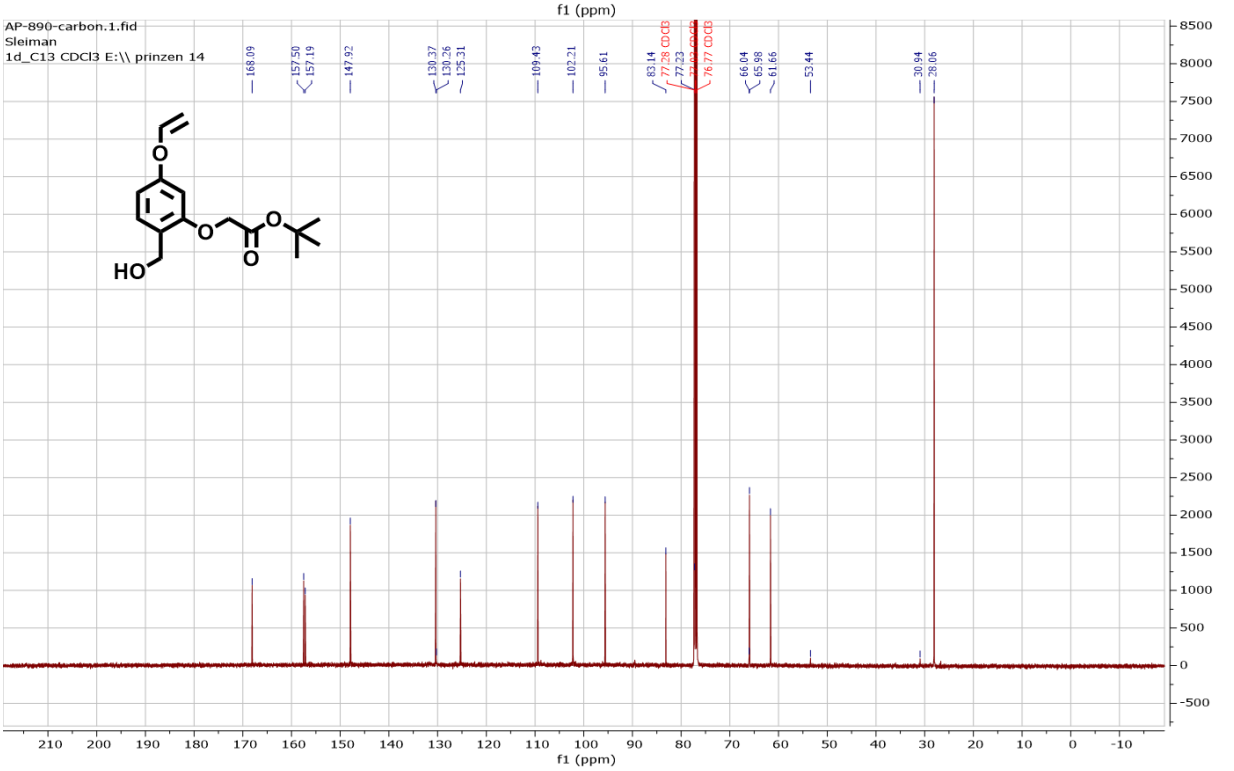

6.3.5. Compound 9

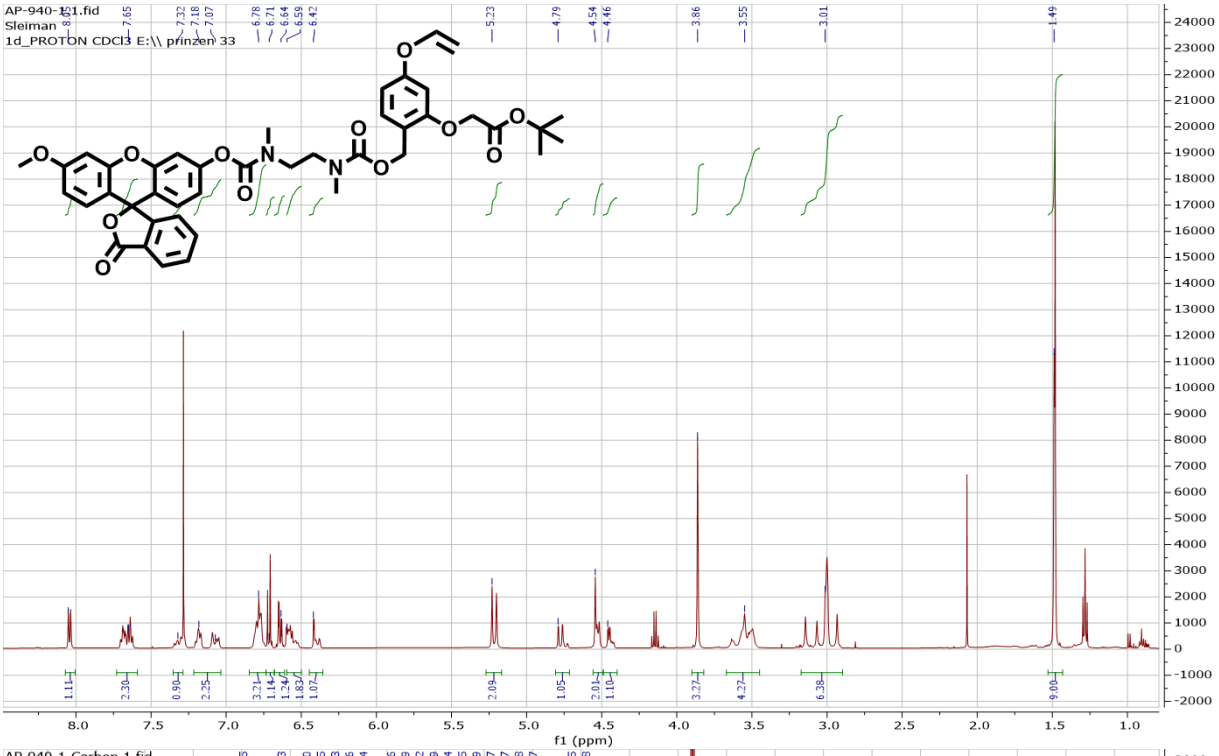

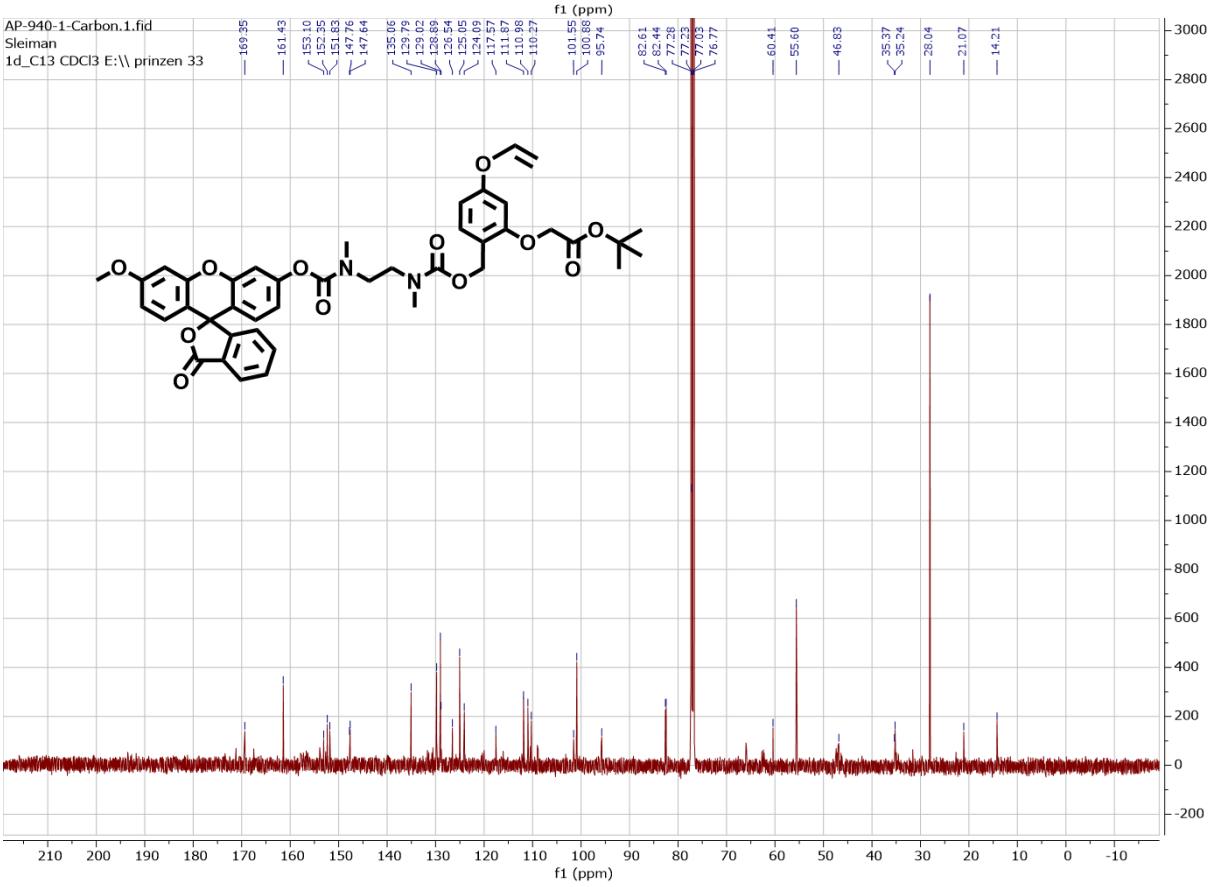

6.4. Molecules from Appendix i.

6.4.1. Compound 1

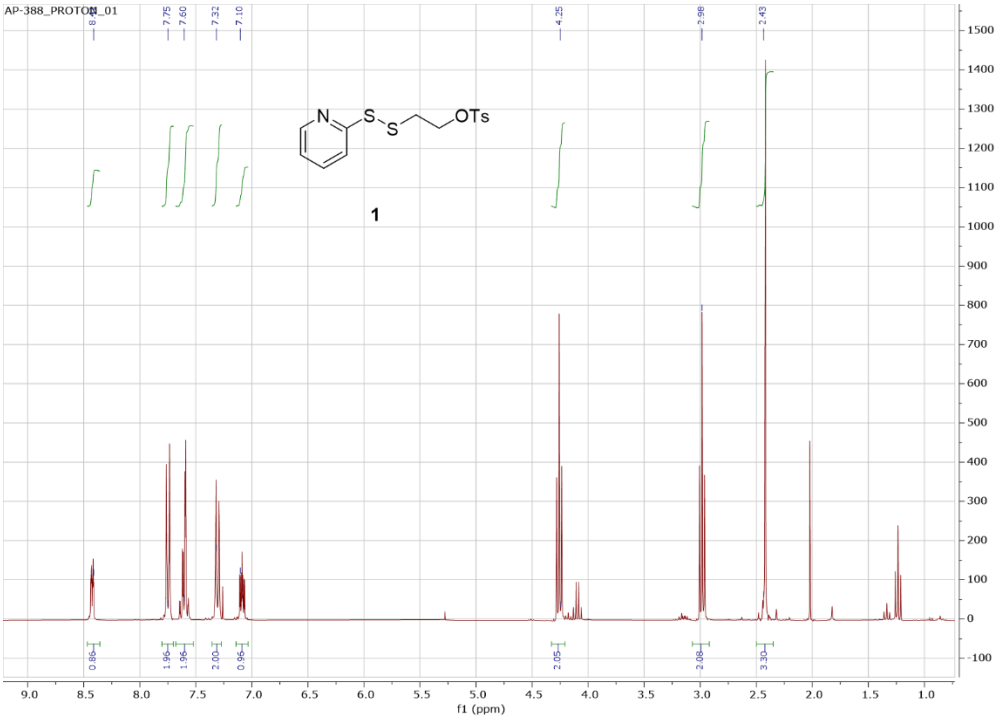

6.4.2. Compound 2

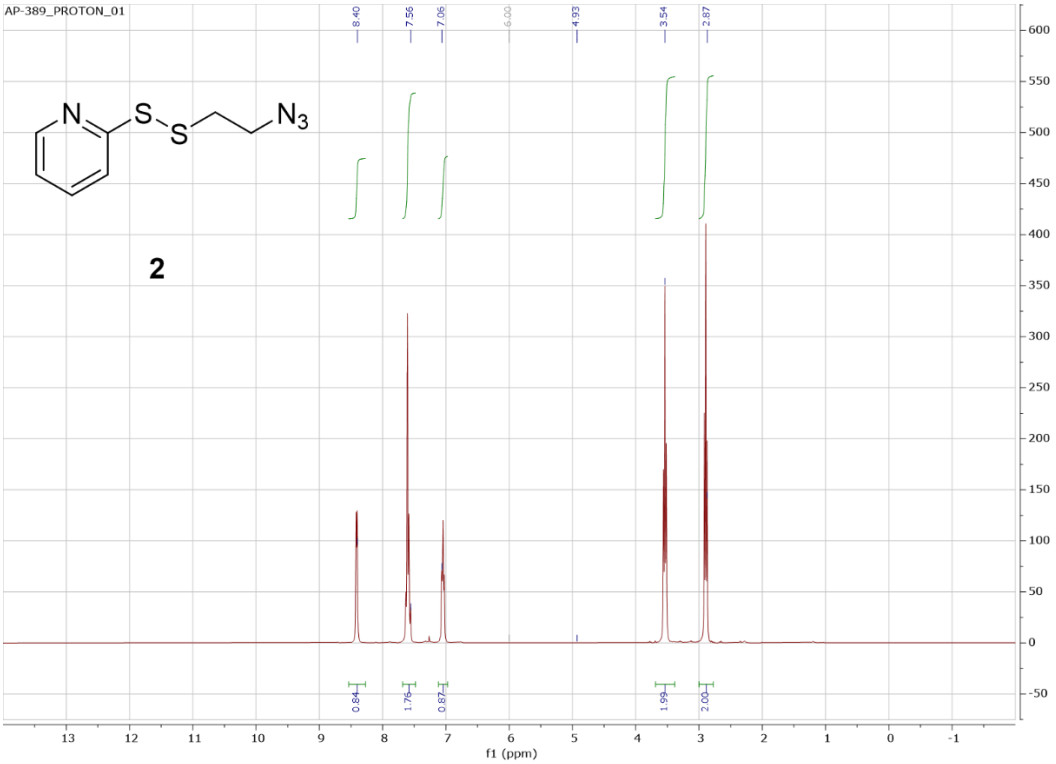

6.4.3. Compound 3

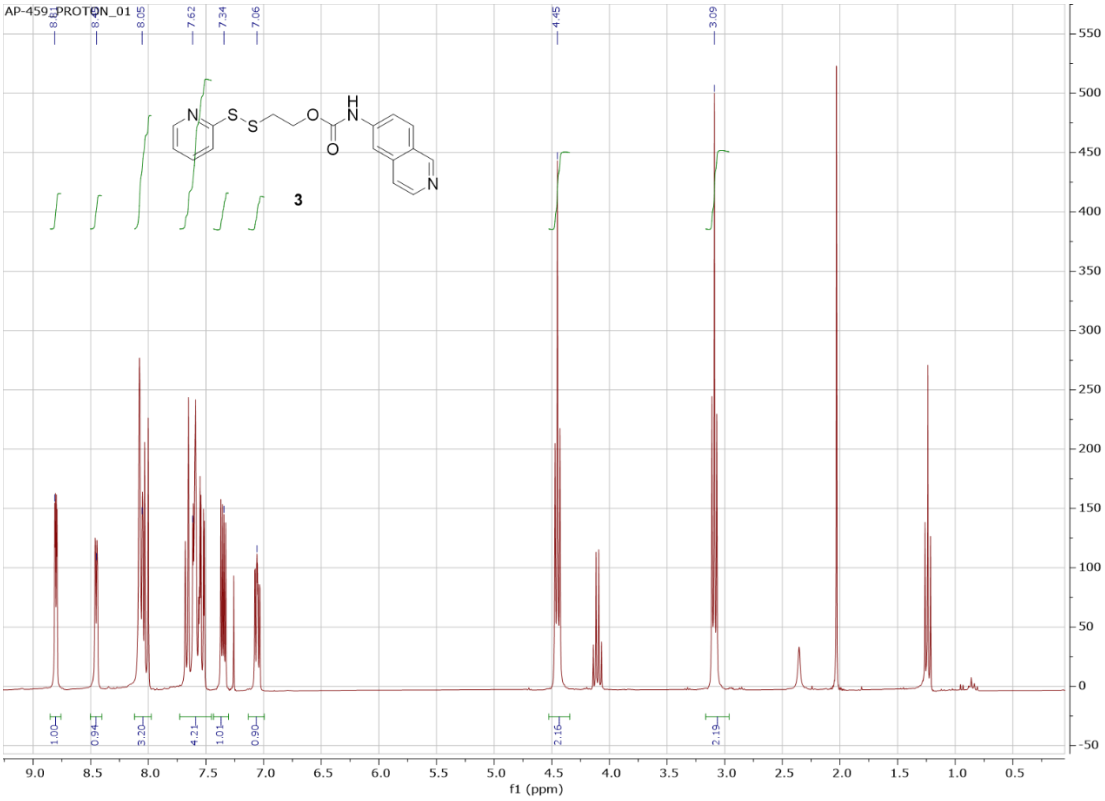

6.4.4. Compound 4

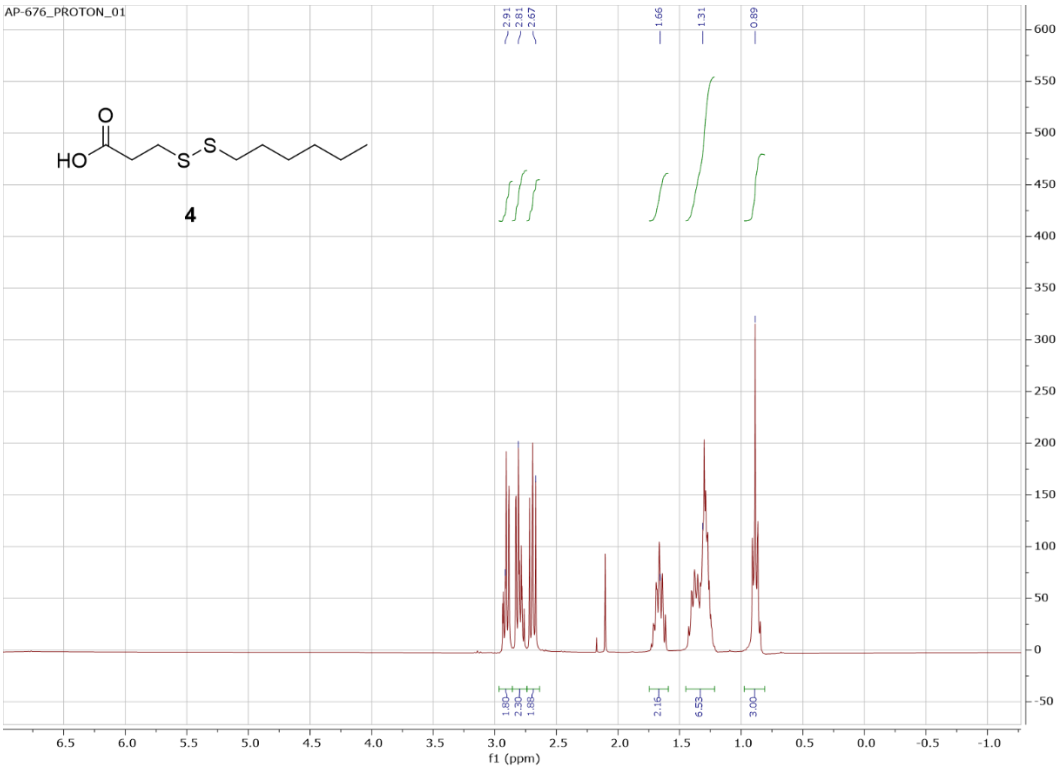

6.4.5. Compound 5

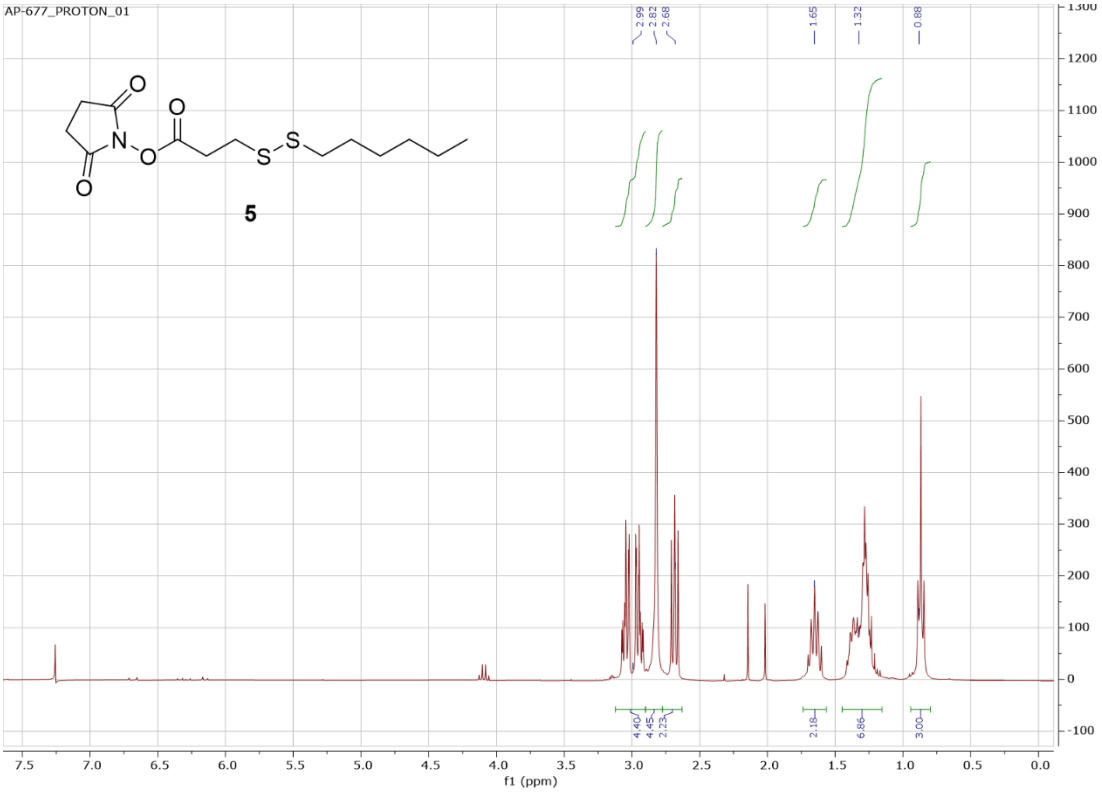

6.4.6. Compound 7

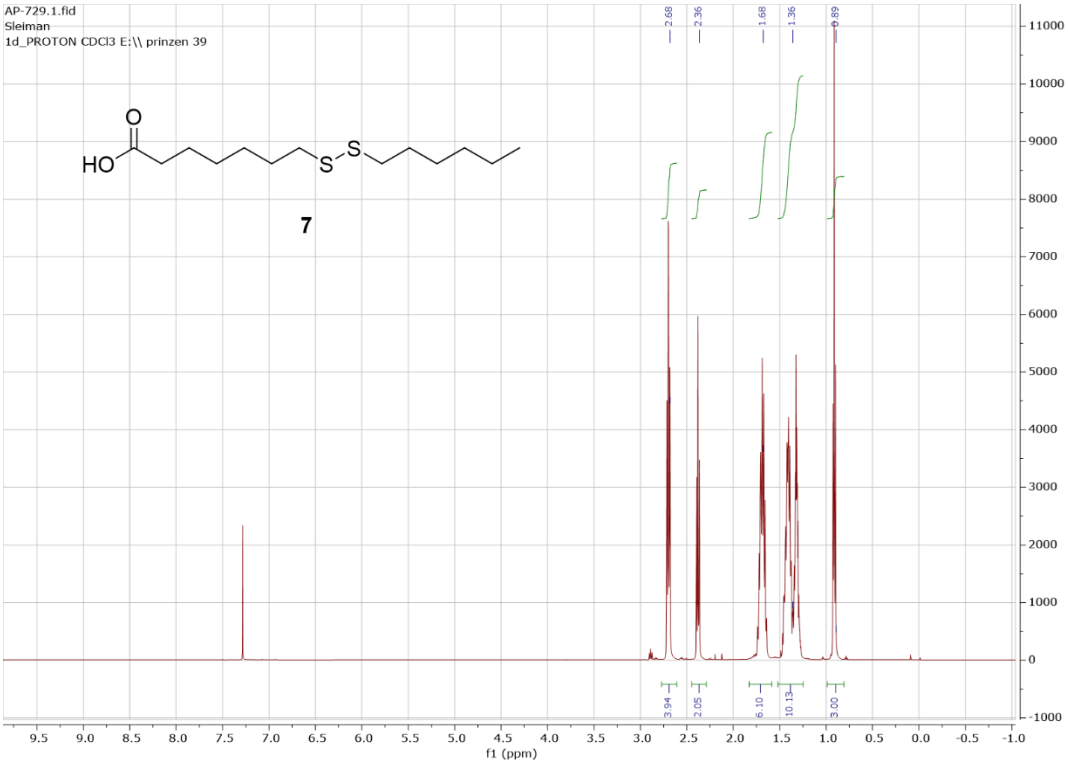

6.4.7. Compound 8

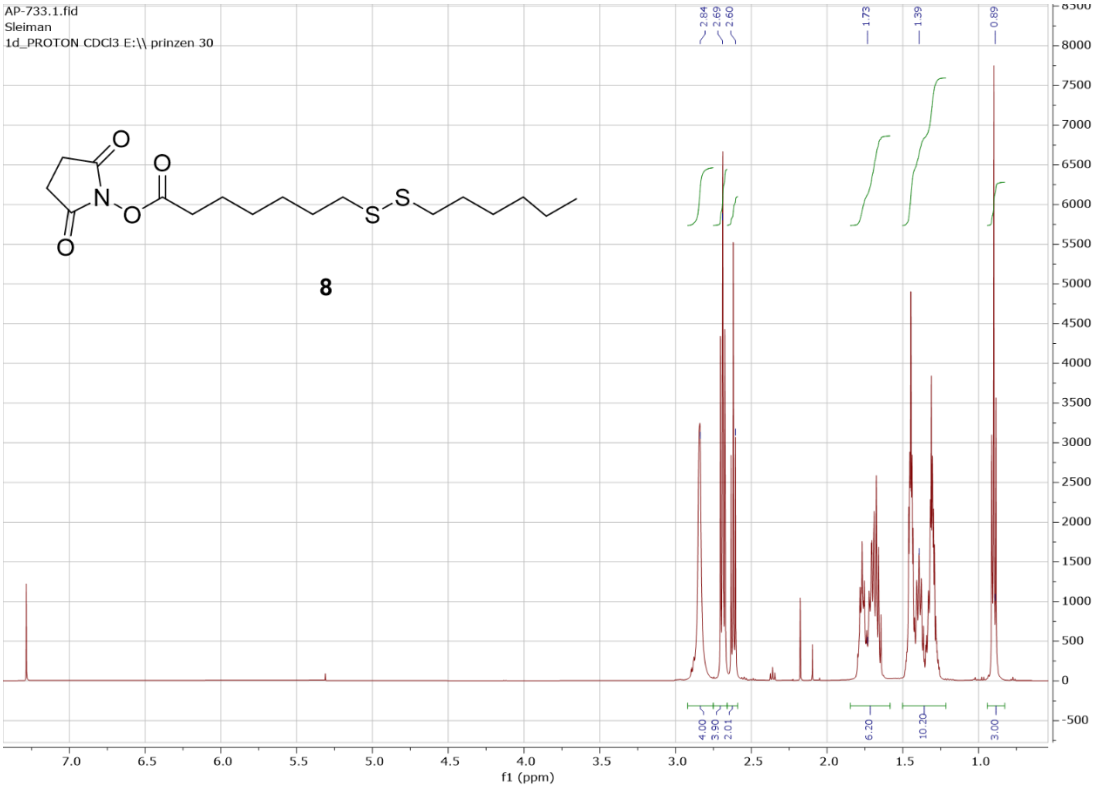

6.4.8. Compound 9

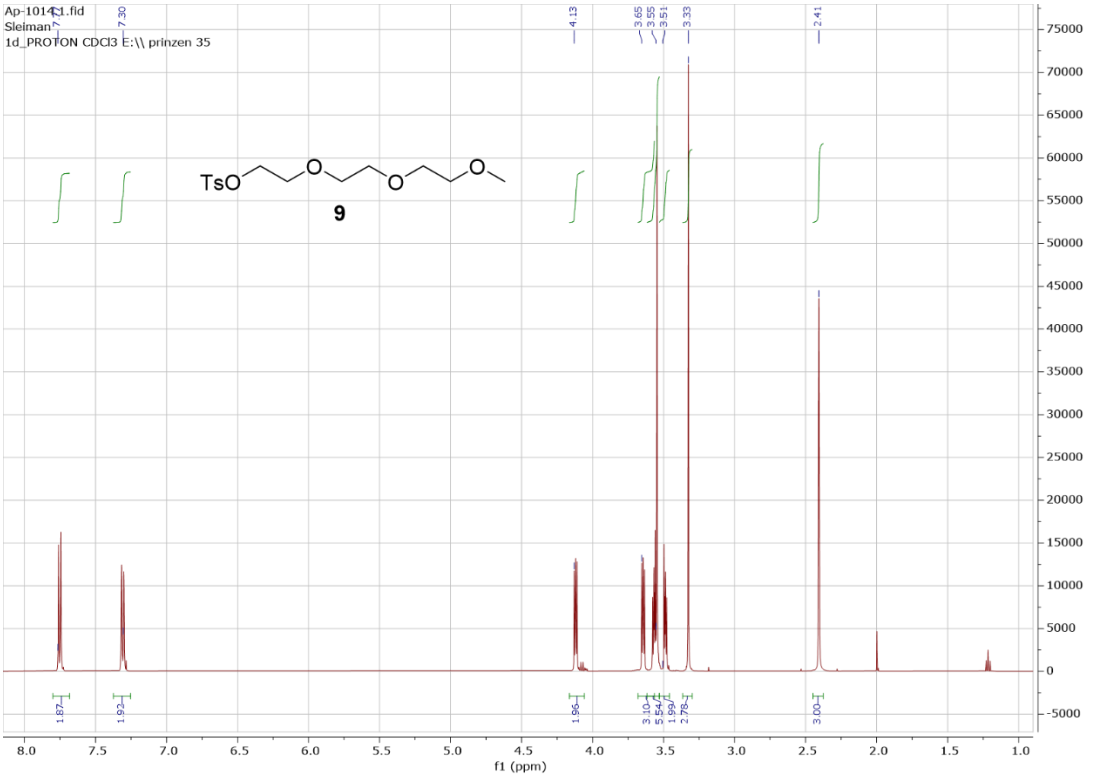

6.4.9. Compound 11

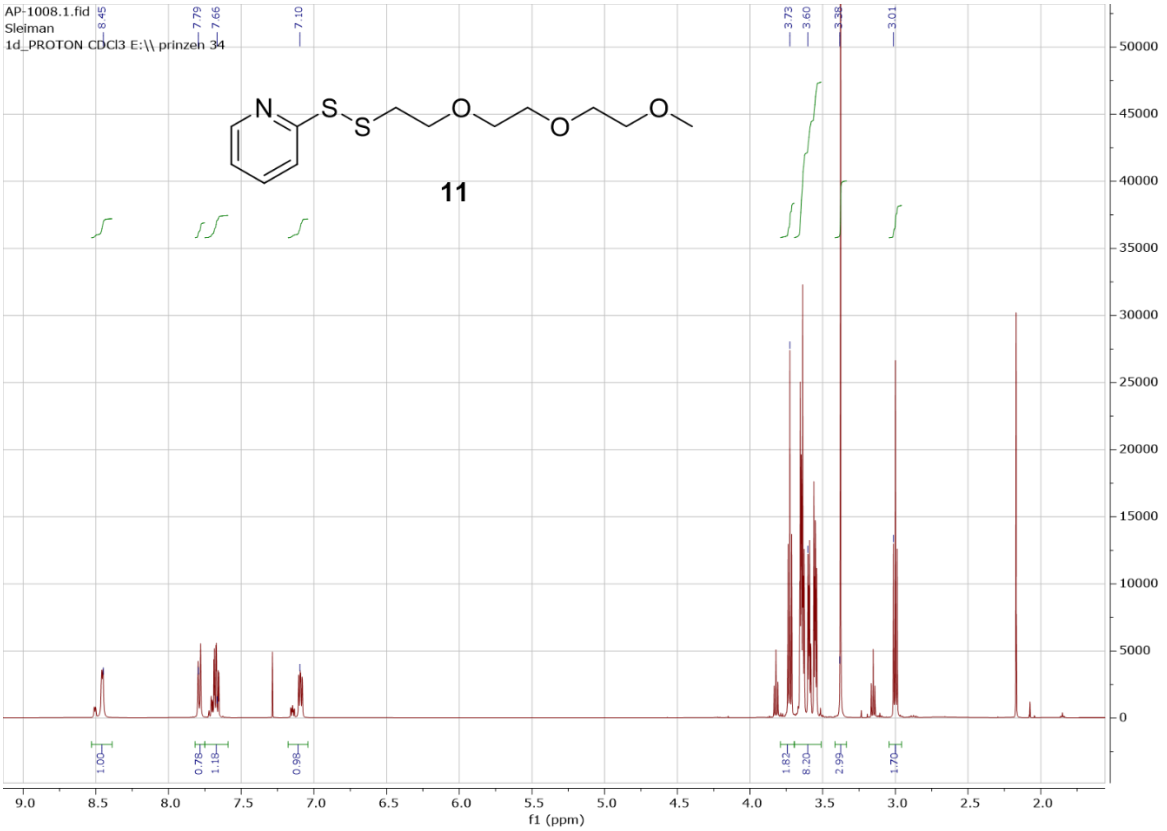

6.4.10. Compound 12

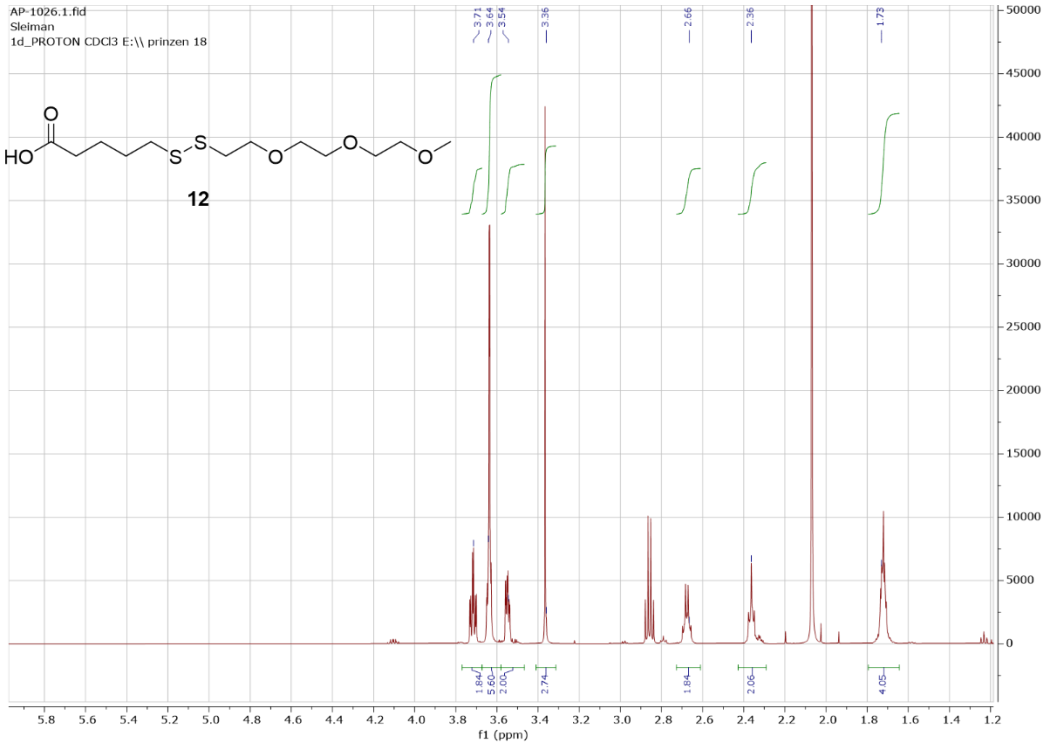

6.5. Molecules from Appendix ii.

6.5.1 Compound 13

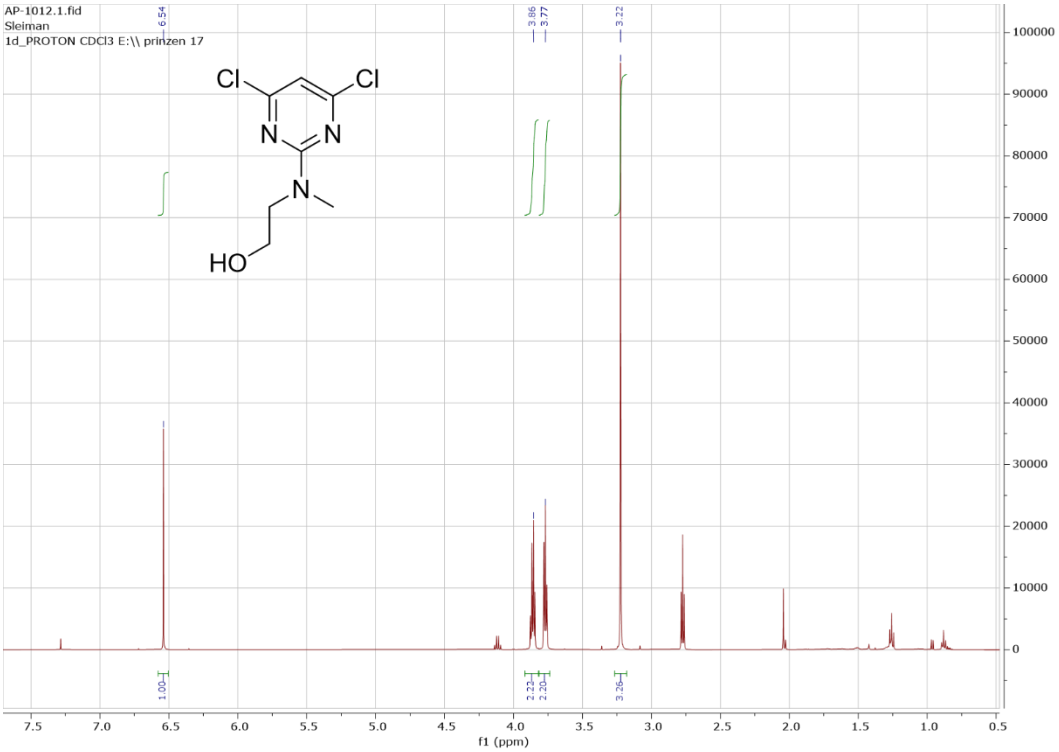

6.5.2 Compound 14

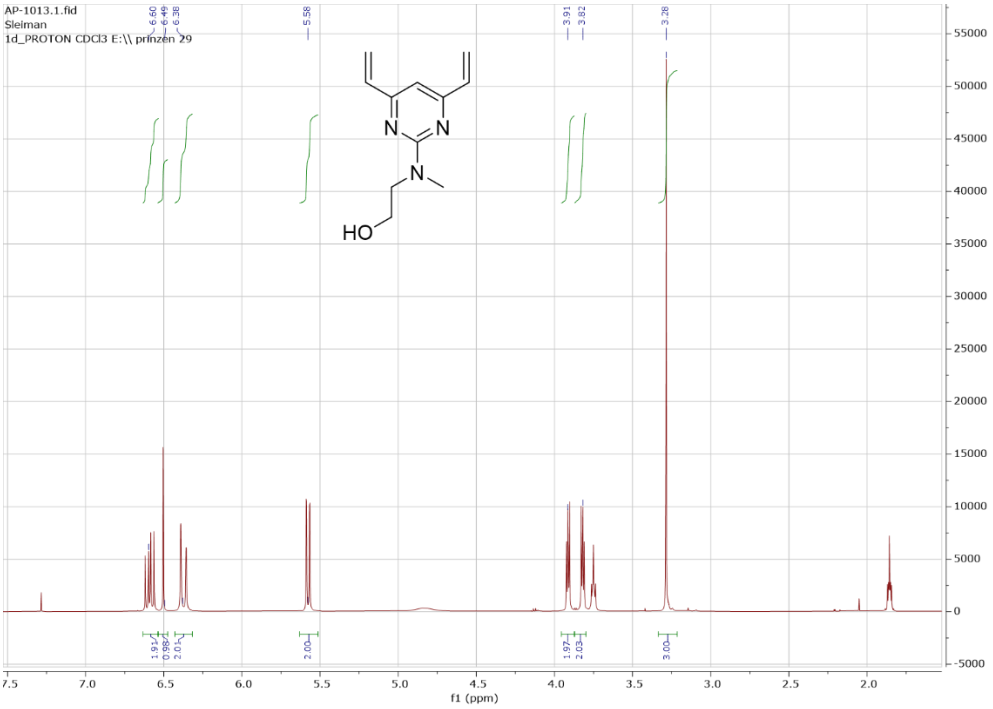

6.6. . Molecules from Appendix iii.

6.6.1 Compound 16

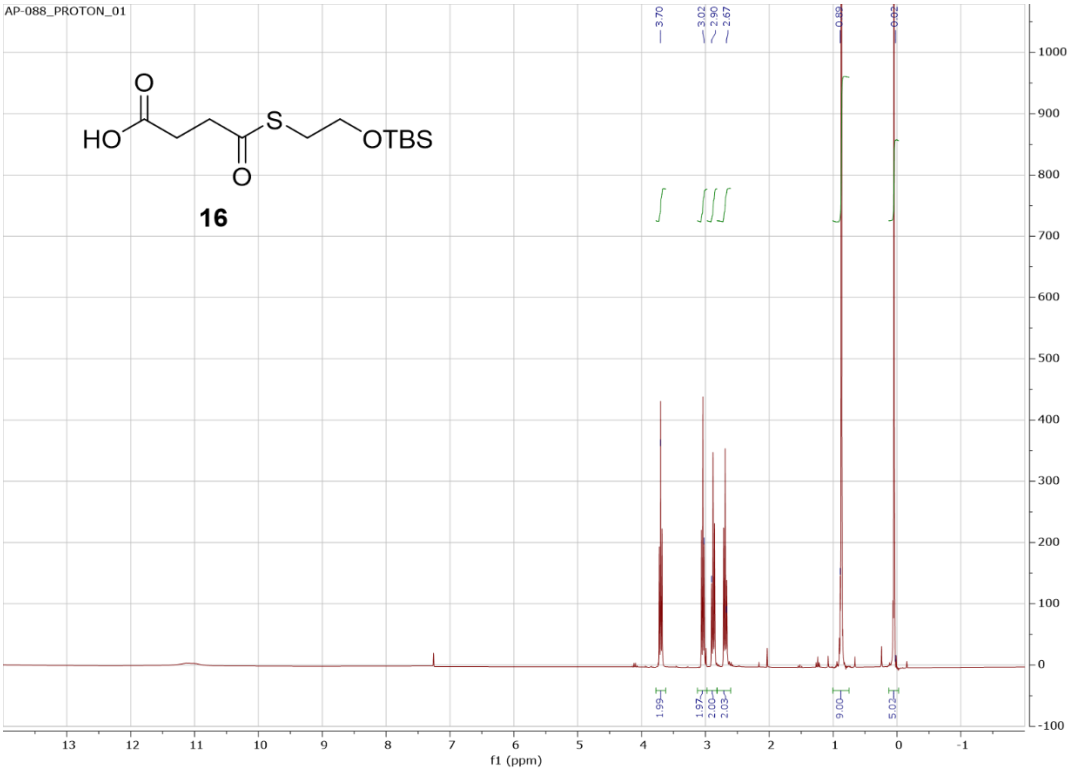

6.6.2 Compound 17

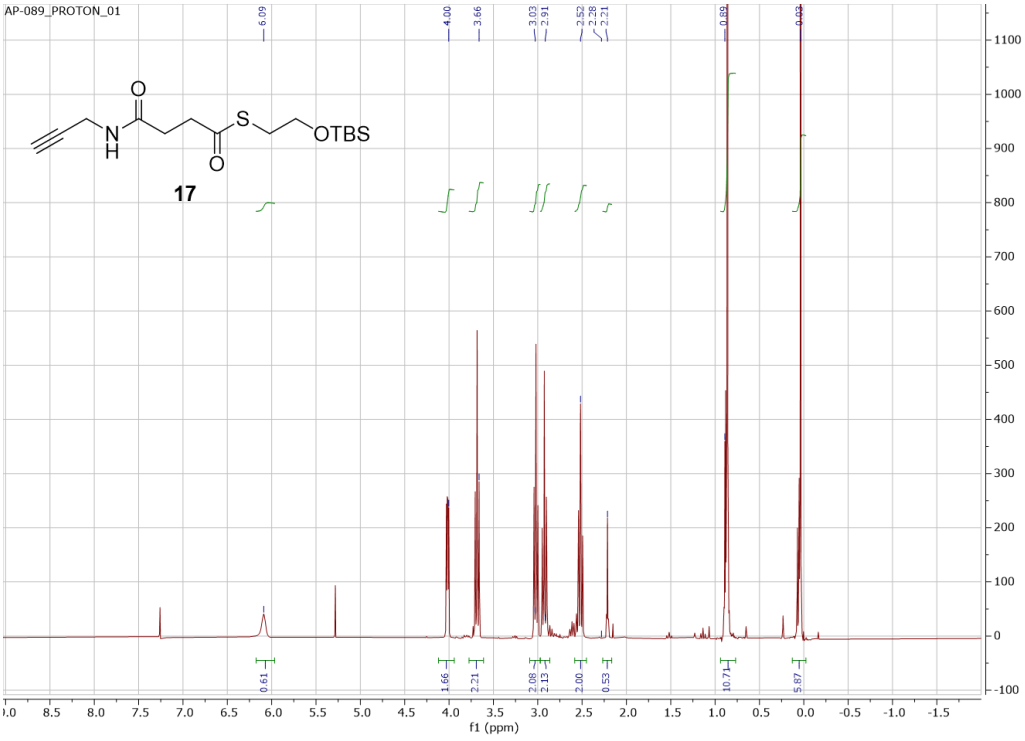

6.6.3 Compound 18

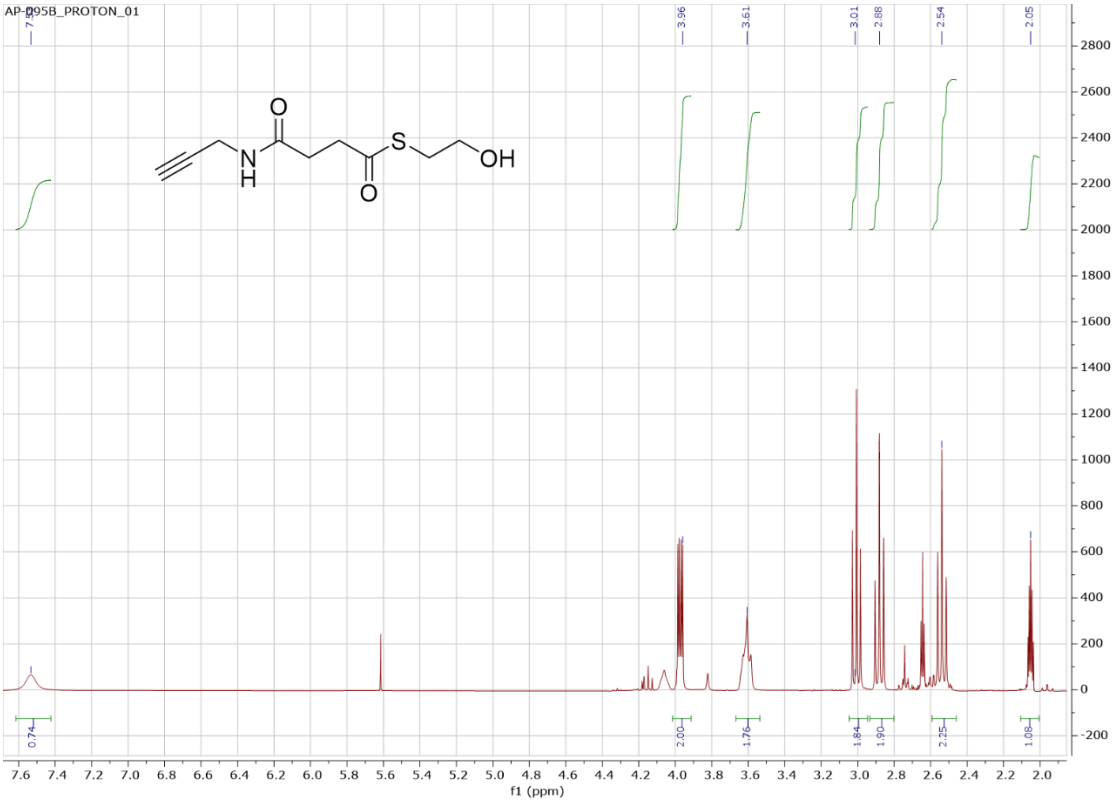

6.6.4 Compound 19

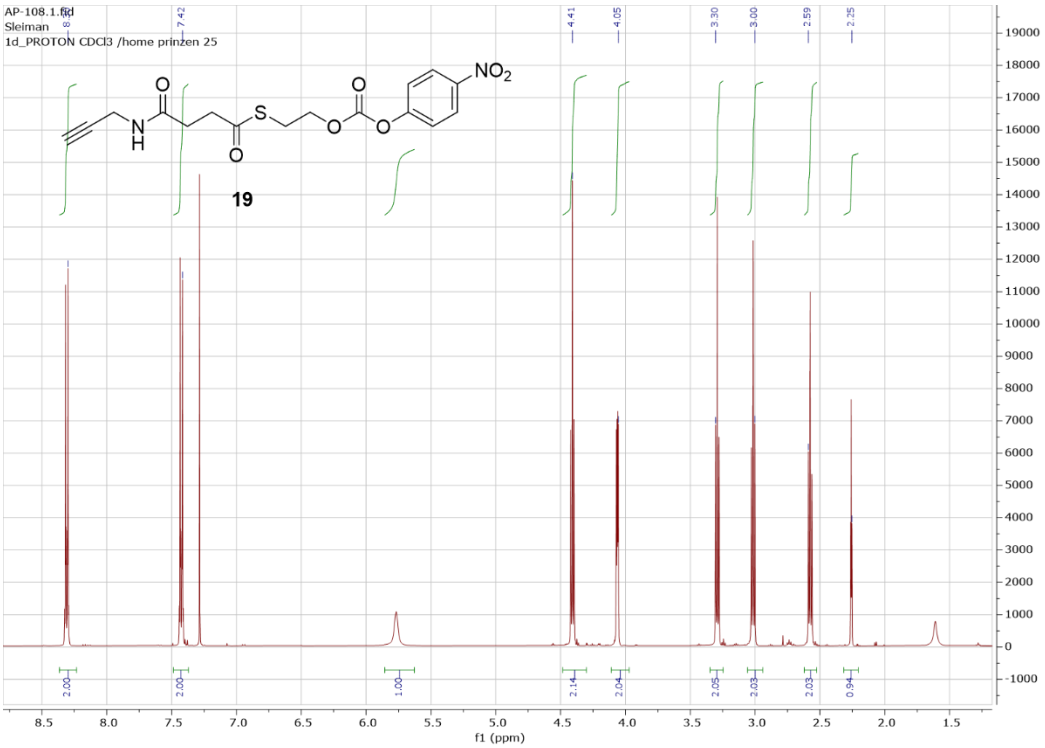

6.6.5 Compound 20

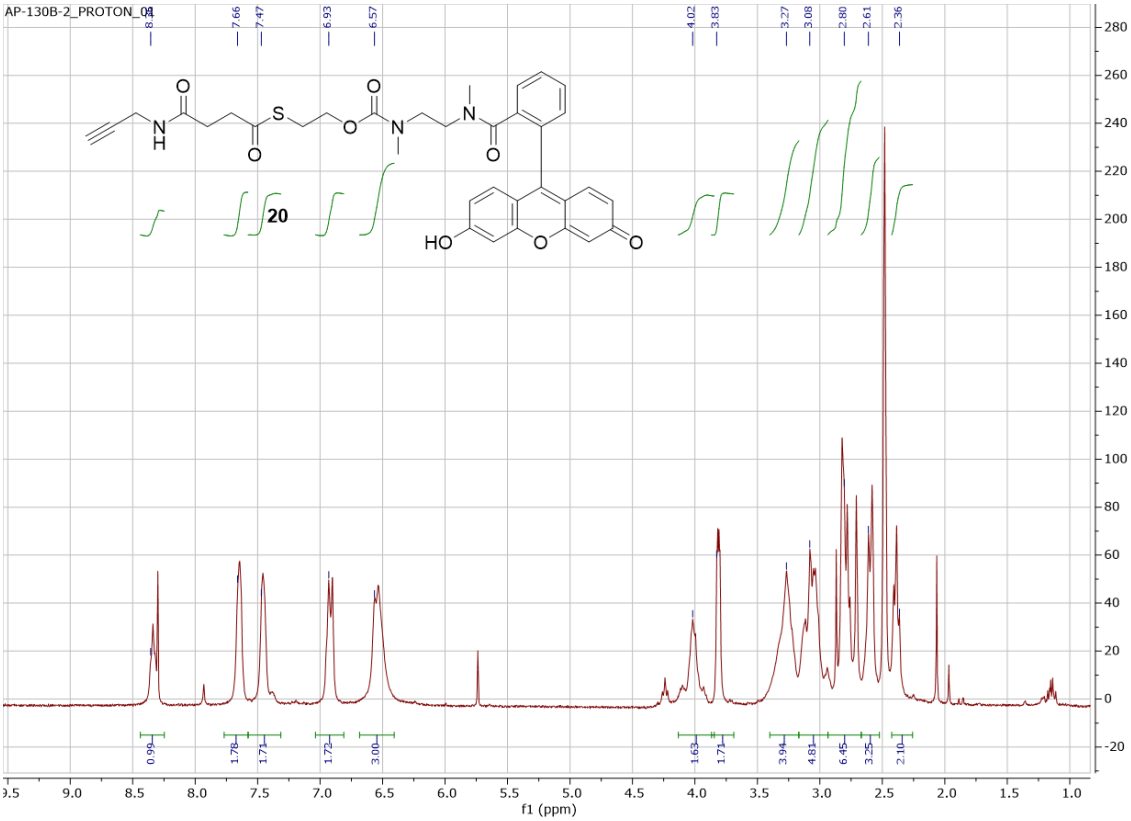

6.6.6 Compound 21

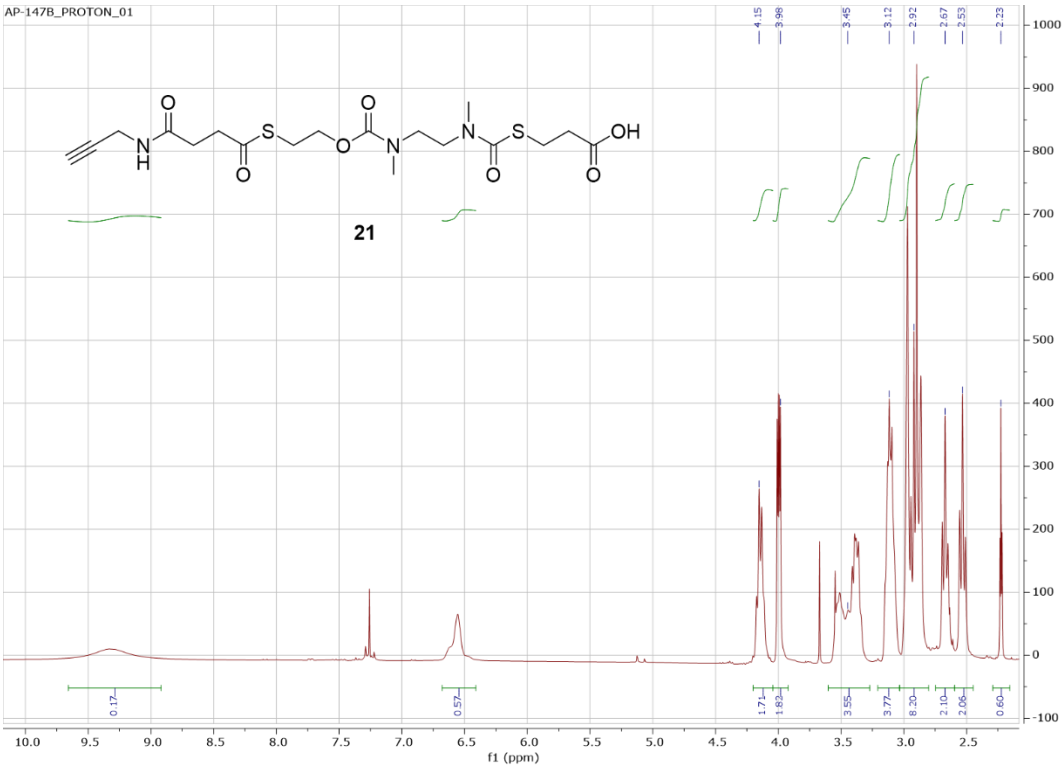

6.6.7 Compound 22

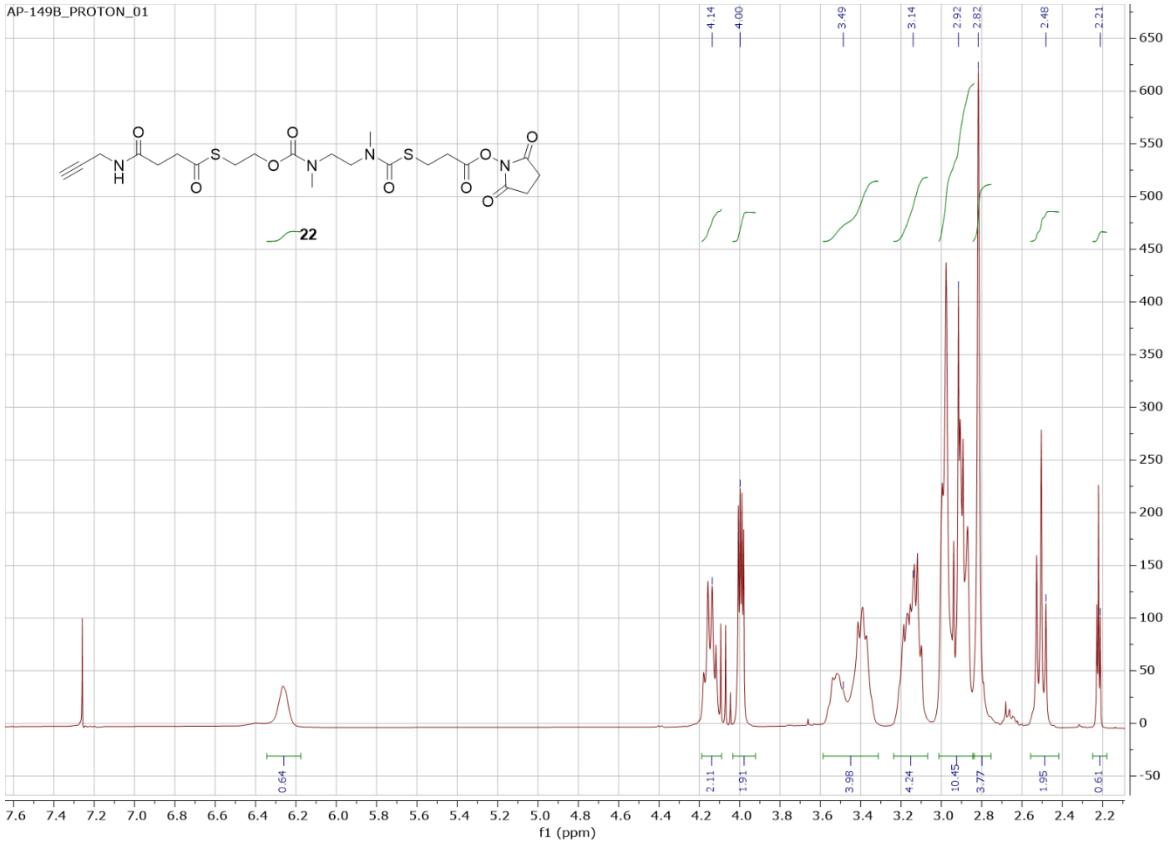

6.7. Molecules from Appendix iv.

6.7.1 Compound 23

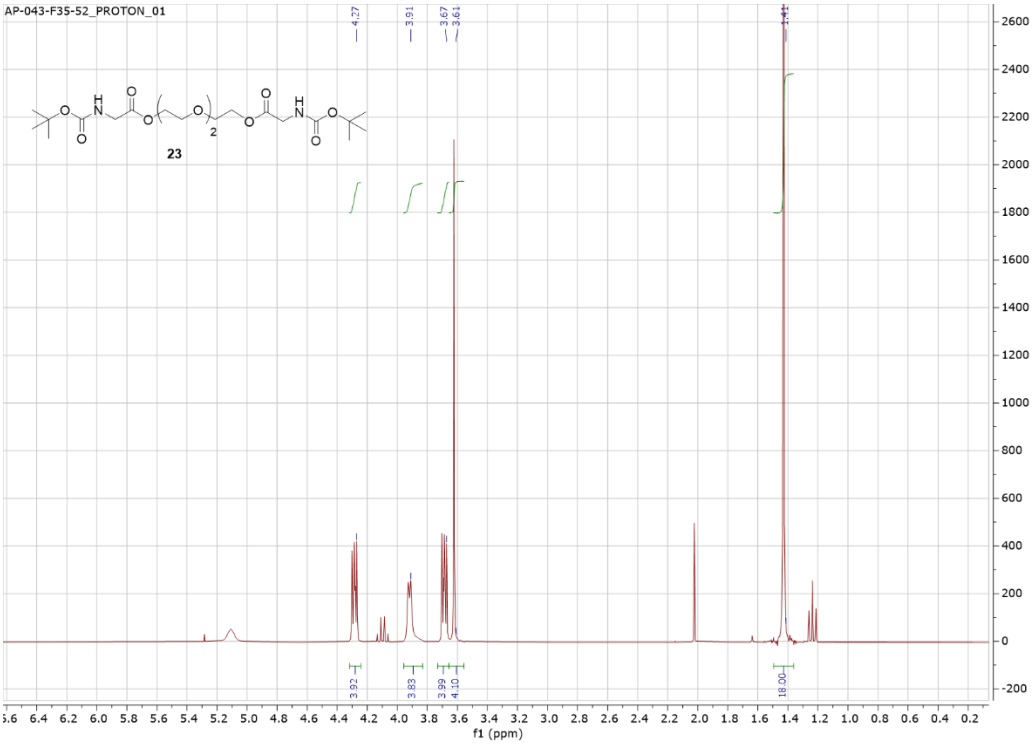

6.7.2 Compound 24

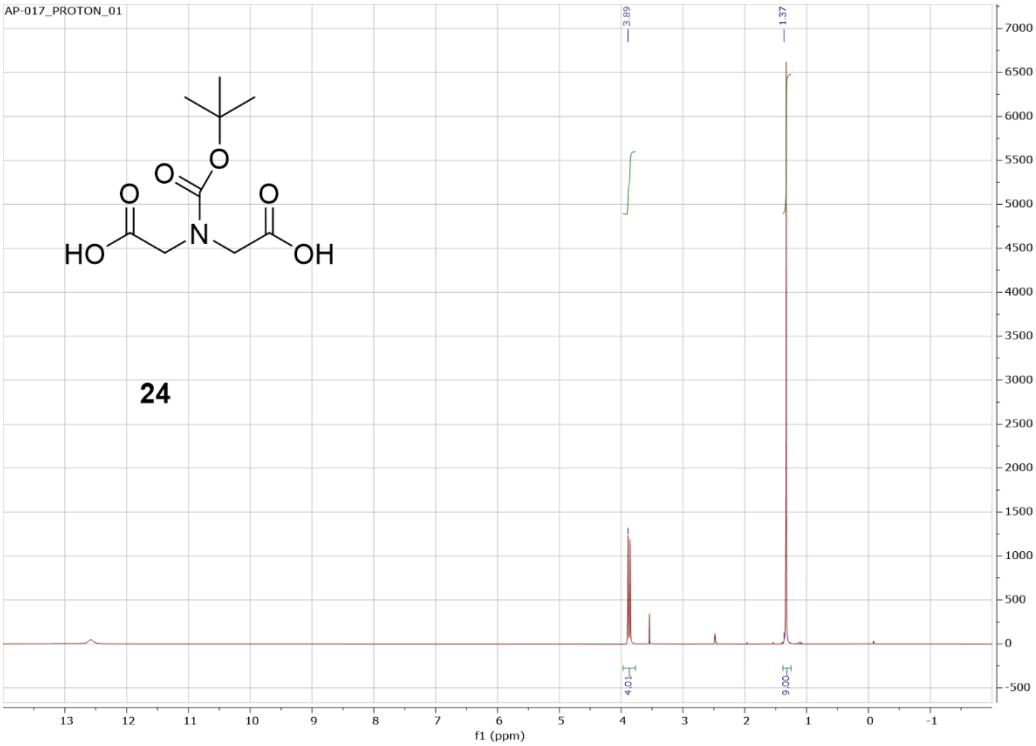

6.7.3 Compound 25

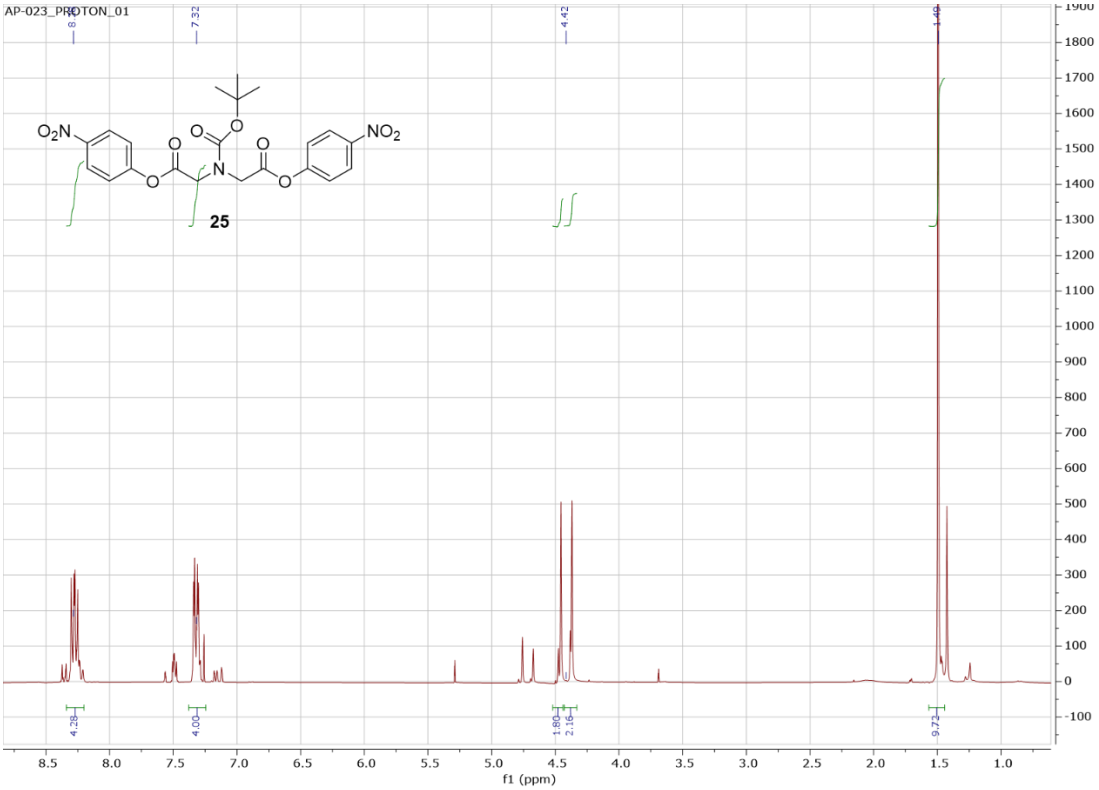

6.7.4 Compound 26

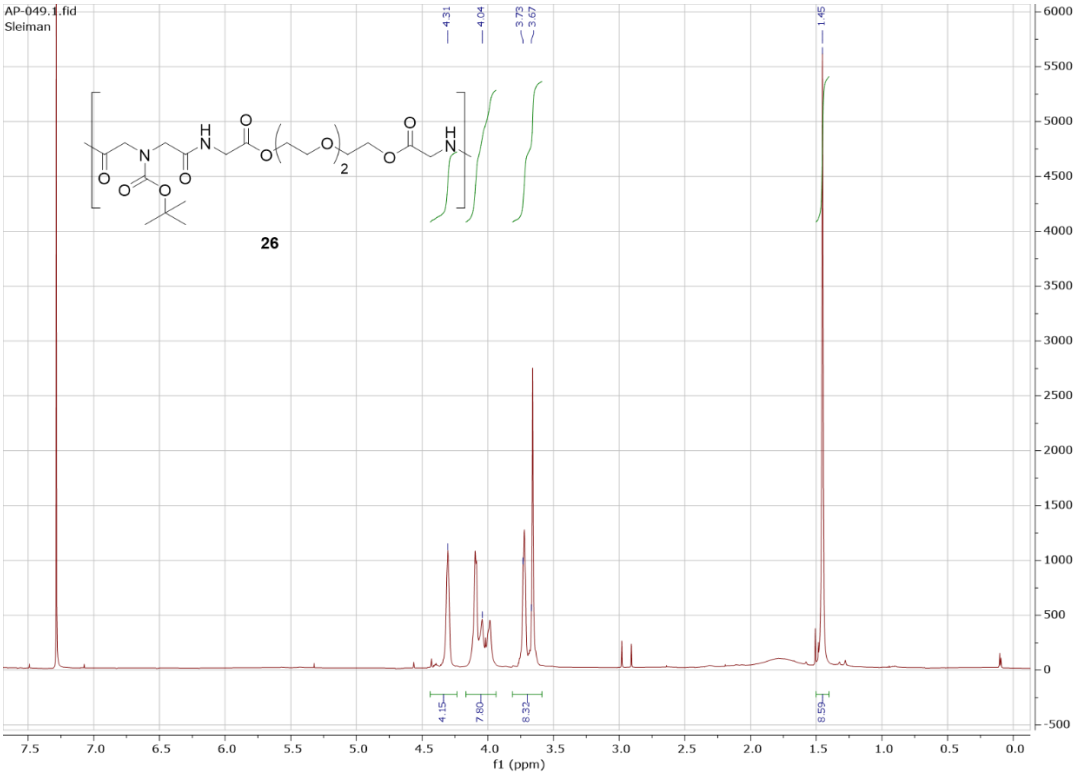

6.7.5 Compound 27

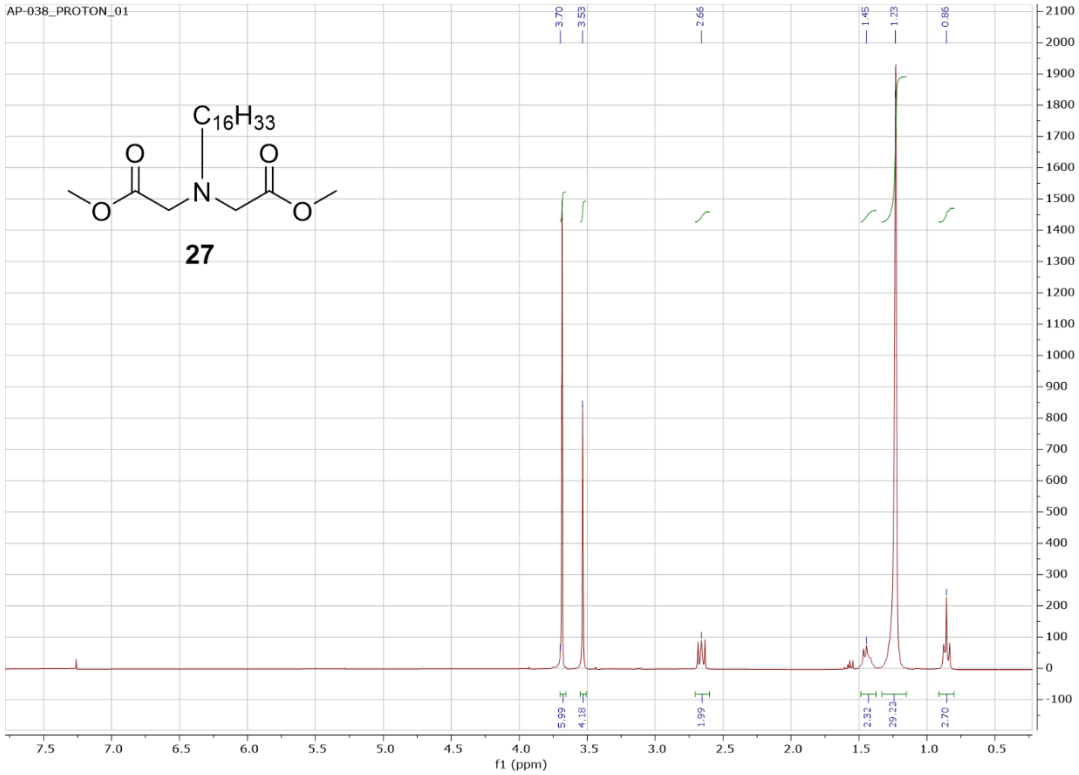

6.7.6 Compound 28

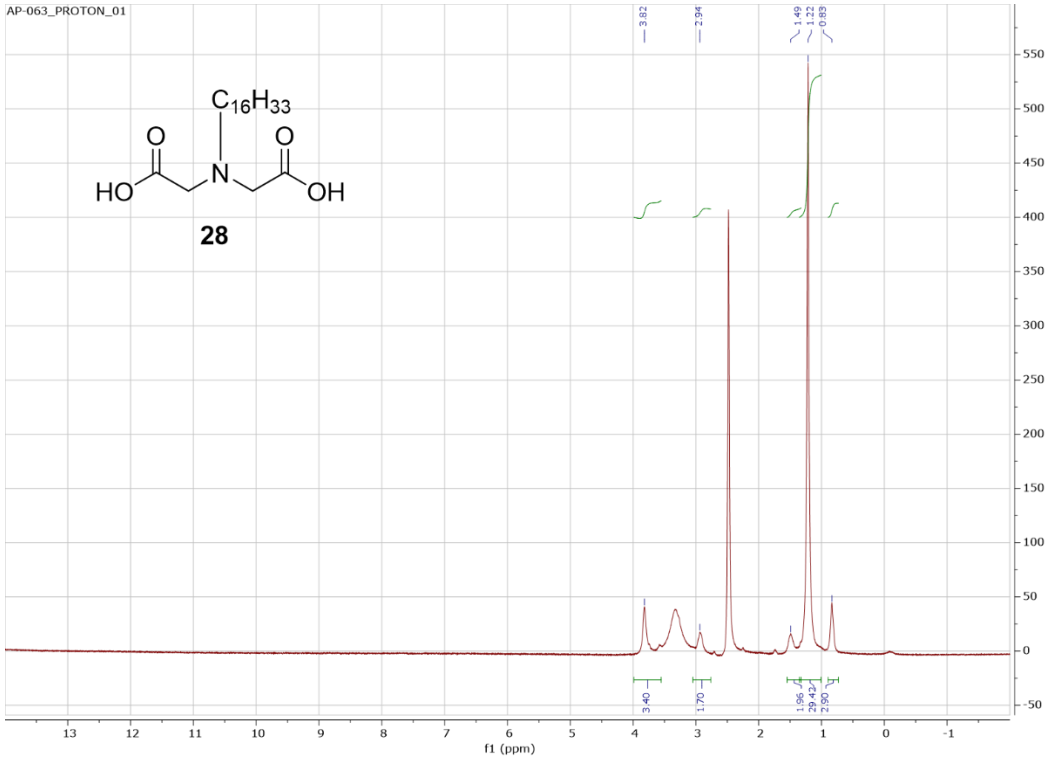

6.7.7 Compound 29

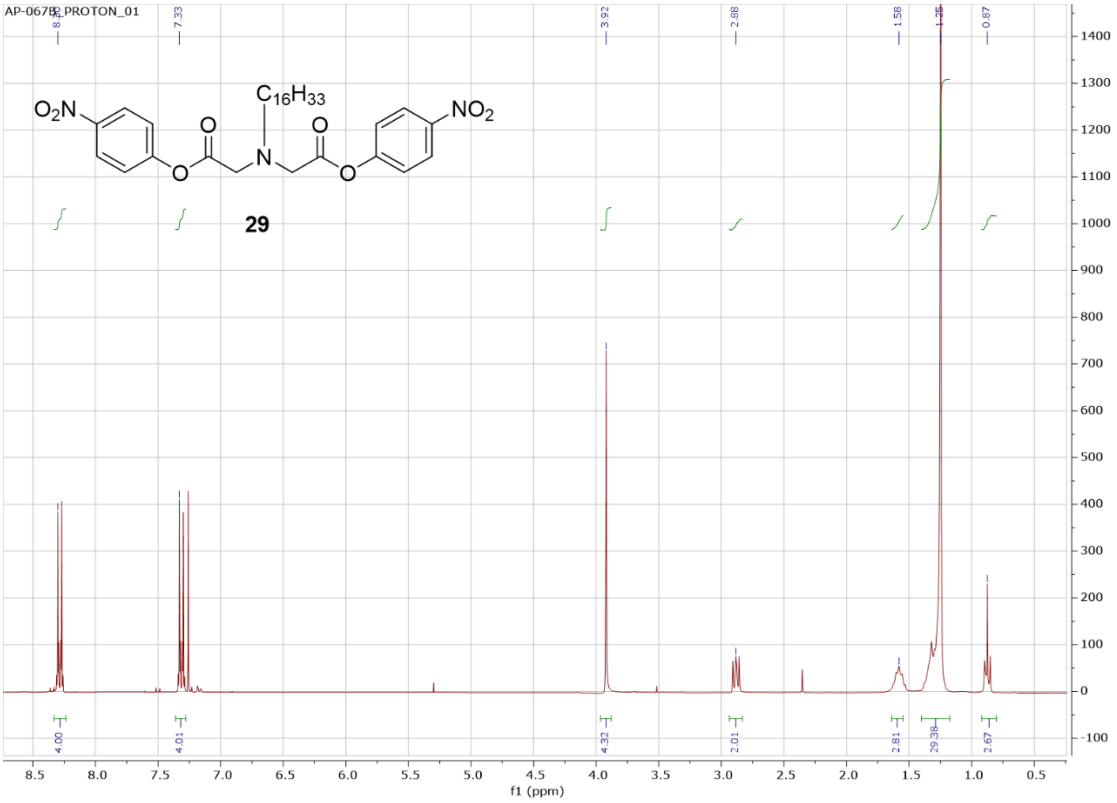

6.7.8 Compound 30

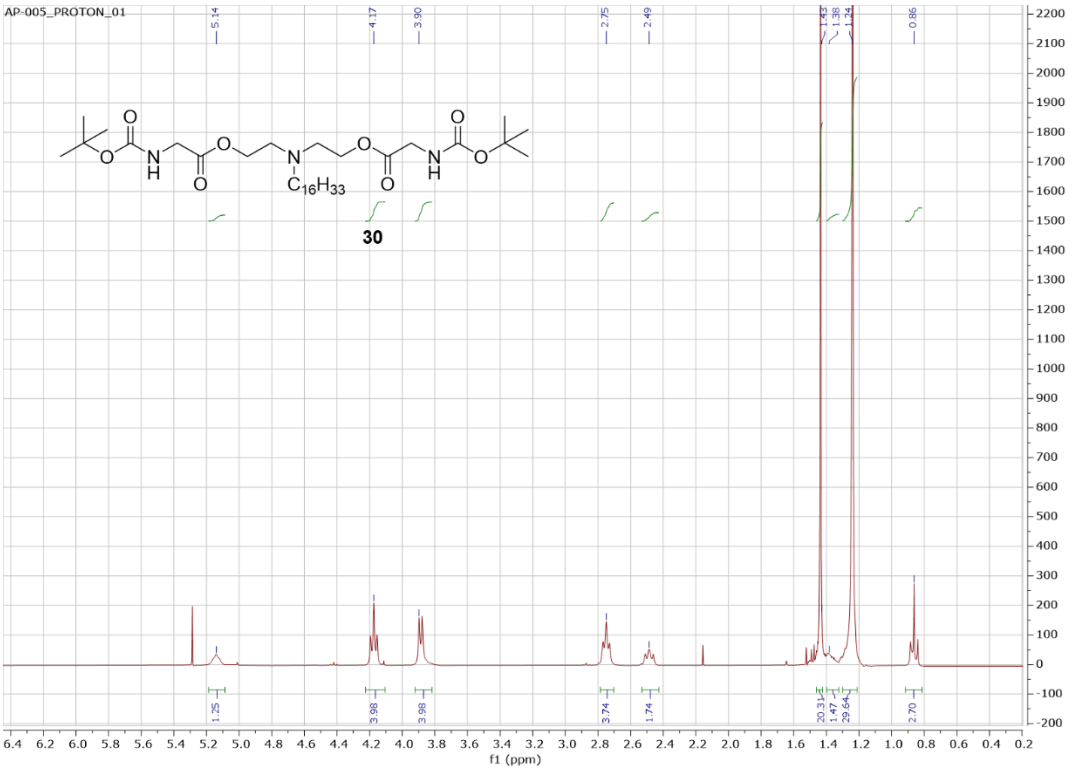

6.7.9 Compound 31

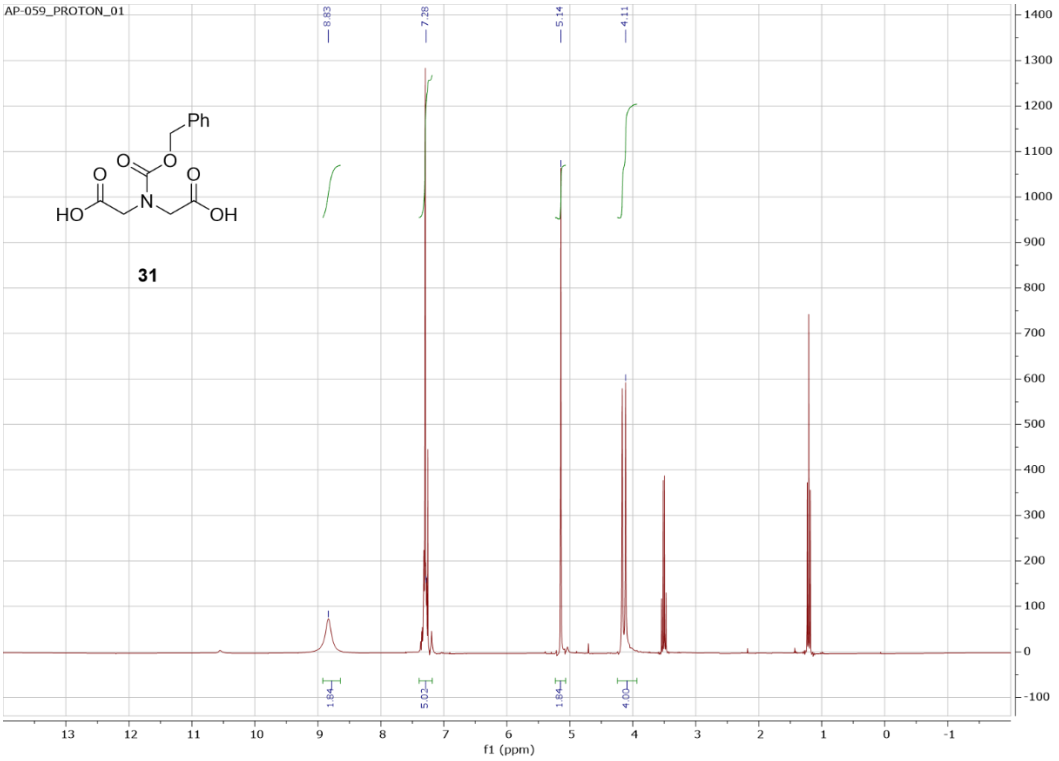

6.7.10 Compound 32

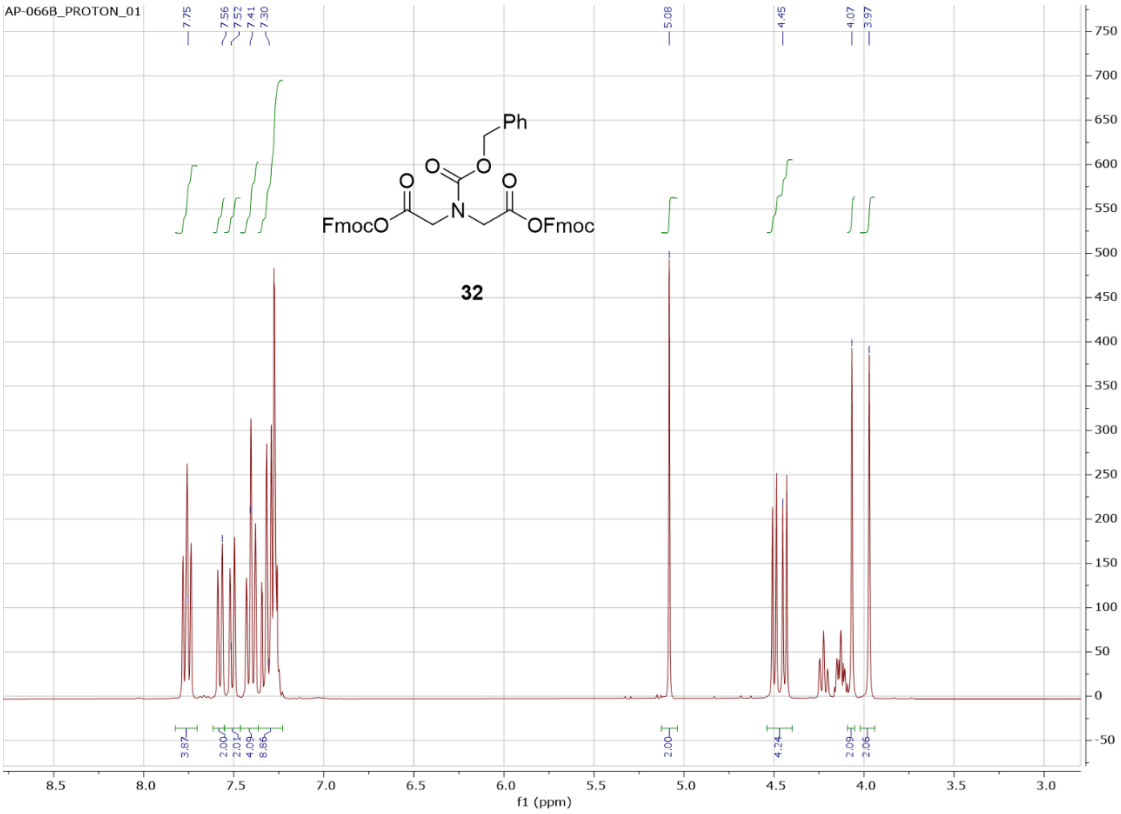

6.7.11 Compound 33

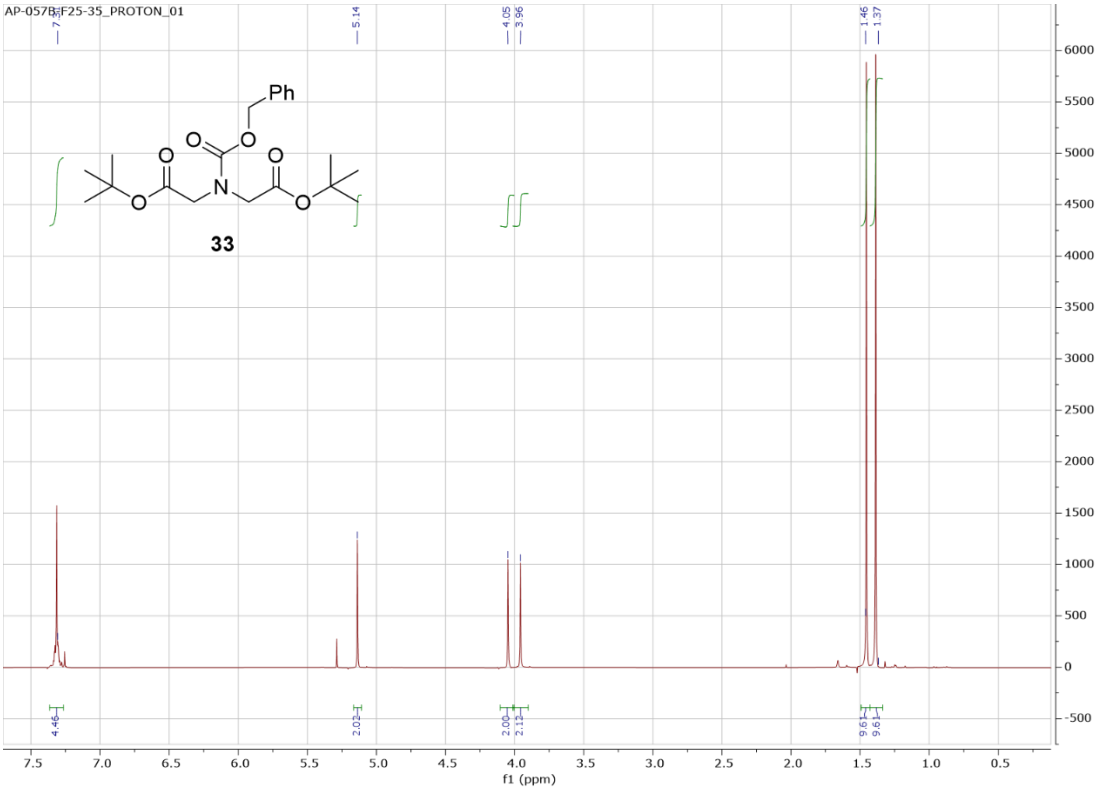

6.7.12 Compound 34

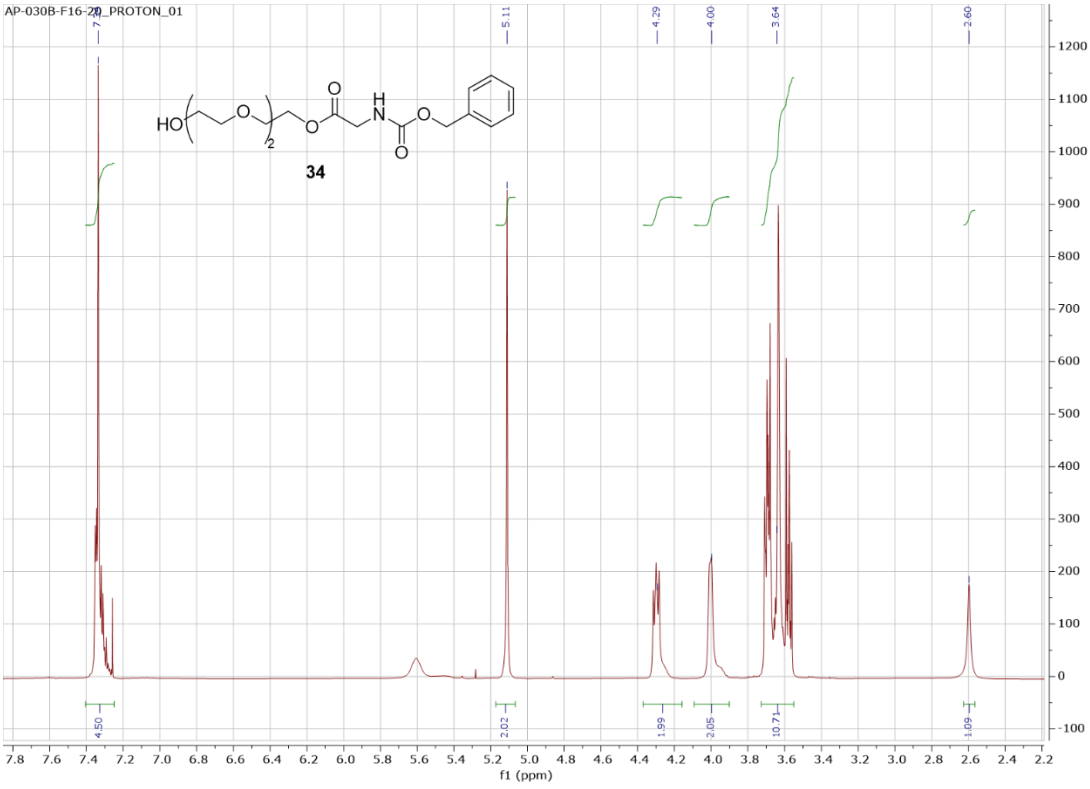

6.7.13 Compound 35

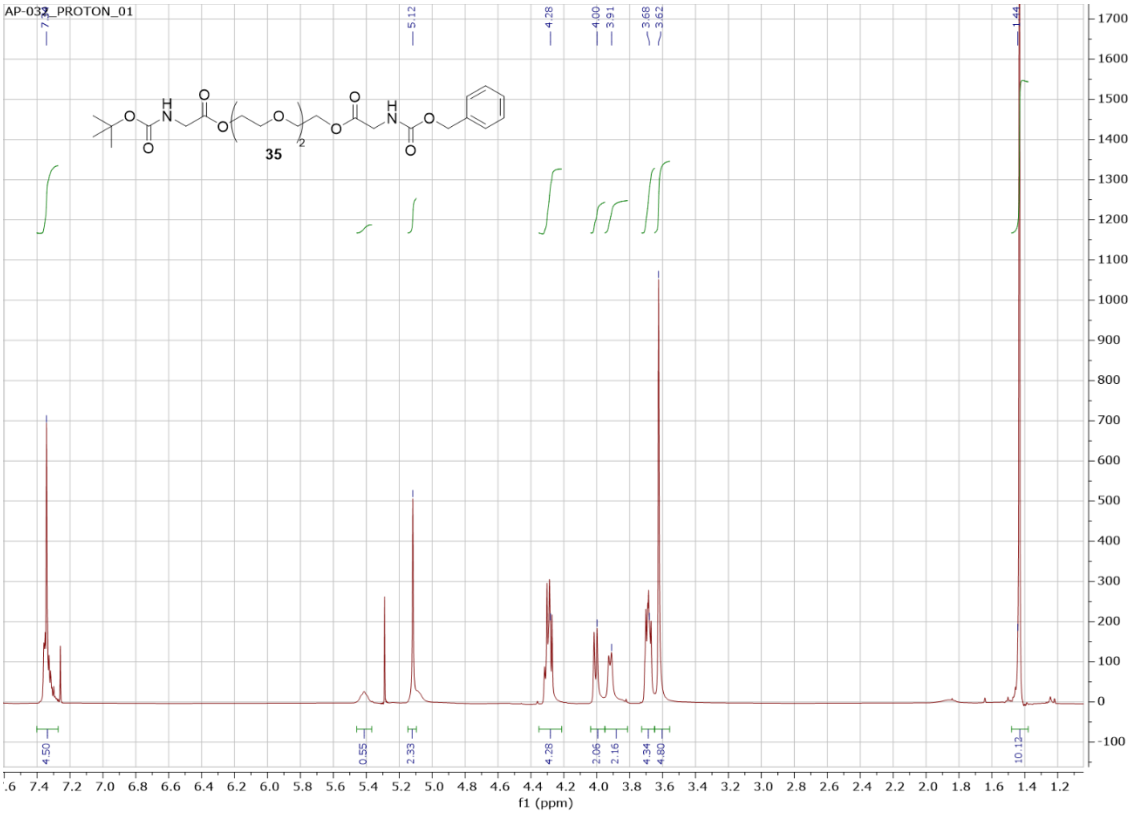

6.7.14 Compound 36

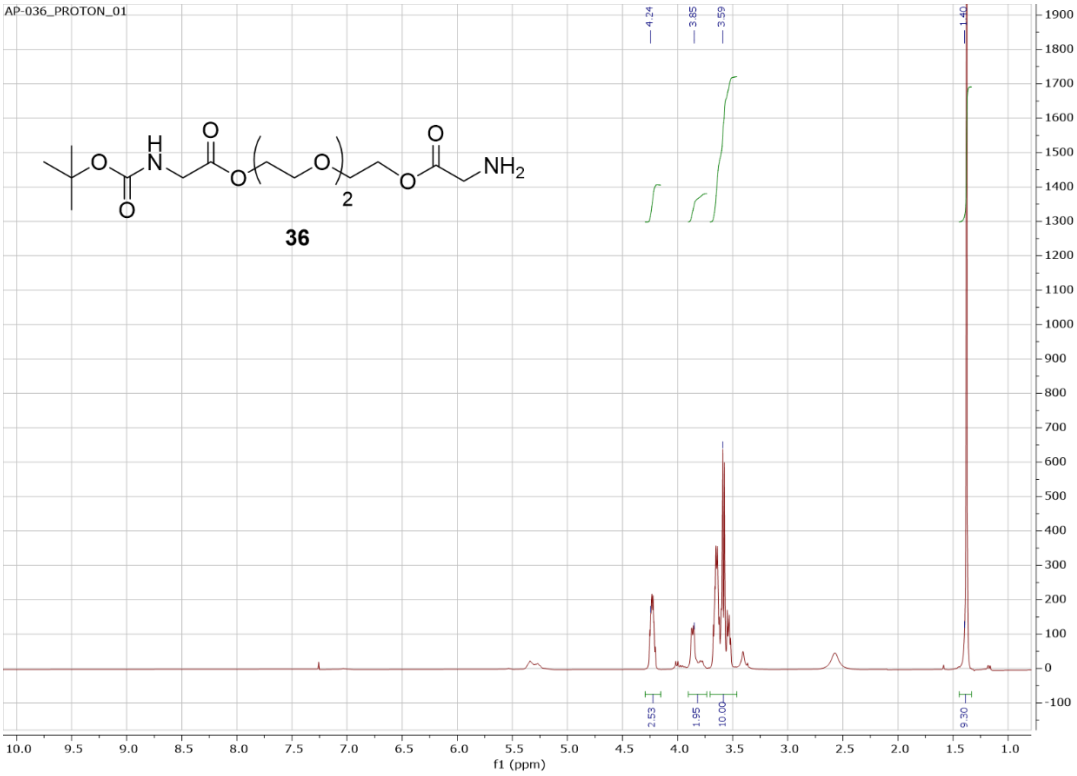

|Appendix|

Appendix i. Synthesis of other Disulfide phosphoramidites and disulfide linkers

Described here are synthetic procedures for the ongoing synthesis of a disulfide phosphoramidite which has a TEG side chain as opposed to a hydrophobic side chain, as well as longer disulfide phosphoramidites with longer chains. A bi-functional disulfide linker with disulfides and an azido group is also presented which could be used as a simple molecule for conjugating two species together with thiol and alkyne functionalities.

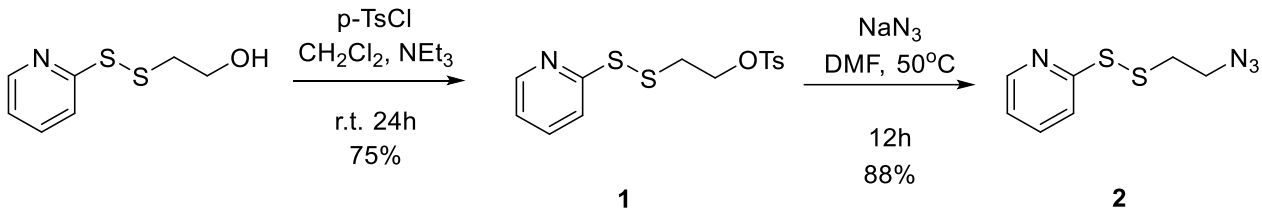

Figure A.I. 1 Synthesis of 2-((2-azidoethyl)disulfaneyl)pyridine

Compound 1:

To a solution of 2-(pyridin-2-yldisulfaneyl)ethan-1-ol (1.00g, 5.34mmol) in CH_2Cl_2 (50mL)was added p-tosyl-chloride (2.04g, 10.68mmol) and NEt_3 (1.93g 10.68mmol). The reaction was reacted at room temperature for 24 hours. After this the solvent was washed with saturated $NaHCO_3$ (50mL) and brine (50mL). The organic phase was dried on $MgSO_4$, filtered and concentrated. The crude material as purified by column chromatography (9:1 Hex/EtOAc to 7:3 Hex/EtOAc) to give the pure compound **1** (1.37g, 75%) ^{1}H NMR (500MHz, $CDCl_3$): δ = 2.43 (s, 3H), 2.98 (t, 2H), 4.25 (t, 2H), 7.10 (m, 1H), 7.32 (m, 2H), 7.60 (m, 2H), 7.75 (m, 2H), 8.47 (m, 1H). HRMS (EI): calc. for $[C_{14}H_{16}NO_5S_3]^+$ $[M]^+$: 342.02, found 342.0298.

Compound 2:

Compound **1** (1.00g, 2.93mmol), was dissolved in DMF (20mL) and sodium azide (600mg, 8,79mmol) was added to this solution. The reaction was heated to 50°C and then left overnight to react. The solution was cooled to room temperature and was then diluted with EtOAc (100mL) and H_2O (100mL). The phases were then separated and the organic phase was extracted with brine (3x 50mL). The collected organic phase was hen dried on $MgSO_4$, filtered and concentrated

in vacuo. Column chromatography was then performed to purify the crude compound (7:3 Hex/EtOAc) and give the pure compound **2** (547mg, 88%). ^{1}H NMR (500MHz, $CDCl_3$): δ = 2.87 (t, 2H), 3.54 (t, 2H), 7.06 (m, 1H), 7.56 (m, 2H), 8.40 (m, 1H). HRMS (EI): calc. for $[C_7H_9N_4S_2]^+$ $[M]^+$: 213.02, found 213.0263.

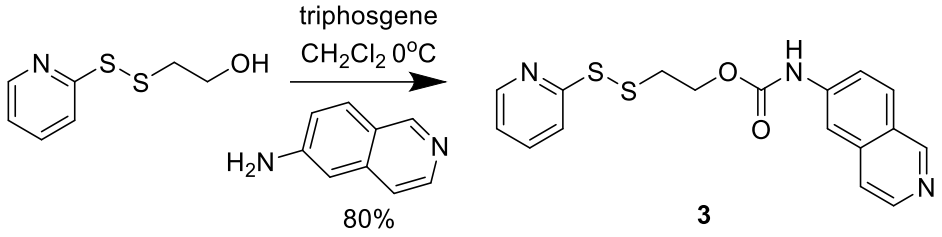

Figure A.I. 2. Synthesis of 2-(pyridin-2-yldisulfaneyl)ethyl isoquinolin-6-ylcarbamate

Compound 3:

First, a solution of triphosgene (160mg, 0.54mmol) was prepared in CH_2Cl_2 (10mL) and cooled to 0°C. Separately, a solution of 2-(pyridin-2-yldisulfaneyl) ethan-1-ol (267mg, 1.53mmol) and NEt_3 (1.00mL, 3.83mmol) in CH_2Cl_2 (5mL) was prepared. This solution was added dropwise to the triphosgene solution and reacted for 2h.Following this, 6-isoquinolinamine (175mg, 0.54mmol) was added to the solution and the mixture was left for 12h. Upon completion the mixture was concentrated in vacuo and purified by column chromatography (1:1 Hex/EtOAc) to give compound **3** (154mg, 80%). ^{1}H NMR (500MHz, $CDCl_3$): δ = 3.09 (t, 2H), 4.45 (t, 2H), 7.06 (m, 1H), 7.34 (m, 1H), 7.62 (m, 4H), 8.05 (m, 3H), 8.49 (m, 1H), 8.81 (m, 1H).

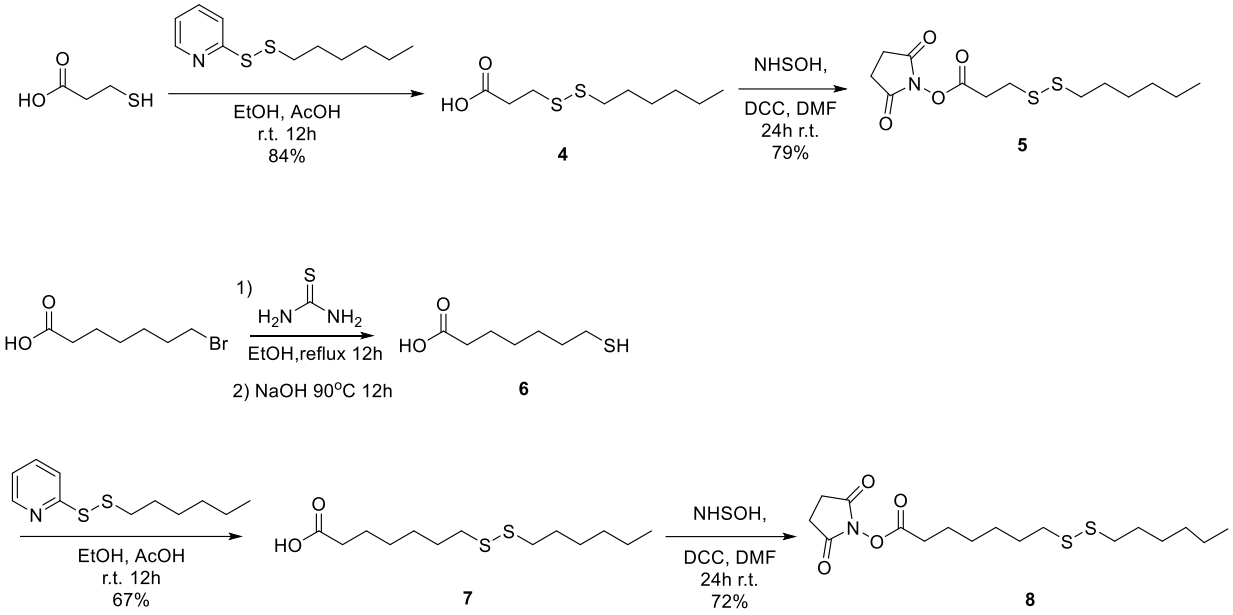

Figure A.I. 3 Synthesis of 2,5-dioxopyrrolidin-1-yl 3-(hexyldisulfaneyl)propanoate and 2,5-dioxopyrrolidin-1-yl 7-(hexyldisulfaneyl)heptanoate

Compound 4:

2-(hexyldisulfaneyl)pyridine (1.10g, 4.84mmol) was dissolved in ethanol (20ml) with acetic acid (2ml). To this 3-mercaptopropanoic acid (470mg, 4.36mmol), was added dropwise and the solution was allowed to react at room temperature for 12 hours. The solution was then concentrated *in vacuo* and the crude material purified by column chromatography (EtOAC/Hex/Acetic Acid 5:94:1) to provide Compound **4** (900mg, 84%). ^{1}H NMR (500 MHz, $CDCl_3$): δ = 0.89 (m, 3H), 1.31 (m, 6H), 1.66 (m, 2H), 2.67 (m, 2H), 2.81 (m, 2H), 2.91 (m, 2H). HRMS (EI): calc. for $[C_9H_{19}O_2S_2]^+$ $[M]^+$: 223.07, found 223.0742.

Compound 5:

Compound **4** (900mg, 4.05mmol) and N-hydroxysuccinimide (920mg, 4.46) were dissolved in DMF (20 ml). To this was added N,N'-Dicycolhexylcarbodiimide (512mg, 4.46mmol) and the mixture was reacted for 24 hours. The solution was then filtered to remove the insoluble urea and diluted with H_2O (100 mL) and extracted with ethyl acetate (3 × 100 mL). The organic phase was washed with saturated $NaHCO_3$ (200 mL), and saturated NaCl (200 mL), and then dried on $MgSO_4$, filtered and concentrated *in vacuo*. The crude material was then purified by column

chromatography (CH_2Cl_2/Hex 7:3) to provide Compound **5** as a colourless oil (1.02g, 79%). ^{1}H NMR (500MHz, $CDCl_3$): δ = 0.88 (m, 3H), 1.32 (m, 6H), 1.65 (m, 2H), 2.68 (m, 2H), 2.82 (s, 4H), 2.99 (m, 4H). HRMS (EI): calc. for $[C_{13}H_{22}NO_4S_2]^+$ $[M]^+$: 320.09, found 320.1003.

Compound 6:

727 To a solution of 7-Bromoheptanoic acid (3.00g, 14.35mmol) in ethanol (50mL) was added thiourea (2.00g, 21.52mmol) and refluxed overnight. The solution was then cooled to room temperature and the solvent evaporated *in vacuo*. Following this, a 7.5M NaOH solution (50mL) was prepared and added to the reaction mixture. The solution was heated to 90^{o}C and left overnight. The solution was then cooled to room temperature, and then cooled further to 0^{o}C. A 2M H_2SO_4 (aq) solution was prepared, and the reaction mixture was adjusted to pH 1. The acidified solution was then extracted with CH_2Cl_2 (9x50mL) and the organic phase collected. The collected organic phase was then dried on $MgSO_4$, filtered, concentrated *in vacuo* and used directly in the synthesis of compound **7.**

Compound 7:

2-(hexyldisulfaneyl)pyridine (1.70g, 7.49mmol), was dissolved in ethanol (50ml) with acetic acid (5ml). To this compound **6** (1.15g, 6.74mmol) was added dropwise and the solution was allowed to react at room temperature for 12 hours. The solution was then concentrated *in vacuo* and the crude material purified by column chromatography (95:5 Hex/AA) to provide Compound **7** (1.40g, 67%). ^{1}H NMR (500 MHz, $CDCl_3$): δ = 0.89 (m, 3H), 1.36 (m, 10H), 1.68 (m, 6H), 2.36 (m, 2H), 2.68 (m, 4H). HRMS (EI): calc. for $[C_{13}H_{27}O_2S_2]^+$ $[M]^+$: 279.14, found 279.1423.

Compound 8:

Compound **7** (1.40g, 5.03mmol) and N-hydroxysuccinimide (640mg, 5.53mmol) were dissolved in DMF (25 ml). To this was added N,N'-Dicycolhexylcarbodiimide (1.14g, 5.53mmol) and the mixture was reacted for 24 hours. The solution was then filtered to remove the insoluble urea and diluted with H_2O (100 mL) and extracted with ethyl acetate (3 × 100 mL). The organic phase was washed with saturated $NaHCO_3$ (200 mL), and saturated NaCl (200 mL), and then dried on $MgSO_4$, filtered and concentrated *in vacuo*. The crude material was then purified by column

chromatography (CH_2Cl_2/Hex 7:3) to provide Compound **8** as a colourless oil (1.36g, 72%). ^{1}H NMR (500MHz, $CDCl_3$): δ = 0.89 (m, 3H), 1.39 (m, 10H), 1.73 (m, 6H), 2.60 (m, 2H), 2.69 (m, 4H), 2.84 (s, 4H). HRMS (EI): calc. for $[C_{17}H_{30}NO_4S_2]^+$ $[M]^+$: 375.15, found 375.1555.

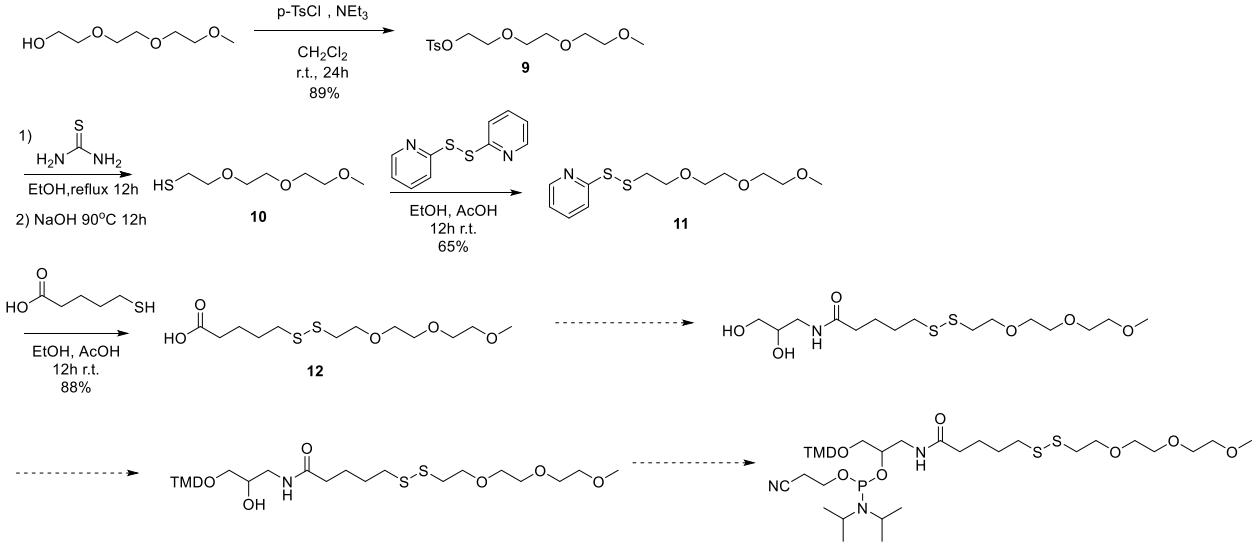

Figure A.I. 4 Synthesis of 2,5,8-trioxa-11,12-dithiaheptadecan-17-oic acid

Compound 9:

Triethylene glycol monomethyl ether (15.00g, 91.4mmol) was dissolved in CH_2Cl_2 (200mL) p-tosyl-chloride (35.00g, 183mmol) and NEt_3 (20.50g 201mmol). The reaction was reacted at room temperature for 24 hours. The crude material was concentrated *in vacuo* and purified by column chromatography (1:1 Hex/EtOAc) to give the pure compound **9** (25.9g, 89%) ^{1}H NMR (500MHz, $CDCl_3$): δ = 3.33 (s, 3H), 3.51 (m, 2H), 3.55 (m, 5H), 3.65 (m, 3H), 4.13 (m, 2H), 7.30 (m, 2H), 7.77 (m, 2H).

Compound 10:

To a solution of compound **9** (23.50g, 73.8mmol) in ethanol (150mL) was added thiourea (8.4g, 110mmol) and refluxed overnight. The solution was then cooled to room temperature and the solvent evaporated *in vacuo*. Following this, a 7.5M NaOH solution (150mL) was prepared and added to the reaction mixture. The solution was heated to 90°C and left overnight. The solution was then cooled to room temperature, and then cooled further to 0°C. A 2M H_2SO_4 (aq) solution was prepared and the reaction mixture was adjusted to pH 1. The acidified solution was then

extracted with CH_2Cl_2 (9x100mL) and the organic phase collected. The collected organic phase was then dried on $MgSO_4$, filtered, concentrated *in vacuo* and used directly in the synthesis of compound **11**.

Compound 11:

Compound **10** (4.60g, 25.60mmol) was dissolved in ethanol (75mL) with acetic acid (7.50ml). To this 2, 2'-dithiopyridine (11.20g, 51.10mmol) was added and the solution was allowed to react at room temperature for 12 hours. The solution was then concentrated *in vacuo* and the crude material purified by column chromatography (1:1 Hex/EtOAc) to provide Compound **11** (4.80g, 65%). ^{1}H NMR (500 MHz, $CDCl_3$): δ = 3.01 (m, 2H), 3.38 (s, 3H), 3.60 (m, 8H), 3.73 (m, 2H), 7.10 (m, 1H), 7.66 (m, 1H), 7.79 (m, 1H), 8.45 (m, 1H). HRMS (EI): calc. for $[C_{12}H_{20}NO_3S_2]^+$ $[M]^+$: 290.08, found 290.0780.

Compound 12:

Compound **11** (4.80g, 16.60mmol) was dissolved in ethanol (75mL) with acetic acid (7.50ml). To this 5-mercaptopentanoic acid (2.00g, 15.80mmol) was added and the solution was allowed to react at room temperature for 12 hours. The solution was then concentrated *in vacuo* and the crude material purified by column chromatography (4:1 Hex/AA with 5%AA) to provide Compound **12** (4.60g, 88%). ^{1}H NMR (500 MHz, $CDCl_3$): δ = 1.73 (m, 4H), 2.36 (m, 2H), 2.66 (m, 2H), 3.36 (s, 3H), 3.54 (m, 2H), 3.64 (m, 6H), 3.71 (m, 2H). HRMS (EI): calc. for $[C_{12}H_{25}O_5S_2]^+$ $[M]^+$: 313.11, found 313.1115.

Appendix II. One Pot Antibody-Oligonucleotide conjugates

Described here are the synthetic procedures towards generating a "dialkene" phosphoramidite for conjugating DNA directly to antibodies without the use of any linkers in one pot.

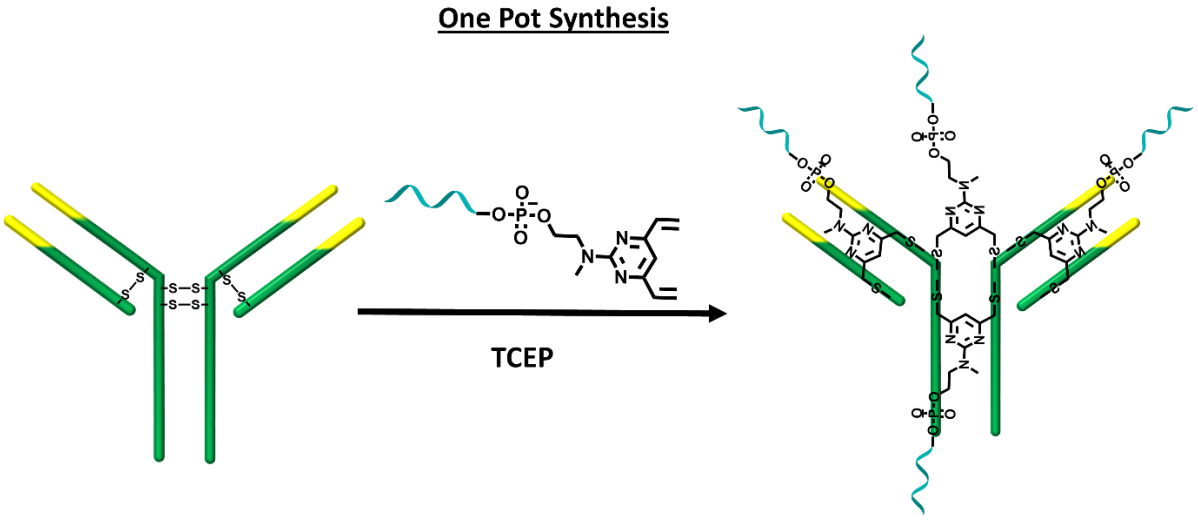

Figure A. II. 1 Scheme for the conjugation of an oligonucleotide to an antibody in one pot

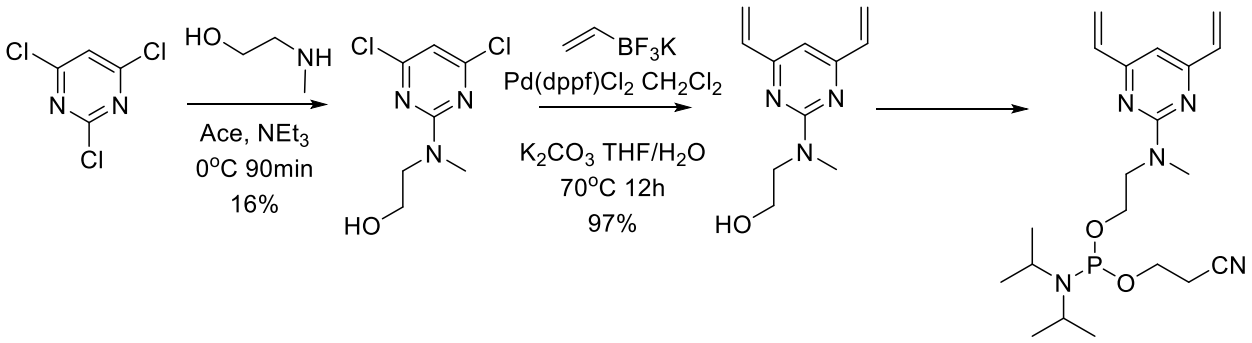

Figure A. II. 2 Synthesis of 2-cyanoethyl (2-((4,6-divinylpyrimidin-2-yl)(methyl)amino)ethyl) diisopropylphosphoramidite

Compound 13:

To a solution of 2,4,6-trichloropyrimidine (5.00 g, 27.30mmol) in acetone (50mL) at 0°C was added 2-(methylamino)-ethanol (2.46g, 32.70mmol), followed by the slow addition of triethylamine (6.88g, 68.1mmol) and the reaction mixture was stirred at 0°C for 90min. Upon completion, the solvent was removed in vacuo, then redisolved in H_2O (50mL) and extracted with

CH_2Cl_2 (4x 50mL). The combined organic fractions were then dried on $MgSO_4$, filtered, concentrated in vacuo and purified by column chromatography (8:2 Hex/EtOAc) to give compound **13** as a white solid (1.20g, 16%). ^{1}H NMR (500 MHz, $CDCl_3$) δ = 3.22 (s, 3H), 3.77 (m, 2H), 3.86 (m, 2H), 6.54 (s, 1H). HRMS (EI): calc. for $[C_7H_{10}OCl_2N_3]^+$ $[M]^+$: 221.01, found 221.0102.

Compound 14:

Compound **13** (1.20g, 4.24mmol)**,** potassium vinyltrifluoroborate (2.80g, 21.2mmol), $Pd(dppf)Cl_2{\cdot}CH_2Cl_2$ (550mg, 0.71mmol) and potassium carbonate (3.80g, 28.7mmol) in THF/H_2O (10:1, 55mL) were heated to 70^{o}C for 12hr. Upon completion, the reaction mixture was filtered through celite® and the solvent removed in vacuo. The crude material was then purified by column chromatography (8:2 Hex/EtOAc) to give compound **14** (840mg, 97%) ^{1}H NMR (500 MHz, $CDCl_3$) δ = 3.28 (s, 3H), 3.82 (m, 2H), 3.91 (m, 2H), 5.58 (m, 2H), 6.38 (m, 2H), 6.49 (s, 1H), 6.60 (m, 2H). ^{13}C NMR (125MHz, $CDCl_3$): δ = 25.61, 36.64, 52.99, 63.24, 67.97, 105.07, 121.62, 135.74, 162.83, 163.30. HRMS (EI): calc. for $[C_{11}H_{16}ON_3]^+$ $[M]^+$: 206.12, found 206.1340.

Compound 15:

Compound 15 was prepared in situ from compound **14** and directly coupled to the 5' end of an oligonucleotide prepared using ultra-mild bases, and deprotected with K_2CO_3 in MeOH.

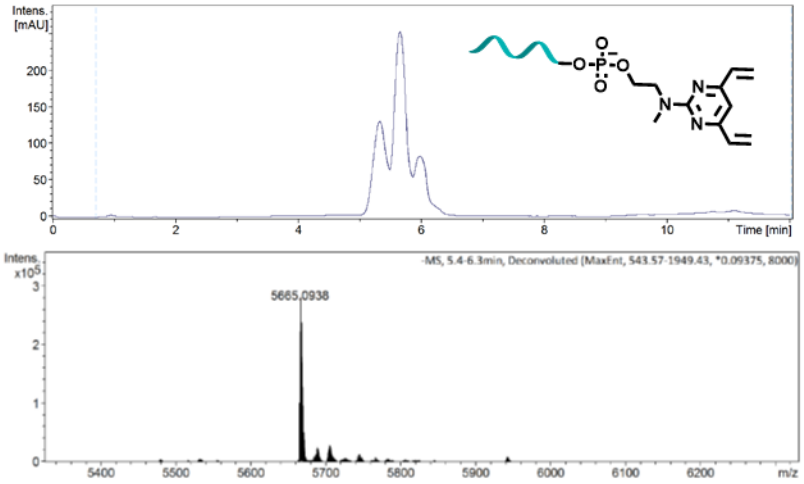

Predicted Mass: 5665.00 found 5665.09

Figure A. II. 3. RP-HPLC and LC-MS characterization of the dialkene conjugated oligonucleotide

Appendix III. DNA Templated Self-Immolative Polymer

Described here are synthetic procedures for molecules designed to be used in a DNA templated self-immolative polymer, in combination with compound 4 from Chapter 1 as the initiator.

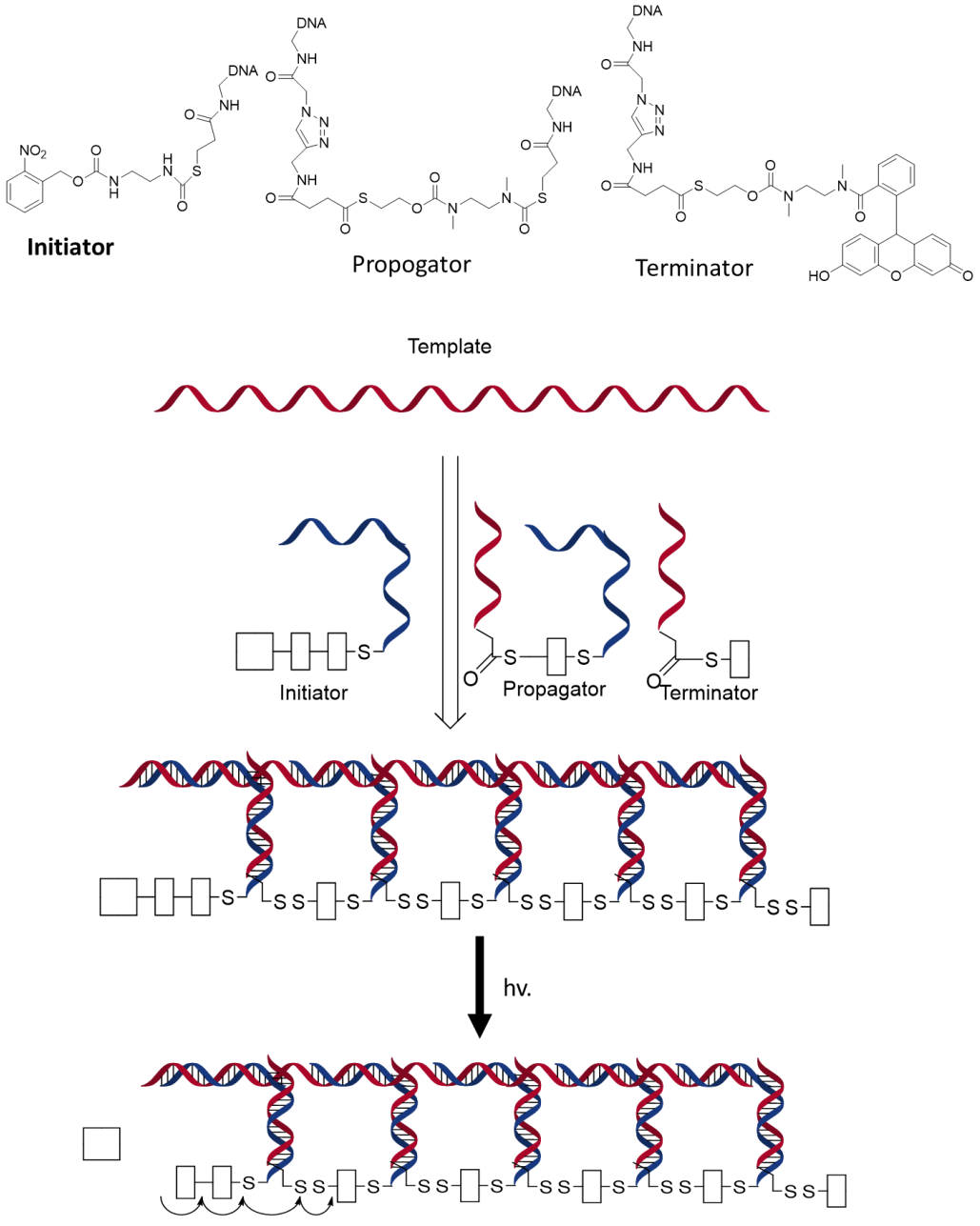

Figure A.III. 1 Representative scheme of DNA templated SIP. Using a series of immolative cyclization's and DNA templated thiol-thioester exchanges the polymer depolymerizes down the length of the DNA template.

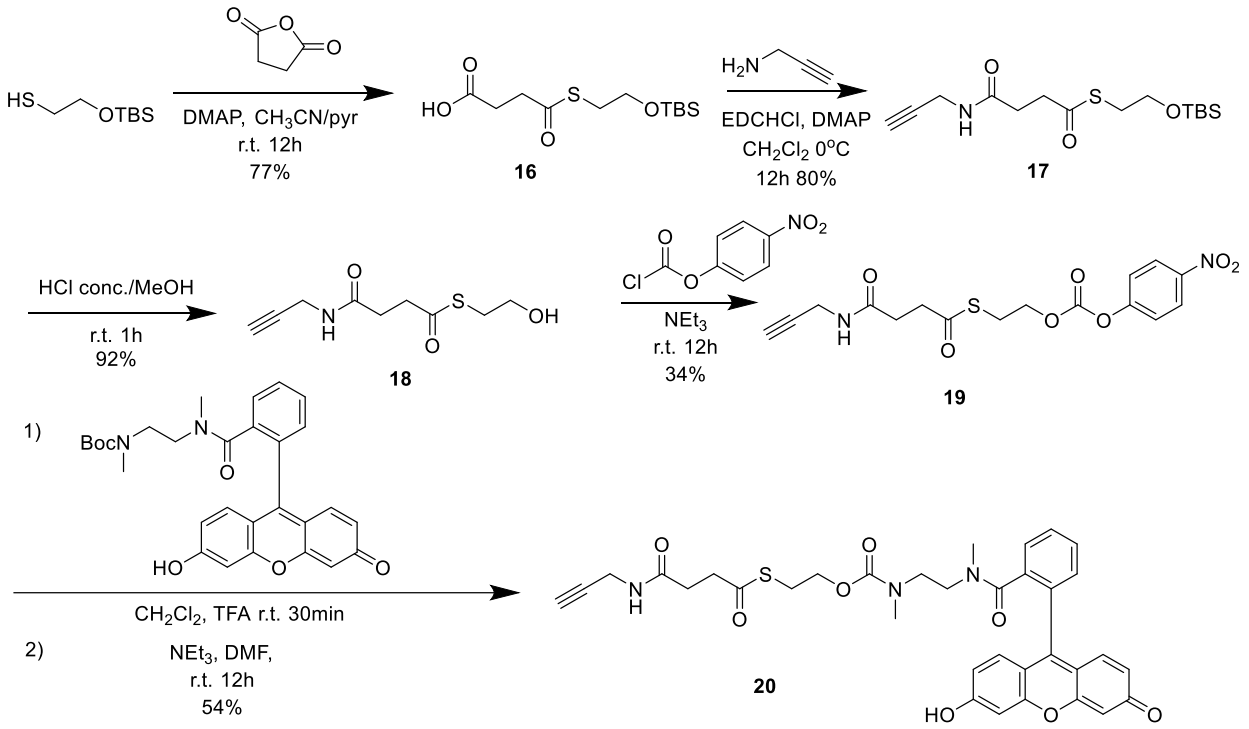

Figure A.III. 2 Synthesis of S-(2-(((2-(2-(6-hydroxy-3-oxo-3H-xanthen-9-yl)-N-methylbenzamido)ethyl)(methyl)carbamoyl)oxy)ethyl) 4-oxo-4-(prop-2-yn-1-ylamino)butanethioate (terminator)

Compound 16:

Succinic anhydride (11.60g, 115mmol) and DMAP (700mg, 5.75mmol), were dissolved in a mixture of CH_3CN and pyridine (9:1 150mL). To this, 2-((tert-butyldimethylsilyl)oxy)ethane-1-thiol (22.20g, 115mmol) was added and the reaction was left for 12hr. Upon completion, the reaction mixture was concentrated in vacuo, and redisolved in EtOAc (100mL). The solution was washed with 1M HCl (3x100mL) and brine (3x100mL), dried on $MgSO_4$, filtered and concentrated in vacuo to give Compound **16** (26.00g, 77%), without any further purification. ^1H NMR (500 MHz, $CDCl_3$): δ = 0.02 (s, 6H), 0.89 (s, 9H), 2.67 (m, 2H), 2.90 (m, 2H), 3.02 (m, 2H), 3.70 (m, 2H).

Compound 17:

A solution of Compound **16** (24.0g, 82.0mmol), EDC·HCl (17.3g 90.0mmol) and DMAP (5.00g, 41.0mmol) was prepared in CH_2Cl_2 (75mL) and stirred for 2hr at room temperature. The solution was then cooled to 0°C, and propargylamine (5.5mL, 86.0mmol), was added slowly. The reaction was warmed to room temperature and left 12hr. Upon completion, the reaction was washed

with 1M HCl (100mL), saturated $NaHCO_3$ (100mL), and brine (100mL). The organic phase was then dried on $MgSO_4$, filtered, concentrated in vacuo and purified by column chromatography (7:3 Hex/EtOAc) to give compound **17** (21.6g, 80%). ^{1}H NMR (500 MHz, $CDCl_3$) δ = 0.03 (s, 6H), 0.89 (s, 9H), 2.21, (s, 1H), 2.52 (m, 2H), 2.91 (m, 2H), 3.03 (m, 2H), 3.66 (m, 2H), 4.00 (m, 2H).

Compound 18:

To a solution of Compound **17** (8.26g, 25.1mmol) in MeOH (100mL) was added HCl conc. (1mL). The reaction was stirred for 1hr at room temperature. Upon completion, H_2O (150mL) was added and solution extracted with EtOAc (3x 150mL). The combined organic phase was then dried on $MgSO_4$, filtered and concentrated in vacuo to provide compound **18** as a white solid (4.96g, 92%) without any further purification. ^{1}H NMR (500 MHz, $CDCl_3$): δ = 2.05 (m, 1H), 2.54 (m, 2H), 2.88 (m, 2H), 3.01 (m, 2H), 3.61 (m, 2H), 3.96 (m, 2H).

Compound 19:

To a solution of Compound **18** (1.84g, 8.54mmol) in THF (50mL) was added triethylamine (6.35mL, 25.6mmol) and p-nitrophenylchloroformate (3.45g, 17.1mmol). The reaction was stirred for 12hr and upon completion quenched with 1M HCl (100mL). The mixture was then extracted with EtOAc (3x 100mL), and the combined organic fractions dried on $MgSO_4$, filterd and concentrated in vacuo. The crude material was purified by column chromatography (1:1 Hex/EtOAc) to give the pure compound **19** (1.10g, 34%) ^{1}H NMR (500 MHz, $CDCl_3$) δ = 2.25 (m, 1H), 2.59 (m, 2H), 3.00 (m, 2H), 3.30 (m, 2H), 4.05 (m, 2H), 4.41 (m, 2H), 7.42 (m, 2H), 8.30 (m, 2H).

Compound 20:

tert-butyl(2-(2-(6-hydroxy-3-oxo-3H-xanthen-9-yl)-N-methylbenzamido)ethyl)(methyl)carbamate (200mg, 0.40mmol) was first dissolved in CH_2Cl_2 (5mL) followed by the dropwise addition of TFA (5mL). The reaction mixture was stirred for 30 min and the CH_2Cl_2 was then evaporated. The solution was re-suspended in CH_2Cl_2 (5mL) and evaporated twice more, to remove any TFA, leaving the TFA salt, which was redisolve in DMF (5mL) and used directly. Next, a solution of **19** (152mg, 0.40mmol) and NEt_3 (0.12mL, 0.44mmol)

was prepared in DMF (5mL). To this, the TFA salt solution was added and the resulting mixture was reacted overnight at room temperature. The crude mixture was concentrated *in vacuo* and purified directly by column chromatography (8:2 EtOAc/MeOH) to give the pure compound **20** (140mg, 54% yield) ^{1}H NMR (500MHz, DMSO D_6): δ = 2.36 (m, 2H), 2.61 (m, 3H), 2.80 (m, 6H), 3.08, (m, 5H), 3.27 (m, 4H), 3.83 (m, 2H), 4.02 (m, 2H), 6.57 (m, 3H), 6.93 (m, 2H), 7.47 (m, 2H), 7.66 (m, 2H), 8.30 (m, 1H). HRMS (EI): calc. for $[C_{34}H_{34}N_3O_8S]^+$ $[M]^+$: 644.20, found 644.01998.

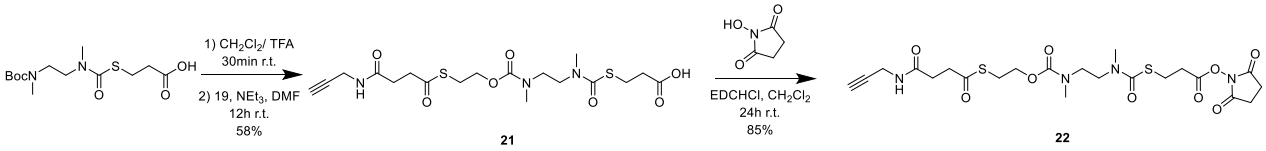

Figure A.III. 3 Synthesis of 2,5-dioxopyrrolidin-1-yl 6,9-dimethyl-5,10,15,18-tetraoxo-11-oxa-4,14-dithia-6,9,19-triazadocos-21-ynoate)(propagator)

Compound 21:

2,2,5,8-tetramethyl-4,9-dioxo-3-oxa-10-thia-5,8-diazatridecan-13-oic acid (227mg, 0.71mmol) was first dissolved in CH_2Cl_2 (5mL) followed by the dropwise addition of TFA (5mL). The reaction mixture was stirred for 30 min and the CH_2Cl_2 was then evaporated. The solution was re-suspended in CH_2Cl_2 (5mL) and evaporated twice more, to remove any TFA, leaving the TFA salt, which was dissolved in DMF (5mL) and used directly. Next, a solution of **19** (300mg, 0.79mmol) and NEt_3 (1.18mL, 4.74mmol) was prepared in DMF (10mL). To this, the TFA salt solution was added, and the resulting mixture was reacted overnight at room temperature. The crude mixture was concentrated *in vacuo* and purified directly by column chromatography (8:2 EtOAc/MeOH) to give the pure compound **21** (190mg, 58% yield) ^{1}H NMR (500MHz $CDCl_3$): δ = 2.23 (m, 1H), 2.53 (m, 2H), 2.67 (2H), 2.92 (m, 8H), 3.12 (m, 4H), 3.45 (m, 4H), 3.98 (m, 2H), 4.15 (m, 2H). HRMS (EI): calc. for $[C_{18}H_{28}N_3O_7S_2]^+$ $[M]^+$: 462.13, found 462.1307.

Compound 22:

Compound **21** (190mg, 0.41mmol), and N-hydroxysuccinimide (52.0mg, 0.45mmol), were first dissolved in CH_2Cl_2 (5mL). To this was added EDC·HCl (86.0mg, 0.45mmol) and the resultant mixture was allowed to react for 24hr at room temperature. The mixture was diluted to 25mL with CH_2Cl_2 then washed with saturated $NaHCO_3$ (25 mL), and saturated NaCl (25 mL). The organic

phase was dried on $MgSO_4$, filtered, concentrated *in vacuo* and the crude product was purified by column chromatography (7:3 EtOAc/Hex) to give compound **22** (195mg, 85% yield) ^{1}H NMR (500MHz, $CDCl_3$): δ = 2.21 (m, 1H), 2.48 (m, 2H), 2.82 (s, 4H), 2.92 (m, 10H), 3.14 (m, 4H), 3.49 (m, 4H), 4.00 (m, 2H), 4.14 (m, 2H). HRMS (EI): calc. for $[C_{22}H_{31}N_4O_9S_2]^+$ $[M]^+$: 559.15, found 559.1563.

Appendix IV. Cationic Polymers as Transfection Agents

Described here are the synthetic procedures towards generating new cationic polymers for use as transfection agents.

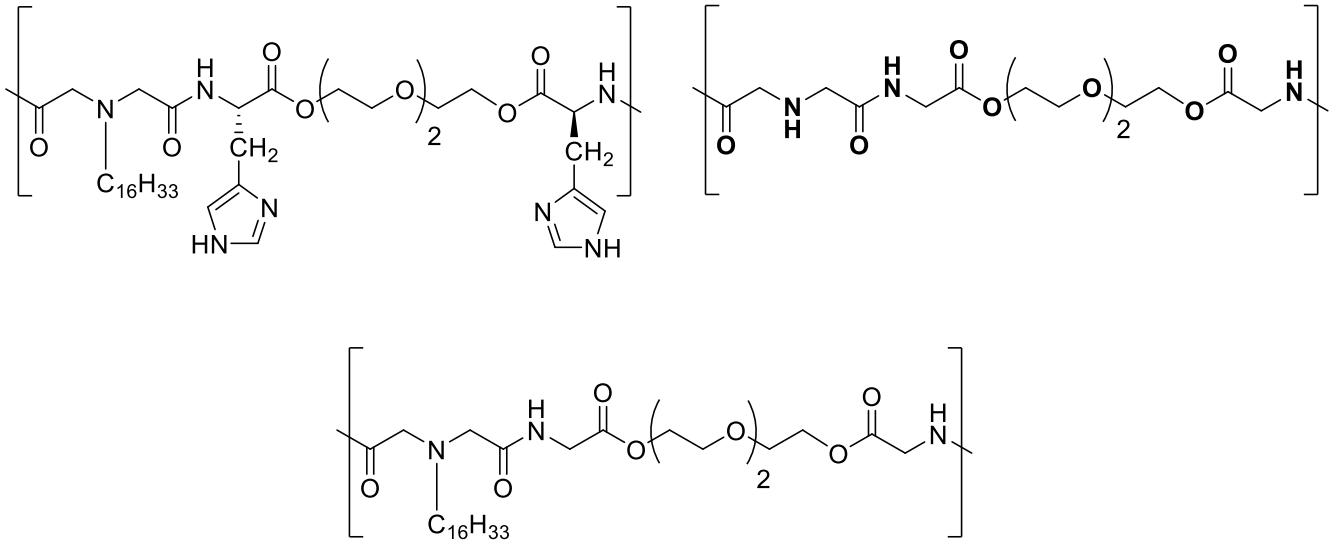

Figure A. IV. 1 . Target polymers for use as transfection agents.

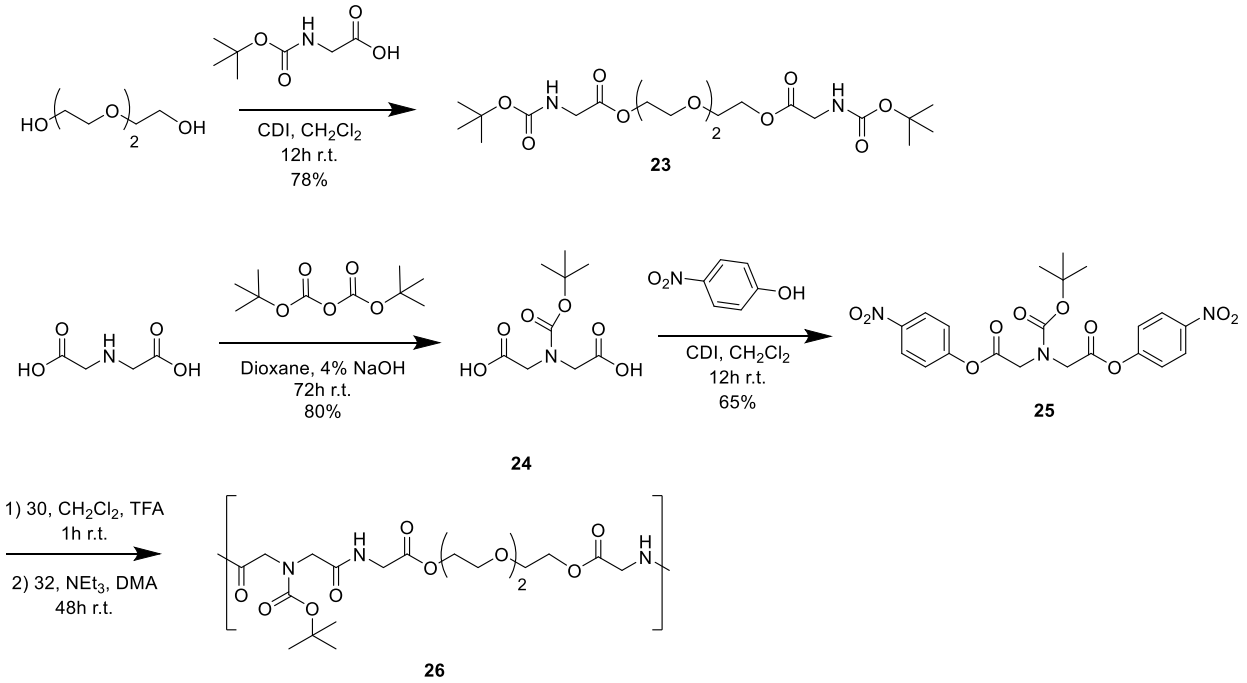

Figure A. IV. 2 Synthesis of Compound 26

Compound 23:

Triethylene glycol (1.00g, 6.66mmol), was dissolved in CH_2Cl_2 (25mL). Separately, Boc-Glycine (3.50g, 19.98mmol) and carbonyl diimidazole (3.24g, 19.98mmol) were dissolved in CH_2Cl_2 (50mL) and reacted for 1h at room temperature. Upon completion, the boc-glycine solution was added dropwise to the solution of triethylene glycol over 6h, and the reaction was allowed to proceed for an additional 12h at room temperature. Upon completion the solution was quenched with 1M HCl (100mL) and the organic phase washed with saturated $NaHCO_3$ (100mL), and brine (100mL). The organic layer was then dried on $MgSO_4$, filtered and concentrated *in vacuo*. The crude material was purified by column chromatography (1:1 Hex/EtOAc) to provide compound **23** (2.41g, 78%) ^{1}H NMR (500MHz, $CDCl_3$): δ = 1.41 (s, 18H), 3.61 (s, 4H), 3.67 (m, 4H), 3.91 (m, 4H), 4.27 (m, 4H).

Compound 24:

To a solution of iminodiacetic acid (5g, 37.57mmol) in dioxane (100mL) was added a 4% NaOH solution (100mL). Following this addition, di-tert-butyl decarbonate (9.02g, 41.32mmol) was added and the reaction proceeded for 72hr at room temperature. The solution was then extracted with diethyl ether (150mL). The aqueous phase was then adjusted to pH 6 with 10% HCl and extracted with EtOAc (3 x 100mL) the combined organic fractions were then washed with brine (3 x 100mL) and then dried on $MgSO_4$, filtered and concentrated *in vacuo.* The crude material was then crystallized from EtOAc/Hexanes to give the pure compound **24** (7.00g, 80%) ^{1}H NMR (500MHz, DMSO D_6): δ = 1.37 (s, 9H), 3.89 (m, 4H).

Compound 25:

Compound **24** (500mg, 2.14mmol) was suspended in CH_2Cl_2 (100mL) and carbonyl diimidazole (800mg, 4.93mmol) was added. This mixture was stirred for 1hr, followed by the addition of a solution of p-nitrophenol (895mg, 6.43mmol) in CH_2Cl_2 (20mL). This mixture was then stirred for 12hr at room temperature. Upon completion the mixture was concentrated in vacuo and purified by column chromatography (1:1 Hex/EtOAc) to give the pure compound **25** (661mg, 65%) ^{1}H NMR (500MHz, $CDCl_3$): δ = 1.49 (s, 9H), 4.42 (m, 4H), 7.32 (m, 4H), 2.28 (m, 4H).

Compound 26:

Compound **23** (92.5mg, 0.20mmol) was first dissolved in CH_2Cl_2 (5mL) and TFA (5mL) was added. The reaction proceeded for 1h followed by the removal of the solvent in vacuo to give the TFA salt of compound **23** which was used directly in the next step. Separately, compound **25** (95mg, 0.20mmol) was dissolved in distilled DMA (2mL). The TFA salt of compound **23** was then added to this solution. NEt_3 (124uL, 0.50mmol) was added and the resulting mixture was stirred for 48 hours. The resulting gel was then dissolved by dilution with DMA (20mL) and dialysed in against DMF and then water using a membrane with a 1 kg mol^{-1} MWCO. Lyophilization provided **26** as a white powder. ^1H NMR (500MHz, $CDCl_3$): δ = 1.45 (s, 9H), 3.67 (m, 8H), 4.04 (m, 8H), 4.31 (m, 4H).

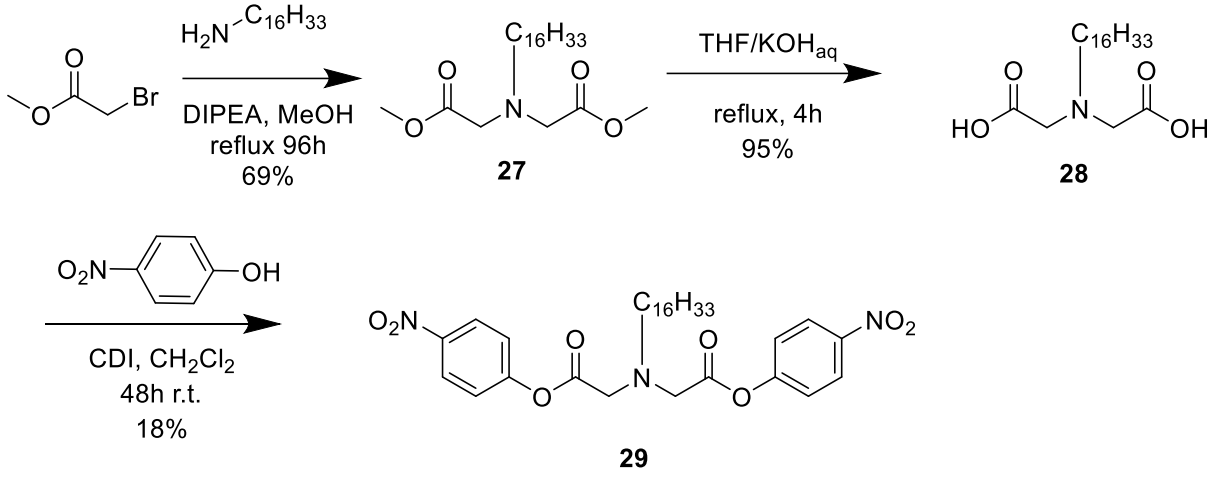

Figure A. IV. 3 Synthesis of bis(4-nitrophenyl) 2,2'-(hexadecylazanediyl)diacetate

Compound 27:

1-hexadecanamine (1.81g, 7.50mmol) was first dissolved in methanol (75mL) and DIPEA (3.92mL, 30mmol) was added. Methyl bromoacetate (2.29g, 15.0mmol) was then added and the solution was refluxed for 96h. Upon completion, the solution was concentrated in vacuo and then redissolved in minimal $CHCl_3$ and purified by column chromatography (5% MeOH in $CHCl_3$) to provide compound **27** (2.00g, 69%) ^1H NMR (500MHz, $CDCl_3$): δ = 0.86 (m, 3H), 1.23 (m, 29H), 1.45 (m, 2H), 2.66 (m, 2H), 3.53 (s, 4H), 3.70 (s, 6H).

Compound 28:

Compound **27** (7.60g, 20.0mmol) was first dissolved in THF (150mL). Separately, a 0.5M KOH solution (100mL) was prepared and then added to the THF solution. The combined solutions were then refluxed for 4h. Upon completion, the solution was cooled to room temperature and the THF was evaporated. The mixture was then acidified to pH 2 with HCl conc. and the resultant precipitate was filtered and collected, giving compound **28** (6.79g, 95%) without any further purification. ^{1}H NMR (500MHz, D_2O): δ = 0.83 (m, 3H), 1.22 (m, 29H), 1.49 (2H), 2.94 (m, 2H), 3.82 (m, 4H).

Compound 29:

Compound **28** (500mg, 1.40mmol) was suspended in CH_2Cl_2 (20mL) and carbonyl diimidazole (1.30g, 8.40mmol) was added. The mixture was stirred for 2h and then p-nitrophenol (1.20g, 8.5mmol) was added and the mixture was reacted for an additional 48 h. Upon completion, the reaction was washed with 1M HCl (50mL) , saturated $NaHCO_3$ (50mL) and brine (50mL). The organic layer was then dried on $MgSO_4$, filtered and concentrated *in vacuo*. The crude mixture was then purified by column chromatography (5:4:1 Hex/Tol/EtOAc) to give the pure compound **29** (150mg, 18%) ^{1}H NMR (500MHz, $CDCl_3$): δ = 0.87 (m, 3H), 1.25 (m, 29H), 1.58 (m, 2H), 2.88 (m, 2H), 3.92 (s, 4H), 7.33 (m, 4H), 8.30 (m, 4H).

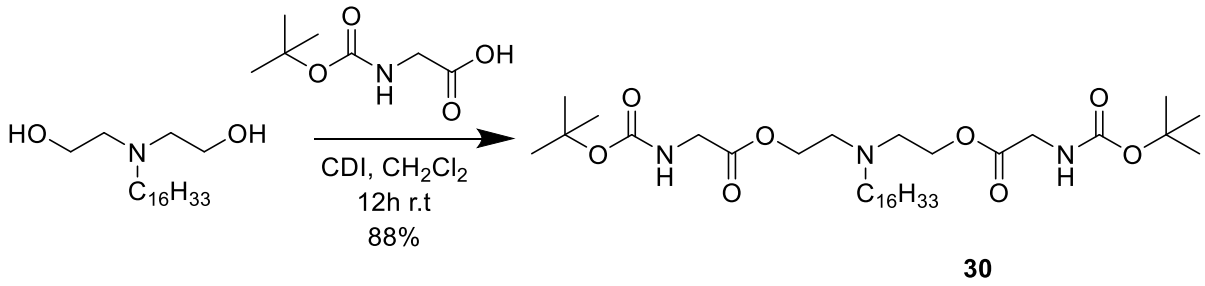

Figure A. IV. 4 Synthesis of (hexadecylazanediyl)bis(ethane-2,1-diyl) bis(2-((tert-butoxycarbonyl)amino)acetate)

Compound 30:

2,2'-(hexadecylimino)bis-ethanol (500mg, 1.50mmol) was dissolved in CH_2Cl_2 (20mL). Separately Boc-glycine (1.59g, 9.10mmol) and carbonyl diimidazole (1.48g, 9.10mmol) were dissolved in CH_2Cl_2 (50mL) and stirred for 1h. Upon completion this solution was then added to the solution of 2,2'-(hexadecylimino)bis-ethanol and reacted for 12 h at room temperature. The reaction was then washed with 1M HCl (100mL) , saturated $NaHCO_3$ (100mL) and brine (100mL) and the organic layer was then dried on $MgSO_4$, filtered and concentrated *in vacuo*. The crude mixture was then purified by column chromatography (9:1 EtOAc:Hex) to provide the pure compound **30** (850mg, 88%) ^{1}H NMR (500MHz, $CDCl_3$): δ = 0.86 (m, 3H), 1.24 (m, 29H), 1.38 (m, 2H), 1.43 (s, 18H), 2.49 (m, 2H), 2.75 (m, 4H), 3.90 (m, 4H), 4.17 (m, 4H).

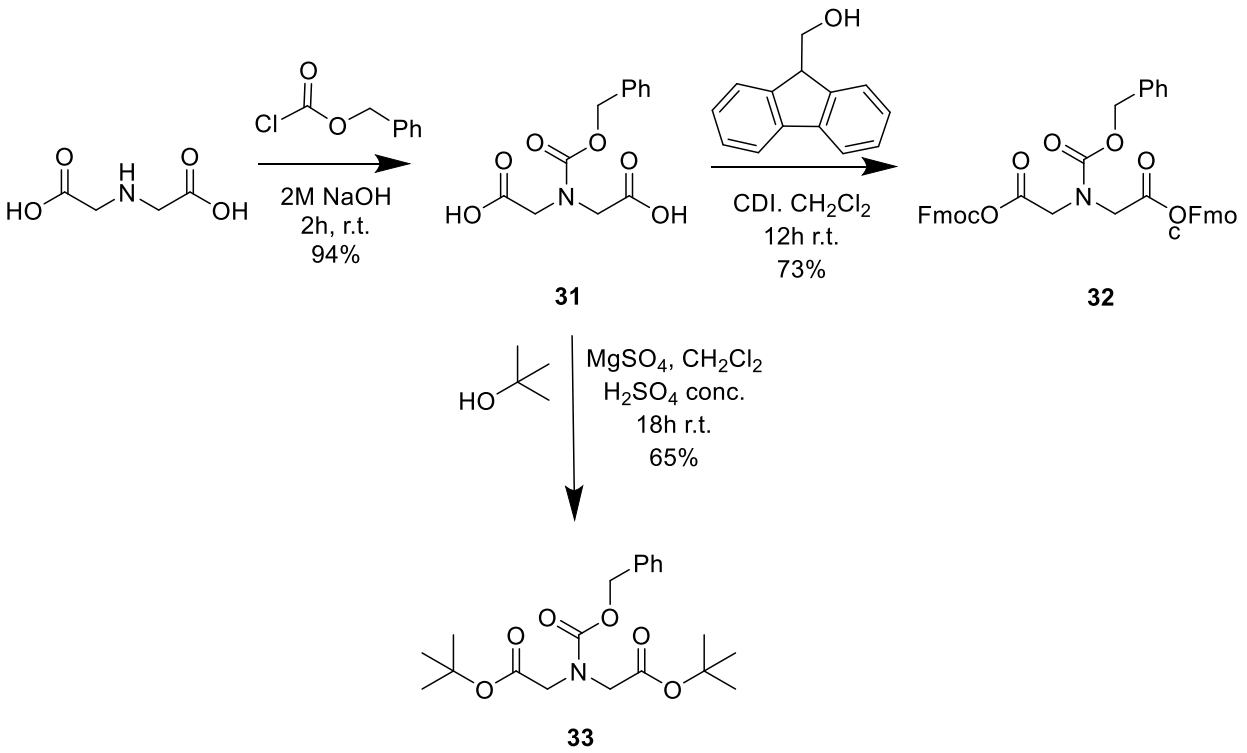

Figure A. IV. 5 Synthesis of di-tert-butyl 2,2'-(((benzyloxy)carbonyl)azanediyl)diacetate and bis((9H-fluoren-9-yl)methyl) 2,2'-(((benzyloxy)carbonyl)azanediyl)diacetate.

Compound 31:

Imidicotimide (5.00g, 37.5mmol) was first dissolved in a solution of 2M NaOH (200mL). To this solution benzyl chloroformate (9.00g, 52.5mmol) was added dropwise and the solution stirred

for 2h. Upon completion, the aqueous solution was extracted with Et_2O (2 x 150mL). The aqueous phase was then cooled to 0°C acidified to pH 2 with HCl conc. The aqueous phase was then extracted with Et_2O (3 x 150mL), dried on $MgSO_4$, filtered and concentrated *in vacuo*, to give compound **31** without any further purification (9.42g, 94%). ^{1}H NMR (500MHz, $CDCl_3$): δ = 4.11 (m, 4H), 5.14 (s, 2H), 7.28 (m, 5H), 8.83 (m, 2H).

Compound 32:

Compound **31** (400mg, 1.50mmol) was dissolved in CH_2Cl_2 (20mL) over 2h. To this solution was added carbonyl diimidazole (973mg, 5.99mmol) and the solution was left for 1h at room temperature. Following this, 9-fluoenylmethanol (1.32g, 6.75mmol) was added and the mixture reacted for 12 h. Upon completion, the organic phase was washed with 1M HCl (50mL), saturated $NaHCO_3$ (50mL) and brine (50mL). The organic phase was then dried on $MgSO_4$, filtered, and concentrated *in vacuo*. The crude mixture was then purified by column chromatography (7.5:2.5 Hex/EtOAc) to give the pure compound **32** (779mg, 73%). ^{1}H NMR (500MHz, $CDCl_3$): δ = 3.97 (s, 2H), 4.07 (s, 2H), 4.45 (m, 4H), 5.08 (s, 2H), 7.30 (m, 9H), 7.41 (m, 4H), 7.52 (m, 2H), 7.56 (m, 2H), 7.75 (m, 4H).

Compound 33:

$MgSO_4$ (2.50g, 21.0mmol) was suspended in CH_2Cl_2 (20mL) and stirred vigorously, H_2SO_4 conc.(433uL, 5.20mmol) was then added dropwise and stirred for 15min. Following this, compound **31** (693mg, 2.60mmol) was added to the solution, followed by the addition of t-BuOH (2.44mL, 26.0mmol), and the solution was stirred for 18h at room temperature. Upon completion the reaction was quenched with saturated $NaHCO_3$ (100mL) to dissolve the $MgSO_4$, and the organic phase was separated, dried on $MgSO_4$, filtered, and concentrated in vacuo. The crude mixture was then purified by column chromatography (100% Hex to 9:1 Hex/EtOAc) to give the pure compound **33** (641mg, 65%). ^{1}H NMR (500MHz, $CDCl_3$): δ = 1.37 (s, 9H), 1.46 (s, 9H), 3.96 (s, 2H), 4.04 (s, 2H), 5.14 (s, 2H), 7.31 (m, 5H).

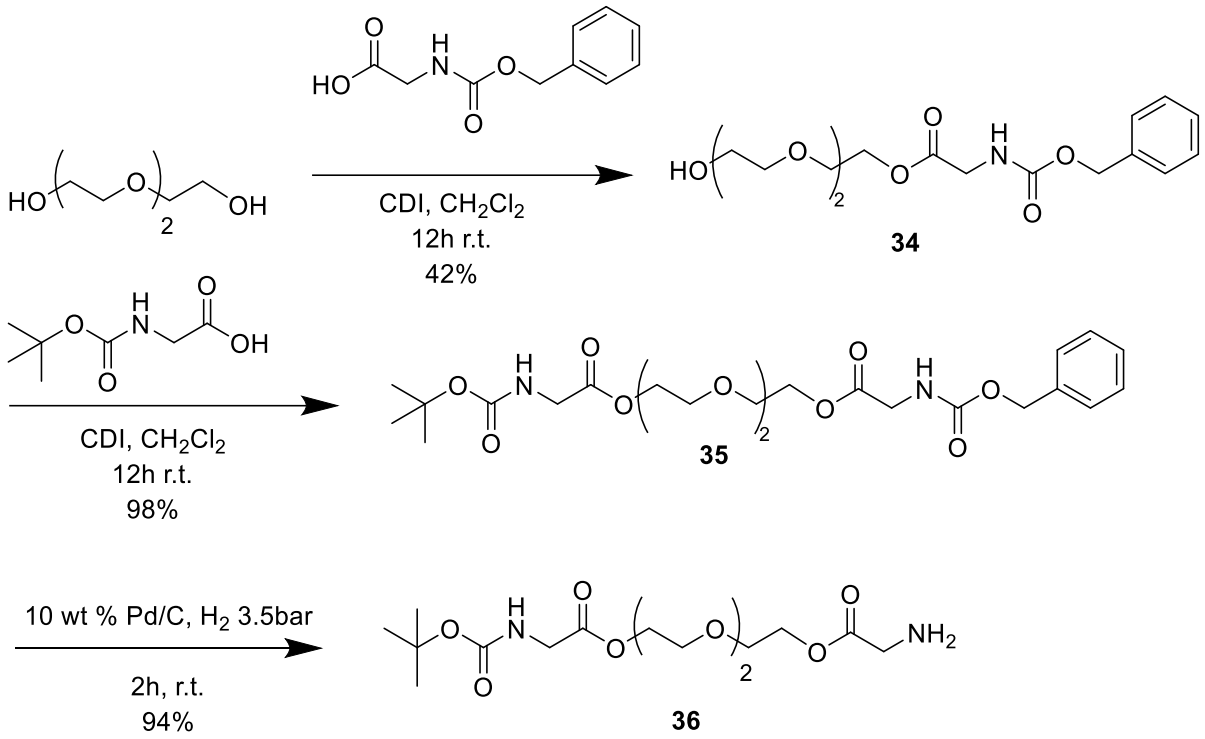

Figure A. IV. 6 Synthesis of 2,2-dimethyl-4,7-dioxo-3,8,11-trioxa-5-azatridecan-13-yl glycinate

Compound 34:

Triethylene glycol (652mg, 4.34mmol), was dissolved in CH_2Cl_2 (25mL). Separately, Cbz-Glycine (1.00g, 4.78mmol) and carbonyl diimidazole (775mg, 4.78mmol) were dissolved in CH_2Cl_2 (25mL) and reacted for 1h at room temperature. Upon completion, the cbz-glycine solution was added dropwise to the solution of triethylene glycol over 6h, and the reaction was allowed to proceed for an additional 12h at room temperature. Upon completion the solution was quenched with 1M HCl (50mL) and the organic phase washed with saturated $NaHCO_3$,(50mL) and brine (50mL). The organic layer was then dried on $MgSO_4$, filtered and concentrated *in vacuo*. The crude material was purified by column chromatography (5% MeOH in CH_2Cl_2) to provide compound **24** (728mg, 42%) ^{1}H NMR (500MHz, $CDCl_3$): δ = 2.60 (s, 1H), 3.64 (m, 10H), 4.00 (m, 2H), 4.29 (m, 2H), 5.11 (2, 2H), 7.34 (m, 5H).

Compound 35:

Compound **34** (500mg, 1.46mmol), was dissolved in CH_2Cl_2 (25mL). Separately, Boc-Glycine (1.50g, 8.79mmol) and carbonyl diimidazole (1.43g, 8.79mmol) were dissolved in CH_2Cl_2 (75mL) and reacted for 1h at room temperature. Upon completion, the boc-glycine solution was added dropwise to the solution of Compound **34** over 6h, and the reaction was allowed to proceed for an additional 12h at room temperature. Upon completion the solution was quenched with 1M HCl (100mL) and the organic phase washed with saturated $NaHCO_3$,(100mL) and brine (100mL). The organic layer was then dried on $MgSO_4$, filtered and concentrated *in vacuo*. The crude material was purified by column chromatography (5% MeOH in CH_2Cl_2) to provide compound **35** (800mg, 98%) ^{1}H NMR (500MHz, $CDCl_3$): δ = 1.44 (s, 9H), 3.62 (m, 4H), 3.68 (m, 4H), 3.91 (m, 2H), 4.00 (m, 2H), 4.28 (m, 4H) 5.12 (s, 2H), 7.34 (m, 5H).

Compound 36:

Pd/C catalyst (80mg, 10 wt %) was added to a solution of **35** (800mg, 1.43mmol) in methanol (25 mL). The resulting solution was stirred under a hydrogen atmosphere (3.5 bar) for 2h, and then the reaction mixture was filtered through celite, and the solvent was removed *in vacuo* providing **36** (490mg, 94%). ^{1}H NMR (500MHz, $CDCl_3$): δ = 1.40 (s, 9H), 3.59 (m, 10H), 3.85 (m, 2H), 4.24 (m, 2H).

Appendix V. Acid sensitive DNA Prism

Displayed here are the design, sequences and assembly for a DNA pentagonal prism which responds to low pH to open using an i-motif.

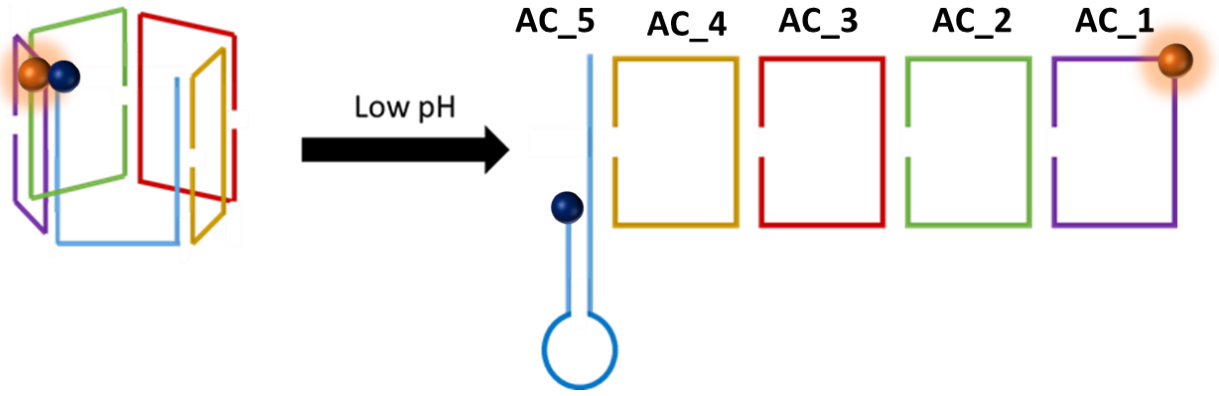

Figure A. V. 1. Mechanism of prism opening under acidic pH

Table A5.1 Sequences used for pH sensitive prism. (Cy3= cyanine 3 phosphoramidite), (HEG=Hexaethylene glycol phosphoramidite), (BHQ2 = 5' Black hole quencher phosphoramidite)

Name	Sequences (From 5' to 3')
AC_1	TCG CTG AGT ATT TTT CCT ATA TGG TCA ACT GCT CTT TTT ATG AGG GGA GGC ATG AG(Cy3) TAT TTT TGT AGT AAT ACC AGA TGG AGT TTT TCA CAA ATC TG
AC_2	CTA TCG GTA GTT TTT CCT ATA TGG TCA ACT GCT CTT TTT ACT CAG CGA CAG ATT TGT GTT TTG TAG TAA TAC CAG ATG GAG TTT TTC AAC TAG CGG
AC_3	CAC TGG TCA GTT TTT CCT ATA TGG TCA ACT GCT CTT TTC TAC CGA TAG CCG CTA GTT GTT TTG TAG TAA TAC CAG ATG GAG TTT TTG GTT TGC TGA

AC_4	CCA CAC TTG CTT TTT CCT ATA TGG TCA ACT GCT CTT TTC TGA CCA GTG TCA GCA AAC CTT TTG TAG TAA TAC CAG ATG GAG TTT TTG TGT GCG TGC
AC_5	(BHQ2)CT CAT GCC TCC CCT CCC CTC CGT TTC CCT CCC CTC CCC TCC TTT GGA GGG GAG GGG AGG (HEG)GC AAG TGT GGG CAC GCA CAC

Assembly Procedure:

AC_1, AC_2, AC_3, AC_4, and AC_5 were prepared as 5uM solutions in 1xTAMg pH 8. Equal volumes of each strand were then mixed and thermocycled from 95°C to 4°C over 12hr.

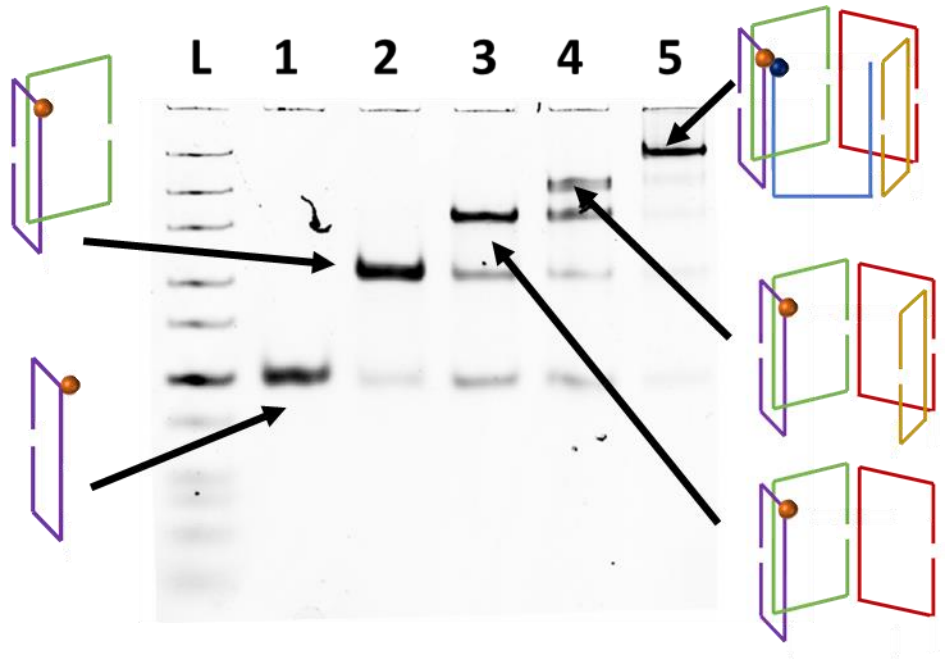

Figure A. V. 2. native PAGE 6% gel of the assembly of the acid responsive DNA prism

Lane 1: AC_1, Lane 2: Lane 1+AC_2, Lane 3: Lane 2: AC_3, Lane 4: Lane 3+ AC_4, Lane 5: Lane 4 + AC_5

Appendix VI. RAFT CTA DNA conjugation:

Described here are the sequences and synthetic procedure and characterization for generating DNA Raft initiator conjugates. This was in collaboration with the O'Reilly group at the University of Birmingham, for them to use as initiators for Polymerization-induced self-assembly (PISA) of oligonucleotides.

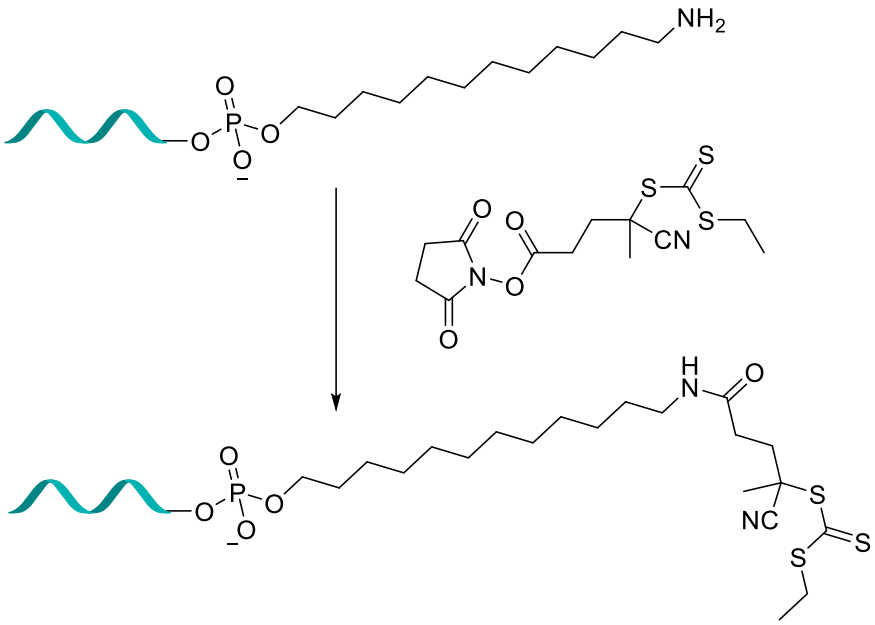

Figure A. VI. 1 Conjugation of a RAFT-CTA initiator to an amino functionalized oligonucleotide

Table A6.1 Sequences used for DNA Conjugates. (MMTNH2C12 = 5'-Amino-Modifier C12 (10-1912) Glen research)

Name	Sequences (From 5' to 3')
RAFT	(MMTNH_2C_{12})TGTAGCGTTGTTGC

RAFT Conjugation procedure

Strand RAFT was prepared as a 106uL, 746uM solution in H_2O. To this was added 11.81 uL of 10xTAMg pH 8, 3.91uL H_2O and 253uL of DMSO. A solution of 2,5-Dioxopyrrolidin-1-yl 4-cyano-4-(((ethylthio)carbonothioyl) thio) pentanoate (ambeed A705653) was prepared by dissolving 100mg in 2.20mL of dry DMSO. 31.8uL of this solution was then added to the RAFT DNA solution and the solution was reacted for 12h. Following this 593uL of H_2O was added to the solution and the solution was filtered through Micro .2µm Nylon Centrifugal Filters. The filtrate was then

dialysed using 1K MWCO dialysis membrane against DMF (24hr replacing dialysate every 6-8hr) and then H_2O (24hr replacing dialysate every 6-8hr). The dialysed solution was then dried by lyophilization to give the RAFT-CTA conjugate.

Table A6.2 calculated and experimental mass spectra of RAFT-CTA

Name:	Calculated	Found
RAFT CTA	4806.90	4806.92

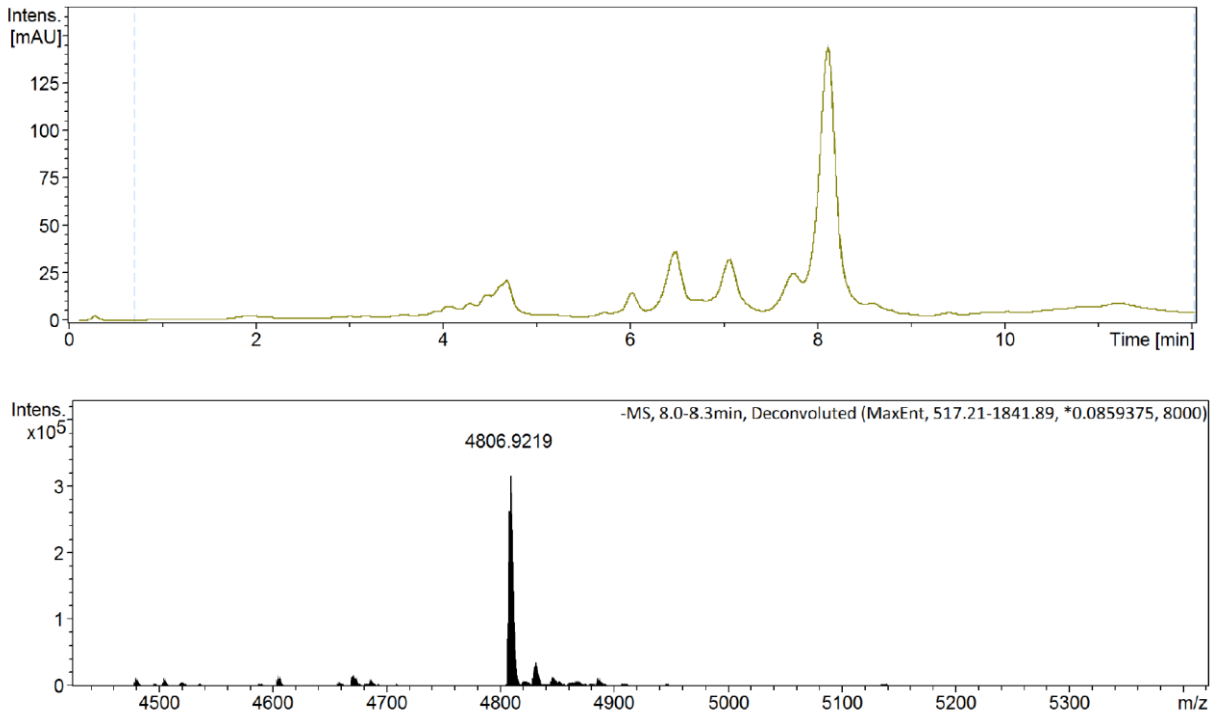

Figure A. VI. 2. RP-HPLC and LC-MS of RAFT-CTA.

Appendix VII. Disulfide Ligated Cube:

Described here are the sequences and characterization of a DNA cube with disulfide modifications at its corners, which we ligated together to increase stability.

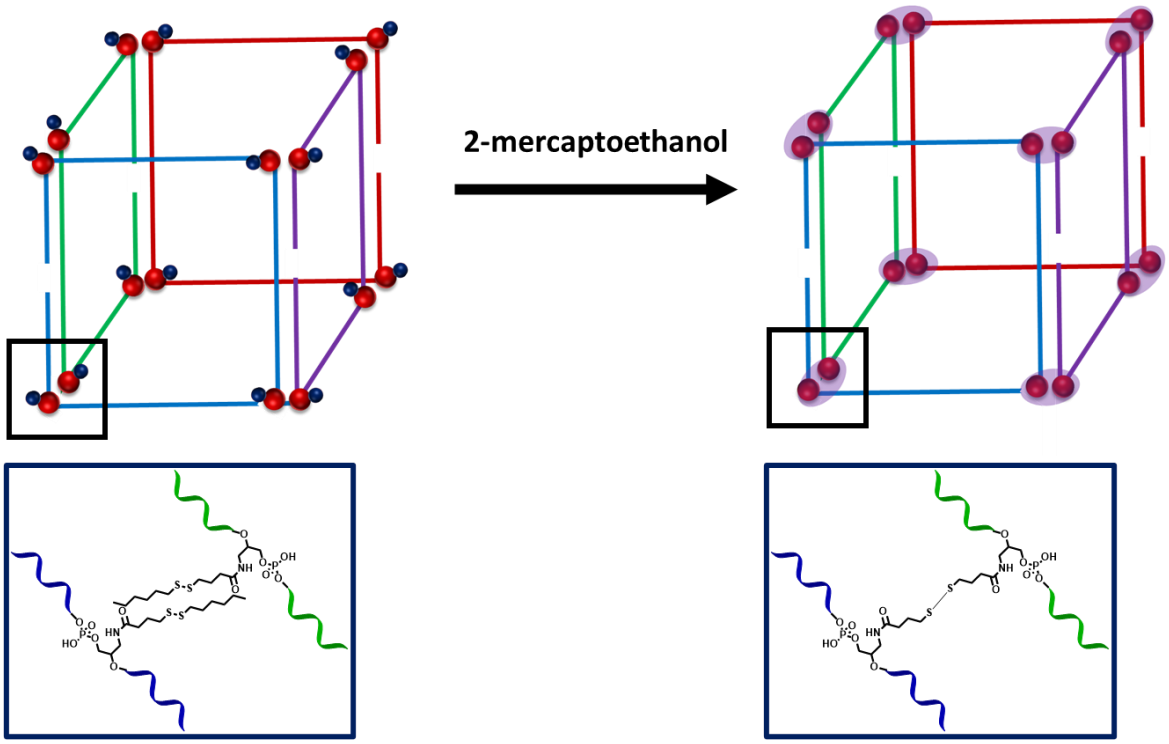

Figure A.VII. 1 Scheme illustrating the ligation of a DNA cube using disulfide bond formation

Table A7.1 Sequences used for disulfide ligated cube (X= disulfide phosphoramidite from chapters 3 and 4),

Name	Sequences (From 5' to 3')
DC_1	TAG CTG AGT ATX TTT TCC TAT ATG GTC AAC TGC TCT TTX TGC AAG TGT TGG AAC GCA CAC TXT TTG TAG TAA TAC CAG ATG GAG TTT TXT CAC AAA TCT G
DC_2	CAA TCG GTA GTX TTT TCC TAT ATG GTC AAC TGC TCT TTX TTA CTC AGC TAC AGA TTT GTG TXT TTG

	TAG TAA TAC CAG ATG GAG TTT TXT CAA CTA GCT G
DC_3	CAC TGG TCA GTX TTT TCC TAT ATG GTC AAC TGC TCT TTX TCT ACC GAT TGC AGC TAG TTG TXT TTG TAG TAA TAC CAG ATG GAG TTT TXT GGT TTG CTT A
DC_4	CAA CAC TTG CTX TTT TCC TAT ATG GTC AAC TGC TCT TTX TCT GAC CAG TGT AAG CAA ACC TXT TTG TAG TAA TAC CAG ATG GAG TTT TXT GTG TGC GTT C

The ligated cube was generated by first preparing a 40x concentrated solution of BME in 1xTAMg pH 8. The clips were first prepared as 1.03uM in 97.5uL in 1x TAMg pH 8 and thermocycled from 95^{o}C to 4^{o}C over 12hr. Following this, 2.5uL of the BME solution was added to the solutions to bring the final volume to 100uL and concentration to 1uM with 1x BME. These solutions were left for 48 hr, and then analysed by native/ denaturing PAGE. We found that at around 50mM of BME in solution that maximum crosslinking occurred as in the denaturing gel the upper band persisted the most. Moving to 200mM of BME lower products can start to be seen increasing in intensity indicating that full reduction is occurring at these higher concentrations.

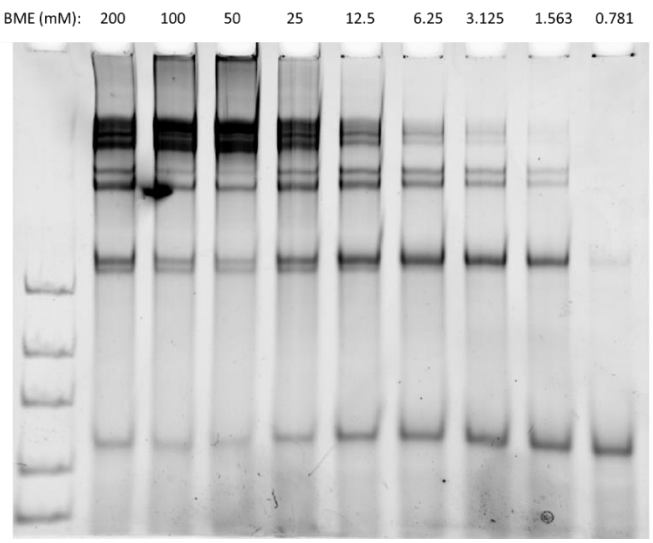

Figure A.VII. 2 Denaturing gel of ligated cube with increasing BME concentration.

Appendix VIII. AND gate design:

Displayed here is the design for a DNA and gate which responds only when two inputs are present.

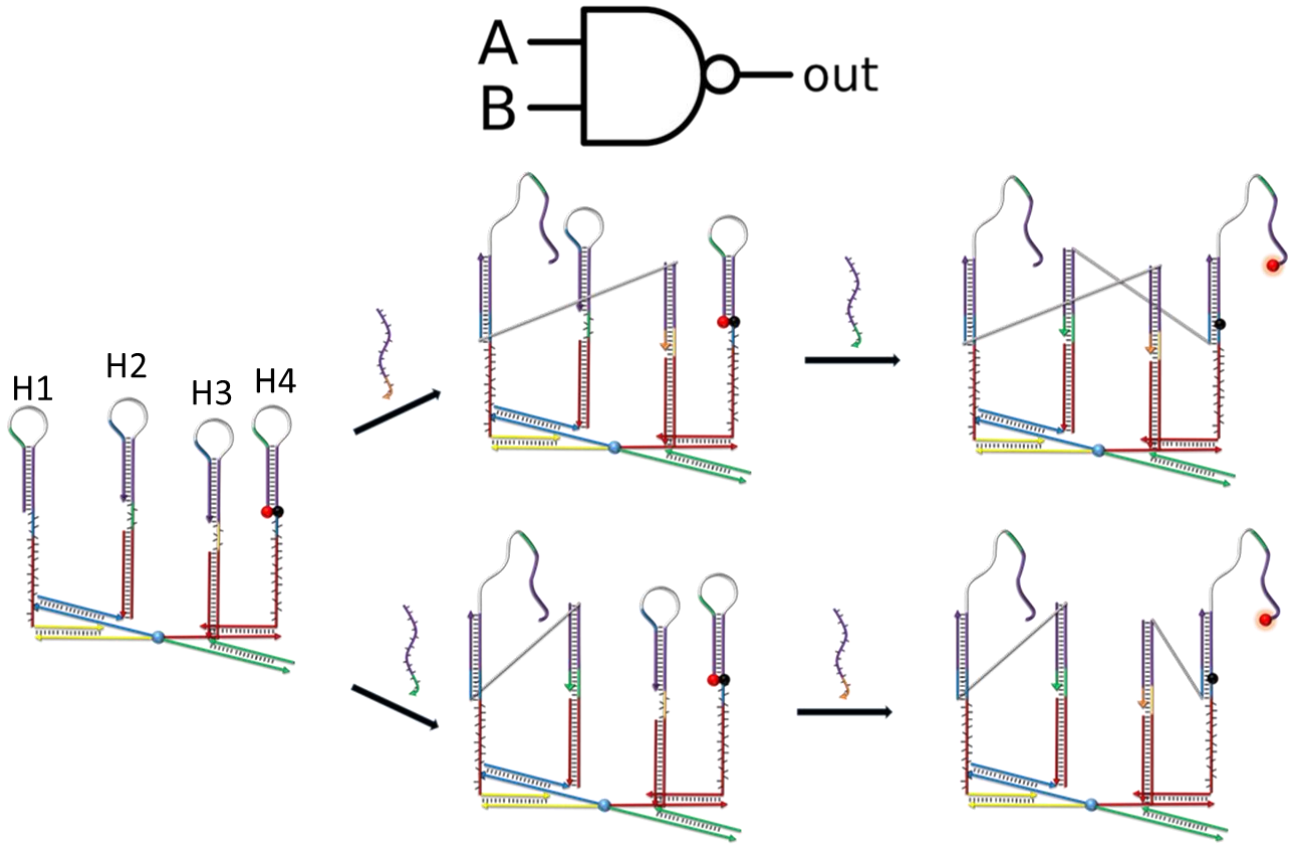

Figure A.VIII. 1 Design of a DNA minimal AND gate.

This design is based off a combination of our OR Gate design and the method used in A spatially localized architecture for fast and modular DNA computing (***Nature Nanotechnology*** *12,* 920-927 *(*2017*)).* Briefly, the output hairpin H4 has a shorter overhang sequence than the sequestering hairpin (H1). When either H2 or H3 is initiated, they preferentially hybridize to the hairpin with the longer overhang region (H1). Only when both initiators are present and H1 has already been hybridized too, does hybridization to H4 occur. Therefore, the initiator for H2 AND the initiator for H3 is needed to open H4, making the AND gate. This design uses a tetramer with four unique sequences connected at a synthetic vertex published by our lab. (***Angew. Chem. Int. Ed.***, 2019, *58*, 3042–3047.)